

**IMPROVING REPEATABILITY OF
LABORATORY-BASED FRICTION AND WEAR
TESTING WITH A MODIFIED RUNNING-IN
PROCEDURE**

Howard Parkin Benadé

**IMPROVING REPEATABILITY OF
LABORATORY-BASED FRICTION AND WEAR
TESTING WITH A MODIFIED RUNNING-IN
PROCEDURE**

By

Howard Parkin Benadé

A thesis submitted in partial fulfilment of the requirements of the degree

Doctor of Philosophy (Chemical Engineering)

In the

Department of Chemical Engineering

University of Pretoria

Pretoria

04 February 2022

IMPROVING REPEATABILITY OF LABORATORY-BASED FRICTION AND WEAR TESTING WITH A MODIFIED RUNNING-IN PROCEDURE

Abstract

Repeatability of friction and wear testing results is a problem often experienced with laboratory-based tests. To determine repeatability of friction and wear testing results on the SRV test rig (Schwingung, Reibung und Verschleiß), the factors that affect repeatability were investigated. Repeatability was improved with a gradual load increase procedure to the test load from the running-in load.

The test method used throughout was based on the American Society for Testing and Materials (ASTM) standard test method as described in ASTM D 6425, using the standard test specimens. This test utilizes a ball-on-disc configuration with sliding oscillating motion. Different base oils with different viscosities were used. A friction modifier and an anti-wear agent were included as additives to enable the friction and wear test to be completed at a load of 200 N. The additives were used separately in the selected test fluid formulations. The factors that affect repeatability are:

- Base oil viscosity.
- Base oil composition. This relates to the viscosity index and polarity of the base oil.
- Additive.
- Step load increase from the running-in load to the operating load.
- Wear scar measurement.

The first 3 factors affect the extent to which the metal surfaces can make direct contact. The better the fluids' ability to prevent contact, the less interactions will occur. This in turn decreases the probability of deviations and so better repeatability will be obtained.

Calculation of the Stribeck curves showed that test procedure used, operates from the boundary to the elastohydrodynamic lubricating regime. Since the ball motion is oscillatory, the ball speed reached a maximum in the middle of the stroke, where the highest Stribeck parameter value was obtained.

The step load increase showed that the apparent contact area increased rapidly once the operating load was reached. This new area contains an area with unworn surface where wear occurs rapidly. This resulted in poor repeatability of the friction coefficient.

The wear scar diameter was adjusted with an image measurement correction technique. This improved repeatability of the friction and wear results for most base oils. The only exception was that the **polyalphaolefin 6 (PAO)**-based oils did not show any improvement. The main contribution of the correction is that it improves the accuracy of the measurement.

When the gradual load increase was implemented, the consistency of the wear profile improved. This in turn resulted in more consistent interactions between the metal surfaces which lead to improved repeatability of the friction coefficient and the extent of wear. The gradual load increase also showed a smooth transition when the load was increased compared to that of the step load increase.

The novelty of the investigation is in identifying the factors affecting repeatability and improving repeatability with a gradual load increase. The gradual load increase improves the consistency of the surface profiles generated. Contributions were also made regarding adjustment of the wear scar diameter toward the accuracy of measurements. An improved method to evaluate the repeatability of the friction coefficient was also developed. This method is based on integration of friction coefficient plots for the entire duration of the test. Furthermore, by also analysing the wear rates, better insight into the duration of the running-in process on the SRV test rig was obtained.

In this investigation, the running-in procedure was extended to 5 minutes at an operating load of 50 N. After 5 minutes the load was stepped up to the operating load of 200 N. The gradual load increase procedure had a gradient of 30 N/min, for the

duration of the running-in procedure. The atmospheric conditions were controlled throughout the test with a humidity of 45 % relative to 22 °C. The block temperature was set at 50 °C and the stroke was 1 mm with a frequency of 50 Hz. Each test was repeated 5 times.

KEYWORDS: friction and wear testing, repeatability, running-in, SRV test rig.

Contents

Abstract	i
Nomenclature	vii
Chapter 1	1
Introduction	1
Chapter 2	6
Literature	6
2.1 Overview	6
2.2 Repeatability	6
2.3 Contact between Two Surfaces	8
2.3.1 Contact Parameters between a Sphere and a Flat Surface	8
2.3.2 Real Contact Area	11
2.3.3 Surface Layers	16
2.3.4 Surface Profiles and Surface Roughness	20
2.3.5 Wear Classification	25
2.3.6 Oxidation Wear	28
2.3.7 Effect of Surface Properties	29
2.4 Transition Processes in Tribology: Running-in	35
2.4.1 Transition Processes in Tribology	35
2.4.2 Definition of Running-in	40
2.4.3 Studies on the Running-in and Wear Process	43
2.4.4 Effect of Load Increase on Friction and Wear	45
2.5 Effect of Water on Friction and Wear	48
2.6 Base Oils	51
2.6.1 Group II and Group III Mineral Oil	51
2.6.2 White Mineral Oil	55
2.6.3 Polyalphaolefin (PAO)	55
2.6.4 Polyalkylene Glycol (PAG)	56
2.6.5 Friction and Wear Behaviour of Base Oils	57
2.6.6 Additives	57
2.6.7 Friction Modifiers	58
2.6.8 Anti-wear Additives	59

2.7	Stribeck Curve.....	62
Chapter 3		66
Experimental		66
3.1	Overview	66
3.2	Test Fluid Selection.....	69
3.3	Apparatus.....	70
3.3.1	Viscosity Measurement.....	71
3.3.2	Ultrasonic Cleaner	72
3.3.3	Mass Balance	73
3.3.4	Friction and Wear Measurement	73
3.3.5	Surface Analysis.....	75
3.3.5.1	Carl Zeiss Optical Microscope.....	75
3.3.5.2	Nanovea Profiler PS50.....	75
3.3.6	Relative Humidity Control	77
3.4	Test Preparation.....	79
3.4.1	Specimen Preparation	79
3.4.2	Sample Blending and Handling	81
3.4.3	Test Start-up.....	82
3.5	Data Analysis	82
3.5.1	Friction Coefficient.....	82
3.5.2	Extent of wear.....	84
3.5.3	Wear Scar Diameter Adjustment	87
3.5.4	Wear Surface Evaluation	90
3.6	Lubricating Regime	91
Chapter 4		92
Results & Discussion.....		92
4.1	Factors Affecting Repeatability.....	92
4.1.1	Test Fluid Characterisation.....	92
4.1.1.1	Base Oil Viscosity.....	92
4.1.1.2	Viscosity Index	94
4.1.1.3	Lubricating Regime	95
4.1.1.4	Base Oil Composition.....	103
4.1.1.5	Amount of Additive	103

4.1.2	Repeatability of Friction and Wear Results.....	105
4.1.3	Influence of Step Load Increase	159
4.1.4	Influence of the Test Disk	164
4.1.5	Summary of Repeatability.....	169
4.2	Improving Repeatability.....	170
4.2.1	Extent of Wear.....	171
4.2.2	Wear Rates.....	186
4.2.3	Friction Coefficient & Wear Surfaces.....	191
4.3	Running-in.....	203
4.4	Correlation between Friction Coefficient and Wear Surface.....	204
4.5	Influence of the Test Disk.....	211
Chapter 5	215
Conclusions & Recommendations	215
Reference List	218
Appendix A: Studies on the Running-in Process	226
Appendix B.1: Friction Coefficient Graphs.....	264	
Appendix B.2: Wear Scar and Wear Track 3 D images.....	272	
Appendix B.3: Wear Surface Profiles	276	
Appendix B.4: Wear Volume Calculations.....	284	
Appendix C.1: Friction Coefficient Graphs: Gradient vs. Step Load Increase	294	
Appendix C.2: Wear Surfaces 3 D Images; Step Load and Gradient Load	306	
Appendix C.3: Wear Surface Images: Step Load and Gradient Load	310	
Appendix C.4: Wear Surface Profiles.....	316	
Appendix C.5: Wear Volume Calculations.....	328	
Appendix C.6: Disk Hardness	341	

Nomenclature

A_r	Real contact area	(m ²)
A_{ellips}	Area of an ellipse	(μm ²)
AVG_{COF}	Average of friction coefficient for 5 repeat runs.	
a	Linear acceleration	(m/s ²)
COF	Friction coefficient	
d_1	Wear scar diameter on the ball parallel to the sliding direction.	mm
d_{1adj}	Adjusted wear scar diameter on the ball parallel to the sliding direction.	mm
d_{1meas}	Measured wear scar diameter on the ball parallel to the sliding direction.	mm
d_2	Wear scar diameter on the ball perpendicular to the sliding direction.	mm
d_3	Total length of the wear track in the sliding direction.	mm
d_4	Width of the wear track.	mm
F	Friction Force	(N)
F_a	Friction force due to adhesion	(N)
F_d	Friction force due to deformation	(N)
F_N	Normal contact force/load	(N)
F_T	Total friction force	(N)
f	Friction coefficient	
h	Liquid film thickness	(m)
h_{min}	Minimum film thickness	(μm)
L	Sample Length	(μm)
p	Peak height relative to average	(μm)
$R_a, CLA \text{ or } AA$	Centre-line average, arithmetic average	(μm)
\bar{R}	Resulting radius of the shape of the wear scar after the test.	mm
R	Initial radius of the ball	mm

R_c	Mean height of peak to valley	(μm)
R_{dc}	Profile section height difference	
R_{ku}	Kurtosis	
R_{mr}	Material ratio of profile	
R_p	Maximum peak height. Maximum peak to mean height	(μm)
R_q or RMS	Root Mean Square	(μm)
R_{sk}	Asperity Skewness	
R_t	Maximum peak to valley height	(μm)
R_v	Maximum valley depth, mean to lowest valley depth	(μm)
R_z	Average peak to valley height	(μm)
S_p	Modified Stribeck parameter	
s	Stroke	(mm)
s_{max}	Sliding distance at maximum velocity	(m)
$STDEV_{COF}$	Standard deviation of friction coefficient.	
t	time	(sec.)
t	Constant for piezoviscosity calculation	
u_i	Initial velocity	(m/s)
U	Speed	(m/s)
U_1	Speed of the ball	(m/s)
U_2	Speed of the disk	(m/s)
U_r	Rolling speed	(m/s)
u_{max}	Maximum velocity	(m/s)
v	Valley depth relative to average	(μm)
W	load per unit length	(N/m)
\bar{W}_{WSD}	Wear Rate: Ball Wear Scar Diameter	($\mu\text{m}/\text{s}$)
\bar{W}_{WVS}	Wear Rate: Ball Scar Wear Volume	($\mu\text{m}^3/\text{s}$)
\bar{W}_{WVT}	Wear Rate: Disk Track Wear Volume	($\mu\text{m}^3/\text{s}$)
WSD	Average wear scar diameter	(mm)
WSD_{meas}	Average wear scar diameter, based on measured values.	(mm)
WSD_{adj}	Average wear scar diameter, based on adjusted values.	(mm)

$W_{q,flat}$	Planimetric wear of the track of the wear track in the middle of the wear track length, seen perpendicular to the sliding direction (cross sectional area of profile).	mm^2
$W_{v,ball}$	Wear volume on the ball	(mm^3)
$W_{v,flat}$	Wear volume on the disk	(mm^3)
y	Constant for piezoviscosity calculation	
z	Height	(μm)

Greek

α	Piezoviscosity coefficient	(GPa^{-1})
β	Fraction of unlubricated area	
η	Dynamic viscosity	$(\text{kg/m}\cdot\text{s}^2)$
η_k	Kinematic viscosity at atmospheric pressure	(mm^2/s)
η_L	Dynamic viscosity of the oil	$(\text{kg/m}\cdot\text{s}^2)$
λ	Specific film thickness	
σ	Composite surface roughness ($\sigma = (\sigma_1^2 + \sigma_2^2)^{1/2}$)	(μm)
σ_1	Surface roughness of body 1	(μm)
σ_2	Surface roughness of body 2	(μm)
μ	Friction coefficient	
τ_a	Average shear strength of a dry contact	(N/m^2)
τ_l	Average shear strength of the lubricant film	(N/m^2)

Chapter 1

Introduction

Friction and wear testing on a laboratory scale is used as screening method to rank candidate lubricants. These tests usually precede field trials and are accelerated tests that can produce a result in a short time. Another advantage is that they are inexpensive (Bhushan, 2013: 615). These tests also form part of specifications and performance criteria required for a lubricant to be approved for specific applications (Rizvi, 2009: 531). For the test results to be reliable, repeatable results is an important requirement.

ASTM test standards D5707 and D6425 describe how friction and wear tests are conducted on the SRV test rig. These tests are used respectively to evaluate lubricating greases and lubricating oils. The repeatability to which test results must conform is specified in the standard according to the limits for the deviations between repeat runs for the friction coefficient and the wear scar diameter. Other standards to determine friction and wear properties on the SRV includes Deutsche Institute für Normung (DIN) 51834 (German), Chinese Standard (NB/SH/T) 0847 and International Organization for Standardization method, ISO 19291.

Cooperative inter-laboratory tests (Round Robin) have also been conducted by the DIN 51834 work group since the late 1990's. The focus of this work group is improving the precision of test standards. During these tests, several test conditions are investigated which include repeatability and running-in. They also look at the determination of the wear volume. These results are used as basis for improving and supplementing the test standards related to testing on the SRV (Woydt, & Weber, 2003, Woydt, 2012, Woydt, 2013, Woydt, 2014, Woydt, 2015, Woydt, 2016 & Woydt 2018).

In a previous study it was seen that the running-in procedure plays a role in repeatability of friction and wear testing results on the SRV test rig. Better repeatability was obtained when the step load increase in the standard procedure was replaced with a gradual load increase procedure. It was also found that relative humidity affects

repeatability. This study was, however limited to a vegetable-based oil with dispersed boron nitride particles (Benadé, 2015).

In test standards ASTM D5707 and D6425, the results that are reported are the friction coefficient and the wear scar diameter. This is for a sliding ball on stationary disk configuration. The wear scar diameter generated on the ball is measured in directions parallel to sliding and perpendicular to sliding. The boundary of the wear scar in the direction parallel to sliding is often poorly defined due to plough marks that exceed the boundary. This results in uncertainty w.r.t the accuracy of the measurement of the wear scar diameter.

These results do not include the wear volume. The standard practice for calculating the wear volume on the test pieces used by the SRV is given in ASTM D7755. Repeatability of the wear volume, however, has not been included in the standards (ASTMD 5707-16 and ASTM D6425-17).

As already mentioned, repeatability can be improved by modifying the load increase method during the running-in procedure on the SRV test rig. Running-in is an important part of the friction and wear process, since it influences the long-term behaviour in terms of friction and wear (Blau, 1989: 269-270). Improving repeatability reduces the uncertainty of friction and wear results.

The extent of wear can only be determined at the end of the test, when the SRV test setup is disassembled. Since alignment errors are made when used test pieces are reassembled, it is difficult to evaluate the wear behaviour during the test. The friction and wear process is also affected by the surface properties such as surface roughness, hardness, and variations in the subsurface microstructure (Bregliozzi et.al., 2003, Mei, et.al., 2019, Reis et.al., 2018, Zambrano et.al., 2019, Joshi et.al., 2019, Wos et.al., 2018, Okamoto et.al., 2016 and Podgursky et.al., 2011).

The objective of this investigation is to determine the factors that affect repeatability of friction and wear testing on the SRV test rig. Special attention is also given to the effect of these factors on running-in and how running-in links in with repeatability of friction and wear results. A technique has also been developed to adjust the wear scar

diameter parallel to the sliding direction. Furthermore, another objective is to study how repeatability is improved when a gradual load increase is implemented during the running-in procedure.

The factors that affect repeatability are limited to the influence of different test fluids, the step load increase during running-in as well as adjustment of the wear scar diameter. Test fluids differed on the API base oil category and the additive used. For the study on the modified procedure, only one test fluid was used while the load was gradually increased.

The friction and wear behaviour related to the 2 ASTM test methods was also evaluated. The focus was on transitions of the friction coefficient and how this related to the wear surface as well as the wear rates. Tests with shorter durations were included for this purpose.

The wear volume on the disk and on the ball was also calculated. This was done to establish repeatability of the wear volume results. The wear volume was also compared to the wear scar diameter, especially for the tests with shorter durations. This compares how the wear rates change during the test and compares the wear rates between the wear scar diameter and wear volume.

Repeatability of the wear surfaces was also determined. This was achieved by comparing microscopic surface images photographed under 10 times magnification. The wear profiles were measured with the aid of the Nanovea™ profiler. The wear profiles were also used to correlate the dependence of repeatability of the friction coefficient and extent of wear with the wear profile.

The lubricants used for this study included base oils with boundary lubricating additives. Simple formulations were used to reduce the number of variables that can affect repeatability. The base oils selected were mineral based oils and synthetic oils. No vegetable oils were used due to their complex chemistries and poor stability. The oils were: mineral oil **API Group II** and **API Group III**, **white mineral oil (Group V)**, **polyalphaolefin (Group IV)** and **polyalkylene glycol (Group IV)**. Two viscosity grades of the Group II mineral oil were also used to verify effects of viscosity.

To complete the friction and wear test on the SRV test rig at an operating load of 200 N, additives were required for all base oils. The additives included a friction modifier that physically adsorbs onto the surface and an additive that reacts to form a tribofilm. The two additives were **diethyl sebacate** (friction modifier) and **zinc dialkyldithiophosphate (ZDDP)** (anti-wear additive). Figure 1.1 is a flow diagram of the experimental design.

The investigation therefore aims to contribute to the understanding of the causes for poor repeatability as well as proving how improved repeatability can be obtained with a gradual load increase. Further contributions are also to improve accuracy of measurements and better interpretation of repeatability of the friction coefficient. The wear rates were also analysed, to gain better insight into the running-in process.

The test method was based on the standard friction and wear test methods described by ASTM D 5707 and ASTM D 6425. The same operating conditions were used (50 Hz, 1 mm stroke) while the block temperature was set at 50 °C and the humidity was controlled at 45 % relative to 22 °C. Standard test specimens were used for a ball-on-disc configuration on the SRV test rig. The test specimens were obtained from the supplier. The atmospheric conditions selected were based on the recommended environments for standard laboratories (ISA-TR52.00.01, 2006).

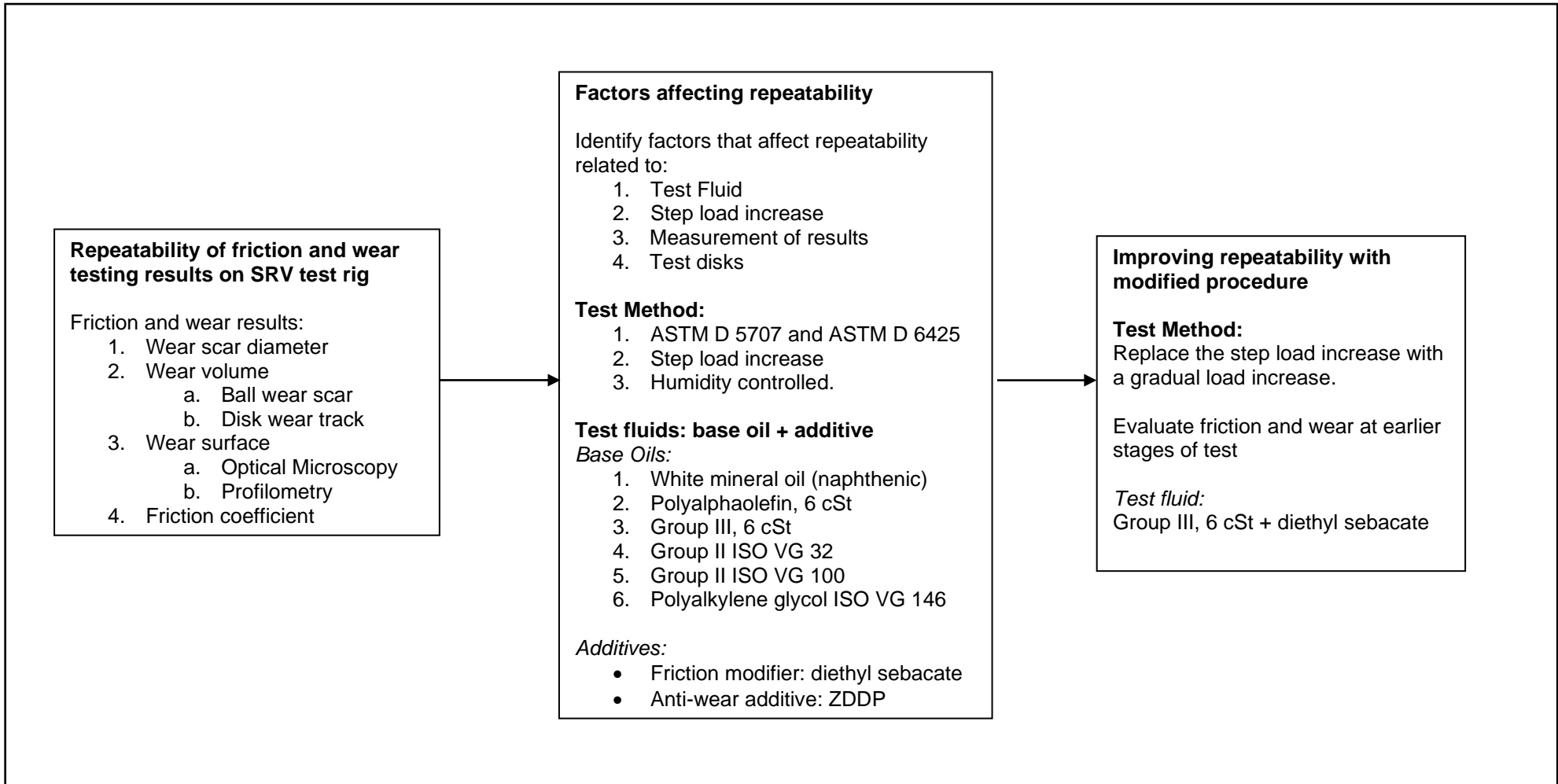


Figure 1.1: Flow diagram summarising the experimental design.

Chapter 2

Literature

2.1 Overview

The literature chapter focuses on the contact between two surfaces, specifically a sphere on flat. This includes the calculation of the contact parameters and the relation between the friction force and the surface interactions. Metal surfaces are characterised in terms of composition, structure, and surface finish.

The next part looks at the transition processes in the friction and wear process. Running-in is defined and this is followed by a summary of studies on the running-in. The effect of water on the wear process has also been included to justify the humidity that was controlled during the experimental investigation.

The properties of base oils and additives are also covered. This includes composition and friction and wear behaviour. Finally, the shifts in the Stribeck curve are explained. These shifts in the curve are due to differences in test fluid properties as well as the influence of surface roughness. However, since the focus of the investigation, this topic will be addressed first.

2.2 Repeatability

Repeatability is defined according to Brown, Tauler and Walczak, 2009 as:

“Repeatability conditions involve independent test results which are obtained with the same method, on identical test items, in the same laboratory, by the same operator, using the same equipment, and within short intervals of time. Thus, repeatability reflects the best achievable internal precision. The results are usually reported in terms of standard deviation, coefficient of variation (CV), or relative standard deviation (RSD).”

Repeatability is one of the key aspects of friction and wear testing. This mainly ensures certainty of friction and wear results. Repeatability is also part of test standards. Repeatability limits for ASTM D 5707 and ASTM D 6425 is specified for the friction coefficient and the wear scar diameter in Table 2.1. The repeatability can only be specified for results obtained by the same operator, on the same apparatus with identical tests materials under constant operating conditions. Furthermore, the limits can only be exceeded for 1 case in 20.

Table 2.1: Repeatability limits according to ASTM D 5707 and ASTM D 6425.

Test Standard	Ball Wear Scar Diameter	Friction Coefficient
ASTM D 5707		
50 °C	0.07 mm	0.012
80 °C	0.07 mm	0.008
ASTM D 6425	0.07 mm	0.010

In an overview paper by Blau (2017), the problem of repeatability is addressed. Different modes of wear were looked at, however of interest here is the lubricated wear as measure for fuel lubricity. In this article, the repeatability on the ball-on-cylinder, lubricant evaluation test rig (BOCLE) was evaluated. During this test, the load is applied onto the ball specimen while the cylinder rotates. The ball is stationary. The wear scar diameter on the ball is then measured (Blau, 2017).

Based on experimental results on different fuel samples, it was found that:

1. Surface finish is a key factor in repeatability (Biddle, Meehan & Warner, 1987).
2. Test chamber humidity needed to be controlled to improve repeatability (Lacey, 1994).

It was found that if the root-mean-square surface roughness (R_q) of the cylinder specimen exceeded 0.2 μm , no difference for the wear results were obtained. Below this value, results differed. The optimum surface roughness to differentiate between fuel samples was 0.04 μm . The effect of humidity is well known and have been investigated by many other researchers. This is addressed in section 2.5.

2.3 Contact between Two Surfaces

2.3.1 Contact Parameters between a Sphere and a Flat Surface

One of the configurations of the SRV test rig is a ball-on-disc configuration or sphere on a flat surface. The focus of this section will therefore be for this specific configuration. For elastic bodies, the contact area in elastohydrodynamic lubrication is circular, as shown in Figure 2.1 (Batchelor and Stachowiak, 2005: 293).

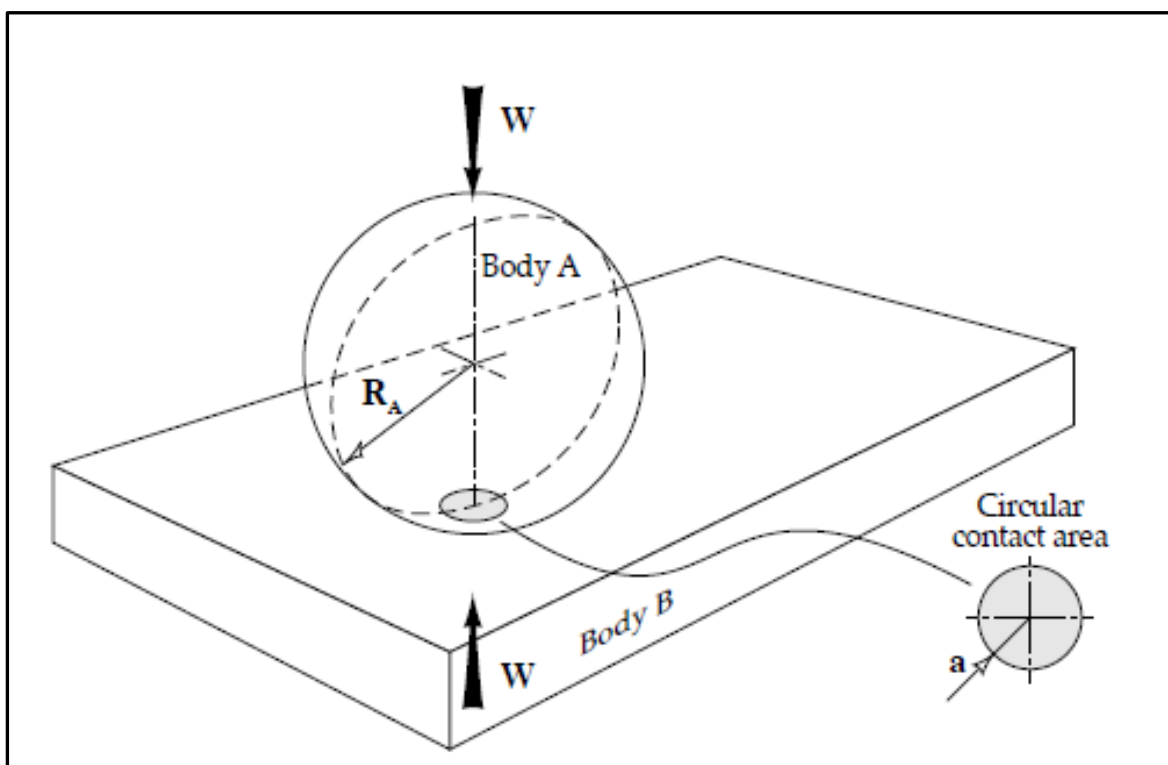


Figure 2.1: Contact between a sphere and a flat surface (Batchelor and Stachowiak, 2005: 293).

The equations to calculate the contact parameters for this geometry are summarised in Table 2.2. This applies to the initial condition on the SRV test rig before any wear has occurred.

Table 2.2: Equations for contact parameters between a sphere and a flat surface (Batchelor and Stachowiak, 2005: 289, 290 & 293-293)

Contact parameter	Description	Equation
Contact area dimension	Circle:	$a = \left(\frac{3WR'}{E'}\right)^{1/3}$
Maximum contact pressure	Hemispherical pressure distribution	$P_{max} = \frac{3W}{2\pi a^2}$
Average contact pressure		$P_{average} = \frac{W}{\pi a^2}$
Maximum deflection		$\delta = 1.0397\left(\frac{W^2}{E'^2 R'}\right)^{1/3}$
Maximum shear stress	At a depth of $z = 0.638a$	$\tau_{max} = \frac{1}{3}P_{max}$

The reduced Young's modulus is defined as:

$$\frac{1}{E'} = \frac{1}{2} \left[\frac{1 - \nu_A^2}{E_A} + \frac{1 - \nu_B^2}{E_B} \right]$$

The reduced radius of curvature for a sphere on a flat surface is defined as:

$$\frac{1}{R'} = \frac{1}{R_x} + \frac{1}{R_y}$$

$$\frac{1}{R'} = \frac{1}{R_{Ax}} + \frac{1}{R_{Bx}} + \frac{1}{R_{Ay}} + \frac{1}{R_{By}}$$

Where: $R_{Bx} = R_{By} = \infty$

And: $R_{Ax} = R_{Ay} = R_A$

Therefore: $\frac{1}{R'} = \frac{2}{R_A}$

Table 2.2: (continued).

Where:

a	Radius of the contact area [m].
W	Normal load [N].
P	Contact pressure (Hertzian stress) [Pa].
δ	Total deflection at the centre of the contact ($\delta = \delta_A + \delta_B$; where ' δ_A ' and ' δ_B ' are the maximum deflections if body 'A' and 'B') [m].
τ	Shear stress [Pa].
z	Depth under surface where the maximum shear stress acts [m].
E'	Reduced Young's modulus [Pa].
R'	Reduced radius of curvature [m].
ν_A and ν_B	Poisson's ratios of the contacting bodies 'A' and 'B'.
E_A and E_B	Young's moduli of the contacting bodies 'A' and 'B'.

By applying these equations to the SRV test configuration, the contact parameters at the start of a test can be determined. The specimens used on the SRV test rig are manufactured from AISI 52100 steel (ASTM D 5706, 5707, 6425 and 7421) and the material properties for this steel are used. The contact parameters are summarised in Table 2.3.

In Table 2.3, a maximum and minimum value for Young's modulus and Poisson's ratio is given. The contact parameters were calculated for both these values. The difference is small and represents the range of the contact parameters. The contact parameters are calculated at 200 N (operating load) as well as 50 N (running-in load).

Table 2.3: Contact parameters for ball-on-disc configuration on the SRV test rig (www.azom.com, 07 April 2016)

Specimen properties	Value	
	<i>minimum</i>	<i>maximum</i>
Young's modulus	190 GPa	210 GPa
Poisson's ratio	0.27	0.30
<hr/>		
Specimen dimensions		
SRV Ball specimen radius	5 mm	
<hr/>		
Operating Loads		
SRV running-in load	200 N	
<hr/>		
Contact parameters		
	<i>Young's modulus = 190 GPa</i>	<i>Young's modulus = 210 GPa</i>
	<i>Poisson's ratio = 0.27</i>	<i>Poisson's ratio = 0.30</i>
	<hr/>	
Reduced Young's modulus	2.060×10^{11} Pa	2.310×10^{11} Pa
Reduced radius	2.500 mm	2.500 mm
<hr/>		
Load = 200 N		
Contact radius (a)	0.194 mm	0.187 mm
Maximum contact pressure (P_{max})	2 533 MPa	2 741 MPa
Average contact pressure ($P_{average}$)	1 689 MPa	1 828 MPa
Maximum deflection (δ)	7.540 μ m	7.000 μ m
Maximum shear stress (τ)	844 MPa	914 MPa
<hr/>		
Load = 50 N		
Contact radius (a)	0.122 mm	0.118 mm
Maximum contact pressure (P_{max})	1 596 MPa	1 727 MPa
Average contact pressure ($P_{average}$)	1 064 MPa	1 151 MPa
Maximum deflection (δ)	2.990 μ m	2.760 μ m
Maximum shear stress (τ)	532 MPa	576 MPa

2.3.2 Real Contact Area

Figure 2.2 shows contact between two flat surfaces. In this figure it can be seen that the contact between the two surfaces is due to contact between the asperities on each surface. The true area of contact will therefore be the sum of all the areas of all the contacting asperities, which is only a small part of the apparent or nominal contact area (Bhushan, 2002: 99-100). This is shown in Figure 2.3.

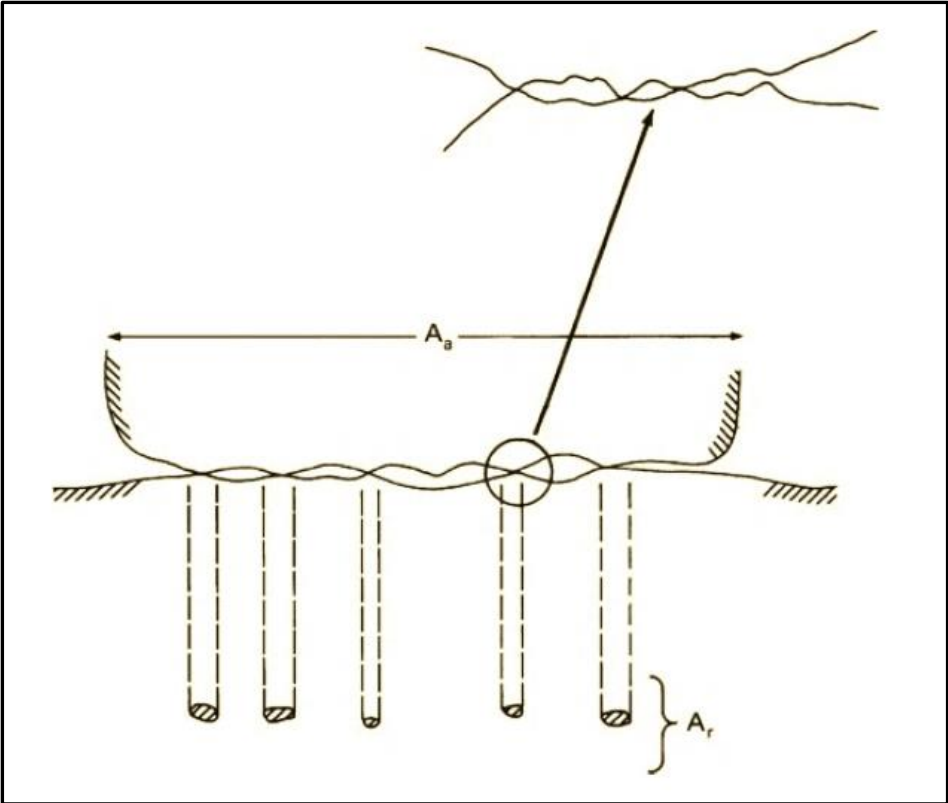


Figure 2.2: Schematic representation of an interface, showing the apparent and real contact areas (Bhushan, 2013: 92).

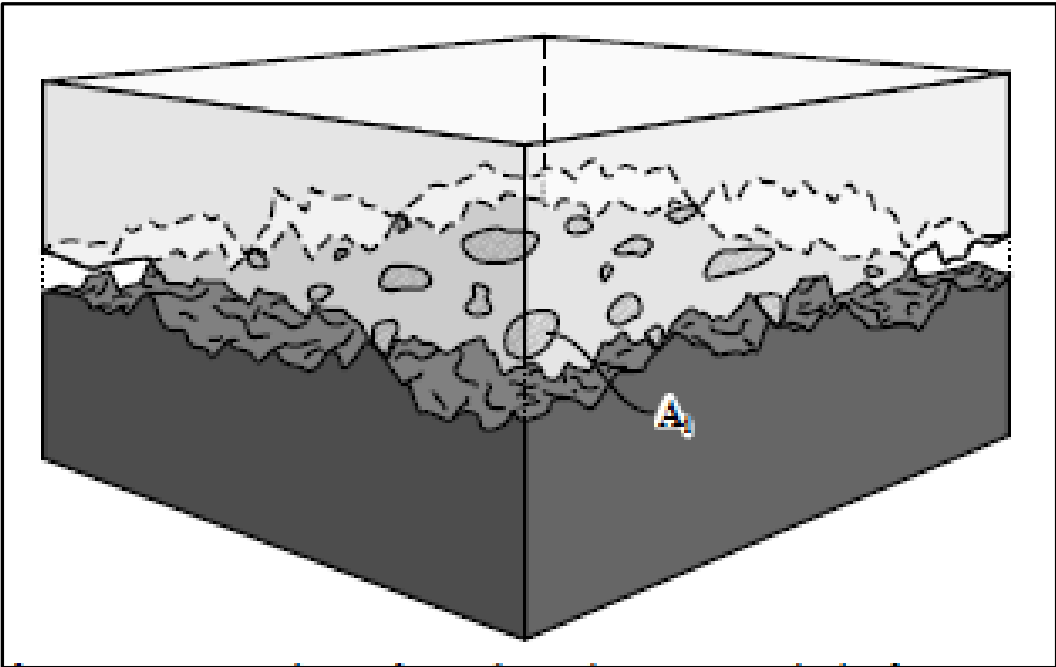


Figure 2.3: Real contact area of rough surfaces in contact (Batchelor & Stachowiak, 2005: 461).

The real area of contact is a function of the (Bhushan, 2013: 91):

- Surface texture
- Material properties
- Interfacial loading conditions

The proximity of the asperities results in adhesive contacts caused by interatomic interactions. When two surfaces move relative to each other, the friction force is determined by adhesion of these asperities as well as other sources of surface interactions. Repeated surface interactions and subsurface stresses developed at the interface result in the formation of wear particles and eventual failure. A smaller real area of contact between asperities results in a lower degree of interaction and lower wear. The problem therefore of relating the friction and wear to the surface texture and material properties generally involves the determination of the real contact area (Bhushan, 2013: 91).

During contact of two surfaces, the contact will initially occur at only a few points to support the normal load. As the normal load is increased, the surfaces move closer to one another and the number of asperities in the contact increases. Deformation also occurs in the region of the contacts establishing stresses that oppose the applied load. The mode of surface deformation which occurs may be (Bhushan, 2013: 91):

- Elastic
- Plastic
- Viscoelastic
- Viscoplastic

The mode of deformation depends on the (Bhushan, 2013: 91):

- Normal and shear stresses
- Surface roughness
- Material properties

It is therefore clear that the surface roughness plays an important role. It is also important to notice that the friction force depends on the normal load and the surface

interactions. An example of the friction force during a test on the SRV test rig is shown in Figure 2.4 for a ball-on-disc configuration.



Figure 2.4: Example of friction force (blue curve) measured during a friction and wear test on the SRV test rig under lubricated conditions. The red graph is the applied load.

In Figure 2.4, the friction force increases as the applied load increases. This is an indication that the number of surface interactions increased. It can also be observed that the friction force is not constant (compared to the applied load), however a steady state is reached after fifteen minutes. Small fluctuations can still be observed, which indicate that small changes occur on the surface.

The friction coefficient is recorded, rather than the friction force. The friction coefficient is a ratio of the friction force divided by the normal, applied load:

$$\mu = \frac{F}{F_N} \quad 2.1$$

Where:

μ Friction coefficient

F	Friction Force	(N)
F_N	Normal applied load	(N)

The friction coefficient graph of Figure 2.4 is given in Figure 2.5.

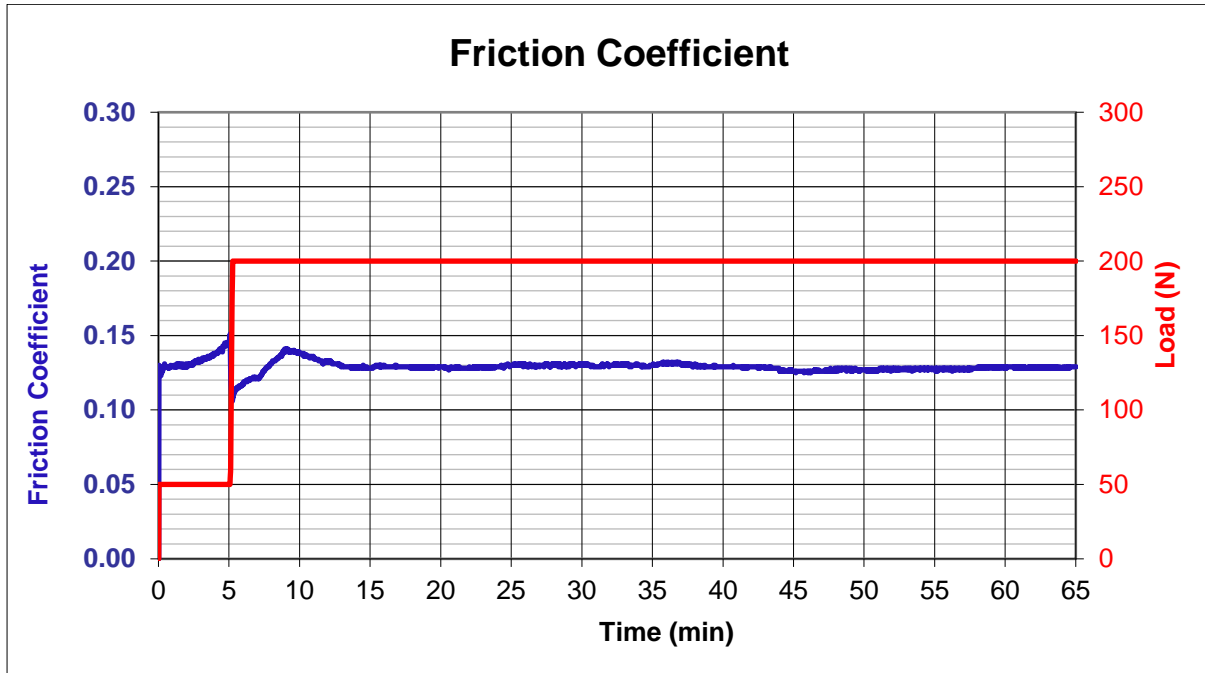


Figure 2.5: Example of friction coefficient measured during friction and wear testing on SRV test rig under lubricated conditions. The red graph is the applied load.

During standard friction and wear testing on the SRV test rig, the load is maintained at a constant value. The friction force, however, is defined as a function of the real contact area and the shear force required to induce motion for a dry contact, according to the classical theory of adhesion (Bhushan, 2013: 208):

$$F_a = A_r \tau_a \quad 2.2$$

Where:

F_a	Friction force due to adhesion	(N)
A_r	Real contact area	(m ²)
τ_a	Average shear strength of a dry contact	(N/m ²)

For a contact with a partial liquid film (Bhushan, 2013: 208):

$$F_a = A_r[\beta\tau_a + (1 - \beta)\tau_l] \quad 2.3$$

Where:

β	Fraction of unlubricated area	
τ_l	Average shear strength of the lubricant film	(N/m ²)

It should be noted that equation 2.3 does not include the formation of tribo-layers on the wear surfaces. These are layers that are formed due to the reaction of the metal surface with water vapour in the atmosphere and reactive compound in liquid formulation. The average shear strength of the liquid film is defined as (Bhushan, 2013: 208):

$$\tau_l = \frac{\eta_l V}{h} \quad 2.4$$

Where:

η_l	dynamic (absolute) viscosity of the lubricant	(kg/m.s ²)
V	Relative sliding velocity	(m/s)
h	Liquid film thickness	(m)

It is assumed that the friction force is due to the adhesion and deformation processes during sliding the total friction force will then be equal to (Bhushan, 2013: 206):

$$F_T = F_a + F_d \quad 2.5$$

Where:

F_T	Total friction force	(N)
F_d	Friction force due to deformation	(N)

2.3.3 Surface Layers

The surface of a solid (metal, alloy or ceramic) consists of layers, as shown in Figure 2.6. Each of these layers will be described briefly:

Deformed layer (Bhushan, 2013: 11)

The layer depends on the forming process with which the material surface was prepared. For grinding, lapping, machining, or polishing, the surface layers are plastically deformed with or without a temperature gradient and become highly strained. The layer is also referred to as the work hardened layer and can also be produced during the friction process.

The amount of material deformed and the degree of deformation that occurs depend on two factors:

- The amount of work or energy that was put into the deformation process.
- The nature of the material.

The deformed layer would be more severely strained near the surface, as can be seen in Figure 2.6. The grain size is also smaller in the deformed zone due to recrystallization of the grains. The individual grains can also re-orientate themselves at the surface. Furthermore, the properties and behaviour of the deformed layer can be entirely different from the metal-worked bulk material.

Beilby layer (Bhushan, 2013: 11)

This layer has an amorphous or microcrystalline structure. It formed by melting and surface flow of molecular layers that are subsequently hardened by quenching as they are deposited on the cool underlying material. The thickness of the layer can be reduced by careful finishing procedures such as lapping or wet polishing.

Chemically reacted layer (Bhushan, 2013: 11-13)

This layer is formed from the reaction of the metal with oxygen in the air. In other environments, other layers can be formed such as nitrides, sulphides, and chlorides. Oxide layers can also be produced during machining or during friction. The heat released increases the rate of oxidation and several type of oxides can be formed. The presence of lubricant and additives causes the formation of solid reaction layers that are important in surface protection.

Oxide layers may be of one or more elemental oxides. For iron, the layer can consist of iron (II) oxide (FeO) and hematite (Fe₂O₃). Other oxides can also be found for alloys, such as chromium oxide (Cr₂O₃) on stainless steel surfaces. It is also important to be aware that the oxide can continue to grow on some metal surfaces. An example of this is where hematite continues to grow in a humid air environment.

Chemisorbed layer (Bhushan, 2013: 13-14)

In this layer, sharing of electrons or electron interchange between the chemisorbed species and the solid surface occurs. The chemisorbed species retain their own individuality and can be recovered with proper treatment. This layer is limited to a monolayer and any subsequent layer formation is either by physisorption or chemical reaction.

Physisorption (Bhushan, 2013: 13)

Here, no exchange of electrons occurs and typically involves van der Waals forces. Examples of physisorption, chemisorption and chemisorption are shown in Figure 2.7.

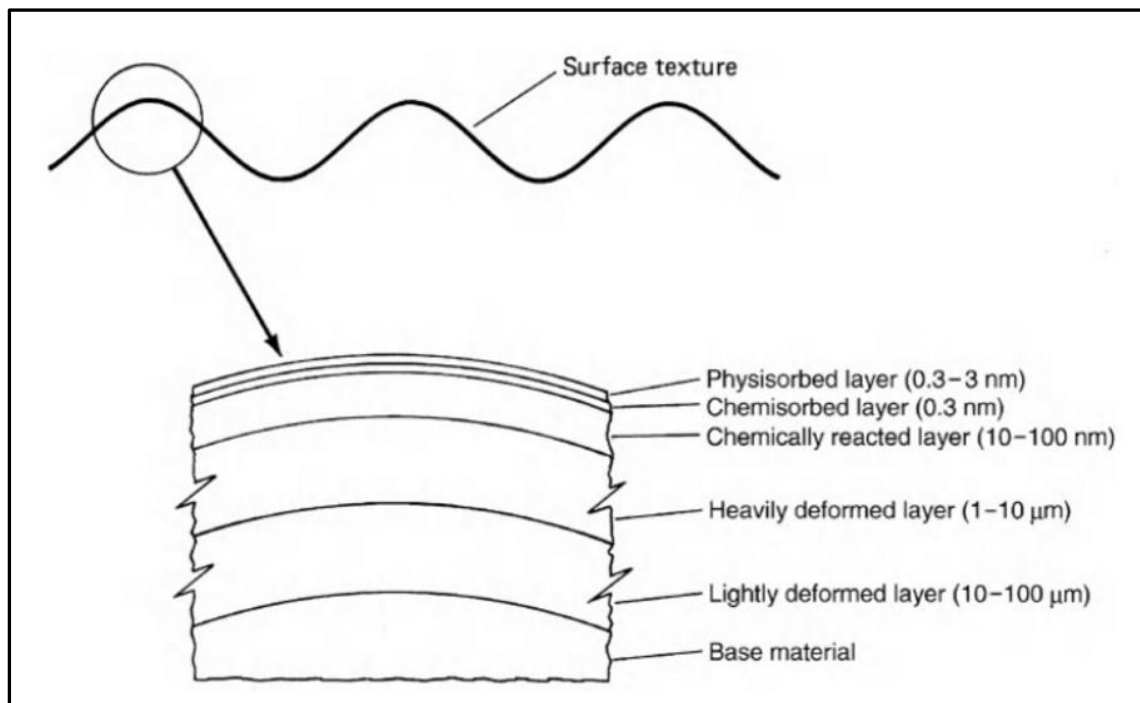


Figure 2.6: Solid surface layers (Bhushan, 2013: 10).

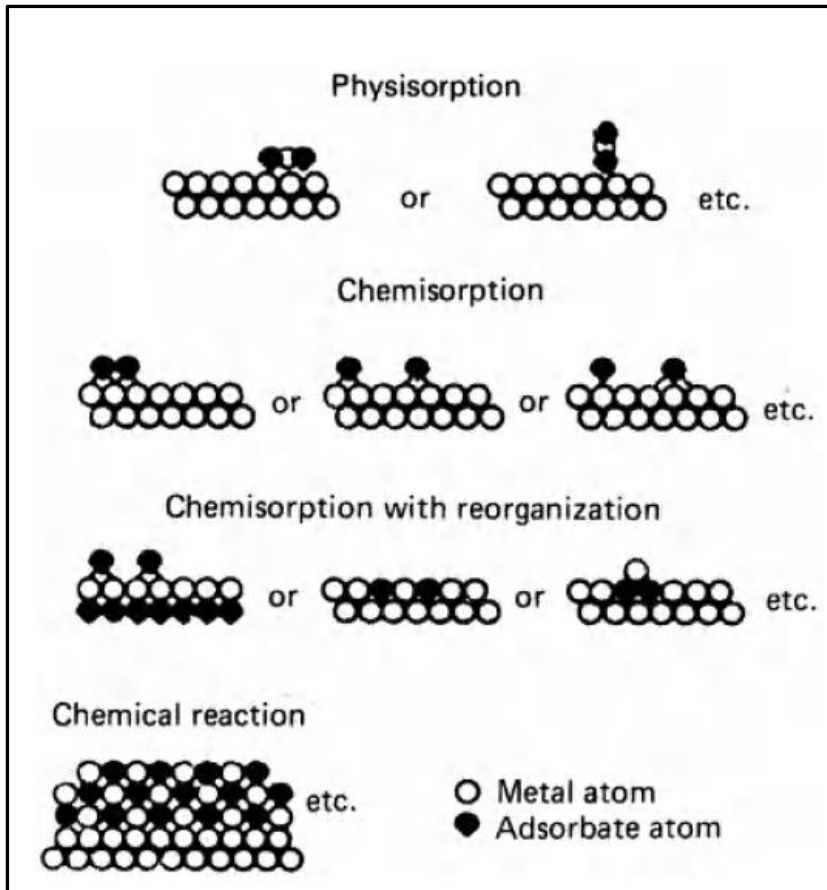


Figure 2.7: Schematic diagrams of physisorption, chemisorption and chemical reaction (Bhushan, 2013: 12).

Methods of characterization of surface layers (Bhushan, 2013: 15)

Matallurgical properties can be determined by sectioning the surface and examining the cross section with:

- High-magnification optical microscope
- Scanning electron microscopy (SEM)
- Transmission electron microscopy (TEM)
- X-ray, high energy, or low energy diffraction techniques

An elemental analysis of a surface layer can be performed by:

- X-ray energy dispersive analyser (X-REDA) – available in most SEM's
- Auger electron spectroscopy (AES)
- Electron probe micro-analyser (EPMA)
- Ion-scattering spectrometer (ISS)
- Rutherford backscattering spectrometer (RBS)

- X-ray fluorescence (XRF)

Chemical analysis can be performed by:

- X-ray photoelectron spectroscopy (XPS)
- Secondary ion mass spectroscopy (SIMS)

Chemical analysis of adsorbed organic layers can be conducted by using surface analytical tools such as:

- Mass spectroscopy
- Fourier transform infrared spectroscopy (FTIR)
- Raman scattering
- Nuclear magnetic resonance (NMR)
- X-ray photoelectron spectroscopy (XPS)

2.3.4 Surface Profiles and Surface Roughness

The surface texture is a representative of random deviation from the normal surface that forms the three-dimensional topography of the surface (Bhushan, 2013: 15).

Surface texture includes:

- Roughness
- Waviness
- Lay
- Flaws

The scale of each of these textures is illustrated in Figure 2.8. The asperities in this figure are referred to as peaks in a two-dimensional profile and summits in a three-dimensional profile. Waviness is the surface irregularity of longer wavelength and is referred to as macro roughness. This may result from factors such as machine or workpiece deflections, vibration, chatter, heat treatment or warping strains. Roughness can be referred to as nano- and micro roughness. The roughness of random profiles is given in Figure 2.9 and height parameters are summarised in Table 2.4.

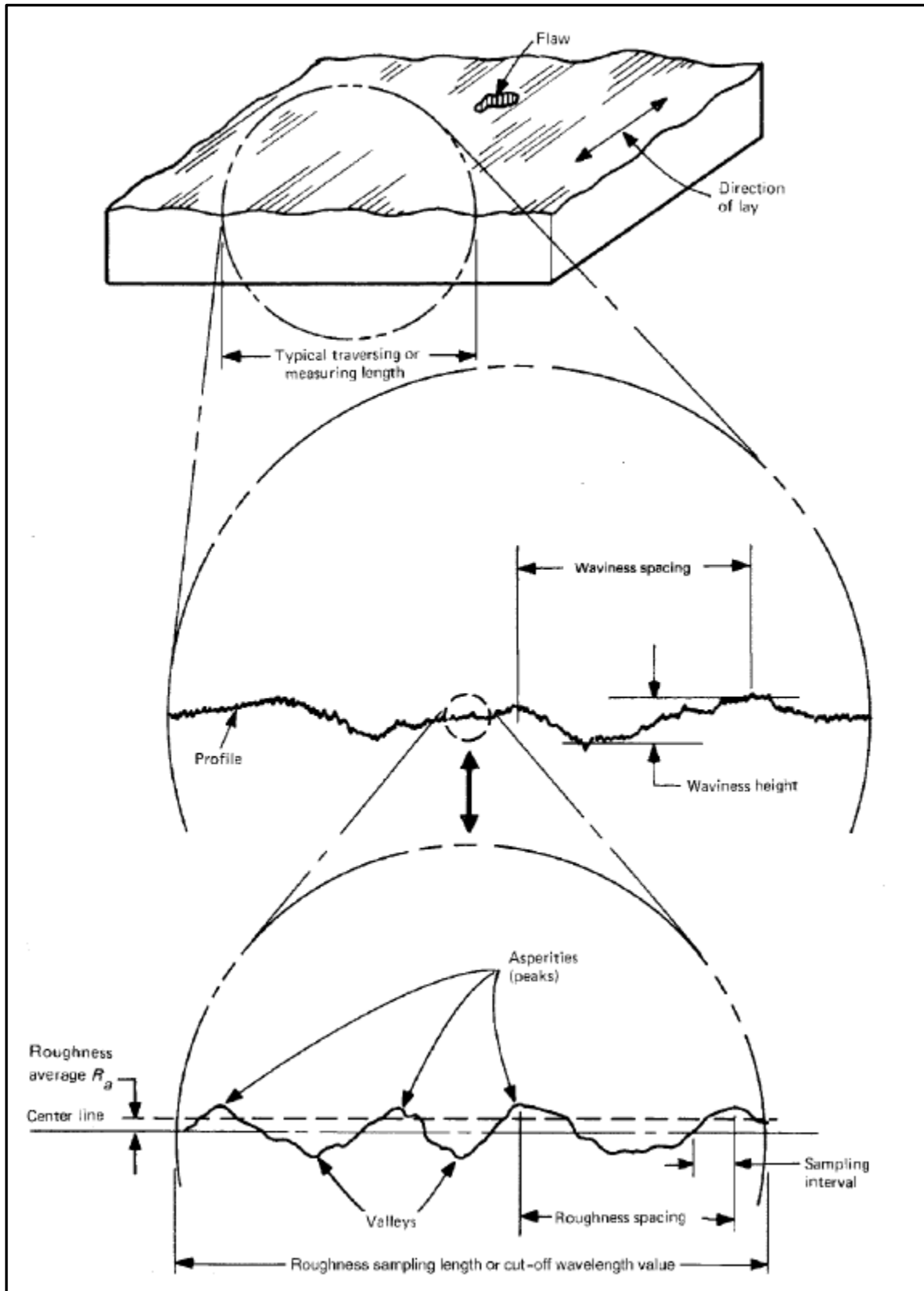


Figure 2.8: Pictorial display of surface texture (Bhushan, 2013: 16).

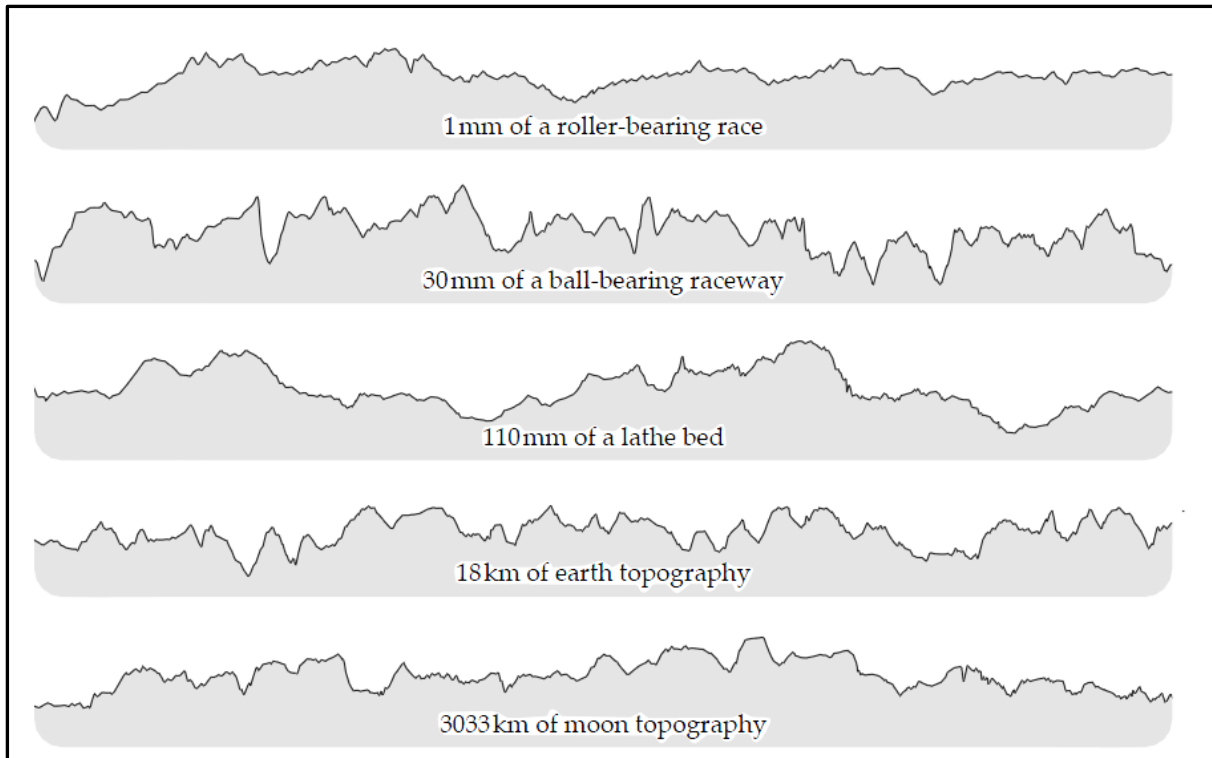
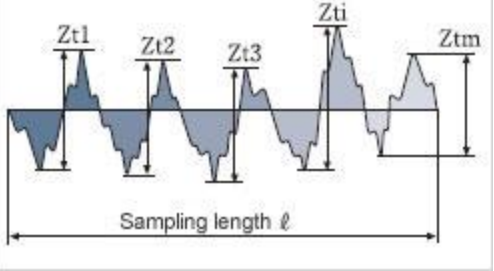
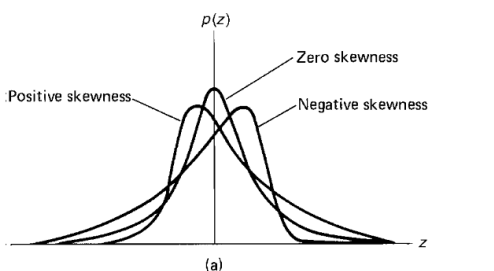
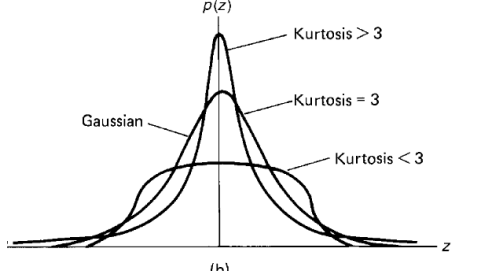
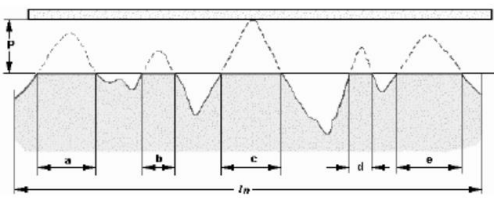
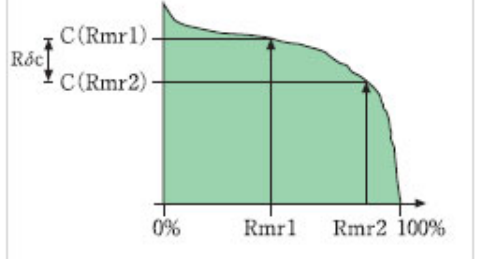


Figure 2.9: Similarities between random profiles of rough surfaces whether natural or artificial (Batchelor & Stachowiak, 2005: 464).

Table 2.4: Summary of surface height parameters.

Parameter	Definition	Equation	Diagram
R_a , <i>CLA</i> or <i>AA</i> **	Centre-line average, arithmetic average	$R_a = \frac{1}{L} \int_0^L z dx$	
R_q or <i>RMS</i> **	Root Mean Square	$R_q = \sqrt{\frac{1}{L} \int_0^L z^2 dx}$	
R_p *	Maximum peak height. Maximum peak to mean height		
R_v *	Maximum valley depth, mean to lowest valley depth		
R_z **	Average peak to valley height	$R_z = \frac{p_1 + \dots + p_5 + v_1 + \dots + v_5}{5}$	
R_t **	Maximum peak to valley height	$R_t = \frac{1}{5} \sum_{i=1}^5 R_{max_i}$	

Table 2.4: (continued).

R_c^*	Mean height of peak to valley	$R_c = \frac{1}{m} \sum_{i=1}^m Z_{ti}$	
R_c^*	Skewness		
R_{ku}^*	Kurtosis		
R_{mr}^*	Material ratio of profile	$\text{Material Ratio (Tp\%)} = \frac{a + b + c + d + e}{l_n}$	
R_{dc}^*	Profile section height difference	$R_{dc} = c(R_{mr1}) - c(R_{mr2})$ $R_{mr1} < R_{mr2}$	 <p>(For a roughness profile)</p>

*Bhushan, 2013: 17

**Batchelor & Stachowiak, 205: 467

2.3.5 Wear Classification

The wear processes that are applicable are summarised below. The focus is on chemical reactions which occur during the wear process. The chemical reactions involve corrosion reactions and corrosive wear.

Chemical and oxidative wear

This cannot strictly be treated as a separate wear mode since chemical reactions can occur on wearing surfaces in almost any environment. This is more one of the contributory processes having a potentially significant effect on the other wear modes. Some of the factors that influence of chemical reactions on wear surfaces are (Blau, 1989: 81):

- Chemical composition and microstructure of the contact surfaces.
- Rugosity and porosity of contact surfaces.
- The presence or absence of surface cracks and grain boundaries.
- The degree to which the contact surface has been work hardened.
- The state of stress in the surface.
- The electrical potentials and current paths between contacting surfaces.
- The temperature and pressure of the tribosystem.
- The reactivity of the medium interposed between contact surfaces.

Corrosive wear is also defined in the ASTM test methods as (ASTM G 40 - 02):

“Wear in which chemical or electrochemical reaction with the environment is significant.”

Oxidation wear, which is also corrosive wear, however, has assumed a particular connotation associated with mild wear. This subject where the interaction of a tribosurface with its environment is addressed is referred to as tribochemistry. This is a complex subject and involves several aspects:

- Mechanical
- Thermal
- Microstructural
- Geometry of surface contact

- Thermochemistry
- Reaction kinetics
- Catalytic processes occurring during wear.

Tribochemistry can also be classified according to subtopics. Here the chemical and oxidative effects on wear will be briefly reviewed in terms of three classes:

- Ambient atmospheric effects
- Corrosive fluid environments
- High temperature effects

The ambient atmospheric effects are applicable, since the effects of the humidity on the wear process have been studied on the HFRR and SRV (Langenhoven, 2015). The formation of oxides and corrosion layer formation have also been actively studied. The chemical and mechanical effects in wear are compared in Table 2.5 (Blau, 1989: 84).

In the Table 2.5, not all chemical effects are negative. For the case of oxidative wear during sliding, a thick oxide film can be formed. This film reduces the shear strength of the interface, which suppresses the wear because of plastic deformation (Quin a, 1983 and Quin b, 1983). The oxides formed during sliding also depend on the operating conditions and the ambient temperature.

At low speeds and temperature, the oxidation occurs on the asperity contacts of steel surfaces and the predominant oxide formed is $\alpha\text{-Fe}_2\text{O}_3$. At intermediate conditions, Fe_3O_4 is formed. At high ambient temperature, the entire surface oxidises and with high operating speeds FeO is formed (Quin, 1983).

Table 2.5: Comparison of chemical and mechanical effects in wear.

Chemical Action	Mechanical Action
Forms surface films.	Wipes surface films away.
Creates scales and cracks to weaken the surface resistance to fracture during wear.	Creates defect structure which permits faster diffusion of reactants into the contact surface.
Creates pits which can act as local stress concentrators.	Puts residual compressive stresses near the surface and tensile stresses below them, compressive stresses often slow corrosion, but tensile stress accelerates it.
Forms lubricious oxides which can reduce friction.	
Forms brittle, hard oxides which can form abrasive debris as they wear off.	Produces a transfer layer of mixed oxide and un-oxidized material.
Reduces the effectiveness of additives.	Distributes corrosion products across the contact surface.
Selectively attack and remove elements added to metal alloys to enhance their wear resistance.	Exposes fresh fracture surfaces to the environment.
Wedges open micro-cracks initiated by mechanical action.	Creates frictional heat which accelerates reaction rates and promotes some reactions which are thermodynamically unfavourable at lower temperature.
Dissolves fine debris creating changes in the pH of the system as time passes.	

2.3.6 Oxidation Wear

So, 1995, investigated the conditions required for oxidational wear on rubbed surfaces. He found that the formation of iron oxides depends on the steel grade, sliding speed and load. The allowable ranges of normal load and sliding speed required to maintain conditions for oxidational wear are wider for alloy steels than cast iron steel.

As the sliding speed increases, the normal load required to maintain the conditions for oxidational decreases correspondingly. The other requirement is that the materials should have enough strength to prevent plastic deformation of the substrate under the areas of real contact. If this is not the case, severe wear will occur.

Cui et.al., 2008, investigated the oxidational wear mechanism of cast steels (no lubricating fluid was used). The objective was to determine whether a correlation exists between oxidation wear and the microstructural changes during sliding wear. Cast steels with different Cr-Mo-V compositions and microstructures were used as test pieces.

It was found that the oxide film increases after the running-in period is completed. Severe wear therefore occurred during the running-in period. The wear rate reduced after the running-in period to the thickness of the oxide layer that increased. This can be seen in Figure 2.10.

When the oxide film reaches a critical thickness, the oxide film on the plateaus become unstable and breaks up to form wear debris because of brittleness and internal stress of oxide. The load then shifts to other load-bearing plateaus where the oxide films are then formed. Steady oxidational wear then continues with alternating oxide layer formation and break down on the contacting plateaus.

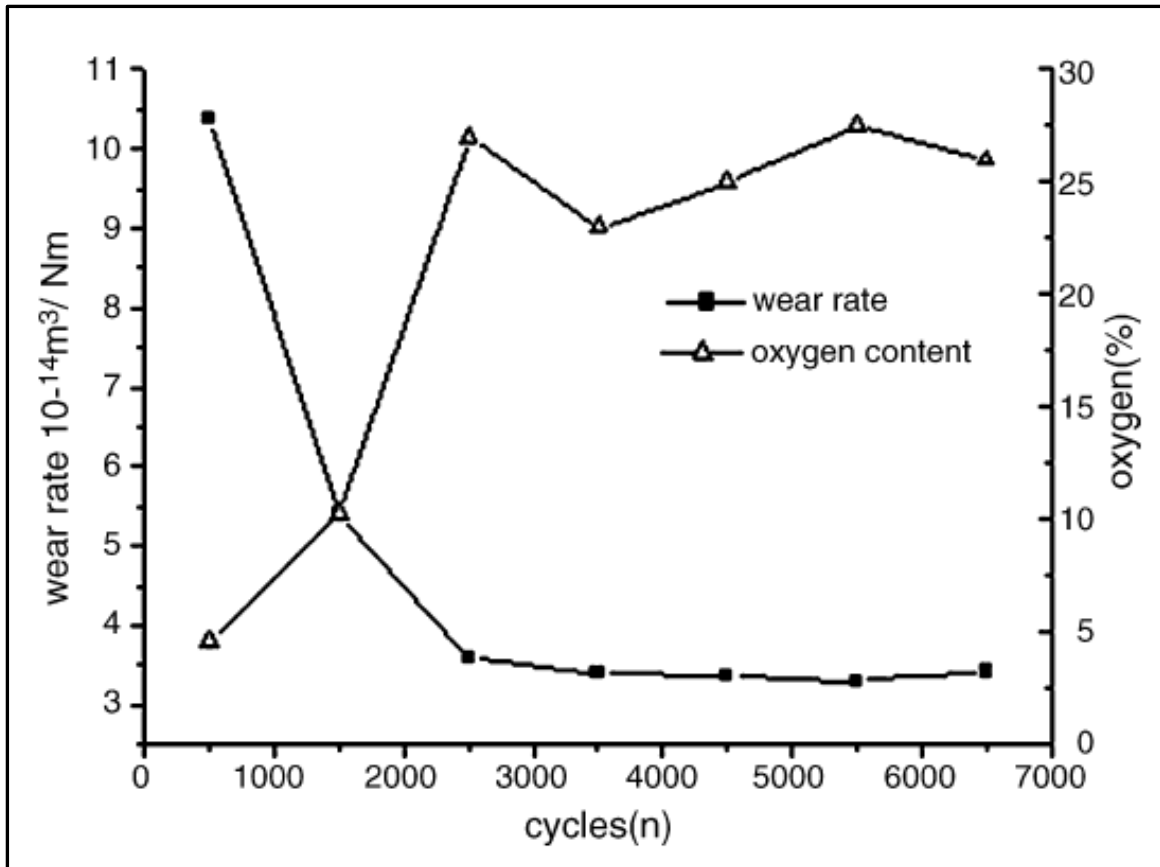


Figure 2.10: Wear rate and oxygen content against rotating cycles at 400 °C and a load of 100 N. The test pieces were produced from cast steel (Cui et.al., 2008).

2.3.7 Effect of Surface Properties

The effect of surface properties has gained a lot of attention by researchers in recent years. Investigations included the effects of certain properties of surfaces on the friction and wear behaviour in tribosystems. These properties include:

1. Grain size
2. Material Mechanical Properties & Microstructure
3. Surface Finish

1. Grain Size

The effect of grain size on the friction and wear of AISI 304 austenitic stainless steel was investigated by Bregliozzi et.al., 2003. They also investigated the effect of humidity, but this effect is discussed in section (section 2.3). Friction and wear tests were conducted on a ball-on-disk tribometer under dry sliding conditions.

Two grain sizes were investigated: 2.5 μm and 40 μm . Smaller grain sizes were obtained by recrystallization after cold rolling. The mechanical properties of steel with a smaller grain size are higher compared to the same steel with larger grain sizes. These properties include hardness, tensile strength, and yield strength. The microstructure of the two grain sizes is given in Figure 2.11.

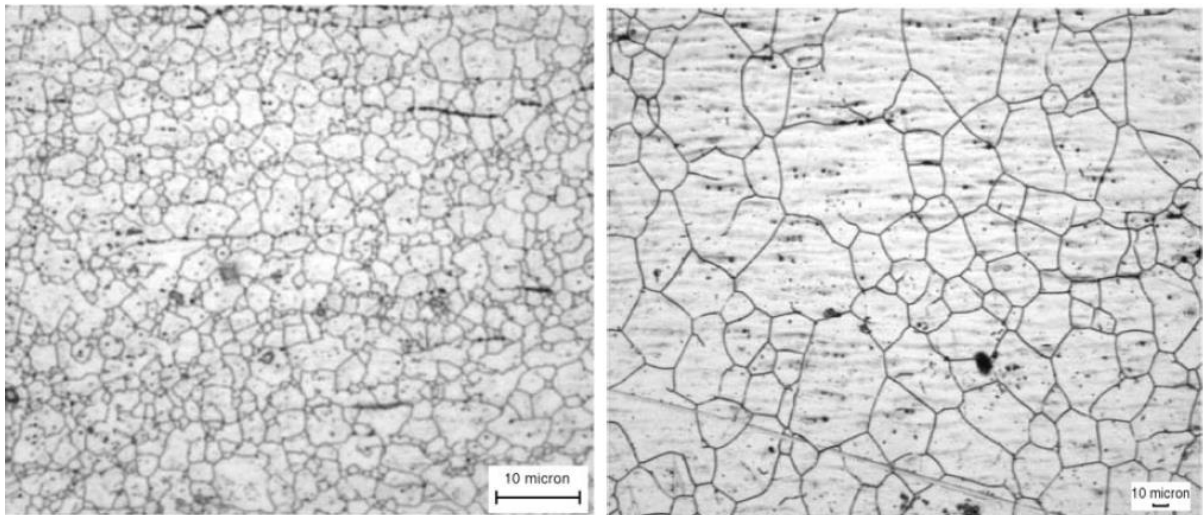


Figure 2.11: Grain size of AISI 304 stainless steel: 2.5 μm and 40 μm (Bregliozzi et.al., 2003).

The friction and wear test results indicate that the friction coefficient as well as the extent of wear decrease with a decrease in the grain size. No further explanation of this is given as to the cause for the reduction in the values. However, the increase in the strength of the material most probably play an important role.

A more recent study was done by Mei, et.al., 2019 where the dry sliding wear behaviour of ultrafine-grained Co-Cr-based alloys was investigated. These alloys already have high wear resistance. This can be further improved with grain refinement, which increases the hardness of the alloy.

In this study it was found that the wear increased at elevated temperatures (600 $^{\circ}\text{C}$) compared to tests done at room temperature. This can be ascribed to grain growth at these temperatures which leads to a decrease in the mechanical properties. The increase in grain sizes can be seen in Figure 2.12 before and after wear testing.

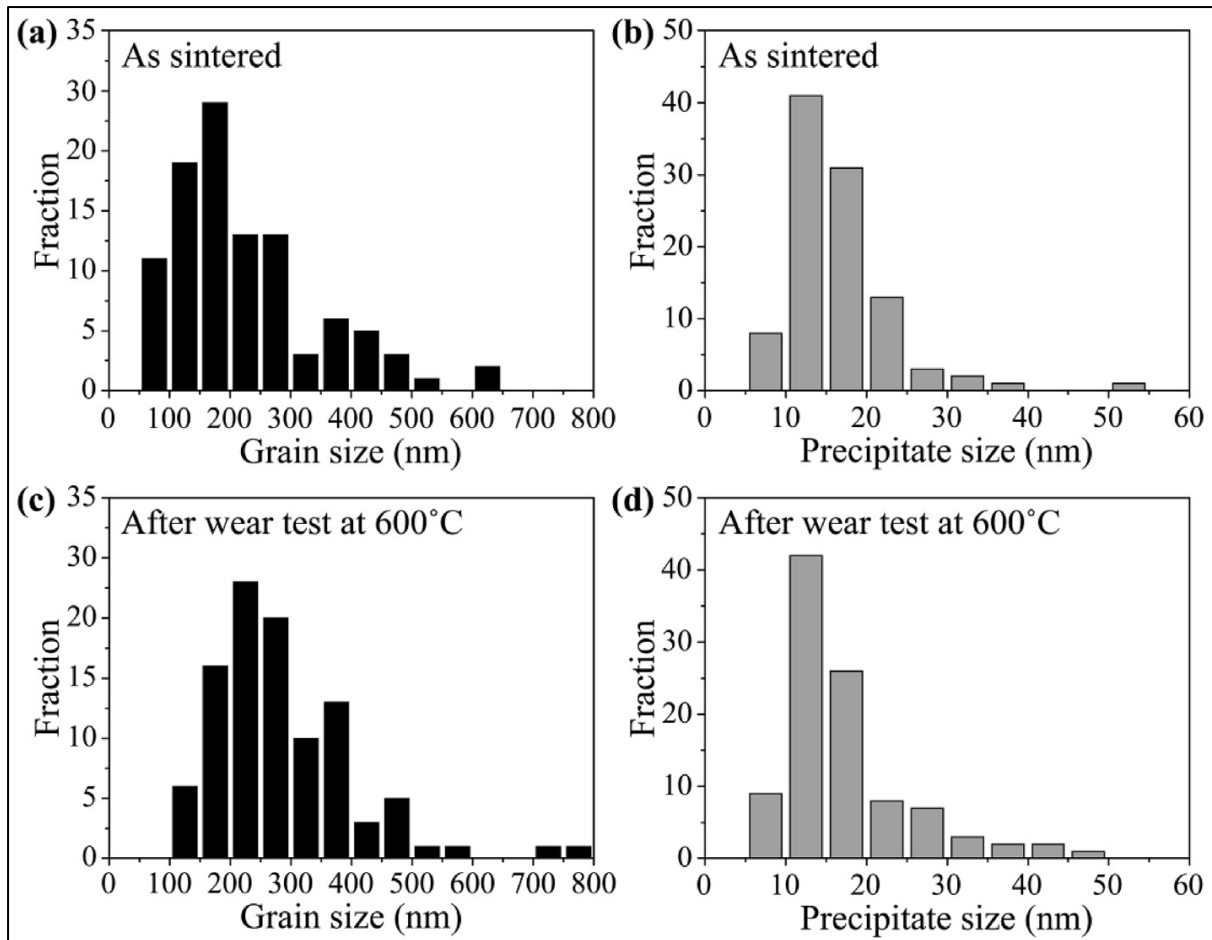


Figure 2.12: Increase in grain size after friction and wear testing at 600 °C of Co-Cr-based alloys (Mei, et.al., 2019).

It was found that a significant reduction in the friction coefficient was obtained when the test temperature was increased to 600 °C. This is shown in Figure 2.13 where the friction coefficient plots are given at both temperatures. For both tests the friction coefficient values increase until a steady state is reached. The test that was done at room temperature can be characterised by a rapid increase until steady state, after which the friction coefficient gradually decreases.

The test conducted at the higher temperature, however, can be characterised by a more gradual increase until steady state is reached. During the steady state the friction coefficient continues to gradually increase. This highlights the effect different test conditions can have on the friction and wear results.

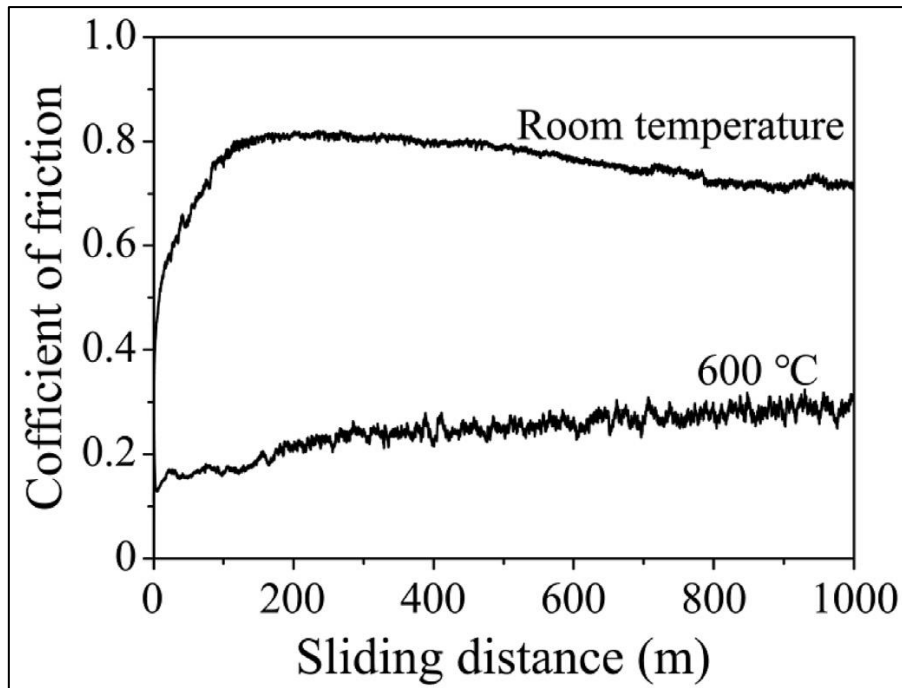


Figure 2.13: Friction coefficients as a function of sliding distance for test conducted at room temperature at different operating temperatures (Mei, et.al., 2019).

Finally, subsurface microstructures of the alloy showed no significant plastic deformation after friction and wear tests. This was attributed to the high hardness of the alloy and limited slip in the hpc system.

2. Material Mechanical Properties

In this section, the effect of the mechanical properties of the materials of components in contact in a friction and wear system is discussed. It has already been mentioned in the previous section that the hardness of the material plays a role. Other properties that also affect the friction and wear process include the tensile strength and the yield strength.

Reis et.al., 2018 investigated the correlation between the wear, hardness, and ultimate tensile strength of aluminium alloys during dry sliding. The mechanical strength of the material is enhanced with an increase in the density of the grain boundaries. The grain boundaries act as barriers to dislocation motion during plastic deformation.

Here two different aluminium alloys with different hardness and ultimate tensile strength were used. These were alloys 752 and 782, where 752 had slightly higher

Brinell hardness and ultimate tensile strength. This material also showed a lower wear rate during dry sliding with a pin-on-disk test rig.

Zambrano et.al., 2019 investigated the sliding wear behaviour of steels with the same hardness, but with different compositions and microstructures. The aim was to determine if these steels would exhibit the same wear behaviour on a block on ring configuration. Three steel rings (AISI 5160, AISI 1045 and AISI O1) were used and a sliding bronze block was used as the slider specimen.

The test was conducted under lubricated conditions, where the lubricant was selected based on its common use in a broad range of industrial applications. SEM images were taken of the materials tested to determine its microstructure. The microstructures for the materials were:

- AISI 5160: Pearlite
- AISI 1045: Ferrite and Pearlite
- AISI O1: Globular Cementite in Ferrite Matrix

The mechanical properties are affected by the microstructure of the material, even though the hardness was the same. The yield strength for instance was the highest for the AISI 5160 steel, followed by the AISI 1045 steel and AISI O1 steel had the lowest yield strength. The order of the strain hardening coefficient, however, was different. Here AISI 1045 had the highest coefficient followed by AISI O1 and AISI 5160.

It was found that the microstructure plays a role in the wear resistance of the material where pearlite showed the best wear resistance, followed by ferritic-pearlite and finally globular cementite embedded in a ferritic matrix. A good correlation was also obtained for the strain hardening coefficient and the deformed volume. Finally, the yield strength had a quadratic relation with the sliding wear resistance. These properties affect the elastic-plastic behaviours of the metals, even though the hardness is the same.

The AISI O1 and AISI 1045 consist of a soft matrix with a small hard phase. For the AISI O1 the soft matrix was ferrite with globular cementite as the hard phase, while for

AISI 1045 the matrix and hard phase were ferrite and pearlite respectively. The ferrite matrix in the AISI 1045 steel does not support the shear stress and the second phase is deformed and fractures. In the AISI O1, the ferrite matrix is deformed with no effect on the colloidal cementite. However, due to the high stiffness of the pearlite in the AISI 5160 steel, the plates fracture. This indicate that the pearlite structure which fractures consumes more energy than mere plastic deformation.

3. *Surface Finish*

The effect of the finish of surfaces on the role of the friction and wear behaviour is also actively being researched. This includes texturing, coatings, and roughness. The effect of coatings is not applicable to this investigation and is therefore not included. With surface texturing surface properties exist that help explain certain behaviour and have therefore been included.

One of the properties of surface texturing is the reduction of the friction coefficient due to micro-holes. Wear debris and lubricant are entrapped in these holes and a smoother surface is obtained. This then results in a decrease in the friction coefficient (Joshi et.al., 2019). Wos et.al., 2018 also ascribed the reduction of friction due to entrapped lubricant on textured surfaces. The opposite effect, however, can also be obtained. Stress intensification can also occur on the edges of the micro holes. This led to an increase in the friction and wear between the surfaces (Joshi et.al., 2019).

Surface texturing also influenced the running-in behaviour (Okamoto et.al., 2016). Here cross-grooved type textured, dimpled textured and mirror finished surfaces were used. For the cross-grooved textured surfaces the highest local contact pressure was obtained. This promoted plastic deformation which accelerated the running-in period. However, no explanation is given as to how the plastic deformation decrease the running-in period.

Finally, Podgursky et.al., 2011 investigated the effect of surface roughness parameters on the friction coefficient during early-stage fretting. They found that the friction coefficient is inversely proportional to the kurtosis of the surface. This means

that a lower value for the kurtosis will lead to an increase in the friction coefficient. The reason for this is that the real contact area increases for a decrease in the kurtosis. This leads to an increase in the friction force and since the load remains constant, the friction force will increase.

To summarise the properties of the materials:

1. The ability of the microstructure to support the shear stresses plays an important role in the prevention of wear. Furthermore, the grain boundary densities and sizes also affect the resistance to wear. This is due to the hardness of the material that increase with an increase in grain boundary density and a decrease in the grain size.
2. Texturing of the surface can lead to increase in local contact stresses. This leads to an increase in the friction and the wear. It also reduces the running-in duration due to enhanced plastic deformation. Furthermore, entrapped wear debris and lubricant results a smoother surface which lead to a decrease in the friction coefficient.
3. The friction coefficient is inversely proportional to the kurtosis of the surface. This is due to the contact area that increases for a decrease in the kurtosis. An increase in the real contact area also result in larger friction forces.

2.4 Transition Processes in Tribology: Running-in

2.4.1 Transition Processes in Tribology

Transition processes in Tribology can occur naturally or can be caused intentionally. The term transition is therefore divided in two categories which are defined below:

Induced transition (intentional): Change in tribological state of a system arising from an externally imposed change of the operating parameters of that system (Blau, 1989: 197).

Non-induced transition (natural): A duration dependent change in the tribological state of a system arising from progressive variations in the geometric, materials, and /or environmental conditions of that system (Blau, 1989: 198).

An example of an induced transition is when the load is increased, and a transition occurs from mild to severe wear. Examples of non-induced transitions are plots of wear, friction, and surface roughness changes during operation (Blau, 1989: 198 - 200).

It is also important to be aware that transitions can be a single occurrence or a cyclic occurrence. Examples of cyclic occurrences are typically found in friction charts, where the coefficient of friction oscillates between one steady state and another (Blau, 1989: 202).

If the definitions of tribological transitions are applied to friction and wear testing on the SRV test rig, the increase in load at the end of the running-in period (see Figure 2.14) will be regarded as an induced single occurrence induced transition.

The transition of the friction coefficient during the first 5 minutes from an unsteady to a steady state will be considered as a non-induced single occurrence transition. When the load carrying capacity of a fluid is determined on the SRV test rig (test methods based on ASTM D 5706 and ASTM D 7421), the increase in the load is considered an induced cyclic occurrence transition process. This is shown in Figure 2.15.

Note the increase in the coefficient of friction at the end of the test in Figure 2.15. It would be easy to assume that with an increase in friction coefficient, the wear would also increase. This is only true for specific cases since there is no universal relationship between friction and wear. The only definite link between friction and wear is that both are interfacial phenomena (Blau, 1989: 212).

Sliding friction and wear, however, can often influence one another interactively. An example of this is when the surface features are smoothed by the wear-in process and eventually reduce the sliding resistance from interlocking asperities. The surfaces can also deteriorate due to transition to severe wear and the roughness effects on asperity

interlocking may bring about an increase in the sliding friction coefficient (Blau, 1989: 212).

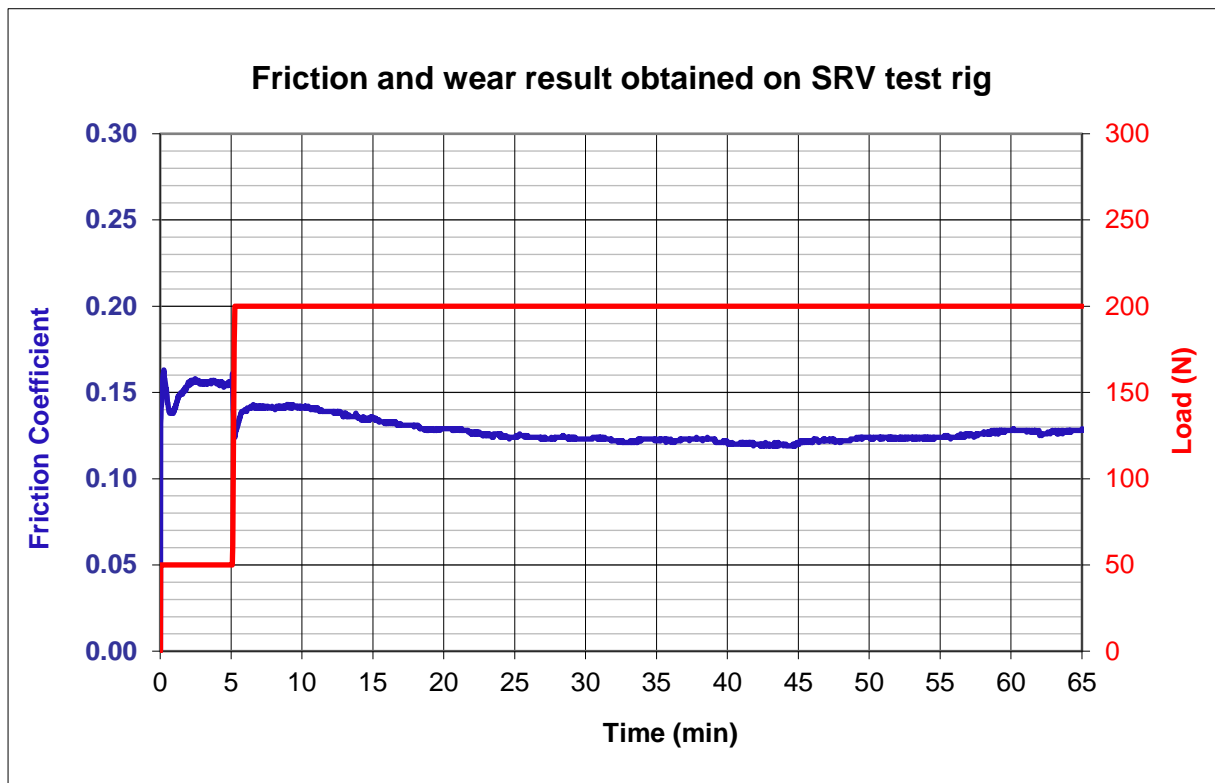


Figure 2.14: Induced single occurrence load transition during friction and wear testing on the SRV test rig. Method based on ASTM D 5707 and ASTM D 6425.

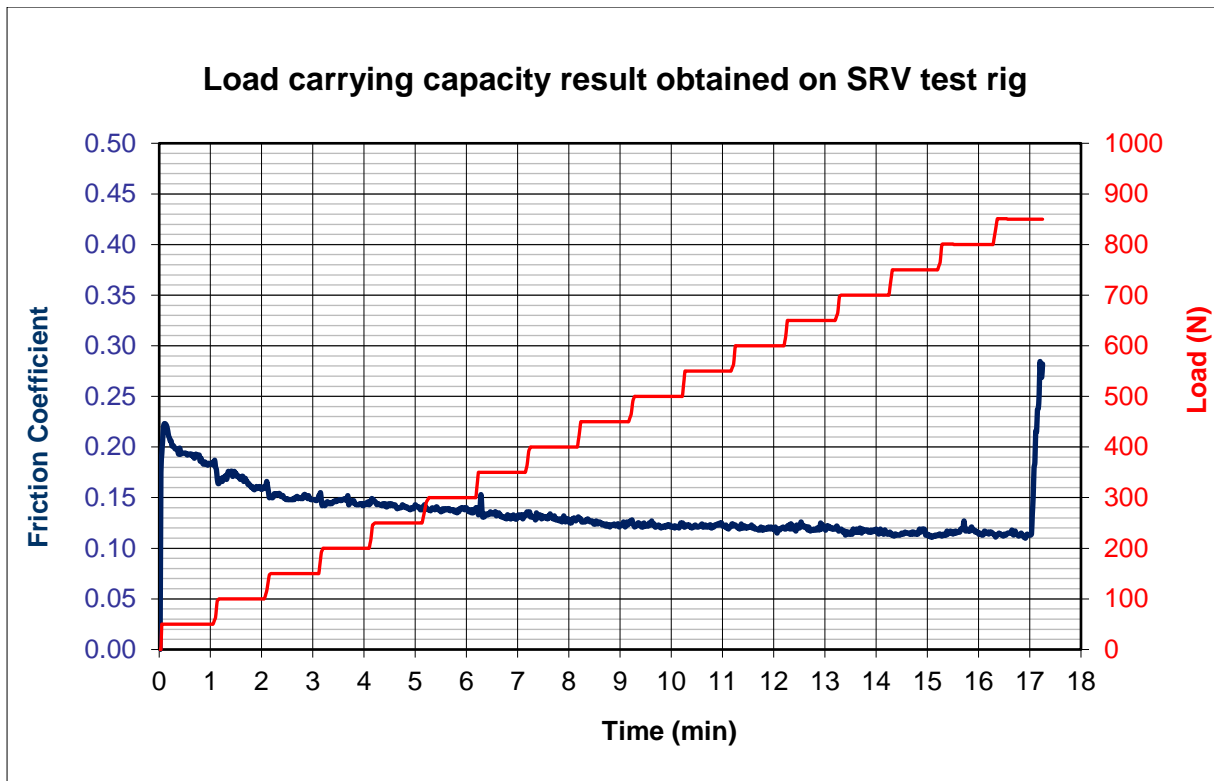


Figure 2.15: Induced cyclic occurrence transition process during load carrying determination on the SRV test rig.

Therefore, the friction coefficient can be an indicator of transition of changes in the wear mode. This would be the case in Figure 2.15 where the coefficient of friction increased rapidly at the end of the test (after 17 minutes), and severe wear occurred. Furthermore, a high friction coefficient during sliding indicates that a relatively large amount of energy is being expended in the contact region to sustain motion. The energy expended would depend on (Blau, 1989: 213):

- The amount of heat produced.
- Energy used to produce wear debris.
- Surface and subsurface deformation.
- Subsurface crack initiation and propagation.
- Tribochemical reactions.

The amount of energy expended on each of the processes above is also likely to vary between tribosystems. The coefficient of friction between two different systems does not imply that they are experiencing the same severity of wear, especially if the

composition of the components varies. The factors that are therefore expected to affect the friction coefficient and wear relationship are (Blau, 1989: 213):

- Thermal conductivities of the sliding materials.
- Fracture toughness and friability (tendency to break into small fractions) of the materials.
- Micro-cutting and ploughing in the materials.
- Presence of debris and/or transfer layers and films to either protect the surfaces, abrade the surfaces, lubricate the surfaces or shear.
- The geometry of the contact regarding heat transfer out of the contact interface.
- Presence of cooling lubricants.
- Formation of tribochemical products.

Transition processes which move the system from one steady state to another during severe wear can be considered as a re-running-in process. This is due to a new rough surface which is formed. This is followed by asperity truncation and deformation processes which is characteristic of running-in. This process is illustrated in Figure 2.16 for sliding, which is based on a model proposed by Blau, 1981.

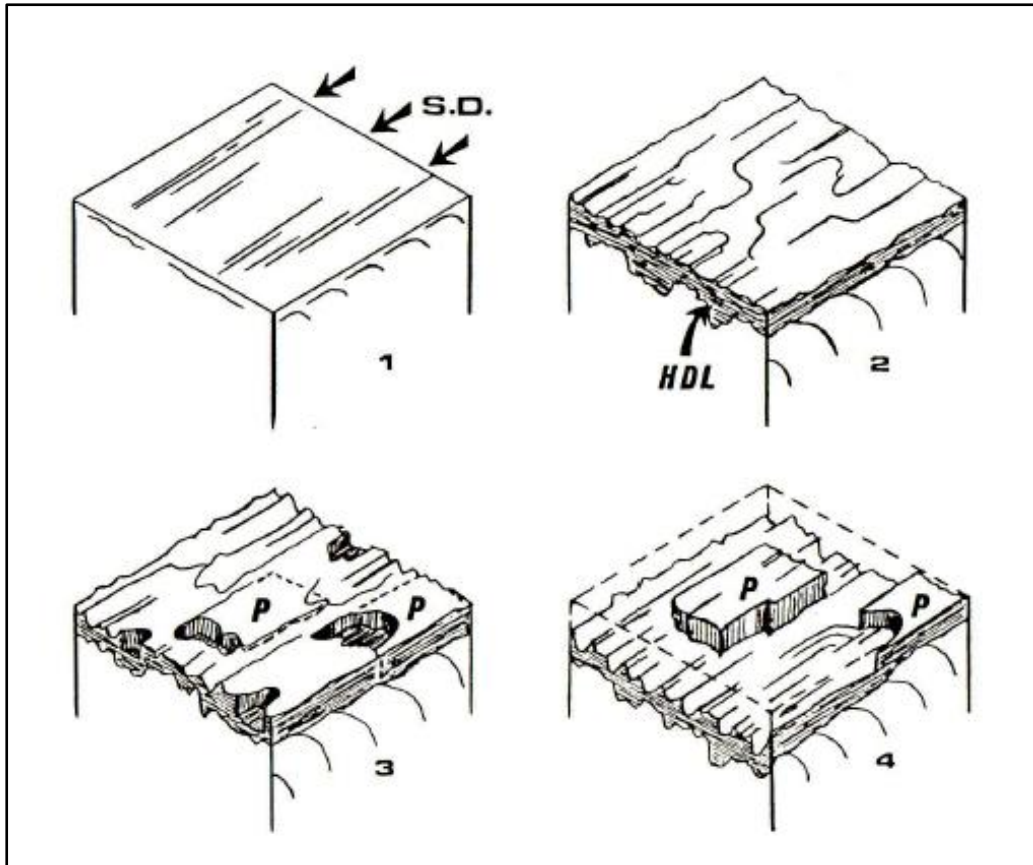


Figure 2.16: Transition process where a rough surface is formed during severe wear. This leads to re-running-in process. The abbreviations in this diagram are S.D: sliding direction; HDL: highly deformed layer; P: plateaus (Blau, 1989: 238).

During this process, pockets are formed in the metal surface due to material removal. This occurs due to surface fatigue or due to transfer to the counter face (diagram 3 in Figure 2.16). More and more material are removed from the surface until load bearing plateaus are formed. The edges of the plateaus tear away and the bearing pressure on the plateaus are gradually increased. When the plateaus can no longer support the load, they are swept away leaving a rough surface. The rough surface then goes through another running-in process (Blau, 1989: 237).

2.4.2 Definition of Running-in

In the previous sections, the terms run-in, running-in and wear-in have been used. These are all transition processes in tribology. The term break-in and running-in are used in some sources interchangeably, despite differences in the meaning according

to other sources. This section will look at the different definitions in running-in. Most importantly, the key characteristics related to running-in for lubricated metal contacts will be summarised.

Blau, 1989 made a clear distinction between run-in and break-in. He also defined terms with special reference to steady state wear. The definitions for run-in, break-in and wear-in from Blau, 1989 p 269-270, are given below:

Break-in (n): Those processes which occur prior to steady state when two or more solid surfaces are brought together under load and moved relative to one another. This process is usually accompanied by changes in macroscopic friction force and/or rates of wear.

Run-in (v): To impose a set of conditions on a tribosystem to reduce the time required to achieve a steady state, improve long-term performance, and/or to cause a steady state of geometric conformity to exist at the contact surfaces in that system.

Wear-in (n): Those processes which precede the acquisition of a constant wear rate.

Wear in (v): To run in specifically for wear conditioning.

Note the important distinction that is made between break-in and run-in. Break-in only refers to the changes in friction forces and wear rates, while the aim of run-in is to reduce the time required to reach steady state and simultaneously ensure improved long-term performance.

He further went on to describe breaking-in, running-in, and wearing-in as examples of tribological transitions, which are characterized by changes in friction and wear with time, numbers of sliding cycles, or sliding distance. These transitions may occur under lubricated or unlubricated conditions. The attributes of friction transitions are (Blau, PJ, 1996: 315):

(a) Changes in the nominal magnitude of the friction force,

- (b) The time that a tribosystem requires to reach steady state or some other distinct condition such as seizure or coating wear-through, and
- (c) The characteristics of short-term fluctuations in the friction force.

Ludema, 1996, defined running-in between 2 metal surfaces as: “The action taken to prepare sliding surfaces for high load-carrying capacity. Generally, new surfaces cannot carry high loads without failure” (Ludema, 1996: 170).

These definitions are quite vague, even though it is specific to the sliding pair composition. For the metal surfaces, however, the definitions refer to improvement of the load carrying capacity, which can be related to the long-term performance as stated by Blau, 1989.

In the ASTM test methods (ASTM D 5706 – 97, D 5707 – 05, D 6425 – 99 and D 7421 – 11) the break-in is defined as:

“An initial transition process occurring in newly established wearing contacts, often accompanied by transients in coefficient of friction or wear rate, or both, which are uncharacteristic of the given tribological system’s long-term behaviour.

Synonyms: run-in, wear-in”

Again, the definition indicates changes in friction coefficient and wear, which is different from the long-term behaviour between the wear surfaces. It is also interesting to note that the test methods apply the same definition to run-in and wear-in.

Svahn, F, 2006, interpreted running-in as an ability to form smooth and conformable surfaces from initially rough ones, while Gohar, 2012: 296 again referred to running-in as a transient process occurring between contacting fresh surfaces that are exposed to relative rolling/sliding motion.

They further state that running-in is often accompanied by transitions in tribological parameters such as coefficient of friction and wear rate. During the running-in process, the surface characteristics of the mating surfaces also continuously change as they undergo relative motion, and the process continues until the surfaces are conformed

to one another. Noticeably, the surface asperities with high slopes and short wavelengths plastically deform and wear away under physical contact.

For the remainder of this document, the term running-in will be used. This will be used to refer to either the running-in procedure, which involves a load increase from the initial load to the operating load or to the running-in period, which refers to the duration until steady state is reached for the friction coefficient and the extent of wear. From definitions above, the following characteristics can be summarised for running-in:

- Proper running-in reduces time to reach steady state of geometric conformity, friction, and wear.
- Transients in coefficient of friction (friction force) and wear occurs, which is uncharacteristic of the long-term behaviour.
- Smooth and conformable surfaces are formed from rough ones.
- Plastic deformation of asperities occurs.
- The long-term performance improves with proper running-in.

2.4.3 Studies on the Running-in and Wear Process

The running-in process is a subject that have been studied by many researchers in detail. Detailed discussions related to studies on running-in can be found in Appendix A. Only a summary will be given here for conciseness. These studies focus on the friction, wear, and surface roughness. The most important findings from these studies are:

Surface properties

- The *surface roughness* obtained at end of test increase with an increase in the load (Ludema & Lee, 1995).
- The mixed lubrication regime is extended for surfaces with a higher roughness (Nogueira, 2002).
- The *surface finish* plays a role in the sensitivity of the system regarding humidity. The higher the surface roughness, the more sensitive the system becomes for changes in humidity (Svahn et.al., 2006).

- The requirements for successful *running-in* depends on the (Svahn et.al., 2006):
 - Macroscopic pressure
 - Smoothing of surfaces
 - Formation of a tribolayer
- Machining affects the running-in, since this affects the subsurface deformation of the test pieces (Linsler et.al., 2016).

Real contact area

- As the ratio of the film thickness divided by the composite surface roughness decreases, the real contact area increases (Ludema & Lee, 1995).

Wear rate

- The *wear rate* depends on the film thickness divided by the composite surface roughness and the test fluid (Ludema & Lee, 1995 and Svahn et.al., 2006).
- *Steady-state wear rate* is reached quicker with an increase in the surface roughness and the load (Kumar et.al., 2002).
- An increase in the *load* results in an increase in the wear rate during steady state (Akbarzadeh & Khonsari, 2010).
- The duration until a *steady wear rate* is obtained decreases with an increase in the *sliding speed* (Akbarzadeh & Khonsari, 2010).

Friction Coefficient

- The *coefficient of friction* decreases with an increase in the sliding speed (Stribeck curve) and an increase in surface roughness (Nogueira, 2002).
- The *friction coefficient* increases with an increase in the humidity for lubricated contact (Svahn et.al., 2006).

Good running-in

- Good *running-in* is obtained by applying the optimum operating conditions for the contact pressure and sliding velocity (Feser et.al., 2013 and Linsler et.al., 2015) and lubricating fluid (Linsler et.al., 2015).
- The *running-in wear rate* increases with an increase in the (Kumar et.al., 2002):

- Load
- Surface roughness
- Temperature
- Contact pressure and surface finish plays an important role in the duration of the running-in period (Okamoto et.al, 2015).

In summary the most important properties that play a role are the surface properties of the test pieces, the operating conditions, and the test fluid. The effect of water (atmospheric humidity) must also be taken into consideration.

2.4.4 Effect of Load Increase on Friction and Wear

As mentioned in section 2.4.3 and in Appendix A, load plays an important role during running-in, which in turn will affect the long-term behaviour. However, changes in the loading conditions were not included in the studies on which section 2.4.3 and Appendix A are based on. This section therefore focuses on changes in loading conditions during friction and wear testing.

A recent study evaluated the tribological behaviour of grease lubricated sliding bearings under variable loads and speeds (Nehme, 2017). A 4-ball tester were utilised with chrome-plated steel balls (Bearing-quality Aircraft Grade E52100). A lithium-based grease was used, and test samples contained MoS₂ and ZDDP respectively.

The load was stepped between 393 N and 786 N during these tests according to 2 schedules. In the first schedule, the initial load was 393 N followed by a step-up to 786 N. This was followed by a step down to 393 N and a final step-up to 393 N. In the second schedule, the order was reversed. The initial load was 786 N which was the stepped down to 393 N, followed by a step-up to 786 N and finally a step down to 393 N.

The effect of the different loading conditions was on the formation of an effective lubricating film. For the test fluids with MoS₂ as additive, a high initial load promoted the formation of a tribolayer. This resulted in a lower friction coefficient. For the test

fluids without MoS₂ a high initial load affected the steady-state friction coefficient, as shown in Figure 2.17.

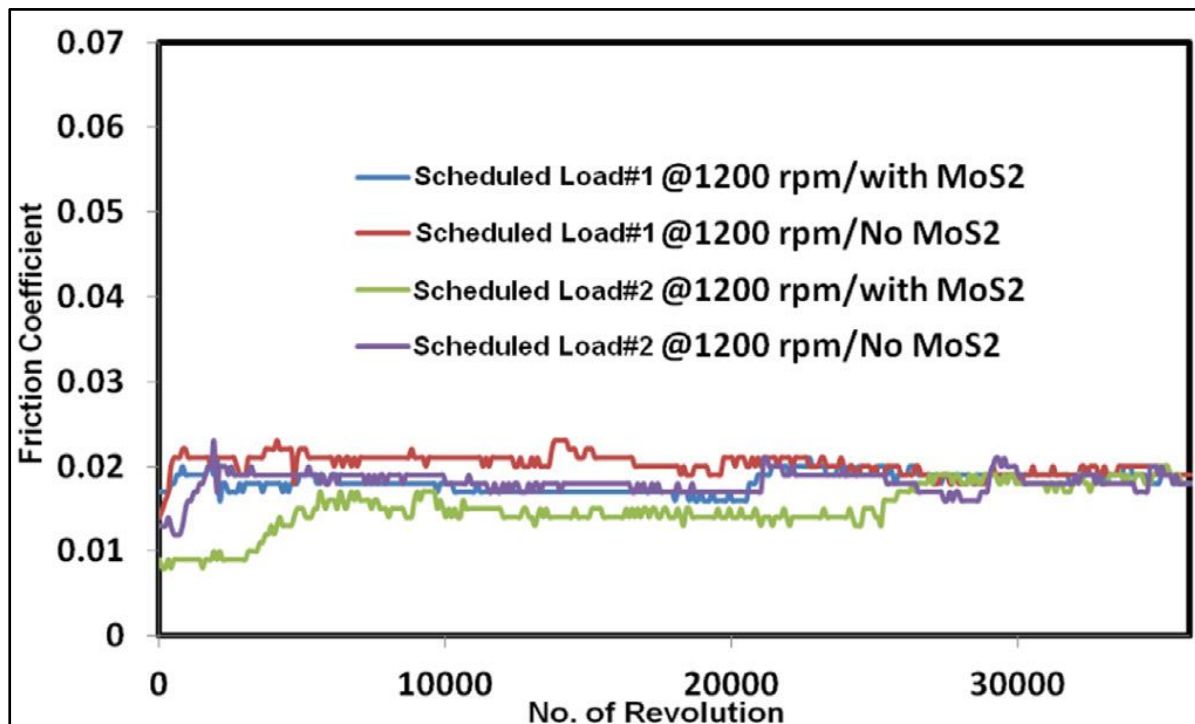


Figure 2.17: Effect of loading conditions on the friction coefficient (Nehme, 2017).

The mechanism of friction and wear in greases under a spectrum of loading conditions were investigated (Bagi & Aswath, 2015). The tests were also conducted on a 4-ball test machine with step up and step-down procedures (Nehme, 2017). They, however, also included test conditions where the duration at a load stage was different. For the one test condition, the duration was 15 minutes at each load stage, while a shorter duration of 7.5 minutes per load stage was used for the other test condition. A grease sample with MoS₂ and a grease sample with ZDDP and polytetrafluoroethylene (PTFE) was used.

They also found that an increase in load resulted in an increase in the friction coefficient. This was only explained for the grease with MoS₂. The lower loads are insufficient to shear the MoS₂ particles and thereby leading to an increase in the friction coefficient. No explanation is given for the greases with ZDDP/PTFE.

It was also found that shorter durations, i.e., higher number of changes per test since the test all had the same number of revolutions, leads to an increase in the extent of wear and friction coefficient. It also resulted in smoother friction coefficient transitions when the load is stepped up. The longer duration at a load stage enables the formation of a stable tribofilm. This limits the abrasion of the surface for the load increase.

Furthermore, changes in loading condition may result in transitions of the wear process (Onsøyen, 1991 & Hsu et.al., 2005). This can cause a change in the wear rate and the system will run in again until a steady wear rate is reached (Onsøyen, 1991). This can also result in failure if the wear rate is too high (Onsøyen, 1991 & Holmberg, 1991).

Finally, surface profiles conform to one another as a test progresses (Suzuki & Ludema, 1987). This is shown in Figure 2.18. The load was slowly applied in 4 N steps, beginning at 4 N, and ending 108 N. Each step had a duration of 10 minutes. Initially, however, the surfaces were not conformed to one another. This occurred at later stages as the test progressed.

The profiles conforming to one another in Figure 2.18 shows the importance of small increase in the load that led to good conformity of the wear surfaces. Furthermore, studies on load increases mentioned here showed the effect load increase has on friction and wear. Therefore, running-in will be affected by load increases. Also, small increases in load are beneficial for the surfaces to properly conform to one another.

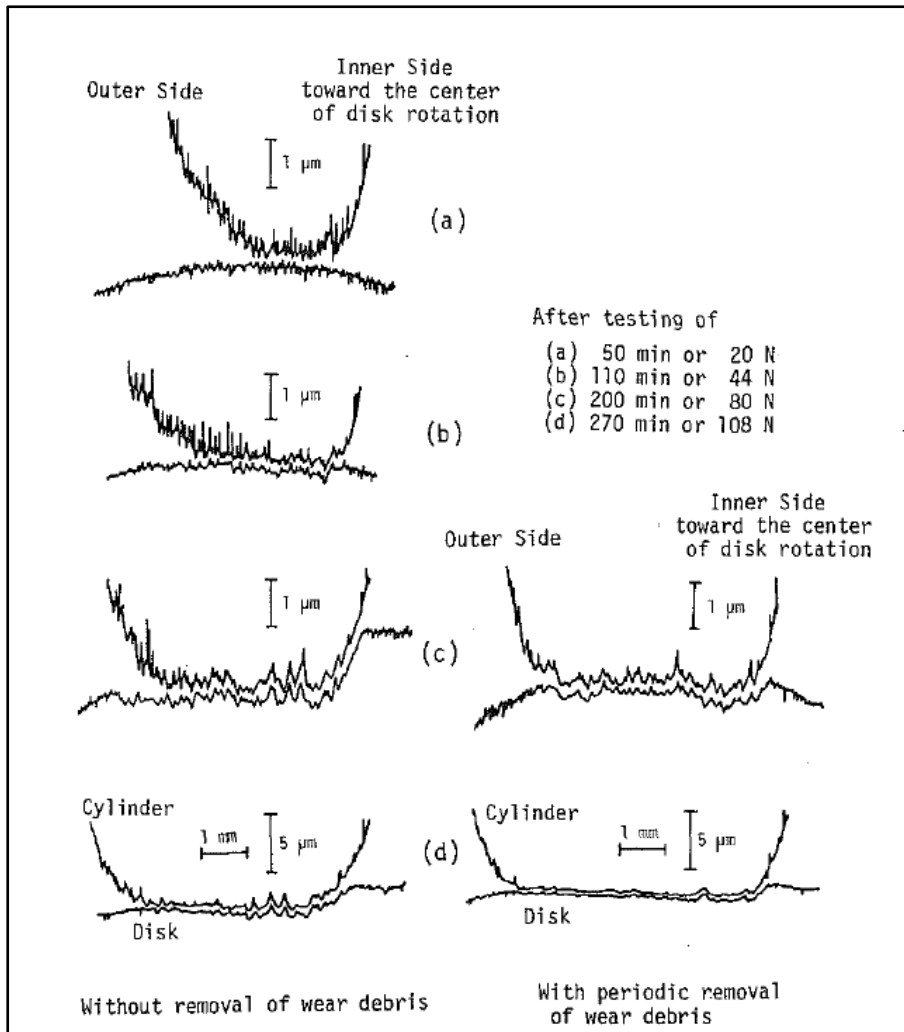


Figure 2.18: Wear profiles conforming to one another during running-in (Suzuki & Ludema, 1987)

2.5 Effect of Water on Friction and Wear

The effect of water on friction and wear have been a field of interest for a long time. Studies have been conducted on the mechanism of how absorption occurs on metal surfaces, its influence on friction and wear during dry sliding and under lubricated conditions. The effect of water is of consequence since active sites are generated during sliding and the composition of the lubricant that can be compromised.

Morimoto et al., 1969 found that water physically adsorbs onto active sites where the formation of a single molecule hydroxyl layer occurs. This layer is stationary. The second layer is formed by water molecules that adsorb onto the hydroxyl layer

through hydrogen bonding. The second layer is mobile. This was confirmed by McCrafferty & Zettlemyer, 1971.

It was also found that hydrogen results in embrittlement of AISI 52100 steel and 440 C steel (Ciruna & Szieleit, 1973). The hydrogen originates from the reaction of water at the bearing surface as well as from decomposition of the lubricant. The hydrogen permeates into the steel which affects the fatigue life of the steel.

During dry fretting, however it was found that the humidity was beneficial in reducing the friction coefficient, but the extent of wear increased with an increase in humidity (Goto and Buckley, 1985). The decrease in the friction coefficient was due to metal oxide layers that was formed which formed smoother surfaces. The increase in wear was due to an increase in corrosive wear with at higher humidity.

Klaffke, 1995, however found that the wear decreased drastically when the relative humidity was increased during dry sliding for a ball on disk. In his study on repeatability of friction and wear results and the influence of humidity he also found that the extent to which the friction coefficient is influenced by humidity was smaller compared to the wear.

He also found that the reduction of wear was larger on the disk compared to the wear on the ball. This was most likely due to the disk, which is periodically exposed to the atmosphere, while the ball is in constant contact with the disk. The higher wear rate on the ball was therefore due to the access of the water molecules being hindered to the surface of the wear scar.

De Baets et.al., 1998 and Bregliozzi et.al., 2003 also found that that the weight loss decreases with an increase in humidity. This is caused by adhesion between metal surfaces that is inhibited with the formation of oxide layers.

Up to now, the effect of humidity with unlubricated contacts have been discussed which gave a basic understanding of how the friction and wear process is influenced. However, in this study the contact was lubricated which is more complicated. The

effect of water on the performance of the lubricant is therefore of main importance and will be the focus for the rest of the section.

In a review article of the effect of water by Lancaster, 1990, the effects of environmental humidity are summarised. According to this article, water vapour can influence the wear process in three distinctive ways:

1. It modifies the adsorption behaviour of long chain organic compounds during boundary lubrication.
2. It affects the interfacial chemistry of protective film by oxygen and/or additives present in the lubricant.
3. It leads to an increase of pitting in rolling elements.

The polarity of water also plays a role since it competes with the other surface-active species in the adsorption process and also reacts with the surface and the lubricant itself.

Lapuerta et.al., 2014 found that wear increased for diesel fuels when the humidity is increased. They also found that paraffinic fuels are more hydrophilic than diesel fuels, but less hydrophilic than biodiesel and alcohol fuels. This led them to investigate the accuracy of the correction factor for the wear scar diameter in the standard HFRR test (EN ISO 12156-1) for biodiesel (Lapuerta 2016). They found that the accuracy of correction factor improves when the number of carbon atoms of the carboxylic acid molecules in the biodiesel is also compensated for. This is due to the amount of water absorbed by the diesel that decreases with an increase in the number of carbon atoms in the molecule.

Water also influences the anti-wear performance of zinc dialkyldithiodiphosphate (**ZDDP**). Cen et.al., 2012, investigated the effect of humidity in lubricated steel-steel contacts under sliding conditions. They found that that the water does not change the bulk properties of the lubricant, but the wear still increased. Reaction of **ZDDP** with water (hydrolysis), however can lead to shorter chain molecules. Consequently, a thinner tribofilm will be formed.

Furthermore, the shorter chain length molecules form in the early stage of the test. This affects the growth rate of the tribofilm which directly impacts the running-in wear. This also affects the steady state wear behaviour (Parsaeian et.al., 2016). Since the steady state wear behaviour is characterised by the steady state wear, consistency in the running-in behaviour becomes more important.

2.6 Base Oils

According to the American Petroleum Institute (API), base oils have been classified into 5 Groups. These Groups are summarised in Table 2.6 (Srivastava, 2009: 17). In this investigation the base oils used were selected to include paraffinic based base oils, naphthenic based oils, and synthetic base oils. For the paraffinic base oils Group II mineral oil and Group III mineral oil was selected. Two synthetic oils were also included, namely polyalphaolefin (PAO) and polyalkylene glycol (PAG). For the naphthenic based oil, a white mineral oil was selected. Each of these base oils will be briefly discussed in sections 2.6.1 to 2.6.4.

Table 2.6: API base oil categories (Srivastava, 2009: 17)

Category	Sulphur	Saturates	Viscosity Index
Group I	>0.03 %	≤90 %	80 to 120
Group II	≤0.03 %	≥90 %	80 to 120
Group III	≤0.03 %	≥90 %	≥120
Group IV	Polyalphaolefins (PAO)		
Group V	All others not included in Groups I to IV		

2.6.1 Group II and Group III Mineral Oil

Group II and Group III mineral oils are refined from base stock which involves hydrotreatment, hydroisomerization and solvent dewaxing. From Table 2.6, these two oils contain less sulphur than Group I mineral oil and have higher degrees of saturation. The Group II and Group III mineral oils are separated by the Group III mineral oil having a higher viscosity index (Srivastava, 2009: 17).

Mineral oils are mainly paraffinic in composition. It therefore has higher viscosity and better oxidation stability compared to naphthenic and aromatic base oils. Paraffinic oils, however, has poor low temperature properties due to wax formation tendencies (Rizvi, 2009: 32-33). The relationship between the hydrocarbon structure and the physical properties of mineral base oils are given in Table 2.7.

Table 2.7: Relationship between hydrocarbon structure and physical properties of mineral base oils (Rizvi, 2009: 39).


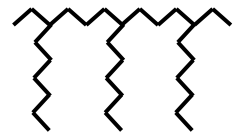
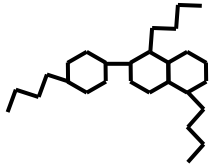
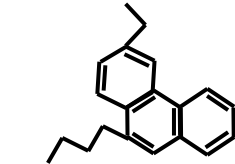
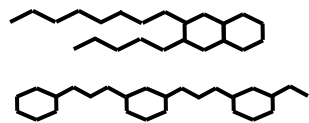
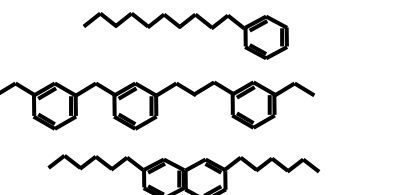
Hydrocarbon	Structure	Main Properties
Straight Chain Paraffin		<ol style="list-style-type: none"> 1. Viscosity varies little with temperature. 2. Good oxidation resistance. 3. High pour point.
Branched Chain Paraffin		<ol style="list-style-type: none"> 1. Viscosity varies little with temperature. 2. Good oxidation resistance. 3. May have low pour point.
Naphthenic Rings with Short Paraffinic Side Chains		<ol style="list-style-type: none"> 1. Viscosity varies greatly with temperature. 2. Becomes a pseudo-plastic at low temperatures. 3. Good oxidation resistance. 4. Low pour point.
Aromatic Rings with Short Paraffinic Side Chains		<ol style="list-style-type: none"> 1. Viscosity varies greatly with temperature. 2. Poor oxidation resistance. 3. Good Thermal stability. 4. Pour point varies according to structure.
Naphthenic Rings with Long Paraffinic Side Chains		<ol style="list-style-type: none"> 1. Viscosity varies little with temperature. 2. Good oxidation resistance. 3. May have low pour point.

Table 2.7: (continued)

<p>Aromatic Rings with Long Paraffinic Side Chains</p>		<ol style="list-style-type: none"> 1. Viscosity varies little with temperature. 2. May have good oxidation resistance if the structure does not contain too many rings. 3. May have low pour point.
--	---	--

2.6.2 White Mineral Oil

These are highly refined oils which consist entirely of saturated components. It can be either paraffinic or naphthenic. All the aromatic compounds have been removed by treatment with fuming sulphuric acid or by elective hydrogenation. They are virtually colourless and are used in medicinal products and in the food industry (Mortier & Orszulik, 1993: 13). The properties have already been discussed in the previous section and the structures are also given in Table 2.7.

2.6.3 Polyalphaolefin (PAO)

Polyalphaolefins (PAO) are synthetic saturated hydrocarbons. They are produced from linear alpha olefins. The production involves a two-step process:

1. Oligomerization of the olefin to yield an unsaturated olefin oligomer.
2. Hydrogenation in the presence of either a nickel or palladium catalyst.

An example of a PAO molecule is given in Figure 2.19. This shown for a PAO produced from 1-decene.

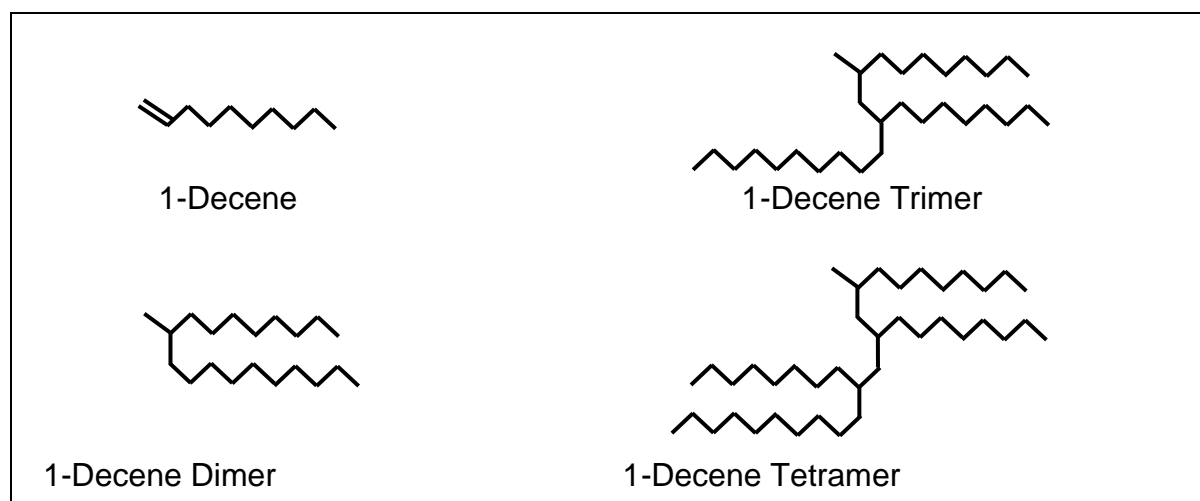


Figure 2.19: Structure of PAO based on 1-decene (Rizvi, 2009: 49).

PAO's have the benefit that they are like mineral base oils, but they do not contain naphthenic and aromatic compounds. These compounds have a negative effect on the viscosity index, volatility, and oxidation stability (Rizvi, 2009: 50). However, they

have poor solubility characteristics regarding additives. Common PAO viscosities are 2, 4, 6, 8, 40 and 100 cSt (measured at 100 °C) (Srivastava, 2009: 50).

2.6.4 Polyalkylene Glycol (PAG)

Polyalkylene glycols (PAG's) are obtained from the polymerization of one or more alkylene oxides. They are also referred to as polyethers and polyglycols. Figure 2.20 contains examples of a few types of PAG structures (Rizvi, 2009: 64).

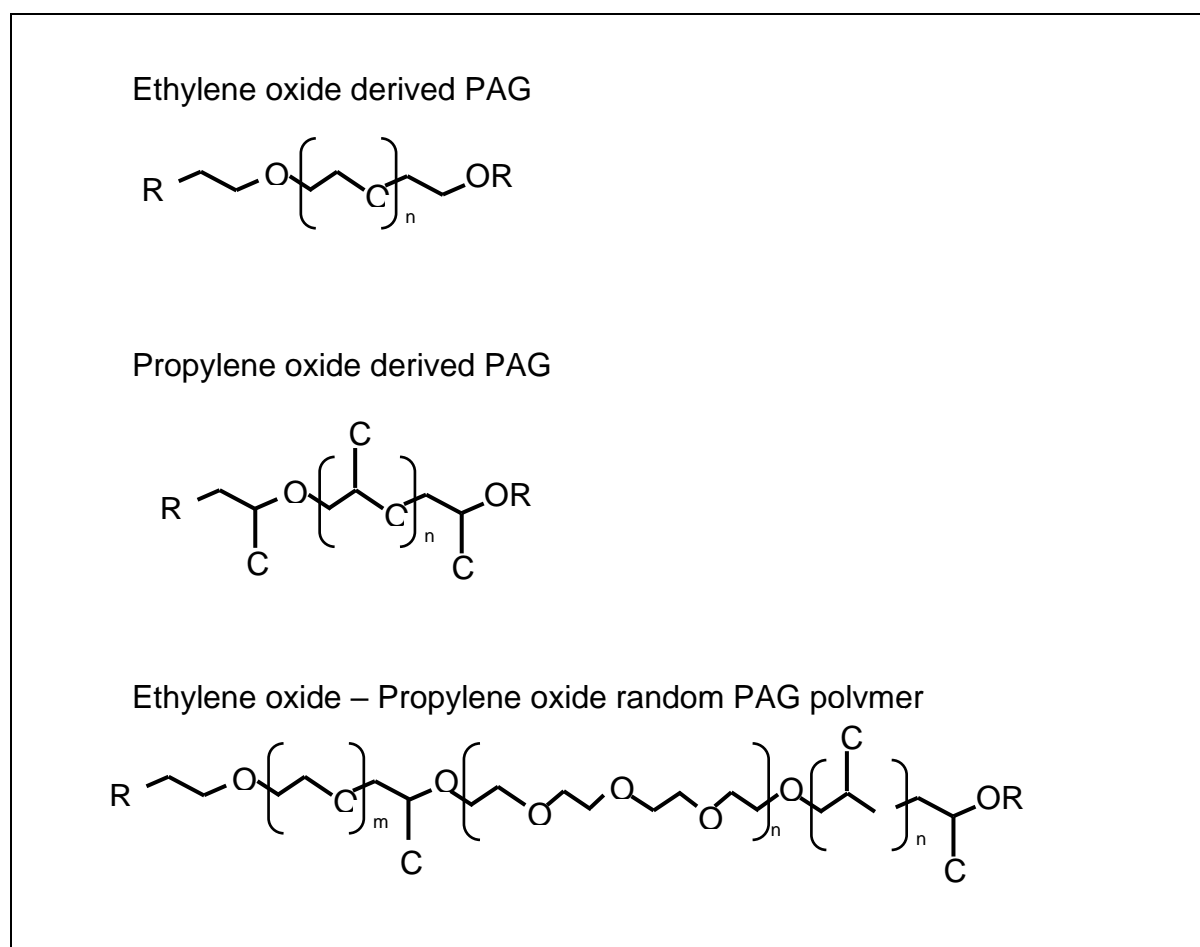


Figure 2.20: Various types of PAG structures (Rizvi, 2009: 64).

PAG's can be divided into two Groups: water soluble and water insoluble. The solubility in water increases with an increase in the ethylene oxide content. The solubility in organic materials increases with an increase in propylene content. The viscosity index also increases when the ethylene oxide/propylene oxide ratio increases (Rizvi, 2009: 64-65).

2.6.5 Friction and Wear Behaviour of Base Oils

The friction and film forming properties of base oils under elastohydrodynamic conditions were investigated by Gonsel, Korcek & Spikes, 1999. The base oils included mineral oils (Group I to III) and polyalphaolefin. They found that the elastohydrodynamic friction coefficient is not independent of the bulk viscosity, which rises proportionally with the log(viscosity).

They also found that the friction coefficient tended to increase with an increase in the pressure-viscosity coefficient. Finally, the composition of the base oil played a role in the friction behaviour. The PAO and mineral oils with a higher degree of refining had a lower friction coefficient.

A similar study was conducted Zhang & Spikes, 2016. The wear protection capabilities of base oils were also investigated. In addition to the base oils in the study referred to above, synthetic esters and polyalkylene glycols were also included. Their most important finding is that the viscosity of the base oil was the predominant factor that affects the friction coefficient and the extent of wear. Their results also indicate that the friction coefficient depends on the molecular structure. Chain structures resulted in lower friction coefficients compared to phenyl Groups.

2.6.6 Additives

Several additives are used in lubricant formulations to perform various functions. These additives include (Rudnick, 2003: vii to viii):

1. Antioxidants
2. Detergents
3. Dispersants
4. Friction Modifiers
5. Anti-wear Additives
6. Extreme Pressure Additives
7. Viscosity Modifiers
8. Tackiness Additives

9. Anti-misting Additives
10. Pour Point Depressants

In this investigation, only two types of additives were used: anti-wear additives and friction modifiers. This section will therefore only be limited to these two types of additives. The friction modifier used in this investigation was **diethyl sebacate** and the anti-wear additive was **Zinc dialkyldithiodiphosphate (ZDDP)**.

2.6.7 Friction Modifiers

Friction modifiers can be found in the following categories (Rudnick, 2003: 208):

1. Carboxylic acids and their derivatives.
2. Amides, imides, amines, and their derivatives
3. Phosphoric or phosphonic acid derivatives
4. Organic polymers

They can also be classified according to their mode of action (Rudnick, 2003: 209):

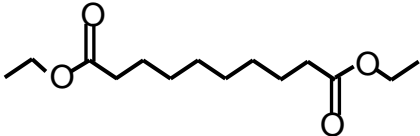
1. Formation of reacted layers
2. Formation of adsorbed layers
3. Formation of polymers
4. Mechanical types (organic polymers)

Friction modifiers normally consist of a straight carbon chain with at least 10 carbon atoms. The molecule also contains a polar head Group. The polar head Group reacts with the metal surface to form a protective layer. This occurs under relatively mild conditions (load and temperature) and a high level of chemical activity is required. The polar head Group can also physically adsorb onto the metal surface to form a protective layer (Rudnick, 2003: 208-209).

In this investigation, a friction modifier that physically adsorbs onto the metal surface was selected, mainly to reduce the number of factors that can influence repeatability of the friction and wear process. It was already mentioned that diethyl sebacate was selected as additive.

Diethyl sebacate is a straight chain molecule with a polar head Group at each end. The physical and chemical properties is summarised in Table 2.8 below. The friction and wear performance of this ester also performed well compared to other esters in study by Anatopoulos et.al., 2001. This study was conducted on diesel fuels with the test performed on the HFRR test rig. Good lubricity was obtained when the concentration of diethyl sebacate was 750 ppm.

Table 2.8: Properties of diethyl sebacate (Chemical Book, 2017).

Property	
CBNumber	CB4852807
Formula	C ₁₄ H ₂₆ O ₄
Structure	
Melting Point	1-2 °C
Boiling Point	312 °C
Density	0.9646 (g/L)
Refractive Index	1.436
Water Solubility	Slightly Soluble

2.6.8 Anti-wear Additives

These additives are used to function as the name suggest as an anti-wear additive. These additives react with surfaces to form a protective layer that prevents contact between surfaces. Extreme pressure additives operate under the same principle, though the anti-wear additives operate under milder conditions. The distinction is not definite, since an additive can be classified as an anti-wear additive for some applications, while it is considered as an extreme pressure additive in others (Rudnick, 2003: 223-224).

One of the most popular additives in this category is Zinc Dialkyldithiodiphosphate. In addition to being an anti-wear agent and mild extreme pressure additive, it is also an

effective oxidation and corrosion inhibitor. Furthermore, it also used in a diverse array of lubricants due to its low cost compared to other additives (Rudnick, 2003: 29). An example of a **ZDDP** molecule is given in Figure 2.21 below.

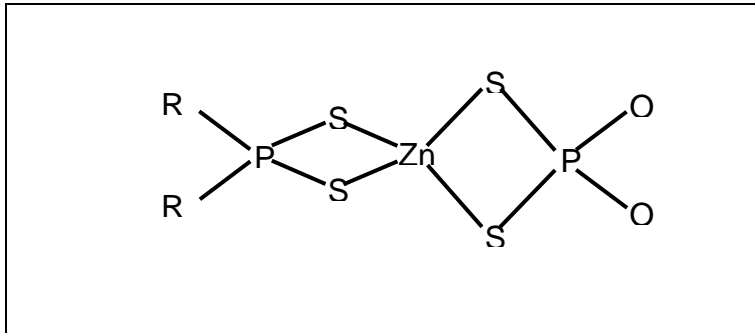


Figure 2.21: Example of a Zinc Dialkyldithiodiphosphate molecule.

The first step when a film is formed on the wear surface is the reaction of sulfur (**ZDDP** thermal degradation products) with the exposed metal surface. This forms a thin iron sulphide layer. This is followed by phosphate that reacts to produce an amorphous layer. This region is also described as a phosphate “glass” (Rudnick, 2003: 38).

This additive has also been the subject of extensive research by various authors. Some of these studies include:

1. Performance of friction modifiers in the presence of **ZDDP** film (Miklozic et.al., 2007).
2. Effect of water on **ZDDP** anti-wear performance (Cen et.al., 2012).
3. Compatibility of **ZDDP** with other surface-active additives (extreme pressure additives and viscosity index improvers) (Vengudusamy et.al., 2013).

These are only a small selection of all the research done on this additive. All of these confirm the superior performance of **ZDDP** as well as the formation of a protective layer. Spikes et.al., 2004 also gives a good overview of the research that was done up to the date when the article was published. The formation of a **ZDDP** film is also shown in Figure 2.22. A surface with no wear is shown on the left and the film starts to form in the second image. The **ZDDP** film is the yellow, brown, and black areas (Zhang & Spikes, 2016).

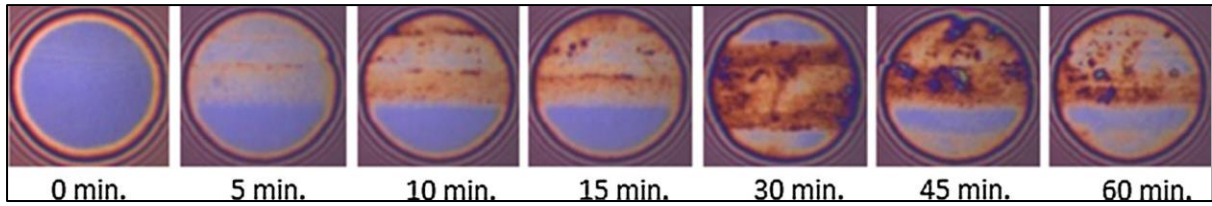


Figure 2.22: Formation of **ZDDP** film on wear surface.

Under closer examination, **ZDDP** forms layers on metal surfaces which prevents metal to metal contact (Rhodes and Stair, 1988). This is shown in Figure 2.23 (Johnson and Hils, 2013). This is formed by reactions, which eliminate the alkyl Groups and much of the sulfur. A tribolayer of zinc polyphosphate is obtained. The layer changes composition, the closer the layers is formed from the metal surface. Closer to the metal surface, the layer becomes glass-like and consist of a mixture of iron and zincphosphate (Martin, 1999). The iron to zinc ratio increases closer to the surface (Yin et.al., 1997). The thickness of the film ranges from 50 nm to 150 nm (Fuller et.al., 2000).

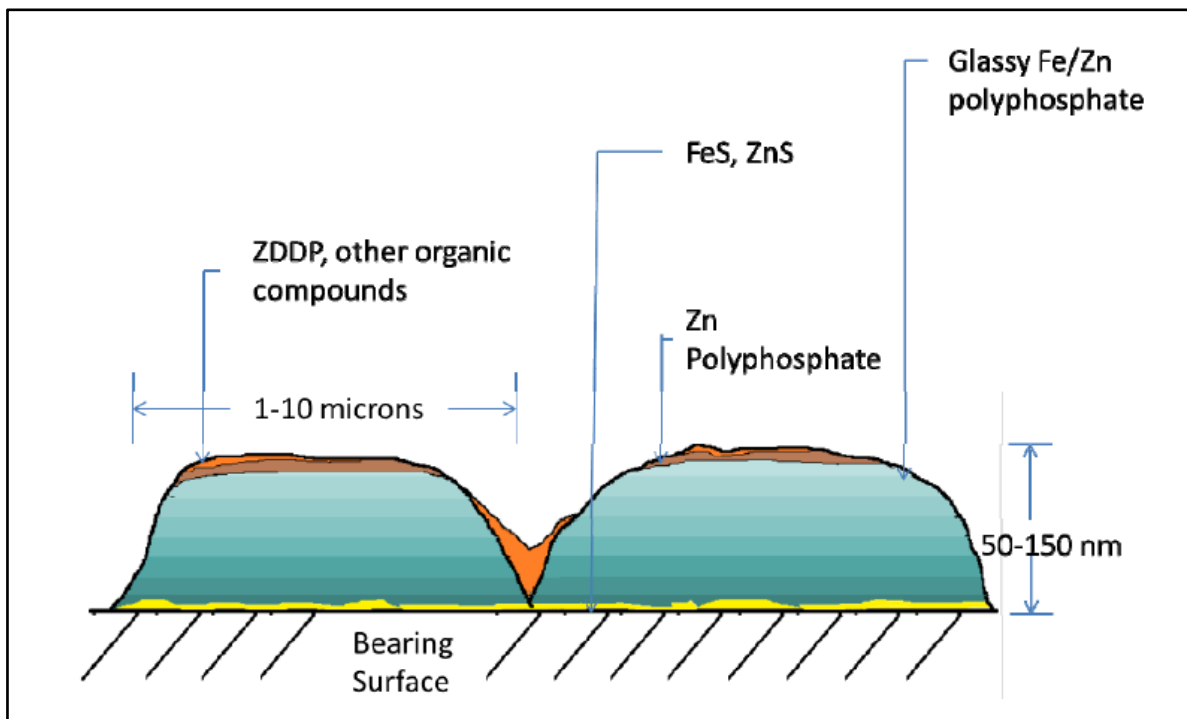


Figure 2.23: Composition of **ZDDP** tribofilm (Johnson and Hils, 2013).

2.7 Stribeck Curve

One of the most well-known tools in the field of Tribology is the Stribeck curve (see Figure 2.24). This is used to determine the lubricating regime in which a system operates. The friction coefficient is plotted as a function of the Hersey or Sommerfeld number or as a function of the specific film thickness:

$$\text{Hersey/Sommerfeld number} = \frac{\eta_L U}{W} \quad 2.6$$

Where:

η_L	Viscosity of the fluid	(N.s/m ²)
U	speed	(m/s)
W	load per unit length	(N/m)

or as a function of the specific film thickness (Bhushan & Gupta, 1991: 2.31):

$$\lambda = \frac{h_{min}}{\sigma} \quad 2.7$$

Where:

λ	Specific film thickness	
h_{min}	Minimum film thickness	(μm)
σ	Composite surface roughness ($\sigma = (\sigma_1^2 + \sigma_2^2)^{1/2}$)	(μm)

In Figure 2.24 it is also indicated that different additives can shift the curve. This diagram, however, does not contain the effect that is caused by viscosity. Anti-wear and EP additives (dotted curve) only play a role in the boundary and mixed lubricating regime. A protective layer is formed on the wear surface with the result that the friction coefficient decreases.

The abbreviation SL in this diagram refers to super lubricity additives. These are additives that expand the range of the lubricating film. They are not applicable to this investigation, but the effect on the Stribeck curve is noteworthy. As can be seen in the

figure, the curve moves to the left, even though the friction coefficient is not reduced. The combined effect of the anti-wear and super lubricity additives is that the friction coefficient will be reduced while the curve moves to the left simultaneously.

The Stribeck curve also shifts before and after running-in. This is, the curve shifts to the left, i.e., the onset of mixed and EHL conditions occur quicker when the surface is run-in. This is due to the surface roughness that decreases because of properly run-in surfaces (Akchurin, Bosman & Lugt, 2017). An example of this shift is given in Figure 2.25. This figure is from the investigation on the generation of wear particles and running-in in mixed sliding contacts. Figure 2.25 contains both experimental values and the model used to predict the friction coefficient.

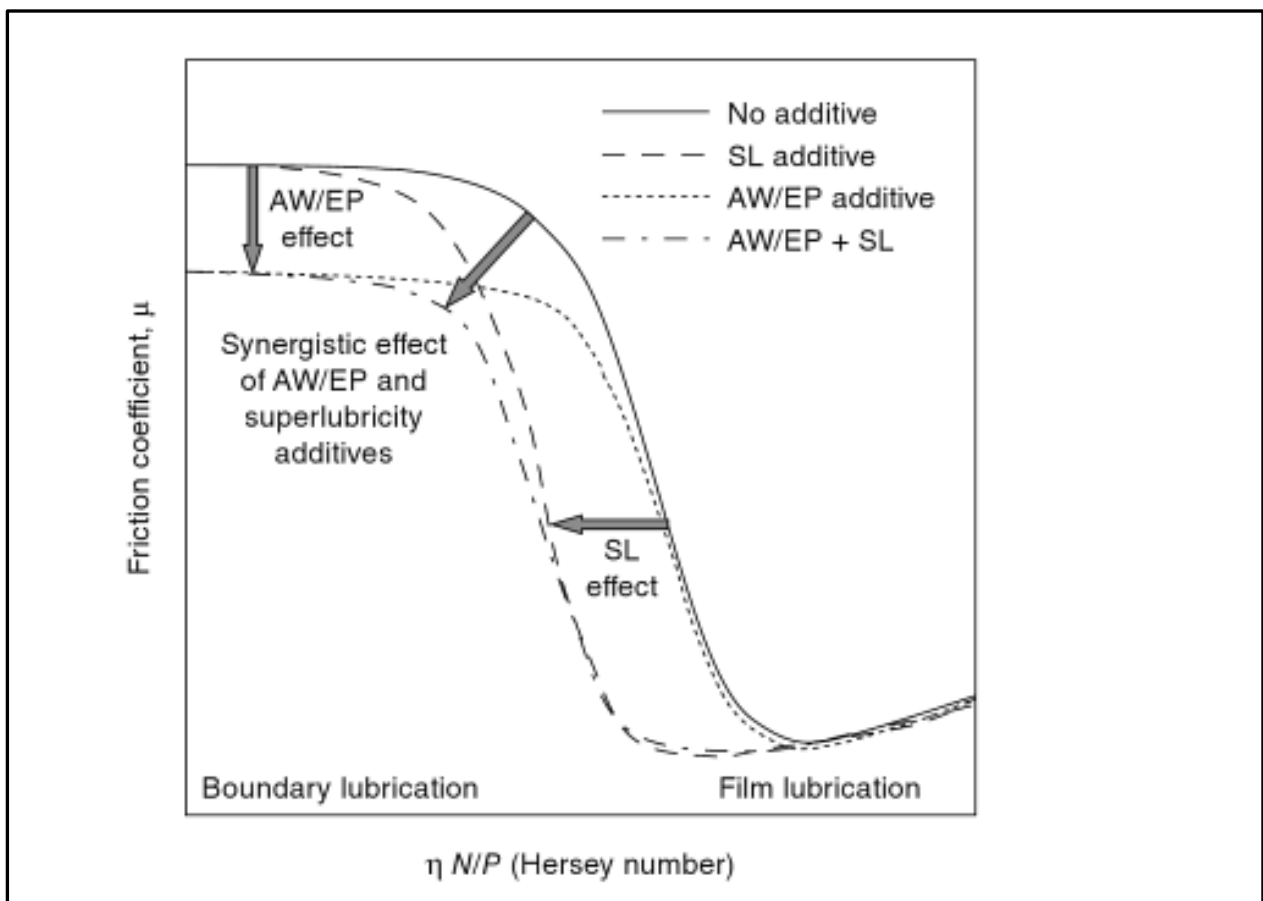


Figure 2.24: Shifts on the Stribeck curve caused by different types of additives (Bart, Cavallano, Gucciardi, 2013: 367).

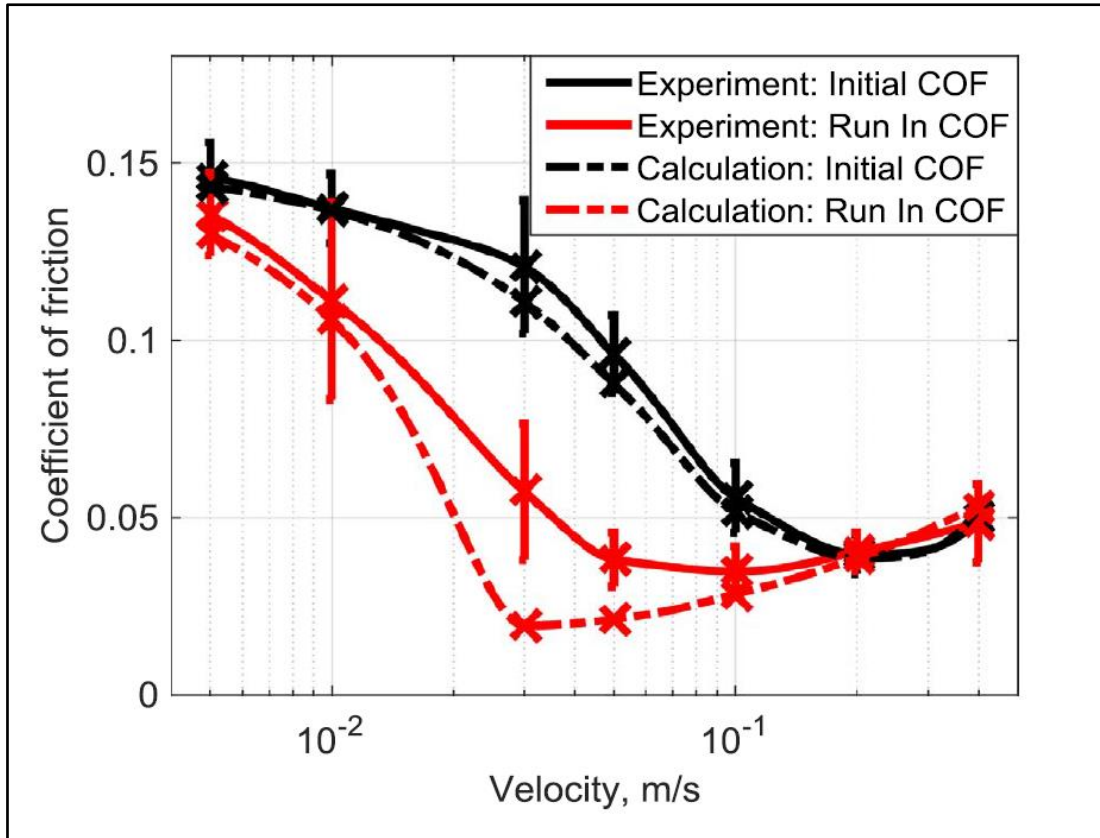


Figure 2.25: Shift in Stribeck Curve before and after running-in (Akchurin, Bosman & Lugt, 2017).

To determine the lubricating regime use is made of the modified Stribeck parameter. The standard Stribeck curve is based on the rolling motion for bearings and consequently a modified parameter is required when sliding occurs. The modified Stribeck parameter also includes the pressure viscosity effects of the fluid (piezoviscosity). The modified Stribeck parameter is defined as (Brandão et.al., 2012):

$$S_p = U_r \cdot \eta_L \cdot \alpha^{1/2} \cdot F_N^{-1/2} \quad 2.8$$

Where:

- | | | |
|----------|------------------------------|------------------------|
| S_p | Modified Stribeck parameter | |
| U_r | Rolling speed | (m/s) |
| η_L | Dynamic viscosity of the oil | (kg/m.s) |
| α | Piezoviscosity coefficient | (s ² .m/kg) |
| F_N | Normal contact force | (N) |

The rolling speed (U_r) is calculated with:

$$U_r = \frac{U_1 - U_2}{2} \quad 2.9$$

Where:

U_1 Speed of the ball (m/s)

U_2 Speed of the disk (m/s)

The piezoviscosity coefficient is determined with (Brandão et.al., 2012):

$$\alpha = y \cdot v^t \quad 2.10$$

Where:

v Kinematic viscosity of the fluid (m^2/s)

y Constant for piezoviscosity ($\text{s}^2 \cdot \text{m}/\text{kg}$)

t Constant for piezoviscosity

Finally, the lubricating regimes are defined as follow:

Elastohydrodynamic regime: $S_p \geq 10^{-7}$

Mixed film regime: $10^{-9} \leq S_p \leq 10^{-7}$

Boundary regime: $S_p \leq 10^{-9}$

Chapter 3

Experimental

3.1 Overview

The aim of the investigation was twofold:

1. Identifying the factors that affect repeatability of friction and wear results and running-in behaviour.
2. Investigating improvement of repeatability with a modified running-in procedure. The tests were conducted on the SRV® 4 test rig.

The different test fluids included 6 base oils from **API Groups II to V**, while **ZDDP** and **diethyl sebacate** were used as additives. Only **API Group III** oil was used when repeatability was improved with the modified running-in procedure. The test procedures are summarised below:

Effect of Different Test Fluids

1. Viscosity of base oils was determined on the Stabinger SVM 3000 viscometer between 25 and 100 °C. This included 40 °C for calculation of viscosity index according to ASTM D2270-16.
2. Friction and wear tests were conducted on the SRV® 4 test rig. The methods were based on ASTM D 5707-16 and ASTM D 6425-17. The load was stepped up from 50 to 200 N at the end of the 5-minute running-in period. Five repeat runs were done for each of the test fluids. The humidity was controlled for each test at 45 % relative to 22 °C.
3. Analysis of friction and wear results:
 - 3.1. Friction coefficient recording plots.
 - 3.2. Photographs of wear scar and wear track taken with a Zeiss Axio Scope A1 optical microscope. Wear surface dimensions also measured with the Axiovision™ software.
 - 3.3. Wear scar diameter adjustment. This was done with an inhouse procedure where wear scars in the images were converted into black and the rest of the image into white. The area of the wear scar image was then determined based

on the fraction of the image that is coloured black. The diameter in the direction parallel to sliding is then calculated from the area of an ellipsoid. This diameter is then the adjusted wear scar diameter.

3.4. Wear profiles scanned with a Nanovea Profilometer PS50. Profiles plotted for scar and track in directions perpendicular to the sliding direction.

3.5. Wear volume of ball scar and disk track calculated according to ASTM D 7755-17.

Modified Running-in Procedure:

1. Only one test fluid used in this section, namely the Group III oil.
2. Friction and wear testing was conducted on the SRV® 4 test rig. The standard and modified load procedures were used. Tests with shorter durations were also done to evaluate wear at earlier stages. For the test runs with shorter durations, each test run was started on an unused surface. After the test run, the wear measurements were taken. An unused surface was then used for the next test run with longer duration. Four repeat runs done for each of the test procedures as well as for every test duration. Humidity was controlled for each test at 45 % relative to 22 °C.
3. Same analysis of results as in 3 above, except the wear scar diameters were not adjusted in this section.
4. Disk analyses were done by a profile of the unworn surface of a disk with the Nanovea Profilometer. Hardness analyses of the disk surfaces were done with a Vickers Hardness Tester FV-700e.

The operating conditions for the investigation are summarised in Table 3.1.

Table 3.1: Operating conditions on the SRV test rig for both parts of the investigation.

Operating Condition	Test Fluids	Modified Running-in
Operating Load	200 N	200 N
Running-in duration	5 min	5 min
Load Increase	Step Load at end of running-in period	Step Load at end of running-in period & Gradual Load increase from start of running-in period to 200 N, 30 N/min
Block Temperature	50 °C	50 °C
Stroke	1 mm	1 mm
Frequency	50 Hz	50 Hz
Humidity	45 % relative to 22 °C	45 % relative to 22 °C
Test Duration (Including running-in)	125 min	125 min 100 min 75 min 40 min 20 min 5 min, after load increase 5 min, before load increase
Base Fluids	White Mineral Oil Group III Mineral Oil Group II Mineral Oil Polyalphaolefin Polyalkylene Glycol	Group III Mineral Oil
Additives	Diethyl Sebacate ZDDP	Diethyl Sebacate
Repeat Runs	5 for every test fluid	5 for every test duration

3.2 Test Fluid Selection

The test fluids selection included a base oil and an additive. Different base oils were selected to investigate the effect of the base oil composition on repeatability. The additives were included to enable the test to operate at 200 N.

Selection of the base oils was based on their use in general applications, such as lubricating greases, hydraulic fluids, engine oils and gear oils. This included mineral and synthetic oils. Highly specialised oils were omitted as well as vegetable base oils, due to the complexity of the composition of vegetable base oils and their high degree of unsaturation.

Group I mineral oils were omitted due to future trends where these oils are being replaced by oils with a higher degree of refining. Group I also have more complex compositions compared to higher refined oils. Naphthenic based white oil was included, which has a higher degree of polarity compared to paraffinic base oils. This was done so that the role of base oil polarity could be determined.

The base oils and their physical properties are summarised in Table 3.2. The numbers following the base oil name for the two **Group II mineral oils** (e.g., **Group II Mineral Oil, 32**) refers to the ISO viscosity grade of the oil at 40 °C. The viscosities of the base oils at 40 °C were different, as can be seen in Table 3.2. Since the base oils were selected from different API groups, two viscosity grades for the **Group II mineral oil** were also included. This was done so that any effects on the repeatability of the results that a change in viscosity between the base oils might have, could be verified. The number (e.g., 6) following the **polyalphaolefin** and **Group III mineral oil** refers to the base oil viscosity at 100 °C. The number 146 for the **polyalkylene glycol** relates to the viscosity of this base oil at 100 °C.

The additives selected included an additive that physically adsorb on to the surface as well as an additive that react with the surface to form a protective anti-wear layer. For the physically adsorbing additive an organic friction modifier was selected; **Diethyl sebacate** (purity > 97.5 %). This was obtained from SIGMA-ALDRICH. According to

the supplier, the remaining < 2.5 % refers to raw materials, solvents, intermediates and by products of the synthesis process. These impurities will therefore not adversely affect the performance of the additive.

A primary **zinc dialkyldithiophosphate (ZDDP)** was selected as the additive that reacts with the surface to form a protective anti-wear layer on the metal surface. **ZDDP** has been in use in industry for a long time and can function as an anti-wear agent, mild extreme pressure agent as well as an effective oxidation and corrosion inhibitor (Rudnick, 2003: 29). This was obtained from Lubrizol and the designation is: Lubrizol®1395. This is **ZDDP** (80 % - 90 %) dispersed in mineral oil (10 % - 20 %).

Table 3.2: Base oils selected for experimental investigation.

Base Oil	Viscosity, 40 °C (mm²/s)	Density, 25 °C (g/cm³)
Group II Mineral Oil, 32	35.004	0.855
Group II Mineral Oil, 100	90.211	0.862
Group III Mineral Oil 6	28.754	0.834
White Mineral Oil, Naphthenic	17.416	0.837
Polyalphaolefin 6	24.218	0.820
Polyalkylene Glycol 146	137.840	0.984

3.3 Apparatus

The apparatus used in this investigation is summarised in Table 3.3. The part of the investigation in which the apparatus was used in also specified in this table.

Table 3.3: Apparatus used in investigation.

Test Function	Apparatus
Oil Viscosity	Stabinger Viscometer SVM 3000/G2
Mass Balance	Metler Toledo XP2003S
Specimen Cleaning	Ultrasonic Cleaner PS-40
Friction and Wear Testing	Optimol SRV ®4
Relative Humidity	In-house Setup

Table 3.3: (continued).

Wear Surface Measurement and Photography	Optical Microscope: Axio Scope A1, supplied by Carl Zeiss Pty (Ltd)
Surface Profile and Roughness	Digital Microscopy camera: AxioCam ERc 5s
Harness Measurement	Nanovea Profilometer PS50 Vickers Hardness Tester FV-700e

3.3.1 Viscosity Measurement

Viscosity measurement of the base oils in this investigation was done with a Stabinger viscometer (model SVM 3000/G2), according to ASTM D 7042. The viscometer works on the principle of a tube that rotates at constant speed. Inside the tube is a rotor with a built-in magnet. The rotor has a low density and floats in the oil sample in the tube. It is centred by centrifugal forces.

As the tube rotates, the rotor will also rotate, and the speed depends on the viscosity of the fluid. The viscosity is determined from the rotating speed of the rotor. The temperature range is -56 °C to 105 °C (Anton Paar, 2011: 14 & 33). A diagram of the tube and rotor is given in Figure 3.1.

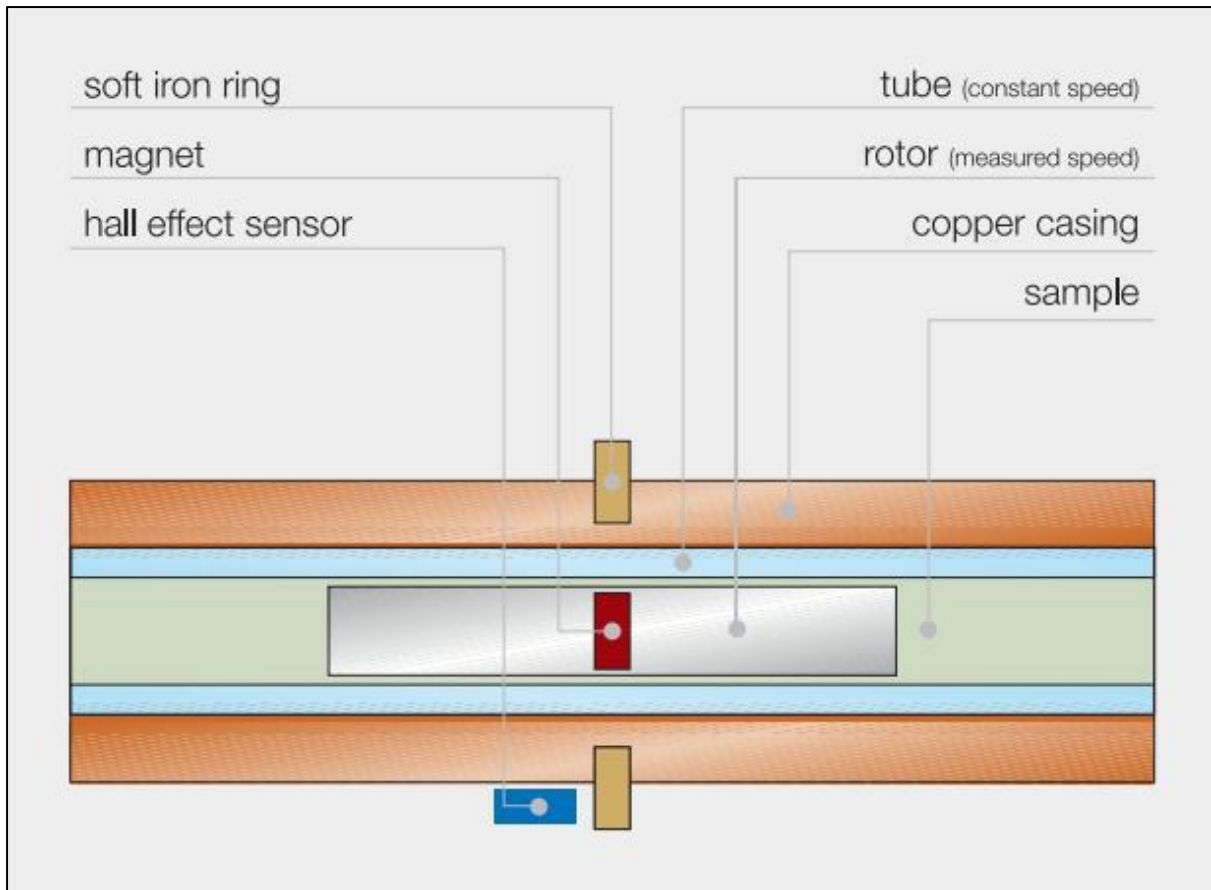


Figure 3.1: Diagram of tube and rotor in the Stabinger viscometer (Krashchitz, 2014).

3.3.2 Ultrasonic Cleaner

An ultrasonic cleaner (PS-40) was used to remove possible contaminants from the test specimens before testing. It's also used to clean the specimens after testing to remove layers from the surface. This is achieved by the cavitation bubbles which are generated by ultrasonic waves that are transmitted through a liquid.

The ultrasonic bath is filled with distilled water and the specimens are placed in a beaker in the ultrasonic bath. Two solvents are used: toluene and acetone. The specimens are kept for 10 minutes in each of the solvents before and for 30 seconds after a test. The specifications of the cleaner are given in Table 3.4. Specimens are cleaned at room temperature and atmospheric pressure.

Table 3.4: Specifications for PS-40 Ultrasonic Cleaner (Ultrasonic cleaners made in China, 2014).

Property	Capacity
Tank Capacity	10 L
Ultrasonic Power	240 W
Heating Power	400 W
Operating Frequency	40 kHz
Mains Power	240 V
Timer	1-30 min & ∞

3.3.3 Mass Balance

A Mettler Toledo XP2003S mass balance was used to weigh the required amount of additive and base oil when the samples were prepared. It has a readability of 1 mg with a maximum load of 2300 g. Repeatability between 10 measurements is also 1 mg. Before a measurement is taken, the drift is corrected with an internal adjustment (Mettler Toledo Operating Instructions, 2005). All measurements were done at room temperature.

3.3.4 Friction and Wear Measurement

The friction and wear tests were conducted on a SRV 4[®] from Optimol Instruments GmbH. A number of assemblies can be used on the SRV 4, such as pin-on-disc, cylinder-on-disc and ball-on-disc. The motion can also be rotating or oscillating. In this investigation, the ball-on-disc configuration with an oscillating motion was used (Optimol Instruments SRV, 2011: 45-102). Figure 3.2 is a diagram of the SRV test rig.

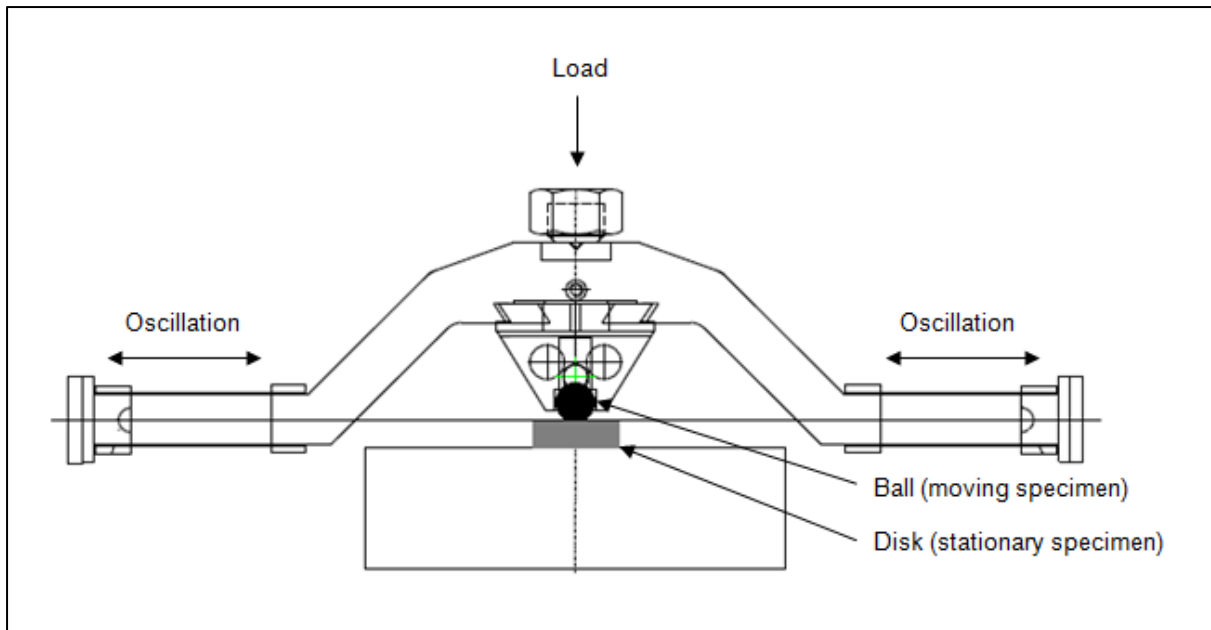


Figure 3.2: Diagram of ball-on-disc assembly with oscillating motion on the SRV test rig (Optimol Instruments SRV, 2011: 47).

The load is applied on the ball assembly with a spring load from the top as indicated in Figure 3.2. The load on the disc is increased with an electric motor, gear and spindle that increases the tension of the spring. The oscillating speed is controlled with the stroke drive and the temperature is controlled by an element in the SRV block.

The friction force is measured with piezoelectric sensors. The friction coefficient is then automatically calculated by the Optimol software by dividing the friction force with the load. The sampling rate at which the friction force was measured was 0.0576 milliseconds. The Optimol software calculates the average value of the friction coefficient for every second which is then displayed. The range for the operating conditions is given in Table 3.5.

Table 3.5: Operating conditions range for the SRV test rig (Optimol-instruments SRV, 2011: 12-25).

Operating Condition	Range
Block Temperature	-35 °C to 350 °C
Load Maximum	2000 N
Frequency	1 to 511 Hz
Stroke Maximum	5 mm
Test Fluid	0.3 mL
Relative Humidity	45 % relative to 22 °C

3.3.5 Surface Analysis

The surface analysis involved comparison of wear surfaces, measurement of wear dimensions, profile scans as well as hardness analysis of the discs. For the wear surface comparison and measurement, a Carl Zeiss optical microscope was used. The profile scans were done with a Nanovea Profilometer PS50 and a Vickers Hardness Tester FV-700e was used to verify the hardness of the test specimens.

3.3.5.1 Carl Zeiss Optical Microscope

An Axiocam ERc 5s digital camera assembled on a Carl Zeiss Axio Scope A1 optical microscope was used to capture images of the wear surfaces. The wear surfaces included wear scars on the ball specimens and the wear tracks on the disk specimens. The wear scar images were captured with 10 x magnification and the wear tracks with 5 x magnification. The captured images were processed with the Zeiss Axiovision Microscope software. The dimensions of the wear scars and tracks were also measured with this software.

3.3.5.2 Nanovea Profiler PS50

The Nanovea Profiler utilizes axial chromatic aberration, i.e., focusing different wavelengths at different distances from the lens (NANOVEA). A diagram illustrating the principle is given in Figure 3.3. In this figure at a certain distance, a specific wavelength will focus on the surface. The lens is also used to receive backscattered

light from the surface into an optical fibre. Due to the confocal arrangement of the lenses, the wavelength that is focused on the surface will be focused to the front of the fibre. The light is then fed through the fibre to a spectrometer. This has a much higher intensity compared to the other wavelengths which is spread over a much bigger area. A wavelength scale can then be calibrated to the distance (Michelt & Schulze, 2005).

The PS50 was fitted with a 300 μm pen and the scan data was processed with Mountains® 7 3D analysis software. This software enables the user to generate 3 D images of wear surfaces, extract surface profiles, calculate surface roughness parameters as well as surface areas. The specifications for the Nanovea Profiler PS50 are summarised in Table 3.6.

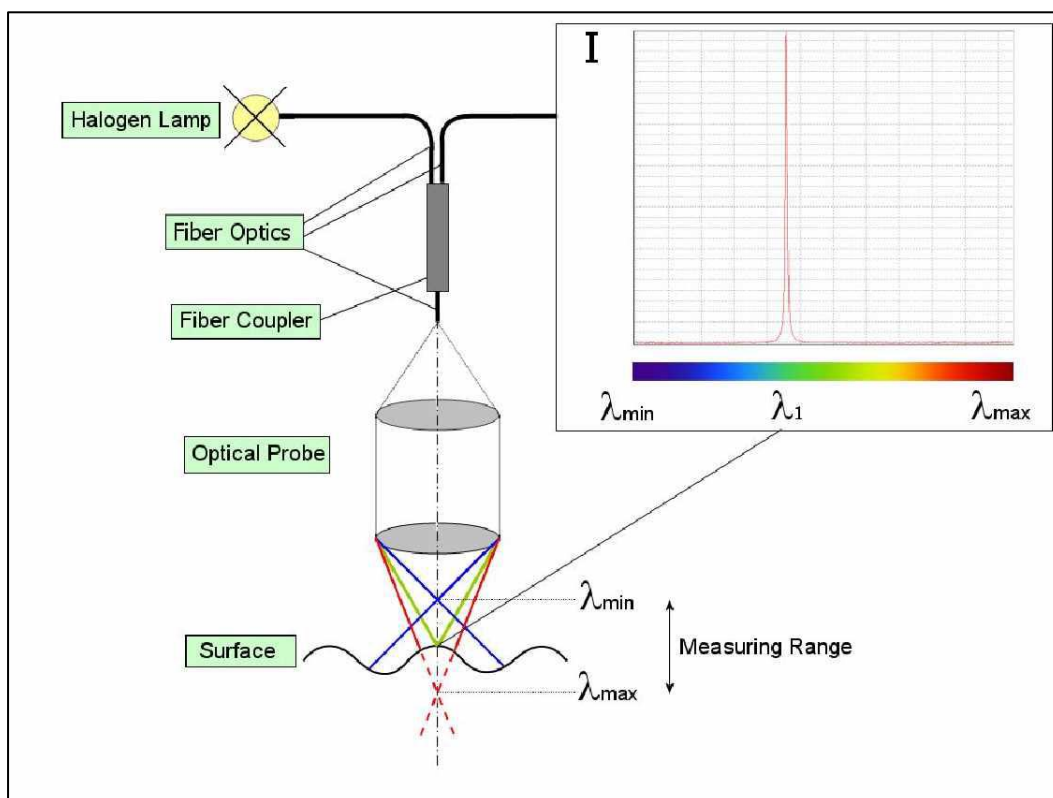


Figure 3.3: Diagram of axial chromatic aberration utilized to measure height (Michelt & Schulze, 2005).

Table 3.6: Specifications for Nanovea Profiler PS50 (NANOVEA).

Specification	Value
<i>Base</i>	
X-Y Axis Travel	50 mm
Z Axis	30 mm
X-Y Axis Resolution	0.1 μm
Maximum X-Y Speed	20 mm/s
<i>Optical Pen</i>	
Measurement Range	300 μm
Working Distance (mm)	11 mm
Vertical Resolution (nm)	8 nm
Vertical Accuracy (nm)	80 nm

3.3.5.3 Vickers Hardness Tester FV-700e

The hardness of the disc surfaces was verified with a Vickers Hardness Tester FV-700e. The hardness is determined from the dimensions of the indentation obtained with a square pyramid diamond tip. The load was 196.1N and the dwell time 10 seconds. The hardness is automatically converted to the Rockwell Hardness C by the Vickers Hardness Tester FV-700e.

3.3.6 Relative Humidity Control

It was found that the amount of water vapour in the atmosphere affects friction and wear during testing (Lapuerta et.,al., 2014, Benadé, 2015, Langenhoven, 2015 Lapuerta et.al., 2016 and Morina et.al., 2017). To eliminate the effect of variation in the atmospheric water content on the friction and wear tests, the relative humidity in the SRV chamber was controlled.

The humidity was controlled with an in-house setup. This utilises compressed air which flows through the humidifier (see diagram in Figure 3.4). Before the compressed air enters the humidifier, it passes through a filter to remove contaminants and particles.

The operating pressure is set at 180 kPa. The total air flowrate is between 3 and 5 L/min.

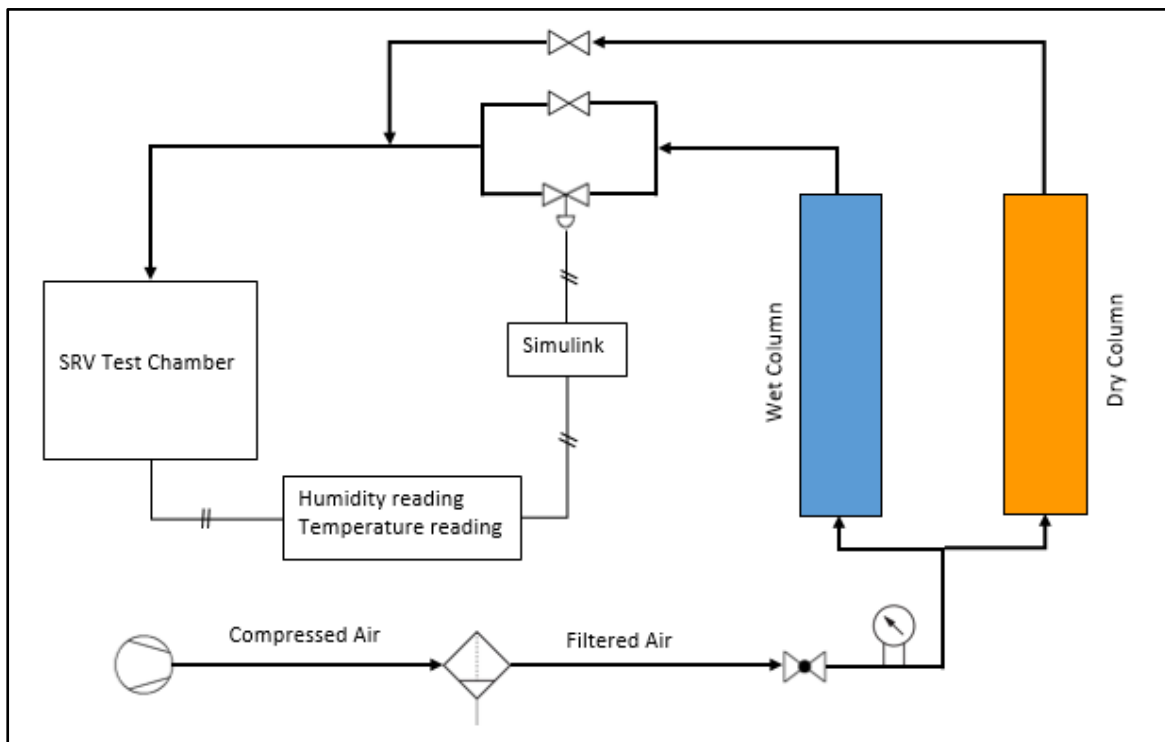


Figure 3.4: Diagram of humidifier to control relative humidity in SRV test chamber.

In the humidifier the air is split and sent through two columns. The one column is filled with silica gel crystals which removes any moisture in the air. In the other column the air is sparged through distilled water. A sparger is used to decrease the diameter of the air bubbles. A reduction in the bubble diameter improves mass transfer. Therefore, a dry air stream and a wet air stream is obtained. These streams are mixed before entering the SRV chamber.

To adjust the amount of water vapour in the chamber atmosphere, the ratio of the dry and wet stream is adjusted (see Figure 3.4). The system has been automated with the implementation of a control valve that adjust the wet air flowrate. Adjustments are made based on feedback control received from a humidity/temperature sensor.

The set point humidity is entered on the Simulink program in Matlab relative to a specified temperature. The program converts the relative humidity to the partial

fraction. The partial fraction is used instead of humidity since humidity is a function of temperature and this is not constant during testing.

3.4 Test Preparation

The preparation procedure for each test and sample was strictly adhered to. The same steps were also repeated in the same order during start-up of every test. This was done to eliminate any possible influence the procedure could have that can affect repeatability of the results.

3.4.1 Specimen Preparation

The test start-up involved cleaning of the specimens, assembling of the ball-on-disc configuration, and stabilizing the humidity in the SRV test chamber. The standard SRV steel specimens, as obtained from the supplier, were used for all tests; AISI 52100 steel. The properties of the specimens are given in Table 3.7. The humidity was set at 45 % relative to 22 °C. This was chosen based on the recommendations for standards laboratories (ISA-TR52.00.01, 2006).

Table 3.7: Specimen Properties (ASTM DD5707-16 & ASTM D6425-17).

Property	Ball	Disc
Material	AISI 52100 steel	AISI 52100 steel
Hardness	60 ± 2 Rockwell C scale	60 ± 2 Rockwell C scale
Surface Finish	0.025 μm ± 0.005 μm <i>Ra</i>	0.500 μm < <i>Rz</i> (DIN) < 0.650 μm 0.035 μm < <i>Ra</i> (C.L.A.) < 0.050 μm 0.020 μm < <i>Rpk</i> < 0.035 μm 0.050 μm < <i>Rvk</i> < 0.075 μm Lapped surface
Dimensions	Diameter = 10 mm	Diameter = 24 mm Thickness = 7.85 mm

The composition of AISI 52100 steel is given in Table 3.8.

Table 3.8: Composition of AISI 52100 steel (AISI 52100 Alloy Steel (UNS G52986), 2012).

Element	Content (%)
Iron (Fe)	96.5 – 97.32
Chromium (Cr)	1.30 – 1.60
Carbon (C)	0.98 – 1.10
Manganese (Mn)	0.25 – 0.45
Silicon (Si)	0.15 – 0.30
Sulfur (S)	≤ 0.025
Phosphorous (P)	≤ 0.025

The cleaning procedure is as follows:

1. Specimens, ball specimen holder, tweezers and hexagonal socket head cap screws are placed in a beaker filled with toluene.
2. The beaker is then placed in the ultrasonic bath for 10 minutes at room temperature.
3. The contents of the beaker are taken out and rinsed with acetone to allow a shorter drying period.
4. It is then placed in a beaker filled with acetone. The beaker is again placed in the ultrasonic bath for 10 minutes.
5. The contents are taken out of the beaker and placed in an oven for drying. The oven temperature must not exceed 90 °C, to prevent surface hardening.
6. After the specimens, ball specimen holder, tweezers and hexagonal socket head cap screws have been dried and allowed to cool down to room temperature, the ball-on disc configuration is assembled in the SRV chamber.

Surgical gloves are worn during the cleaning procedure to prevent any possible contamination of the test fluid and the specimens. This also protects the operator from accidental spills when the toluene is being handled.

3.4.2 Sample Blending and Handling

To prevent the effects of degradation and oxidation of the test fluid to affect the results, samples were replaced after 7 days, and a new sample was prepared. Consequently, small sample sizes were used (5 g). Samples were blended by first weighing the required amount of additive in a sterile injection glass vial, followed by adding the base oil. The vials were rinsed with hexane and dried in an oven before use. The scale was reset with an internal adjustment before every sample was blended (section 3.3).

After each test fluid had been added, the vial was closed with a rubber stopper. This was done to form an airtight plug which prevented oxygen and water vapour from entering the vial. The remaining air in the vial was replaced with nitrogen to obtain an inert atmosphere. This also prevents the sample from degradation.

The vial was shaken and placed in the ultrasonic bath to allow proper mixing of the additive. The sample was then left overnight before it was used. The amount of test fluid required for each test was 0.3 mL. This was drawn up with a 1 mL glass syringe (without removing the stopper) and transferred onto the test disk. The syringe was thoroughly rinsed with hexane and acetone and dried in an oven after every test. The sample was also vigorously shaken 5 to 10 minutes before the 0.3 mL was drawn up. The mass of additive and base oil for each of the test fluids are given in Table 3.9.

Table 3.9: Mass of base oil and additive for each of the test fluids.

Test Fluid	Base Oil (g)	Base Oil Name/ API Classification	Diethyl Sebacate (g)	ZDDP (g)
TF 1	4.975	White Mineral Oil	0.025	-
TF 2	4.850	PAO 6 cSt	0.150	-
TF 3	4.900	Group III 6 cSt	0.100	-
TF 4	4.900	Group II, ISO VG 32	0.100	-
TF 5	4.900	Group II, ISO VG 100	0.100	-
TF 6	4.975	PAG 146 cSt	0.025	-
TF 7	4.975	PAO 6 cSt	-	0.025
TF 8	4.975	PAG 146 cSt	-	0.025

3.4.3 Test Start-up

The procedure followed during start-up incorporates the cleaning procedure described in section 3.1 and the sampling handling described in section 3.2. The focus here will be the steps followed before a test is started:

1. While the cleaning procedure is in progress, the humidity in the SRV test chamber is adjusted to the desired operating conditions. The air flow rates are fine-tuned during this stage.
2. After the specimen-cleaning procedure, the SRV test chamber is opened, and the ball-on-disk configuration is assembled. The ball and disk are tightened. The humidity in the SRV test chamber changes again to the humidity in the laboratory, since the SRV chamber is open.
3. The test fluid is then transferred onto the disk. The ball is then loosened and allowed to drop onto the disk. The load is applied onto the ball. After the load is applied, the disk is also loosened. This ensures that the clamping of the disk and ball do not result in misalignment and that proper contact is obtained between the ball and disk as well as the disk and the test block. The disk is clamped again followed by clamping of the ball.
4. After the load is released, the disk and ball are tightened.
5. The load is applied, and the test chamber is closed.
6. Once the humidity stabilizes again at the set point, the test is started.

3.5 Data Analysis

The analysis of the results from the friction and wear tests are described in this section. This is divided into three categories: friction, extent of wear and surface finish. The calculation of the lubricating regime in which the tests operate is also included.

3.5.1 Friction Coefficient

The friction coefficient is recorded continuously throughout the duration of a test. This is plotted on a graph as a function of time. The load is also plotted on this graph. The

data recorded during friction and wear testing were also used to obtain the friction coefficients at specified times as described in ASTM D6425-17. These times are: f_{min} , f_{max} , f_{15} , f_{30} , f_{90} and f_{120} . These values are used to compare repeatability between the repeat runs.

Repeatability described in ASTM D6425-17 is defined so that the difference between the friction coefficient values should not exceed a value of 0.01 between consecutive runs. These criteria apply only to results obtained by the same operator on the same test apparatus with the same test materials. The difference of 0.01 can be exceeded for only one case in 20. For ASTM D5707-17 the same criteria apply except that the difference must not exceed 0.012. Only the minimum friction coefficient value is required for ASTM D5707-16.

To quantify repeatability of the friction coefficient, the friction coefficient plots were integrated. Essentially the area between the average of friction coefficient and the standard deviation for the friction coefficient is then calculated for every data point. A smaller area calculated will be due to smaller standard deviations for every data point. Since it is an integration, the areas for all the data points are summed. Therefore, a smaller total area is due to smaller standard deviations. Smaller standard deviations were obtained for tests with better repeatability. This method gives a better overall indication of repeatability as opposed to only single values. This was derived as follows:

- The average of the friction coefficient for 5 repeat runs was determined.
- The standard deviation from the average of the friction coefficient was also determined.
- To integrate the friction coefficient plot, the standard deviation was subtracted from the average of the friction coefficient. Mathematically, this equates to

$$\int AVG_{COF} - STDEV_{COF} dt$$

This integration was done by calculating the area between average of the friction coefficient and the standard deviation of the friction coefficient. From the SRV, a

friction coefficient value is recorded for each second. By dividing the plot into time intervals of 1 second, the total area was calculated. To calculate the area, the average of the friction coefficients for all the repeat runs minus the standard deviation for each time interval was multiplied with the time interval. This is shown in equation 3.1:

$$\int AVG_{COF} - STDEV_{COF} dt = \sum_{t=0}^{t=7500} [AVG_{COF} - STDEV_{COF}] \times [t_{n+1} - t_n] \quad 3.1$$

3.5.2 Extent of wear

The extent of wear is determined for both the ball and the disk specimens used during testing. The wear scar refers to the wear surface on the ball specimen and wear track to the wear surface on the disk.

Wear Scar Diameter

The wear scar diameters on the ball specimens were determined by calculating the average of the diameter parallel to the sliding direction (d_1) and the diameter perpendicular to the sliding direction (d_2):

$$WSD = \frac{d_1 + d_2}{2} \quad (3.2)$$

Wear Volume

As already mentioned, the friction and wear test methods are based on the ASTM test standards. Therefore, the wear volume on the scar and on the track is calculated according to the method described in ASTM D 7755-17. Furthermore, this is also the calculation of the wear volume for ASTM D 6425 and ASTM D 5707 during the Round Robin test series (Woydt, 2015 & Woydt, 2016).

This method utilized dimensional measurements from the scar as well as the wear track. The cross-sectional area of the wear profile was also included. The variables

used to calculate the wear volume are given in Figure 3.5 (dimensions) and in Figure 3.6 (profile area). It is assumed that the profile of the wear scar is the same as the profile of the wear track:

Wear Scar Volume (ball):

$$W_{v,ball} = \frac{\pi(d_1^2 \cdot d_2^2)}{64} \left(\frac{1}{R} - \frac{1}{\bar{R}} \right) \quad (3.3)$$

\bar{R} is calculated with:

$$\bar{R} = \frac{d_2^3}{12W_{q,flat}} \quad (3.4)$$

Where:

\bar{R}	Resulting radius of the shape of the wear scar after the test.	mm
R	Initial radius of the ball	mm
d_1	Wear scar diameter on the ball parallel to the sliding direction.	mm
d_2	Wear scar diameter on the ball perpendicular to the sliding direction.	mm
$W_{q,flat}$	Planimetric wear of the wear track in the middle of the wear track length, seen perpendicular to the sliding direction (cross sectional area of profile).	mm ²

Wear Track Volume (disk):

$$W_{v,flat} = \frac{\pi d_4^2 (d_3 - s)^2}{64} \cdot \frac{1}{\bar{R}} + s \cdot W_{q,flat} \quad (3.5)$$

\bar{R} is calculated with:

$$\bar{R} = \frac{d_4^3}{12W_{q,flat}} \quad (3.6)$$

Where:

- \bar{R} Resulting radius of the shape of the wear track after the test. mm
- d_3 Total length of the wear track in the sliding direction. mm
- d_4 Width of the wear track. mm
- s Stroke mm

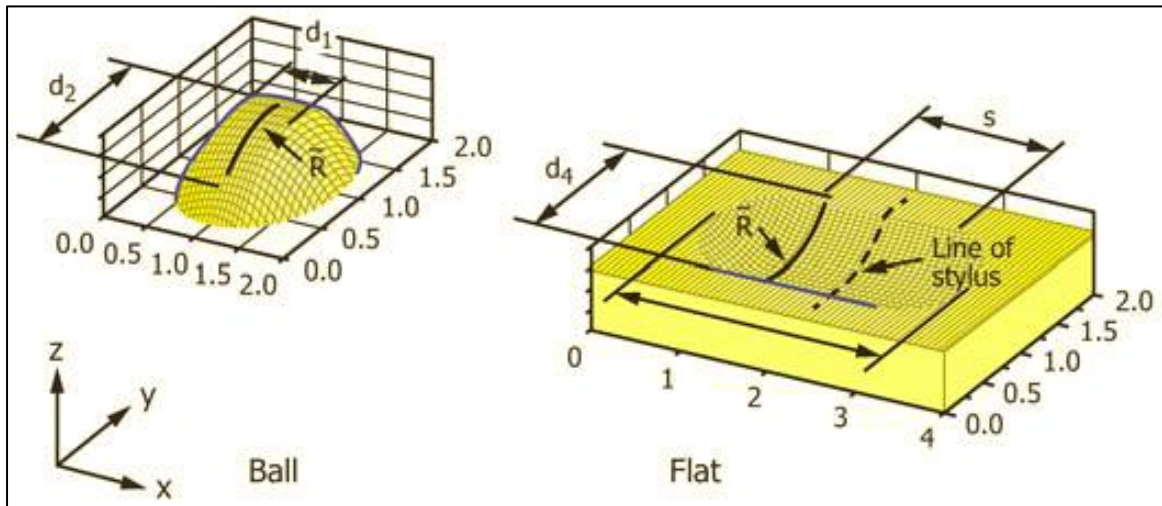


Figure 3.5: Dimensions used to calculate wear volume on the ball and disk (ASTM D7755-17).

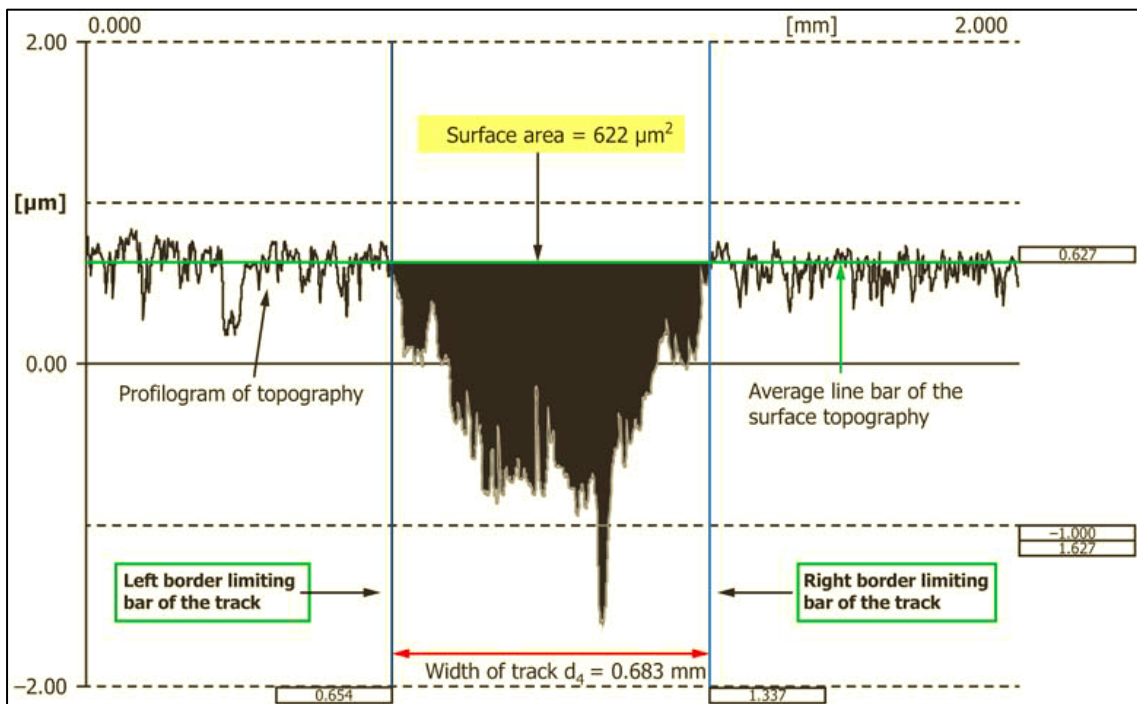


Figure 3.6: Profile cross sectional area used to calculate wear volume on the ball and disk (ASTM D7755-17).

The wear rates were calculated with:

$$\bar{W}_{WSD} = \frac{\text{Wear Scar Diameter at time}_t}{\text{time}_t} \quad (3.7)$$

$$\bar{W}_{WVS} = \frac{\text{Ball Wear Scar Volume at time}_t}{\text{time}_t} \quad (3.8)$$

$$\bar{W}_{WVT} = \frac{\text{Disk Wear Track Volume at time}_t}{\text{time}_t} \quad (3.9)$$

In equation 3.7, 3.8 and 3.9, the extent of wear refers to either the wear scar diameter (WSD), ball wear scar volume ($W_{v,ball}$) or the disk wear track volume ($W_{v,flat}$). The wear rate can therefore be seen as either the rate of change of the wear scar diameter or the rate of change of the wear volume on either the ball or on the disk.

3.5.3 Wear Scar Diameter Adjustment

For the diameter in the direction parallel to sliding direction, there is a degree of uncertainty in the accuracy of the measurement. This is due to the edge of the wear scars that are poorly defined in this direction. An example is given in Figure 3.7. To correct for this, the wear scars were adjusted. The wear scar adjustment is explained below.

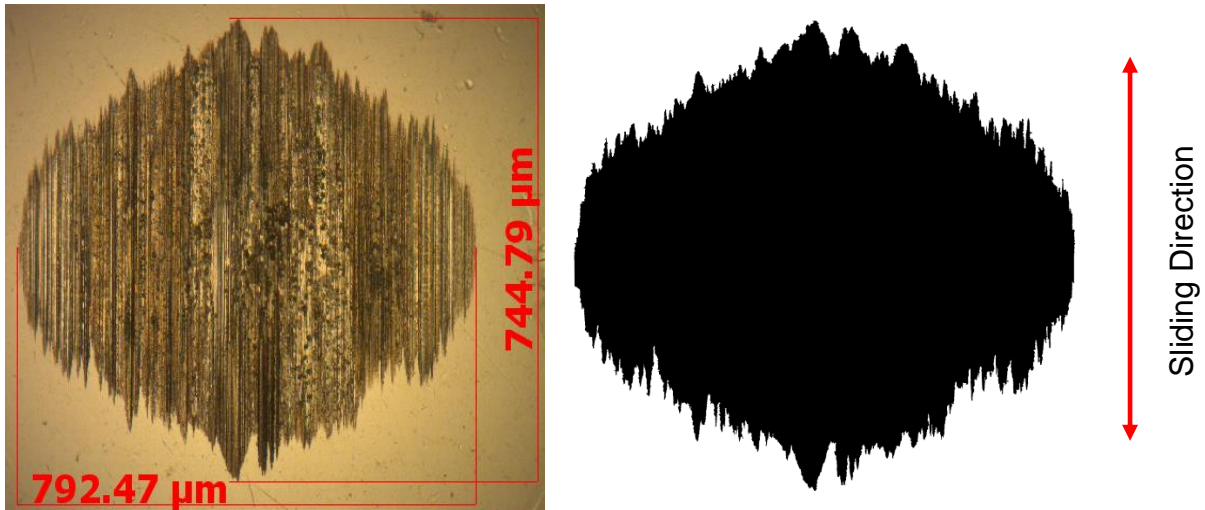


Figure 3.7: Example of a wear scar with a poorly defined diameter in the direction parallel to the sliding direction.

The steps followed to adjust the wear scar diameter were:

1. The wear scar image is converted to a black and white image with GIMP 2.10.6 image manipulation program. This is freeware that is available online (Kimball & Mattis, 1996).
2. The fraction of the image that is black (scar) is also determined with the software.
3. The dimensions for every image taken with the microscope under 10 times magnification are 1131.09 μm x 845.45 μm (i.e., rectangular). From these dimensions, the area of the image was calculated. The area of the wear scar was determined by multiplying the area fraction of the wear scar with the total area of the image.
4. The adjusted wear scar diameter is determined by assuming the shape of the wear scar as an ellipse. The area of an ellipse is then used to calculate the diameter parallel to the sliding direction.

$$d_{1\ adj} = \frac{4 \cdot A_{ellips}}{\pi \cdot d_2} \quad (3.10)$$

An example of how the wear scar adjustment was done is given in Table 3.10.

Table 3.10: Example of wear scar diameter adjustment (wear scar from Figure 3.7), parallel to the sliding direction.

Wear Scar Dimensions:

$d_1 = 744.790 \mu m$ – diameter parallel to the sliding direction, poorly defined

$d_2 = 792.470 \mu m$ – diameter perpendicular to the sliding direction, well defined

Rectangular Area of Image:

$$\begin{aligned} Area_{image} &= width \times length \\ &= 1131.090 \mu m \times 845.450 \mu m \\ &= 956280.041 \mu m^2 \end{aligned}$$

Wear Scar Fraction of Area of the Image:

(GIMP 2.10.6 image manipulation program)

Wear Scar Area Fraction = 0.402

Thus, Area of the Wear Scar:

$$\begin{aligned} Area_{wear\ scar} &= Area_{image} \times Wear\ Scar\ Area\ Fraction \\ &= 956280.041 \times 0.402 \\ &= 384424.576 \mu m^2 \end{aligned}$$

Adjusted Wear Scar Diameter (equation 3.8):

Assume: $Area_{wear\ scar} = Area_{ellips}$

Thus:

$$\begin{aligned} d_{1\ adj} &= \frac{A_{ellips}}{\pi \cdot d_2} \\ &= \frac{4 \times 384424.576}{\pi \cdot 792.470} \\ &= 617.644 \mu m \end{aligned}$$

Measured Wear Scar Diameter vs Adjusted Wear Scar Diameter

Measured Wear Scar Diameter

$$\begin{aligned} WSD_{meas} &= \frac{d_{1\ meas} + d_2}{2} \\ WSD_{meas} &= \frac{744.790 + 792.470}{2} \\ WSD_{meas} &= 768.630 \mu m \end{aligned}$$

Adjusted Wear Scar Diameter

$$\begin{aligned} WSD_{adj} &= \frac{d_{1\ adj} + d_2}{2} \\ WSD_{adj} &= \frac{617.644 + 792.470}{2} \\ WSD_{adj} &= 705.057 \mu m \end{aligned}$$

3.5.4 Wear Surface Evaluation

Wear Surface Images

The wear surfaces between runs are based on the following characteristics:

1. Consistency of surface damage between runs. This includes plough marks and smoother areas.
2. Uniformity of the wear scars, i.e., differences in depth.
3. Comparing the roundness of the scars. This is determined from the ratio of the two measured wear scar diameters. A ratio = 1 indicates that the surface is round.

Wear Profiles

The wear profiles of the scar and track was measured with the NANOVEA Profiler PS50. For both surfaces an area was scanned that included the entire wear surface. The step size of the scans was 0.8 μm in both x and y direction. The scan data was processed with the Mountains® 7 3D analysis software (Digital Surf, 1996). This included:

1. Profile of the wear scar, perpendicular to the sliding direction (in the middle of the wear scar).
2. Profile of the wear track, perpendicular to the sliding direction (in the middle of the wear track).
3. 3D image of the wear surfaces.

The profiles between the repeat runs were compared and deviations between the profiles were carefully taken note of. The 3D images assisted with the observations of the wear surface images. The disk surfaces with no wear tracks were also scanned. This was used to determine the surface roughness of the disk surfaces.

3.6 Lubricating Regime

The lubricating regime was determined with the modified Stribeck numbers (Gold et.al., 2001 & Brandão et.al., 2012). Equations 2.8 to 2.10 described in section 2.7 in Chapter 2 was used to calculate the modified Stribeck numbers.

To determine the maximum sliding speed, the equations of motion were used. It was assumed that the maximum velocity is reached at half the stroke length and that acceleration is constant:

$$u_{max} = u_i + a \cdot t \quad (3.11)$$

$$u_{max}^2 = u_i^2 + 2 \cdot a \cdot s_{max} \quad (3.12)$$

$$s_{max} = u_i \cdot t + \frac{1}{2} \cdot a \cdot t^2 \quad (3.13)$$

Chapter 4

Results & Discussion

This chapter is divided into 2 sections. This is so that the objectives of the study can be addressed separately. Section 4.1 focuses on the factors that affect repeatability of friction and wear results while Section 4.2 focuses on improving repeatability of friction and wear results. This is followed by sections that focus on running-in, the role of the test disk and the surface finish.

4.1 Factors Affecting Repeatability

The factors affecting repeatability are the test fluid, wear scar diameter adjustment, the step load increase, and the test disk. The effects of the test fluid and the wear scar diameter adjustment are discussed in section 4.1.2. The step load increase and the test disk results are discussed in sections 4.1.3 and 4.1.4. However, the test fluids will first be characterised in section 4.1.1.

4.1.1 Test Fluid Characterisation

The test fluid characterisation comprises the following properties of the test fluids:

1. Base oil viscosity
2. Base oil viscosity index
3. Lubricating regimes for each base oil under running-in load and operating load.
4. Base oil composition (polarity)
5. Amount of additive required for each base oil.

4.1.1.1 Base Oil Viscosity

The viscosity of each of the base oils is given in Figure 4.1 as a function of temperature. Since the block temperature on the SRV test rig was controlled at 50 °C, the viscosity of each base oil at this temperature was also determined.

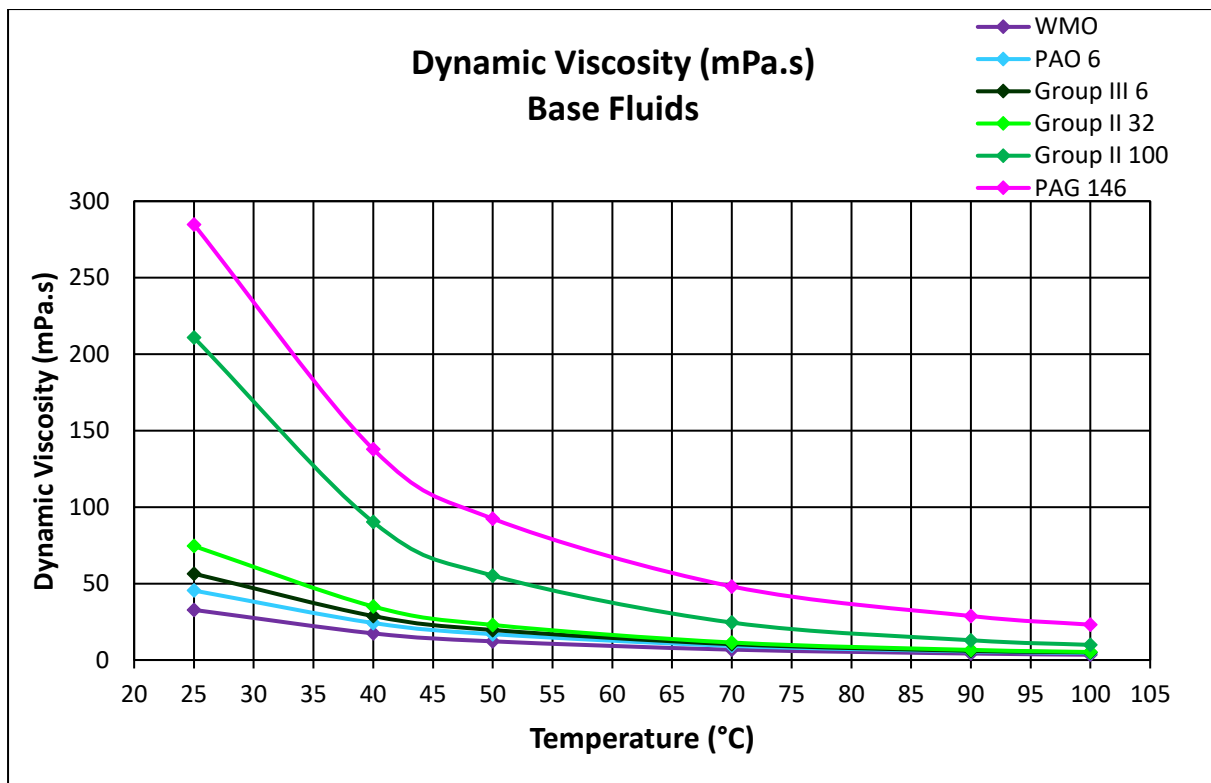


Figure 4.1: Base fluid viscosity of base oils, 25 °C to 100 °C. Measured with Stabinger viscometer, SVM 3000.

It should also be noted that **PAO 6**, **Group II 32**, and **Group III 6** all have viscosities at 50 °C that are close to one another. However, **Group III** oil's viscosity is slightly higher at lower temperatures. Furthermore, the difference between the viscosity of these 3 oils is small compared to the viscosity difference of **Group II 100** and **PAG 146**.

The base oils in Figure 4.2 are listed in order of ascending viscosity. The order in which the base oils appear in this figure will be used throughout the subsequent sections.

This order is:

1. White mineral oil; **WMO**
2. Polyalphaolefin, 6 cSt; **PAO 6**
3. Group III mineral oil, 6 cSt; **Gr III 6**
4. Group II mineral oil, ISO VG 32; **Gr II 32**
5. Group II mineral oil, ISO VG 100; **Gr II 100**
6. Polyalkylene glycol, 146; **PAG 146**

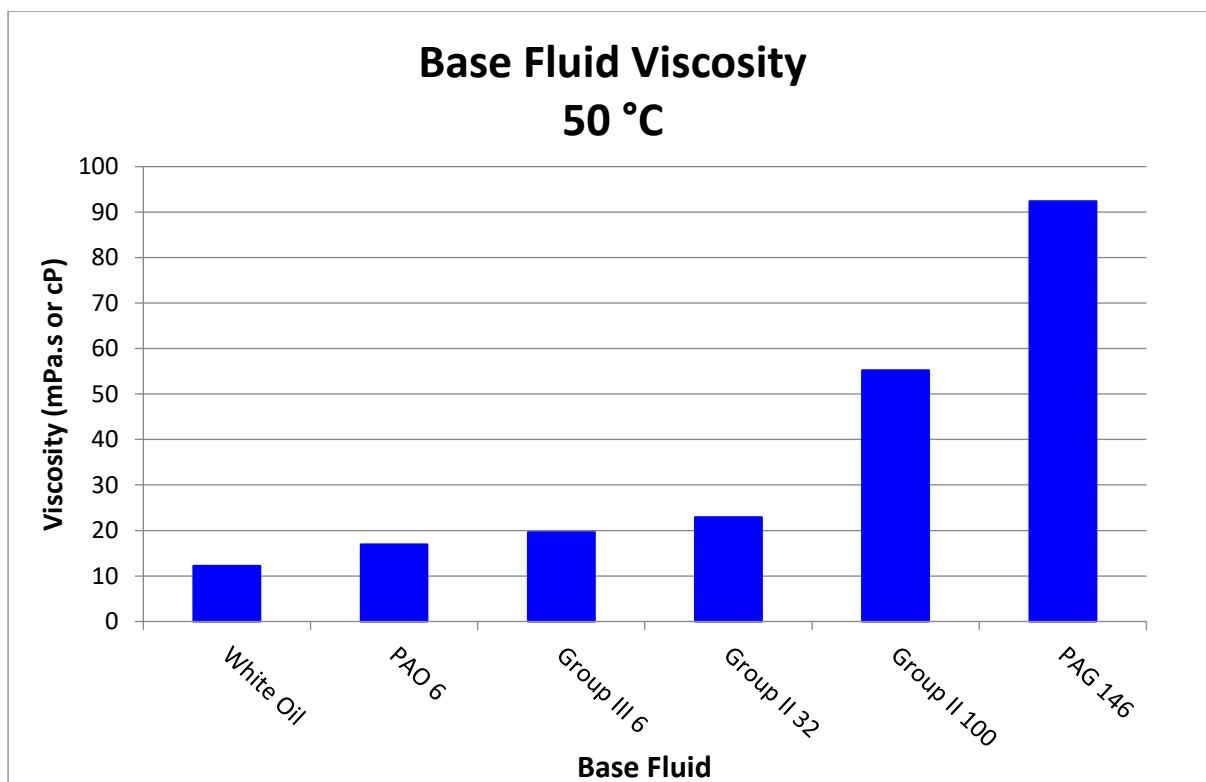


Figure 4.2: Base fluid viscosity at 50 °C. Measured with Stabinger viscometer, SVM 3000.

4.1.1.2 Viscosity Index

The viscosity index for the base oils was calculated according to ASTM D 2270-16 and are given in Figure 4.3. The order of the base oils is still in ascending order of viscosity (see section 4.1.1).

From Figure 4.3 the highly refined **Group III oil** and the **2 synthetic oils** had higher viscosity indexes compared to the mineral base oils. The **white mineral oil** is refined from a naphthenic crude oil source. However, it had a viscosity index above 100. This is due to the high degree of refinement. In general, all the base oils had viscosity indexes greater than 100. The **2 Group II mineral oils** had the lowest viscosity indexes.

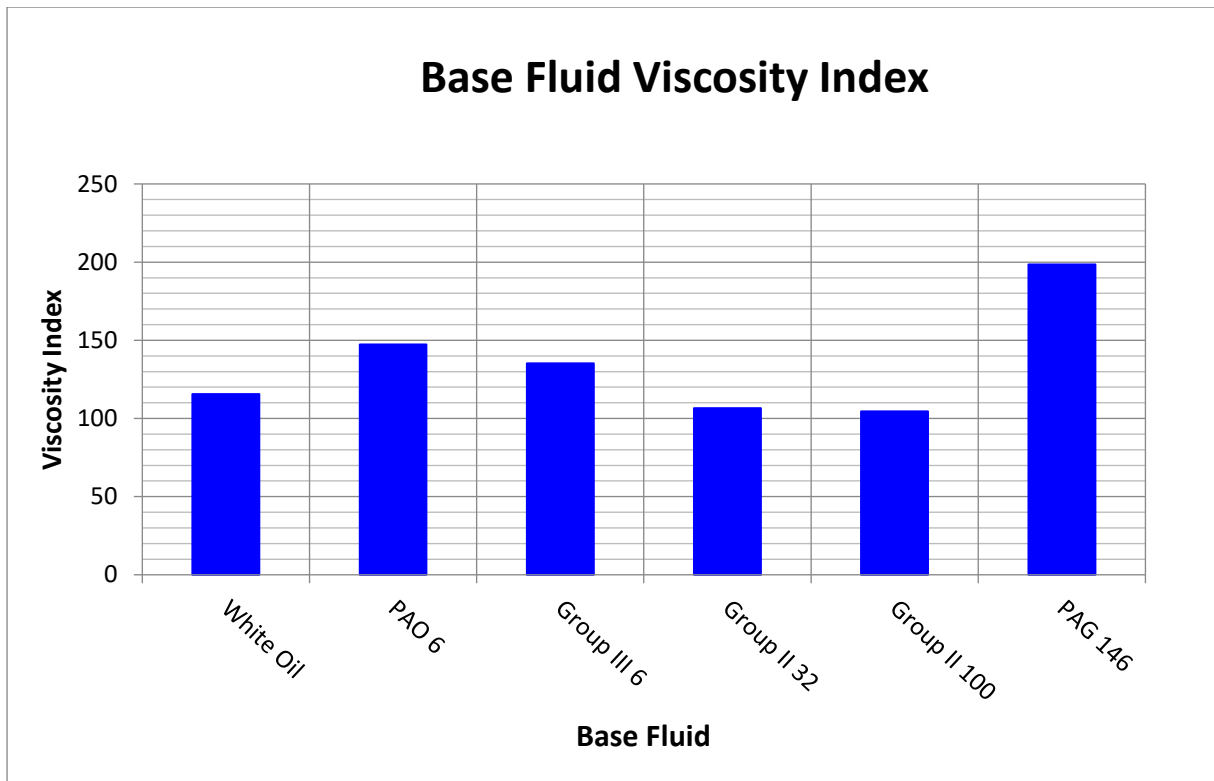


Figure 4.3: Base fluid viscosity index of base oils, calculated according to ASTM D 2270 – 16.

4.1.1.3 Lubricating Regime

The Modified Stribeck numbers (Gold et.al., 2001 & Brandão et.al., 2012) for each of the test fluids was calculated with equations 2.8 to 2.10 in section 2,7 in Chapter 2. The Stribeck numbers together with the lubricating regime is given in Table 4.1. The calculations are based on the viscosity of the base oils at 50 °C. The lubricating regime was determined under the operating load of 200 N as well as the running-in load of 50 N. The lubricating regimes for the modified Stribeck parameter (S_p) are defined as (Brandão et.al., 2012):

1. Boundary film lubrication: $S_p \leq 1 \times 10^{-9}$
2. Mixed film lubrication: $1 \times 10^{-9} \leq S_p \leq 1 \times 10^{-7}$
3. Elastohydrodynamic lubrication: $S_p \geq 1 \times 10^{-7}$

It is important to note that the motion on the SRV is oscillatory. The ball accelerates from zero to its maximum speed after which it decelerates to zero to change direction.

This occurs at a frequency of 50 Hz. 1 Oscillation therefore occurs in 0.02 seconds and 1 stroke in 0.01 seconds.

The lubricating regime was therefore determined at the average speed as well as the maximum speed. The average speed was simply calculated by dividing the stroke length (1 mm) with the time for 1 stroke to be completed. The maximum speed was determined by assuming that the maximum speed is reached in the middle of the stroke, i.e., 0.5 mm after 0.005 seconds. This was then determined by solving the equations of motion (equations 3.11 to 3.13) simultaneously.

For a load of 200 N, it was found that each base oil operates in the mixed regime when the average speed is used. Both the viscosity and the boundary lubrication properties of the oil are therefore of importance. However, since the speed is increasing and then decreasing, the lubricating regime will change. This is shown in Table 4.1 where the Stribeck parameters increase when the maximum speed is reached. It is also noticeable that the **Gr II 100** and **PAG 146** are estimated to operate in the EHL regime, where the influence of viscosity becomes even more of importance. It should also be noted that the pressure viscosity coefficient for the synthetic test fluids is lower compared to the mineral base oils.

For the running-in load of 50 N, the lubricating regime for **Gr II 100** and **PAG 146** is elastohydrodynamic for both the average and the maximum speed. The rest of the base oils all operate under mixed lubrication conditions.

The lubricating regimes are also plotted as the speed increases from zero to the maximum speed at half the stroke length (0 mm to 0.5 mm). The regimes for the running-in load are plotted in Figure 4.4 and for the operating load in Figure 4.5. In both these figures the main lubricating regime for **WMO**, **PAO 6**, **Gr III 6** and **Gr II 32** is the mixed lubricating regime. A small portion during the stroke, however, also operates in the boundary regime.

The lubricating regimes for **Gr II 100** and **PAG 146** extends from the boundary lubricating regime to the elastohydrodynamic regime, in both figures. For the operating

load, the main regime in which the system is still the mixed lubricating regime. However, during the running-in procedure, the system operates mainly in the EHL regime for these 2 fluids.

Table 4.1: Lubrication regime for base oils at the average and maximum linear speed.

Base Oil	Visc., 50°C mm ² /s	Piezo Viscosity Constants			Lubricating Regime 200 N				Lubricating Regime: Running-in 50 N			
		s	t	α	Average Speed (0.1 m/s)		Maximum Speed (0.2 m/s)		Average Speed (0.1 m/s)		Maximum Speed (0.2 m/s)	
					Sp (x10 ⁻⁸)	Regime	Sp (x10 ⁻⁸)	Regime	Sp (x10 ⁻⁸)	Regime	Sp (x10 ⁻⁸)	Regime
WMO	14.864	12.517	0.180	20.363	1.232	Mixed	2.464	Mixed	2.464	Mixed	4.928	Mixed
PAO 6	21.013	7.382	0.134	11.085	1.259	Mixed	2.517	Mixed	2.517	Mixed	5.035	Mixed
Gr III 6	23.991	9.904	0.139	15.404	1.723	Mixed	3.446	Mixed	3.446	Mixed	6.891	Mixed
Gr II 32	27.318	9.904	0.139	15.685	2.031	Mixed	4.061	Mixed	4.061	Mixed	8.123	Mixed
Gr II 100	65.184	9.904	0.139	17.700	5.194	Mixed	10.387	EHL	10.387	EHL	20.774	EHL
PAG 146	95.785	5.489	0.149	10.807	6.794	Mixed	13.588	EHL	13.359	EHL	27.176	EHL

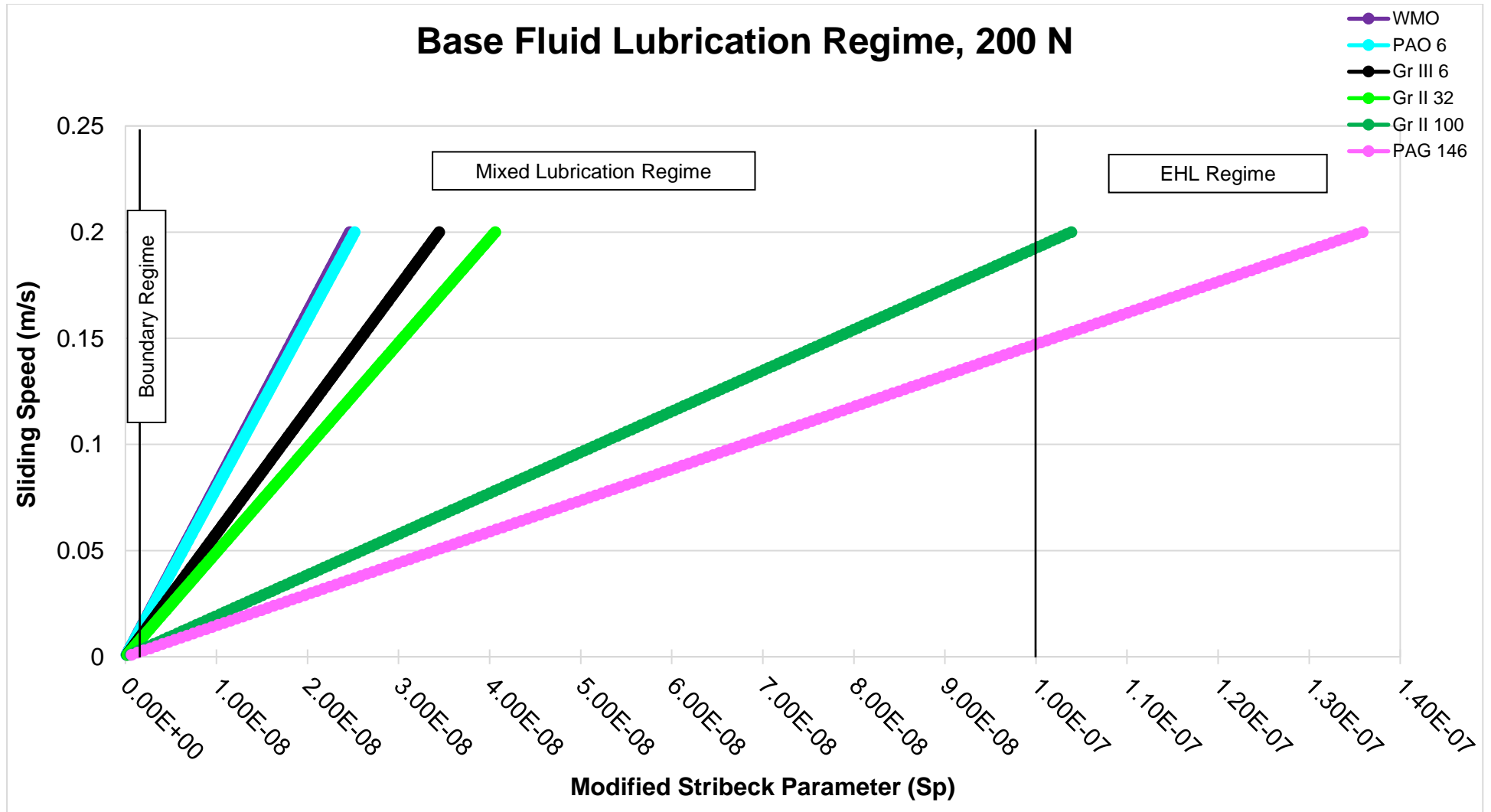


Figure 4.4: Change in lubrication regime of base fluids with sliding speed under operating load of 200 N.

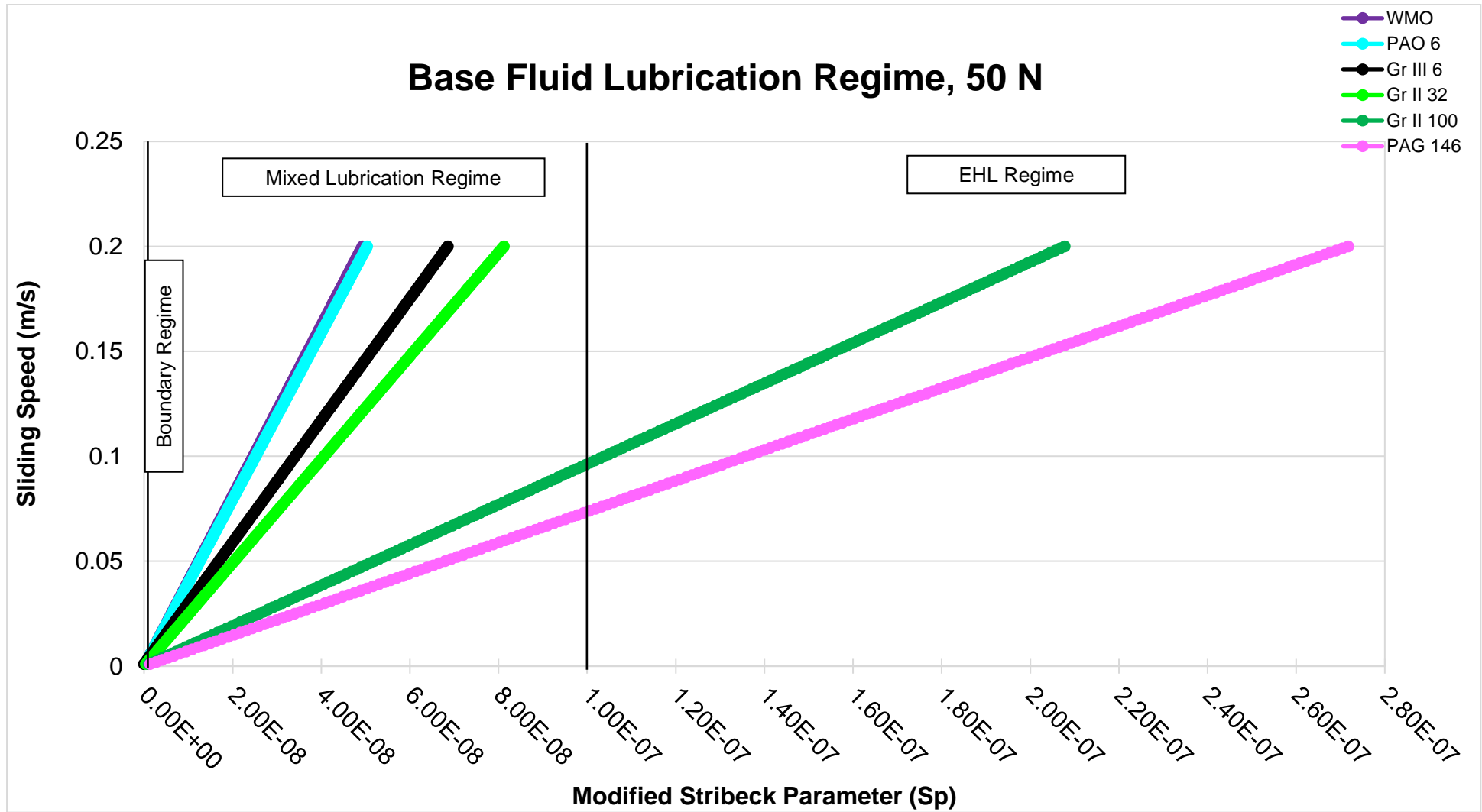


Figure 4.5: Change in lubrication regime of base fluids with sliding speed under operating load of 50 N.

The change in lubricating regime can therefore be illustrated as shown in Figure 4. 6. The lubricating begins in the boundary lubricating regime and moves into the mixed lubricating regime as the speed increases from zero to the maximum (blue arrow labelled 1). For the high viscosity base fluids, the lubricating regimes extends into the elastohydrodynamic lubricating regime. When the speed is then decreased to zero towards the end of the stroke, the lubricating regime moves back towards the boundary lubricating regime (blue arrow labelled 2).

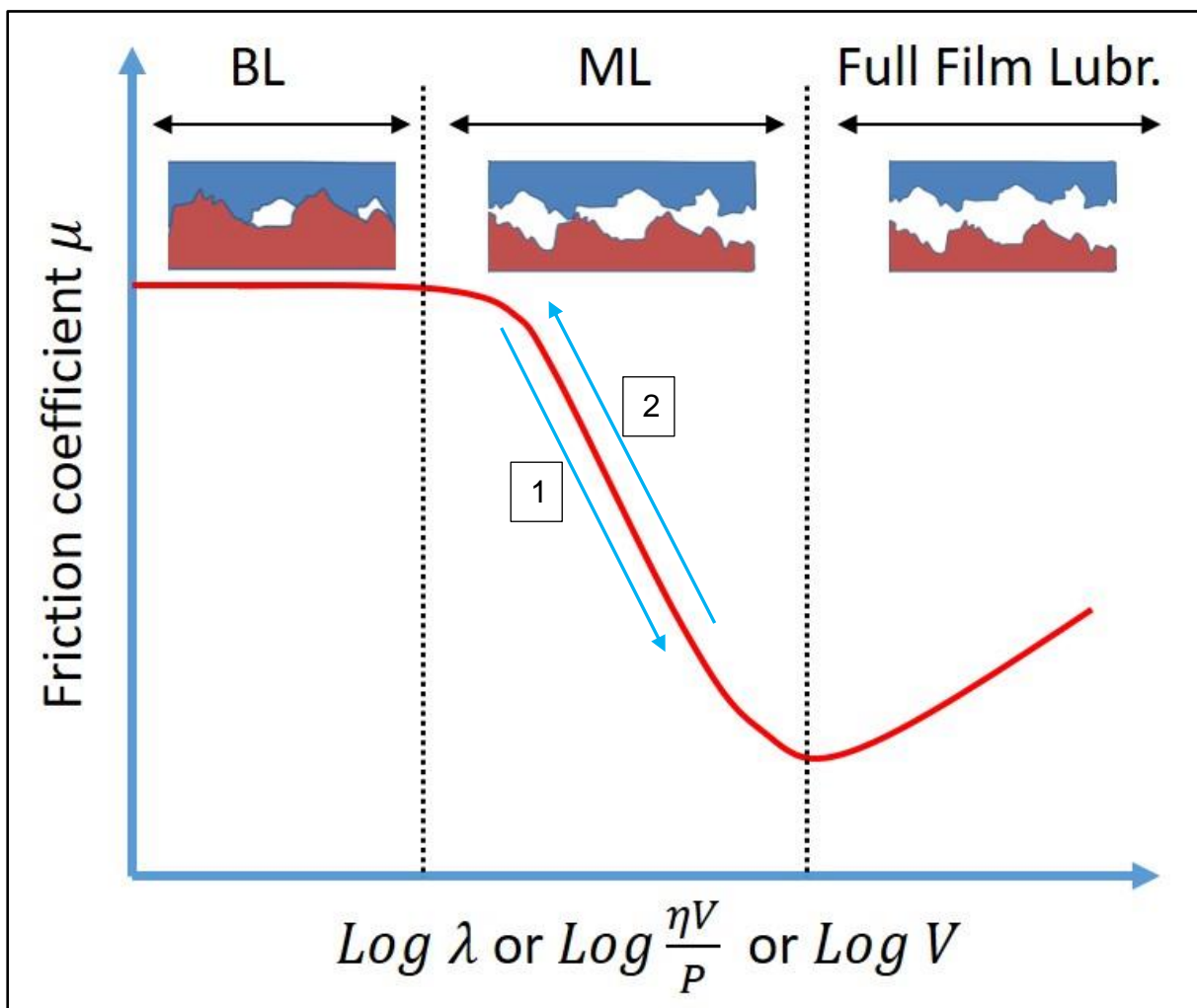


Figure 4.6: Change in lubricating regime with change in sliding speed during one stroke (Tribonet.org, 2021).

As discussed in section 2.7, the viscosity of the base oils also shifts the Stribeck curve. The elastohydrodynamic/hydrodynamic regimes are extended for higher viscosity base oils and the system will operate in these regimes at lower speeds. Also, the additive (in this case friction modifier and mild antiwear additive) will decrease the

friction coefficient in the boundary lubricating regime (refer to Figure 2.23). This is shown in Figure 4.7.

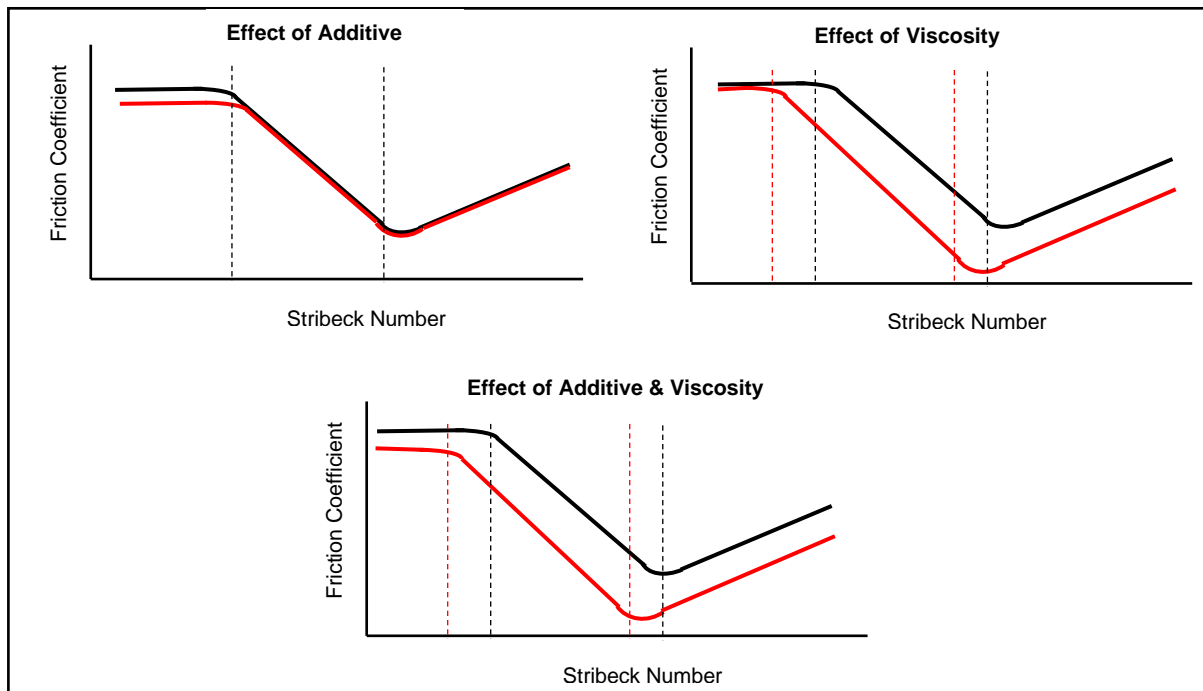


Figure 4.7: Shifts in Stribeck curve due to fluid viscosity and additive, friction modifier and anti-wear additive.

During the test, the apparent contact area of the wear surface increase as the test progress. Consequently, the load, which is constant, will be distributed over a larger area. This mean that the load between 2 contacting asperities will decrease, which also applies to all contacting asperities. This in turn will affect the film thickness, i.e., the film will become thicker and provide better protection. Asperities are also worn away during sliding and the surface becomes smoother. This is an effect of running-in of wear surfaces (Akchurin, Bosman & Lugt, 2017). This also contributes to the load being distributed over a larger area. Therefore, as the test progress the system will also move towards the elastohydrodynamic regimes and away from the boundary regime.

4.1.1.4 Base Oil Composition

As mentioned in Chapter 3, the base oils all fall in **API Group II to Group V**. The chemistry of the **2 Group II base oils** and the **Group III base oils** are predominantly paraffinic in nature and are therefore closest to one another. The main difference between **Group II and Group III** is viscosity index (Table 2.5). This means that there are fewer branched molecules in **Group III oil**. Based on the nature of the molecules in **Group II and Group III**, the polarity will be the same.

The white mineral oil is naphthenic base and therefore falls in **Group V**. The naphthenic nature of the white mineral oil contributes to its polarity. The naphthenic base oil is therefore more polar compared to the **Group II and Group III oils**. **PAO**, however, is an oligomer of known structure. **PAO** is also non-polar, and normally requires significant amounts of ester during formulation of lubricants. This is to assist with dissolving the additive packages required for its end purpose. Finally, **PAG's** water solubility depends on the ethylene oxide content. For **PAG's** to be water soluble, polarity is required. Even when the **PAG** is not water soluble, there is still some level of ethylene oxide in the molecular structure. Ultimately, this also contributes to the polarity of **PAG-based** fluids.

4.1.1.5 Amount of Additive

As stated in the experimental section two additives were used in the test fluid formulations. Additives are required for the test fluid to ensure that the lubricating film does not fail with an operating load of 200 N. The two additives used are:

- **Diethyl sebacate (DES)** – friction modifier
- **Zinc dialkyldithiodiphosphate (ZDDP)** – antiwear additive

Diethyl sebacate was added to all 6 base oils, while **ZDDP** was only added to the 2 synthetic base oils. **ZDDP** was included as a control, i.e., to verify that the effect of the base oil is measured and not only the effect of the additives. The composition of synthetic oils is much simpler, compared to mineral oils. By only adding the **ZDDP** to

the 2 synthetic oils, the number of variables that can influence results is therefore reduced.

The amount of additive blended into each of the test fluids had to comply with 2 criteria. The first was that the film must not fail for the duration of the test. The film fails when the friction coefficient exceeds a value of 0.3 or if the friction coefficient is larger than 0.2 for longer than 20 seconds (ASTM D 5707 and ASTM D 6425).

The second criterion was that the dosage level of the additive must not be too high so that the friction and wear behaviour is dominated by the additive. This enables the study of the effect of the base fluid on repeatability of the friction and wear results. In each of the samples an initial amount of 0.5 % (mass basis) of additive was added. The amount of additive was increased up to 1 % if failure occurred at 0.5 %, and thereafter by increments of 1 % until the film did not fail during the friction and wear test. The amount of additive in each of the base oils is summarised in Table 4.2.

Table 4.2: Amount of additive used during friction and wear testing.

	Base Oil	Abbreviation	Additive	Mass %
1	White Mineral Oil	WMO	Diethyl Sebacate	0.5
2	Polyalphaolefin	PAO	Diethyl Sebacate	3
3	Group III Mineral Oil	Gr III	Diethyl Sebacate	2
4	Group II Mineral Oil Low Viscosity	Gr II LV	Diethyl Sebacate	2
5	Group II Mineral Oil High Viscosity	Gr II HV	Diethyl Sebacate	2
6	Polyalkylene Glycol	PAG	Diethyl Sebacate	0.5
7	Polyalphaolefin	PAO	ZDDP	0.5
8	Polyalkylene Glycol	PAG	ZDDP	0.5

From this table, the white mineral oil required the least amount of additive (**diethyl sebacate**) to prevent film break down. **PAG 146** also only required 0.5 % (mass basis) **diethyl sebacate**. Both these fluids have a stronger polarity compared to the other base oils. This is due to the naphthenic rings in the white oil and due to the ethylene oxide monomers in the **PAG 146** polymer backbone. They would therefore also contribute to the boundary film and consequently, less additive was required.

PAO 6, however, was the least polar of all the base oils. Therefore, the highest additive level was required, i.e., 3 %. The 3 paraffinic mineral oils only required 2 % of additive.

This indicates that they are more polar than the **PAO 6**, but not to the same extent as the **white mineral oil** (naphthenic) and **PAG 146**.

4.1.2 Repeatability of Friction and Wear Results

The friction and wear results include the extent of wear, the wear surface, and the friction coefficient. Each of these will be looked at separately with the focus on repeatability. The same order in which the base oils are arranged in Table 4.1 is adhered to in the rest of this chapter. The effect of adjusting the wear scar diameter in the direction parallel to sliding will also be focused on in section 4.1.2.1. Finally, the running-in will be closely looked at in the friction coefficient results (section 4.1.2.3).

4.1.2.1 Extent of wear

The extent of wear includes the ball wear scar diameter, the ball wear volume, and the disk wear volume. The wear volume is included since the wear scar diameter does not take the effect on the extent of wear of the wear surface profile into consideration. The change in extent of wear with time is also non-linear since the wear occurs on a spherical object.

The extent of wear (wear scar diameter, ball wear scar volume and disk wear track volume) has also been included in the results. This is due to each test fluid that will produce different wear results. Even though the focus is on repeatability, the relationship between the test fluid properties and repeatability is identified through the extent of wear. This also holds for the friction coefficient, which is discussed in section 4.1.2.3.

4.1.2.1.1 Wear Scar Diameter

The average wear scar diameters with their standard deviations for the test fluids are given in Figure 4.8. The blue bars represent the wear scars that were measured, and the red bars represent the adjusted wear scar diameters (described in section 3.5.3). The wear scar diameters in Figure 4.8 are given in Appendix B.4 Table B.4.1. **Note that the viscosity of the base oils increases from left to right.**

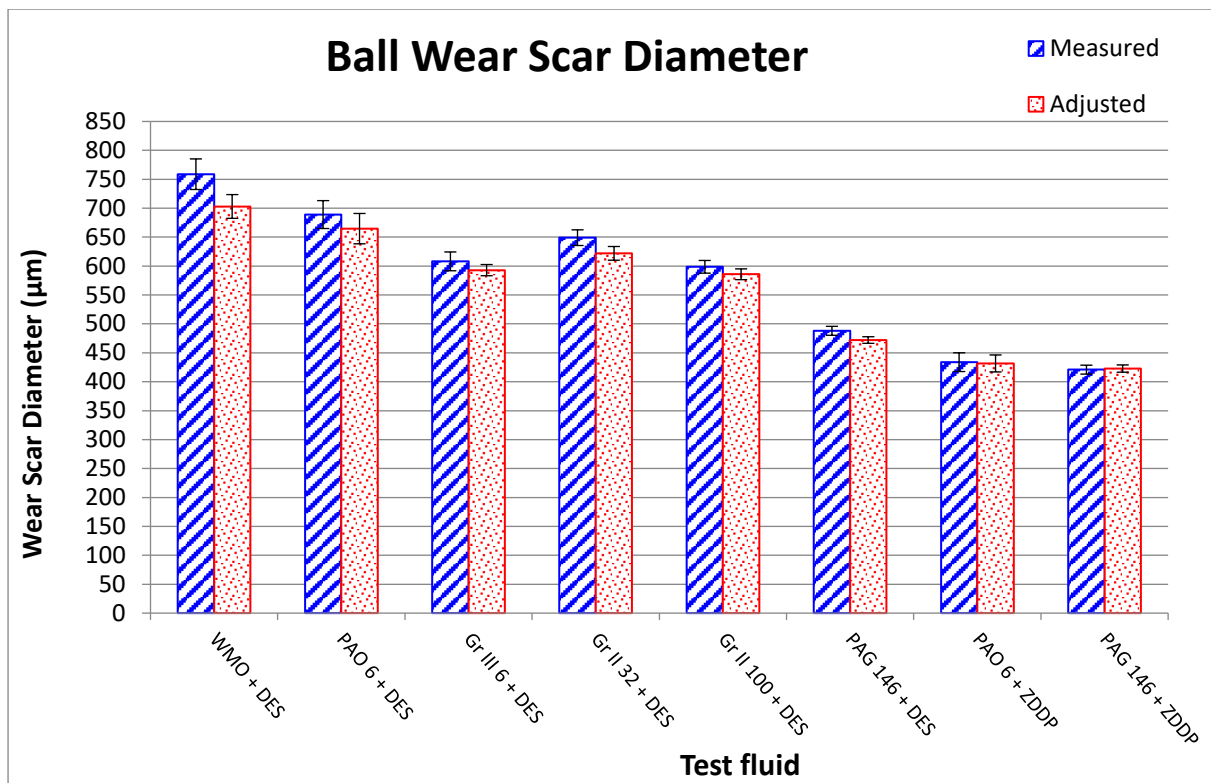


Figure 4.8: Wear scar diameters for test fluids evaluated on the SRV test rig according to ASTM D 5707 and ASTM 6425.

In Figure 4.8 it can be seen that:

1. The extent of wear decreases with an increase in the base oil viscosity. This confirms the results obtained by Zhang, et.al., 2016.
2. **PAO 6, Group III 6, and Group II 32** have small differences in viscosity compared to the other base oils. The smallest wear scar diameter, however, is obtained for **Group III mineral oil**, while **PAO 6 + 0.5 % DES** had the largest wear scar diameter.
3. When **DES** is replaced by **ZDDP** as additive, the wear scar diameter decreases considerably for **PAO 6**. However, with **ZDDP** as additive, the base oil viscosity does not affect the diameter of the wear scar when **PAO 6 + 0.5 % ZDDP** and **PAG 146 + ZDDP** are compared.
4. There was a small change in the average wear scar diameter when the diameter parallel to the sliding direction was adjusted. The most significant decrease in WSD was seen for the **WMO-based** test fluid. No change was observed for the two base oils with **ZDDP** as additive. This will be discussed in section 4.1.2.8.

The statistical standard deviation was calculated to evaluate repeatability and are given in Figure 4.9. From this figure it can be seen that:

1. Repeatability improves when the wear scar diameter decreases.
2. The standard deviation calculated for the wear scar diameter for the **Group III-based oil and Group II 32-based oil** was smaller compared to **PAO 6**. Furthermore, **Group III** had the best repeatability when the wear scar is adjusted for these 3 oils.
3. Repeatability improved for **PAO** when **ZDDP** was used as additive, but no difference was seen for the **2 PAG-based fluids**.
4. An improvement in repeatability (smaller deviation) can be observed for the test fluids when the wear scar diameter is adjusted, except for the **PAO-based fluid** with **DES** as additive. This will be discussed later.

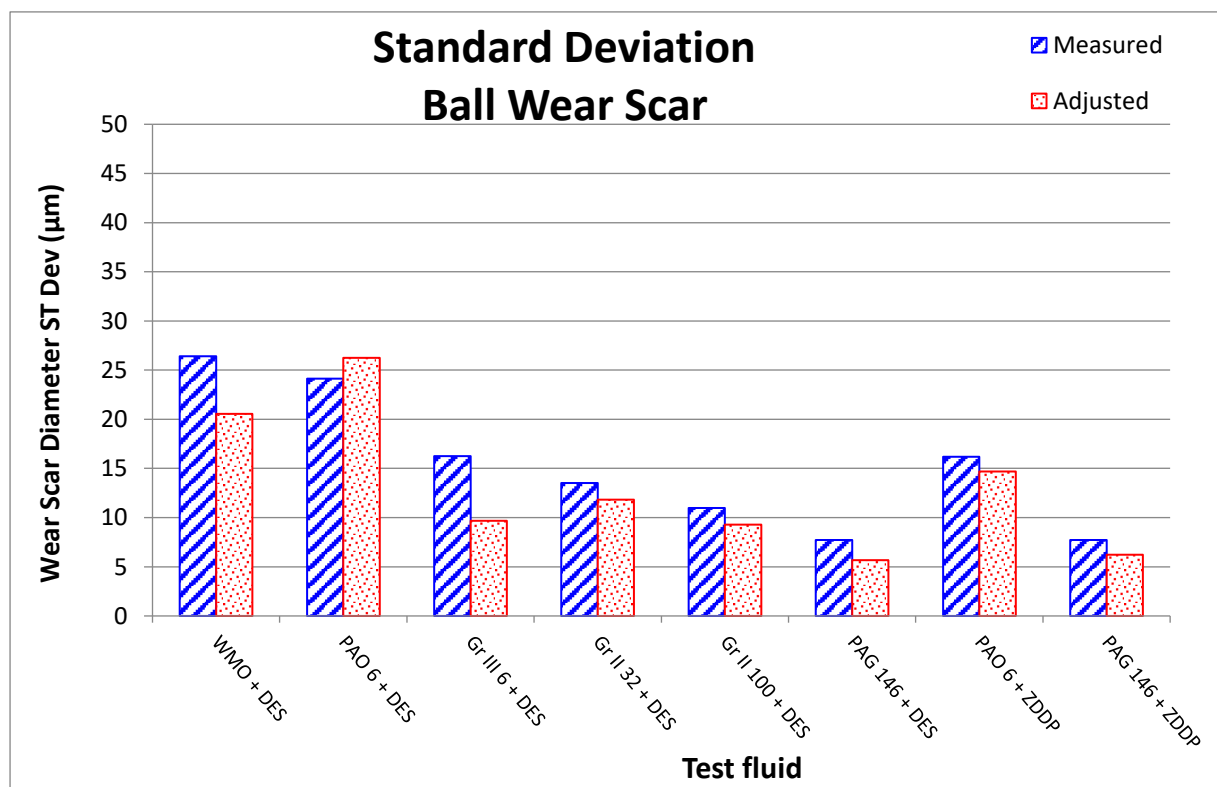


Figure 4.9: Standard deviation of wear scar diameters for test fluids evaluated on the SRV test rig (error bars in Figure 4.8).

4.1.2.1.2 Wear Volume

The wear volume was calculated for the ball wear scar volume and the disk wear track volume. The calculation was done according to ASTM D 7755-17, as described in section 3.5.2. The calculations are given in Appendix B.4.

The calculation of the wear volume for the scar is a function of the diameter parallel to the sliding direction (d_1), the diameter perpendicular to the sliding direction (d_2), and the planimetric wear area (W_q). Since d_1 was adjusted, the wear volumes calculated on the scar was also adjusted.

The wear track volume, however, is not a function of the diameter parallel to the sliding direction (adjusted wear scar diameter, d_1) and therefore no adjusted values were calculated. The wear volumes for the ball scar are given in Figure 4.10.

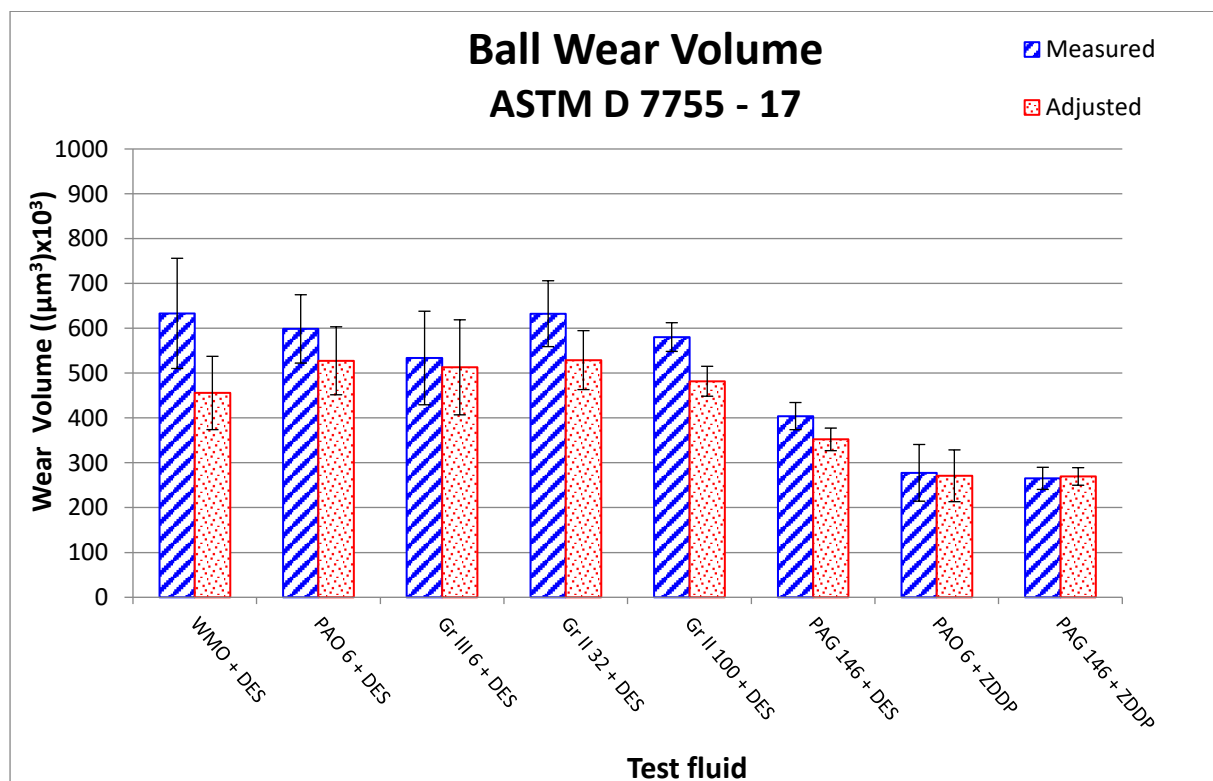


Figure 4.10: Ball wear scar volumes calculated according to ASTM D 7755 – 17 for test fluids evaluated on the SRV test rig.

From this figure it can be seen that:

1. When only the measured values are considered (blue bars), the wear volume decreases with an increase in viscosity, since there was a definite decrease in the average wear volume between **Group II 32, Group II 100, and the PAG-based oil**. However, for the lower viscosity fluids (**WMO, PAO 6, Group III 6 and Group II 32**), the trends flattens and there is no difference between the wear volumes. At 50 °C these base oils have viscosities of respectively: 12.211 mPa.s, 16.907 mPa.s, 19.630 mPa.s and 22.930 mPa.s. The same trend is seen for the adjusted wear scar diameter (red bars).
2. **Group III + 2 % DES** had a smaller average volume based on the measured values (blue bars) compared to **PAO 6 + 3 % DES and Group II 32 + 2 % DES**. The adjusted wear volume for the **white mineral oil** (red bars) had a considerable effect on the wear volume.
3. The wear volume for the test fluids with **ZDDP** was the same, irrespective of the base oil or wear scar diameter adjustment.
4. For the base oils with **DES** as additive, the adjustment of the wear scar diameter resulted in a decrease of the wear volume.

The standard deviation of the wear scar volume is plotted in Figure 4.11. From this figure it can be seen that:

1. Repeatability improves with a decrease in the wear volume (increase in viscosity) for the test fluids with **DES** as additive. The **Group III-based** test fluid, however had poorer repeatability compared to **PAO 6 + DES and Group II 32 + DES**.
2. The adjusted wear scar diameter had a small effect on repeatability for all the test fluids, except for **WMO + 0.5 % DES**. This will be discussed in section 4.1.2.8.
3. For the test fluids with **ZDDP** as additive, a significant difference in repeatability can be seen based on the base oil viscosity. Here the higher viscosity fluid (**PAG**) had much better repeatability compared to the lower viscosity fluid (**PAO 6**). Furthermore, **ZDDP** also improved repeatability for both fluids.

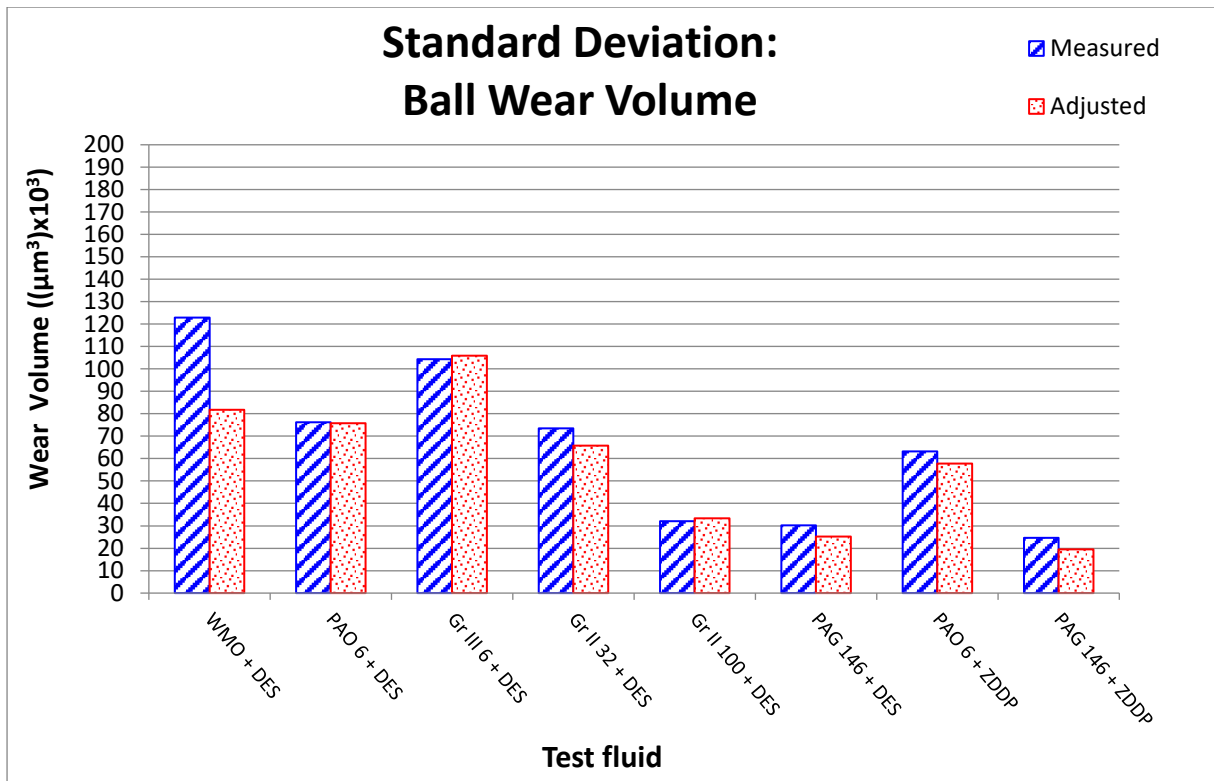


Figure 4.11: Standard deviation calculated for wear scar volumes for test fluids evaluated on the SRV test rig (error bars in Figure 4.10).

The average values of the wear volumes on the disk are plotted in Figure 4.12. As mentioned before, no adjusted values were calculated for the wear tracks. From this figure it can be seen that:

1. The wear volume decreases when the viscosity increases and when **DES** is replaced with **ZDDP** as additive.
2. As was found for the wear scar diameter, **Gr III mineral oil** had a lower wear volume compared to the trend.
3. The wear volumes continued to increase with a decrease in viscosity, even though the differences were slight between **Group II 32, Group III 6 and PAO 6**. **WMO** also had the highest wear volume This is the opposite of the trend observed for the wear volume on the ball. For the ball, no further increase in wear volume was observed for the low viscosity fluids.

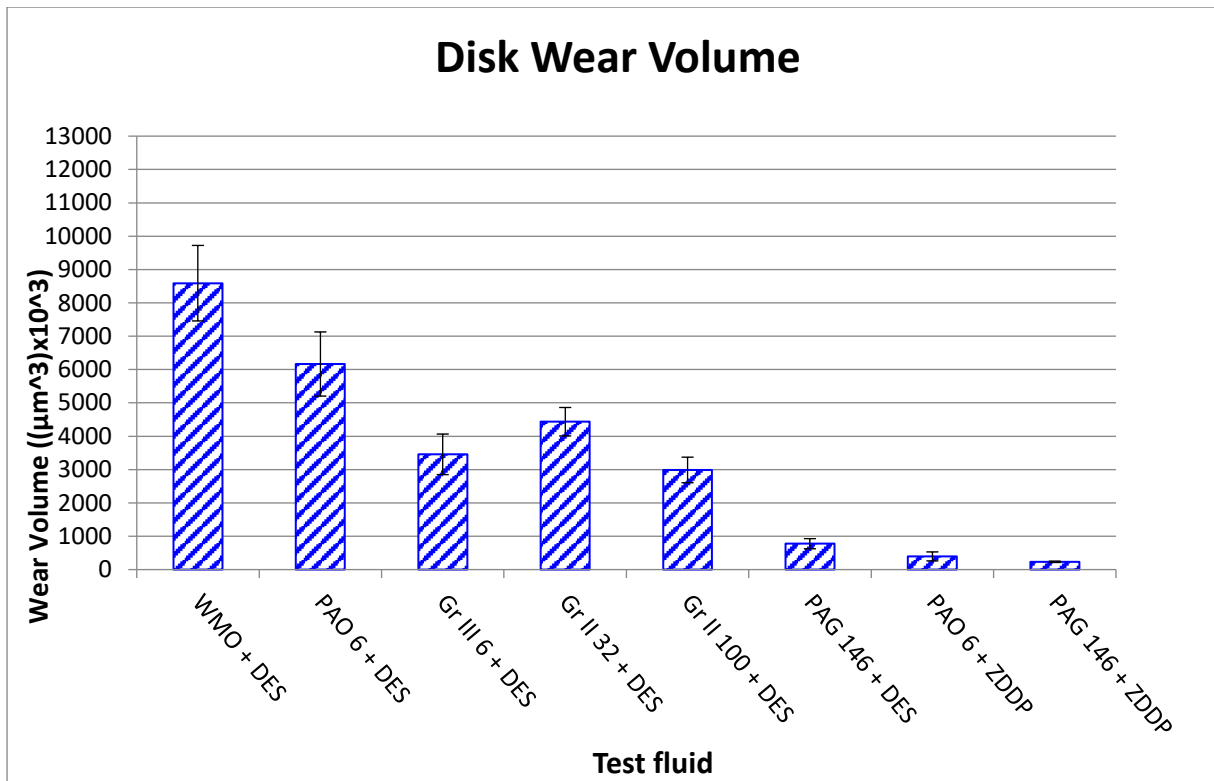


Figure 4.12: Wear track volumes calculated according to ASTM D 7755 – 17 for test fluids evaluated on the SRV test rig.

The standard deviation for the wear volumes in Figure 4.12 is plotted in Figure 4.13. In this figure it can be seen that:

1. The standard deviation decreases when the wear volume decreases.
2. A significant difference can be seen between the two **PAG-based** test fluids. Repeatability for the **PAG 146 + ZDDP** was exceptionally good and performed much better than the **PAG 146 + DES** in terms of repeatability. Only a small difference was observed for repeatability on the ball scar wear volume.
3. Repeatability for the **PAO + 0.5 % ZDDP** was also exceptionally good.
4. No deviations from the trend were observed for the wear volume on the disk. This is also different compared to the wear volume and wear scar diameter on the ball, where deviations from the trends were observed. This will be discussed in section 4.1.2.6.

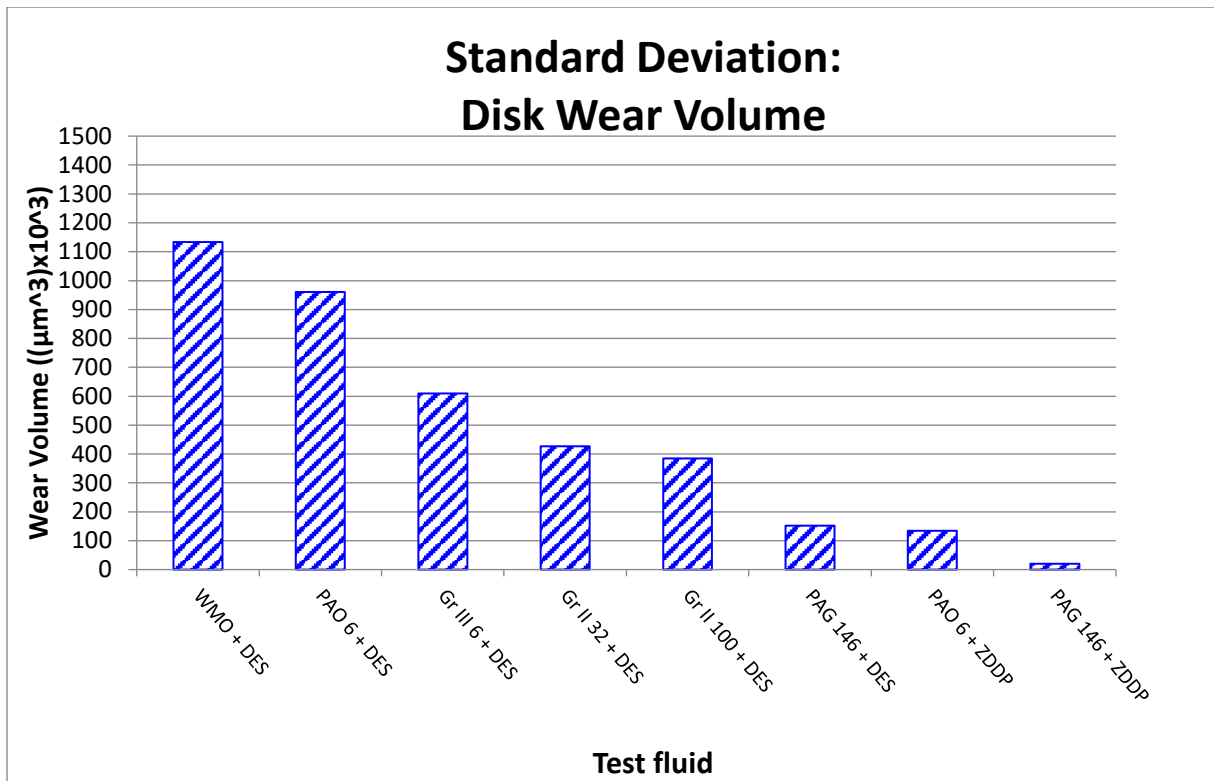


Figure 4.13: Standard deviation calculated for wear track volumes for test fluids evaluated on the SRV test rig (error bars in Figure 4.12).

Up to this point, **Group III 6-based test fluid** performed well in terms of repeatability for the wear scar diameter but showed poor repeatability for the ball wear scar volume. The wear volumes in Figure 4.10 and Figure 4.12 are calculated with the aid of 2 wear parameters (equations 3.3 to 3.6): the wear scar profile radius and the planimetric wear area. The latter is determined on the disk. Therefore, to include the effect of these parameters on repeatability, the ball wear scar profile radius, the disk wear track profile radius and the planimetric wear area on the disk are given in Figures 4.14, 4.16 and 4.18 respectively. The standard deviation for each of the results represented in these figures is also plotted in Figures 4.15, 4.17 and 4.19. From these Figures:

1. The wear surface profile radius (Figures 4.14 and 4.16) increases with a decrease in wear. This means that the wear surface is flatter when the extent of wear is smaller.
2. The profile radius for **Group III 6 + 2% DES** is flatter compared to **Group II 32 + 2% DES**.
3. The planimetric wear area tends to decrease for a decrease in wear (Figure 4.18). However, the planimetric wear area for **Group III 6 + 2% DES** is smaller than for

Group II 32 + 2% DES. Based on the trend, it would be expected that the **Group III 6-based fluid** would have a larger planimetric wear area.

4. The standard deviations of the wear track profiles increase as the profile radii increase (Figures 4.15 and 4.17). **PAO 6 + 0.5% ZDDP** had by far the worst repeatability. **Group III 6 + 2% DES** also had poorer repeatability than **Group II 32 + 2% DES**.
5. The standard deviation for the planimetric wear area decreases as the extent of wear decrease (Figure 4.19).

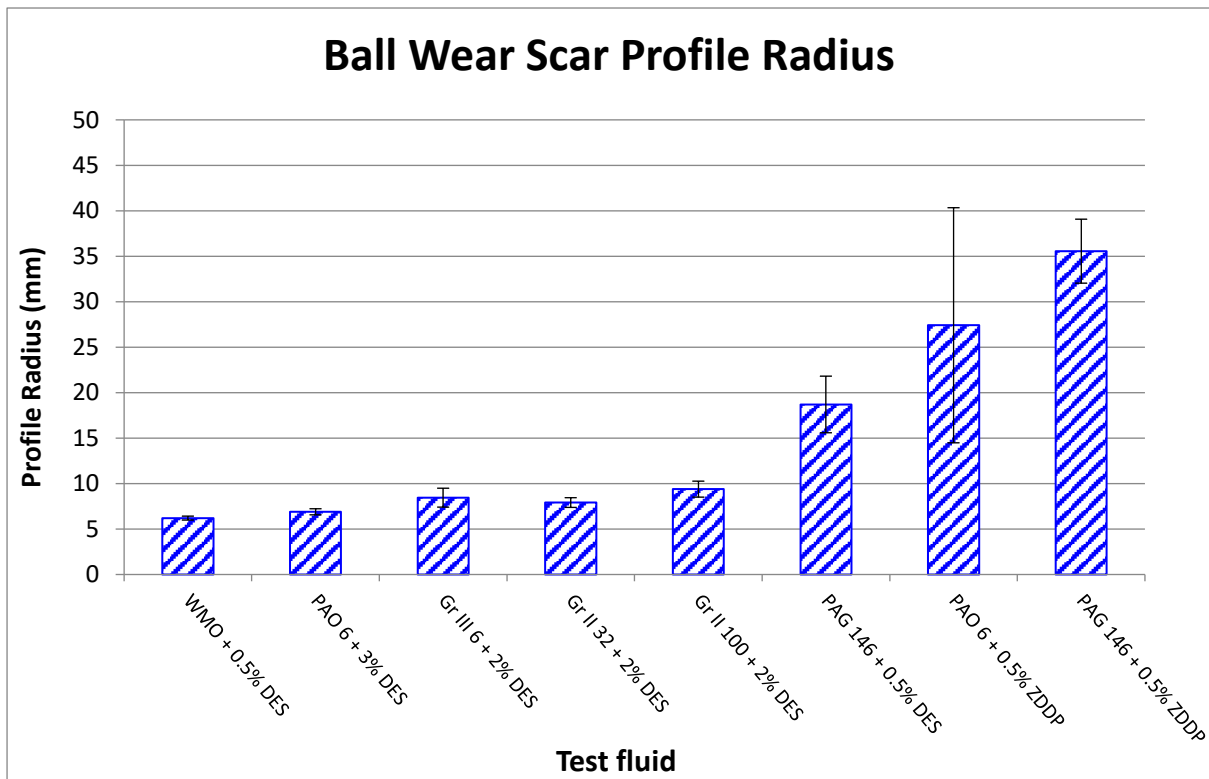


Figure 4.14: Ball wear scar profile radius.

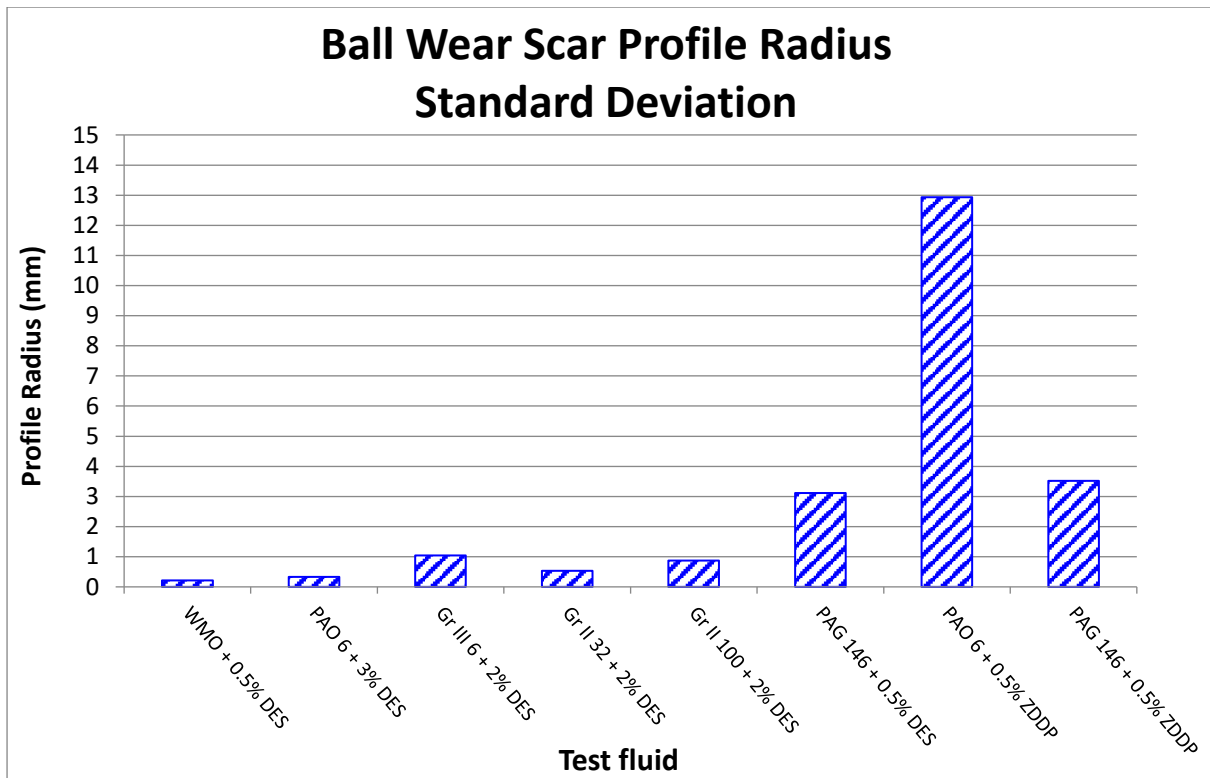


Figure 4.15: Standard deviation ball wear scar profile radius (error bars Figure 4.14).

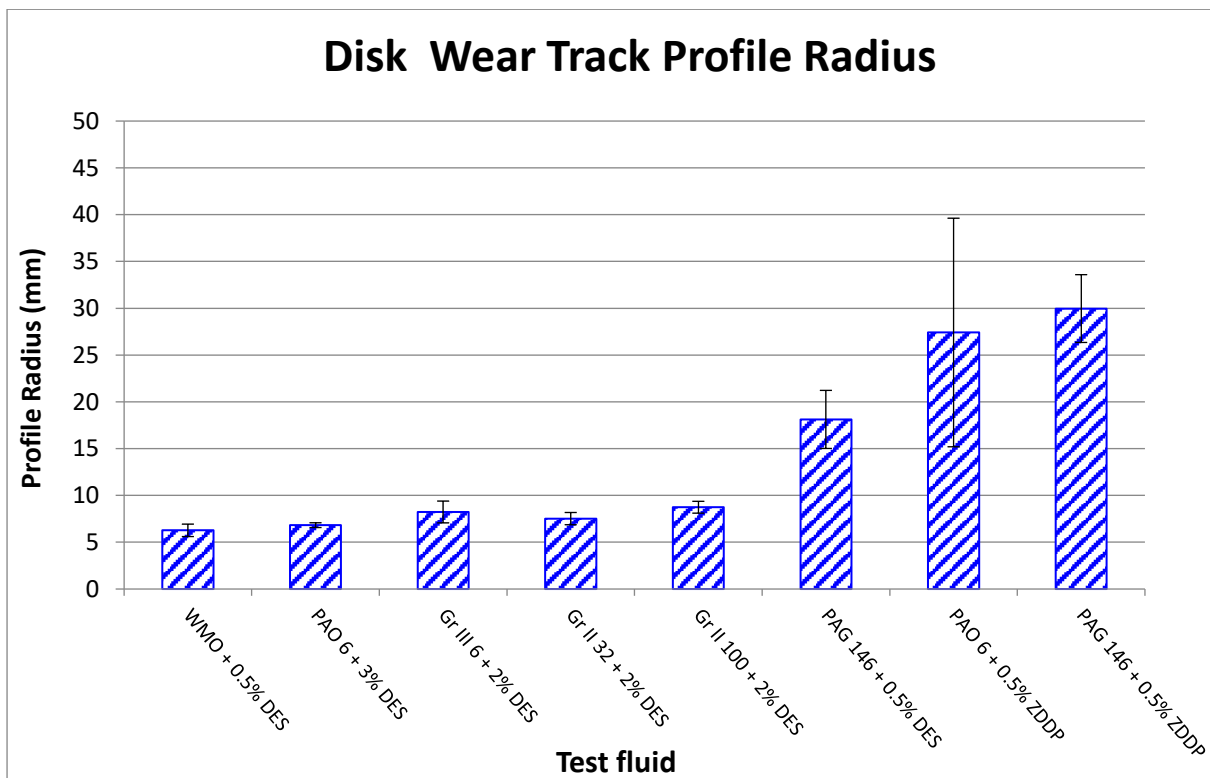


Figure 4.16: Disk wear track profile radius.

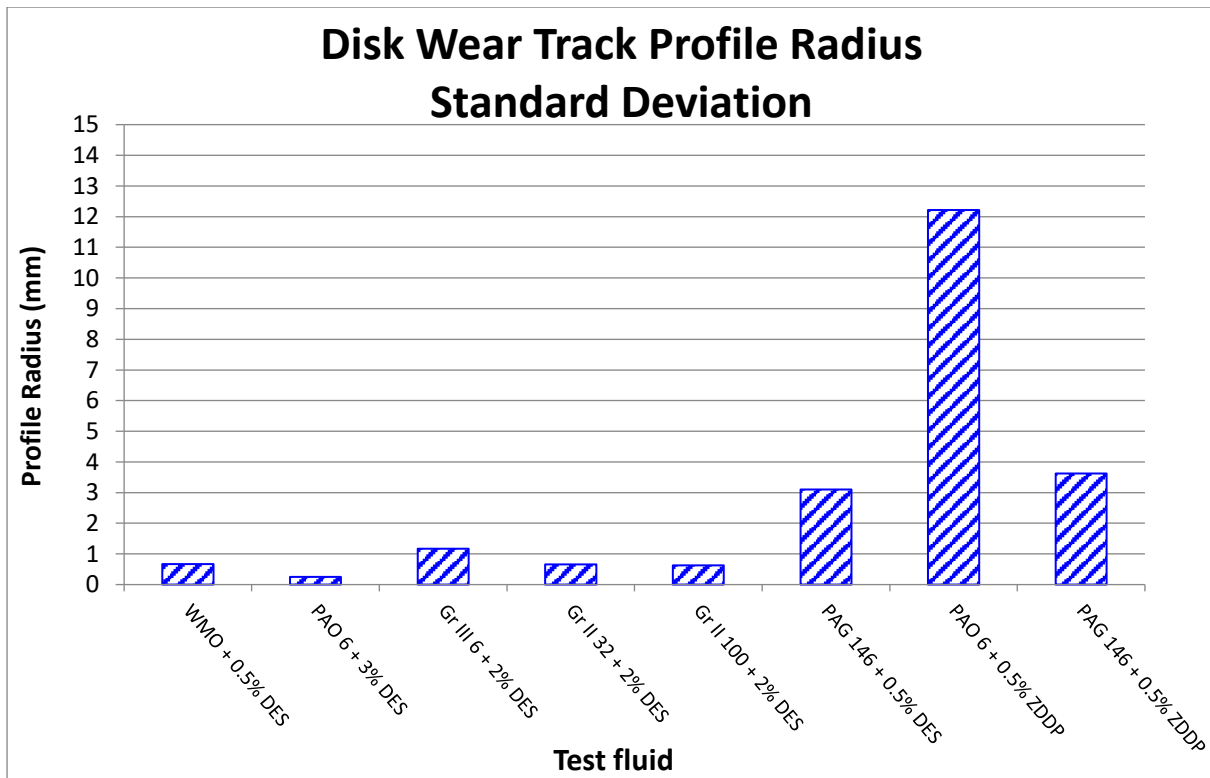


Figure 4.17: Standard deviation disk wear track profile radius (error bars Figure 4.16).

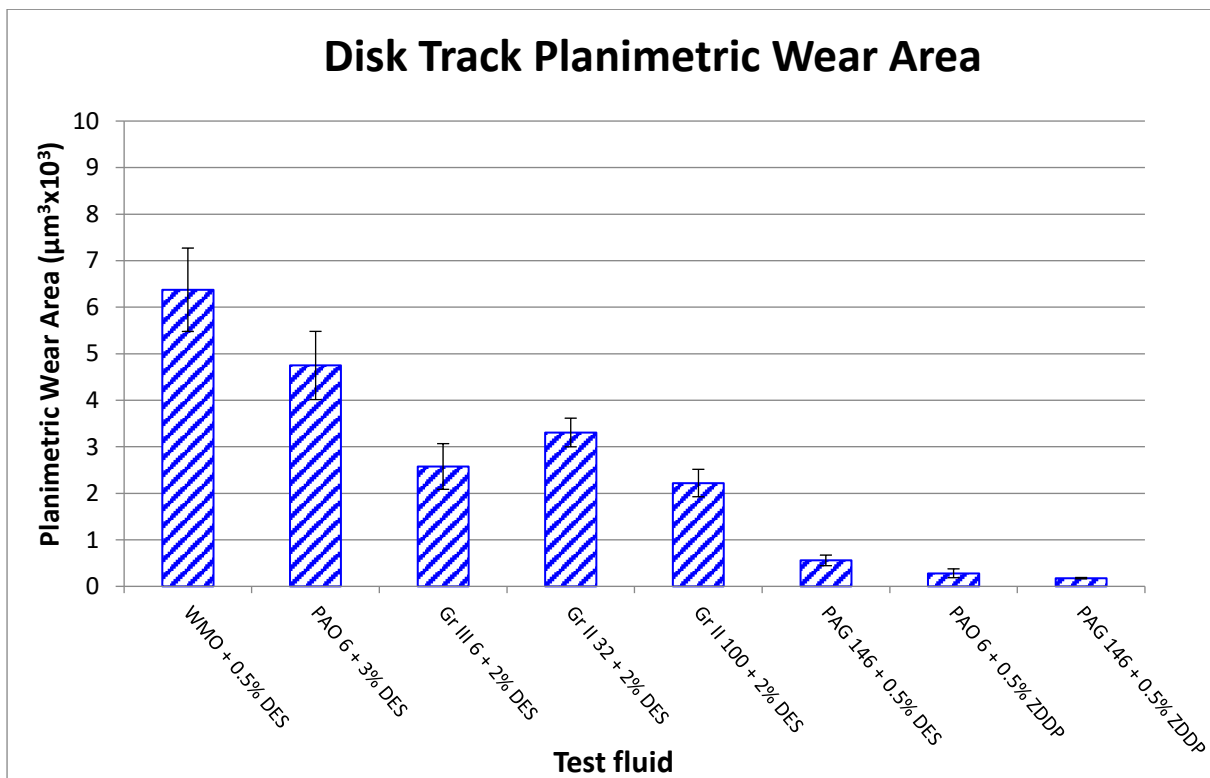


Figure 4.18: Disk planimetric wear area.

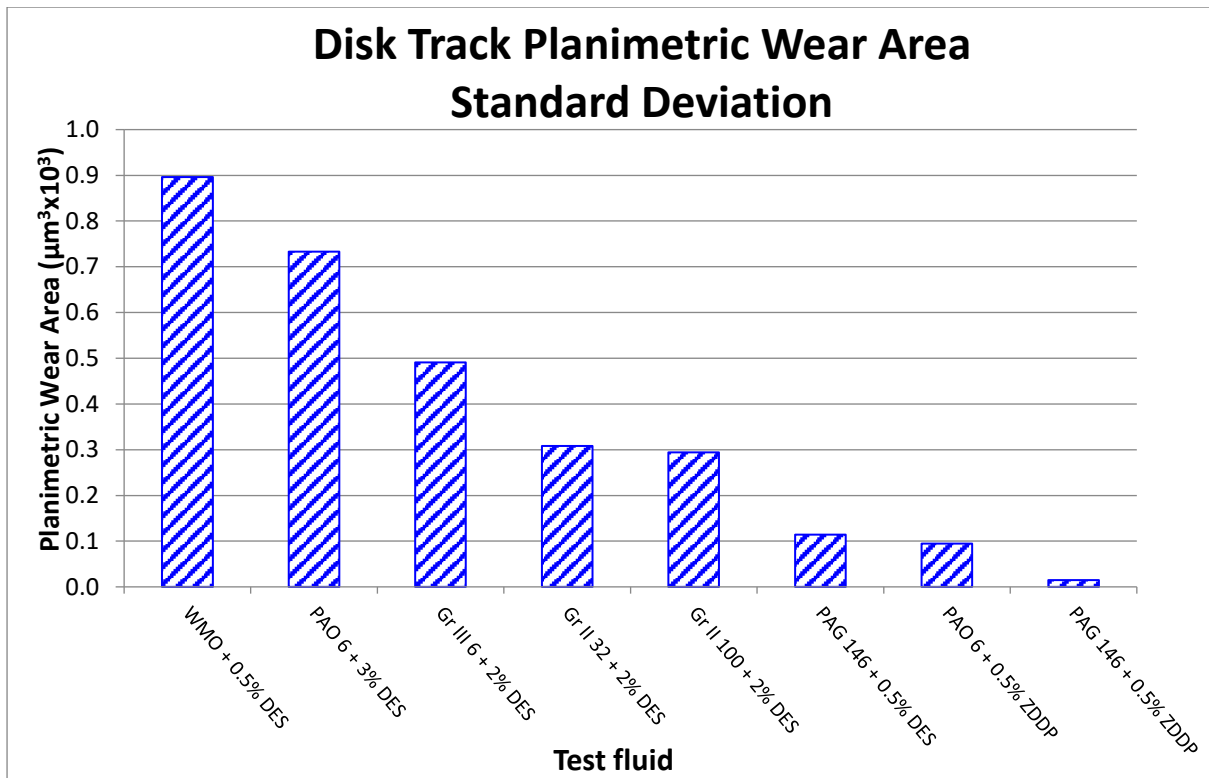


Figure 4.19: Standard deviation disk planimetric wear area (error bars Figure 4.18).

Extent of wear Summary

From the extent of wear results, it was seen that:

1. *Repeatability improves with increase in base oil viscosity:*

The trend for the wear scar diameter and the wear track volume is that wear decreases with an increase in viscosity. For the wear scar volume, the wear volume only decreases when there are significant differences in the viscosity. For lower viscosity base oils, the extent of wear is unaffected by the base oil viscosity. Repeatability improved with an increase in viscosity. This will be discussed in section 4.1.2.4.

2. **ZDDP** *improves repeatability, while viscosity is the main property of the base oil that affects the extent of wear on the disk:*

For the ball wear scar, when **DES** was replaced with **ZDDP** the wear scar diameter and wear scar volume decreased. However, when the 2 fluids with **ZDDP** as additive are compared, no difference in the extent of wear was observed and the viscosity of the base oil did not play a role. For the wear track volume however, the base oil did affect the extent of wear for the fluids with

ZDDP as additive. This was due to the **PAG-based fluid** that had a smaller wear track volume compared to the **PAO-based fluid**.

Repeatability of the extent of wear improves for the **PAO-based test fluid**. For the **PAG-based oils**, only repeatability of wear track volume showed a significant improvement with **ZDDP** as additive. A small improvement is seen for the wear scar volume and no effect is seen for the scar diameter.

3. ***Group III mineral oil deviates from the trend:***

The **Group III mineral oil** had smaller amounts of wear for the wear scar diameter, wear scar volume and the wear track volume compared to the trend. Poor repeatability for the ball wear scar volume was obtained due to variations of the planimetric wear area.

4. ***Base oil composition affects repeatability.***

For the deviation of the wear scar volume, the **PAO + 3 % DES** fluid deviated from the trend for the measured wear scar diameters as well as the adjusted values. The **Group III + 2 % DES** had poorer repeatability for the wear scar volume than expected.

5. ***Wear scar adjustment only had a significant effect on white mineral oil:***

For the test fluids with **DES** as additive a small decrease in the extent of wear scar diameter was observed when the diameter parallel to the sliding direction was adjusted. A more significant decrease was seen for the wear scar volume for the **WMO-based fluid**. The white mineral oil-based fluid also showed improvement in repeatability when the wear scar diameter is adjusted. No effect on the extent of wear was observed for the 2 fluids with **ZDDP** as additive.

A final point to add to this section is to compare repeatability of the wear scar diameters according to the criteria described in the ASTM test methods (ASTM D5707-16 and ASTM D 6425-17). This criterion evaluates repeatability on the difference between the wear scar diameters between 2 consecutive runs. The difference can only exceed a value of 70 μm for 1 case in 20. The wear scar diameters for all the test fluids are given in Table 4.3.

In this table, the values in brackets indicate the difference in the wear scar diameter from the previous run. None of the consecutive wear scars exceeded 70 μm and are

within the limit described in the ASTM test methods. However, discerning between the test fluids in terms of repeatability it is quite difficult when this criterion is used.

Table 4.3: Differences between consecutive wear scar diameters (μm) for test fluids evaluated on the SRV test rig.

Run	WMO	PAO	Gr III	Gr II LV	Gr II HV	PAG	PAO	PAG
	0.5 % DES	3 % DES	2 % DES	2 % DES	2 % DES	0.5 % DES	0.5 % ZDDP	0.5 % ZDDP
1	705	623	576	618	578	479	432	426
2	738 (33)	656 (33)	600 (26)	625 (7)	577 (1)	465 (14)	456 (24)	432 (6)
3	690 (48)	677 (21)	596 (4)	635 (10)	597 (10)	469 (4)	421 (33)	422 (10)
4	696 (6)	676 (1)	598 (2)	604 (31)	595 (2)	472 (3)	419 (4)	419 (3)
5	687 (9)	691 (15)	594 (4)	628 (24)	583 (12)	477 (5)	427 (8)	416 (3)

4.1.2.2 Wear Surface

Repeatability of the wear surfaces includes the wear surface on the ball (scar) and the wear surface on the disk (track). The focus is on the appearance of the wear surfaces, the shape of the wear surfaces and the profile of the wear surfaces.

4.1.2.2.1 Surface Appearance and Shape of the Wear Surfaces

Table 4.4.1 to Table 4.4.8 contains photographs of the wear scars and wear tracks for all the repeat runs for all 8 test fluids. This table also contains black and white images for the wear scars. The black and white images were obtained by processing the wear scar images with the GIMP 2.10.6 image manipulation program. The black and white images assisted with the comparison of the wear shapes. Repeatability of the wear surfaces is summarised in Table 4.5. The 3-dimensional images for all the wear surfaces are given in Appendix B.2.

In these tables, the following shape deviations are compared:

- 1. Severity of wear*

This focus on the appearance of the wear surface. Properties of the surface include plough marks and the formation or absence of a tribofilm. The tribofilm is a black deposit on the wear scars and tracks.

- 2. Deviation of the surface appearance*

Deviations between repeat runs are evaluated based on the distribution of the tribofilm and notable surface features.

- 3. Boundary parallel to the sliding direction: wear scars*

This compares the boundary parallel to the sliding direction. The degree to which this boundary is exceeded by plough marks and consequently how well this boundary is defined is of importance. This is important for the accuracy of the wear scar diameter and the wear volume. An example of how the boundary is exceeded by plough marks is given in Figure 4.20.

4. Shape of the wear scars

Here the shape of the outline of the wear scars is compared. This does not include the deviations on the edges (see 5 below). It will only be indicated in Table 4.5 which repeat runs had similar shapes and which repeat runs had different shapes.

5. Deviation of the edges

This compares the deviation of the length of the edges with the rest of the wear scar in the direction parallel to the sliding direction (left side and right side of the wear scar). This is indicated in Figure 4.20.

6. Ratio of the diameters

The ratio of the diameter parallel to the sliding direction (d_1) and the diameter perpendicular to the sliding direction (d_2) is evaluated. This indicates the deviation of the wear scar from a circular shape.

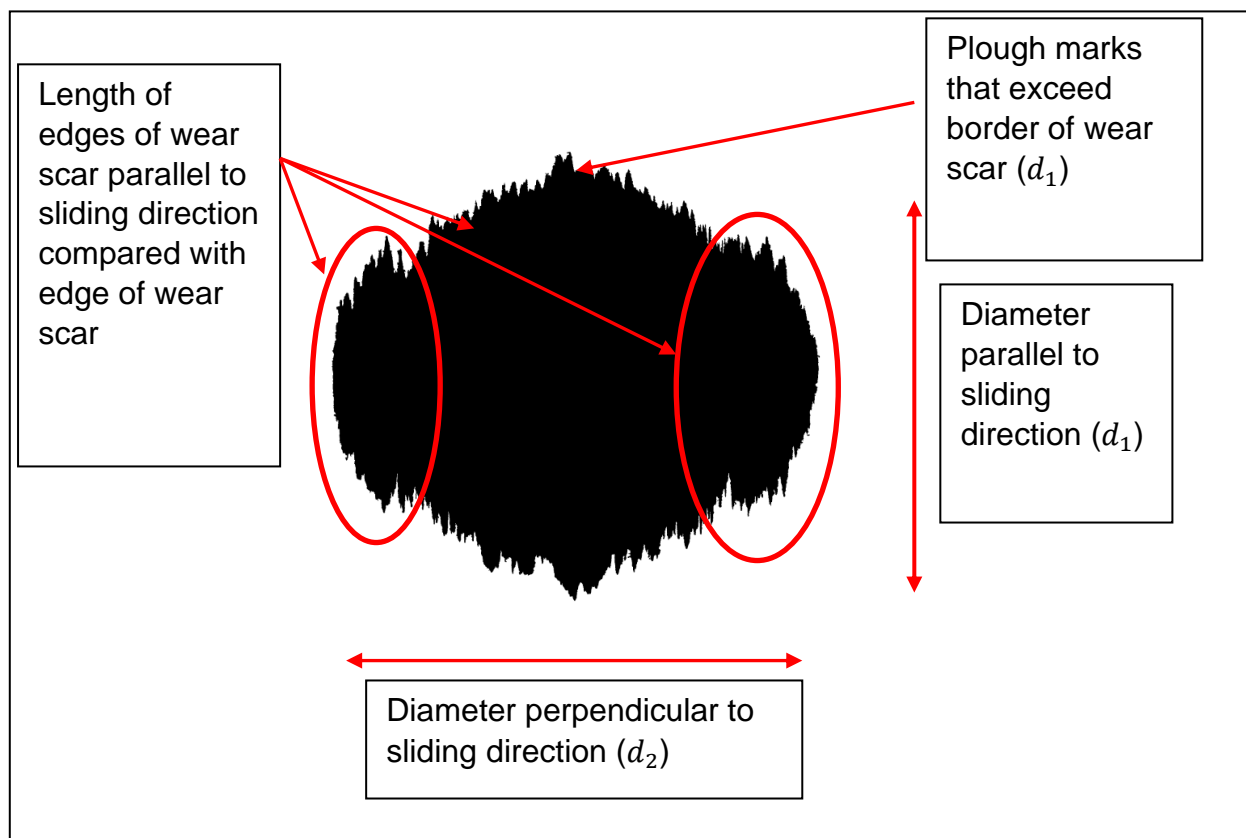


Figure 4.20: Shape deviations of wear scars that are compared for test fluids evaluated on the SRV test rig.

Table 4.4.1: Wear surface images for **white mineral oil (WMO) with 0.5 % DES.**

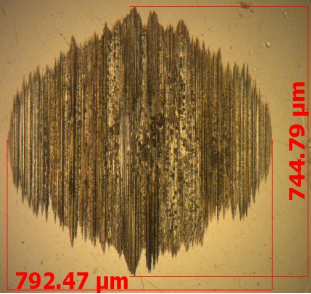
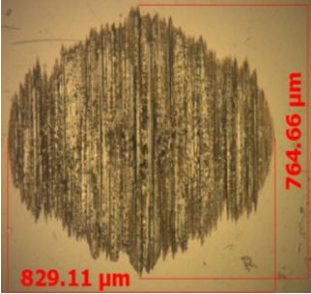
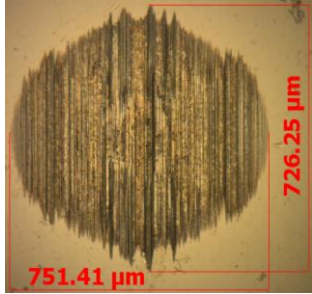
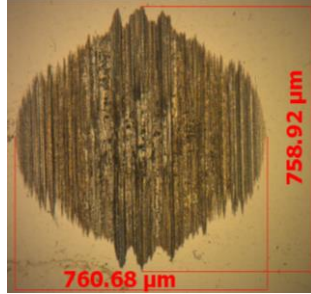
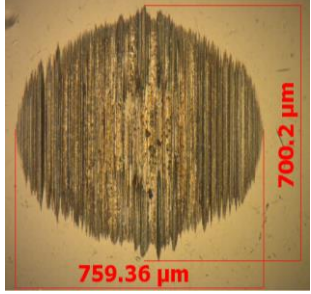

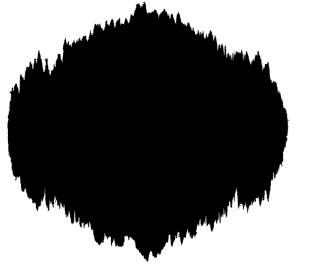




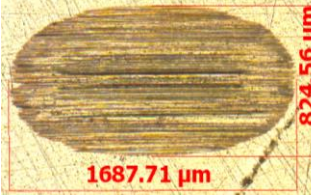
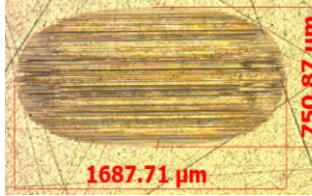
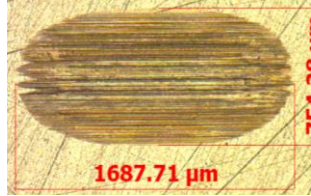
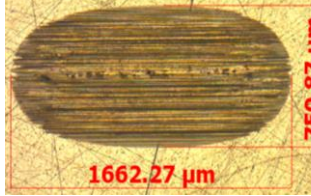
	Run 1	Run 2	Run 3	Run 4	Run 5
Wear Scars	 792.47 μm (width), 744.79 μm (height)	 829.11 μm (width), 764.66 μm (height)	 751.41 μm (width), 726.25 μm (height)	 760.68 μm (width), 758.92 μm (height)	 759.36 μm (width), 700.2 μm (height)
Wear Scars: Black & White					
Wear Tracks	 1669.29 μm (width), 783.33 μm (height)	 1687.71 μm (width), 824.56 μm (height)	 1687.71 μm (width), 750.87 μm (height)	 1687.71 μm (width), 754.38 μm (height)	 1662.27 μm (width), 750.87 μm (height)

Table 4.4.2: Wear surface images for polyalphaolefin (PAO) with 3 % DES.

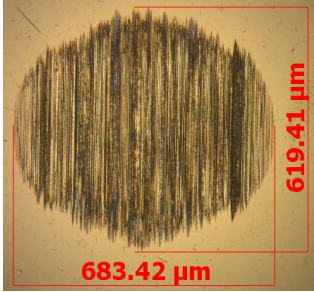
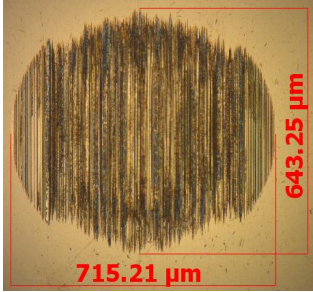
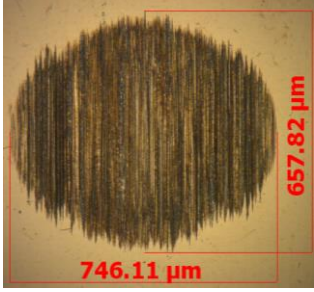
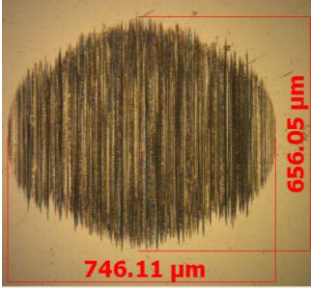
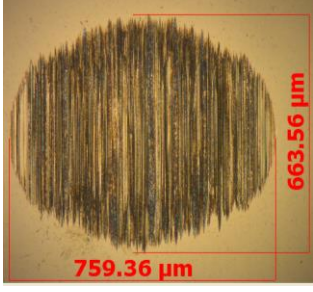

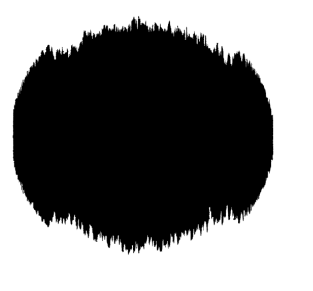
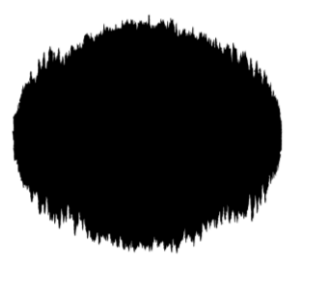
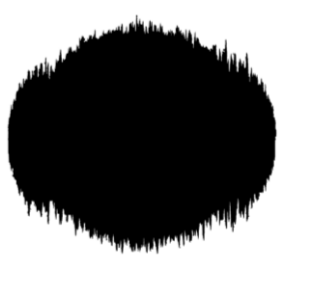
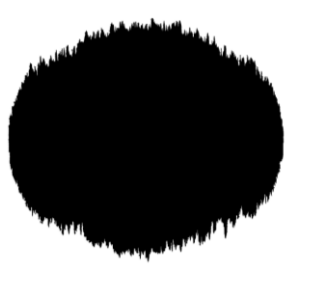
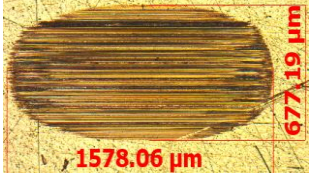
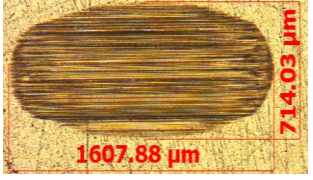
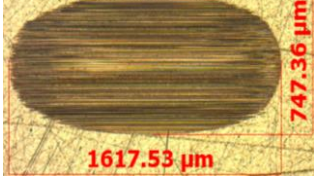
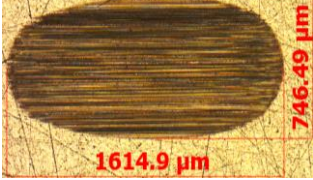
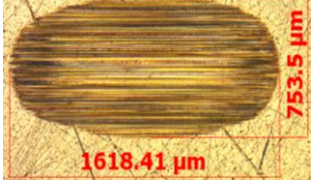
	Run 1	Run 2	Run 3	Run 4	Run 5
Wear Scars					
Wear Scars: Black & White					
Wear Tracks					

Table 4.4.3: Wear surface images for **Group III mineral oil (Gr III) with 2 % DES.**

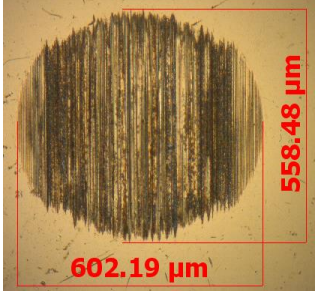
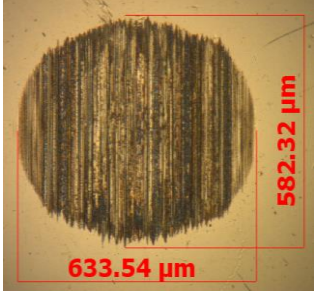
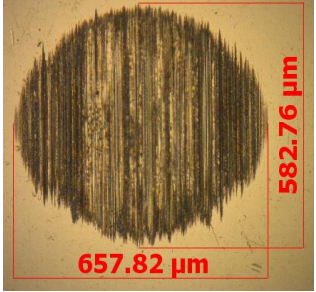
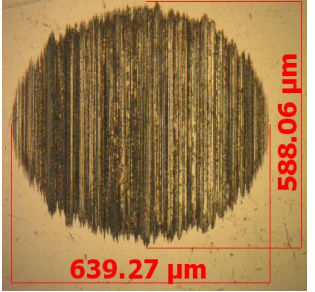
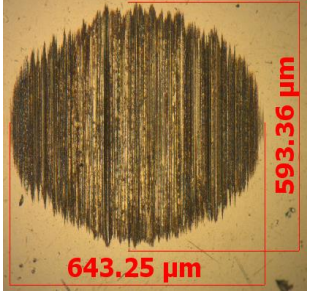
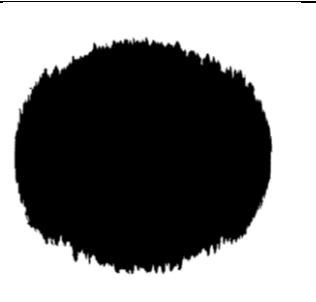
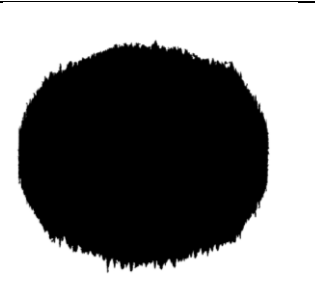
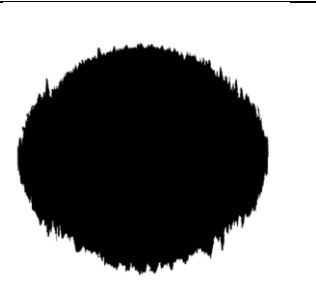
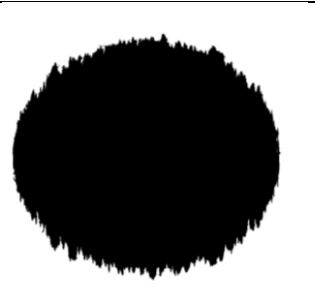
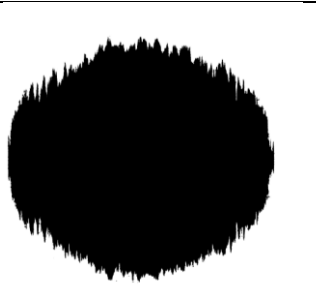
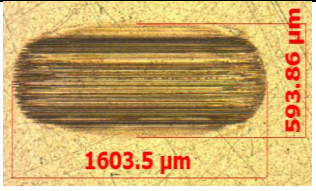
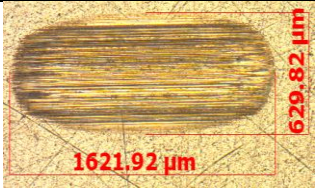
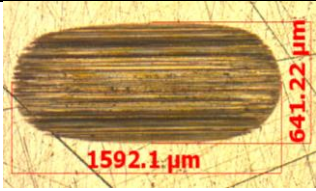
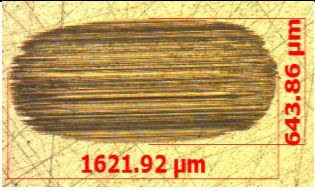
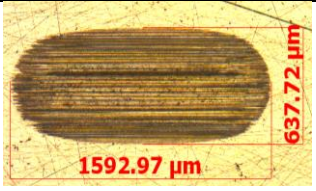
	Run 1	Run 2	Run 3	Run 4	Run 5
Wear Scars					
Wear Scars: Black & White					
Wear Tracks					

Table 4.4.4: Wear surface images for Group II mineral oil, ISO VG 32 (Gr II 32) with 2 % DES.

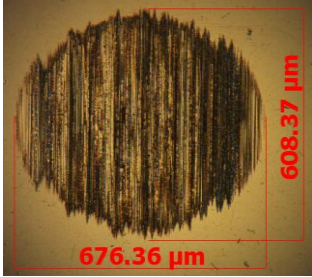
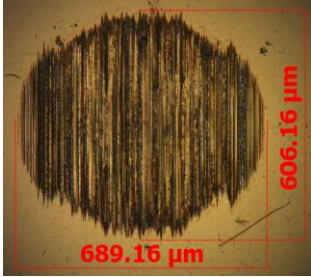
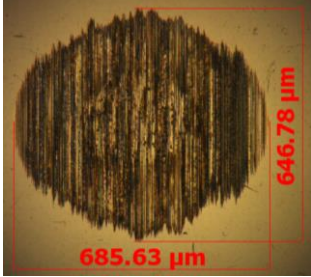
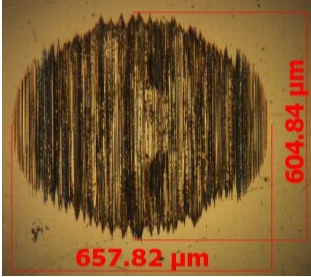
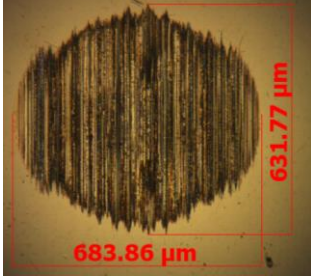
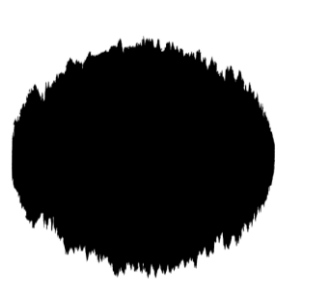
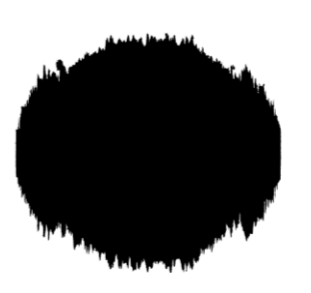

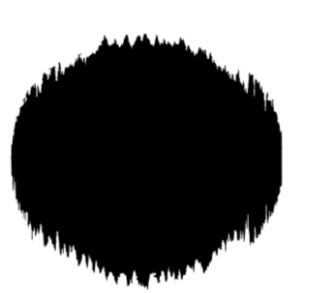
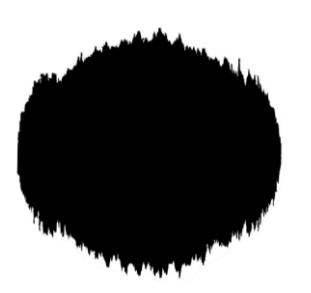

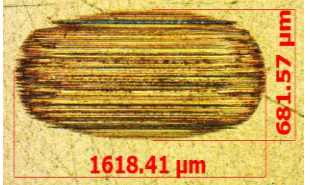
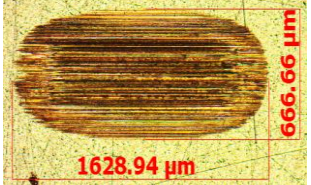
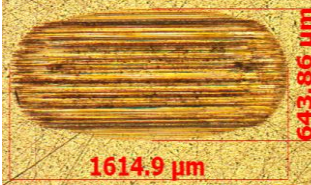
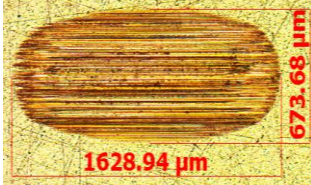
	Run 1	Run 2	Run 3	Run 4	Run 5
Wear Scars					
Wear Scars: Black & White					
Wear Tracks					

Table 4.4.5: Wear surface images for **Group II mineral oil, ISO VG 100 (Gr II 100) with 2 % DES.**

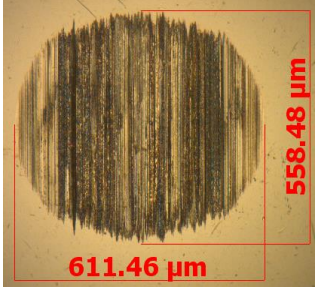
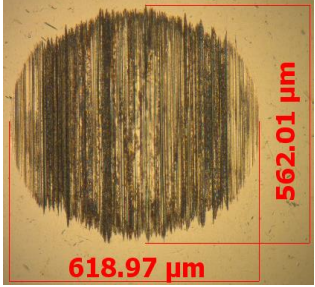
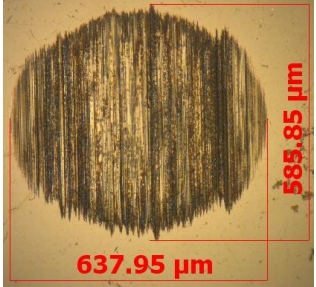
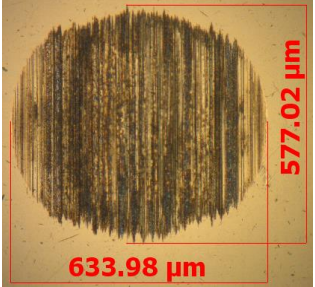
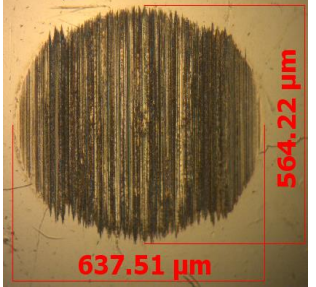





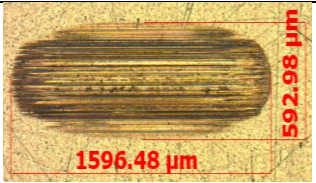
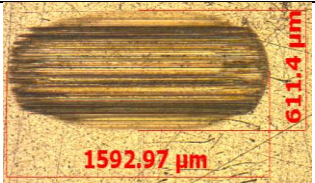
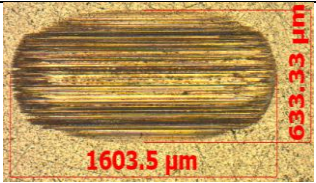
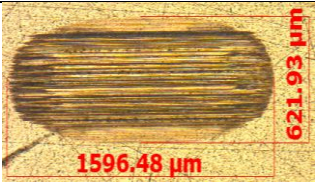
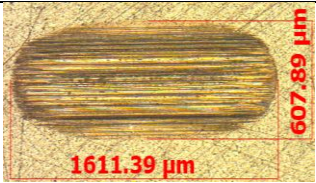
	Run 1	Run 2	Run 3	Run 4	Run 5
Wear Scars	 611.46 μm (width), 558.48 μm (height)	 618.97 μm (width), 562.01 μm (height)	 637.95 μm (width), 585.85 μm (height)	 633.98 μm (width), 577.02 μm (height)	 637.51 μm (width), 564.22 μm (height)
Wear Scars: Black & White					
Wear Tracks	 1596.48 μm (width), 592.98 μm (height)	 1592.97 μm (width), 611.4 μm (height)	 1603.5 μm (width), 633.33 μm (height)	 1596.48 μm (width), 621.93 μm (height)	 1611.39 μm (width), 607.89 μm (height)

Table 4.4.6: Wear surface images for polyalkylene glycol (PAG) with 0.5 % DES.

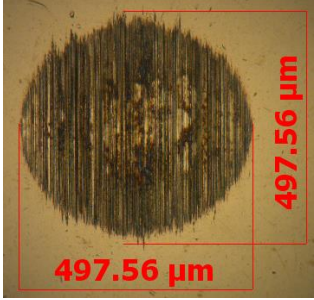
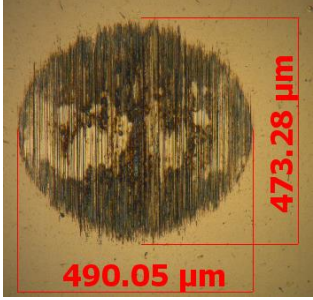
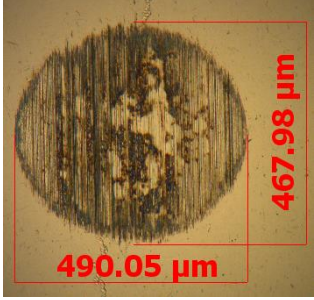
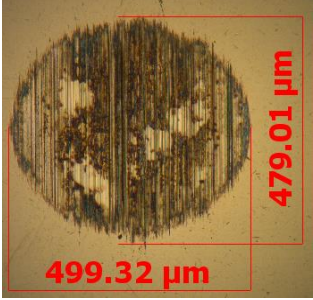
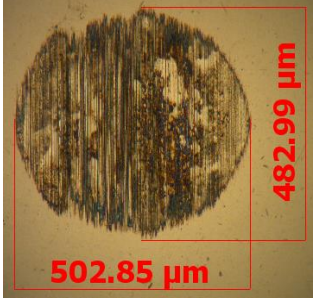

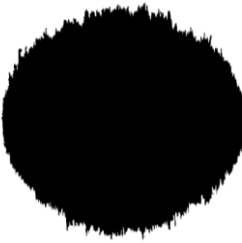
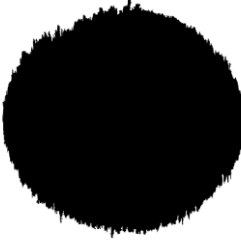
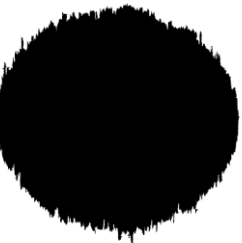
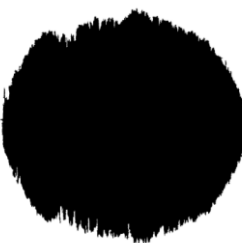
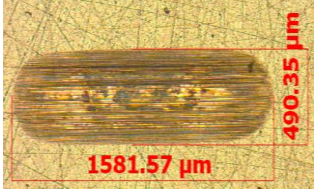
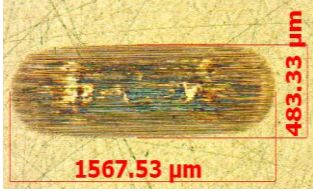

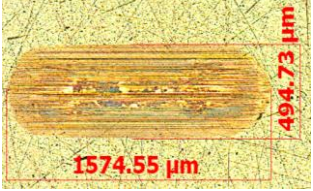
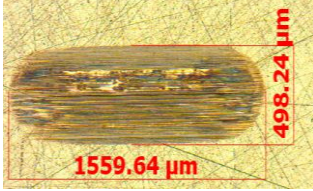
	Run 1	Run 2	Run 3	Run 4	Run 5
Wear Scars	 497.56 μm 497.56 μm	 473.28 μm 490.05 μm	 467.98 μm 490.05 μm	 479.01 μm 499.32 μm	 482.99 μm 502.85 μm
Wear Scars: Black & White					
Wear Tracks	 490.35 μm 1581.57 μm	 483.33 μm 1567.53 μm	 486.84 μm 1566.66 μm	 494.73 μm 1574.55 μm	 498.24 μm 1559.64 μm

Table 4.4.7: Wear surface images for polyalphaolefin (PAO) with 0.5 % ZDDP.

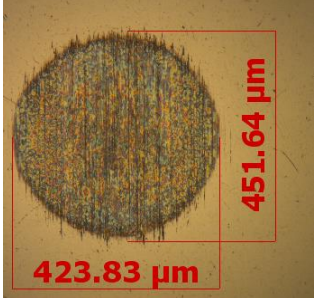
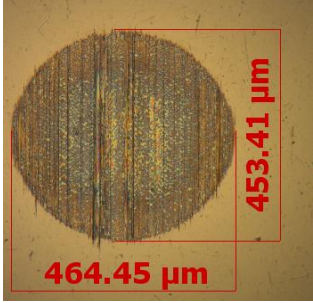
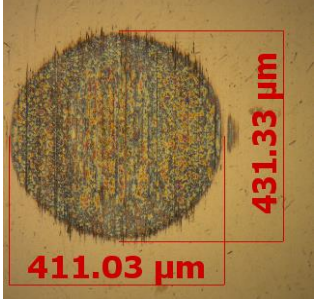
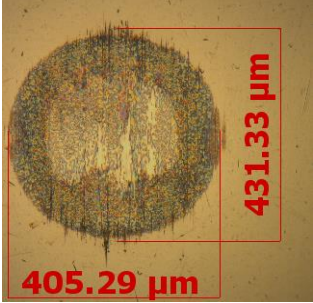
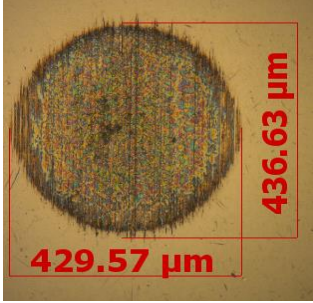

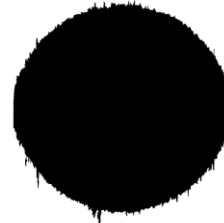
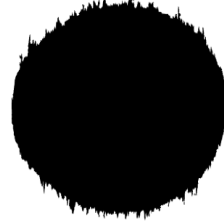


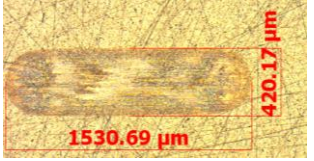
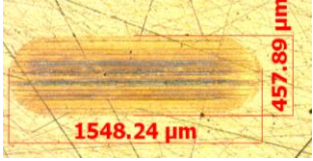
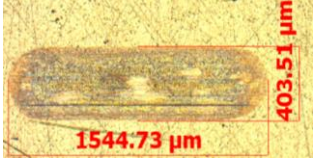
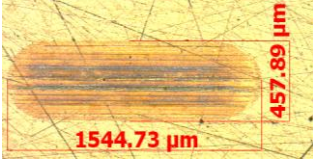
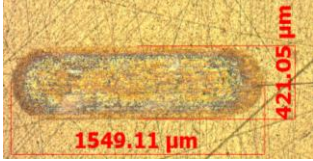
	Run 1	Run 2	Run 3	Run 4	Run 5
Wear Scars	 <p>423.83 μm (width) 451.64 μm (height)</p>	 <p>464.45 μm (width) 453.41 μm (height)</p>	 <p>411.03 μm (width) 431.33 μm (height)</p>	 <p>405.29 μm (width) 431.33 μm (height)</p>	 <p>429.57 μm (width) 436.63 μm (height)</p>
Wear Scars: Black & White					
Wear Tracks	 <p>1530.69 μm (width) 420.17 μm (height)</p>	 <p>1548.24 μm (width) 457.89 μm (height)</p>	 <p>1544.73 μm (width) 403.51 μm (height)</p>	 <p>1544.73 μm (width) 457.89 μm (height)</p>	 <p>1549.11 μm (width) 421.05 μm (height)</p>

Table 4.4.8: Wear surface images for polyalkylene glycol (PAG) with 0.5 % ZDDP.

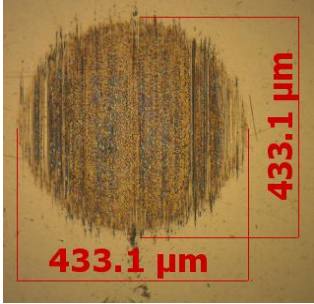
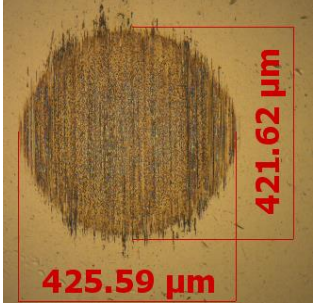
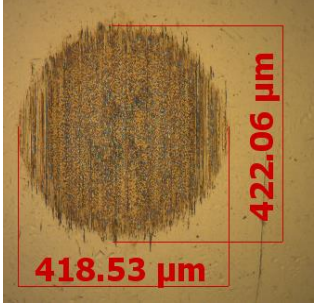
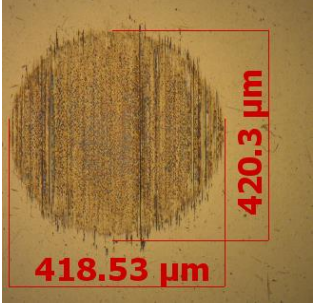
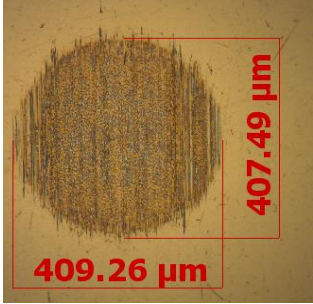
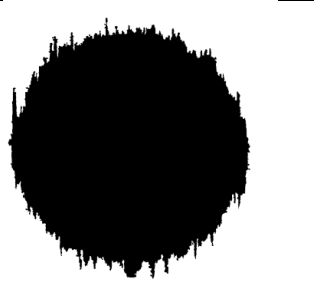
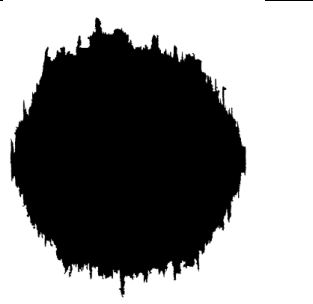
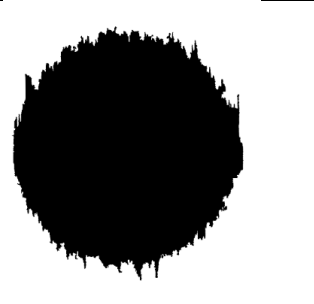
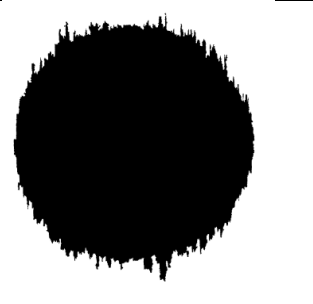
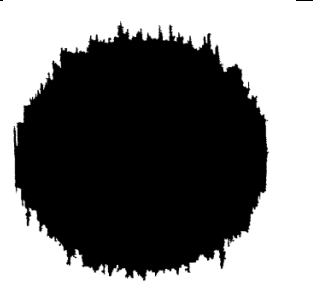
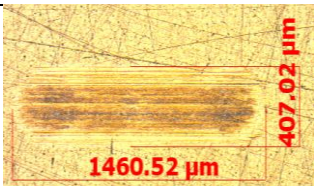

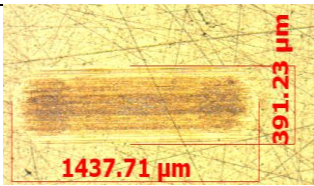

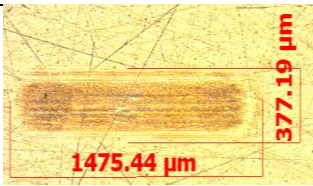
	Run 1	Run 2	Run 3	Run 4	Run 5
Wear Scars					
Wear Scars: Black & White					
Wear Tracks					

Table 4.5: Summary of repeatability of the wear surface appearance and the wear surface shape of wear scars.

Test Fluid	Wear Surface	Surface Deviation	d_1 Boundary	Shapes	Edge Deviation	d_1/d_2
WMO + 0.5 % DES	Severe plough marks	All Similar	Exceeds boundary Poorly defined	Run 1,2 & 4 similar Run 3 and 5 different	All 5 runs	$d_1 < d_2$
PAO 6 + 3 % DES	Severe plough marks	All Similar	Exceeds boundary Poorly defined	Run 1,3 & 4 similar Run 2 & 5 similar	All 5 runs	$d_1 < d_2$
Gr III 6 + 2 % DES	Severe plough marks	All Similar	Exceeds boundary	Run 1 & 2 similar Run 3,4 & 5 similar	Run 1 & 2	$d_1 < d_2$
Gr II 32 + 2 % DES	Severe plough marks	All Similar	Exceeds boundary poorly defined	All 5 runs have similar shapes	All 5 runs, uneven balanced	$d_1 < d_2$
Gr II 100 + 2 % DES	Severe plough marks	All Similar	Exceeds boundary poorly defined	All 5 runs have similar shapes	All 5 runs, uneven balanced	$d_1 < d_2$
PAG 146 + 0.5 % DES	Clear areas. Plough marks	Run 1 – clear areas to lesser degree	Exceeds boundary poorly defined	All 5 runs have similar shapes	Run 4 and 5	$d_1 < d_2$
PAO 6 + 0.5 % ZDDP	Clear areas. Plough marks	Run 4 – lighter inner area	Small degree exceeds boundary	All 5 runs have similar shapes	None	$d_1 = d_2$
PAG 146 + 0.5 % ZDDP	Clear areas. Plough marks	All Similar	Exceeds boundary	All 5 runs have similar shapes	None	$d_1 = d_2$

From Tables 4.4.1 to 4.4.8 and Table 4.5:

1. *Wear surface*

All the surfaces indicate that plough marks were present. For the three fluids with the smallest extent of wear (**PAG 146 + DES**, **PAG 146 + ZDDP** and **PAO 6 + ZDDP**) variations in the surface appearance could be seen. The severity of the wear decreased for fluids with higher viscosity and when **ZDDP** was used as an additive. Furthermore, for the test fluids with **ZDDP** a translucent green layer can be seen. This is shown in Figure 4.21.

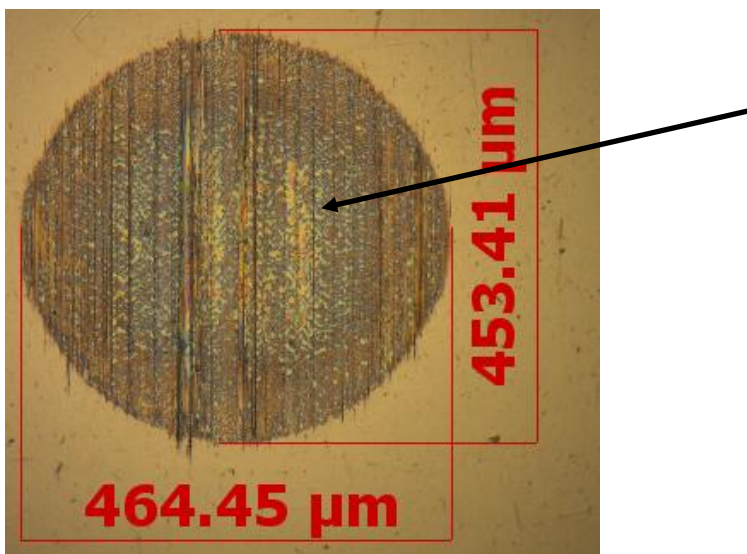


Figure 4.21: Translucent green layer observed on wear scar for **PAO 6 + 0.5 % ZDDP**, run 2.

2. *Surface Deviations*

Deviations between the surface appearances could only be seen for the **PAO 6 + ZDDP** and **PAG 146 + DES**. For the rest of the surfaces, where excessive wear occurred, the surfaces were similar.

3. *d₁ Boundary*

All the wear scars indicate that the boundary parallel to the sliding direction have been exceeded by plough marks. For **PAO 6 + 0.5 % ZDDP**, however the boundary was well defined. The boundary for **Group III mineral oil** was not as poorly defined compared to **Group II 32 mineral oil**.

4. Wear Scar Shapes

Variation was obtained for the wear scar shapes for the test fluids with the highest extent of wear. These were for white mineral oil, **PAO 6** and **Group III mineral oil**, all with **DES** as additive. The wear shapes for the other fluids showed good repeatability.

5. Edge Deviation

Deviation of the edges occurred for all the wear scars except for the test fluids with **ZDDP**. This deviation also increased when the extent of wear increased.

6. Ratio of the diameters

The diameter ratios are plotted in Figure 4.22. The diameter ratios for the adjusted wear scar diameters are also included. For all the test fluids with **DES** as additive, the d_1 diameter was smaller than the d_2 diameter. For the two test fluids with **ZDDP**, the scars were circular since the diameter ratio was 1.

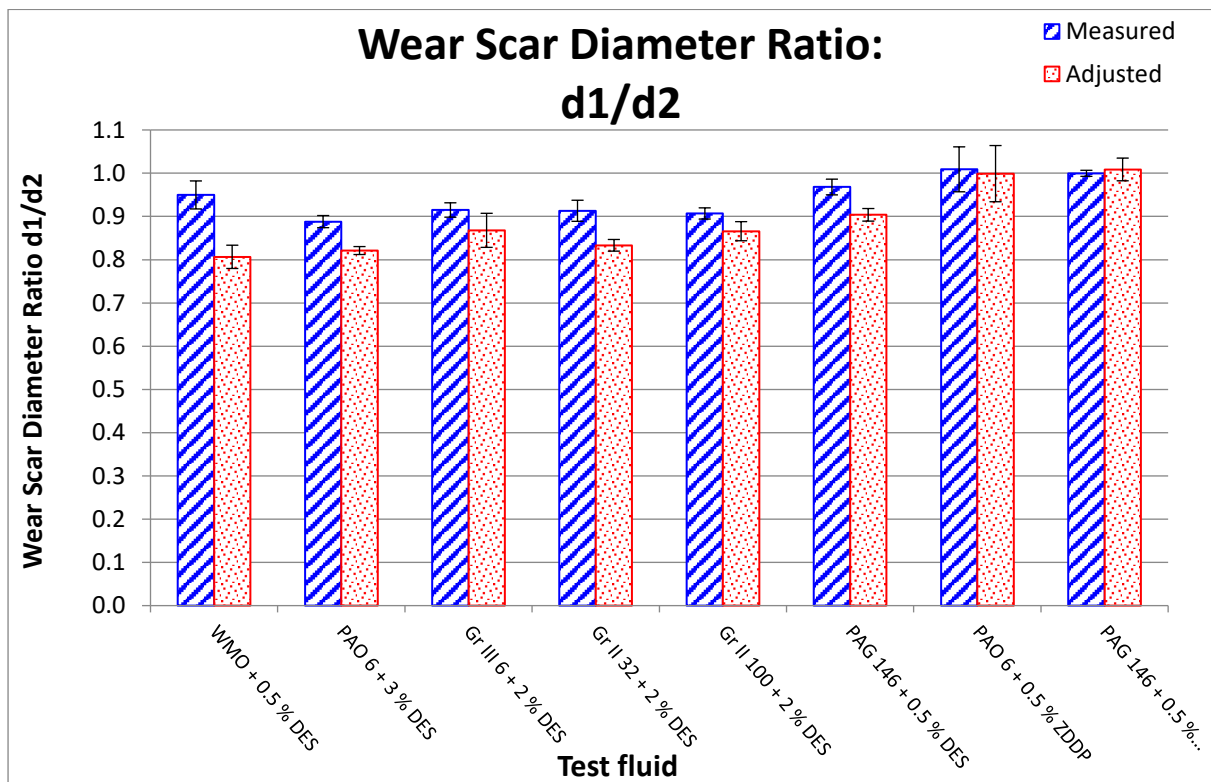


Figure 4.22: Wear scar diameter ratio: diameter parallel to the sliding direction (d_1) and the diameter perpendicular to the sliding direction (d_2).

In Figure 4.22 the ratio increased as the viscosity of the base oil increased. The ratio for the **Group III 6 oil**, however, is higher compared to **PAO 6 and Group II 32**. Also, the ratio decreased when the wear scar diameter was adjusted, i.e., the wear scar shape is more ellipsoidal than circular. This observation only applies to test fluids with **DES** as additive and not when **ZDDP** is the additive.

4.1.2.2.2 Wear Profiles

The wear profiles on the scar only included the profiles perpendicular to the sliding direction. This was done since the selection of the profile parallel to the sliding direction can easily be subjected to bias, since it depends where the operator selects the profile to be measured. Furthermore, the distribution of the plough marks is random and the edges poorly defined. This makes comparison difficult. The same holds for the profile on the track parallel to the sliding direction.

The profiles for all the wear surfaces are given in Appendix B.3. Only a selection of the wear profiles will be included here. Observations from these figures are summarised:

1. As the wear increase, deviations in the wear profiles also increase.
2. For the **PAO 6 and PAG 146** dosed with **ZDDP**, the **PAO 6** had more profile deviations even though the extent of wear was the same (Figures 4.23 and 4.24).
3. When the **2 PAG 146-based oils** are compared, the test fluid with **DES** as additive had a larger variation for the surface profiles.
4. All the wear profiles for the scars obtained for the test fluids with **DES** as additive had indents on the edges, which corresponds to the edge deviations that was observed on the wear scars images. This is shown in Figure 4.25. These indents cannot be seen for the base oils with **ZDDP** as additive.
5. The profiles for the **PAO 6 + 3 % DES** (Figure 4.27) fluid had better repeatability compared to the **WMO + 0.5 % DES** (Figure 4.26) and the **Gr III + 2 % DES** (Figure 4.28) test fluids. For the **WMO-based fluid** the largest deviations of the profile can be observed.

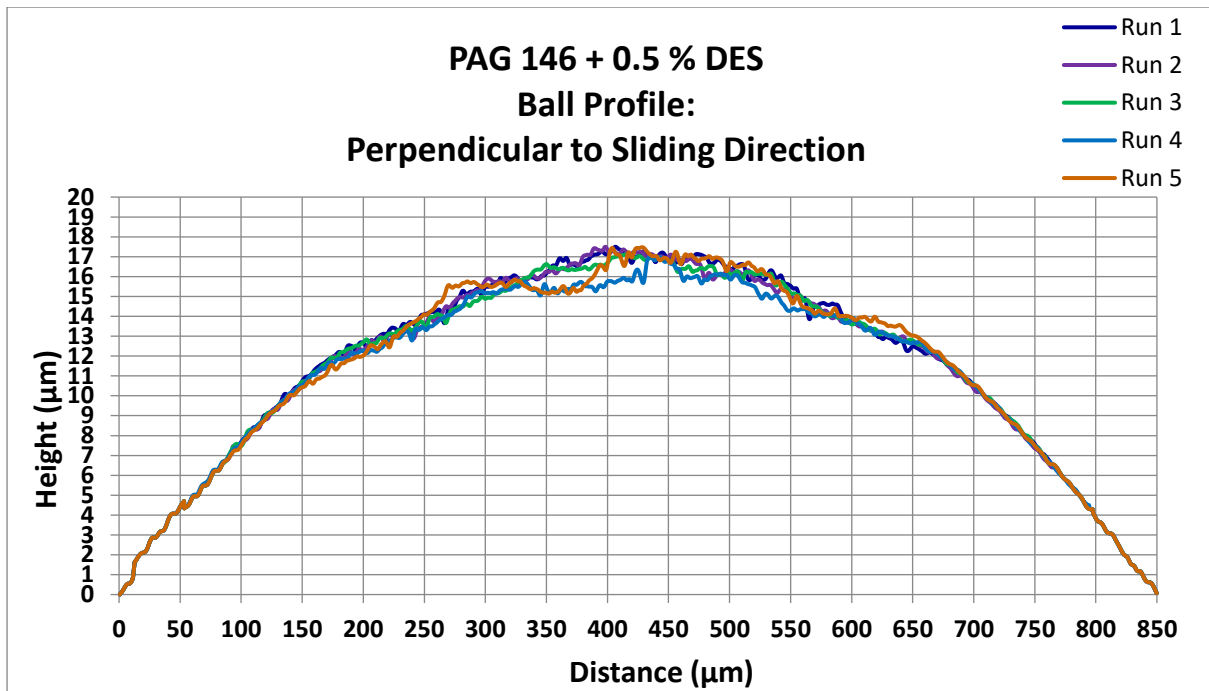


Figure 4.23: Wear scar profiles perpendicular to sliding direction for **PAG 146 + 0.5 % DES**.

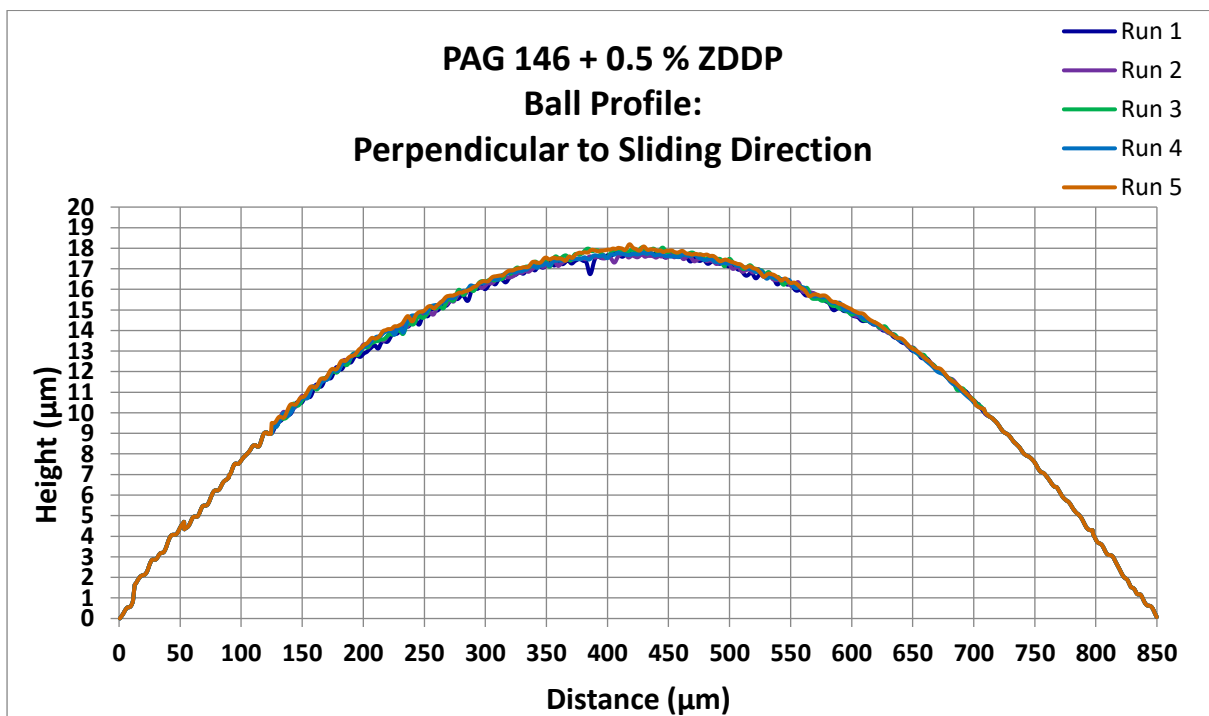


Figure 4.24: Wear scar profiles perpendicular to sliding direction for **PAG 146 + 0.5 % ZDDP**.

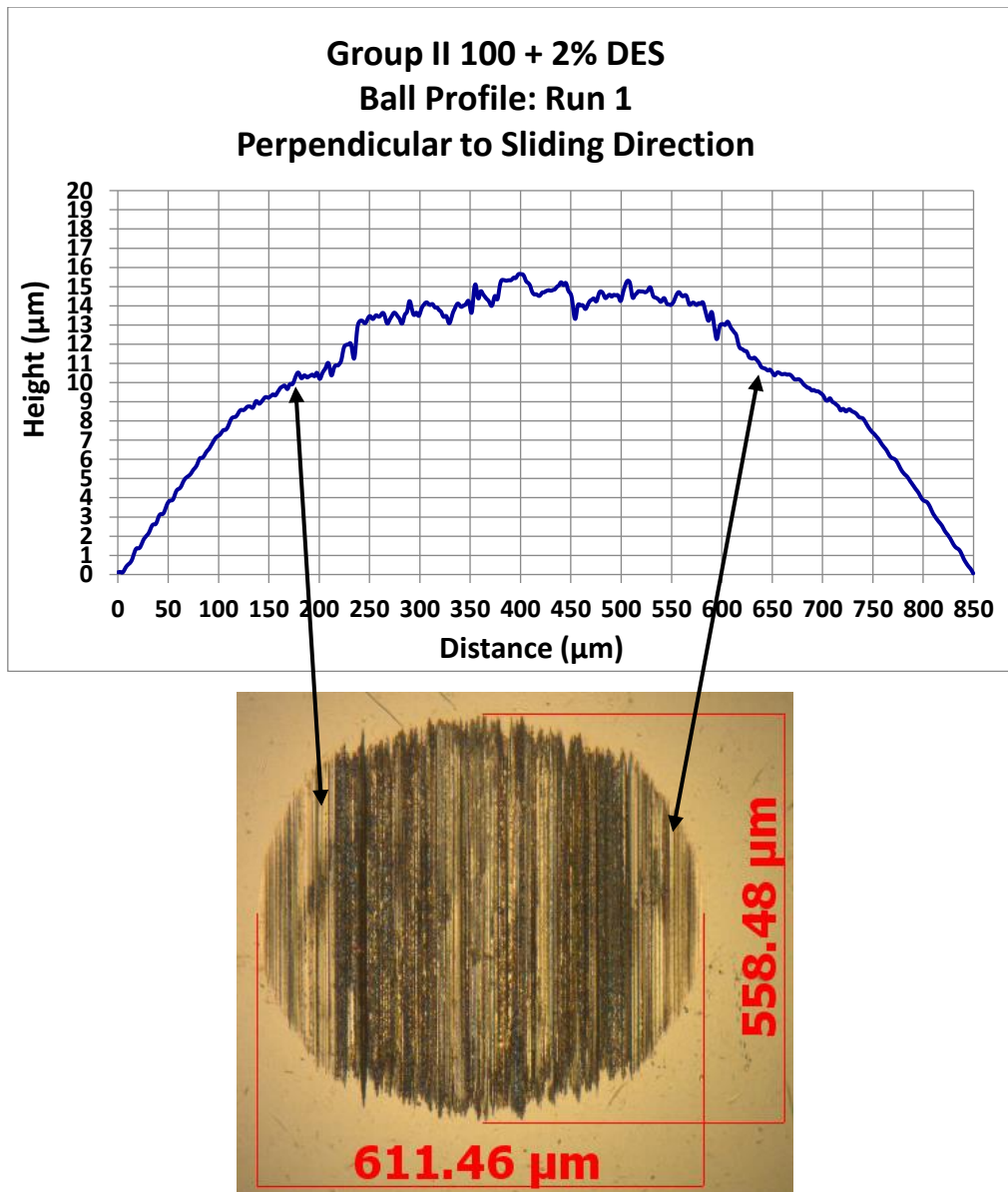


Figure 4.25: Indents observed on the edges of the wear scars. Profile compared to wear scar image.

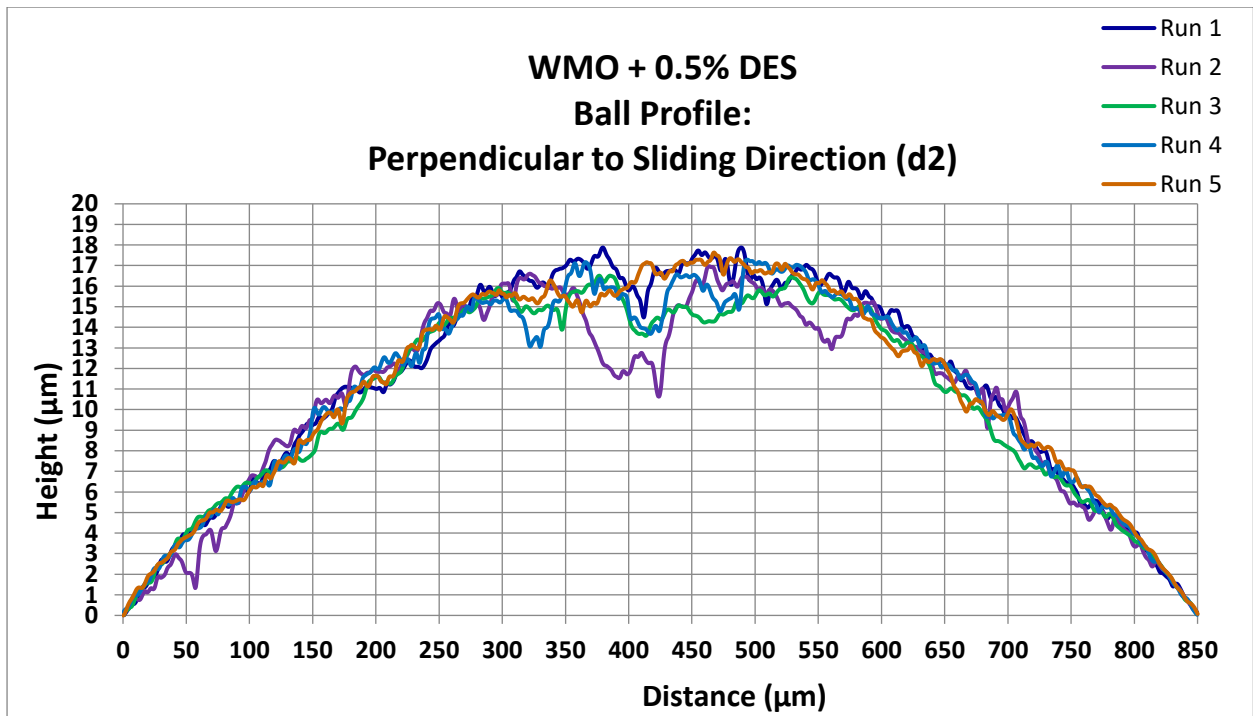


Figure 4.26: Wear scar profiles perpendicular to sliding direction for **WMO + 0.5 % DES**.

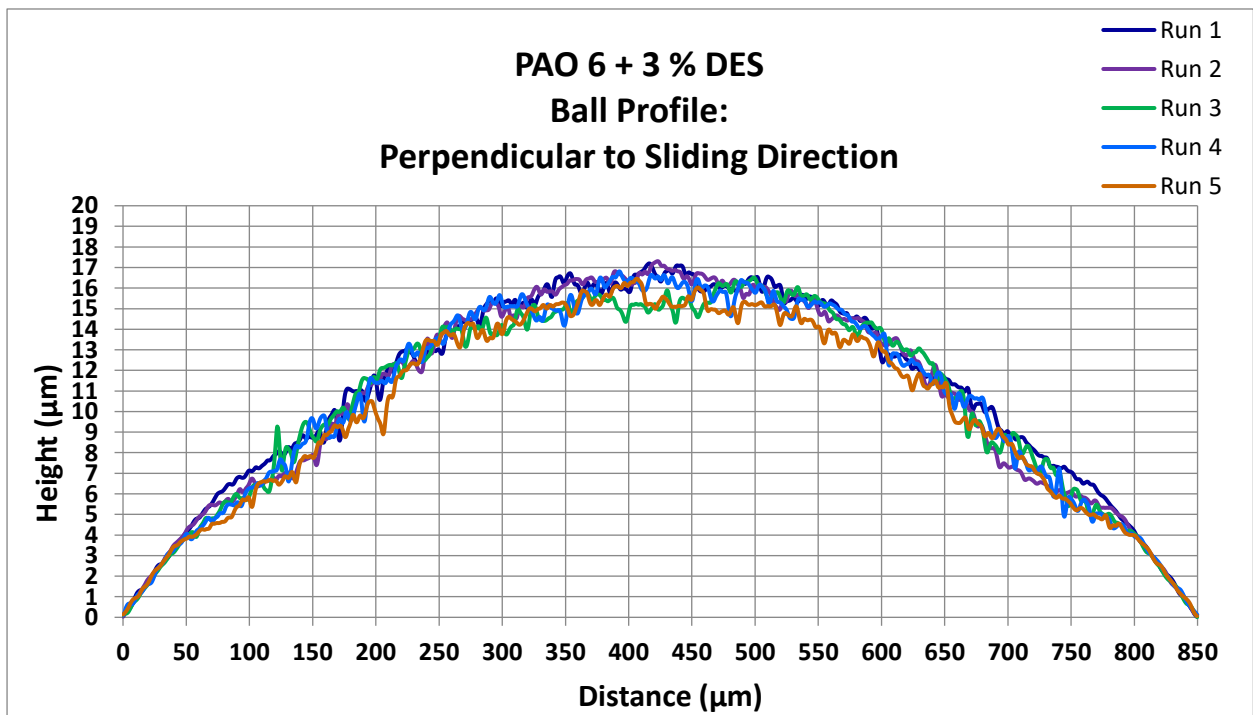


Figure 4.27: Wear scar profiles perpendicular to sliding direction for **PAO 6 + 3 % DES**.

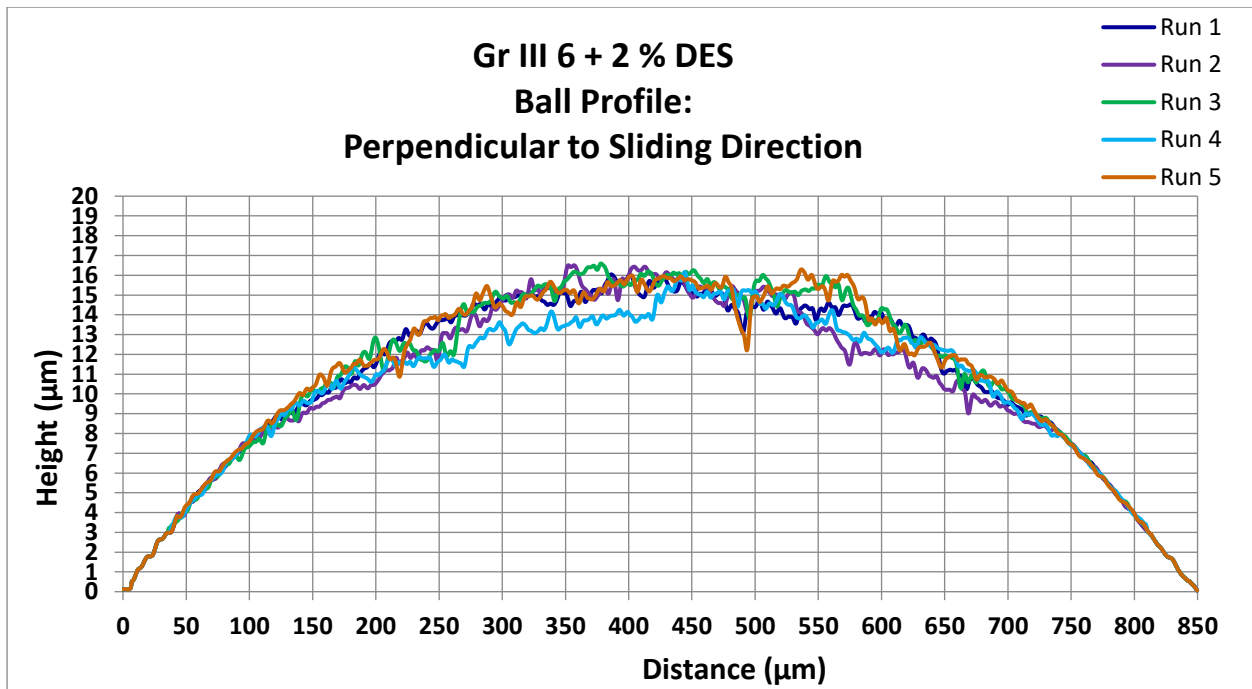


Figure 4.28: Wear scar profiles perpendicular to sliding direction for **Gr III 6 + 2 % DES**.

4.1.2.2.3 Wear Surface Summary

1. Viscosity

For higher viscosity oils, the surface appearance indicates that less severe wear occurred. The appearance of these surfaces, however varied to a greater extent. This was limited to the distribution of areas on the wear scars where layers were scraped away. Deviations in the shape and on the edges as well as the wear profile decreased with an increase in the viscosity. Finally, when the diameter ratio is considered, an increase in the viscosity resulted in the ratio moving closer to 1, i.e., the profiles become more circular.

2. Edge Deviations

The profiles for the wear scar indicate that the deviations observed for the edges correspond to indents on the profile. The edge deviations were only observed with DES as additive.

3. Effect of **ZDDP**

The addition of **ZDDP** resulted in a significant improvement on the wear surface appearance as well as on the shape, edge deviation and wear profile. With **ZDDP** as additive, circular wear scars were also obtained compared to ellipsoidal scar fluids with **DES** as additive.

4. Effect of Base Oils

For the most part, the viscosity of the base oil seems to play the dominant role. Deviations from the trend by **Group III** as base oil, however, indicate that the viscosity of the oil is not the only contributing factor. The boundary of the wear scar in the direction parallel to the sliding direction (d_1) was much better defined for **Group III 6** compared to the scars for the **Group II 32-based test fluid**.

Finally, the **WMO-based oil** was characterised by extreme wear with poorly defined boundaries in the direction parallel to the sliding motion. The wear profiles also showed the largest standard deviations.

5. Effect of Wear Scar Diameter Adjustment

The wear scar diameter adjustment decreased the ratio between the diameter parallel to the sliding direction and the diameter perpendicular to the sliding direction, i.e., the wear scars became more ellipsoidal. This was only observed for wear scars of fluids with **DES** as additive. No effect was seen on the ratio for the fluids with **ZDDP**.

4.1.2.3 Friction Coefficient Repeatability

The criteria used to evaluate repeatability for the friction coefficient during testing are defined in the relevant ASTM test methods. In the ASTM D5707-16 standard test method the primary result to report is the minimum coefficient of friction. Repeatability of the minimum friction coefficient is restricted in the standard to a difference smaller than 0.012 between successive results for an operating temperature of 50 °C. This criterion applies to results obtained by the same operator on the same test apparatus with the same test materials. The difference of 0.012 can be exceeded for only one case in 20.

Repeatability described in ASTM D6425-17 is defined in a similar way as in ASTM D5707-16, but the difference between the friction coefficient values should not exceed a value of 0.01. For this test however, no temperature is specified, while six friction coefficient values are reported: f_{min} , f_{max} , f_{15} , f_{30} , f_{90} and f_{120} .

In terms of specifications, these single values are adequate. However, when only single values are reported, changes in the friction coefficient cannot be compared between repeat runs. This includes the transition of the friction coefficient measurement after the load is increased to the operating load or the duration until steady state is reached.

For these reasons, the friction coefficient recordings between repeat runs were plotted on a single graph. An example is given in Figure 4.29, where the test fluid was **PAO + 3 % DES**. The friction coefficient graphs for all the test fluids evaluated on the SRV test rig are given in Appendix B.1.

It is clear from this figure that deviations occurred between repeat runs, for the entire test duration. The extent of the deviations can also be seen when the average value as well as the standard deviation for all 5 repeat runs are plotted on a single graph. This is shown in Figure 4.30, also for **PAO 6 + 3 % DES**.

In Figure 4.30, poor repeatability occurred during and after the running-in procedure. After about 12 minutes into the test, the deviation is small, and good repeatability is obtained. After 38 minutes, the deviations increase again and remain constant for the remainder of the test. The average of the friction coefficient recordings with standard deviations for the rest of the test fluids are given in Appendix B.1.

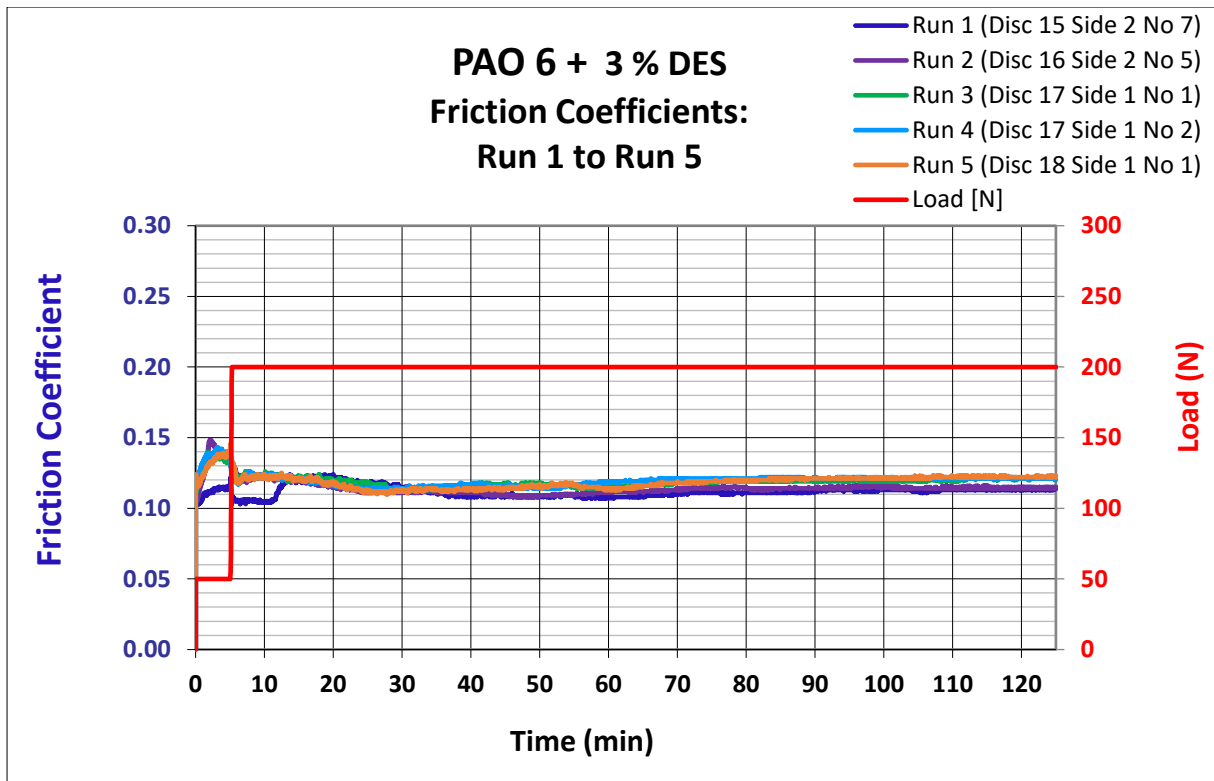


Figure 4.29: Friction Coefficient recording for 5 repeat runs done on the SRV test rig. The test fluid is **PAO 6 + 3 % DES**.

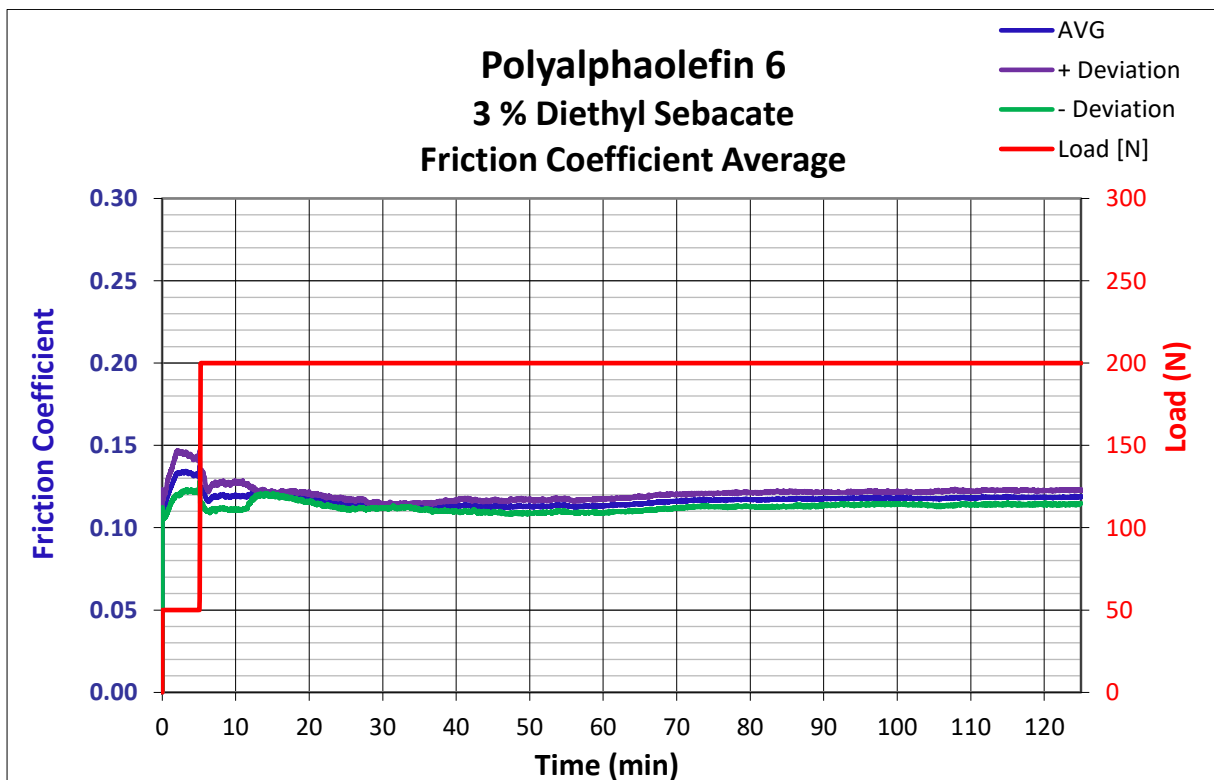


Figure 4.30: Average and standard deviation for friction coefficient recordings during evaluation of **PAO 6 + 3 % DES** on the SRV test rig.

Figure 4.30 enables the visual determination where poor repeatability occurred between repeat runs. The average friction coefficient with standard deviation for **white mineral oil with 0.5 % diethyl sebacate** are also given in Figure 4.31. In this figure repeatability was good during the running-in procedure and for most of the test up to 92 minutes. After 92 minutes, however, the values started deviating from the average value.

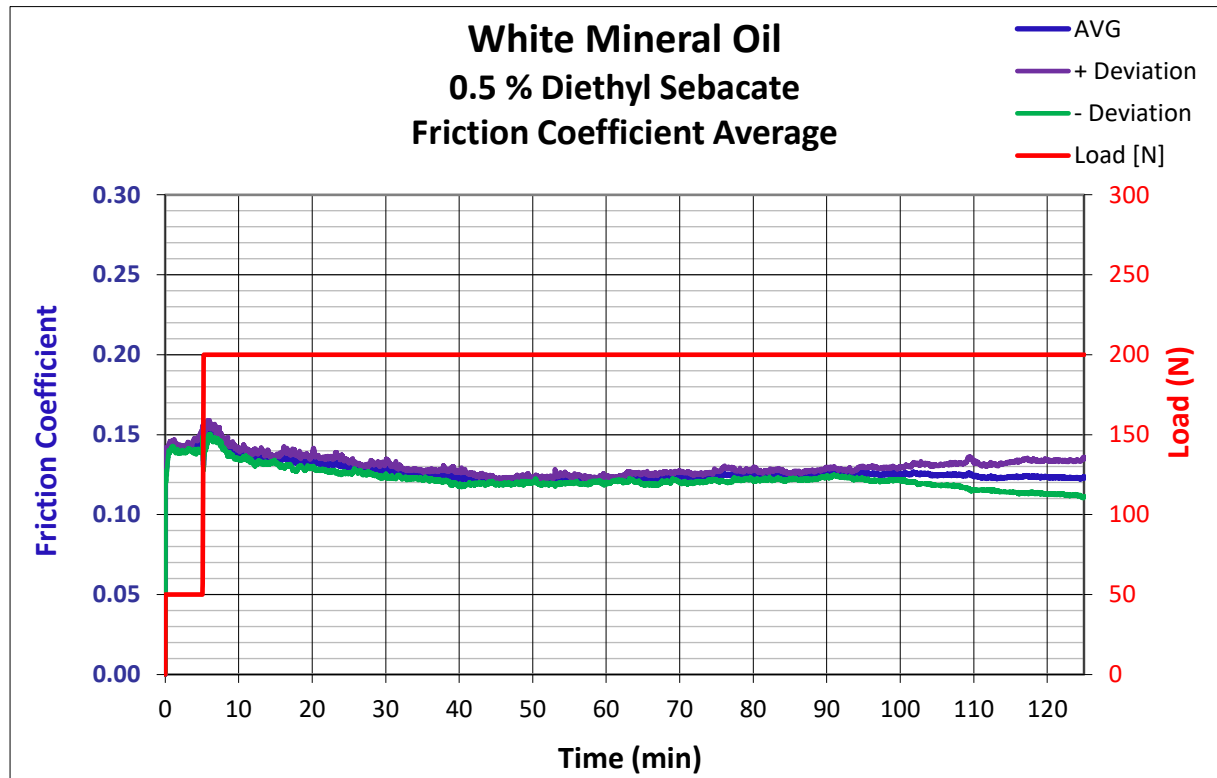


Figure 4.31: Average and standard deviation for friction coefficient recordings during evaluation of **WMO + 0.5 % DES** on the SRV test rig.

To quantify repeatability, the difference between the average and the standard deviation of the friction coefficient was integrated. This is obtained by calculating the area between the positive and negative deviation. This is done by summing the area for each time interval, i.e., the sum of the difference between the positive and negative deviation multiplied with time interval duration for each time interval (equation 3.1). The integrals of the standard deviation from the average of the friction coefficient for all the test fluids are given in Figure 4.32.

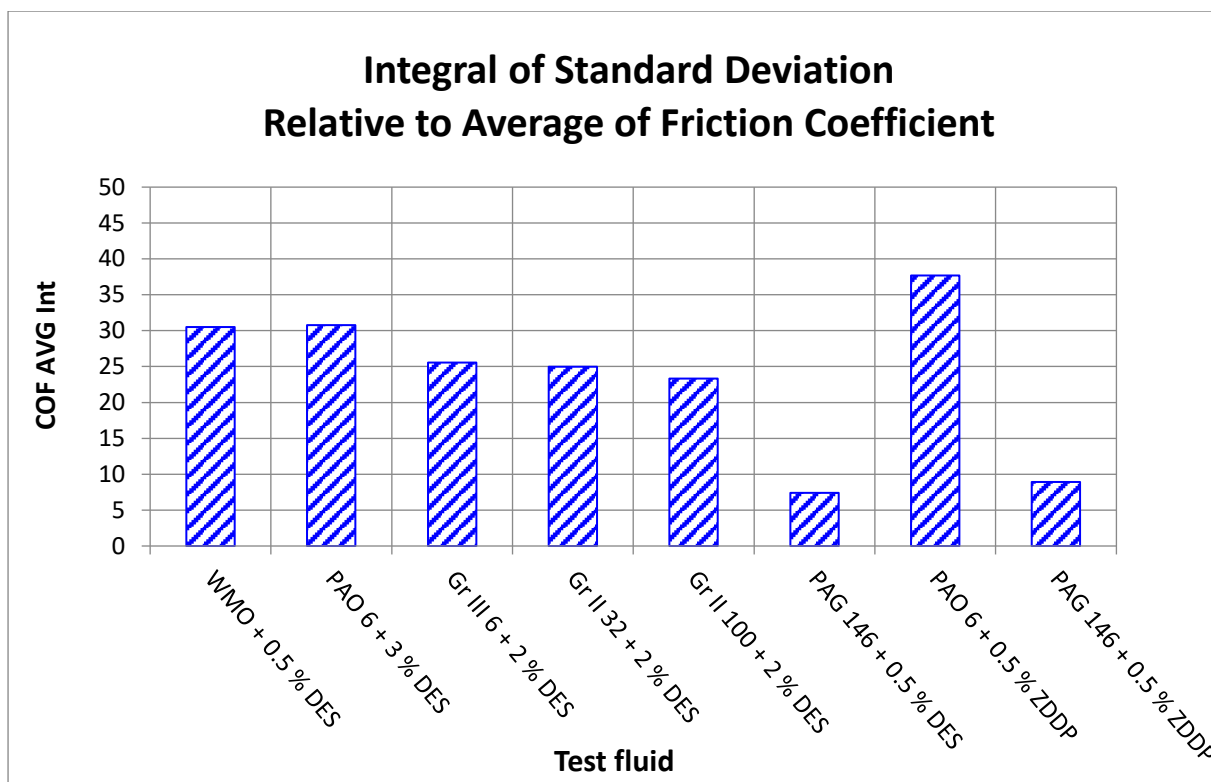


Figure 4.32: Repeatability of friction coefficient of base oils, based on 5 repeat runs on the SRV test rig.

In Figure 4.32 it is immediately evident that repeatability of the friction coefficient also improves with an increase in the base oil viscosity. The **PAO 6 based oil** had the poorest repeatability of all the test fluids. This was irrespective of the additive used. Furthermore, for the **2 synthetic fluids**, repeatability was poorer when **ZDDP** was used as additive instead of **DES**. There was also a small difference between repeatability of **Group III 6 and Group II 32**.

The final value for the friction coefficient recorded for each of the test fluids is given in Figure 4.33. This is an average value calculated from the final values of the 5 repeat runs for each of the fluids. These values were used, to relate the friction coefficient to the extent of wear and the wear surface profile, both of which were measured at the end of the test.

In Figure 4.33, for the test fluids with **DES** as additive, the lowest friction coefficient was obtained with **Group II 32**. **PAG 146** had the highest friction coefficient. Furthermore, for the 2 test fluids with **ZDDP** as additive:

- No effect was seen for the **PAG 146-based test fluids**.
- **ZDDP** decreased the friction coefficient for **PAO 6**.

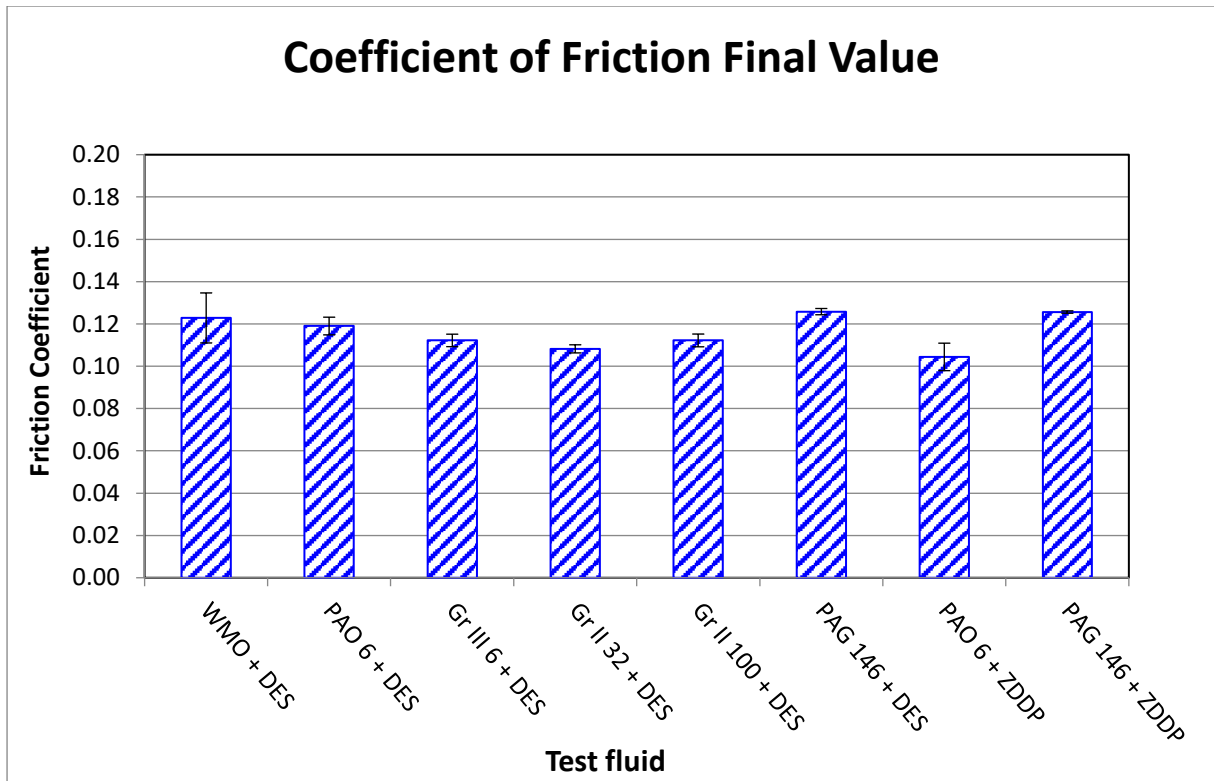


Figure 4.33: Average of the final friction coefficient value between 5 repeat runs.

The standard deviation for the final value of the friction coefficients is given in Figure 4.34. From this figure:

1. The standard deviation for the **WMO + 0.5 % DES** test fluid was much larger compared to the rest of the test fluids.
2. The standard deviation decreases as the viscosity increases, with one exception. The standard deviation for the **Group II 100 + 2 % DES** base fluid was higher than the test fluids with lower viscosity.
3. The standard deviation for the **PAG-based oil** improved when the **DES** was replaced with **ZDDP**. The opposite is true for the **PAO-based oils**.

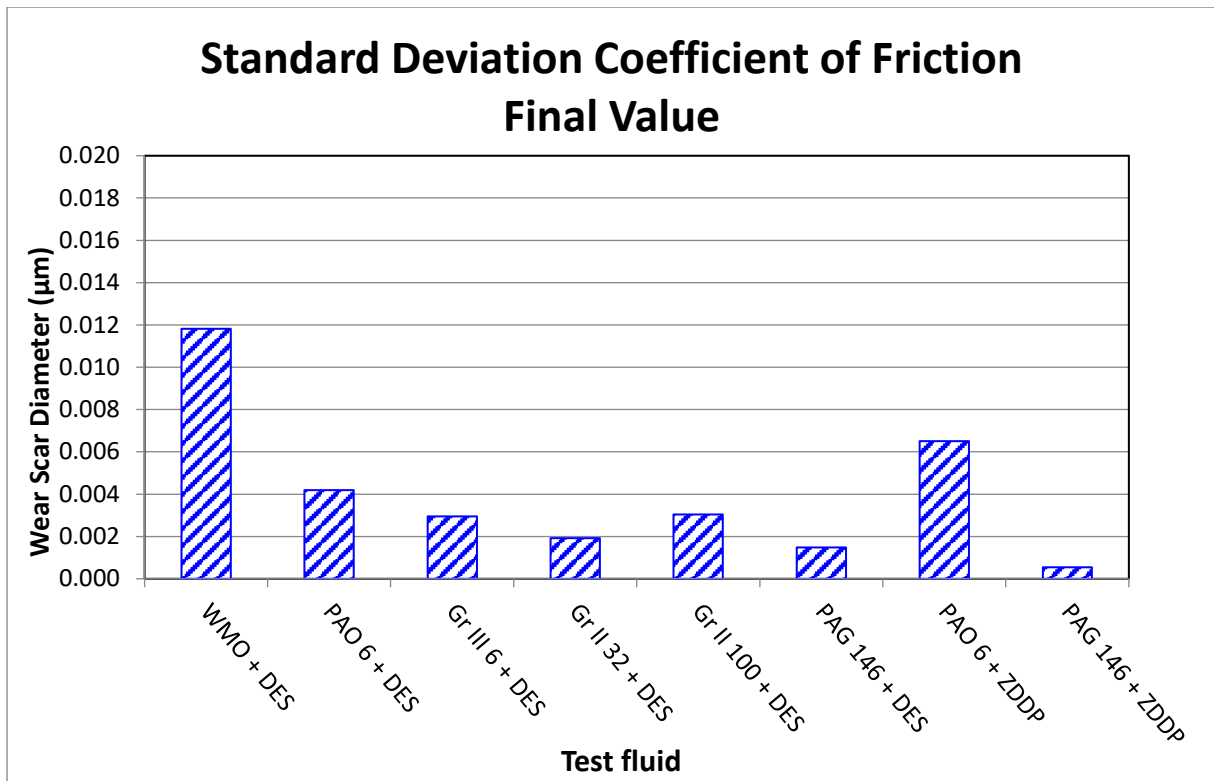


Figure 4.34: Standard deviation of the final friction coefficient value between 5 repeat runs (error bars from Figure 4.33).

When Figure 4.32 and 4.34 are compared, both have the same trends with a few exceptions:

- **WMO + 0.5 % DES** had the worst repeatability in Figure 4.34, while **PAO 6 + 0.5 % DES** had the poorest repeatability in Figure 4.32.
- **Group II 100** had poorer repeatability compared to Group II 32 and Group III 6 in Figure 4.34. In Figure 4.32, it had better repeatability.
- **ZDDP** improved repeatability in Figure 4.34 for the **PAG-based fluids**, but not in Figure 4.32.

The exceptions above highlight that care must be taken when interpreting repeatability of friction and wear results, since it depends on how the results are presented.

In Figures 4.29 to 4.31 the friction coefficients reach a point in the test whereafter the value is constant. This will be referred to as a steady state. Before steady state, the friction coefficient undergoes a few transitions. The first is the changes in the friction coefficient during the first 5 minutes at the running-in load of 50 N. This is followed by

an induced transition when the load is increased to 200 N and the friction coefficient drops rapidly. After increasing the load to 200 N, the friction coefficient increases to a maximum. Variations can also be observed between the friction coefficients between repeat runs for some fluids after the step load increase. This is followed by a steady decline until the constant value is reached.

In the figures in Appendix B.2, the duration until steady state is reached is different for each of the test fluids. This is summarised in Table 4.6. The base oil viscosity and **ZDDP** decrease the duration until steady state is reached.

Table 4.6: Duration until friction coefficient steady state.

Test Fluid	Duration Until Steady State	COF Steady State Value
WMO + 0.5 % DES	80 min	0.123
PAO 6 + 3 % DES	70 min	0.119
Group III 6 + 2 % DES	75 min	0.112
Group II 32 + 2 % DES	75 min	0.108
Group II 100 + 2 % DES	60 min	0.112
PAG 146 + 0.5 % DES	10 min	0.126
PAO 6 + 0.5 % ZDDP	20 min	0.104
PAG 146 + 0.5 % ZDDP	5 min	0.126

Summary of Friction Coefficient Repeatability

1. The general trend is that repeatability improves with an increase in base oil viscosity.
2. The additive only had a positive effect with **PAG**. For **PAO**, poorer repeatability was obtained when **ZDDP** was used in instead of **DES**.
3. From the graphs, the friction coefficient goes through a few transitions until steady state is reached. The first is during the first 5 minutes at the running-in load of 50 N. This is followed by an induced transition when the load is increased to 200 N. After the induced transition, the friction coefficient increases to a maximum value. It then decreases until steady state is reached.
4. The duration until steady state was reached was different for most of the test fluids and depended on the base oil viscosity and the additive.
5. The step load increase resulted in variations in the friction coefficient after the load was increased.

Summary of repeatability of Friction and Wear Results

The results so far indicate that properties of the test fluid do not only affect the friction coefficient, the extent of wear and the surface finish, but also affect repeatability.

These properties are:

1. The viscosity of the base oil played a significant role. The general trend for the viscosity observed was an improvement in repeatability with an increase in the viscosity. The extent of wear decreased with an increase in viscosity, while the minimum friction coefficient had a minimum value for **Gr II 100**, which had the second highest viscosity.
2. The additive also played an important role. In general, an improvement was seen when **diethyl sebacate** was replaced with **ZDDP**.
3. The differences in behaviour between **PAO 6, Group III 6 and Group II 32** indicate that composition of the base oil also plays a role.
4. Wear scar adjustments can also affect the outcome in terms of repeatability, though not in all cases.
5. The step load increase caused a rapid change in the friction coefficient. This will be looked at further in the next section.
6. The duration until steady state for the friction coefficient is obtained depends on the base oil viscosity and the additive.

In Section 4.1.2.4 to 4.1.2.8, the role that the base oil viscosity, the composition of the base oil, the effect of the additive and the wear scar diameter plays on repeatability are discussed. The step load increased will be looked at in more detail in section 4.1.3. Up to this point, the role of using more than one test disk to complete all the runs was not included. This will be looked at in section 4.1.4.

4.1.2.4 Effect of the Base Oil Viscosity

The effect of the base oil viscosity on the friction and wear process has already been documented by other researchers, so the discussion will not focus too much on this property (Zhang & Spikes, 2016). It was, however, confirmed in this study that the

base oil viscosity is the predominating factor that affects friction and wear performance.

Furthermore, the increase in friction coefficient for the **PAG 146** in Figure 4.33 indicates that the lubricating regime moves into the elastohydrodynamic regime as indicated by Figure 4.4. In this regime the fluid viscosity also contributes to the friction coefficient. This can be seen for the test fluids with **DES** as additive and with **ZDDP** as additive.

The effect of the viscosity on repeatability is also evident in Figures 4.9, 4.11, 4.13, 4.32 and 4.34 as well as Tables 4.4.1 to 4.4.8. Repeatability improves with an increase in base oil viscosity. The explanation is simply that a higher viscosity base fluid has a better ability to prevent surface interactions, i.e., the system moves away from the boundary and mixed lubricating regimes and toward the hydrodynamic regimes. Higher degrees of surface interactions increase the probability of surface deviations between repeat runs. The friction and wear between 2 surfaces depend on these interactions and surface deviations therefore lead to poor repeatability. For larger extents of wear, the degree of surface interactions increases. With an increase in the surface interactions, the probability of surface deviations also increases, and this leads to poorer repeatability.

This is further verified by the 2 test fluids with **ZDDP** as additive. Both had extents of wear of similar magnitude while the viscosity of the 2 synthetic base oils were significantly different. The **PAO 6 + 0.5% ZDDP**, with the lower viscosity, had poorer repeatability on both the disk and the track, while the higher viscosity fluid (**PAG 146-based**) performed very well.

4.1.2.5 Composition of the Base Oil

The three base oils: **PAO 6, Group III 6 and Group II 32** all have similar viscosities at the operating temperature. However, there were still some differences in performance between the 3 base oils. This indicates that base oil composition also plays a role during testing on the SRV test rig.

Wear results for the **Group III mineral oil** indicate that the extent of wear obtained for this base oil was lower than the expected trend. This can be seen in Figures 4.8, 4.10 and 4.12 respectively for the wear scar diameter, wear scar volume and the wear track volume. The 3 test fluids (**PAO 6, Group III 6 and Group II 32**) had small differences in their viscosities. Therefore, the test method on the SRV test rig is highly sensitive to the base oil viscosity.

The difference between the **Group III and Group II mineral oils** is that the **Group III** has undergone severe hydrocracking. It is therefore predominantly straight chain paraffinic molecules. Consequently, the viscosity index for **Group II** is higher. Furthermore, the temperature in the contact point can very easily exceed that of the operating temperature of 50 °C. The **Group III 6** sample will therefore have higher viscosity at higher temperature and provide better protection.

When repeatability is considered, **Group III 6** had poorer repeatability for the ball wear scar volume, while the ball wear scar diameter had good repeatability. Since the ball wear scar volume calculation also includes wear surface parameters, the poor repeatability for the wear volume indicate that these parameters also have poor repeatability. This was also confirmed in Figures 4.15, 4.17 and 4.19.

In equation 3.4, the profile radius of the scar calculation includes the planimetric wear area. Consequently, if the planimetric wear area varies between repeat runs, the profile radius will also vary. This will also affect the wear volume calculation in equation 3.3.

The reason why repeatability of the wear volume for **Group III 6** was poorer than expected was due to the planimetric wear area for run 5 that was much larger compared to the other 4 repeat runs (see Appendix B.4.3). The wear profiles in Appendix B.3 also indicate that the wear area is larger for run 5 which resulted in poor repeatability.

When the friction coefficient graph is considered, the 5th run deviated from the other repeat runs just after the step load increase. This is shown in Figure 4.35. Initially, just after the load was increased, the friction coefficient was lower. After about 22 minutes,

a non-induced transition occurred where the friction coefficient increased. However, the friction coefficient recovered and had the steady state behaviour was similar compared to the other runs. This increase indicates a rapid change in the surface interactions which resulted in the higher extent of wear for this run.

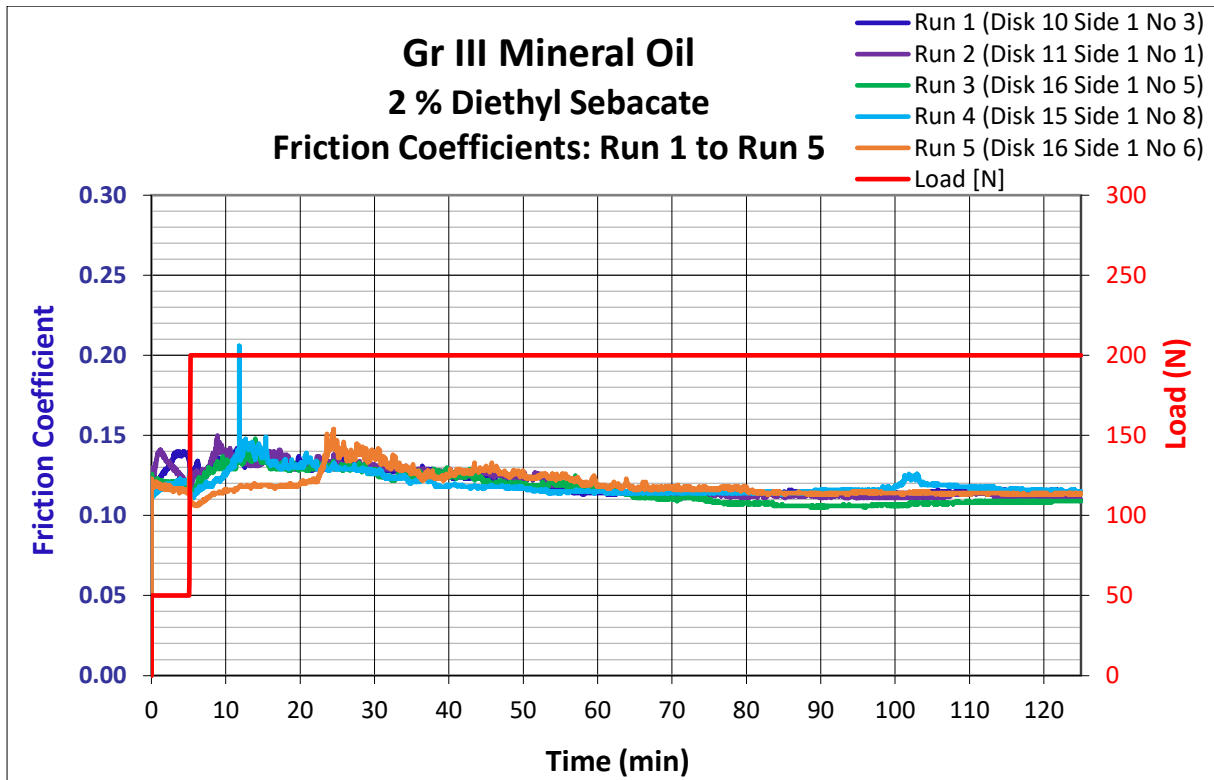


Figure 4.35: Friction coefficient plots for **Group III 6 + 2% DES**.

4.1.2.6 Repeatability of Wear Volume on Ball and on Disk

In Figure 4.11 (section 4.1.2.1.2), both **Gr III + 2 % DES** and **PAO + 0.5 % ZDDP** deviated from the trend, i.e., had higher standard deviations than the trend. However, this was not the case for the standard deviations on the disk (Figure 4.13).

When the calculations are considered, both these fluids' poor repeatability was due to run number 5 that deviated the most from the average, as seen in Tables 4.7 and 4.8. This was due to Run 5 for each fluid which had the biggest deviation for $W_{q,flat}$, compared to the other 4 runs.

When the wear volumes are considered on the ball and on the disk, it is important to notice that there is a difference of 1 order between the magnitude of volume on the disk and on the ball. For instance, compare 4.82×10^{-4} for the ball and 3.46×10^{-3} on the disk. The wear volume on the disk is therefore 10 times higher compared to the ball.

Since both calculations uses the same $W_{q,flat}$, the effect of a deviation of $W_{q,flat}$ will be more pronounced on the ball wear scar volume. Consequently, the deviation in $W_{q,flat}$ was only seen on the ball and not on the disk. The disk wear volume is therefore not as sensitive to deviations in $W_{q,flat}$ compared to the ball wear volume.

For both fluids, the friction coefficient plots indicate that run 5 deviated from the other 4 runs. This is shown in Figures 4.36 and 4.37. In Figure 4.36 run 5 had the lowest friction coefficient after the load increase. After about 22 minutes into the test, the friction coefficient increased rapidly, which most likely lead to a rapid increase in wear. It can also be seen on the profile of the wear track that run 5 had the largest $W_{q,flat}$ (Figure 4.38).

In Figure 4.37, no sudden event occurred for the friction coefficient of run 5. Run 5 however, had the lowest friction coefficient. As was the case for **Gr III + 2 % DES**, the profile on the wear track also deviated from the other 4 repeat runs (Figure 4.39).

Table 4.7: Wear volumes for scars and tracks for **Group III mineral oil, 6 cSt, (Gr III 6) with 2 % diethyl sebacate**. Values highlighted in green indicate largest deviation from the average.

Run	Scar Dimensions		Track Dimensions			Scar Calculations				Track Calculations	
	d_1 (mm)		d_2	d_3	d_4	$W_{q,flat}$	\bar{R}_s	$W_{v, ball}$ (mm ³)		\bar{R}_t	$W_{v, flat}$
	Meas.	Adj.	(mm)	(mm)	(mm)	(mm ²)	(mm)	Meas.	Adj.	(mm)	(mm ³)
1	0.558	0.550	0.602	1.604	0.594	0.00209	8.723	4.74E-04	4.60E-04	8.366	2.84E-03
2	0.582	0.567	0.634	1.622	0.630	0.00224	9.467	6.31E-04	5.98E-04	9.302	3.05E-03
3	0.583	0.535	0.658	1.592	0.641	0.00295	8.035	5.45E-04	4.59E-04	7.442	3.90E-03
4	0.588	0.556	0.639	1.622	0.644	0.00237	9.169	6.31E-04	5.64E-04	9.368	3.21E-03
5	0.593	0.545	0.643	1.593	0.638	0.00323	6.865	3.89E-04	3.28E-04	6.690	4.28E-03
AVG	0.581	0.551	0.635	1.607	0.629	0.00258	8.452	5.34E-04	4.82E-04	8.234	3.46E-03
STDEV	0.013	0.012	0.021	0.015	0.020	0.00049	1.038	1.04E-04	1.06E-04	1.168	6.08E-04

Table 4.8: Wear volumes for scars and tracks for **polyalphaolefin, 6 cSt, (PAO 6) with 0.5 % ZDDP**. Values highlighted in green indicate largest deviation from the average.

Run	Scar Dimensions		Track Dimensions			Scar Calculations			Track Calculations		
	d_1 (mm)		d_2	d_3	d_4	$W_{q,flat}$	\bar{R}_s	$W_{v, ball}$ (mm ³)		\bar{R}_t	$W_{v, flat}$
	Meas.	Adj.	(mm)	(mm)	(mm)	(mm ²)	(mm)	Meas.	Adj.	(mm)	(mm ³)
1	0.424	0.424	0.452	1.531	0.420	0.000375	20.460	2.72E-04	2.72E-04	16.474	5.23E-04
2	0.453	0.453	0.464	1.548	0.458	0.000260	32.217	3.68E-04	3.68E-04	30.871	3.59E-04
3	0.431	0.431	0.411	1.545	0.404	0.000360	16.113	2.13E-04	2.13E-04	15.244	5.15E-04
4	0.431	0.431	0.405	1.545	0.458	0.000273	20.358	2.26E-04	2.26E-04	29.358	3.77E-04
5	0.437	0.437	0.430	1.549	0.421	0.000138	47.900	3.09E-04	3.09E-04	45.106	1.96E-04
AVG	0.435	0.435	0.432	1.544	0.432	0.00028	27.410	2.78E-04	2.78E-04	27.41	3.94E-04
STDEV	0.011	0.011	0.025	0.007	0.024	0.00009	12.929	6.33E-05	6.33E-05	12.21	1.34E-04

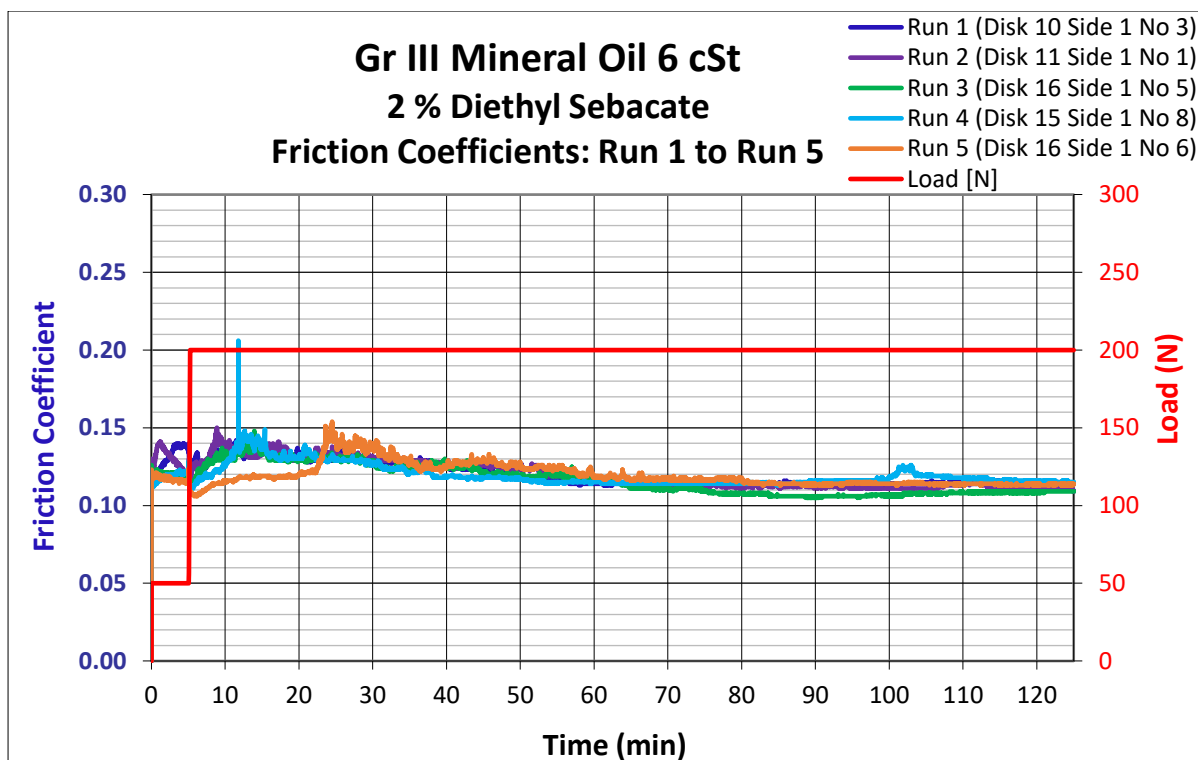


Figure 4.36: Friction coefficient measurements for **Group III mineral oil 6 cSt (Gr III 6)** with **2 % (mass basis) diethyl sebacate**.

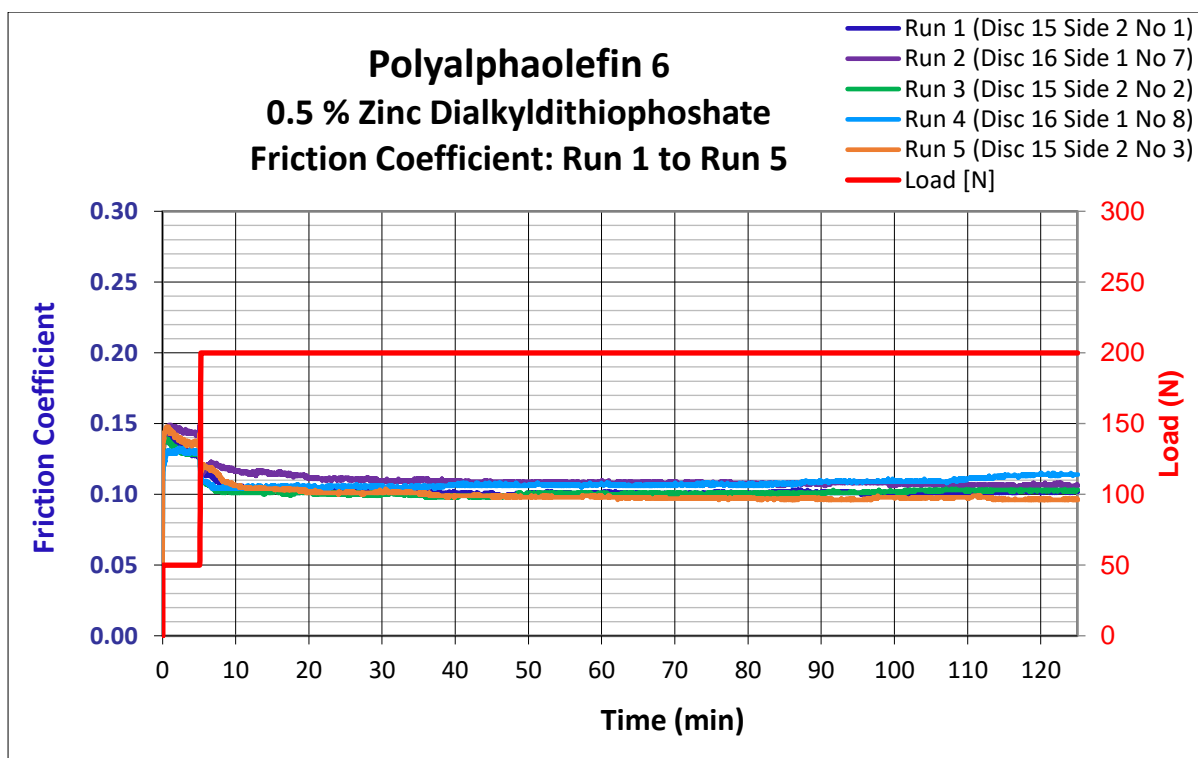


Figure 4.37: Friction coefficient measurements for **polyalphaolefin, 6 cSt, (PAO 6)** with **0.5 % (mass basis) ZDDP**.

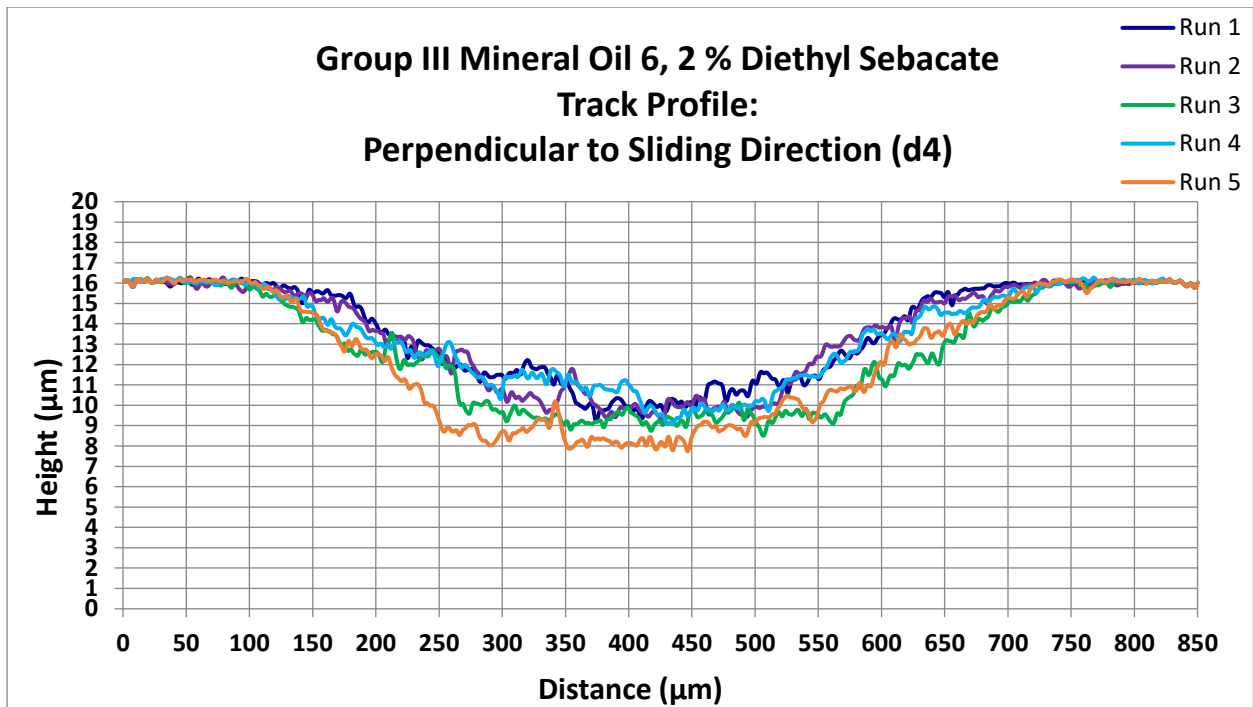


Figure 4.38: Wear track profiles perpendicular to sliding direction for **Group III mineral oil, 6 cSt, (Gr III 6) with 2 % diethyl sebacate.**

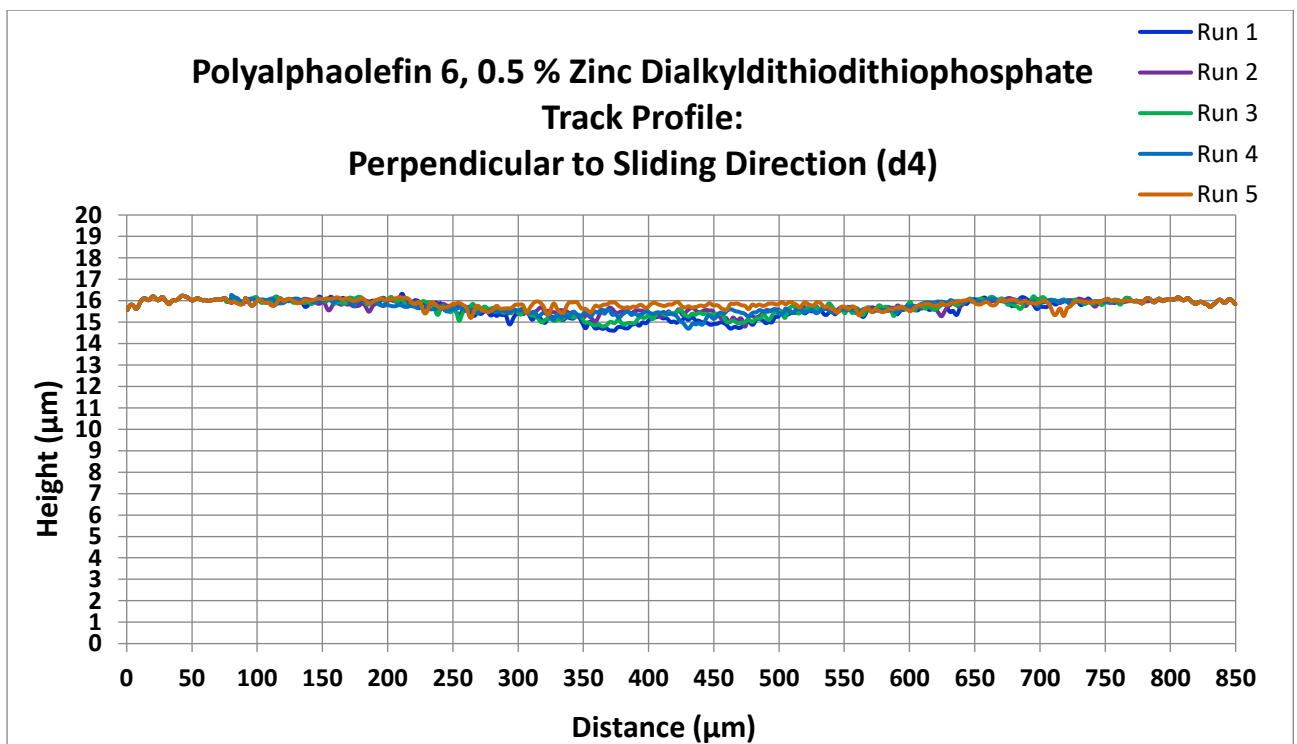


Figure 4.39: Wear track profiles perpendicular to sliding direction for **polyalphaolefin, 6 cSt, (PAO 6) with 0.5 % ZDDP.**

4.1.2.7 Effect of the Additive

This section will only focus on the four test fluids with synthetic base oils:

1. **PAO 6 + 3 % DES**
2. **PAO 6 + 0.5 % DES**
3. **PAG 146 + 0.5 % DES**
4. **PAG 146 + 0.5 % ZDDP.**

The effects of the additive that have been observed will be discussed. These are:

1. Effect on repeatability on the extent of wear.
2. Effect on the wear profile repeatability.
3. Effect on the friction coefficient repeatability.
4. Effect on the wear surface.
5. Effect on the wear scar diameter ratios.

In terms of repeatability of the extent of wear on the wear scar as well as the wear track volume, no real effect was seen for the **PAG-based oil** when **DES** was replaced with **ZDDP**. This was most likely due to the high viscosity of the base oil. For the **PAO-based oils**, repeatability of the extent of wear was better for the test fluid with **ZDDP**.

ZDDP chemically bonds to the metal surface and therefore forms a stronger boundary film compared to **DES**. This provides better protection of the surfaces and reduce surface interactions. The same principle applies as for the viscosity of the test fluid, where the reduction of surface interactions decreases the probability of surface deviations. Consequently, better repeatability is obtained.

When the wear surface profile radii are compared (Figures 4.15 and 4.17), the **PAO 6 + 0.5% DES** showed by far the worst repeatability. Since this base oil has a lower viscosity compared to **PAG 146**, it will certainly have more surface interactions and so poorer repeatability. Also, the values of radii are much larger compared to the **DES** fluids and **PAG 146** also had a larger radius. In general, deviations for larger values may appear more severe compared to deviations of smaller values. Care must therefore be taken when interpreting these results. The effect of poor repeatability for

the profile radius of **PAO 6 + 0.5% ZDDP** is reduced by the better repeatability of the wear scar diameters. The wear volumes in equations 3.3 and 3.5 are directly proportional to the square of both wear scar diameters (parallel and perpendicular to sliding) and indirectly proportional to the wear profile radius.

The wear profiles for the **PAG 146 base fluids** show how the **ZDDP** resulted in smoother profiles with better repeatability. This also confirms the better protection that is provided by **ZDDP** which reduces the surface interactions. Furthermore, the improvement in repeatability of the final value of the friction coefficient between **PAO 6 + 0.5% ZDDP** and **PAG 146 + 0.5% ZDDP** indicates that the consistency of the wear profile is important for good repeatability.

The most notable effects of the additives on the wear surface are the of severity of wear, the extent to which the wear scar border is exceeded and the translucent green layer. **ZDDP's** superior boundary performance compared to **DES** is responsible for the lower degrees of severity and extent to which the scar border is exceeded. The translucent green layer is the glassy Fe/Zn polyphosphate layer (Johnson & Hills, 2013).

When the diameter ratio of the wear scar diameters is considered (Figure 4.22), the ratio obtained for the test fluids with **ZDDP** is equal to 1, i.e., circular. The wear scar ratios for the test fluids with **DES** as additive, however, was more ellipsoidal. Therefore, wear on the scars for the fluids with **DES** as additive was pronounced in the direction perpendicular to the sliding direction. On the wear scars for the **ZDDP** containing fluids the wear was equal in both directions.

The reason for the wear that occurs predominantly in the direction parallel to the sliding direction is due to the centre area of the scar that is in constant contact with the track (see Figure 4.40). This is due to the sliding, reciprocating motion. The ability of the tribofilm to resist the shear forces and prevent metal to metal contact then plays an important role. The **ZDDP** reacts with the surface to form a tribofilm which is much more effective than the **diethyl sebacate** that only physically adsorbs onto the surface. Consequently, the extent of wear for the **DES** containing fluids was more pronounced in the direction perpendicular to the sliding direction.

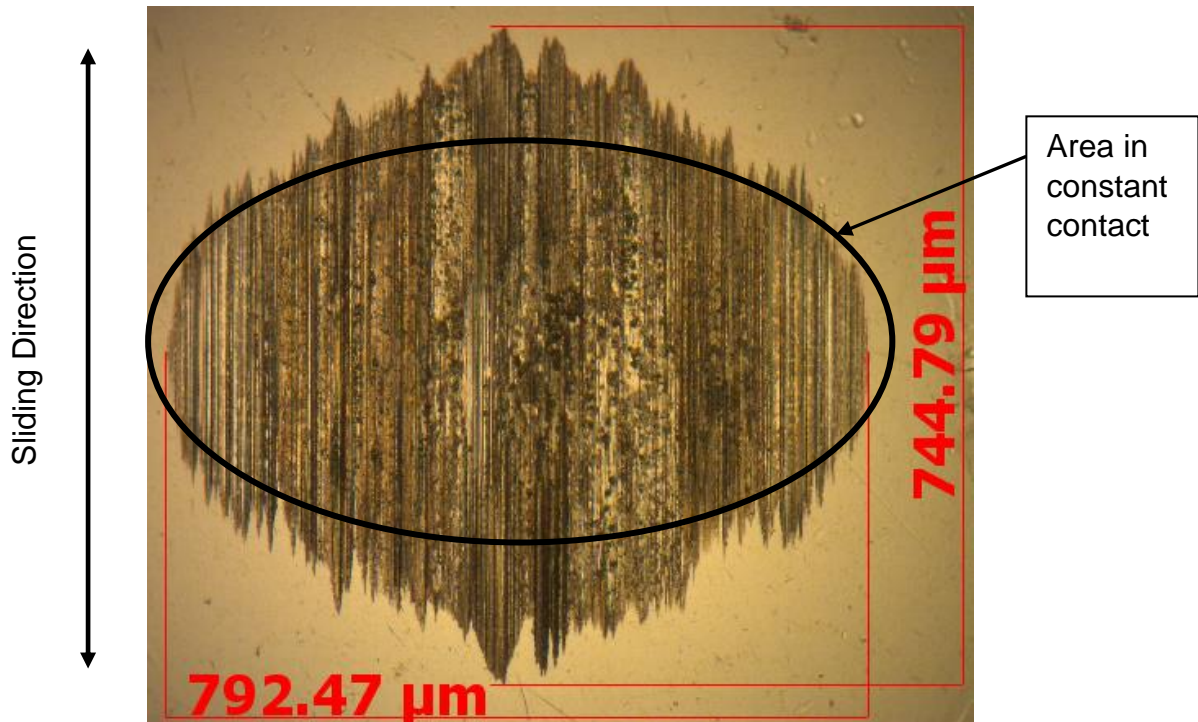


Figure 4.40: Estimation of the area of wear scar that is in constant contact with the wear track.

The circular shape of the test fluids with **ZDDP** can also be related to the size of the apparent contact area for a sphere on a flat at the start of the test. The apparent contact area diameter for a sphere on a flat is determined by the equations described in Batchelor & Stachowiak, 2003: 289-293. This is for an unlubricated contact with no motion. Even though the surfaces are in relative motion, this will give an indication of the apparent area. The contact parameters for the operating conditions on the SRV are calculated in Table 2.2.

The apparent contact area diameter at 200 N is estimated to be equal to 374 to 388 μm. The wear scar diameters for the two **ZDDP** containing fluids were 430 μm (**PAO 6**) and 420 μm (**PAG 146**). These values were only slightly larger than the apparent contact area. This indicates that wear occurred mainly on the apparent contact area and that the wear predominantly occurred during early stages of the test.

4.1.2.8 Wear Scar Diameter Adjustment

When the wear scar was adjusted with the method as described in section 3.5.3, in the direction parallel to the sliding direction, repeatability of the wear scar diameter and the ball wear scar volume showed a small improvement. This was also the case for the **PAG 146-based oils**, which already have good repeatability.

The wear scar diameter improvement was not as effective for the ball wear scar volume. This is due to the volume calculation which also includes the wear profile area and the planimetric wear area. Deviations in these 2 parameters will also contribute to repeatability.

The biggest improvement in repeatability was seen for the **WMO + 0.5 % DES**. From Tables 4.4.1 to 4.4.8, the boundary was exceeded to the highest degree for **WMO + 0.5 % DES**. Furthermore, the biggest decrease in WSD was also seen for this fluid.

PAO 6-based oils, however, had poorer repeatability with the wear scar adjustment. This shows that the method does not necessarily improve repeatability of the extent of wear. It does contribute to the certainty and accuracy of the extent of wear. This is due to the wear scar diameter that will be overestimated if the diameter is measured from tip to tip. This is shown in Figure 4.41.

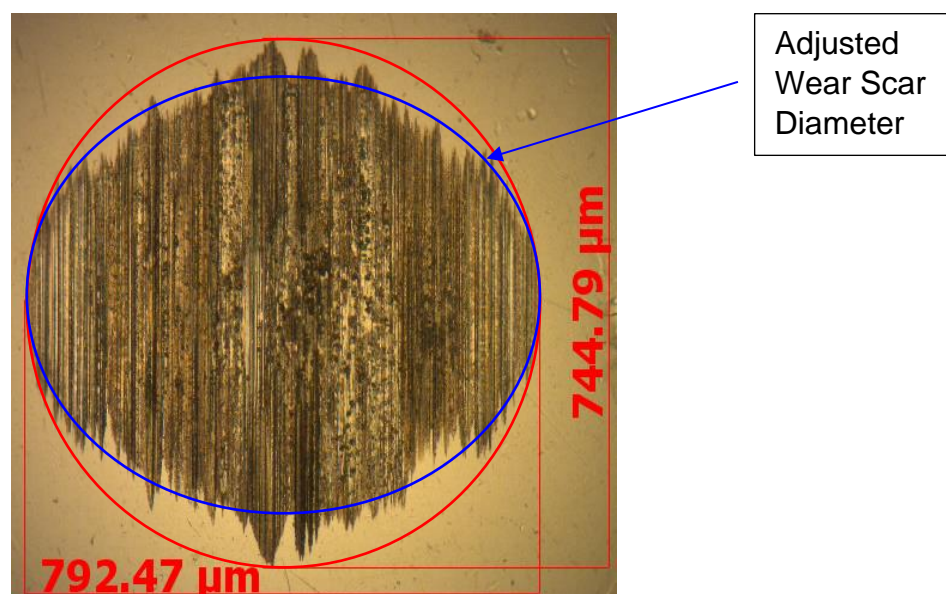


Figure 4.41: Adjustment of wear scar diameter.

4.1.3 Influence of Step Load Increase

In this section, the effect of the step load increase will be discussed. In Figure 4.42.a to h, the first 40 minutes of the friction coefficient graphs is presented. The friction coefficient range on the y-axis is limited to 0.1 to 0.2 (compare to 125 minutes where the friction coefficient range is 0 to 0.3 in Appendix B.1). The load is not represented in these graphs, but all 5 repeat runs are given:

Run 1 = dark blue

Run 2 = purple

Run 3 = green

Run 4 = light blue

Run 5 = orange

From these graphs certain characteristics can be identified for each of the test fluids. Some of the characteristics were the same for all the test fluids while others were fluid specific:

1. After the load was increased to 200 N, all the friction coefficient graphs were subjected to a step decrease. This was true irrespective of the base oil or the additive used.
2. After the step decrease, the value of the friction coefficient increased again to a maximum. The duration until the maximum value was reached was different for all the test fluids and depended on the viscosity of the base oil and the additive used. The friction coefficient graphs also went through a few transitions until the maximum value was reached, except for the **PAG-based oil with ZDDP**.
3. After the maximum friction coefficient value was reached, a gradual decrease could be seen. For the two **PAG-based fluids**, however steady state was reached shortly after the running-in period. Steady state was not reached by the end of 40 minutes for the other test fluids.
4. The behaviour during the first 5 minutes (running-in period) were different between the repeat runs for **Group III 6 + 2 % DES, PAO 6 + 3 % DES, Group II 100 + 2 % DES** and **PAO 6 + 0.5 % ZDDP**. The behaviour between the repeat runs for the other 4 test fluids were similar (**WMO + 0.5 % DES, Group II 100 + 2 % DES, PAG 146 + 0.5 % DES** and **PAG 146 + 0.5 % ZDDP**).

5. White mineral oil and the two **PAG-based oils** showed good repeatability for the first 40 minutes.
6. The polarity of the base oils played a role in repeatability of the friction coefficient after the step load increase. The base oils with higher polarity (**WMO and PAG 146**) showed better repeatability compared to the less polar base oils.

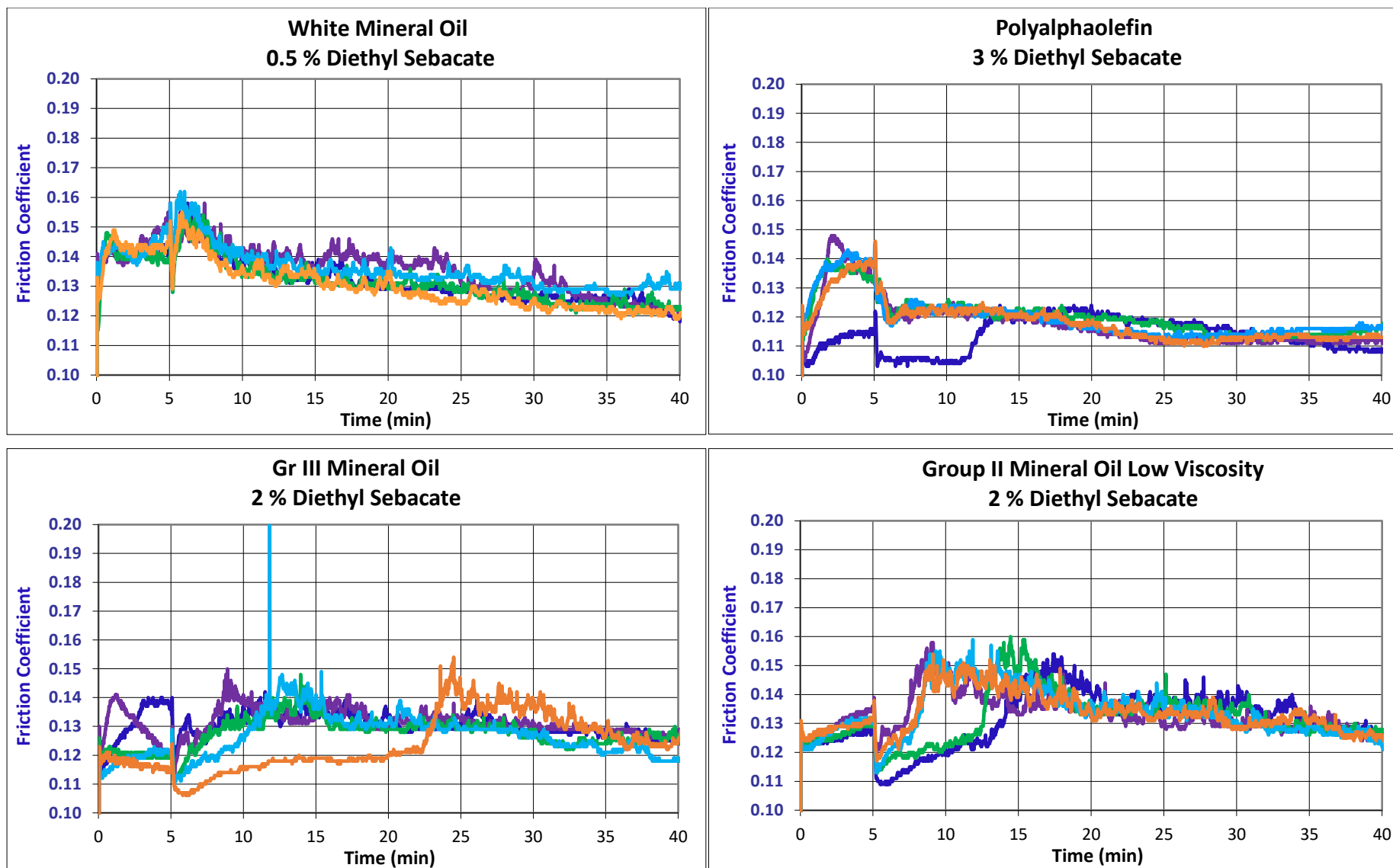


Figure 4.42.a-d: Friction coefficient graphs for repeat runs, first 40 minutes.

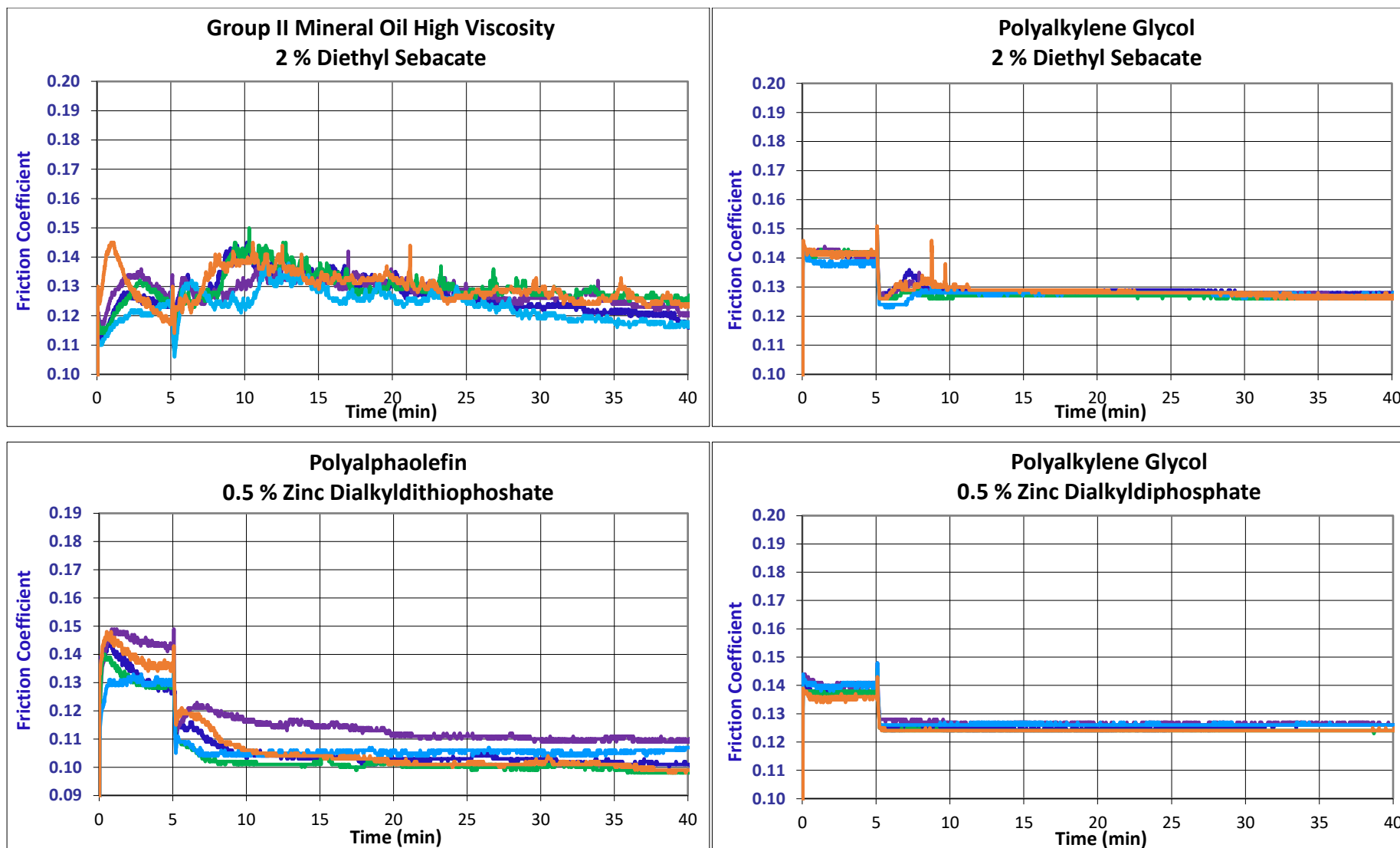


Figure 4.42.e-h: Friction coefficient graphs for repeat runs, first 40 minutes.

The friction coefficient is a ratio of the friction force and the load. The decrease in the friction coefficient after the load is increased, is therefore due to a decrease in the friction force. At this stage a few items need to be taken into consideration:

1. The friction force depends on the surface interactions and the viscosity of the oil (equation 2.3)
2. The apparent contact area diameter for a sphere on flat changes from 244 μm to 388 μm when the load is increased from 50 N to 200 N (Table 2.2).
3. When the load is distributed over a larger area, the load experienced between two contacting asperities experience will be smaller.
4. As the wear process progresses, the asperities shapes change from sharp peaks to more rounded peaks, i.e., the kurtosis decreases. Consequently, the load is supported by larger real contact areas between peaks.

When the load is rapidly increased, the apparent contact area therefore also increases. There is also an area between the circumferences of the apparent contact area at 50 N and the apparent contact area at 200 N where wear will now also occur. This is illustrated in Figure 4.43.

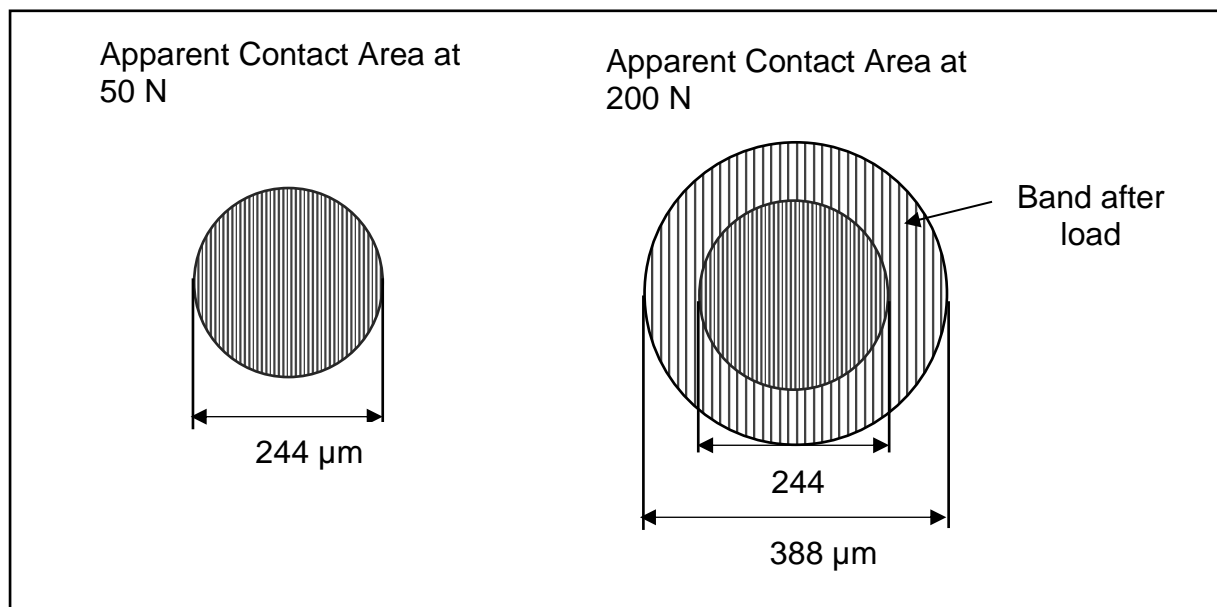


Figure 4.43: Apparent contact area at 50 N and 200 N for a sphere on a flat surface.

This unworn area is less rough than the apparent contact area at 50 N. At the same time the load is distributed over a larger area. Both these effects will reduce the friction force. As wear occurs on the new surface and the surface becomes rougher the friction

coefficient will increase. At a certain point, the friction coefficient reaches a maximum and then decrease. To understand what is happening at this stage, more information is required w.r.t the extent of wear and the wear profile.

However, the effect of the step load on the friction coefficient is that poor repeatability is obtained. This indicates that the interactions between the wear surfaces are not consistent between repeat runs. This was especially applicable for the less polar base oils. The less polar base oils' ability to form a boundary layer is not as effective as that of the more polar base oils. Consequently, the surface interactions for less polar oils will increase. This in turn will increase the probability for deviations to occur.

Rapid wear will also occur during the step load increase. This, together with the sudden change in the apparent contact area will result in the changes in the wear surface to be less controllable and will result in poor repeatability. Furthermore, high wear rates can also influence the microstructure of the metal surfaces (Pan et.al., 2018). Rapid wear leads to sub-surface plastic deformation of which the extent is non-uniform. This leads to variation of the surface hardness. Since the hardness also affects the friction and wear behaviour (Sadowski & Stupkiewics, 2019), variation in the friction coefficient can be obtained.

4.1.4 Influence of the Test Disk

In section 2.1.7 the influence of variations of test specimen surface properties on friction and wear results was summarised. The position of the wear scar on the disk specimen was therefore noted down for every test. The order in which the subsequent tests were done on a disk surface are shown in Figure 4.44. Both sides of the disk were used.

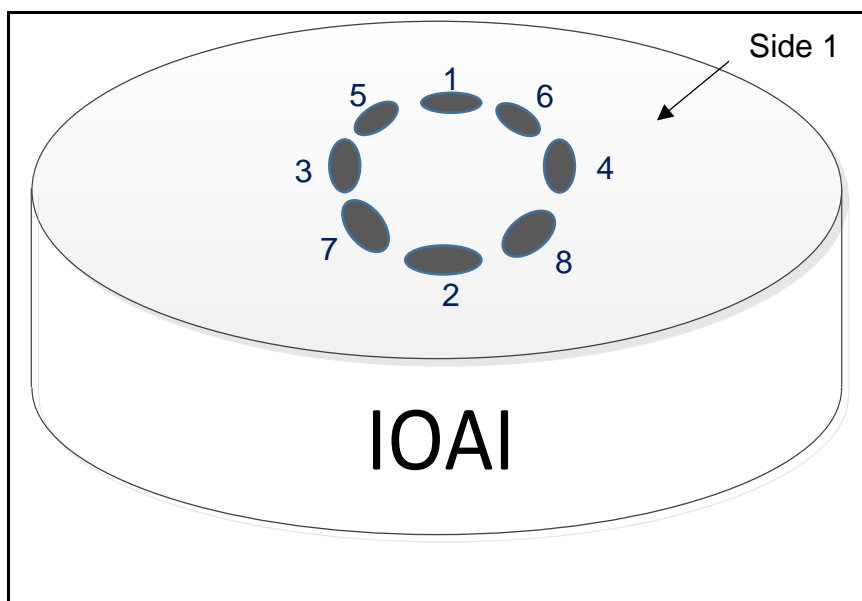


Figure 4.44: Position of wear scars on disk specimen, side 1.

The position of the wear scar on the disk as well as the friction and wear results for each repeat run for all the test fluids is given in Table 4.9. The format for the disk code in the second column is: disk number, side of disk and disk position. For instance, the disk code for the first run for **WMO + 0.5 % DES** is 6.1.8. This indicates that disk number 6 was used, on side 1 and position 8. The disk number is just an arbitrary number assigned to each disk used to differentiate between them.

In Table 4.9, the results for the extent of wear and the wear profiles are presented. For the friction coefficient and the wear surface, a number is assigned. This number indicates whether subsequent runs have similar results to that of the first one or not. These results include the friction coefficient graphs in Appendix B.1 and the wear surface images. For the first run the number 1 is assigned. If run 2 is similar to run 1, the number 1 is also assigned to run 2. If the friction coefficient graph or wear scar for the second run deviates from the second graph, the number 2 is assigned. Run 3 is compared to both run 1 and 2 and the number is assigned to which one it corresponds to. If it deviates from both, the number 3 is assigned. The same principle is applied to run 4 and run 5.

The repeat runs done on the same disk have been highlighted in light blue and pink in Table 4.9. For each of the test fluids the following can be observed:

1. **WMO + 0.5 % DES:** The extent of wear and wear profile showed better repeatability for the 2 runs done on the same disk. This was not true for the friction coefficient and wear scar appearance.
2. **PAO 6 + 3 % DES:** The two runs conducted on the same disk showed better repeatability for all the results compared to the other runs.
3. **Group III 6 + 2 % DES:** The two runs conducted on the same disk only showed good repeatability for the wear scar diameter and wear scar appearance.
4. **Group II 32 + 2 % DES:** All repeat runs were done on the same disk. Run 3 had wear volumes and wear profiles that varied considerably from the other repeat runs.
5. **Group II 100 + 2 % DES:** This fluid was evaluated on 2 disks. The wear volumes and the wear profiles for the runs done on disk 10 side 1 showed considerable variation. The rest of results indicated good repeatability.
6. **PAG 146 + 0.5 % DES:** All the results showed good repeatability except for the wear surface appearances for the test done on disk 12 side 1 (distribution of areas with no film).
7. **PAO 6 + 0.5 % DES & PAG 146 + 0.5 % ZDDP:** No effect of the disk could be seen.

From these observations, it seems that the disk does play a role in repeatability of the friction and wear results. This is true for test fluids with **DES** as additive. When **ZDDP** was used as additive, no effect was seen. The effect of the disk was also less evident with an increase in the viscosity. Inconsistencies are however also present, since the results obtained for test done on the same disk had poor repeatability.

Table 4.9: Influence of disk on test result. Disk code: Disk number, side of disk, position on disk.

Test Fluid	Disk	Friction Coefficient	Extent of wear			Wear Scar Appearance	Wear Profile	
			Wear Scar Diameter	Wear Scar Volume	Wear Track Volume		Profile Radius	Cross Sectional Area
			μm	$\times 10^{-3} \mu\text{m}^3$	$\times 10^{-3} \mu\text{m}^3$		mm	μm^2
WMO + 0.5 % DES								
Run 1	6.1.8	1	705	376	9296	1	5.95	6966
Run 2	7.2.5	2	738	554	10207	1	6.23	7630
Run 3	6.2.1	3	690	486	7472	2	6.43	5502
Run 4	6.2.2	4	696	496	7839	1	6.41	5725
Run 5	9.1.7	3	687	365	8130	3	6.03	6049
PAO 6 + 3 % DES								
Run 1	15.2.7	1	623	450	4740	1	7.24	3672
Run 2	16.2.5	2	656	531	5600	2	7.10	4292
Run 3	17.1.1	3	677	483	6854	1	6.57	5270
Run 4	17.1.2	3	676	463	6909	1	6.50	5322
Run 5	18.1.1	3	691	636	6724	2	7.05	5176
Group III 6 + 2 % DES								
Run 1	10.1.3	1	576	460	2840	1	8.72	7428
Run 2	11.1.1	2	600	598	3048	1	9.47	7284
Run 3	16.1.5	3	596	459	3903	2	8.03	7328
Run 4	15.1.8	3	598	564	3215	2	9.17	7450
Run 5	16.1.6	4	594	328	4280	2	6.87	9225
Group II 32 + 2 % DES								
Run 1	12.1.3	1	618	538	4243	1	8.09	3186
Run 2	12.1.4	2	626	588	4355	1	8.33	3273
Run 3	12.1.5	1	635	452	5169	1	7.01	3830
Run 4	12.1.6	2	604	467	4062	1	7.86	3018
Run 5	12.1.7	2	628	592	4344	1	8.26	3228

Table 4.9: (continued).

Test Fluid	Disk	Friction Coefficient	Extent of wear			Wear Scar Appearance	Wear Profile	
			Wear Scar Diameter μm	Wear Scar Volume $\times 10^{-3} \mu\text{m}^3$	Wear Track Volume $\times 10^{-3} \mu\text{m}^3$		Profile Radius mm	Cross Sectional Area μm^2
Group II 100 + 2 % DES								
Run 1	10.1.6	1	578	579	2404	1	10.73	1776
Run 2	10.1.7	1	577	493	2870	1	9.22	2144
Run 3	11.1.4	1	597	509	3399	1	8.52	2539
Run 4	10.1.8	1	595	522	3242	1	8.76	2425
Run 5	11.1.5	1	583	542	3025	1	9.72	2220
PAG 146 + 0.5 % DES								
Run 1	12.1.6	1	479	281	231	1	19.09	538
Run 2	12.1.7	1	465	298	211	2	17.28	568
Run 3	12.1.8	1	469	263	239	3	22.38	438
Run 4	12.2.1	1	472	254	264	2	20.52	506
Run 5	14.1.2	1	476	252	219	3	14.25	743
PAO + 0.5 % ZDDP								
Run 1	15.2.1	1	438	272	523	1	20.46	375
Run 2	16.1.7	2	459	368	359	1	32.22	259
Run 3	15.2.2	1	421	213	515	1	16.11	359
Run 4	16.1.8	3	418	226	377	2	20.36	273
Run 5	15.2.3	4	433	309	196	1	47.90	138
PAG + 0.5 % ZDDP								
Run 1	15.1.2	1	426	281	231	1	38.34	177
Run 2	16.1.1	1	432	298	211	1	39.77	162
Run 3	15.1.3	1	422	263	239	1	32.88	186
Run 4	16.1.2	1	419	254	264	1	31.46	194
Run 5	15.1.4	1	416	252	219	1	35.35	162

4.1.5 Summary of Repeatability

The factors that affect repeatability of the friction and wear results include the properties of the base oil and factors related to the test method. It was seen that the disk also plays a role. Another factor that has not been included in this investigation was the humidity in the atmosphere. This has already been investigated and proven that it does affect the friction and wear behaviour. It was therefore only controlled at a constant value.

The properties of the test fluid determine the extent of surface interactions. An increase in the amount of surface interactions increases the probability of surface deviations. This in turn can lead to surface deviations, which result in poorer repeatability. These properties are the base oil viscosity and viscosity index, base oil polarity and additive.

The method related factors that affect repeatability are the step load increase and the adjustment of the wear scar diameter in the direction parallel to the sliding direction. The sudden change in the apparent contact area and the rapid wear rate leads to poor repeatability. The wear scar adjustment improved repeatability, with a few exceptions. It can, however, also result in poorer repeatability. It does, however, improve the accuracy of the measurement.

4.2 Improving Repeatability

In this section, it is shown how the repeatability of the friction and wear test can be improved by replacing the step load increase with a gradual load increase. The load is gradually increased from 50 N to 200 N during the 5-minute running-in period at a rate of 30 N/min. This is shown in Figure 4.45. Runs with shorter durations are also included to determine how the extent of wear and the wear surface finish progress throughout the test. Only one test fluid was used, **Group III 6 with 2 % diethyl sebacate** and 4 repeat runs were done per test.

Each test was started on an unused surface, including the tests with shorter durations. The extent of wear was determined at the end of each test run. The next test run was done on a new surface. Each run for every test duration was also started on an unused surface. This is to prevent misalignment errors. The effect of the wear scar adjustment for **Group III** in section 4.1.2 was minimal. The wear scars were therefore not adjusted in this section.

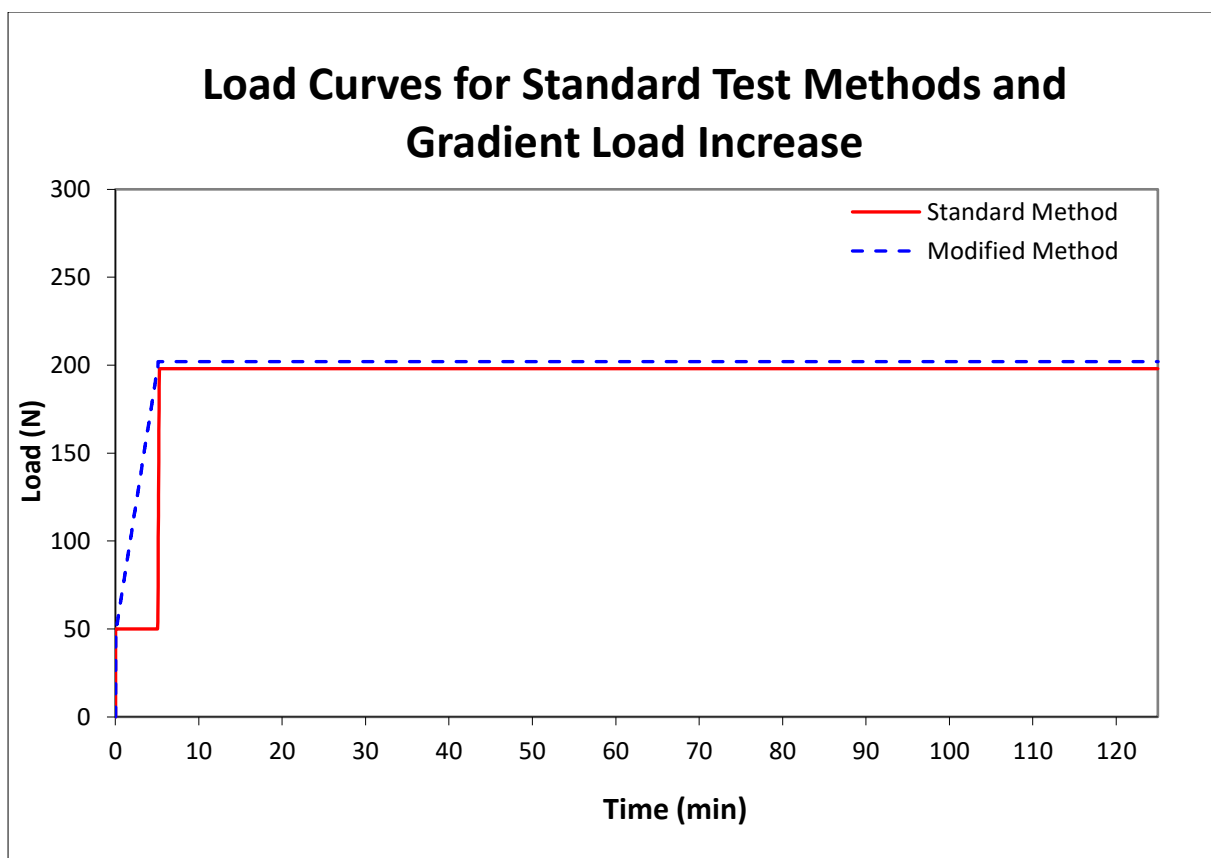


Figure 4.45: Load curves for the 2 test methods: standard test method (red) and gradient load increase (blue).

4.2.1 Extent of Wear

The extent of wear was calculated using equations 3.2 to 3.6. It is important to notice that the wear scar diameter is determined from the scar dimensions which are measured values. The wear volumes on the disk and ball, however, are calculated values. This includes the measured dimensions of the ball wear scar and disk wear track as well as the planimetric wear area of the disk. The planimetric wear area is determined perpendicular to the sliding direction from the profile of the disk wear track. The Mountains® 7 3D Analysis software was used for this purpose (see section 3.3.7).

4.2.1.1 Ball Wear Scar Diameter

The average for the ball wear scar diameters is given in Figure 4.46 for both the step load increase and the gradient load increase methods. In this figure, the diameter of the ball wear scars compared well for the 2 methods in terms of magnitude. The modification of the load increase procedure therefore did not increase the wear.

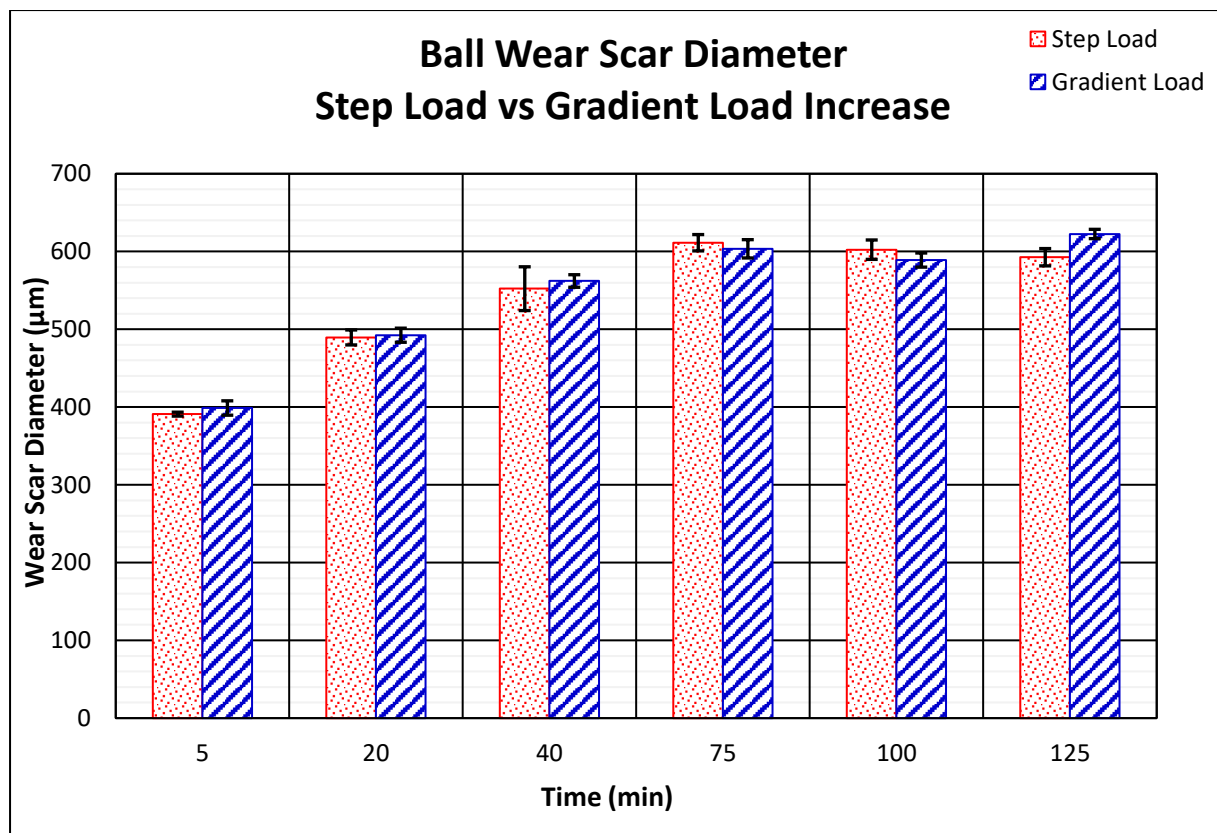


Figure 4.46: Average ball wear scar diameters for step and gradient load increase methods on the SRV test rig.

The standard deviation for the ball wear scar diameter is given in Figure 4.47. Repeatability improved when the modified method was used, with 2 exceptions. After 5 minutes there was a big difference and at 75 minutes, the step load had slightly better repeatability.

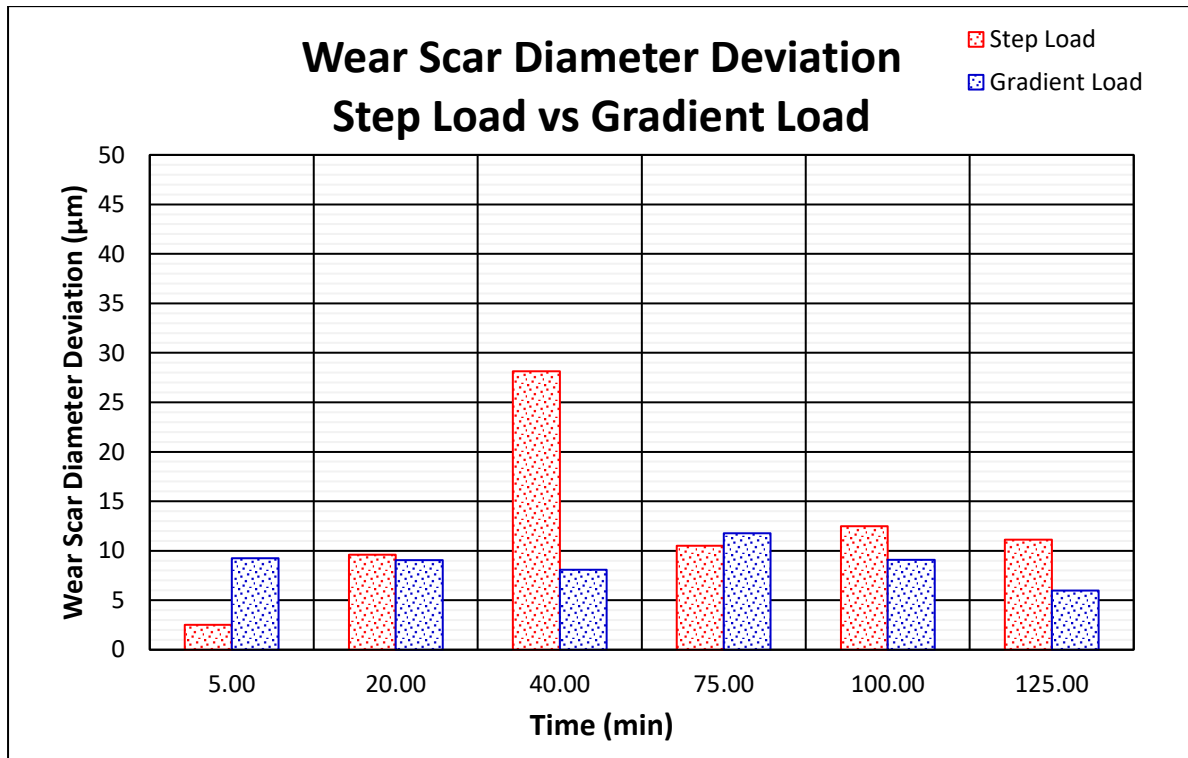


Figure 4.47: Standard deviation of ball wear scar diameter step load vs. gradient load (i.e., error bars from Figure 4.46).

4.2.1.2 Ball Scar Wear Volume

The wear volumes calculated for the ball wear scars are given in Figure 4.48. The wear volumes for both test methods were also similar in magnitude, as was the case for the ball wear scar diameters in Figure 4.46.

Deviations from the trend was observed for the wear volumes after a test duration of 75 minutes, i.e., the wear volume was lower than expected. It is important to take note that, due to the large number of tests that were performed (48), several disks were used to complete the test runs. The standard deviation for the ball wear scar volumes is given in Figure 4.49. Overall, repeatability for the gradient load was better than for the standard test method. The only exception to this is the smaller standard deviation obtained after 5 minutes for the step load as mentioned earlier.

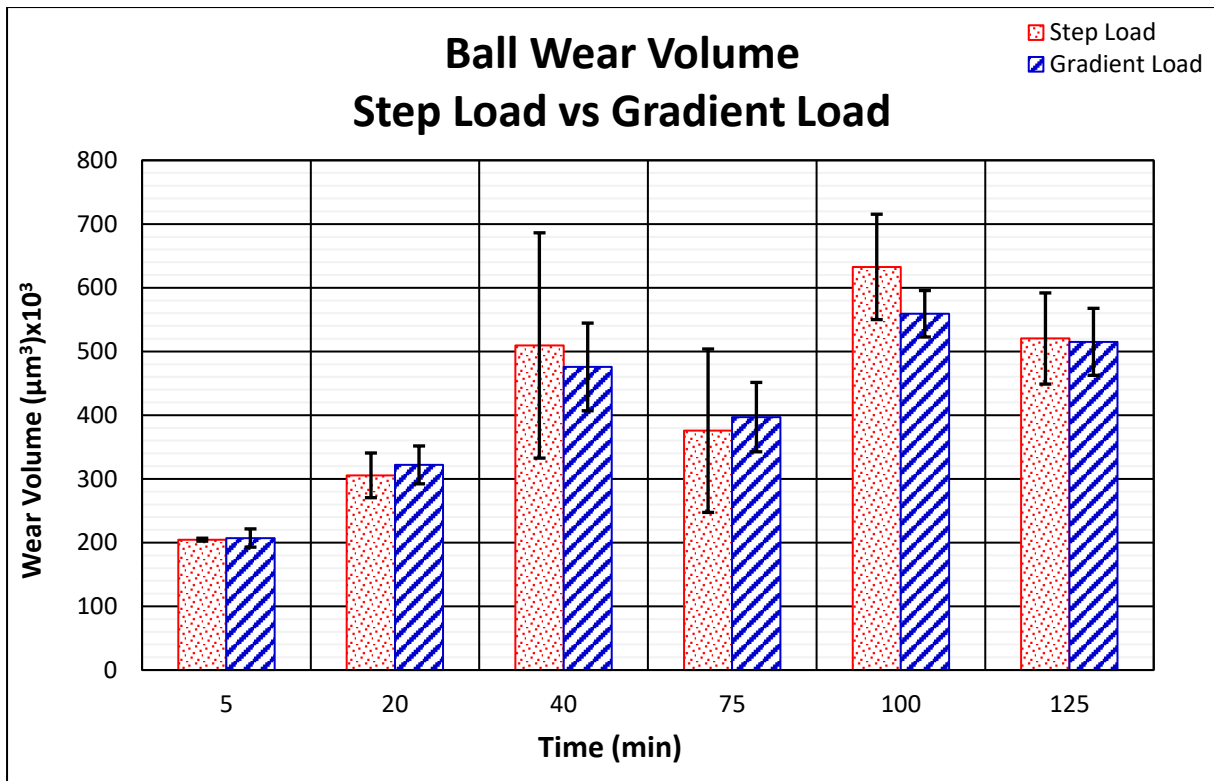


Figure 4.48: Wear volumes on the ball scar for step and gradient load increase methods.

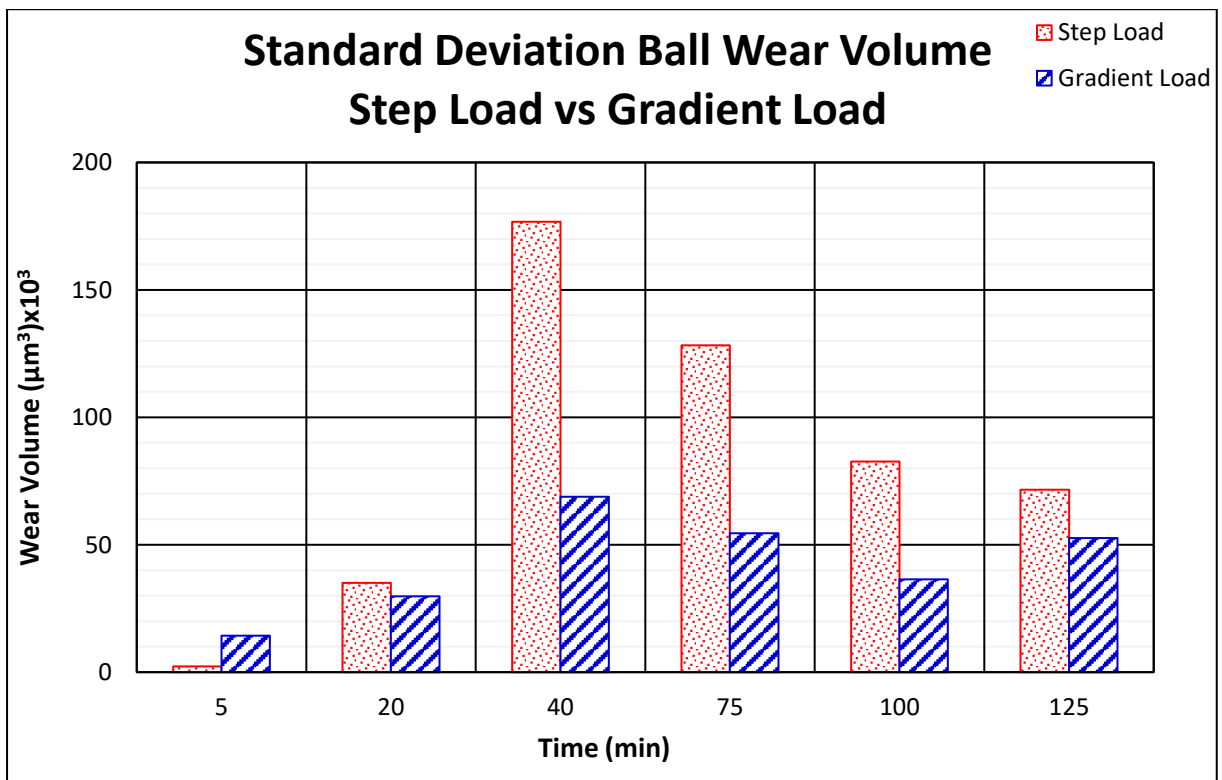


Figure 4.49: Standard deviation of wear volumes on the ball scar for step and gradient load increase methods (i.e., error bars from Figure 4.48).

4.2.1.3 Disk Track Wear Volume

The wear volumes calculated for the disk wear tracks are given in Figure 4.50 and repeatability gradient load increase in Figure 4.51. In Figure 4.51, repeatability at longer durations were better for the gradient load increase. The only exceptions were at 5 minutes and at 40 minutes. Also, the load increase did not affect the end results, since the magnitude of the wear volume calculated for both test methods were of the same order. Only for test duration of 100 minutes a significant difference was obtained in terms of the wear volume.

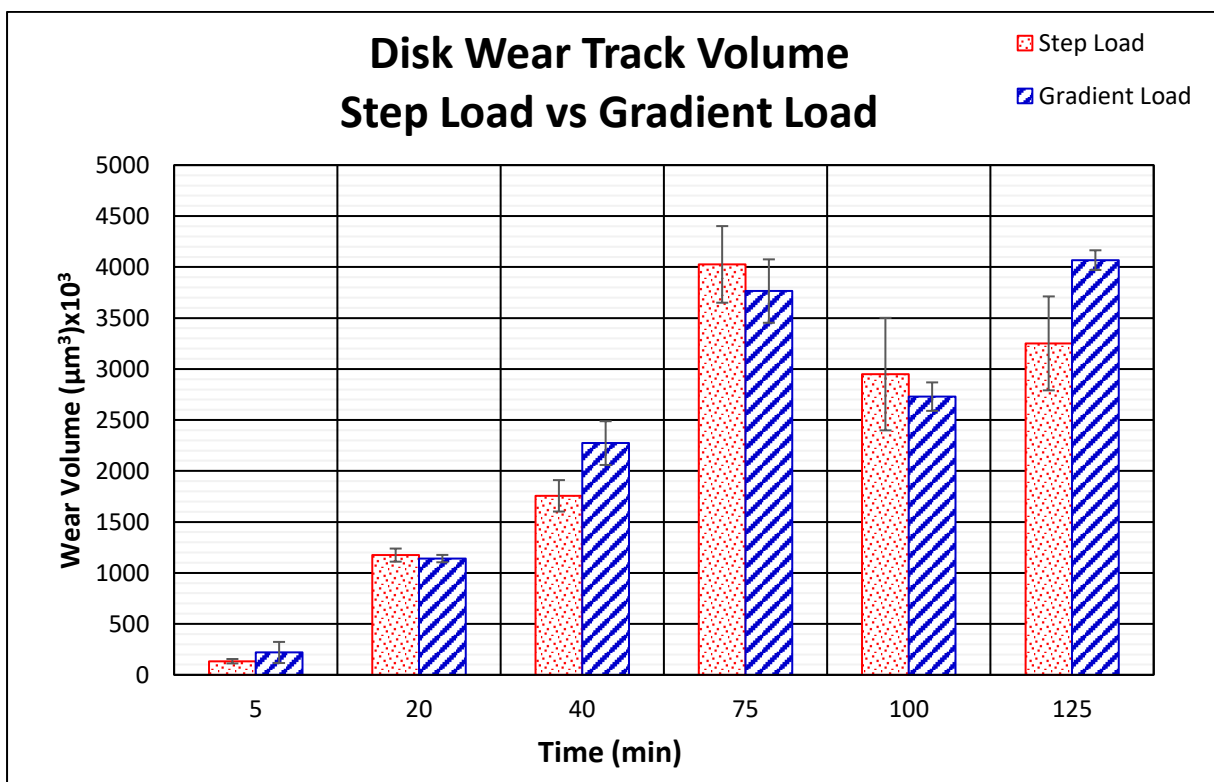


Figure 4.50: Disk wear track volumes on the track for step and gradient load increase methods.

During testing, all the procedures were meticulously followed, while the same test fluid was used for all test runs. The atmosphere in the test chamber was also controlled. Despite controlling the external factors that can affect results, deviations in the wear volume repeatability results on the disk were obtained.

The deviations in the wear volume results therefore indicate that there is still another factor that affects repeatability. As mentioned in the experimental section, multiple

disks were used to complete all the test runs. This therefore leaves a question about the effect of the test disks on the results, which will be addressed.

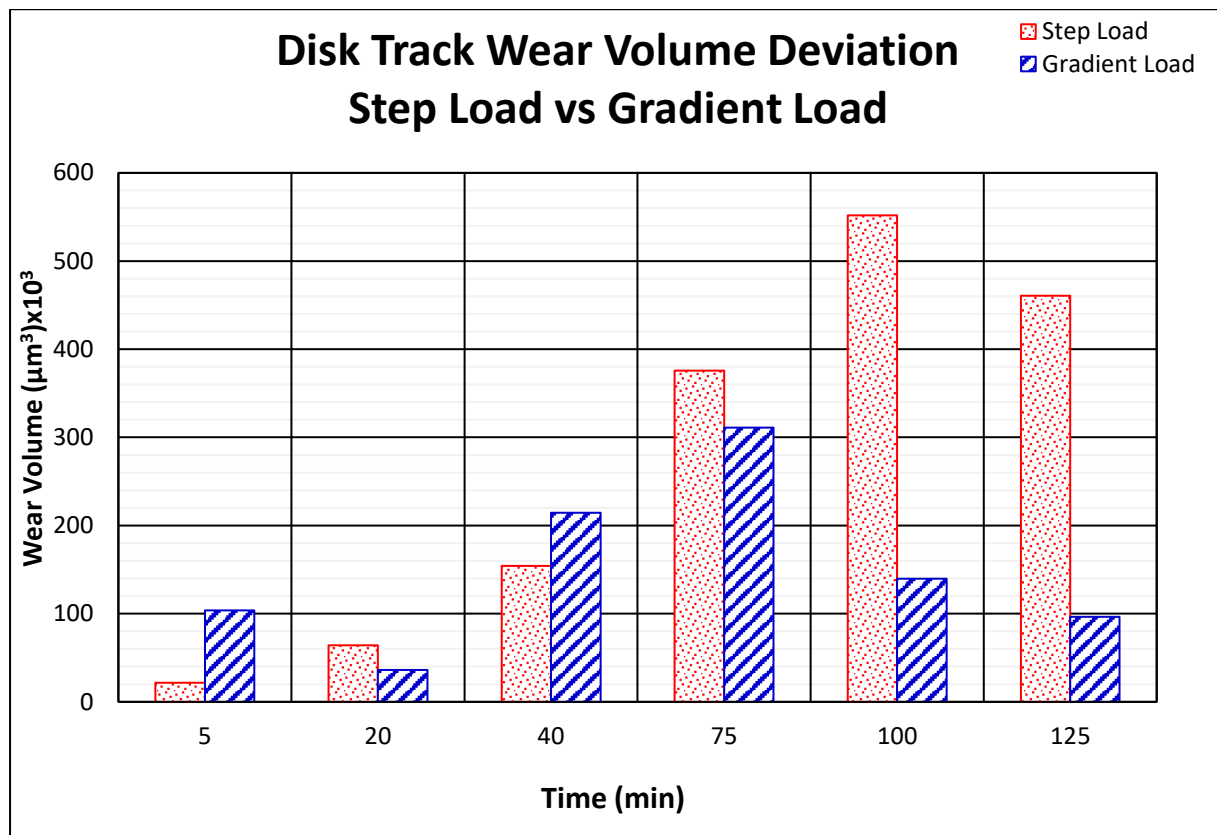


Figure 4.51: Standard deviation of wear volumes on the track for step and gradient load increase methods (error bars plotted from Figure 4.50).

4.2.1.4 Repeatability of Wear Volume Parameters

Overall, both the wear scar volume and the disk wear track had better repeatability with the gradual load increase. The wear volume calculation also includes wear profile radius and the planimetric wear area and not only the wear scar diameters. Therefore, repeatability of the parameters used to calculate the wear volumes will also be evaluated. This is:

1. Resulting radius of the shape of the wear profile (\bar{R}) of the ball wear scar.
2. Resulting radius of the shape of the wear profile (\bar{R}) disk wear track.
3. Planimetric wear area on the disk wear track, seen perpendicular to the sliding direction ($W_{q,flat}$).

These parameters for the 2 test methods are compared in Figures 4.52, 4.54 and 4.56. The standard deviations for each of these parameters are plotted in Figures 4.53, 4.55 and 4.57.

From these figures:

1. For the ball wear scar, the profile radius is initially large. It then rapidly decreases and do not change much from 20 minutes onward (Figure 4.52). The gradient load also had better repeatability, with the exception at 5 minutes test duration (Figure 4.53).
2. The same observation as in point 1 above is also true for the profile radius on the disk wear track (Figure 4.54 and Figure 4.55). The wear profile is therefore “flatter” initially and become more rounded as the test progresses. The biggest change, however, occurs before 20 minutes.
3. As it would be expected, the disk planimetric wear area increases as the test progress (Figure 4.56). There is notably a difference in the rate of change before and after 75 minutes. The biggest change occurs before 75 minutes. The gradient method also had better repeatability compared to the step load method (Figure 4.57). The only exceptions were at 5 minutes and at 40 minutes.

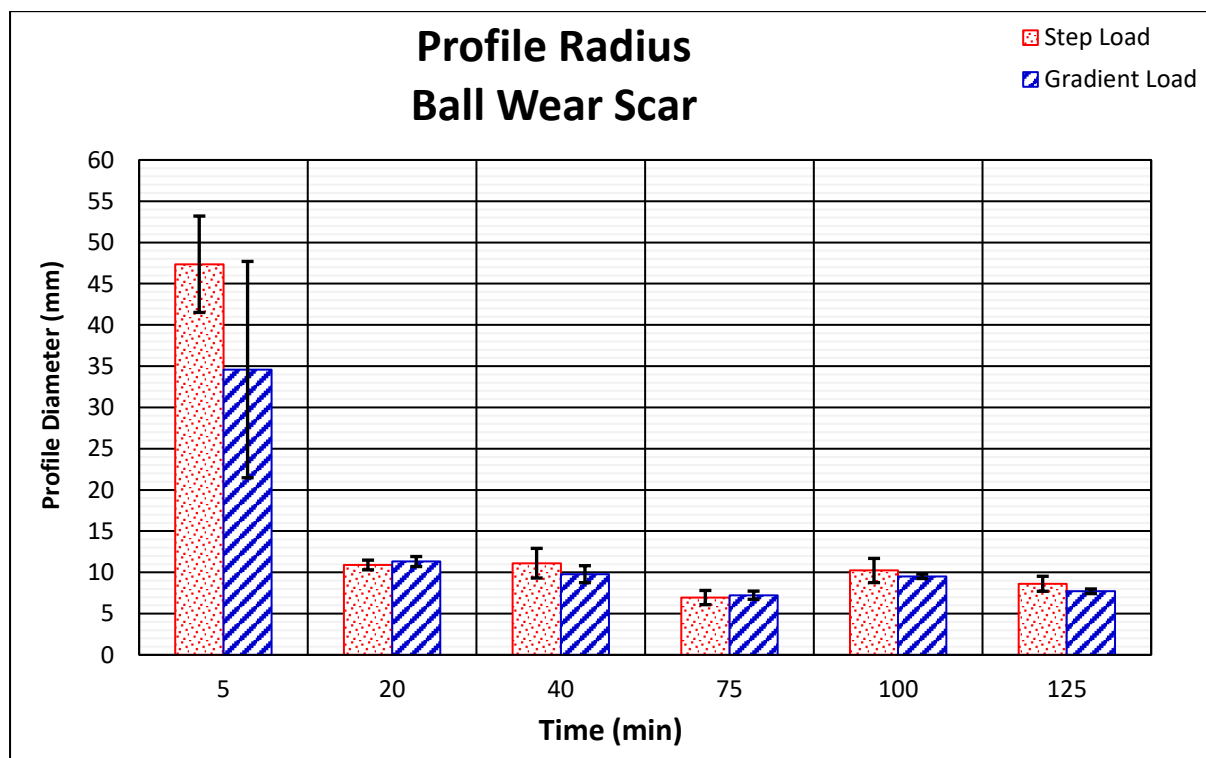


Figure 4.52: Ball wear scar profile radius.

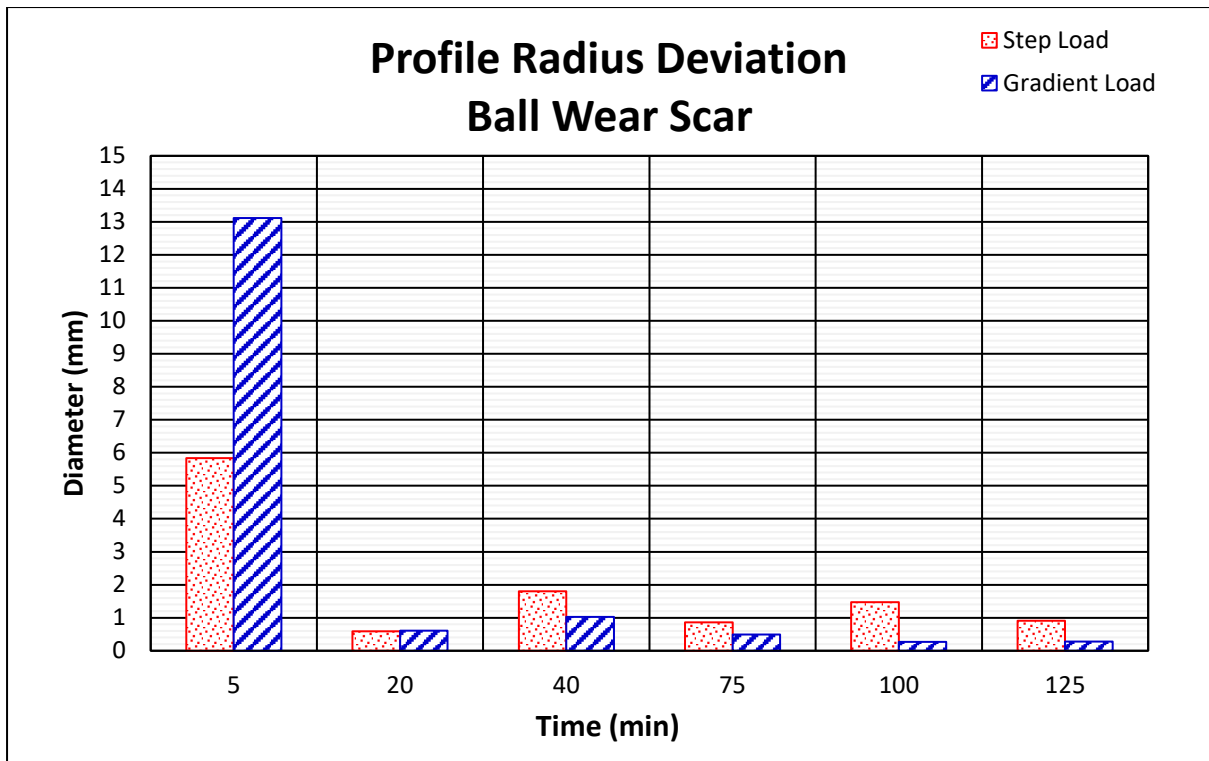


Figure 4.53: Standard deviation ball wear scar profile radius (error bars from Figure 4.52).

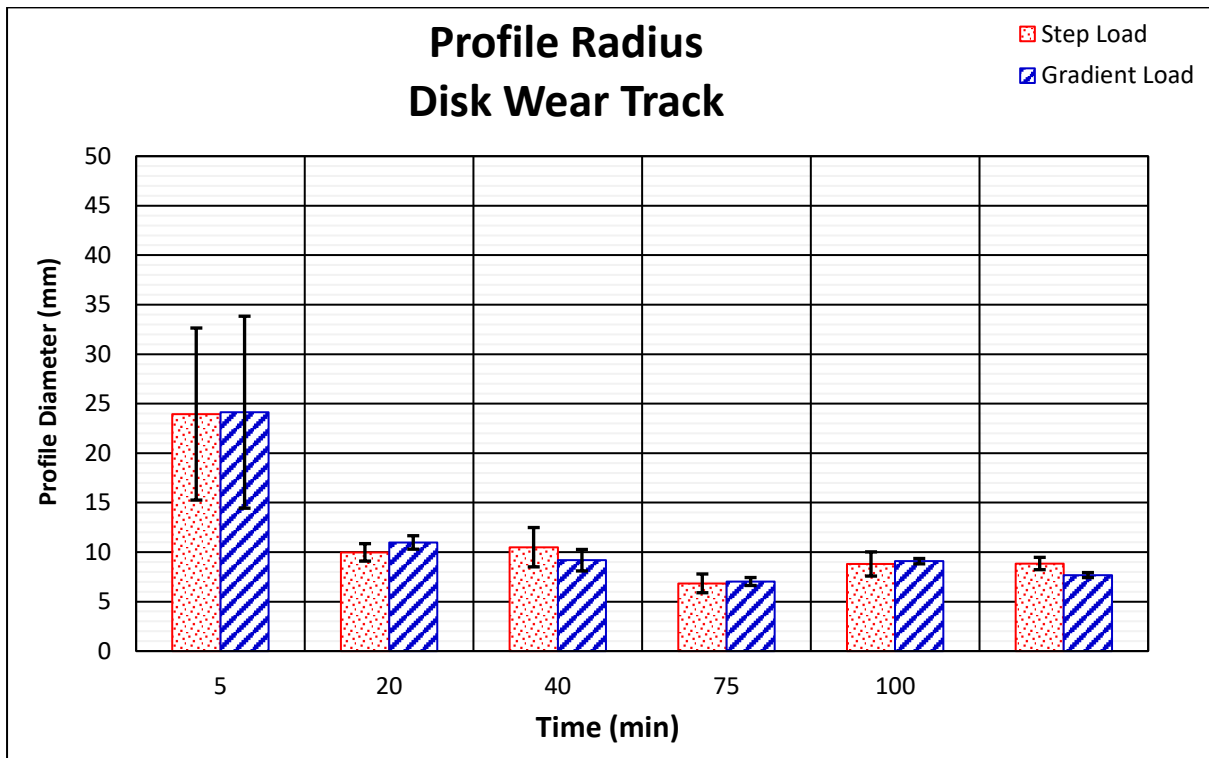


Figure 4.54: Disk wear track profile radius.

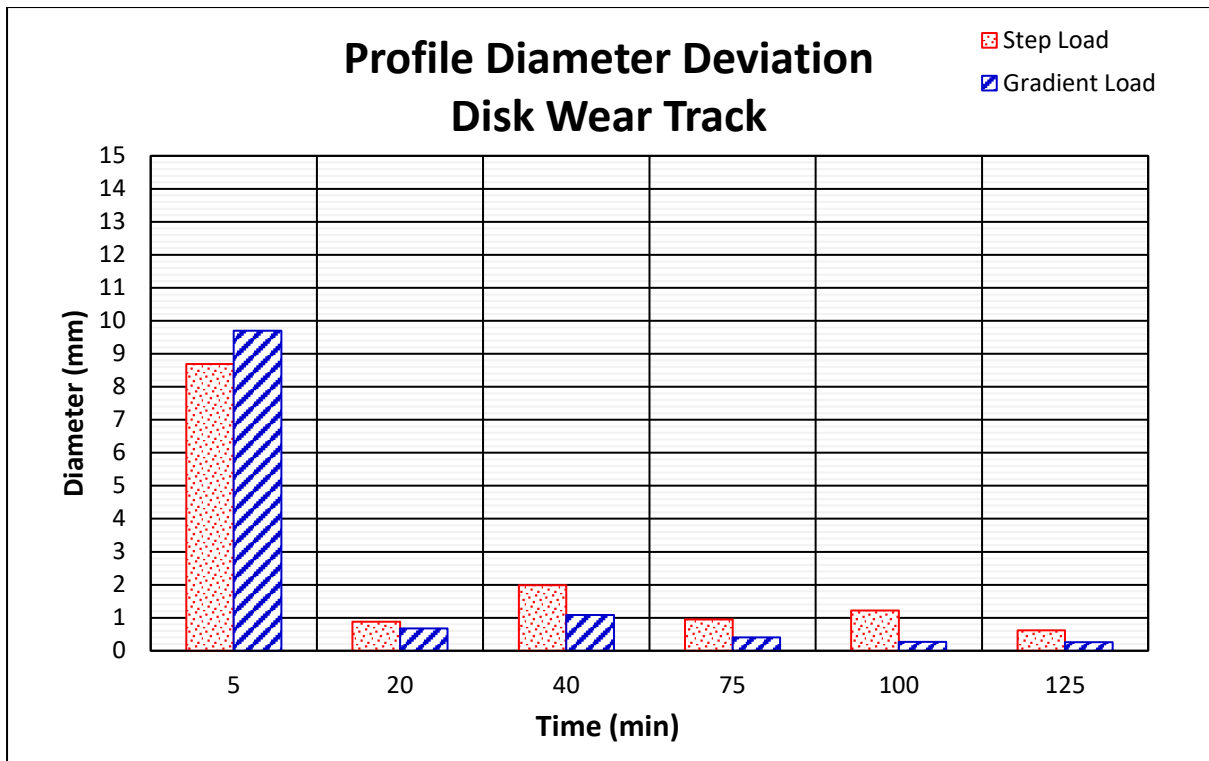


Figure 4.55: Standard deviation disk wear track profile radius (error bars from Figure 4.54).

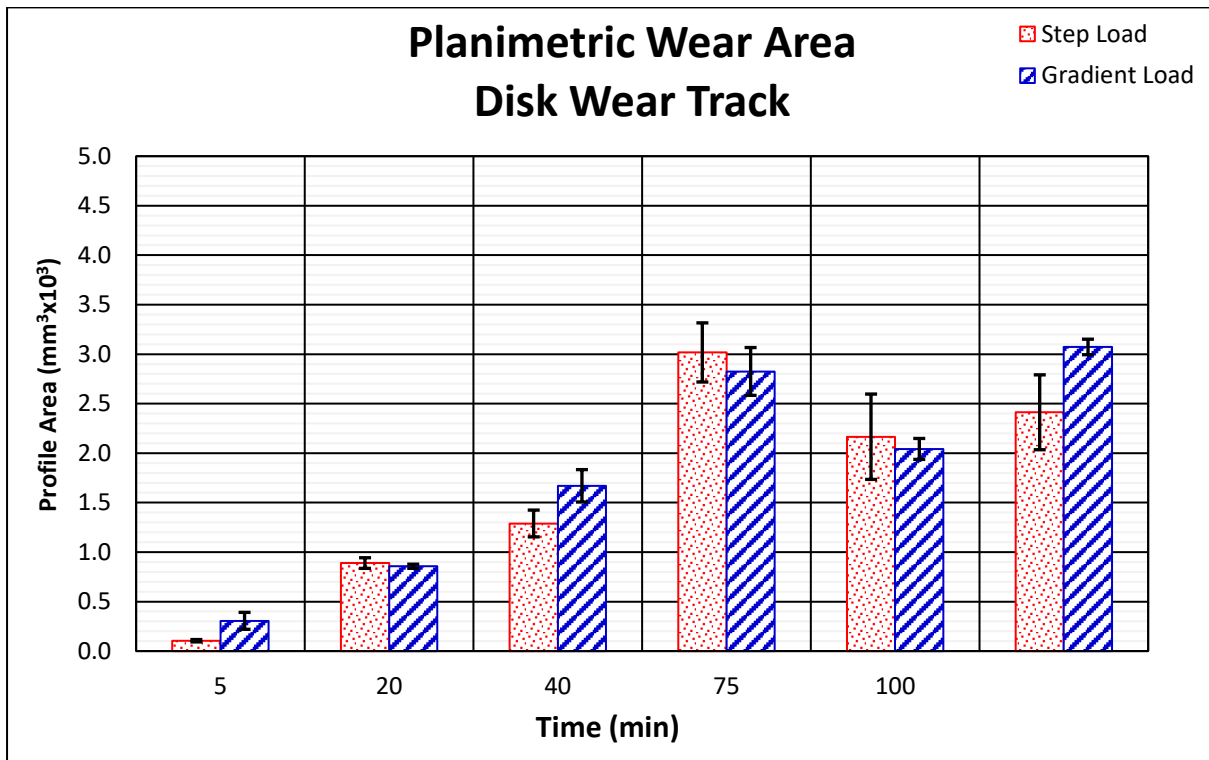


Figure 4.56: Planimetric wear area on the disk.

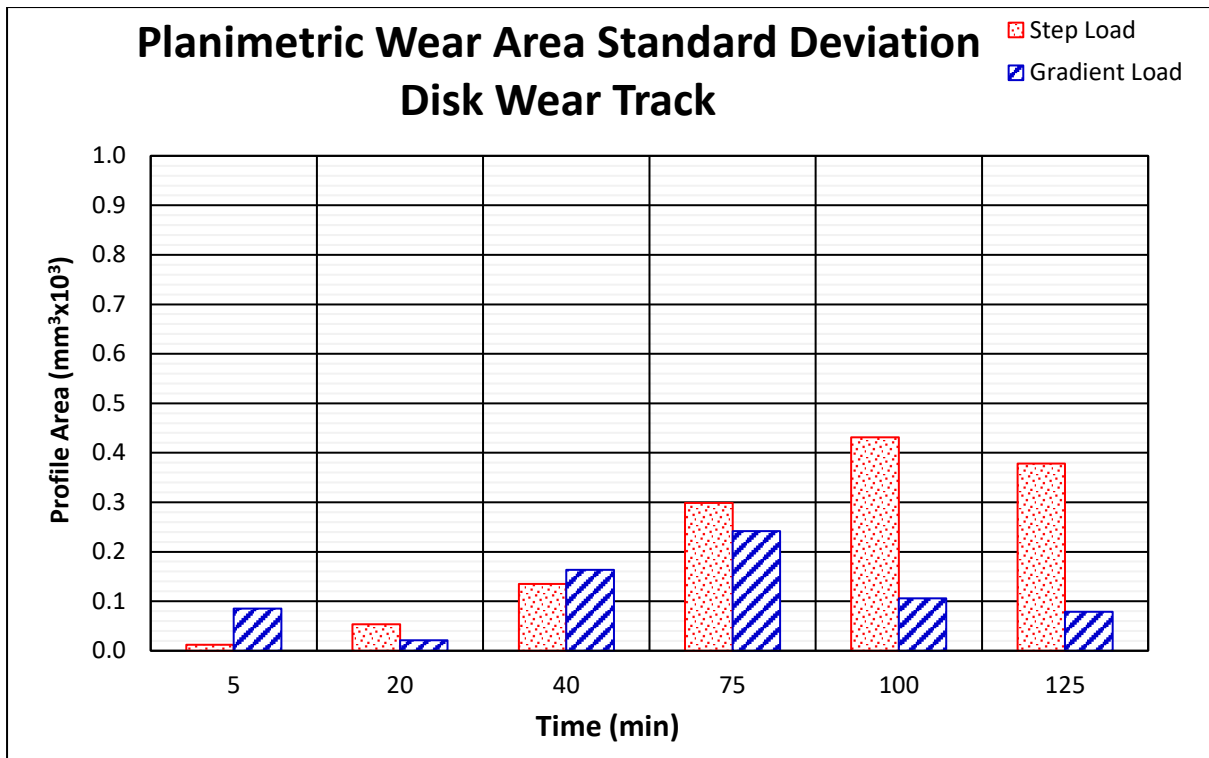


Figure 4.57: Standard deviation planimetric wear area on the disk (error bars from Figure 4.56).

4.2.1.5 Discussion: Repeatability of Extent of Wear

The results in the preceding sections indicate that the gradual load increase improves repeatability of the ball wear scar volume and disk wear track improved, as shown in Figure 4.47 and Figure 4.49. This was due to the wear profile variables that had better repeatability as shown in Figure 4.53, Figure 4.55, and Figure 4.57. The gradual load increase therefore improved the consistency of the wear profile. Since the wear scar diameter does not include the profile variables, the improvement in the wear scar diameter (Figure 4.47) was therefore not as significant as for the wear volumes.

Some exceptions for repeatability were also observed for test runs with duration 5 minutes, 40 minutes, and 75 minutes. These exceptions do not apply to every measurement technique. Each of these will be discussed below:

Test Duration: 5 minutes

For this test duration, the wear scar diameter, wear scar volume and the wear track volume had poorer repeatability for the gradient load increase. For the wear scar diameter, the measurement taken for the 1st run deviated from the other 3 and was responsible for the poorer repeatability. See Table 4.10 (Appendix C.5.12). This is also reflected in the wear scar volume.

For the wear track volume, run 2 and run 4 deviated from the other 3 test runs. For these 2 test runs, the planimetric wear area also deviated the most from the average. This can also be seen in Figure 4.58 for the wear profiles on the track. The profiles indicate that run 1 had the smallest $W_{q,flat}$.

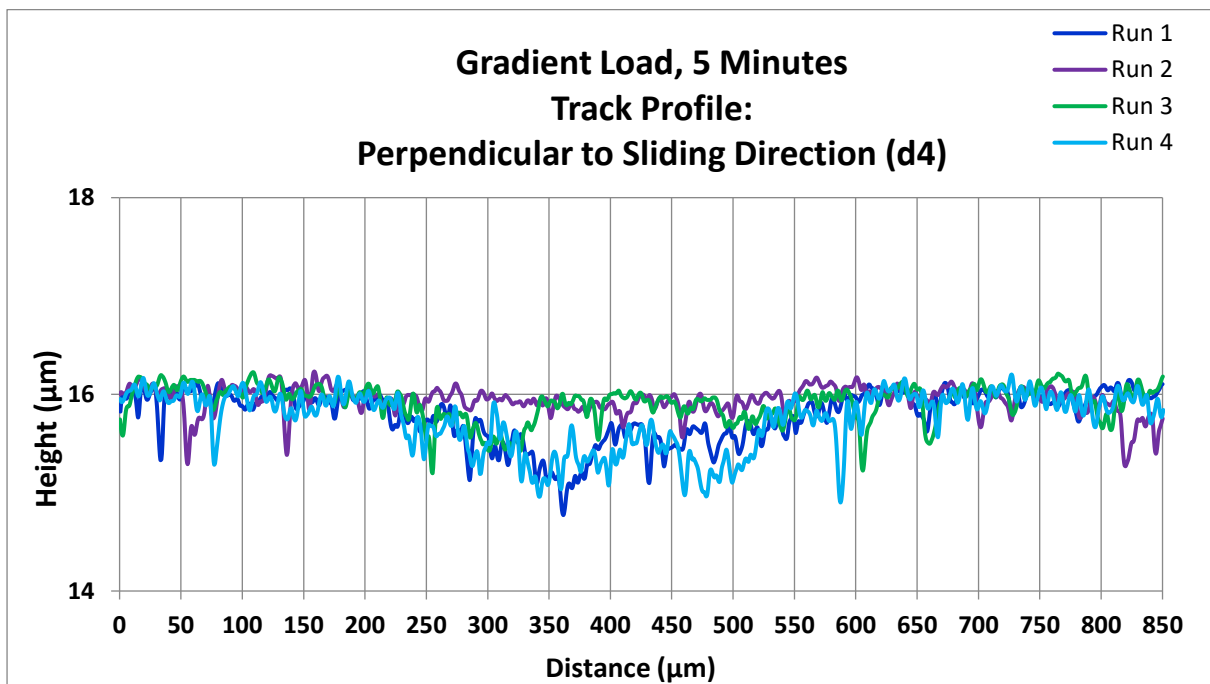


Figure 4.58: Wear track profiles on the disk for test duration of 5 minutes.

For convenience, the calculations of the wear volume on the ball and disk are repeated:

Wear Scar Volume (ball):

$$W_{v,ball} = \frac{\pi(d_1^2 \cdot d_2^2)}{64} \left(\frac{1}{R} - \frac{1}{\bar{R}} \right) \quad (3.3)$$

\bar{R} is calculated with:

$$\bar{R} = \frac{d_2^3}{12W_{q,flat}} \quad (3.4)$$

Where:

\bar{R}	Resulting radius of the shape of the wear scar after the test.	mm
R	Initial radius of the ball	mm
d_1	Wear scar diameter on the ball parallel to the sliding direction.	mm
d_2	Wear scar diameter on the ball perpendicular to the sliding direction.	mm
$W_{q,flat}$	Planimetric wear of the track of the wear track in the middle of the wear track length, seen perpendicular to the sliding direction (cross sectional area of profile).	mm ²

Wear Track Volume (disk):

$$W_{v,flat} = \frac{\pi d_4^2 (d_3 - s)^2}{64} \cdot \frac{1}{\bar{R}} + s \cdot W_{q,flat} \quad (3.5)$$

\bar{R} is calculated with:

$$\bar{R} = \frac{d_4^3}{12W_{q,flat}} \quad (3.6)$$

Where:

\bar{R}	Resulting radius of the shape of the wear track after the test.	mm
d_3	Total length of the wear track in the sliding direction.	mm
d_4	Width of the wear track.	mm
s	Stroke	mm

To establish the relationship between the wear scar and track dimensions with the wear volumes, equation 3.4 is substituted into equation 3.3 and 3.6 is substituted into equation 3.5. This yield:

$$W_{v,ball} = \left(\frac{\pi \cdot d_2^2}{64 \cdot R} - \frac{3\pi \cdot W_{q,flat}}{16 \cdot d_2} \right) \cdot d_1^2 \quad (4.1)$$

And

$$W_{v,flat} = \left(\frac{3\pi \cdot (d_3 - s)^2}{16 \cdot d_4} + s \right) \cdot W_{q,flat} \quad (4.2)$$

From equation 4.2, the wear volume on the disk is directly proportional to $W_{q,flat}$. The relationship between the ball scar wear volume and $W_{q,flat}$, however, is much more complex, as can be seen in equation 4.1. In this equation, the predominating value will be the diameter perpendicular to the sliding direction (d_1) and the relation between $W_{q,flat}$ and d_1 and the ball wear volume is more complex. The relationship between the disk wear track volume and d_3 and d_4 is also much simpler compared to equation 4.1. Also note that it is possible that a deviation in one variable, can offset a deviation in another variable.

Test Duration: 40 minutes

For this test duration, only the disk wear track volume had poorer repeatability. This was also mainly due to deviations in $W_{q,flat}$, as shown in Table 4.11. Here Run 2 had the smallest $W_{q,flat}$ and smallest wear volume and Run 4 the largest $W_{q,flat}$ and largest wear volume. In Figure 4.59, both Run 1 and 3 had a small sharp peak at around 5 minutes, while this did not occur for Run 2 and Run 4. This indicates that there was a change in the surfaces interactions for Run 1 and Run 3 at these 2 moments. Because this did not occur for Run 2 and 4, the wear surfaces for these 2 runs varied from Run 1 and 3. Consequently, the planimetric wear area will also deviate.

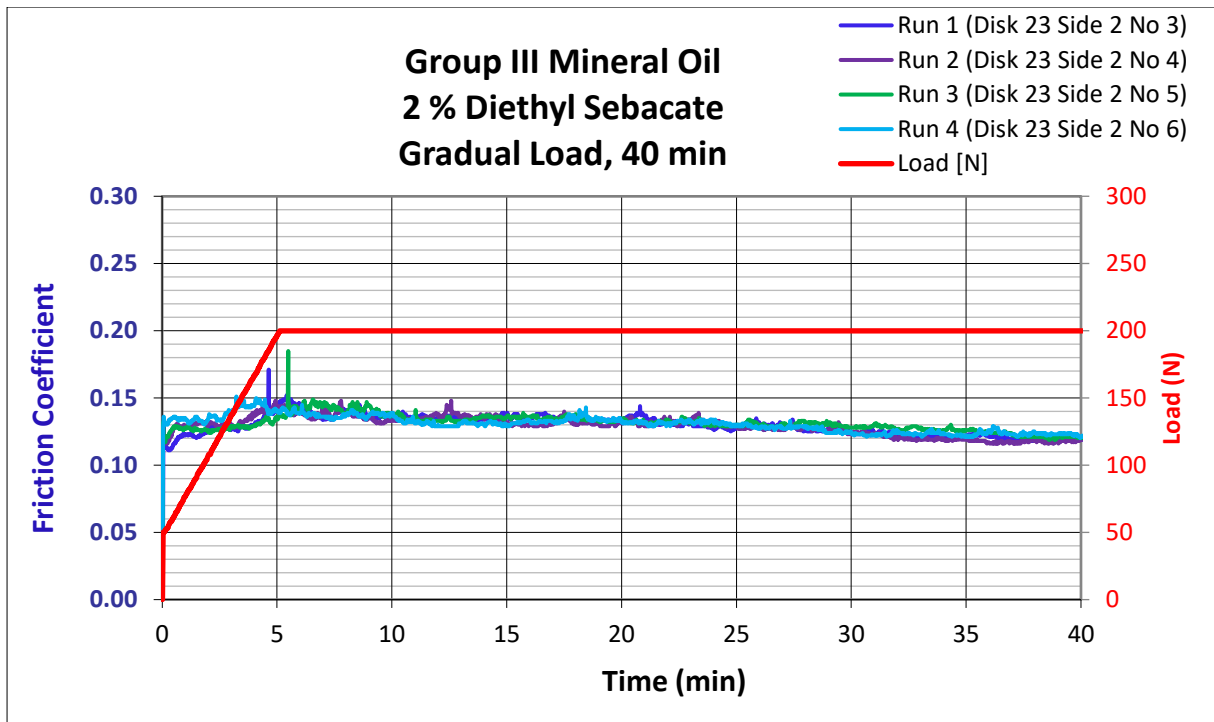


Figure 4.59: Friction coefficient graphs for gradual load, 40 minutes.

Table 4.10: Wear volume calculations for scars and tracks obtained with gradual load increase, 5 min. Values highlighted in green deviated the most from the average.

Run	Scar Dimensions		Track Dimensions			Scar Calculations		Track Calculations	
	d_1 (mm)	d_2 (mm)	d_3 (mm)	d_4 (mm)	$W_{q,flat}$ (mm ²)	\overline{R}_s (mm)	$W_{v, ball}$ (mm ³)	\overline{R}_t (mm)	$W_{v, flat}$ (mm ³)
1	0.415	0.402	1.454	0.388	1.87E-04	28.950	2.26E-04	26.021	2.45E-04
2	0.396	0.390	1.329	0.268	1.00E-04	49.323	2.11E-04	15.888	1.24E-04
3	0.389	0.389	1.420	0.377	1.21E-04	40.651	1.97E-04	37.074	1.54E-04
4	0.411	0.398	1.449	0.385	2.71E-04	19.416	1.95E-04	17.558	3.55E-04
AVG	0.399	0.392	1.399	0.343	1.64E-04	36.463	2.01E-04	23.507	2.11E-04
STDEV	0.011	0.005	0.063	0.065	9.33E-05	15.387	8.72E-06	11.779	1.26E-04

Table 4.11: Wear volume calculations for scars and tracks obtained with gradual load, 40 minutes. Values highlighted in green deviated the most from the average.

Run	Scar Dimensions		Track Dimensions			Scar Calculations		Track Calculations	
	d_1 (mm)	d_2 (mm)	d_3 (mm)	d_4 (mm)	$W_{q,flat}$ (mm ²)	\overline{R}_s (mm)	$W_{v, ball}$ (mm ³)	\overline{R}_t (mm)	$W_{v, flat}$ (mm ³)
1	0.540	0.566	1.589	0.556	1.73E-03	8.712	3.91E-04	8.265	2.37E-03
2	0.546	0.597	1.589	0.586	1.85E-03	9.554	4.96E-04	9.039	2.50E-03
3	0.543	0.573	1.589	0.553	1.62E-03	9.688	4.61E-04	8.688	2.22E-03
4	0.549	0.582	1.593	0.575	1.47E-03	11.181	5.55E-04	10.740	2.00E-03
AVG	0.546	0.584	1.590	0.571	1.65E-03	10.141	5.04E-04	9.489	2.24E-03
STDEV	0.003	0.012	0.002	0.017	1.91E-04	0.903	4.75E-05	1.098	2.51E-04

Test Duration: 75 minutes

Here, only the wear scar diameter had slightly poorer repeatability. The measurement for Run 1, was higher compared to the other 3 runs (see Table 4.12).

Table 4.12: Wear scar diameters for repeat runs with gradual load increase, 75 minutes.

Run	Scar Dimensions		
	d_1 (mm)	d_2 (mm)	WSD (mm)
1	0.604	0.636	0.620
2	0.575	0.611	0.593
3	0.571	0.625	0.598
4	0.577	0.629	0.603
AVG	0.574	0.622	0.604
STDEV	0.003	0.009	0.011

4.2.2 Wear Rates

To evaluate the wear behaviour, wear rates were also determined. Results of the wear rate calculations are shown in Table 4.13. The wear rates were calculated according to equation 3.7. The wear rates are also plotted in Figures 4.60, 4.61 and 4.62.

Table 4.13: Wear rates for all test durations on the ball scar and disk track.

Dur. (min)	Ball WSD (μm)		Ball WSV (μm^3) $\times 10^3$		Disk WSV (μm^3) $\times 10^3$	
	Step	Grad	Step	Grad	Step	Grad
5	390.9	398.8	204.6	207.2	133.7	219.5
20	489.5	492.4	305.6	322.0	1174.5	1140.2
40	552.2	562.1	509.4	475.8	1756.1	2273.5
75	611.3	603.5	375.6	397.0	4026.0	3764.4
100	602.4	589.0	632.7	559.1	2950.0	2729.1
125	592.7	622.6	520.3	515.1	3251.3	4067.9
Dur. (min)	Wear Rate Ball WSD ($\mu\text{m}/\text{min}$)		Wear Rate Ball WSV ($\mu\text{m}^3/\text{min}$) $\times 10^3$		Wear Rate Disk WSV ($\mu\text{m}^3/\text{min}$) $\times 10^3$	
	Step	Grad	Step	Grad	Step	Grad
5	78.2	79.8	40.9	41.4	26.7	43.9
20	24.5	24.6	15.3	16.1	58.7	57.0
40	13.8	14.1	12.7	11.9	43.9	56.8
75	8.2	8.1	5.0	5.3	53.7	50.2
100	6.0	5.9	6.3	5.6	29.5	27.3
125	4.7	5.0	4.2	4.1	26.0	32.5

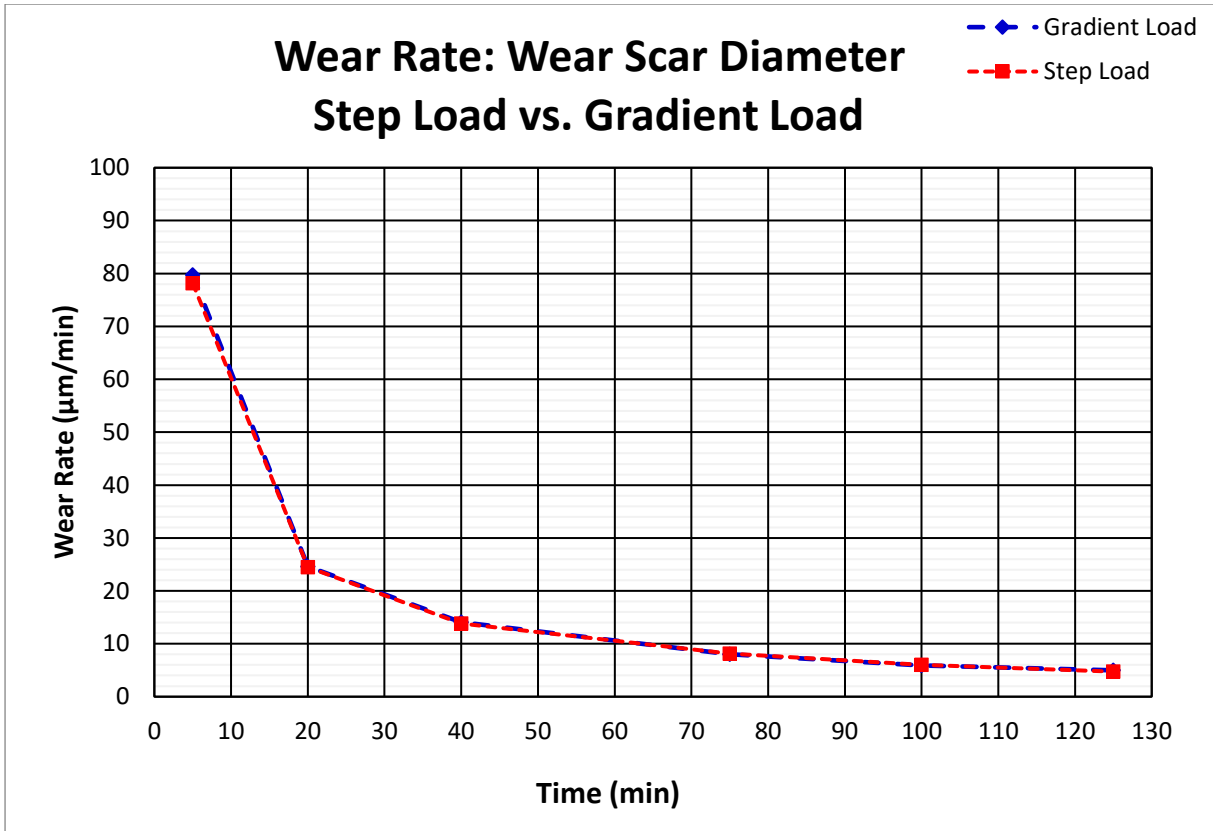


Figure 4.60: Ball wear scar diameter wear rate.

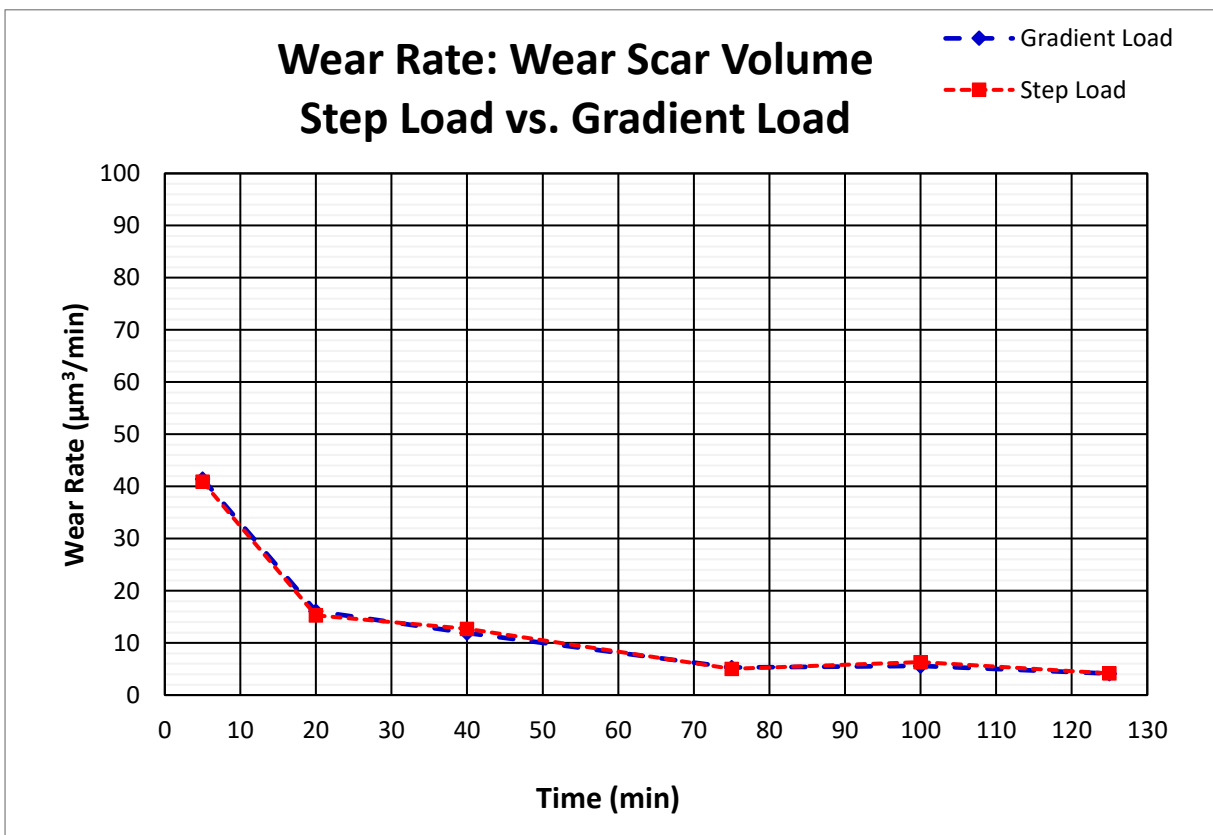


Figure 4.61: Ball wear scar volume wear rate.

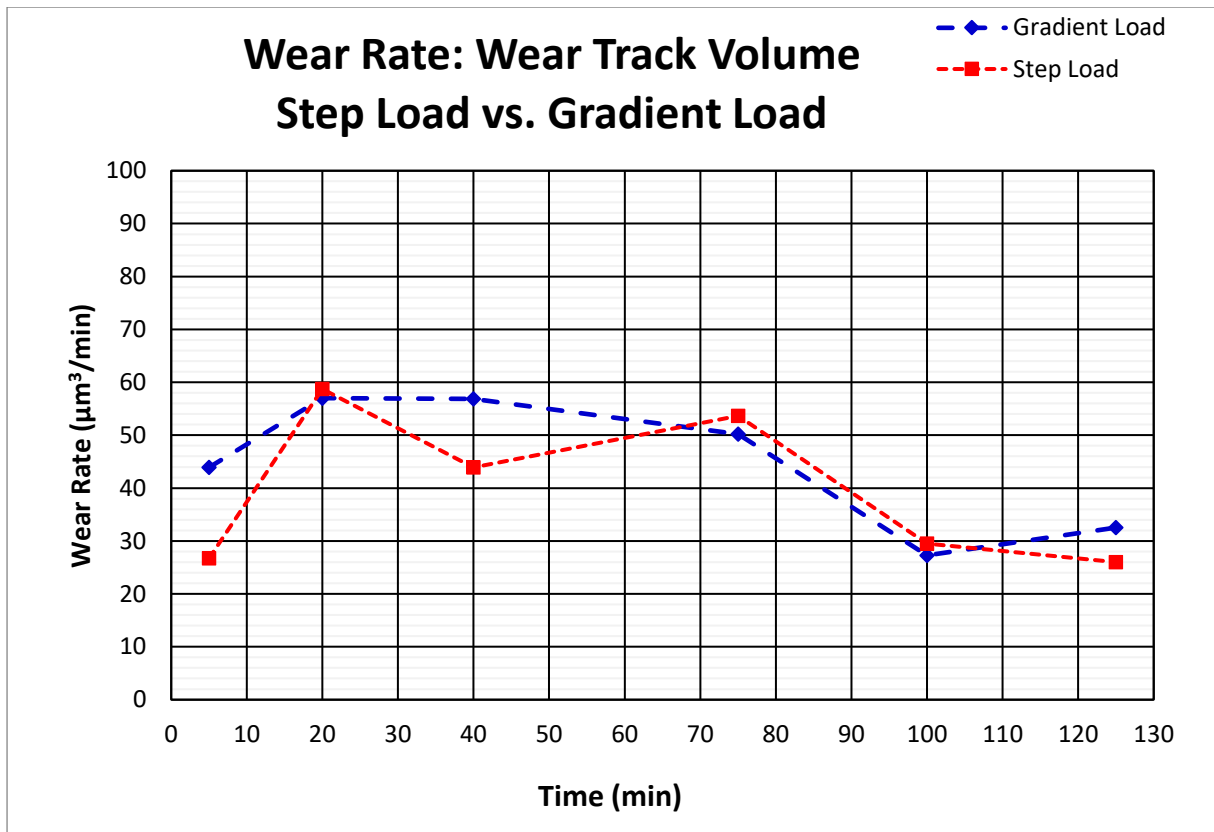


Figure 4.62: Disk wear scar volume wear rate.

In Figures 4.60 and 4.61, the initial wear rates after 5 minutes are the highest on the ball. The wear rate then has a steady decline until the end. For the wear rates after 5 minutes to 75 minutes, a non-linear decrease in the wear rates is obtained. The decrease in wear rate between the last 3 data points, however, is linear. The wear rates can therefore be divided into 3 regimes:

1. Regime with high wear rate: 0 min. to 5 min.
2. Regime where the wear rate decreases non-linearly: 5 min. to 75 min.
3. Regime with linear decrease in wear rate: 75 min. to 125 min.

The wear rates on the disk (Figure 4.62) showed different behaviour compared to the ball. The initial wear rate was lower, and the highest wear rate was measured at 20 minutes. After this it steadily declined.

Furthermore, the wear rate on the disk after 125 minutes is the same as the wear rate on the disk after 5 minutes. Both are also the lowest wear rates. On the ball, however, the lowest wear rates occurred only at the end. This then indicates that most of the

wear on the ball occurs during the first 5 minutes followed by a non-linear regime (5 to 75 minutes). Most of the wear on the disk, however, does not occur during the first 5 minutes, but from 5 minutes to 75 minutes.

On the ball, little wear occurs from 75 minutes onward, while a substantial amount of wear still occurs on the disk for the remainder of the test. The wear rates on the disk also tended to deviate from trends, while a smoother trend was observed for the wear rates calculated on the ball.

The regimes described above can therefore be summarised as follows:

1. *Load Increase Regime* characterised by high wear rates on the ball, 0 to 5 minutes.
2. *Running-in Regime* characterised by high wear rates, 5 to 75 minutes.
3. *Steady State Regime* characterised by low wear rates which occur predominantly on the disk.

The varying wear rates (Table 4.13) for the ball wear scar diameter and the wear volume (on the scar and the track) indicate that the direction of the wear varies for each wear regime. The wear regimes in terms of the ball wear scar diameter, ball wear scar volume and disk wear track volume are illustrated in Figure 4.63. The 3 methods with which the extent of wear is determined have been normalised, i.e., the extent of wear is the same. This is to easily compare the wear rates.

The direction of the wear can also be divided into the lateral direction (ball wear scar diameter) and perpendicular to the wear surface (wear profile). Wear occurs in both directions for each wear regime. The extent of wear for either of these directions, however, depends on the wear regime. This is illustrated in Figure 4.64, where the extent of wear is represented by the length of the arrows.

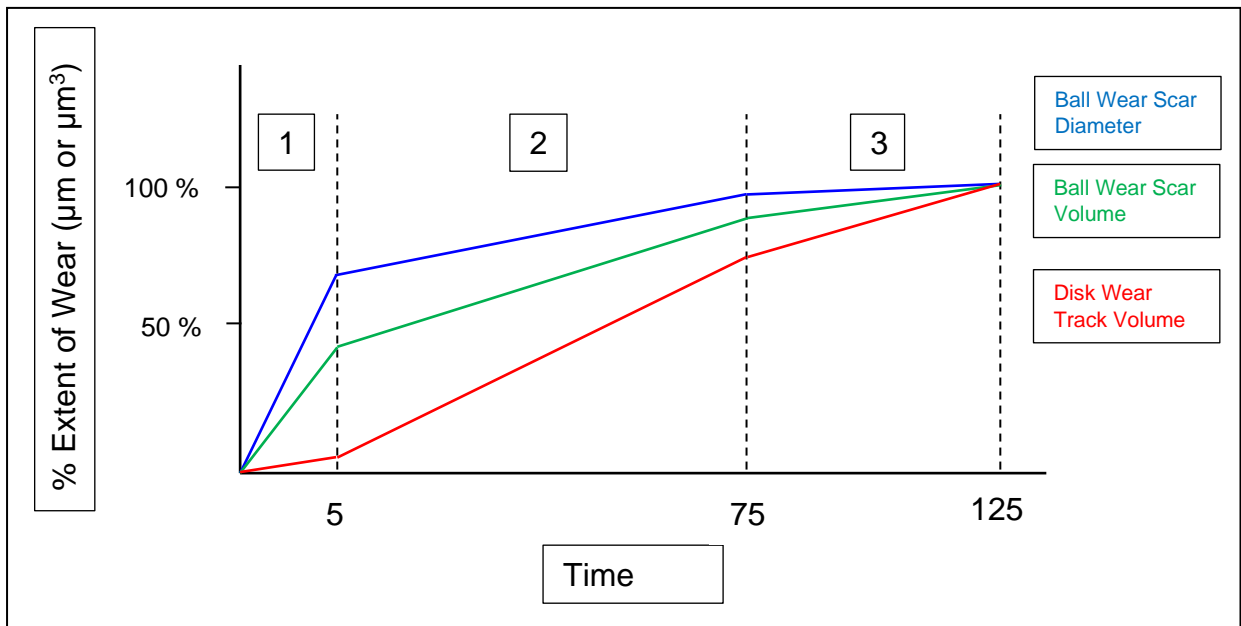


Figure 4.63: Extent of wear for the ball wear scar diameter, ball wear scar volume and disk wear track volume, normalised to 100 %.

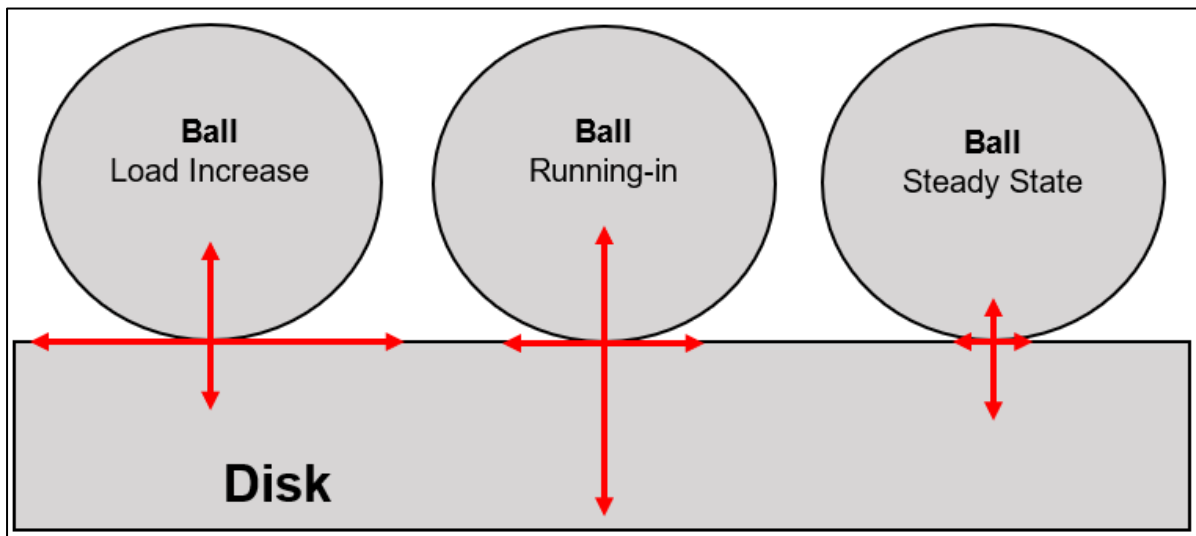


Figure 4.64: Directions in which wear predominantly occurs for each regime: load increase (0 to 5 minutes), running-in period (5 to 75 minutes) and steady state (75 to 125 minutes).

From Figures 4.63 and 4.64 the wear can be summarised as follows:

Load Increase Regime: The highest extent of wear occurs in the lateral direction (wear scar diameter). However, wear rates calculated for the ball wear volume, indicate that a substantial extent of wear also occurs in the perpendicular direction into the ball.

Running-in Regime: This regime is characterised by the highest extent of wear determined for the disk, while a substantial amount of wear still occurs on the ball. Most of the wear occurs in the perpendicular direction.

Steady State Regime: In this regime, the system is run-in and the majority of the wear occurs on the disk in the perpendicular direction. The extent of wear for the ball is small.

It should also be noted that the wear volume calculation gives a more accurate indication of the extent of wear that occurred, since this is a 3-dimensional calculation which takes the wear profile into account. The ball wear scar diameter is only a two-dimensional measurement on a spherical object and can easily give the incorrect impression of the wear rate.

4.2.3 Friction Coefficient & Wear Surfaces

The friction coefficient graphs for the 4 repeat runs for each of the test methods can be found in Figure 4.65 (step load increase) and Figure 4.66 (gradient load increase). The test duration was 125 min.

In these figures repeatability was better for the gradient load increase during the steady state regime. Like the wear rates, the friction coefficient plots can also be divided into 3 regimes, as seen in section 4.2.2 above.

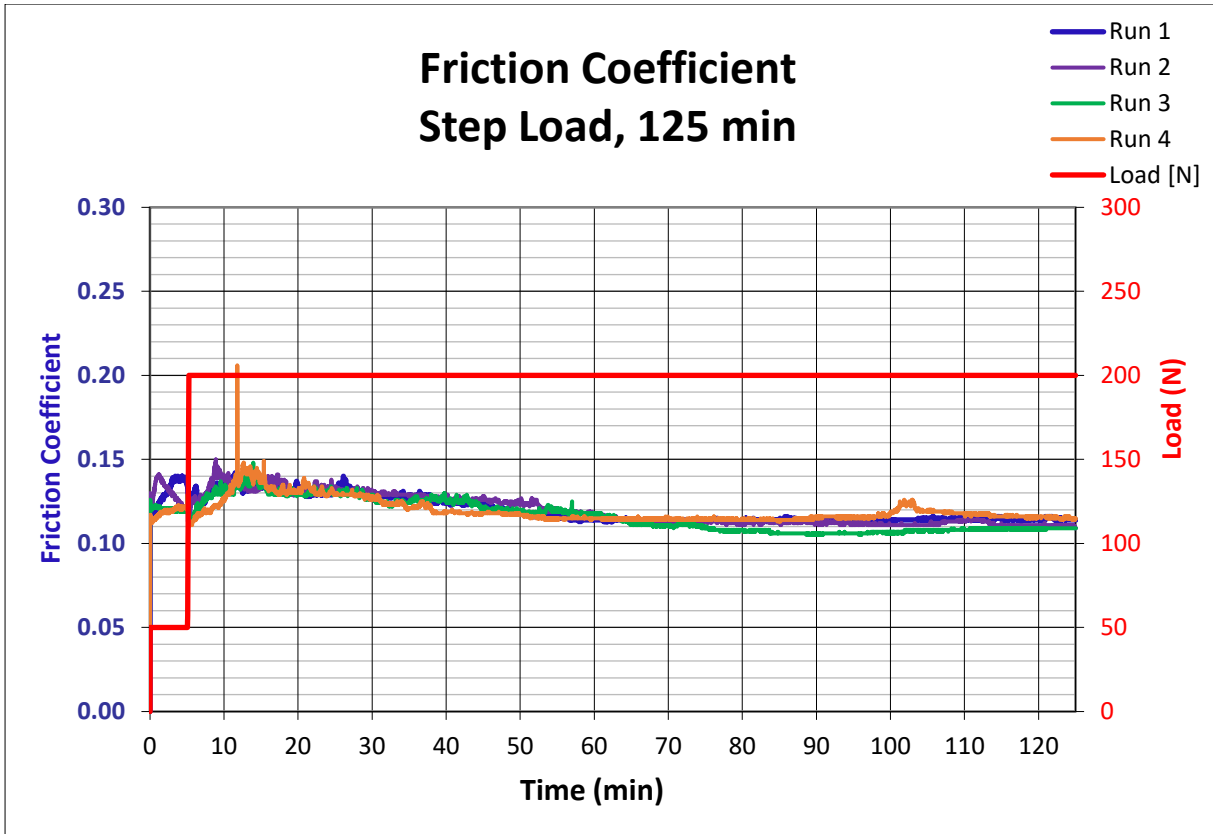


Figure 4.65: Friction coefficient graphs for step load, 125 minutes.

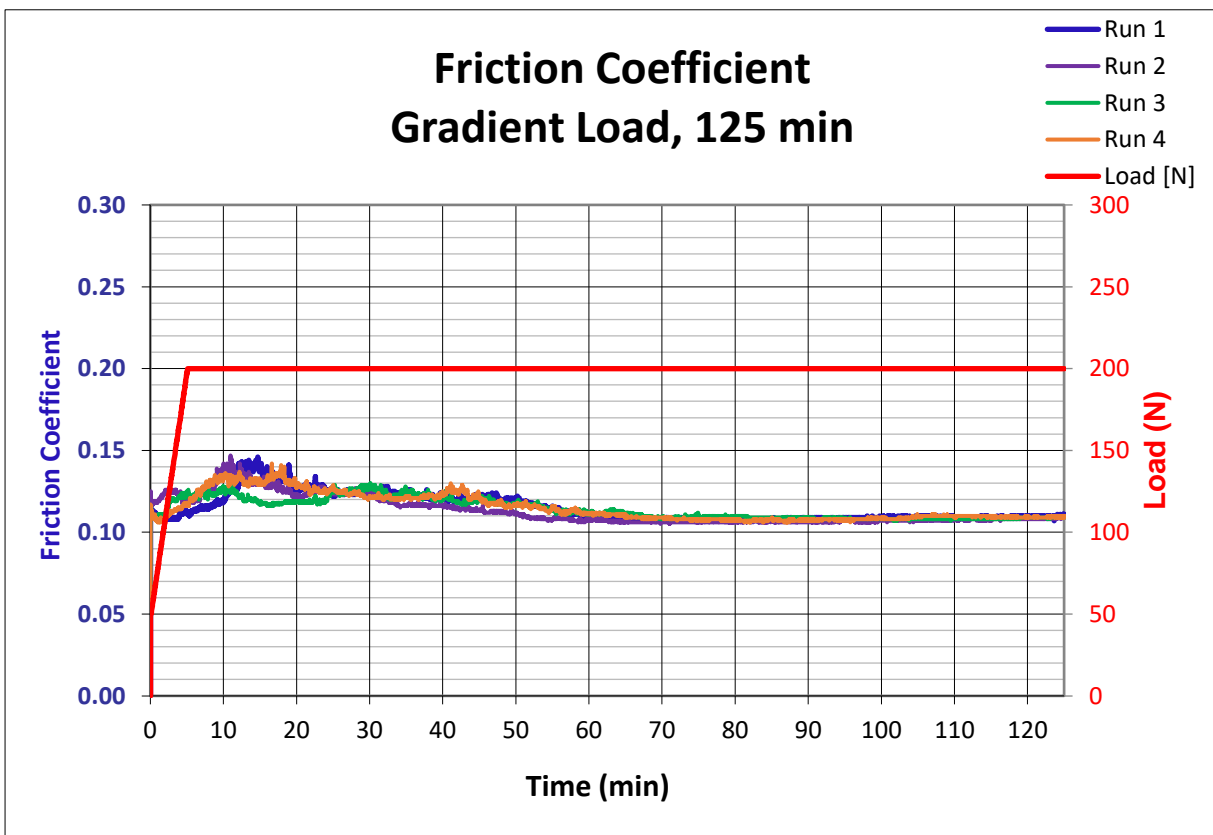


Figure 4.66: Friction coefficient graphs for gradient load increase, 125 minutes.

During the first 5 minutes, when the load is increased, variations in the friction coefficient are obtained. After the operating load is reached (5 minutes) the friction coefficient increases, and a maximum value is reached. The friction coefficient then steadily decreases until a constant value is reached. The constant value is reached after about 75 minutes.

This compares well to the regimes observed for the wear rates:

1. 0 – 5 minutes: high wear rate (ball) and deviations in friction coefficient.
2. 5 – 75 minutes: non-linear decrease in wear rate as well as decrease in friction coefficient after a maximum value.
3. 75 – 125 minutes: linear decrease in wear rate and constant friction coefficient.

When the 2 test methods are compared, the transition of the friction coefficient for the gradient load increase was also smoother after the load was increased to 200 N. For the step load increase a sudden decrease after the load increase occurred.

To quantify repeatability for the friction coefficient, the integral between the standard deviation and the average was determined according to equation 3.1. The integrals are given in Figure 4.67. The integral for the tests runs with shorter durations are also included. Again, the gradient load increase method had better repeatability for tests with longer durations. Repeatability for the 5 minute and 20-minute tests were about the same.

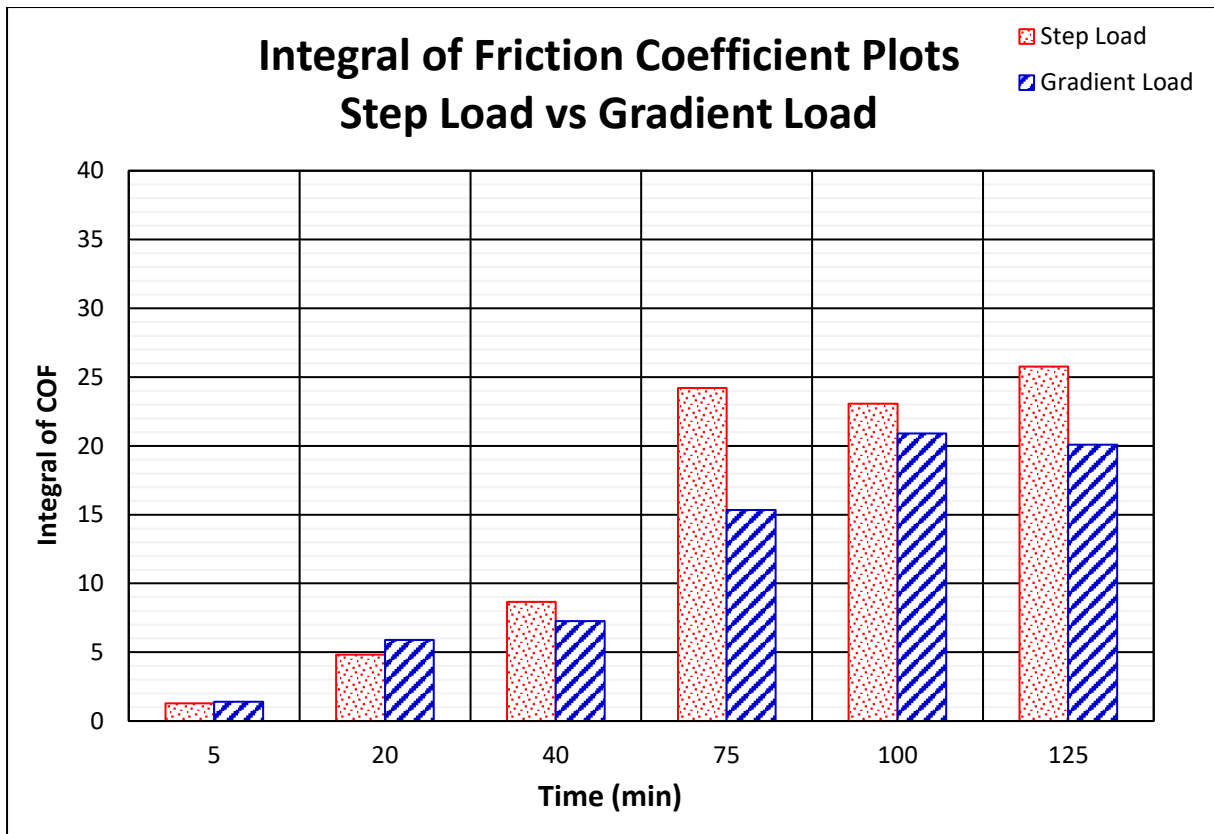
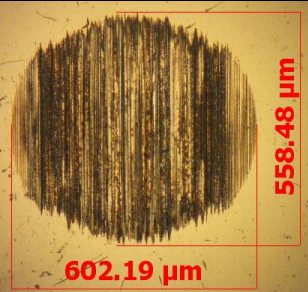
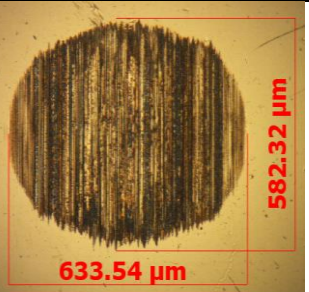
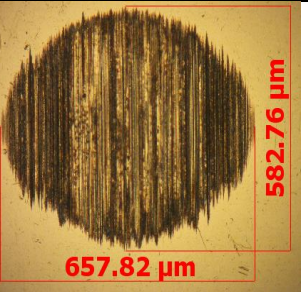
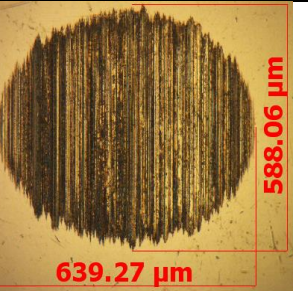
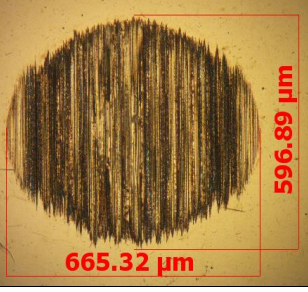
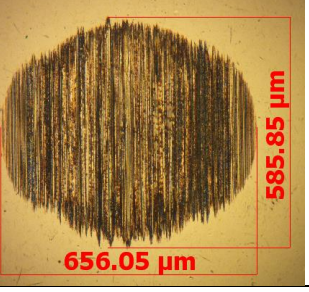
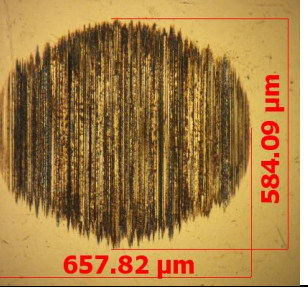
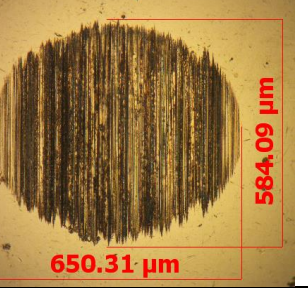
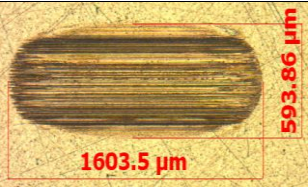
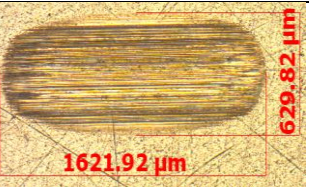
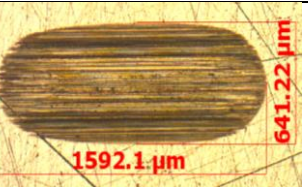
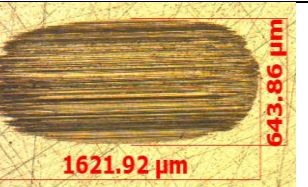
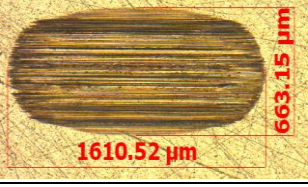
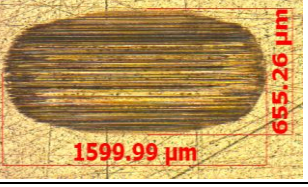
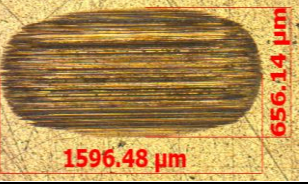
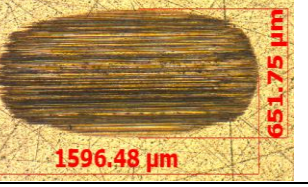


Figure 4.67: Integral of friction coefficient plots.

From these figures, repeatability of the friction coefficient improved with the modified procedure (Figures 4.65, 4.66 and 4.67). To understand what happens with the friction coefficient, the wear surfaces were evaluated.

The wear scar and track images are given in Table 4.14 for the step load and the gradient load test methods. For both, excessive occurred with no real difference between the surface finish between the repeat runs for each method. The shapes for the gradient load are however more uniform compared to the shapes of the wear surfaces for the step load.

Table 4.14: Wear surfaces for the step and gradient load procedure for **Group III 6 + 2 % diethyl sebacate**.

Load Increase	Wear Scars			
	Run 1	Run 2	Run 3	Run 4
Step Load				
Gradient Load				
	Wear Tracks			
Step Load				
Gradient Load				

The wear profiles for the scars obtained from both test methods are given in Figure 4.68 and 4.69 and in Figure 4.70 and 4.71 for the profiles of the wear tracks are given. From Figures 4.68 and 4.70 the profiles for the step load tended to have indents at the edges. This can be seen for Run 3 that had a peak at 550 μm , while the entire left half of the profile for run 4 was lower than the other 3 runs.

For the gradient load (Figures 4.70 and 4.71), only run 1 deviated from the other 3 runs, but to a lesser extent compared to the step load. The same effect can be seen on the wear tracks, where indents tend to occur toward the edges for the step load procedure.

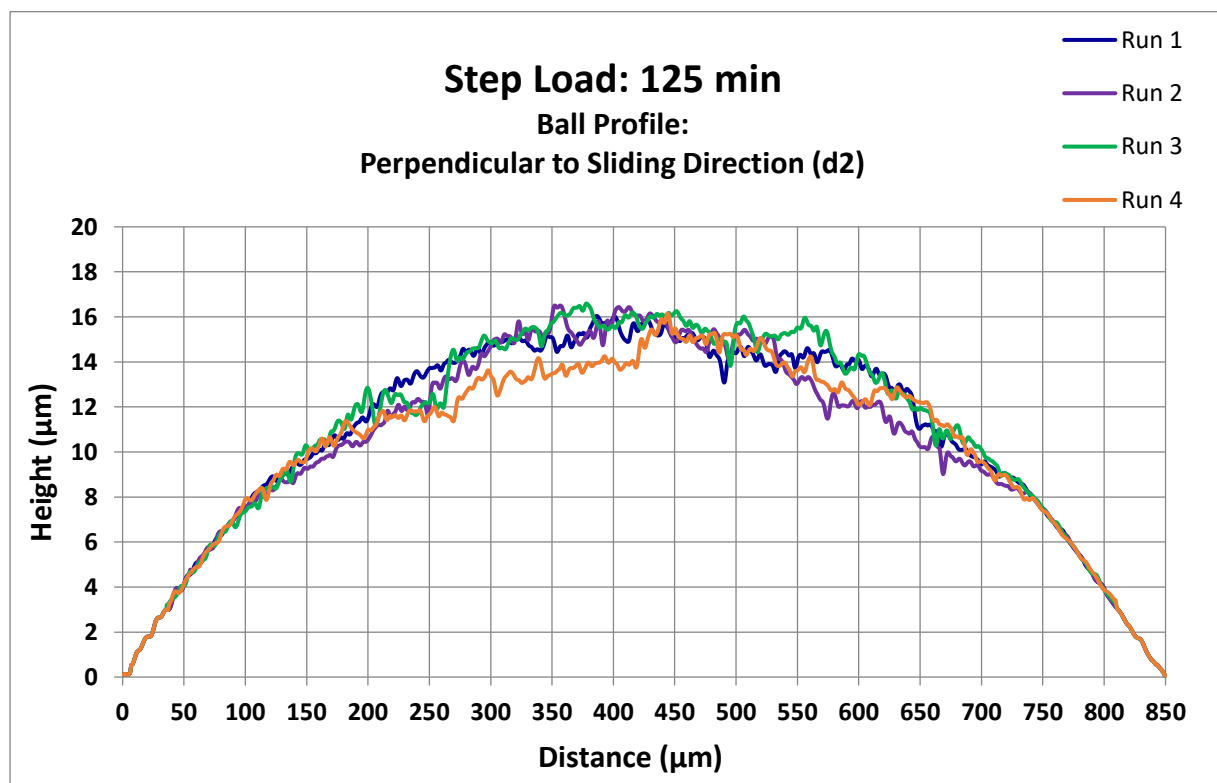


Figure 4.68: Scar profiles perpendicular to the sliding direction for scars obtained with the step load increase with **Group III 6 + 2 % diethyl sebacate**.

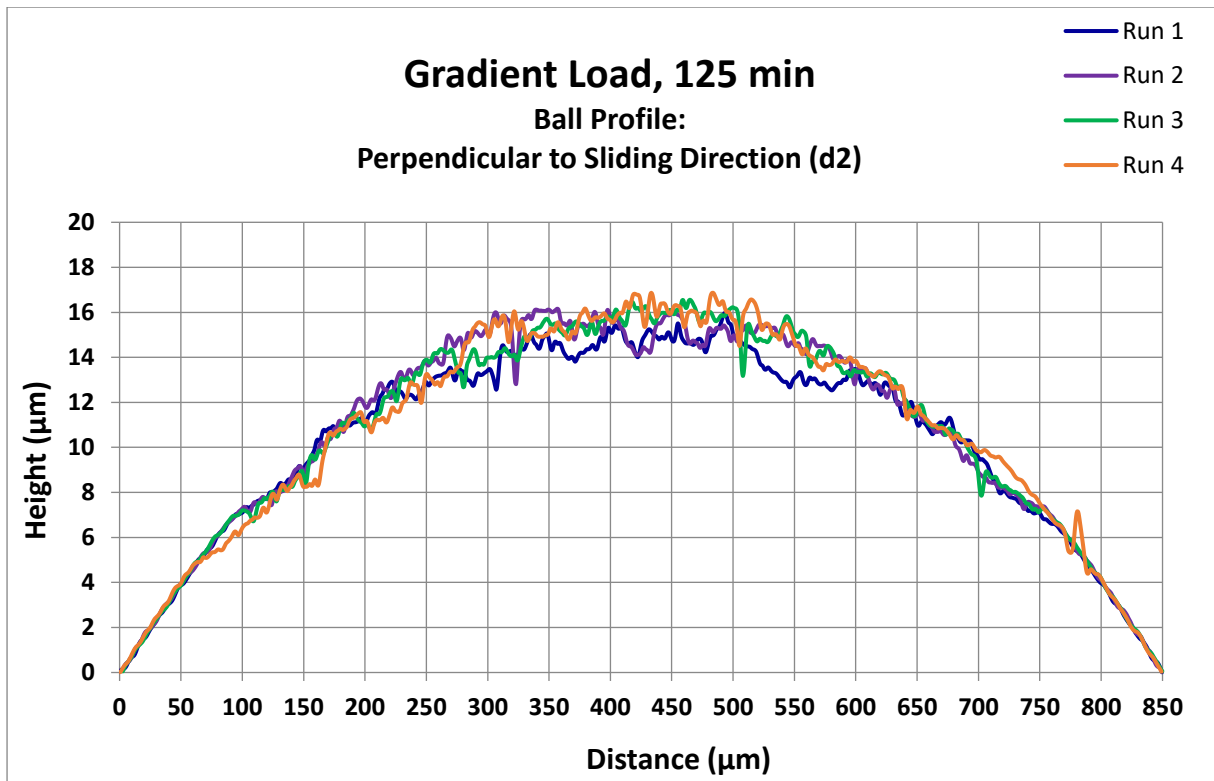


Figure 4.69: Scar profiles perpendicular to the sliding direction for scars obtained with the gradual load increase with **Group III 6 + 2 % diethyl sebacate**.

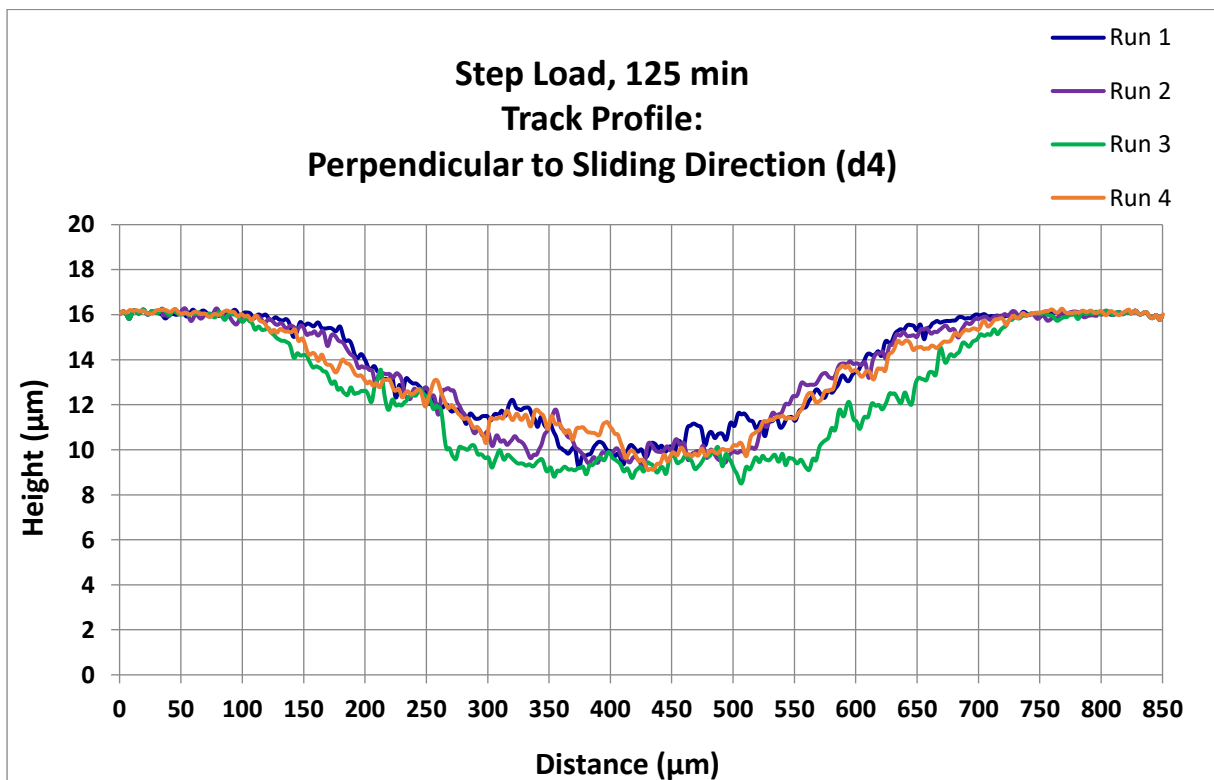


Figure 4.70: Track profiles perpendicular to the sliding direction for scars obtained with the step load increase with **Group III 6 + 2 % diethyl sebacate**.

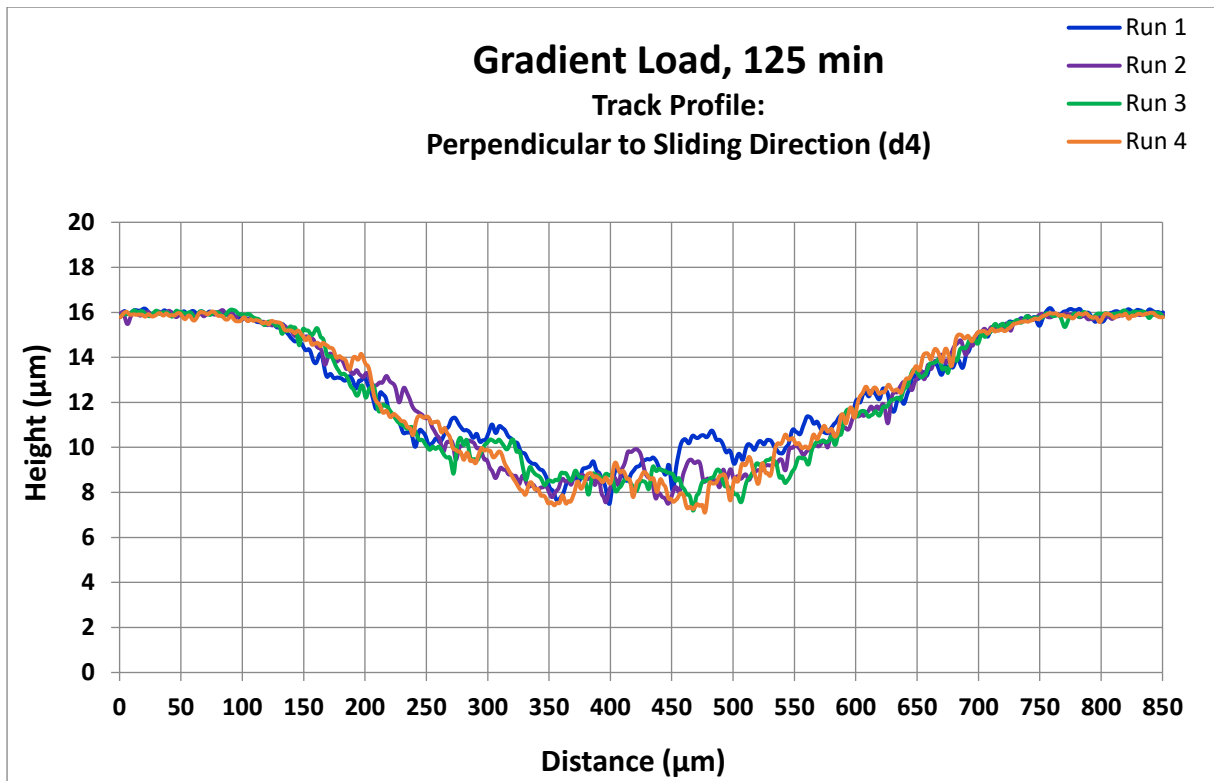


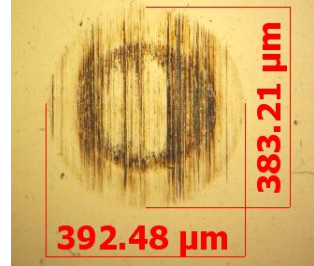
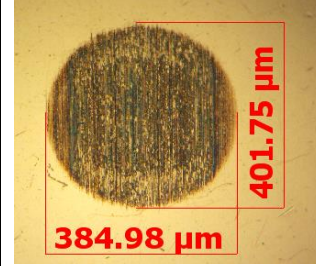
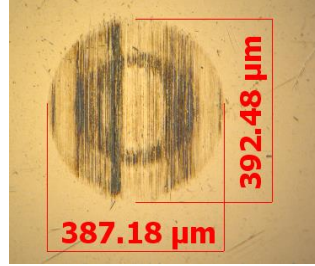
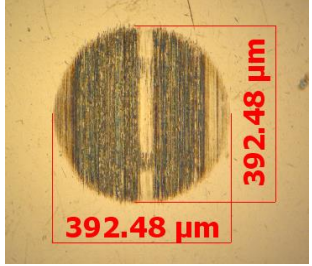
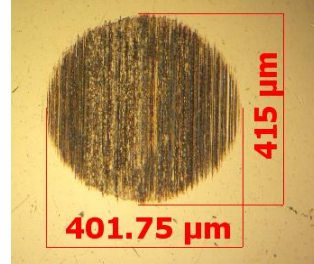
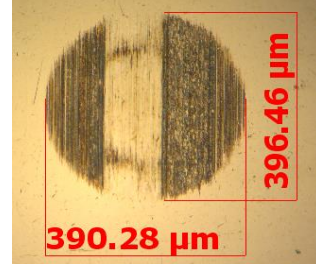
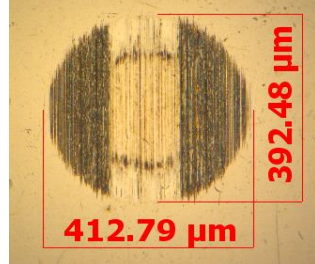
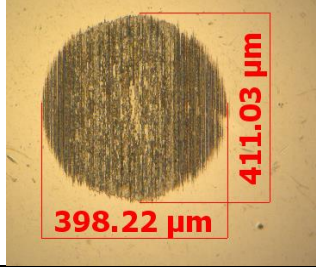
Figure 4.71: Track profiles perpendicular to the sliding direction for scars obtained with the gradual load increase with **Group III 6 + 2 % diethyl sebacate**.

The average for the profile radius of the ball wear scar for step load and gradual load, (see Appendix C.5) was 8.619 mm and 7.709 mm, respectively. This indicates that the profiles for the gradual load was slightly more curved compared to the profiles for the step load. The standard deviation was also smaller for the gradual load (0.278 mm compared to 0.909).

The rest of the wear surfaces can be found in Appendix C.3. They have not been included in this section since the differences between the two methods are insignificant. The 3-dimensional surfaces can also be found in Appendix C.2.

Table 4.15 contains the wear scar images at 5 minutes. For both load increase procedures, excessive wear is already observable. For the step load an inner wear circle is visible after the load increase. All 4 scars differed in its appearance for each load increase procedure. Run 2 and 3 for the gradual load increase method were different than the other 2 runs.

Table 4.15: Wear scar surface images before and after load increase for step and gradual load increase.

	Run 1	Run 2	Run 3	Run 4
Step Load	 <p>383.21 μm 392.48 μm</p>	 <p>401.75 μm 384.98 μm</p>	 <p>392.48 μm 387.18 μm</p>	 <p>392.48 μm 392.48 μm</p>
Gradient Load	 <p>415 μm 401.75 μm</p>	 <p>396.46 μm 390.28 μm</p>	 <p>392.48 μm 412.79 μm</p>	 <p>411.03 μm 398.22 μm</p>

An inner ring can also be seen on run 2 and 3 for the gradual load after the load increase. This ring is however less well defined for the gradual load increase compared to the step load increase. The wear profiles for all the scars in Table 4.15 is given in Figure 4.72 for the step load and in Figure 4.73 for the gradual load (the rest of the profiles at shorter durations can be found in Appendix C.4).

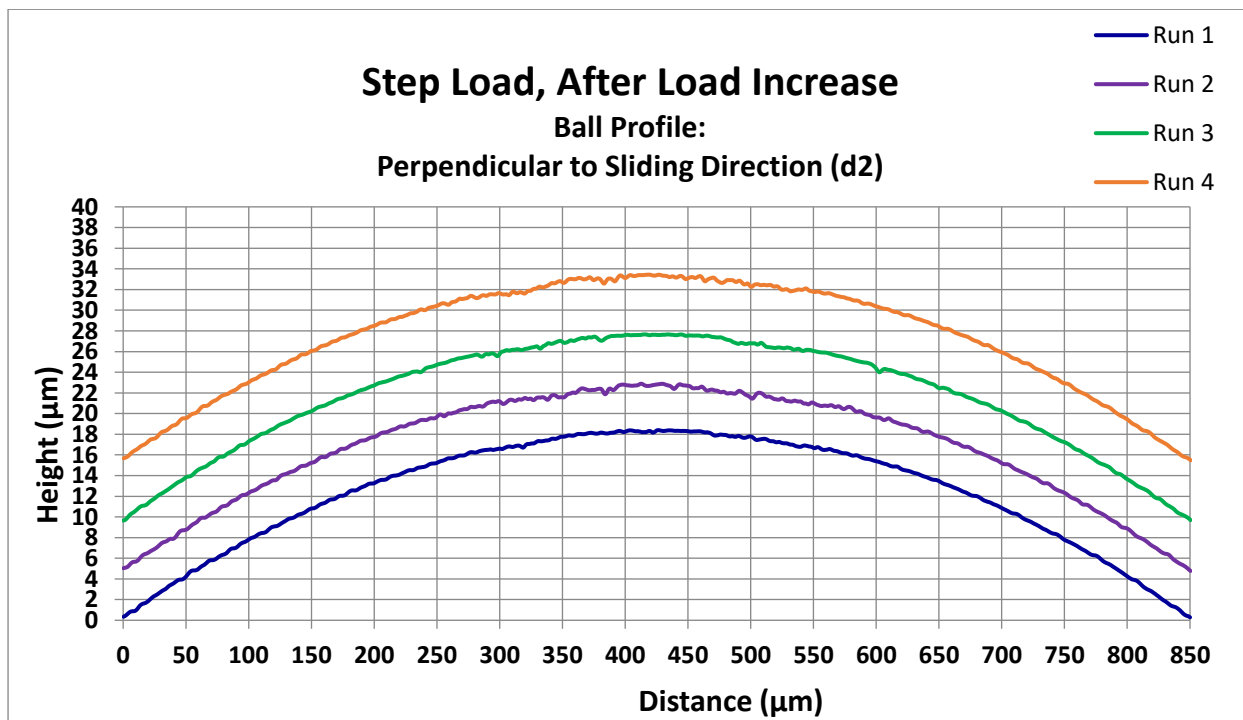


Figure 4.72: Scar profiles perpendicular to the sliding direction for scars obtained with the step load increase with **Group III 6 + 2 % diethyl sebacate**. Test stopped after load increase.

In Figure 4.72, no significant difference can be seen between the wear profiles. In Figure 4.73, however the lighter sections in the scars in Table 4.15 corresponds to smoother sections on the wear profile. The profiles, however, do not indicate any difference between the two test methods.

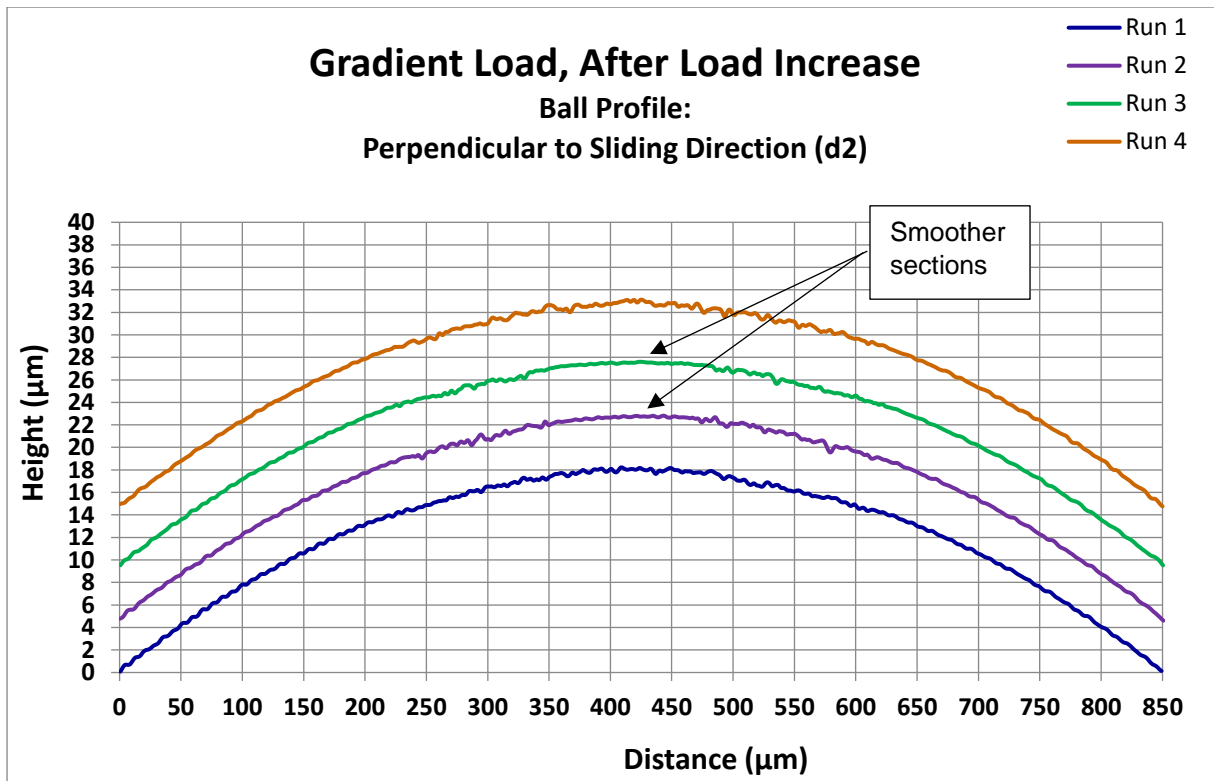


Figure 4.73: Scar profiles perpendicular to the sliding direction for scars obtained with the gradual load increase with **Group III 6 + 2 % diethyl sebacate**. Test stopped after load increase.

A more consistent wear surface profile was obtained with the gradual load increase. The friction coefficient, however, is a function of the surface interactions. Surface interactions in turn depend on the load, speed, lubricant, and real contact area. Since the same operating conditions and lubricant were used, improved consistency of the wear profiles therefore indicate that the consistency of the real contact area also improved between test runs for the gradual load increase procedure. This resulted in fewer deviations and repeatability improved.

The gradual load also shows a smooth transition in the friction coefficient during the load increase procedure. This indicates that there is a smoother transition of the wear surface.

The friction coefficient can also be divided into the 3 regimes as described for the wear rates in the section above. The duration for the regimes for the friction coefficient also coincides with the duration of the regimes obtained for the wear rates:

Load Increase Regime: the friction coefficient is characterised by changes and transitions, either increasing or decreasing.

Running-in Regime: A maximum friction coefficient is reached which is followed by a gradual decrease.

Steady State Regime: A constant friction coefficient is obtained.

As the test progresses and the surfaces are run-in, the load is distributed over a larger area. This will therefore decrease the friction coefficient since the contact force between asperities will decrease. The friction force will therefore depend less on the shear forces between the surfaces and more on the real contact area. This is if it is assumed that the viscosity of the fluid remains unchanged during sliding.

The more consistent wear profile and wear scar which results in improved repeatability of the friction coefficient, therefore, indicate that the parameters contributing to the friction force is more consistent. Since wear also occurs due to deformation and adhesion, the better consistency will also result in improved repeatability for the extent of wear.

Finally, the inner circle observed in the wear scar surfaces for scars obtained from the step load increase in Table 4.15, confirms the initial apparent contact area that rapidly increases as the load is stepped up to the operating load. The inner circle in Figure 4.74 correlates well with the diameters calculated in Table 2.2:

- 50 N: Apparent contact area = 236 to 244 μm
- 200 N: Apparent contact area = 374 to 388 μm

Note that in Table 2.2 the radius of the apparent contact area was calculated.

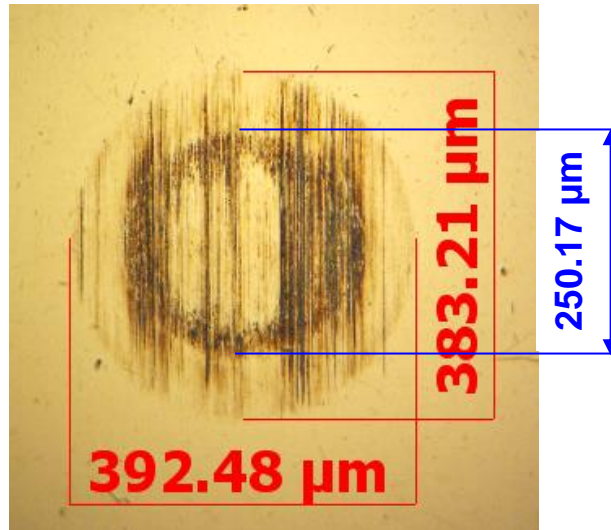


Figure 4.74: Apparent contact area before and after the step load increase.

The inner circle of the wear scars obtained with the gradual load increase was less well defined compared to the step load increase. This was due to the load which was increased from the start of the test with the gradual load increase.

Finally, the magnitude of the final value of the friction coefficient compared well for the 2 test methods. This was also seen for the extent of wear. The modification of the test method therefore did not change the results, but only improved repeatability.

4.3 Running-in

In this section, findings related to running-in from both section 4.1 and section 4.2 are consolidated into a single discussion. It therefore includes the effect of the test fluid and load increase procedure.

In Table 4.6, the duration until steady state for the friction coefficient for each of the base oils is given. The duration until steady state was reached increased with a decrease in the base oil viscosity while the additive also played a role. In section 4.2.3, steady state was reached after 75 minutes for **Group III 6 + 2 % DES**. This corresponds to the time from which wear predominantly occurs into the disk (section 4.2.2 and Figure 4.64).

As the test progresses and the apparent contact area increases, the deformation and adhesion forces decrease between the surfaces. This is due to 2 effects. The first is that asperities are worn away and become smoother (Akchurin, Bosman & Lugt, 2017). The second is that as the contact area increases and asperities become smoother, the load distribution will also increase. This will result in reducing the force between asperities of the 2 surfaces in relative motion. The system is therefore run-in when the surface can support the load and most of the wear occurs into the disk. During this stage, the wear scar diameter only has a slight increase in size.

4.4 Correlation between Friction Coefficient and Wear Surface

This section looks at the correlation between surface phenomena and the friction coefficient. It was already discussed in section 4.2.3 how repeatability of the friction and wear results correlates to the wear surface finish. This section will focus on shape and surface deviations and how they relate to the surface profile. The deviation in the friction coefficient for **WMO + 0.5 % DES** will also be explained.

Surface Appearance

Most of the wear scar surface images indicate the presence of plough marks on the surfaces. This can easily be seen on the 3 D image as shown in Figure 4.75. This is a severely worn surface obtained with **PAO 6 + 3 % DES**.

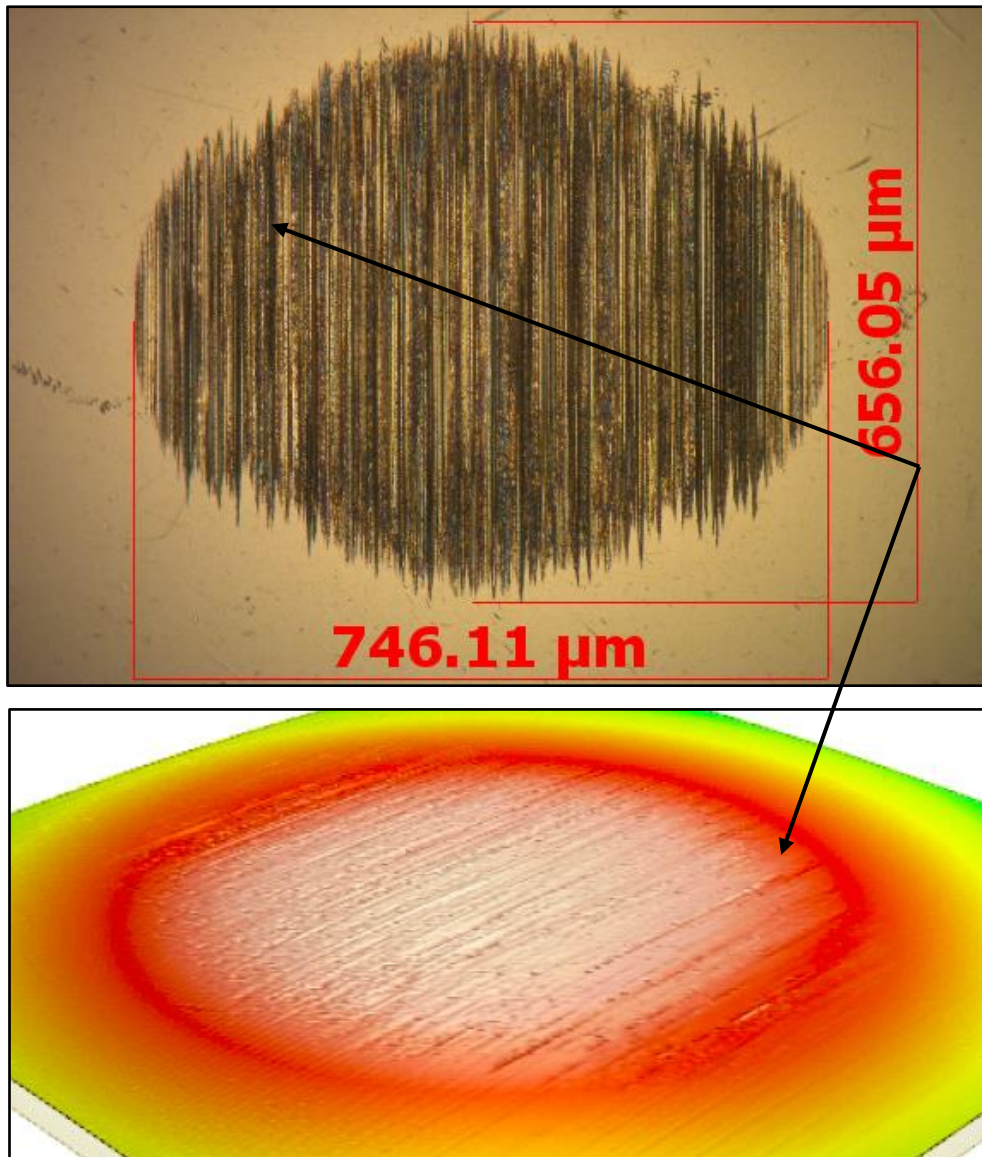


Figure 4.75: Wear scar photo and 3 D image for **PAO 6 + 3 % DES**, Run no.4.

In Table 4.4.6, surface irregularities for the **PAG 146 + 0.5 % DES** were observed. These were areas that were clearer. The tribofilm on the wear surface are darker areas. Therefore, on the clear areas no film is present. These areas also correlate with smooth areas on the 3 D image. This is shown in Figure 4.76.

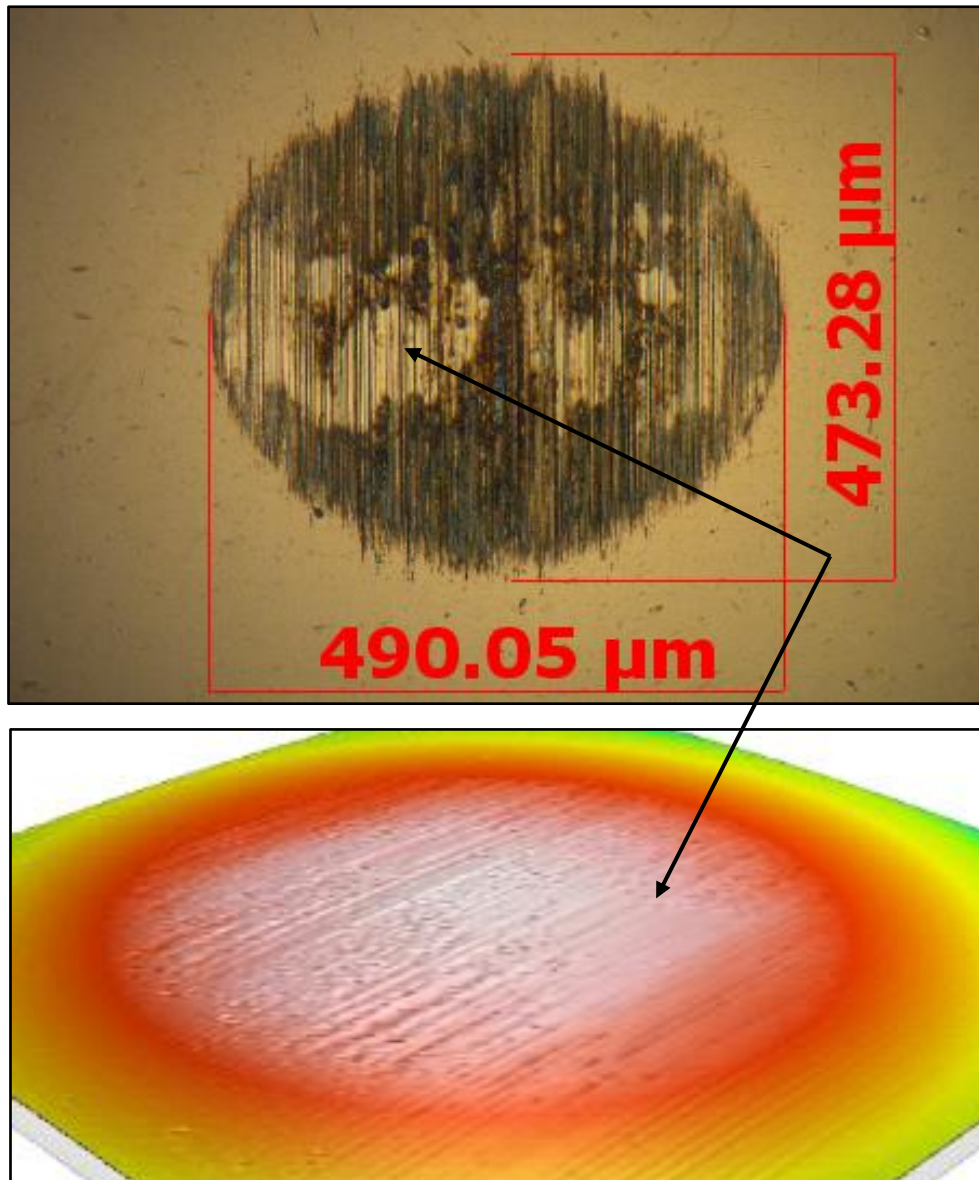


Figure 4.76: Wear scar photo and 3 D image for **PAG 146 + 0.5 % DES**, Run no.2.

The areas where no film is present tend to be in the centre of the wear scar image, parallel to the sliding direction i.e., areas on the wear scar that is in constant contact with the disk. The film will get worn away and has a lighter colour. The surface irregularities (smoother areas) were also obtained for the **PAO + 0.5 % ZDDP** (Figure 4.77). This is different compared to the irregularities in Figure 4.76. A continuous smooth circular area in the middle of the wear scar instead of irregular distribution of smooth areas was obtained. This only occurred on the scar obtained for run 4, and to a lesser extent on the scar for run 2. This indicates that most of the contact occurs in this inner area.

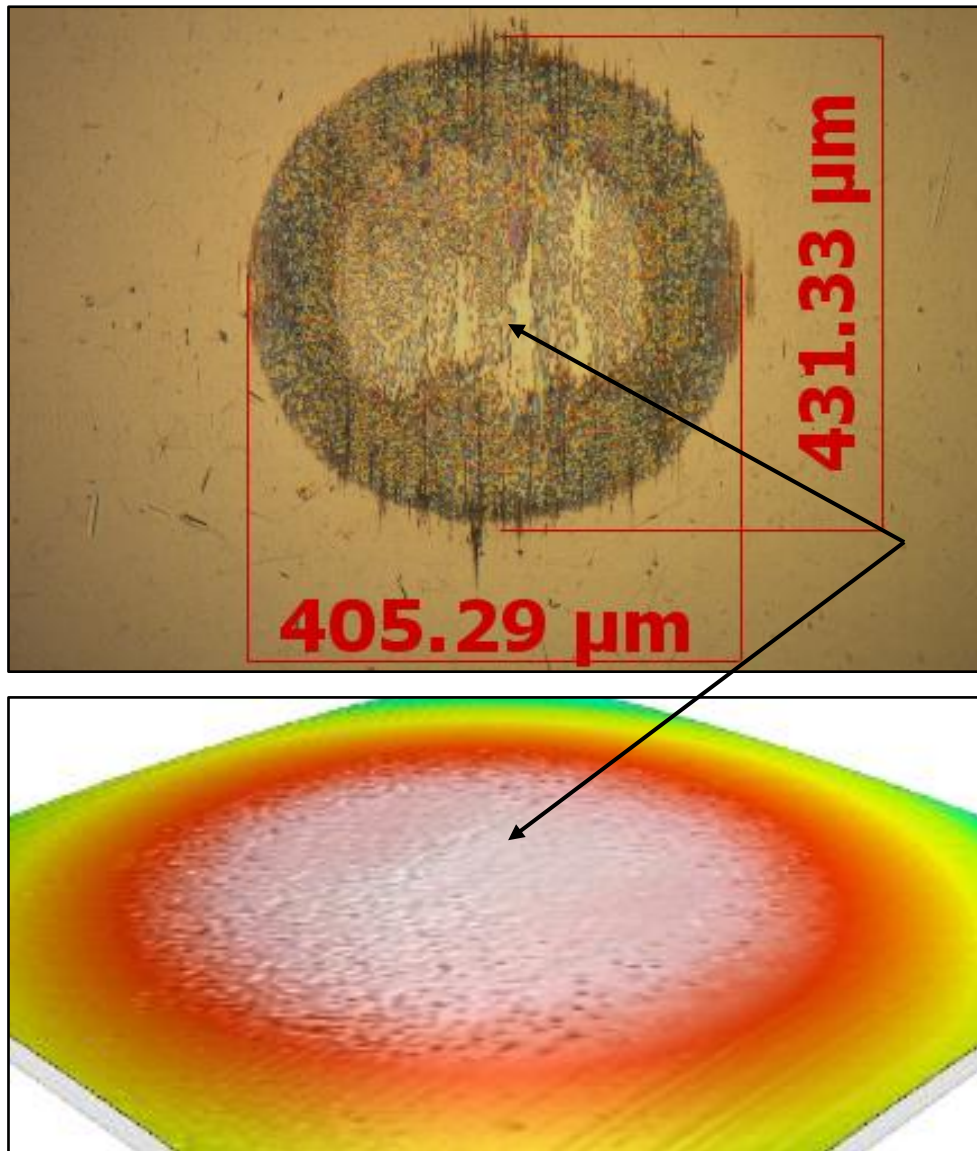


Figure 4.77: Wear scar photo and 3 D image for **PAO 6 + 0.5 % ZDDP**, Run no.2.

Friction Coefficient dependence on Wear Profile

The friction coefficient plot for the **WMO + 0.5 % DES** test fluid is given in Figure 4.78 and the corresponding wear profiles are given in Figure 4.79. The order of the friction coefficients from high to low is:

1. Run 2
2. Run 1
3. Run 4
4. Run 3 and Run 5

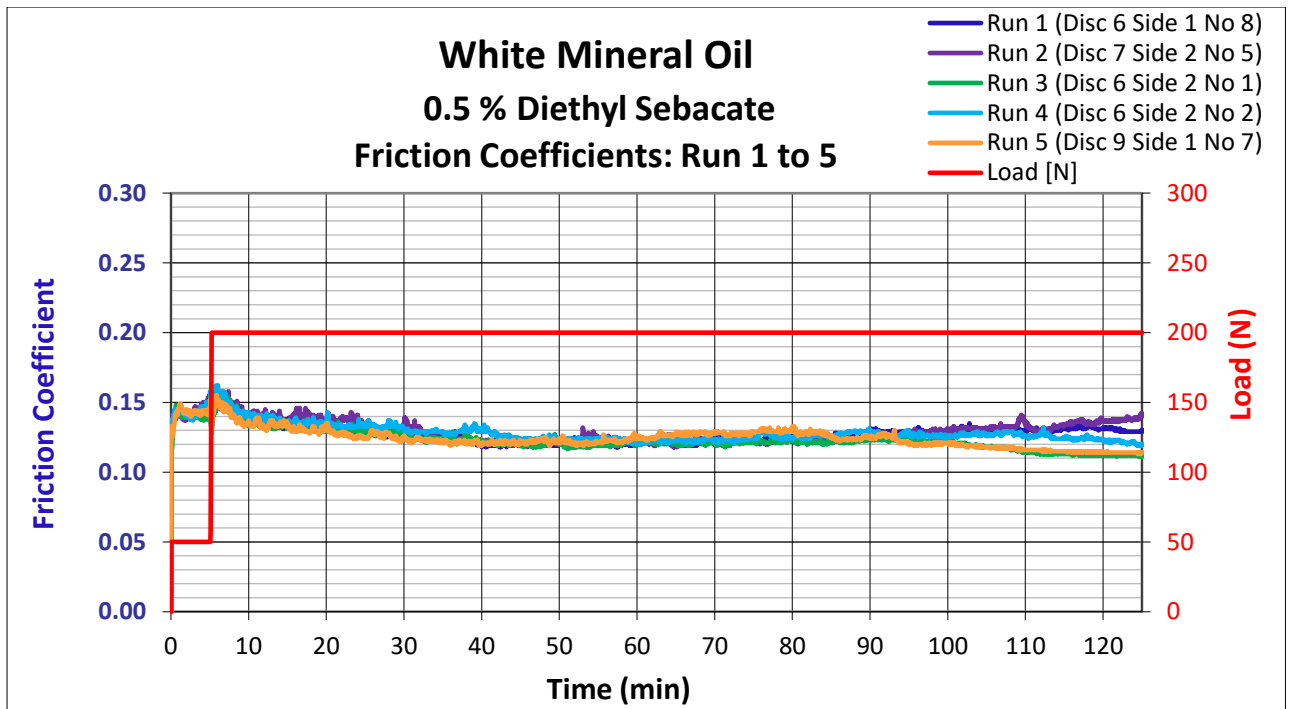


Figure 4.78: Friction coefficient recordings for **WMO + 0.5 % DES** during friction and wear testing on the SRV test rig.

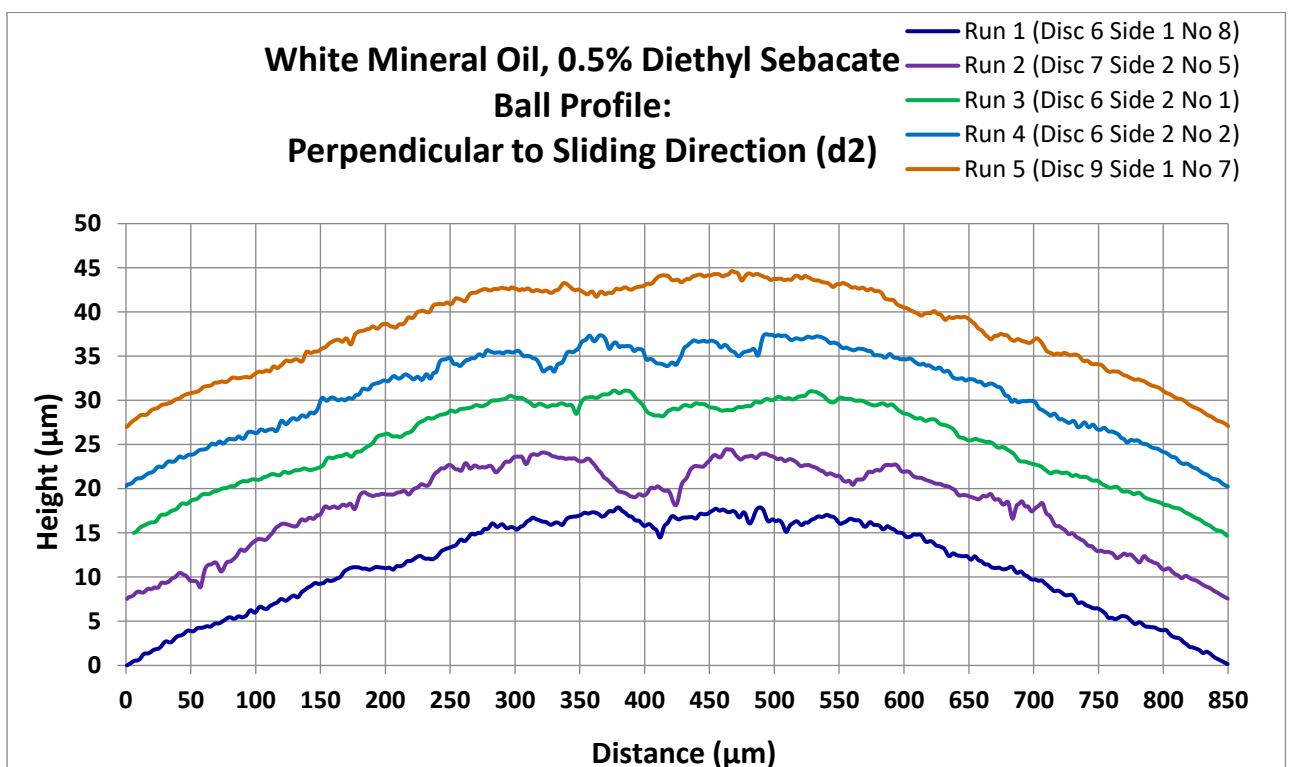


Figure 4.79: Wear profiles for **WMO + 0.5 % DES** measured on wear scars from friction and wear testing on the SRV test rig.

In Figure 4.79 it can be seen that the runs where the profiles were characterised by sharp peaks and valleys (Run 1 and 2), the friction coefficient was higher in Figure 4.79. For both these runs sharp peaks were found between 350 μm and 450 μm . The other three runs were characterised by smoother profiles, though they were still irregular. This then indicates that the sharp peaks increase the friction coefficient, since the load will be concentrated on these areas.

Shape Deviation

The characteristic where the edges of the wear scar parallel to sliding deviated from the rest of the wear scar (Figure 4.20) was only observed for the test fluids with **diethyl sebacate** as additive. In Figure 4.80, an example of a wear scar with this characteristic is given. This was the wear scar photographed for **PAO 6 + 3 % DES**. The corresponding wear profile in the direction perpendicular to the sliding direction is given in Figure 4.81. In this figure the enlarged edges formed a step or indent on the profile.

Finally, when the scar profile is fitted onto the track profile, as seen in Figure 4.82, the step is caused by wear from the edges of the wear track. A slight deflection is also observed at the edges, i.e., the surfaces do not lie 100 % on top of one another. This is due to deflection caused by elastic deformation (Batchelor & Stachowiak, 2003: 290-292).

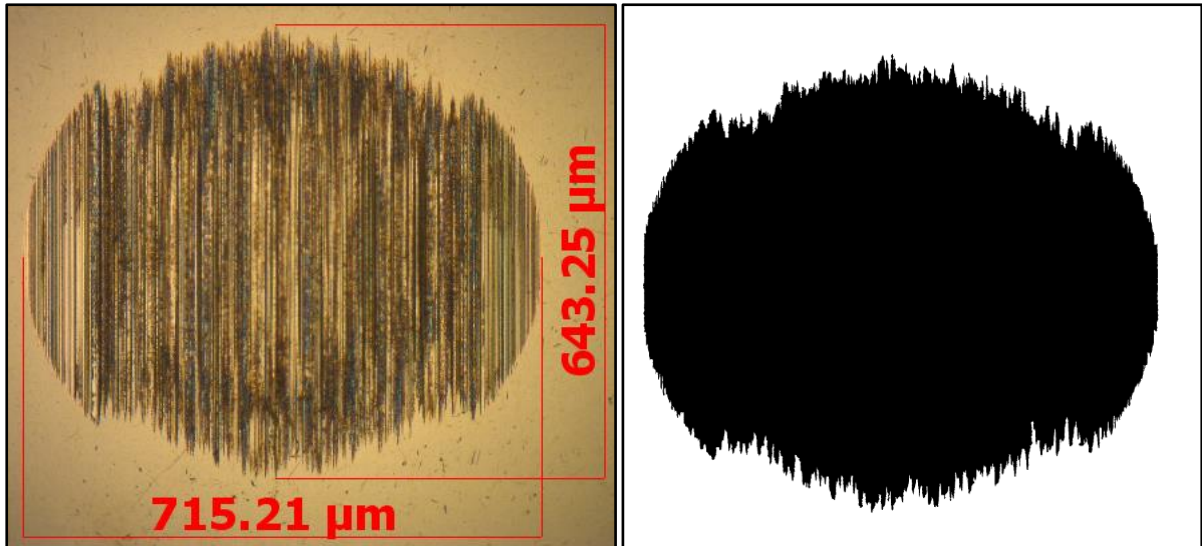


Figure 4.80: Example of a wear scar with enlarged edges. This wear scar was obtained from **PAO 6 + 3 % DES**, run 2.

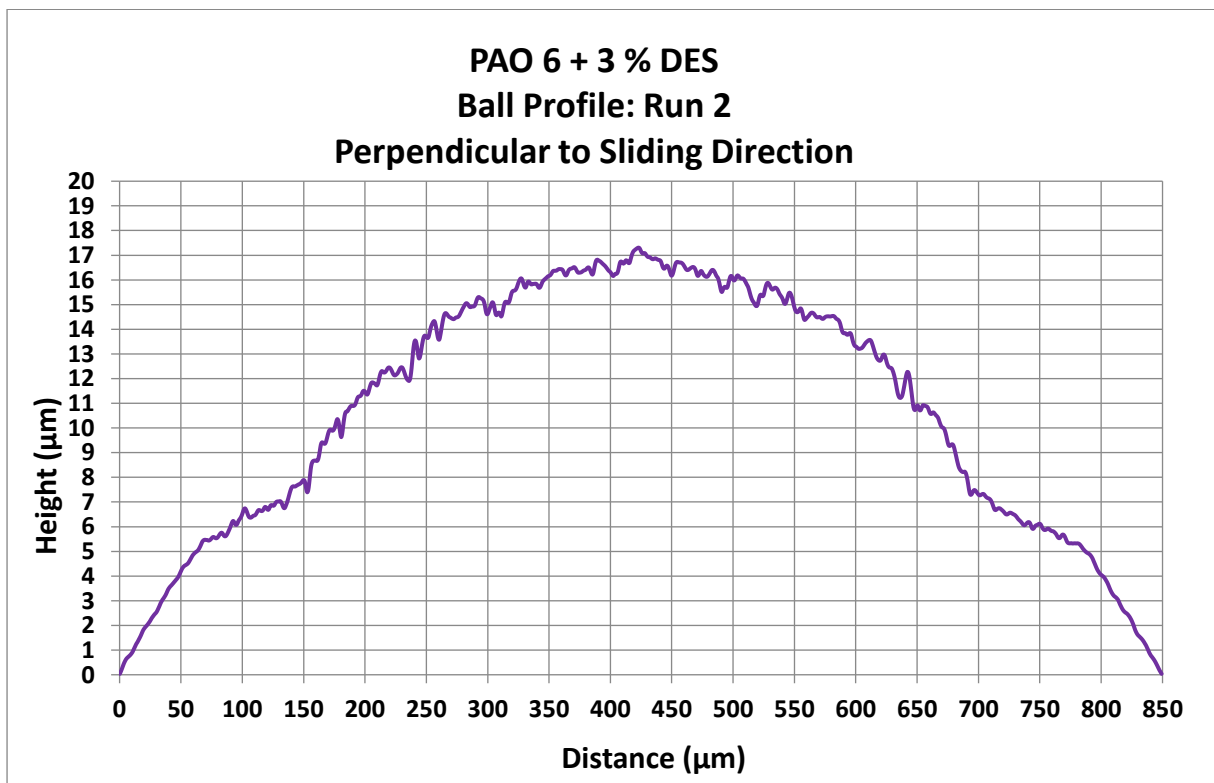


Figure 4.81: Wear surface profile perpendicular to sliding direction for wear scar obtained for 2nd run with **PAO + 3 % DES**.

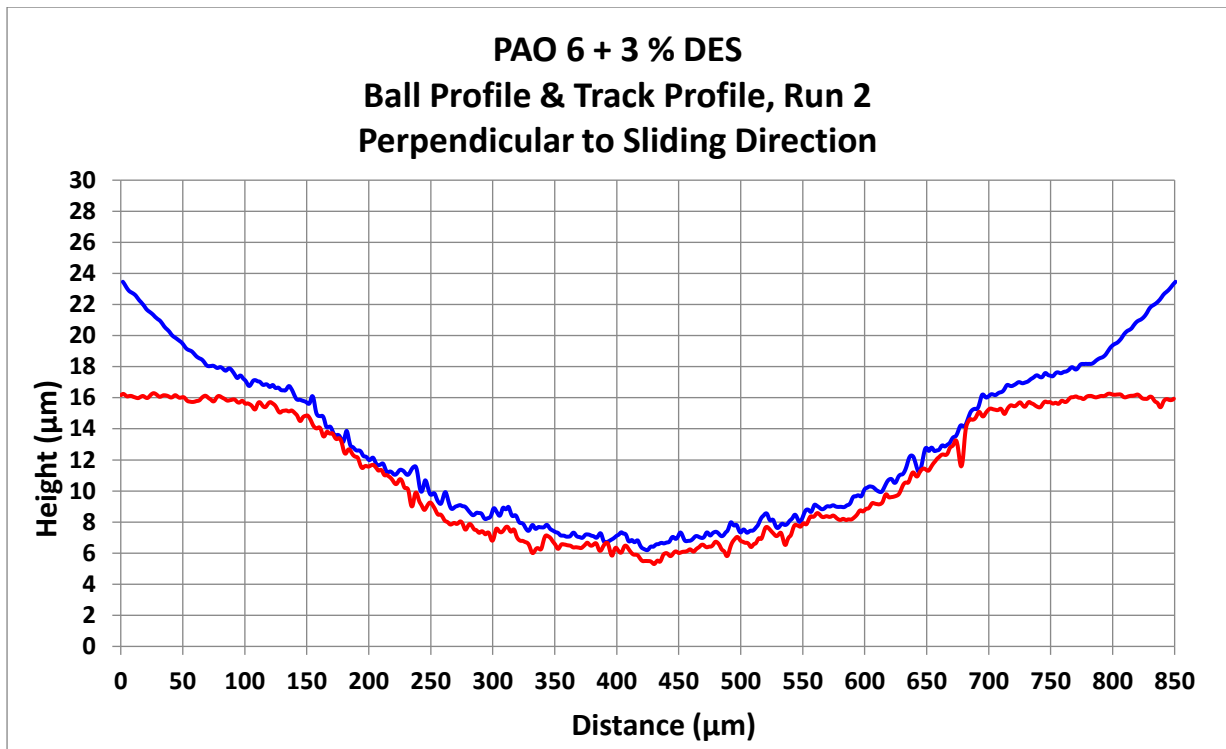


Figure 4.82: Wear surface profile on scar and track perpendicular to sliding direction for wear scar obtained for 2nd run with **PAO 6 + 3 % DES**.

4.5 Influence of the Test Disk

This section looks at the role of the test disk. This is due to the high number of disks that were used. A total of 8 repeat runs can be done on each face of the disk. Consequently, more than one disk had to be used to complete all the test runs (24 for each test method and 48 in total).

The effect of using multiple disks is shown in Figure 4.83. Here 4 disks were used. All 4 disks were from the same batch of test pieces. These disks will be referred to as A, B, C and D and all complied with the requirements as described in ASTM D 6425. From this figure:

- The friction coefficient plot for the run done on Disk B shows that the test failed after about 38 minutes.
- For Disk C, the friction coefficient was higher compared to Disk A.
- The friction coefficient plot obtained for Disk D compared very well with Disk A.

The ball wear scar diameters in Table 4.16 also indicate that good repeatability was obtained between Disk A and D. A larger ball wear scar diameter was obtained on Disk C.

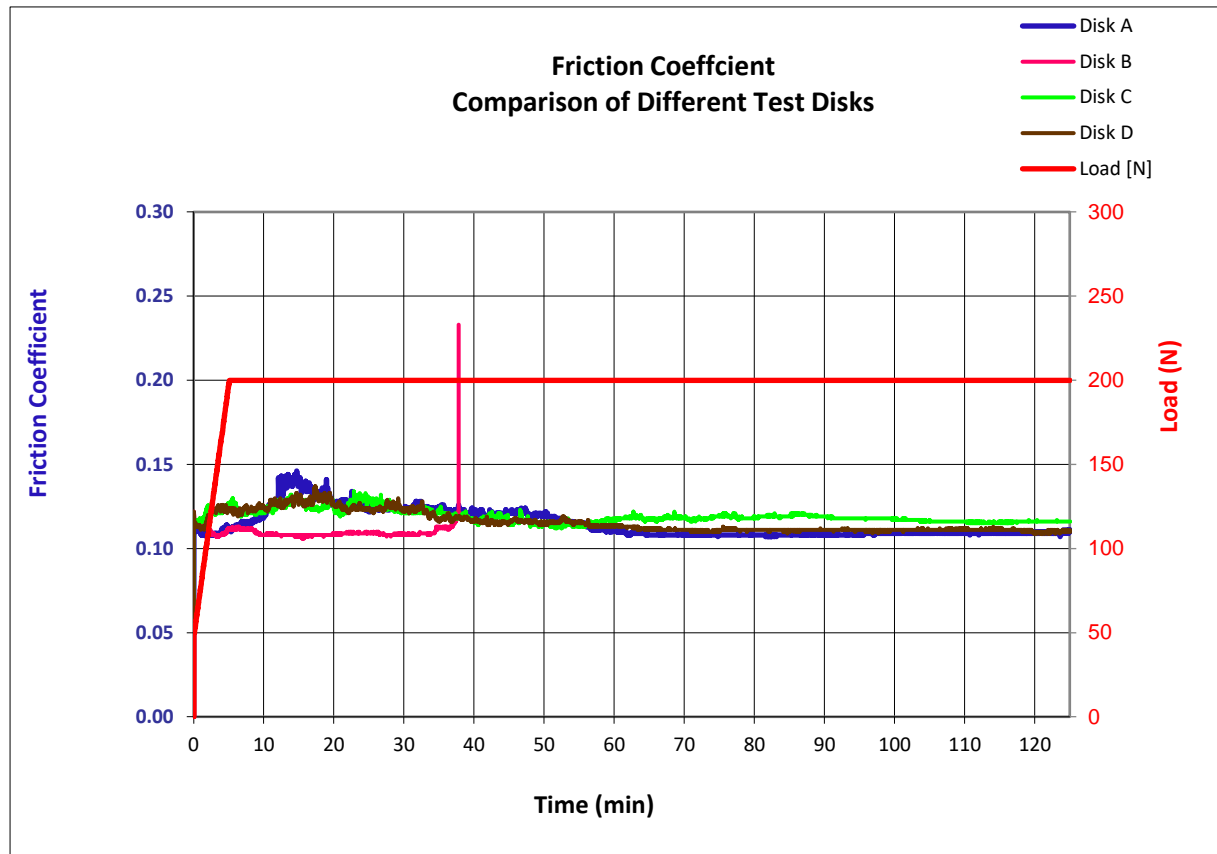


Figure 4.83: Comparison of friction coefficient plots for different test disks.

Table 4.16: Ball wear scar diameters measured for test runs conducted on different disks.

Disk	Ball Wear Scar Diameter		
	d_1	d_2	AVG
A	597	665	631
B	N/A*	N/A*	N/A*
C	641	722	682
D	598	664	631

* Due to seizure which resulted in test failing, no wear scar diameter was measured.

The surface roughness parameters of the 4 test disks are compared in Table 4.17. This was obtained with a detailed scan of the disk surface with the surface profiler:

Area = 3 mm x 3 mm

Step size = 0.8 μm

These parameters were determined along an arbitrary x and y axis on the disk. The reference point for the x-axis was the disk code, as indicated in Figure 4.84.

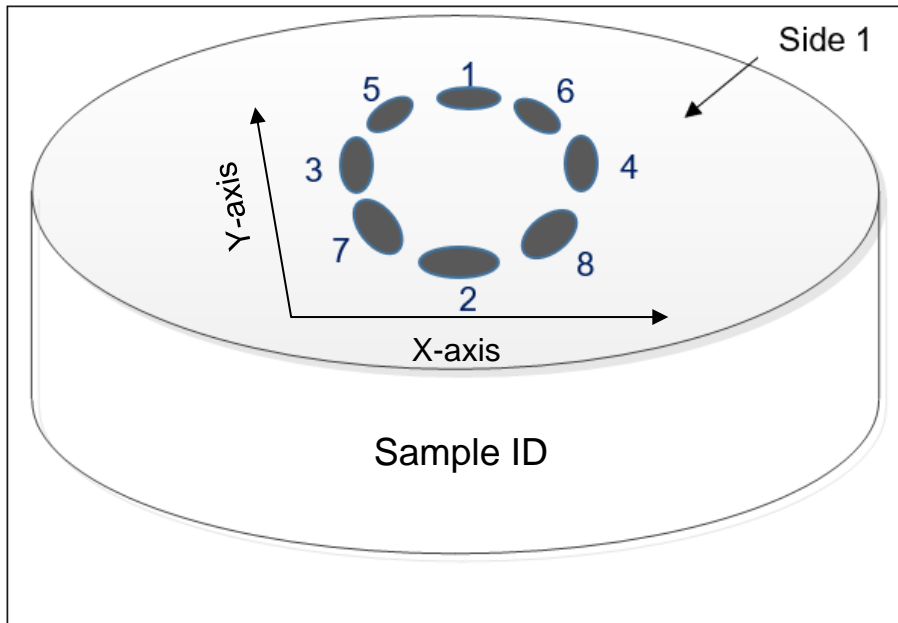


Figure 4.84: Position of the x-axis and y-axis along which the surface roughness parameters were determined.

Table 4.17: Surface roughness parameters determined for disk A to D.

	Disk A		Disk B		Disk C		Disk D	
	x	y	x	y	x	y	x	y
R_q (μm)	0.10	0.10	0.15	0.10	0.13	0.08	0.10	0.10
R_{Sk}	-1.25	-1.49	-2.75	-1.15	-2.84	-1.14	-0.92	-1.17
R_{Ku}	5.23	7.18	13.93	4.59	15.03	5.44	3.99	4.67
R_z (μm)	0.62	0.71	1.08	0.62	1.00	0.53	0.57	0.59
R_a (μm)	0.08	0.07	0.10	0.08	0.02	0.06	0.08	0.08

In Table 4.17 the root mean square (R_q) values measured on the x-axis were higher on Disk B and C compared to Disk A and D. This was also the case for the skewness (R_{sk}), kurtosis (R_{ku}) and average peak to valley height (R_z). The arithmetic average (R_a) on Disk C also had a larger value on the y-axis of the disk, while the R_a values in both directions on Disk C were smaller.

The root mean square and the average peak to valley height are measures of the surface roughness. On both Disk B and C, it was found that these values were higher. The friction coefficients as well as the wear scar diameters for these 2 disks also deviated from Disk A and Disk D. In the case of Disk A, the test was stopped prematurely due the friction coefficient which exceeded 0.3. No wear scar diameters were therefore measured.

The skewness is an indication of the degree to which a peak deviate from the vertical axis. If a peak does not deviate from the vertical axis, the skewness is equal to zero. Both Disk B and C had skewness that deviated more compared to the peaks on Disks A and D. This indicates that the orientation of the peaks also affects the results.

The last surface parameter deviated was the kurtosis. This is an indication of the sharpness of the peaks. The higher the kurtosis, the sharper the peak. The kurtosis was 2 to 3 times higher on Disk B and C compared to Disk A and D. Disks B and C therefore had sharper peaks. This can have an effect on the plastic deformation of the peaks, since the load is carried by a smaller area.

The effect of the microstructure of steel was investigated by several researchers in recent years. This included grain size (Bregliozzi et.al., 2003) and microstructures such as pearlite and cementite (Coronado et.al., 2019) and how the wear rate affect these properties. The higher loads carried by the sharper peaks can therefore alter the microstructure of the wear surface, which will influence the friction and wear process.

The Rockwell C hardness of the 4 disks was also measured (see Appendix C.6). These measurements indicate that the hardness between the disks was consistent. All the measurements taken on the surfaces at various positions had hardness values between 58.4 HRC and 60.3 HRC. This falls within conformance requirements of the test disks. Therefore, the hardness did not affect repeatability of friction and wear results.

Chapter 5

Conclusions & Recommendations

The factors that affect repeatability of the friction and wear test related to the test fluid are:

- The base oil viscosity.
- The base oil composition. This relates to the viscosity index and polarity of the base oil.
- The boundary lubricating additive.

All these factors affect the extent to which the metal surfaces can make direct contact. The better the fluids' ability to prevent contact, the smaller degree of asperity interactions. This in turn reduces the probability of deviations and so better repeatability will be obtained. Furthermore, the additive also plays an important role in the final shape of the wear scar.

Viscosity played an important role since the tests operate from the boundary to the elastohydrodynamic lubricating regime, as indicated by the modified Stribeck parameter. The system goes through the lubricating regimes with each stroke. This is due to the oscillating motion where the speed is zero at the start of each stroke and then accelerates to reach a maximum speed in mid-stroke. At this point, the highest Stribeck parameter is obtained. After this, the speed decreases again to zero to the end of the stroke.

The step load increase showed that the apparent contact area increased rapidly once the operating load is reached. This new area contains a band with unworn surface where wear occurs rapidly. High wear rates can change the microstructure of the metal and so cause variation in the wear surface. This can lead to poor repeatability.

The wear scar diameter adjustment improved repeatability of the friction and wear results for most base oils. The only exception was that the PAO 6-based oils did not

show any improvement. The main contribution of the adjustment is, however, that it improves the accuracy of the measurement.

The gradual load increase improves the consistency of the wear profile. This in turn results in more consistent interactions between the metal surfaces which result in improved repeatability of the friction coefficient and the extent of wear. The gradual load increase also showed a smooth transition when the load was increased compared to the step load increase.

The tests with shorter durations revealed that there are 3 regimes present:

Load Increase Regime: The highest extent of wear occurs in the lateral direction (wear scar diameter). However, wear rates calculated for the ball wear volume, indicate that a substantial extent of wear also occurs in the perpendicular direction into the ball. The friction coefficient is characterised by changes and transitions, either increasing or decreasing.

Running-in Regime: This regime is characterised by the highest extent of wear determined for the disk, while a substantial amount of wear still occurs on the ball. Most of the wear occurs in the perpendicular direction. A maximum friction coefficient is reached which is followed by a gradual decrease. The gradual decrease is due to the adhesion and deformation forces that decrease.

Steady State Regime: In this regime, the system is run-in and the majority of the wear occurs on the disk in the perpendicular direction. The extent of wear for the ball is small and a constant friction coefficient is obtained.

The system is therefore run-in when the wear surface can support the load without excessive increase in the wear scar diameter. The duration until running-in is completed and steady state is reached also depends on the properties of the test fluid: base oil viscosity, composition, and additive.

This section of the wear surface not only correlated surface phenomena to the wear profile, but also highlights the dependence of the friction coefficient on the wear profile. Larger friction coefficients are obtained for surfaces with sharper peaks.

Finally, the effect of the test disk cannot be excluded. The main influences of the test disk on repeatability of the test results include deviations of the surface roughness as well as the degree of skewness and the kurtosis (shape) of the asperities.

The novelty of the investigation is in identifying the factors affecting repeatability and improving repeatability with a gradual load increase. The gradual load increase improves the consistency of the surface profiles generated. Contributions were also made regarding adjustment of the wear scar diameter toward the accuracy of measurements. An improved method to evaluate the repeatability of the friction coefficient was also developed. This method is based on integration of friction coefficient plots for the entire duration of the test. Furthermore, by also analysing the wear rates, better insight into the duration of the running-in process on the SRV test rig was obtained.

Scope for further work would be to investigate the role that the disk plays on repeatability. It was seen that the disk surface finish affects friction and wear behaviour, however, other properties such as subsurface microstructures and grain sizes also influences results.

Reference List

1. AISI 52100 Alloy Steel (UNS G52986) (2012) AISI 52100 Alloy Steel (UNS G52986), Written by Azom.
2. Akbarzadeh, S and Khonsari, MM (2010) "On the prediction of running-in behaviour in mixed-lubrication line contact", *Journal of Tribology ASME*, 132, 032102-1.
3. Akchurin, A, Bosman, R & Lugt, PM (2017) "Generation of wear particles and running-in in mixed lubricated sliding contacts", *Tribology International* 110: 201-208.
4. Anastopoulos, G, Lois, E, Zannikos, F, Kalligeros, S & Teas, C (2001) "Influence of aceto acetic esters on diesel fuel lubricity" *Tribology International* 34: 749-755.
5. Anton Paar (2011) Instruction manual: SVM 3000/G2, Stabinger viscometer, Anton Paar GmbH, Austria.
6. ASTM D 2270 (1998) "Standard Practice for calculating viscosity index from kinematic viscosity at 40 and 100 °C", ASTM Int.
7. ASTM D 5707 (2016) "Standard test method for measuring friction and wear properties of lubricating grease using a high frequency, linear-oscillation (SRV) test machine", ASTM Int.
8. ASTM D6425 (2017) "Standard test method for measuring friction and wear properties of extreme pressure (EP) lubricating oils using SRV test machine", ASTM Int.
9. ASTM D 7042 (2016) "Standard test method for dynamic viscosity and density of liquids by Stabinger Viscometer (and the calculation of kinematic viscosity)", ASTM Int.
10. ASTM D7755 (2017) "Standard practice for determining the wear volume on standard test pieces used by high-frequency, linear-oscillation (SRV) test machine", ASTM Int.
11. ASTM G40 (2002) "Standard Terminology Relating to Wear and Erosion", ASTM Int.
12. AZO Materials (2000) "Physical properties: AISI 52100 steel", <http://www.azom.com> [7 April 2016].
13. Bagi, SD & Aswath, PB (2015) "Mechanism of friction and wear in MoS₂ and ZDDP/f-PTFE greases under spectrum loading conditions", *Lubricants* 3, 687 -711.

14. Bart, JCJ, Cavallano, E and Gucciardi, S (2013) *Biolubricants Science and Technology*, Woodhead Publishing, Oxford.
15. Batchelor, AW & Stachowiak, GW (2005) *Engineering Tribology*, Butterworth-Heinemann, USA.
16. Battez, AH and Gonzalez, R (2008) "CuO, ZrO₂ and ZnO nanoparticles as antiwear additive in oil lubricants", *Wear*, 265: 422–428.
17. Benadé, HP (2015) *Evaluating repeatability of friction and wear testing on a lubricant with dispersed hexagonal-boron nitride nanoparticles*, Dissertation for Master's degree, University of Pretoria, Pretoria, South Africa.
18. Biddle, TB, Meehan, RJ & Warner, PA (1987) *Standardization of lubricity test*, Air Force Wright Aeronautical Laboratories Report. AFWAL-TR-87, p. 40.
19. Blau, PJ (1981) "Mechanisms for transitional friction and wear behavior of sliding metals", *Wear*, 72: 55 – 66.
20. Blau, PJ (1989) *Friction and wear transition of materials*, Noyes Publications, USA.
21. Blau, PJ, (2005) "On the nature of running-in", *Tribology International*, 38: 1007 – 1012.
22. Blau, PJ (1996) *Friction science and technology*", Marcel Dekker, New York.
23. Blau, PJ (2017) "Lessons learned from the test-to-test variability of different types of wear data", *Wear* 376 – 377: 1830-1840.
24. Bhushan, B & Gupta, BK (1991) *Handbook of Tribology*, McGraw-Hill, USA.
25. Bhushan, B (2013) *Introduction to Tribology*, John Wiley & Sons, Ltd., New York.
26. Brandão, JA, Meheux, M, Ville, F, Seabra, JHO & Castro, J (2012) "Comparative overview of 5 gear oils in mixed and boundary film lubrication" *Tribology International* 47: 50-61.
27. Bregliozzi, G, Di Schino, A, Kenny, JM & Haefke, H (2003) "The influence of atmospheric humidity and grain size on the friction and wear of AISI 304 austenitic stainless steel" *Materials Letters* 57: 4505-4508.
28. Brown, SD, Tauler, R & Walczak, B (2009) *Comprehensive Chemometrics Chemical and Biochemical Data Analysis*, Elsevier.
29. Cen, H, Morina, A, Neville, A, Pasaribu, R & Nedelcu, I (2012) "Effect of water on ZDDP anti-wear performance and related tribochemistry in lubricated steel/steel pure sliding contacts" *Tribology International* 56: 47-57.
30. Chemical Book (2017) "Chemical Book: Diethyl Sebacate", <https://chemicalbook.com> [29 July 2019].

31. Cui, XH, Wang, SQ, Wang, F and Chen, KM, (2008) "Research on oxidation wear mechanism of the cast steels", *Wear*: 265, 468 – 476.
32. Ciruna, JA & Szieleit, HJ (1973) "The effect of hydrogen on the rolling contact fatigue life of AISI 52100 and 440C steel balls" *Wear*, 24: 107-118.
33. De Baets, P, Kalacska, G, Strijckmans, K, Van de Velde, F & Van Peteghem, AP (1998) "Experimental study by means of thin layer activation of the humidity influence on the fretting wear of steel surfaces" *Wear* 216: 131-137.
34. Digital Surf (1996) "MountainsMap® surface analysis software for profilometers", <http://www.digitalsurf.com> [14 August 2019].
35. Feser, T, Stoyanov, P, Mohr, F and Dienwiebel, M (2013) "The running-in mechanisms of binary brass studied in-situ topography measurements", *Wear*, 303: 465-472.
36. Farr, LPG (1975) "Molybdenum disulphide in lubrication: a review", *Wear*, 35: 1-22.
37. Fuller, ML, Fernandez, LR, Massoumi, GR, Lennard, WN, Kasrai, M and Bancroft, GM (2000) "The use of X-ray absorption spectroscopy for monitoring the thickness of anti-wear films from ZDDP", *Tribology Letters*, 8:187-192.
38. Gohar, R & Rahnejat, H (2012) *Fundamentals of Tribology*, 2nd edition, Imperial College Press, London.
39. Gold, PW, Schmidt, A, Dicke, H, Loos, J, & Assmann, C (2001) "Viscosity-Pressure-Temperature behaviour of mineral and synthetic oils", *Journal of synthetic lubrication* 18 (1).
40. Goto, H & Buckley, DH (1985) "The influence of water vapour in air on the friction behaviour of pure metals during fretting" *Tribology International* Vol 18 No 4.
41. Guo, F, Wang, W & Wong, PL (2004) "Application of partial elastohydrodynamic lubrication analysis in dynamic wear study for running-in", *Wear*, 257: 823 – 832.
42. Holmberg, K. (1991), *Tribological Bases for Accelerated Testing, in Operational Reliability and Systematic Maintenance by K.Holmberg and A.Folkesson (editors)*, Elsevier, p. 31-50.
43. Hsu, SM & Shen, MC (2005), *Wear Mapping of Materials, in Stachowiak, GW (Ed.), Wear – Materials, Mechanisms and Practise*, John Wiley and Sons, 369 – 423.
44. ISA-TR52.00.01 (2006) Recommended Environments for Standards Laboratories, Technical Report, Research Triangle Park, USA.

45. Johnson, DW and Hills, JE (2013) "Phosphate Esters, Thiophosphate Esters and Metal Thiophosphates as Lubricant Additives", *Lubricants* 1: 132-148.
46. Joshi, GS, Putignano, C, Gaudioso, C, Stark, T, Kiedrowski, T, Ancona, A & Carbone, G (2018) "Effects of the micro surface texturing in lubricated non-conformal point contacts", *Tribology International* 127: 296-301.
47. Kimball, S & Mattis, P (1996) "GIMP GNU manipulation program", <http://www.gimp.org> [03 September 2018].
48. Klaffke, D (1995) "On repeatability of friction and wear results and on the influence of humidity in oscillating sliding of steel-steel pairings" *Wear* 189: 117-121.
49. Kong, XL, Liu, YB, Qiao, LJ (2003) "Dry sliding tribological behaviors of nanocrystal-line Cu–Zn surface layer after annealing in air", *Wear*, 256: 747–753.
50. Kraschitz, E (2014) "Stabinger Viscometer", <http://www.anton-paar.com> [2014, July 26].
51. Kumar, R, Prakash, B and Sethuramiah, A (2002) "A systematic methodology to characterise the running-in and steady state wear process", *Wear*, 252: 445-453.
52. Lacey, PI (1994) *Wear mechanism evaluation and measurement of fuel-lubricated components*. US Army Contract Interim Report # BFLRF 286, Southwest Research Institute San Antonio, TX, p.40.
53. Lancaster, JK (1990) "A review of the influence of environmental humidity and water on friction, lubrication and wear" *Tribology International* Vol 23 No 6.
54. Langenhoven (2015) *The effects of humidity and soluble water content on the lubricity testing of a n-hexadecane and palmitic acid test fluid*, Dissertation for Master's degree, University of Pretoria, Pretoria, South Africa.
55. Lapuerta, M, Sánchez-Valdepeñas & Sukjit, E (2014) "Effect of ambient humidity and hygroscopy on the lubricity of diesel fuels" *Wear* 309: 200-207.
56. Lapuerta, M, Sánchez-Valdepeñas, J, Bolonio, D & Sukjit, E (2016) "Effect of fatty acid composition of methyl and ethyl esters on the lubricity at different humidities", *Fuel* 184: 202-210.
57. Ludema, KC and Lee, Y (1990) "The shared-load wear model in lubricated sliding: scuffing criteria and wear coefficients", *Wear*, 138: 13-22.
58. Ludema, KC (1996) *Friction, wear, lubrication*. CRC Press LLC, London.
59. Martin, JM, Le Mogne, T, Chassagnette, C & Gardox, MN (1992) "Friction of hexagonal boron nitride in various environments", *Tribology Transactions*, 35: 463 – 472.

60. Martin, JM (1999) "Antiwear mechanisms of zinc dithiophosphate: A chemical hardness approach", *Tribology Letters*, 6: 1-8.
61. Masilela, SR (2018) Assessment of the Friction Behaviour of selected Base Oils under Oscillatory Sliding Conditions, Dissertation: Master of Engineering (Chemical Engineering), University of Pretoria, Pretoria.
62. McCafferty, E & Zettlemoyer, AC (1971) "Adsorption of water vapour on α -Fe₂O₃", *Discussions of the Faraday Society*, Volume 52: 239-254.
63. Mei, Q, Ren, F, Zhao, C & Zhou, J (2019) "Microstructure and dry sliding wear behavior of ultrafine-grained Co-30 at% Cr alloy at room and elevated temperatures", *Journal of Alloys and Compounds* 770: 276-284.
64. Mettler Toledo Operating Instructions (2005) Operating Instructions: Mettler Toledo Excellence Plus XP Comparator Balances XP2004S, XP2003S, XP5003S, XP10003S, Mettler-Toledo GmbH.
65. Michelt, B, Schulze (2005) "The spectral colours of nanometers", Reprint from the *Journal Mikroproduktion* 3.
66. Miklozic, KT, Forbus, TR and Spikes, HA (2007) "Performance of friction modifiers on ZDDP-generated surfaces" *Tribology Transactions*, 50: 328-335.
67. Morina, A, Nedelcu, I, Neville, A, Soltanahmadi, S & Van Ejjik, MCP (2017) "Tribochemical study of micropitting in tribocorrosive lubricated contacts: the influence of water and relative humidity", *Tribology International* 107: 184-198.
68. Morimoto, T, Nagao & Tokuda, F (1969) "The relationship between the amounts of chemisorbed and physisorbed water on metal oxides" *The Journal of Physical Chemistry* Volume 73, Number 1.
69. Mortier, RM & Orszulik, ST (1993) *Chemistry & Technology of Lubricants*, Blackie Academic and Professional, Great Britain.
70. NANOVEA, NANOVEA® A Better Measure (pdf. Version of Product Brochure available online) [2016, July 27].
71. Nehme, GN (2017) "Tribological behavior and wear prediction of molybdenum disulfide grease lubricated rolling bearings under variable loads and speeds via experimental and statistical approach", *Wear* 376 – 377, 876 - 884.
72. Nogueira, I, Dias, AM, Gras, R and Progrid, R, (2002) "An experimental model for friction during running-in", *Wear*, 253: 541 – 549.

73. Okamoto, M, Jibiki, T, Ito, S and Motoda, T (2016) "Role of cross-grooved type texturing in acceleration of initial running-in under lubricated fretting", *Tribology International* 100: 126-131.
74. Onsøyen, S (1991) "Accelerated testing of components exposed to wear, in operational reliability and systematic maintenance by K. Holmberg and A Folkesson (editors)", Elsevier, p. 51 to 77.
75. Optimol Instruments SRV (2011) "SRV Test System Operating Manual", Optimol Instruments, Germany.
76. Pan, R, Ren, R, Zhao, X and Chen, C (2018) "Influence of microstructure evolution during the sliding wear of CL65 steel", *Wear* 400-401: 169-176.
77. Parsaeian, P, Ghanbarzadeh, A, Wilson, M, Van Eijk, MCP, Nedelcu, I, Dowson, D, Neville, A & Morina, A (2016) "An experimental and analytical study of the effect of water and its tribochemistry on the tribocorrosive wear of boundary lubricated systems with ZDDP-containing oil" *Wear* 358-359: 23-31.
78. Patir, N (1978) "A numerical procedure for random generation of rough surfaces", *Wear*, 47: 263 – 277.
79. Podgursky, V, Adoberg, E, Surženkov, A, Kimmari, E, Viljus, M, Mikli, V, Hartelt, M, Wäsche, R, Šíma, M & Kulu, P (2011) "Dependence of the friction coefficient on roughness parameters during early stage fretting of (Al, Ti) N coated surfaces", *Wear* 271: 853-858.
80. Quin, TFJ (1983a) "Review of oxidational wear – Part I: The origins of oxidational wear", *Tribology international*, 16: 257 – 271.
81. Quin, TFJ (1983b) "Review of oxidational wear – Part II: Recent developments and future trends in oxidational wear research", *Tribology international*, 16: 305 – 315.
82. Reis, BP, Lopes, MM, Garcia, A & dos Santos, CA (2018) "The correlation of microstructure features, dry sliding wear behaviour, hardness and tensile properties of Al-2wt%Mg-Zn alloys", *Journal of Alloys and Compounds* 764: 267-278.
83. Rhodes, KL & Stair, PC (1988) "The surface chemistry of zinc dialkyldithiophosphate, an antiwear additive on oxidized iron and steel foils", *Journal of Vacuum Science and Technology A*, 6: 971-974.
84. Rizvi, SQA (2009) *A Comprehensive Review of Lubricant Chemistry, Technology, Selection and Design*. ASTM International, USA.

85. Rudnick, LR (2003) *Lubricant Additives Chemistry and Applications*, Marcel Dekker, Inc., New York.
86. Sadowski, P & Stupkiewics, S (2019) "Friction in lubricated soft-on-hard, hard-on-soft and soft-on-soft sliding contacts", *Tribology International* 129: 246 – 256.
87. Savage, RH (1948) "Graphite lubrication", *Journal of Applied Physics*, 19: 1-10.
88. So, H (1995) "The mechanism of oxidational wear", *Wear*, 184: 161 – 167.
89. Spikes, HA (2004) "The history and mechanisms of ZDDP" *Tribology Letters* Vol. 17, No 3.
90. Soltanahmadi, S, Morina, A, van Eijk, MCP, Nedelcu, I & Neville, A (2017) "Tribocchemical study of micropitting in tribocorrosive lubricated contacts: the influence of water and relative humidity", *Tribology International* 107: 184-198.
91. Srivastava, SP (2009) *Advances in Lubricant Additives and Tribology*, Tech Books International, New Dehli, India.
92. Suzuki, M & Ludema, KC (1987) "The wear process during the 'running-in' of steel in lubricated sliding", *Journal of Tribology*, Vol. 109/587.
93. Tribonet (2021) "Stribeck Curve", <https://www.tribonet.org/wiki/stribeck-curve> [2021, July 19]
94. Svahn, F, Kassman-Rudolphi, A and Hogmark, S (2006) "On the effect of surface topography and humidity on lubricated running-in of a carbon based coating", *Wear*, 261: 1237 – 1246.
95. Ultrasonic cleaners made in China (2014) "Jenken ultrasonic cleaner limited", <http://www.ultrasoniccleaners-en-made-in-china.com> [2014, July 26].
96. Vengudasamy, B, Grafl, A, Novotny-Farkas, F, Schimmel, T & Adam, K (2013) "Tribological behaviour of antiwear additives used in hydraulic applications: synergistic or antagonistic with other surface-active additives?" *Tribology International* 67: 199-210.
97. Winer, WO (1967) "Molybdenum disulphide as a lubricant: a review of the fundamental knowledge", *Wear*, 10: 422 – 452.
98. Wos, S, Koszela, W, Pawlus, P, Drabik, J & Rogos, E (2018) "Effects of surface texturing and kind of lubricant on the coefficient of friction at ambient and elevated temperatures", *Tribology International* 117: 174-179.
99. Woydt, M & Weber, H (2003) "Improving the precision of specifications by evaluating the influence of test parameters on tribological results- a synthesis from

a series of international Round Robin tests”, report on Round Robin test conducted in 1997, 1998, 1999, 2000, 2001, 2002 and 2003, Munich.

100. Woydt, M & Ebrecht, J (2012) “Tribological testing on the translator oscillation apparatus”, Minutes of the annual meeting of the DIN 51835 work Group, Munich.
101. Woydt, M & Ebrecht, J (2013) “Tribological testing on the translator oscillation apparatus”, Minutes of the annual meeting of the DIN 51835 work Group, Munich.
102. Woydt, M & Ebrecht, J (2014) “Tribological testing on the translator oscillation apparatus”, Minutes of the annual meeting of the DIN 51835 work Group, Munich.
103. Woydt, M & Ebrecht, J (2015) “Tribological testing on the translator oscillation apparatus”, Minutes of the annual meeting of the DIN 51835 work Group, Munich.
104. Woydt, M & Ebrecht, J (2016) “Tribological testing on the translator oscillation apparatus”, Minutes of the annual meeting of the DIN 51835 work Group, Munich.
105. Woydt, M & Ebrecht, J (2018) “Tribological testing on the translator oscillation apparatus”, Minutes of the annual meeting of the DIN 51835 work Group, Munich.
106. Yin, Z, Kasrai, M, Fuller, M, Bancroft, GM, Fyfe, K and Tan, KH (1997) “Application of soft X-ray absorption spectroscopy in chemical characterization of antiwear films generated by ZDDP part1: The effects of physical parameters”, *Wear*, 202: 172-191.
107. Zambrano, OA, Gómez, JA, Coronado, JJ & Rodríguez (2019) “The sliding wear behaviour of steels with the same hardness”, *Wear* 418-419: 201-207.
108. Zhang, J, Yamaguchi, E & Spikes, H (2013) “Comparison of three laboratory tests to quantify mild wear rate” *Tribology Transactions*, 56: 919-928.
109. Zhang, J & Spikes, H (2016) “On the mechanism of ZDDP antiwear film formation” *Tribol Lett* 63:24.
110. Zhang, XA, Zhao, Y, Ma, K & Wang, Q (2016) “Friction behaviour and wear protection ability of selected base lubricants”, *Friction* 4(1): 72-83.

Appendix A: Studies on the Running-in Process

This section consists of summaries of results reported by various authors about the running-in process. This considers the factors and operating conditions that affect this process. The results are categorised according to the year of publication.

Nomenclature

A	Nominal area	(m ²)
d	Diameter of the pin	(m)
F_N	Normal contact force/load	(N)
P_i	Initial power density	(W/m ²)
R_A	Arithmetic mean of the height of the profile	(μm)
R_{pm}	average distance of five maximal peak heights to the mean line of the profile	(μm)
R_q	Root Mean Square	(μm)
r	Track radius on the disk	(m)
v	Sliding velocity	(m/s)

Greek

μ_i Initial friction coefficient

Other

Λ Ratio of film thickness divided by composite surface roughness

1. Ludema, KC and Lee, Y (1990) “The shared-load wear model in lubricated sliding: scuffing criteria and wear coefficients” *Wear*, 138, 13-22.

The objective of this study was the exploration of several time-dependent events in lubricated sliding where ratio of film thickness divided by composite surface roughness (Λ) ranges from 3 to 0.005. Λ values greater than 1 would imply that few asperities contact each other. A cylinder on disk setup was used with a sliding, unidirectional motion. The lubricants used were:

- Laboratory grade mineral oil – in an air atmosphere
- Synthetic automotive engine oil + additives – in an air atmosphere
- Vacuum pump oil – in a N₂ atmosphere

The investigation was conducted in the elastohydrodynamic to boundary lubricating regime. The variables that were measured were:

- Surface roughness
- Electrical contact resistance – indication of real area of contact
- Wear rate

The tests were started at high Λ values of about 3.0 and progressing stepwise to lower values. Each test was done at a specified Λ value. Lower values were obtained by adjusting the load and the speed. The surface roughness was also measured before each test to ensure that the desired Λ value was obtained.

The duration of each test run was 3 minutes. The surface roughness was again determined at the end of each test with a surface tracer system. Unfortunately, no other specifications are given about the surface analysis system. These tests were referred to as the progressive loading system.

The electrical contact resistance was used as an indication of the real area of contact by assuming that intermediate resistance values imply partial asperity contact. The intermediate resistance values refer to resistance values obtained for thin films and resistance values obtained for metallic contact.

Some tests were also done under conditions for Λ smaller than 1 without running-in. This was done to determine whether the tests would survive longer than 15 minutes. These are referred to as the intermediate loading tests. It is not specified with what is implied with running-in.

From these tests it was found that:

- The *surface roughness* became rougher for the progressive loading conditions for all the lubricants. The vacuum pump oil in nitrogen atmosphere, was not able to adequately lubricate at Λ values less than 1 (Figure A.1).
- *Electric contact resistance* decreased as Λ values decreased. This indicates that the assumption that metallic contact increases as film thickness decreases is true and that real contact area increases at smaller Λ values. This is true for Λ values between 1 and 3. Below Λ values of 1, no observable change in ECR was observed (Figure A.2).
- The wear rate was found to be linear until just below $\Lambda = 1$ for mineral oil, where after the change in wear rate decreased with decreasing Λ (Figure A.3).
- The linear region in terms of wear rate for engine oil was well below Λ value of 1 (see Figure A.3).

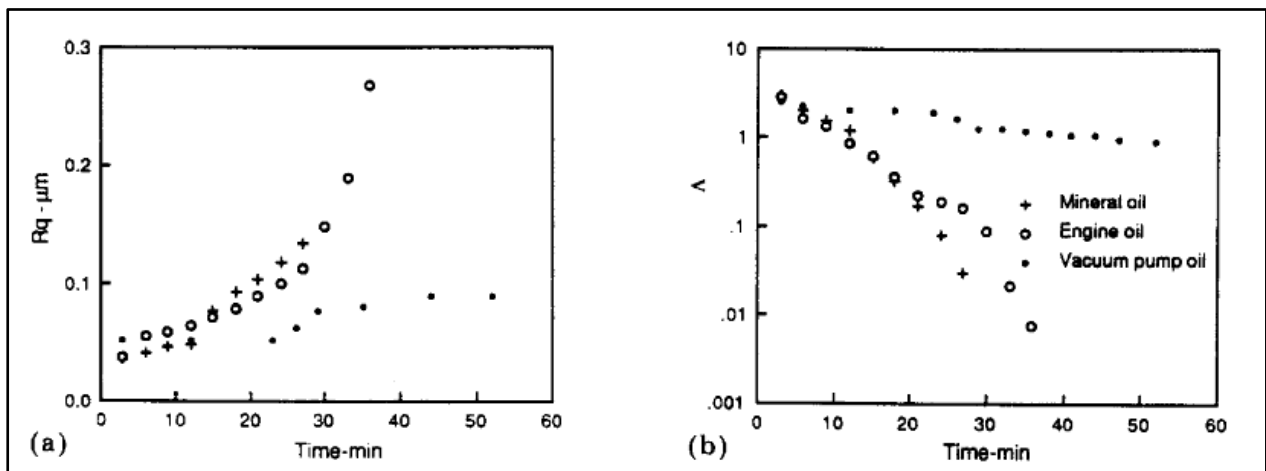


Figure A.1: Changes in (a) surface roughness and (b) Λ with time.

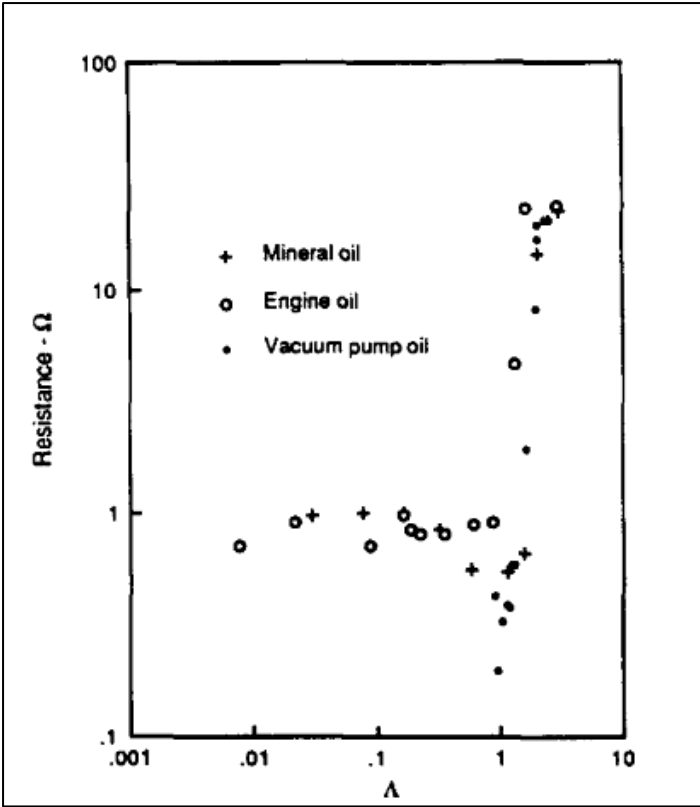


Figure A.2: Variation of contact resistance with Λ .

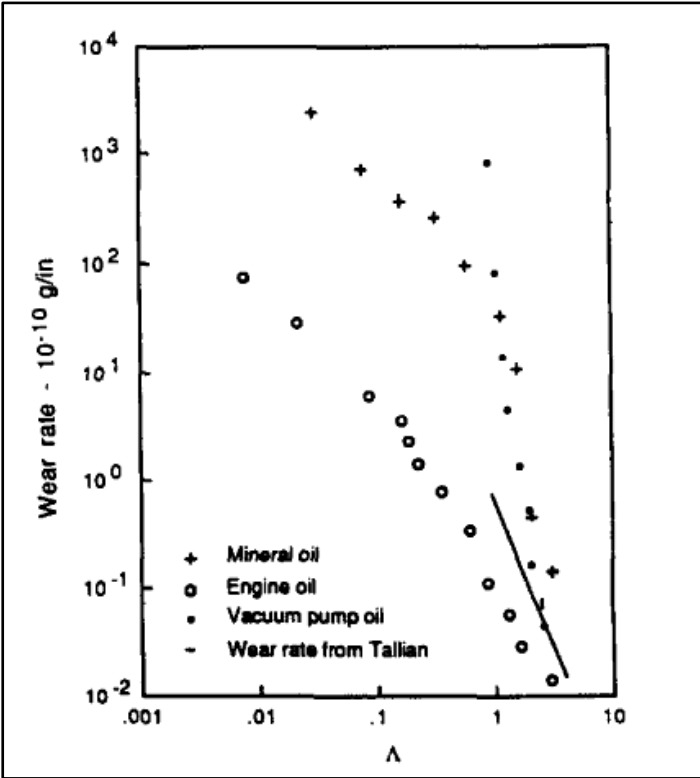


Figure A.3: Variation of wear rate with Λ .

1. Kumar, R, Prakash, B and Sethuramiah, A (2002) “A systematic methodology to characterise the running-in and steady state wear process” *Wear* 252, 445-453.

The objective in this study was to develop an improved methodology to characterise running-in and steady state wear processes (see Figure A.4). This was achieved by developing empirical relations for:

- Running-in wear rate
- Running-in period wear rate and
- Steady state wear rate

The wear rates were determined as functions of:

- Load
- Surface roughness
- Temperature

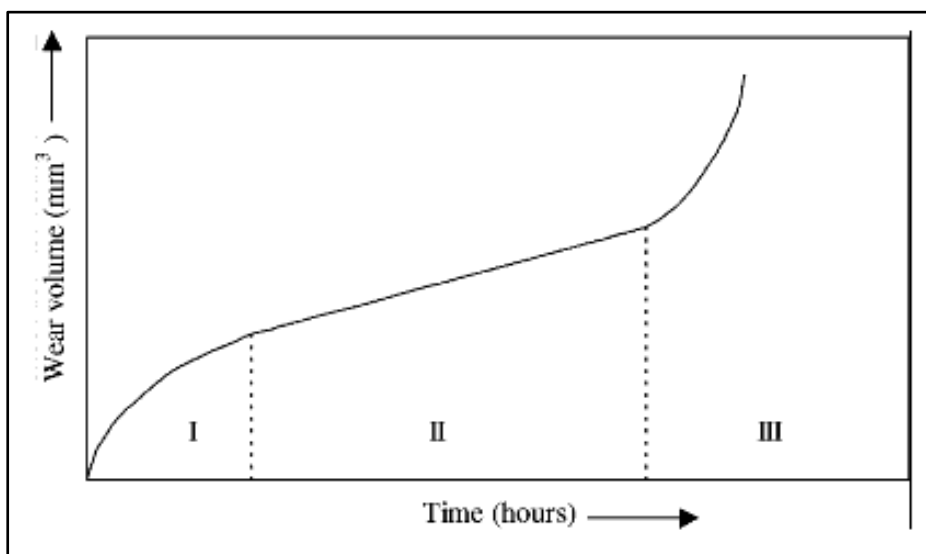


Figure A.4: Wear behaviour of a new component in its life span. (I) Running-in zone; (II) steady state wear zone; (III) wear out zone.

The investigation was done on the SRV tester with EN 31 steel specimens. The test setup was a ball-on-disk configuration with oscillating motion. The test fluid consisted of commercial engine oil which contains zinc dithiophosphate. The test fluid was only

applied to the contact surface at the start of each test. The parameters for this experimental investigation are summarised in Table A.1.

Table A.1: Test parameters on SRV

Parameter	Value
Frequency	50 Hz
Stroke	1 mm
Test Fluid Volume	0.1 cm ³
Test duration	10, 20, 30, 60 and 120 minutes
Load	20, 40 and 60 N
Temperature	50, 100 and 150 °C
Surface roughness (R_q)	0.35, 0.55 and 0.75 μm

From this study it was found that

- The running-in wear rate increase with increase in the load, surface roughness and temperature.
- Steady state is reached faster with rougher surfaces, and therefore the running-in duration decrease with increase in surface roughness. The same is true for an increase in the load.
- The wear rate also increased with increasing initial surface roughness. The final surface roughness reached a value of about 0.15 μm , regardless of the initial surface roughness.
- Wear rate decrease with decrease in temperature. This is considered to be due to reaction films which are formed.

2. Nogueira, I, Dias, AM, Gras, R, and Progri, R, (2002) “An experimental model for friction during running-in” *Wear* 253, 541 – 549.

A model is proposed whereby the friction coefficient is controlled by a single hydrodynamic parameter (modification of Stribeck hydrodynamic parameter). This hydrodynamic parameter considers the elastic deformation of asperities. This model

is based on experimental results which considered a wide variety of factors influencing the conditions in which the contact operates. This is divided into three categories:

1. Functional parameters
 - a. Normal load
 - b. Sliding speed
 - c. Viscosity
2. Contact pairs mechanical properties
 - a. Elastic modulus
 - b. Poisson's ratio
3. Surface microgeometry
 - a. Expressed by standardized roughness parameters

This was conducted with a pin on rotating (uni-direction) disk tribometer. The test fluid was 100 Neutral solvent oil which is a mineral paraffin-based oil without any additives. The composition for the test specimen pairs was also varied.

Two series of test were conducted on the tribometer. In the first series, the speed was varied sequentially as a step function (minimum 0.1 m.s^{-1} and maximum 3.0 m.s^{-1}). This can also be seen in Figure A.5. The coefficient of friction as a function of the speed are also given in Figure A.6.

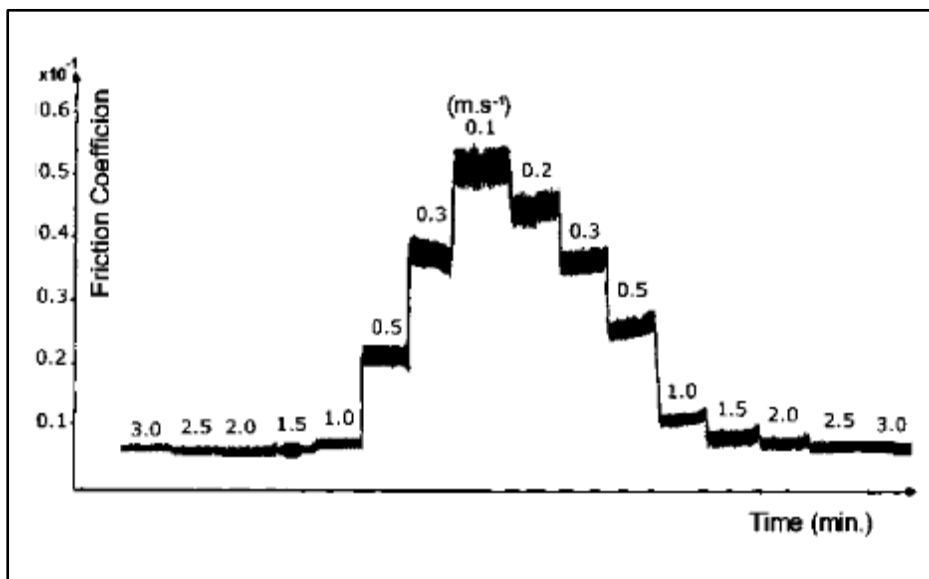


Figure A.5: Friction coefficient measured at variable speed as a step function.

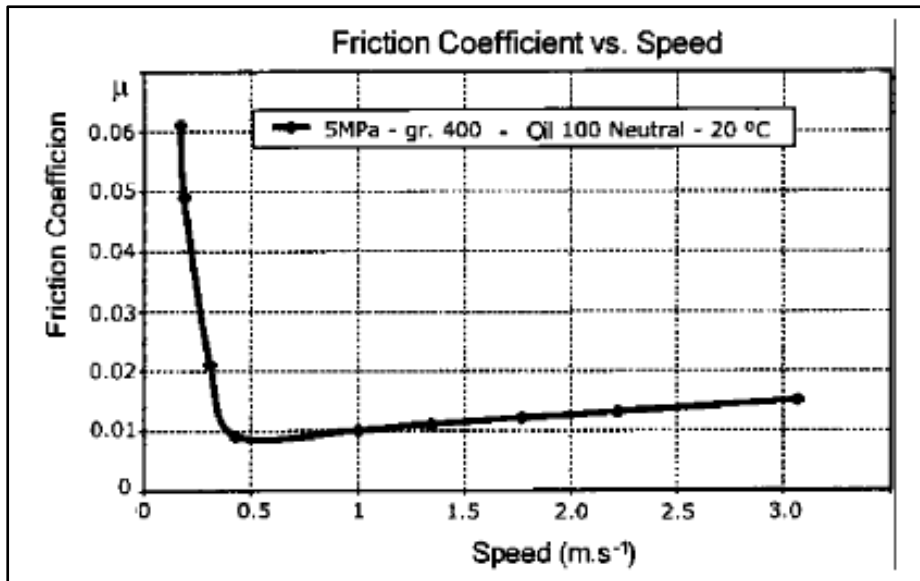


Figure A.6: Coefficient of friction as a function of speed.

The operating conditions for the tests on the pin-on-disk tribometer are summarised in Table A.2. The materials used are also given in this table. The disk material was ball bearing steel AFNOR C.

From these results it was found that:

- The friction coefficient decreases with increasing sliding speed. This is due to placement on the Stribeck curve which moves to mixed and elastohydrodynamic lubricating regime as the speed is increased.
- Smaller values for surface finish resulted in lower friction coefficient.
- The transition from mixed to hydrodynamic lubrication is more abrupt with fine finishes. This is due to a larger mixed lubrication regime for rougher surfaces.
- More ductile materials have a smaller hydrodynamic parameter, i.e., full film regime onset occurs quicker.
- Profile analysis of the surfaces during the running-in period indicates that plastic deformation occurs.

Table A.2: Test parameters on pin on rotating disk tribometer

Parameter	Value	
Sliding speed	0.1 m.s ⁻¹ to 3.0 m.s ⁻¹	
Speed stage duration	1 min	
Load	5 and 10 MPa	
Temperature	20 °C	
Surface roughness: disks		
R_a	0.04 µm	
R_{pm}	0.12 µm	
Surface roughness: pins (R_{pm})		
	Sandpaper 400	Sandpaper 80
Aluminium AFNOR Al 6082	1.41	4.86
Brass AFNOR UZ 40 M3A	0.79	4.56
Stainless steel AFNOR Z6 CND17-12	0.45	2.11
Spring steel AFNOR	0.74	1.73
Carbon steel AFNOR XC 42	0.81	2.59
Alloyed steel AFNOR 35 NCD	0.53	1.48
Alloyed steel AFNOR 40 CD	0.83	2.21

* R_A refers to the arithmetic mean of the height of the profile and R_{pm} refers to the average distance of five maximal peak heights to the mean line of the profile.

4. Blau, PJ, (2005) “On the nature of running-in” Tribology International 38, 1007 – 1012.

This paper is a summary of theory which focuses on running-in. Most of the theory discussed in this paper has already been included in the literature study. However,

some additional theory has also been added. This includes a summary of the factors that influence the changes that occur in friction and wear during running-in:

1. Surface roughness alterations
2. Changes in surface composition
3. Microstructure
4. Third-body distribution
5. Contact alignment
6. Surface preconditioning

It is also stated that:

“Appropriate running-in practices during friction testing can improve repeatability of results and enhance the ability of a test to detect subtle changes in lubricant condition.”

The 8 types of break-in/running-in curve shapes are also given in this paper, which can also be seen in Figure A.7. The purpose of these curves is to assist with the identification of the transitions which occurs during running-in.

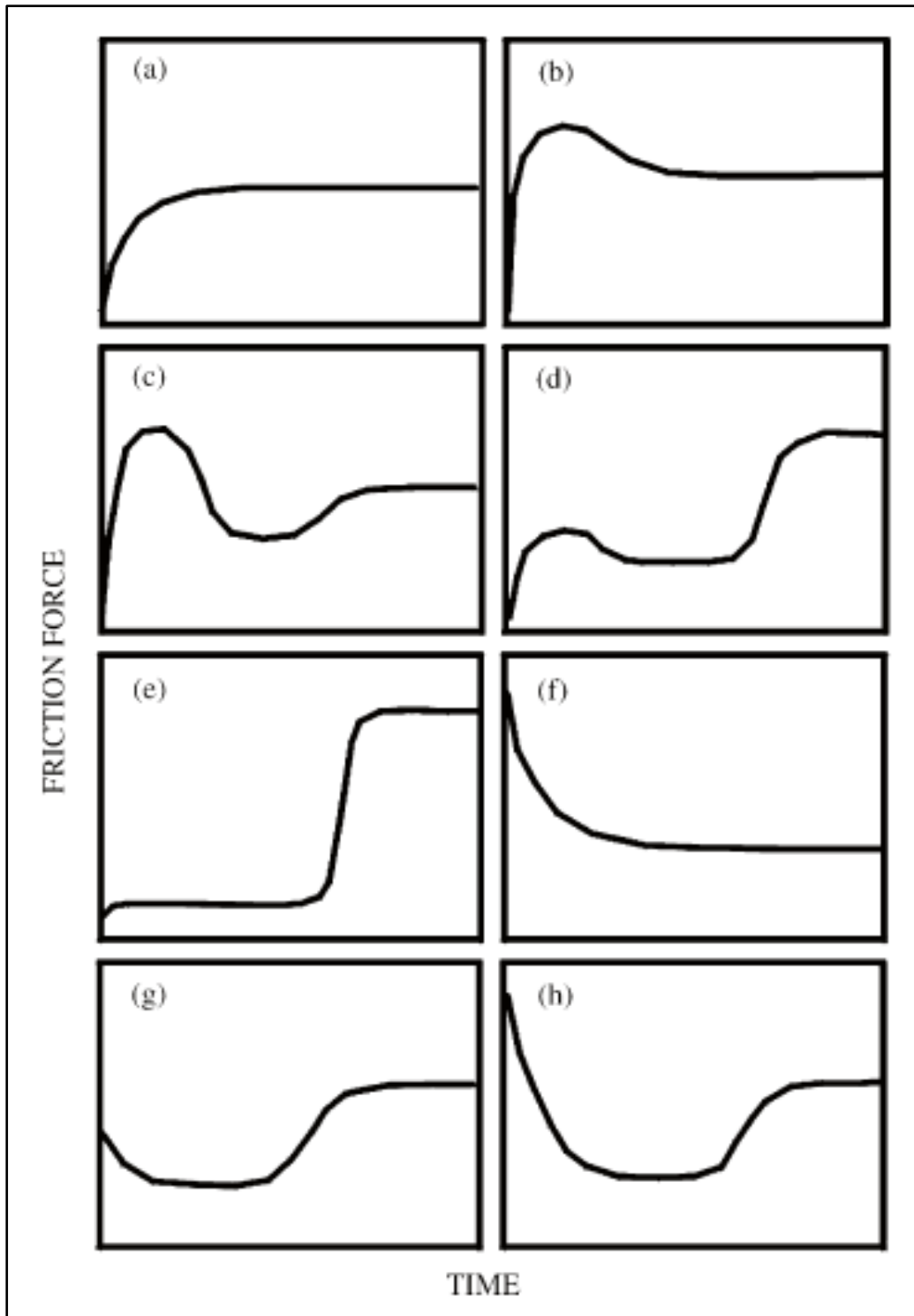


Figure A.7: Types of running-in curves. Friction force is on the vertical axis and time, or number of cycles is given on the horizontal axis.

The characteristics of some of the curves are:

- a: Dry, non-intentionally lubricated metal couple having a small amount of surface contamination, oxide or adsorbed species that is quickly worn away to cause a greater degree of adhesion and a rise in friction.
- b: Common for boundary lubricated or even non-lubricated metals (example steel on steel) in which the initial roughness of the surface produce a momentary rise in friction until surface conformity and smoothing occurs, reducing the friction.
- c & d: These curves are a combination of curve b and a second transition to a new steady state which occurs. The only difference between c and d is the relative heights of the first peak and the second steady state friction force value (Blau, 1989: 277).
- e: This curve relates more to transition in behaviour than running-in. The first part before a steady state is reached is the running-in period and a transition occurs to a new steady state. These types of curves have been observed for self-lubricating polymers and liquid or solid lubricant which degrades.
- f: This curve is the opposite of a. This curve is obtained in sliding of very clean metals in a vacuum. It also occurs for surface which are initially rough and that conforms to form smoother surfaces. This curve has also been observed for tribosystems which are restarted (Blau, 1989: 279).
- g & h: These two curves are essentially the same. Both begins as type f, but a transition occurs before steady state is reached, and a higher friction value is obtained. For curve g, the initial friction value is below the final steady state value and for curve h, the opposite is true. These two curves are quite uncommon but can be observed for flat-on-flat surfaces (Blau, 1989: 279).

3. Svahn, F, Kassman-Rudolphi, A and Hogmark, S (2006) “On the effect of surface topography and humidity on lubricated running-in of a carbon based coating” *Wear* 261, 1237 – 1246.

The objective of this study was to determine the effect of surface roughness and humidity on the running-in of non-hydrogenated carbon coatings. A sputtered carbon coating (a-C-Cr) was deposited on substrates (disks) with 4 different surface treatments. The surface treatment on the disks was:

- Polished

- Ground
- Wet-blasted
- Blasted with dry sand

It is important to mention that a sufficient humidity is required for carbon coatings to obtain a low coefficient of friction in sliding. A too dry atmosphere may cause high friction coefficient values and failure in unlubricated conditions. Therefore, effect of humidity in lubricated sliding was therefore also included in the scope.

Four different oils were used in this investigation:

- Polyalphaolefin (PAO)
- Paraffinic mineral oil
- Complex ester
- Fully formulated engine oil (Mobil Delvac HP-F 10W-30)

The rest of the test parameters are given in Table A.3.

Table A.3: Test parameters for tests on ball on disk tribometer.

Parameter	Value
Sliding speed	0.05 m.s ⁻¹
Rotational radius	25 mm
Revolutions	115000
Load	30 N
Temperature	20 °C
Amount of lubricant	0.2 g
Surface roughness: disks (R_q)	
Polished	3 nm
Ground	150 nm
Wet-blast	200 nm
Dry-blast	1000 nm
Surface roughness: ball (R_q)	
	30 – 40 nm
Humidity	
Normal	50 – 60 %
Low	5%

Friction coefficient

It was observed in the results that the steady state friction coefficient was lower for the test done in a dry atmosphere, except when formulated engine oil was used as test fluid on wet-blasted surfaces. This shown in Figure A.8.

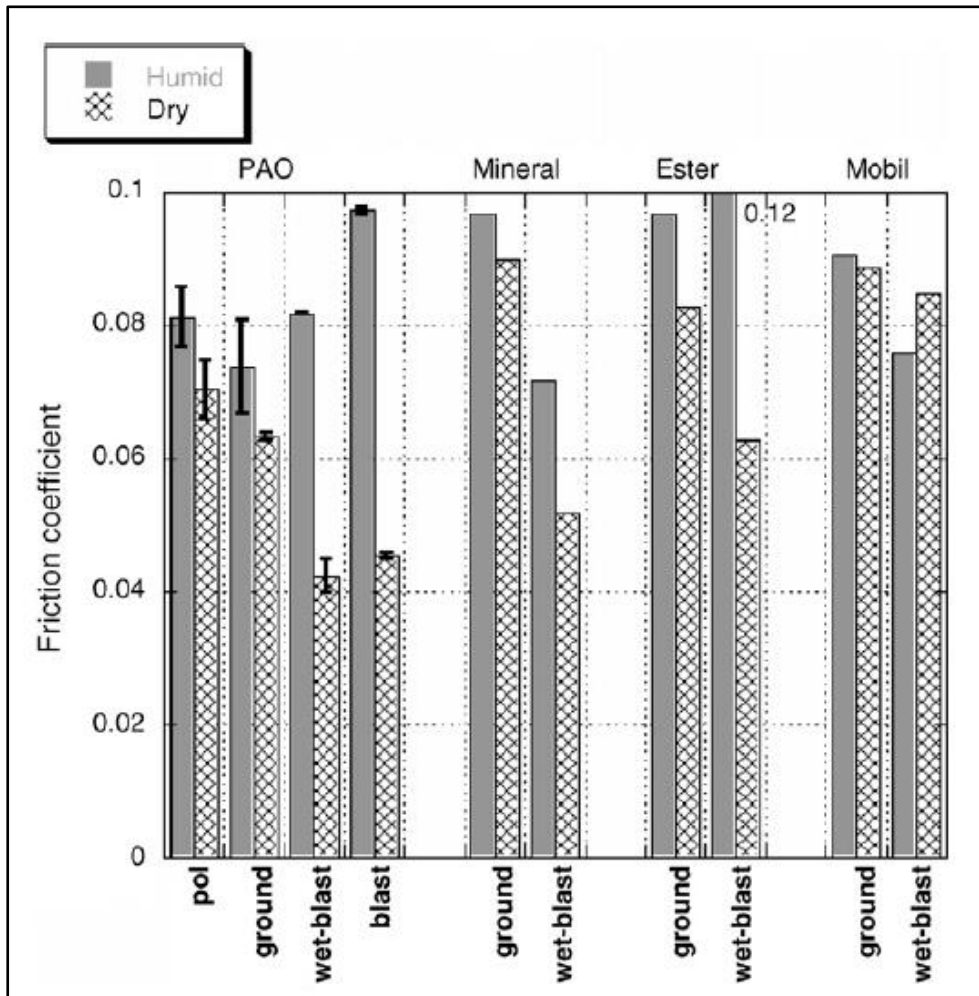


Figure A.8: Steady state friction coefficients obtained during testing

As mentioned earlier, the presence of water vapour improves the lubricity of coated surfaces in the absence of liquid lubricants. The result of the polished finished surface is given in Figure A.9. This result is the exact opposite that is obtained for liquid lubricants.

It has been observed by Winer, 1967, Farr, 1975, Savage, 1948 and Martin et.al., 1992 that the performance of solid lubricants depends on the absence or presence of certain chemical species. Water for instance weakens the residual bonds between layers for

graphite, H_3BO_3 and h-BN. This then is most likely the reason for the poor performance of the coated surfaces in Figure A.9.

It has also been observed that the humidity increases the friction coefficient (de Vaal and Langenhoven, 2015: 114 - 119). It should also be noted here that the composition of the test fluid consisted of n-hexadecane and palmitic acid. The effect of water vapour on the friction value may differ with composition of test fluid.

The surface finish also influences the shape of the friction coefficient curve (see Figure A.10). When the surface becomes rougher from ground to wet-blasted, the shapes changes completely, especially when the running-in period is considered.

Furthermore, the effect of humidity seems to become more pronounced with an increase in surface roughness when Figures A.10 a and b are compared. The difference for grounded surfaces is almost insignificant, while it is much more pronounced for wet-blasted surfaces.

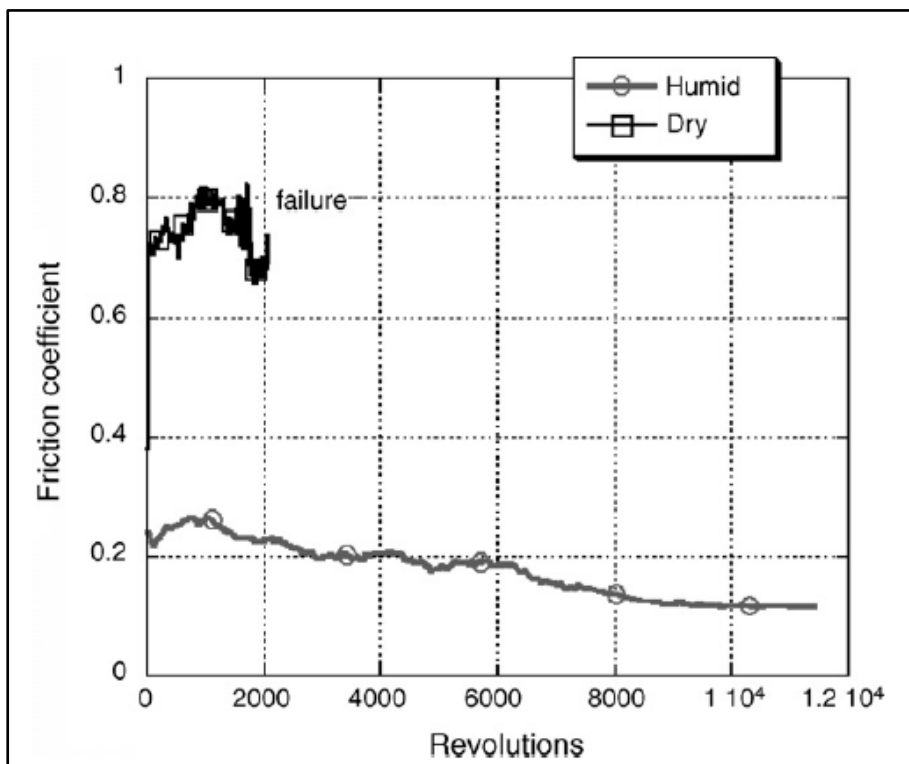


Figure A.9: Friction coefficient obtained in unlubricated contact. The surfaces were polished.

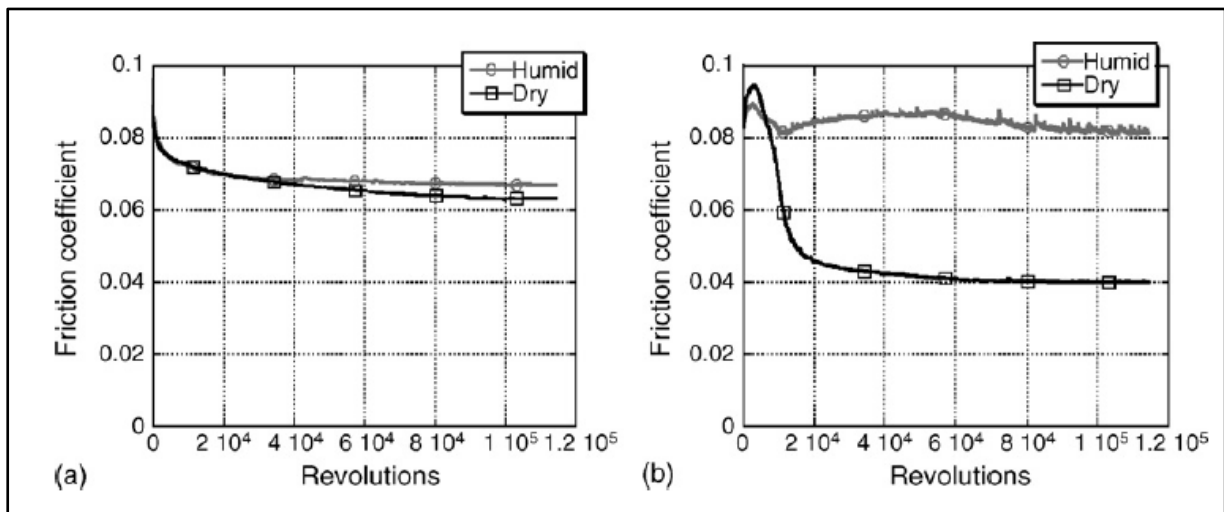


Figure A.10: Coefficient of friction curves for ground (a) and wet-blasted (b) surfaces in dry and humid atmospheres. The test fluid used in these figures was polyalphaolefin.

Wear

The results of wear rates on the ball specimen are given in Figure A.11. The trends about the lubricant are:

If test fluid and humidity are constant, but roughness varied.

- PAO: Small difference between polished and ground surface. Increase in wear rate much higher with increase in roughness.
- Mineral oil, ester, and Mobil engine oil: increase in surface roughness result in increase in wear rate.

If test fluid and roughness are constant, but humidity is varied.

- PAO: It seems that the trend is that the wear rate decreases with a decrease in humidity, except with polished surfaces.
- For the mineral oil, ester and Mobil engine oil, the trend seems to depend on the test fluid, as well as the magnitude of the wear rate difference between the humid and dry conditions.

If humidity and roughness are constant, but test fluids are compared – humid conditions

- The PAO and fully formulated engine oil had the lowest wear rates with grounded surfaces.
- The wear rate increased considerably for Mobil engine oil on a wet-blasted engine oil.

If humidity and roughness are constant, but test fluids are compared – dry conditions

- POA outperformed the other lubricants in dry conditions, regardless of the surface roughness.

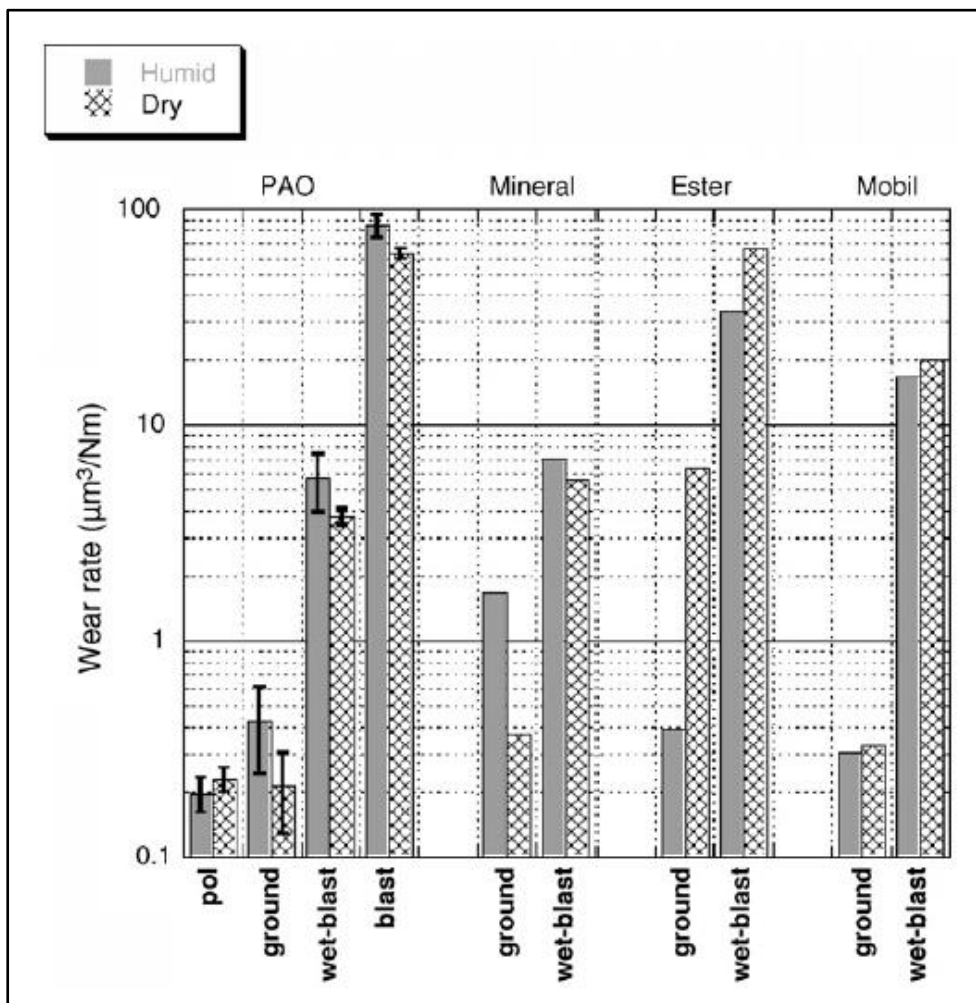


Figure A.11: Summary of ball wear rates from coated lubricated ball-on-disk tests.

When the wear rate during a test is considered, it is seen that the wear rate is initially high but declines as the test proceeds. This can be seen in Figure A.12. The wear rate during the first 200 cycles can be referred to as the running-in period. Again, the humidity has a significant effect on the wear rates.

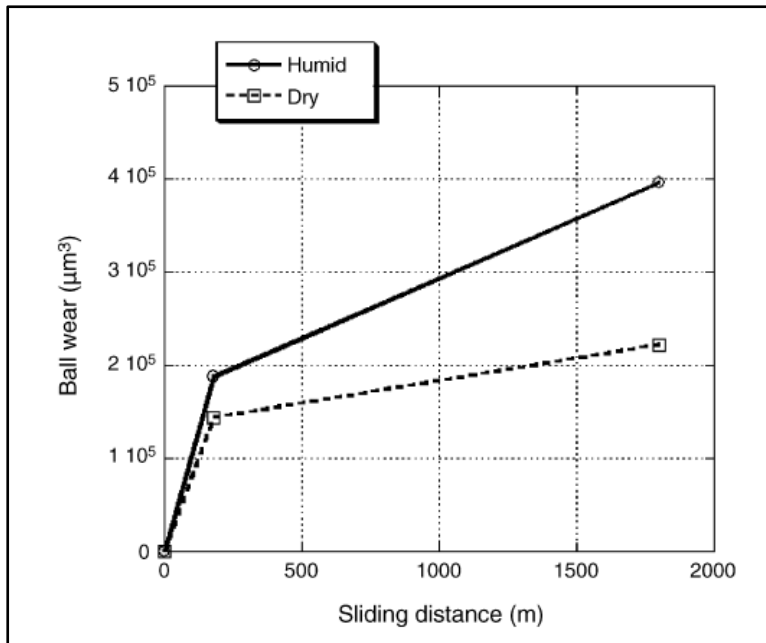


Figure A.12: Wear (on ball) progress during testing of PAO with coated wet-blasted surfaces.

XPS

XPS depth profiles revealed that both wear surfaces for humid and dry conditions on coated surfaces displayed an increase amount of O, C and Cr toward the surface. The increase in Cr indicates a material transfer from coating to the surface. The oxygen atoms observed indicates that an oxide layer was formed on the surface. The XPS results are given in Figure A.13.

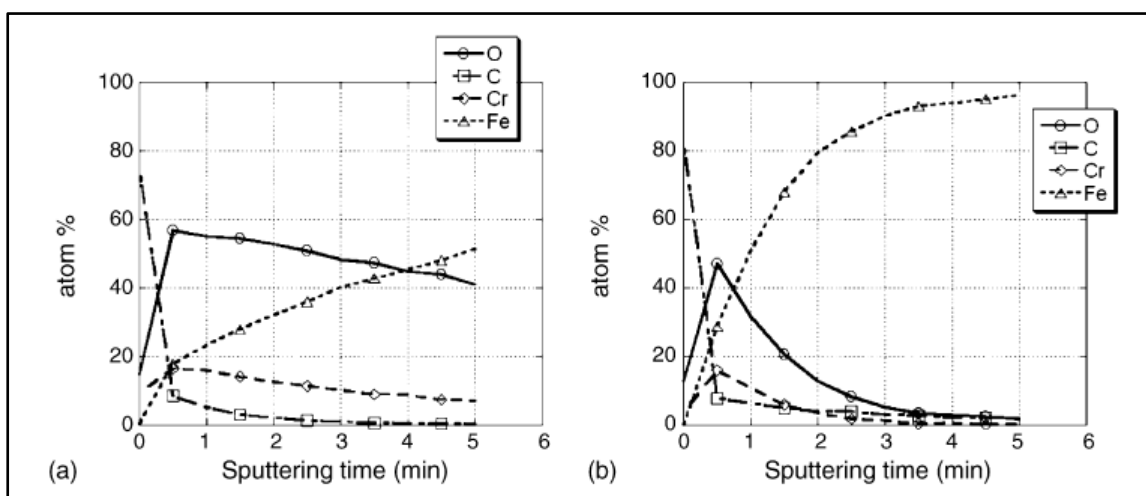


Figure A.13: XPS depth profiles of wear surfaces of ball-on-coated wet-blasted surface. Test fluid was PAO, and conditions were a. dry air and b. humid atmosphere.

This investigation indicates that the requirements for successful running-in are:

- Macroscopic pressure reduction
- Smoothing of the surfaces
- Formation of tribolayer.

Such running-in should result in substantial decline in the friction coefficient with sliding distance and low steady state wear. Macroscopic pressure reduction is obtained due to flattening of the ball surface caused by wear. The effect of the wear surface on the macroscopic pressure is shown in Figure A.14.

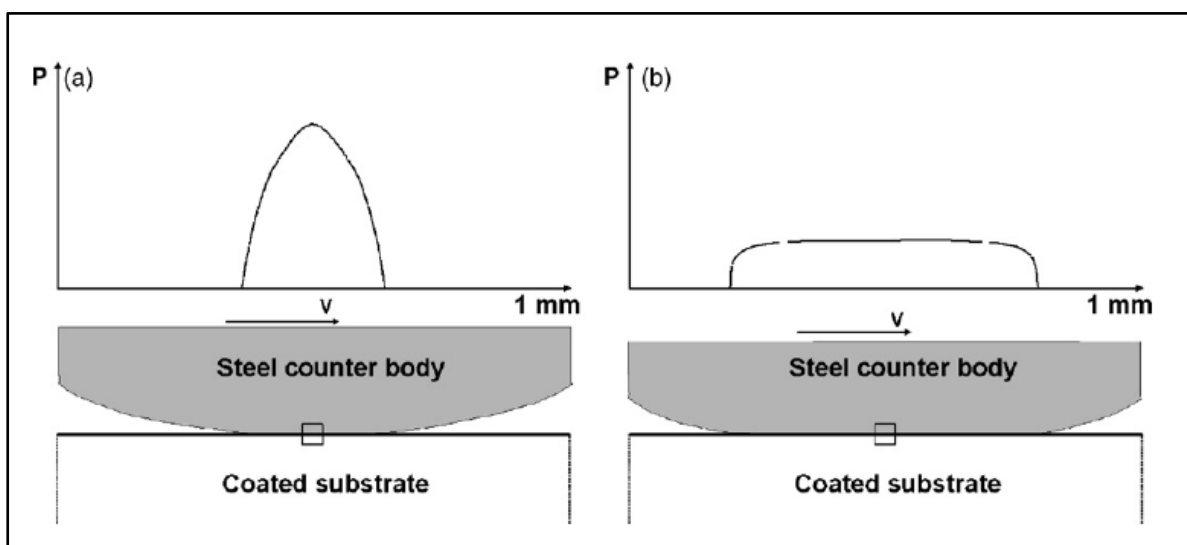


Figure A.14: Illustration of macroscopic pressure reduction due to wear of the uncoated ball: a. prior to running-in and b. after running-in.

Smoothing of the surfaces due to wear on a much finer scale will increase the value of the film parameter (Λ) and increase the separation of peaks. The formation of a tribolayer may also have a beneficial effect since it will contribute to the smoothing, as well as protect the surface from additional wear. This is shown in Figure A.15.

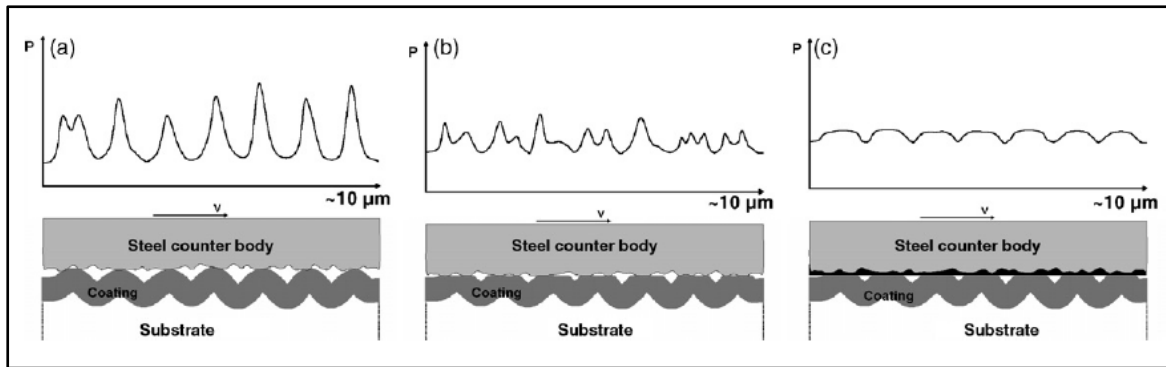


Figure A.15: Illustration of fine scale smoothing wear and corresponding contact pressures. A. Prior to running-in. b. after running-in without the formation of a tribolayer. c. After running-in with the formation of a tribolayer.

4. Akbarzadeh, S and Khonsari, MM (2010) “On the prediction of running-in behaviour in mixed-lubrication line contact.” Journal of Tribology ASME, 132, 032102-1.

A model is presented which predicts the behaviour of the running-in process in mixed lubrication line contact. This model combines the plastic deformation of asperities with the mixed-lubrication load-sharing concept. The model was also compared with experimental results obtained by Guo et.al., 2004.

Surface roughness was also a variable that was incorporated in this model. This was achieved by numerically generated surface patterns (based on algorithm of Patir, 1978). The surfaces generated were:

- Transverse
- Isotropic
- Longitudinal

These surfaces are also diagrammatically illustrated in Figure A.16.

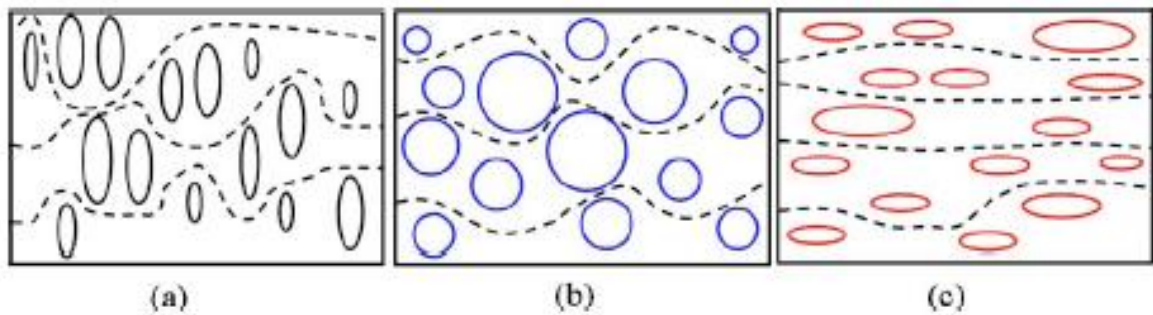


Figure A.16: Different surface patterns. a. Transverse b. Isotropic c. Longitudinal.

From the simulation of the friction coefficient during running-in (see Figure A.17), surface pattern affects the friction coefficient. A larger friction coefficient is observed for transverse surface patterns. This is probably due to the lubricant flow which is impeded. Furthermore, as the asperities polish, the contribution of asperities in carrying the load as well as the real contact area decreases. This results in a gradual decrease in friction coefficient until it reaches steady state.

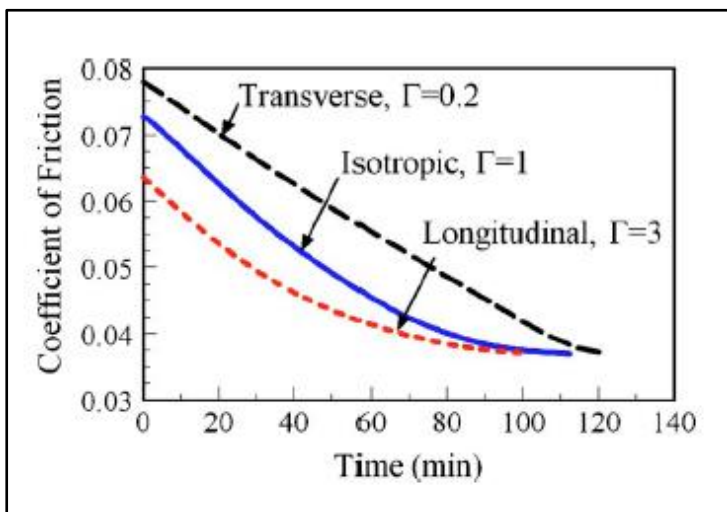


Figure A.17: Variation of friction coefficient during running-in.

When the rolling speed is increased, the time to reach steady state was reduced in terms of friction coefficient and wear volume. The steady state values also decreased with increase in rolling speed. This was due to the thickness of the film that increased with an increase in the speed. When the speed was reduced, the speed was decreased; the film thickness was reduced causing an increase in the extent of wear. This is shown in Figure A.18.

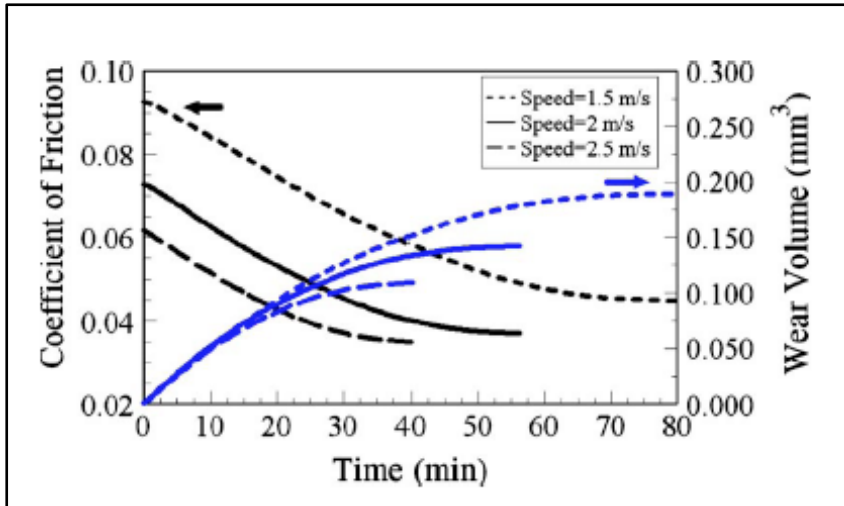


Figure A.18: Variation in friction coefficient and wear volume during running-in.

The effect of the operating load on the running-in period is an increase in the operating load resulted in an increase in the steady state wear rate and surface roughness. This is shown in Figure A.19.

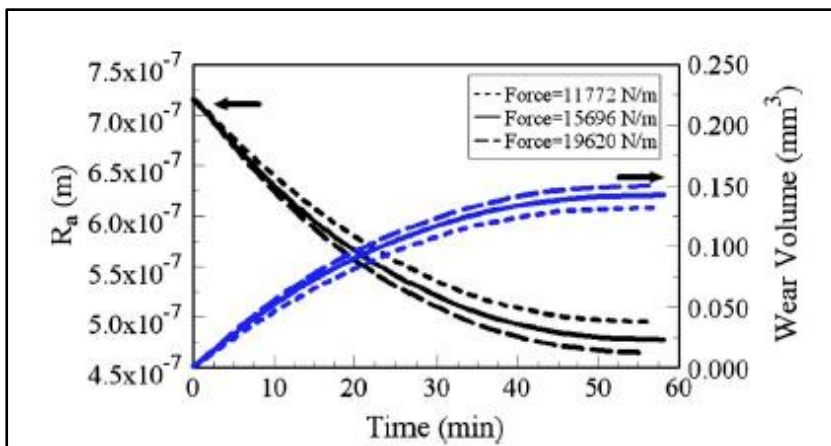


Figure A.19: Variation in surface roughness and wear volume during the running-in period.

**5. Feser, T, Stoyanov, P, Mohr, F and Dienwiebel, M (2013) “The running-in mechanisms of binary brass studied in-situ topography measurements.”
Wear, 303: 465-472.**

The purpose of this investigation was to determine the influence of contact pressure and sliding velocities on the running-in behaviour of brass. This was achieved by conducting test on pin-on-plate tribometer. This tribometer can determine holographic imaging throughout sliding experiments. The operating conditions are given in Table A.4.

Table A.4: Operating conditions during experimental investigation.

Parameter	Value
Stroke	120 mm
Velocity	10 to 20 mm/s
Load	1 to 5 MPa
Temperature	35 °C
Humidity	50%

Test procedure

The test fluid used was polyalphaolefin (PAO-8). The upper specimen consisted of 100Cr6 spheres of which the one side was grinded and polished to obtain a flat surface. The running-in procedure was evaluated as either good or poor, depending on the ability on the system to reach steady state. The steady state considered here only applies to the friction coefficient.

The friction coefficient graphs for both good and poor running-in are given in Figure A.20. In both graphs the initial friction coefficient starts at a low value, which rapidly increases. The friction coefficient value decrease and reach steady state for proper running-in. For poor running-in, however, the friction coefficient value oscillates and do not reach steady state.

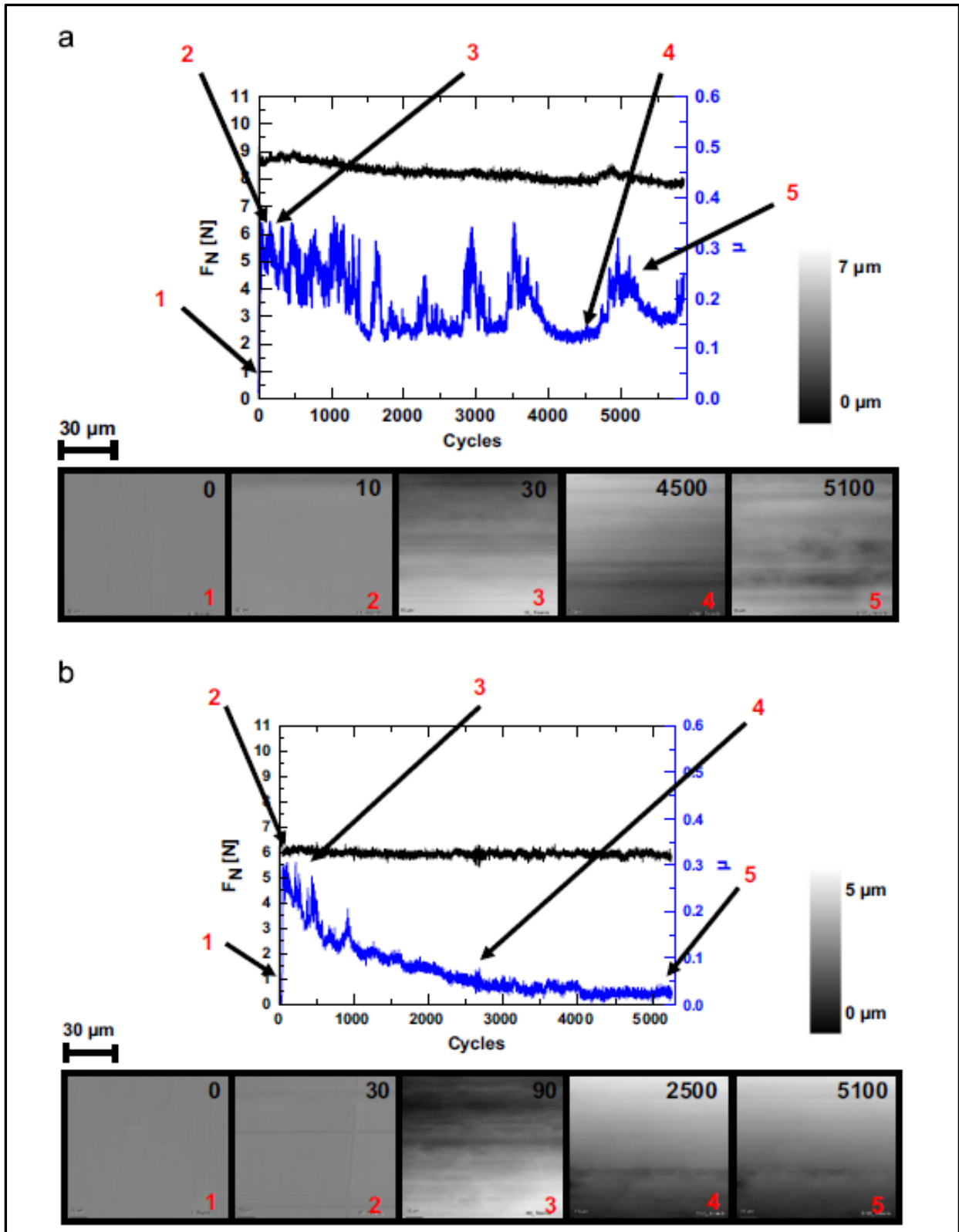


Figure A.20: Friction coefficient for poor (a) and good running-in (b).

The surface roughness of the wear surface is given in Figure A.21 as a function of the number of cycles. The surface roughness for good running-in reaches a steady state

while the surface roughness for poor lubricity oscillates. The wear profile for the track obtained during good and poor lubricity are given in Figure A.22, where a significant difference can be observed between the two conditions.

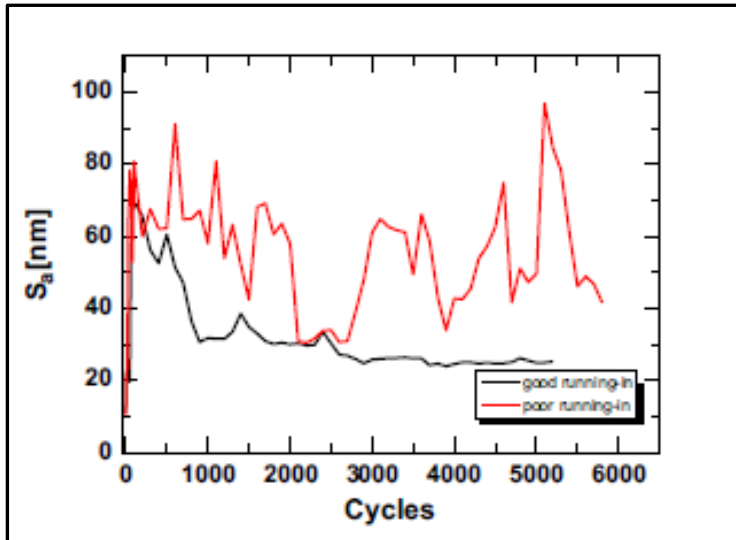


Figure A.21: Surface roughness of wear surface for good and poor running-in.

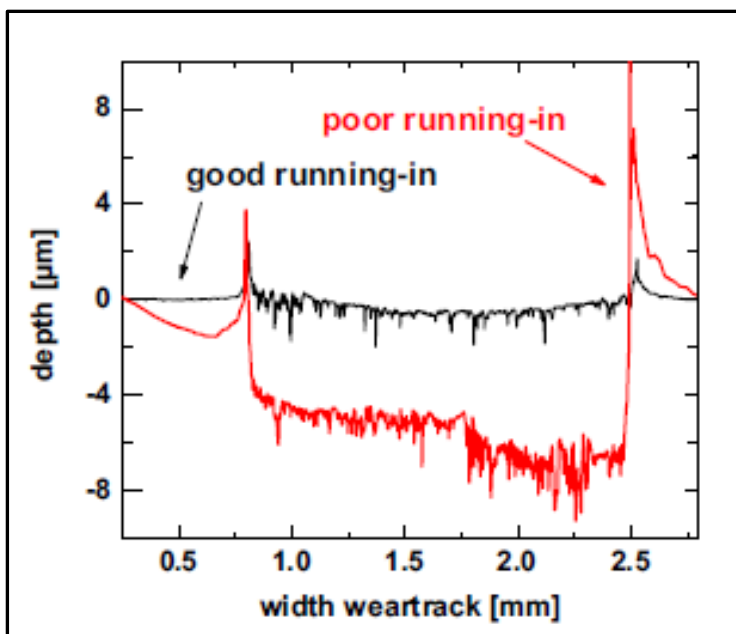


Figure A.22: Depth of wear track for good and poor running-in.

Up to this point, the friction and wear results from good and running-in have been reported. The question now is, how are poor and good running-in obtained? Good running-in was obtained by operating at the optimum contact pressure and sliding velocity. For this investigation, it was found to be:

- Contact pressure: 2.3 to 2.9 MPa
- Sliding velocity: 20 mm/s

The difference between good and poor running-in is thought to be caused by the difference in transfer film build-up. Poor running-in is obtained when the transfer film is continuously formed and broken down. This transfer film would consist of a brass film transferred to the steel surface.

It has also been observed in this study that thinner transfer films result in good running-in. The formation of zinc and copper oxides on the wear surfaces also aided the running-in process. This is due to the good lubricating properties of these oxides (Kong et.al., 2003 and Battez, et.al., 2008). The presence of oxides has been verified by XPS analysis of the wear surfaces.

**6. Okamoto, M, Jibiki, T, Ito, S and Motoda, T (2015) “Role of cross-grooved type texturing in acceleration of initial running-in under lubricated fretting”
Tribology International, 100: 126-131.**

Fretting tests under lubricated conditions were conducted with cross-grooved texture, dimpled texture and mirror finished surfaces. Examples of surfaces with cross-grooved and dimple texturing are shown in Figures A.23 and A.24. The purpose of texturing is to minimise fretting by ensuring even lubricant distribution with the aid of oil grooves and pockets as well as removing wear particles away from the surface. The focus was on the running-in period.

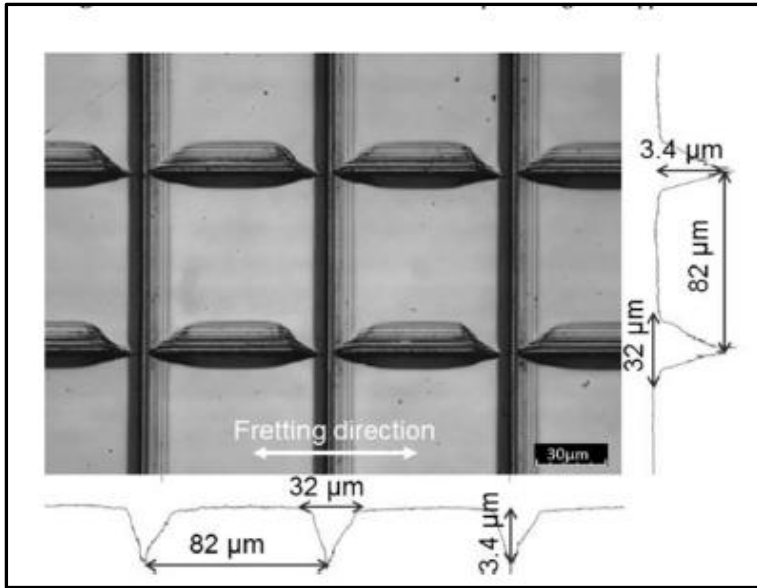


Figure A.23: Micrograph of cross-grooved type texturing.

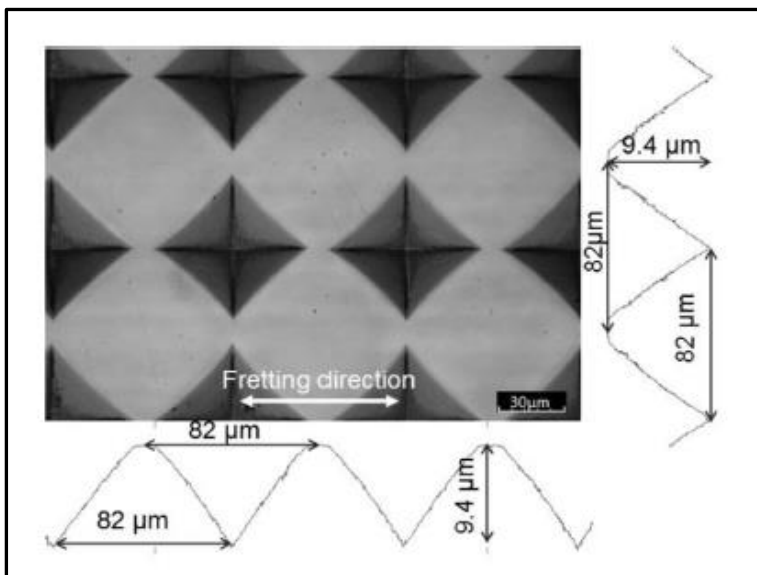


Figure A.24: Micrograph of dimple texturing.

This investigation applies, as the title indicates, to fretting conditions. Fretting occurs wherever short amplitude reciprocating sliding contacting surfaces are sustained for many cycles. It results in two forms of damage; surface wear and deterioration of fatigue life (Batchelor & Stachowiak, 2005: 593). The test conditions are given in Table A.5.

Table A.5: Operating conditions during fretting tests

Parameter	Specification
Specimens	
Upper specimen	Flat bearing steel (HV760)
Lower specimen	Ball bearing steel (HV760), dia = 9.525 mm
Configuration	Ball on flat point contact
Fretting Stroke	30- 200 μ m
Normal load	9.8 N
Lubricant	Polyalphaolefin
Test duration	2×10^5 cycles
Frequency	7.0 Hz
Temperature	24 °C
Humidity	45%

From the fretting experiments it was seen that:

- Running-in is completed for cross-grooved and dimple textured surfaces before the running-in is completed for polished surfaces.
- This is due to the contact pressures that are generated on textured surfaces resulting in shortest running-in period.

7. Linsler, D, Scherge, M and Schlarb (2015) “The running-in corridor of lubricated metal-metal contacts.” *Wear*, 342-343: 60-64.

Here the possibility of a “corridor” that results in good running for metal contacts are investigated. The “corridor” refers to a specific energetic range in which the tribological system is able to develop ultra-low wear rates and small coefficients of friction. This corridor is associated with the formation of a third body. The width of the corridor depends on the:

- External tribological stressing conditions
- Materials
- Lubricants
- Initial friction coefficient.

During the running-in period three scenarios can occur:

Case 1: The system can quickly develop low friction and wear rate.

Case 2: Maintain constant friction and wear.

Case 3: Catastrophic failure due to exponential increase in friction and wear.

Case 1 refers to proper running-in, while overstressing results in high wear and high friction (case 3). Under-stressing can also be harmful since the system does not receive enough energy to develop the third body and friction and wear remain high (case 3).

Third bodies, also refer to interfaces, can be defined in a material sense as zones which exhibits a marked change in composition from that of the rubbing specimens. It can also be defined in a kinetic sense as the thickness across which the difference in velocity between solids is accommodated (Godet, M, 1990).

The parameters that were varied in this investigation were:

- Composition of specimens
- Normal load
- Sliding velocity

Two test fluids were also used. The test fluids were Fuchs Titan 5W30 and Castrol Edge FST 5W30, both which are engine oils. The test configuration was a pin on rotating disk. The variables are given in Table A.6.

Table A.6: Test parameters and variables during running-in tests.

Pin Material and diameter	Disk material	Lubricant	
Cr, 3 mm	Gray cast iron (GG25) -band finished	Fuchs 5W30	Titan
100Cr6, 5 mm	AISI (AISI9Cu3)		

Variables	Values
Load	Up to 1000N
Sliding velocity	0.1 m/s to 5 m/s
Oil temperature	70°C and 90°C

The running-in strongly depends on the friction power density (friction power dissipated) acting on the initiating surfaces. The initial friction power density is determined from the equation below. It is at this stage not certain where this equation was obtained since no reference was given. The dimensional analysis, however, indicates that the equation is correct.

$$P_i = \frac{\mu_i v F_n}{A} \quad \text{A.1}$$

Where:

P_i	Initial power density	(W/m ²)
μ_i	Initial friction coefficient	
v	Sliding velocity	(m/s)
F_N	Normal contact force/load	(N)
A	Nominal area	(m ²)

The nominal area was calculated from:

$$A = 2\pi r d \quad \text{A.2}$$

Where:

- | | | |
|-----|--------------------------|-----|
| r | Track radius on the disk | (m) |
| d | Diameter of the pin | (m) |

The final coefficient of friction plotted as a function of the initial friction power density is given in Figure A.25. The plots for both metals were generated by varying the sliding velocity and the normal load. In this figure it can clearly be seen that the width of low final friction coefficient values differs for material pairs. This indicates that a running-in corridor exists.

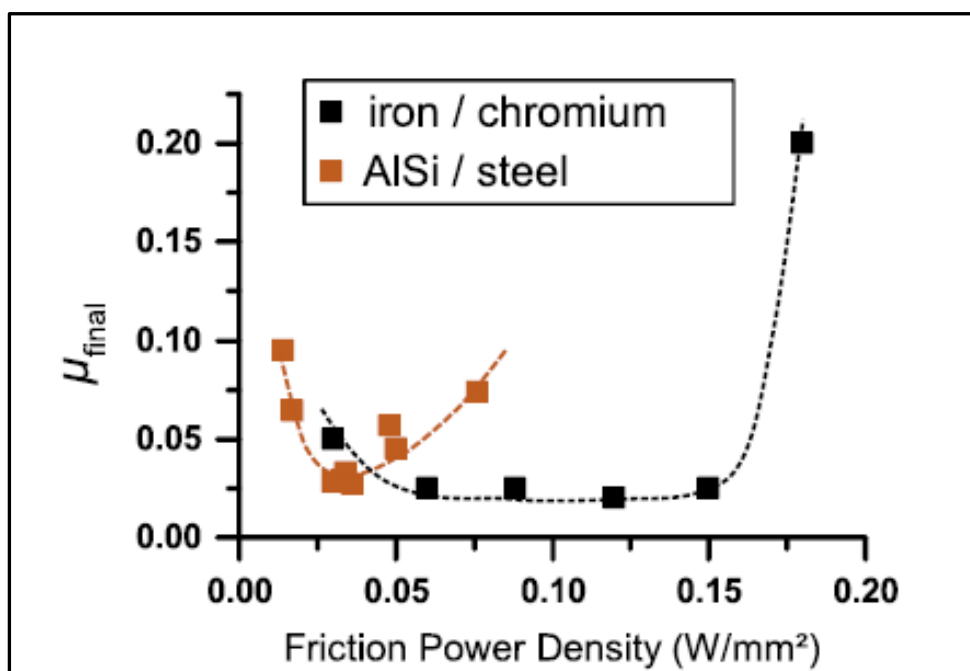


Figure A.25: Final friction coefficient as a function of the initial friction power density for iron/chromium and AISi/steel pairs.

It was also found that the surface finish plays an important role on the width of the running-in corridor. It was found that the rougher surface resulted in a wider “corridor”. This indicates that for surfaces with a rougher surface finish, the sensitivity of the system becomes smaller.

The role of the lubricant will affect the initial friction coefficient. This will depend on the viscosity in elastohydrodynamic and hydrodynamic lubricating regimes or the composition (anti wear additives etc.) in mixed and boundary lubricating regimes. This

in turn affects the initial power density and will determine the location in the corridor. This concept is similar to the position of a system on a Stribeck curve.

- 8. Linsler, D, Scherge, M and Schröckert, F (2016) “Influence of subsurface plastic deformation on the running-in behavior of a hypoeutectic AISi alloy” Tribology International,**
<http://dx.doi.org/10.1016/j.triboint.2016.01.033>.

The aim of this study was to examine the influence of different subsurface microstructures, introduced by machining, on the tribological behaviour of hypoeutectic AISi₉Cu₃ alloy. The subsurface microstructures were obtained by machining the disks with:

- Monocrystalline diamond cutting insert. This exerted small ploughing forces. This was referred to as FM1.
- Wiper cutting insert which exert a ploughing force of approximately 29N. This surface was referred to as FM 2.
- Wiper cutting insert which exert a ploughing force of approximately 45N. This surface was referred to as FM 3.

The operating conditions of the experimental investigation are summarised in Table A.7. A detailed explanation of the test method has been omitted by the authors of this study. It is the opinion that it is not necessary for the overall understanding.

Table A.7: Operating conditions.

Parameter	Specification
Configuration	Pin-on-disk
Lubricant	Castrol Edge FST 5W30, oil circuit filled with 2.5l
Running-in conditions	
Duration	32 hrs.
Sliding velocity	0.8 m/s
Contact pressure	35 MPa
Test conditions	
Total duration	48 hrs.
Sliding velocity variation	0.1 to 2 m/s
Contact pressure variation	15 to 35 MPa
Temperature	70 °C

The hardness with depth of indentation is given in Figure A.26. The depth of deformation caused by machining is indicated in the legend (FM1 – 0.5 μm , FM2 – 5 μm and FM3 – 9 μm). From the hardness result the surfaces with larger depths of deformation had higher hardness values.

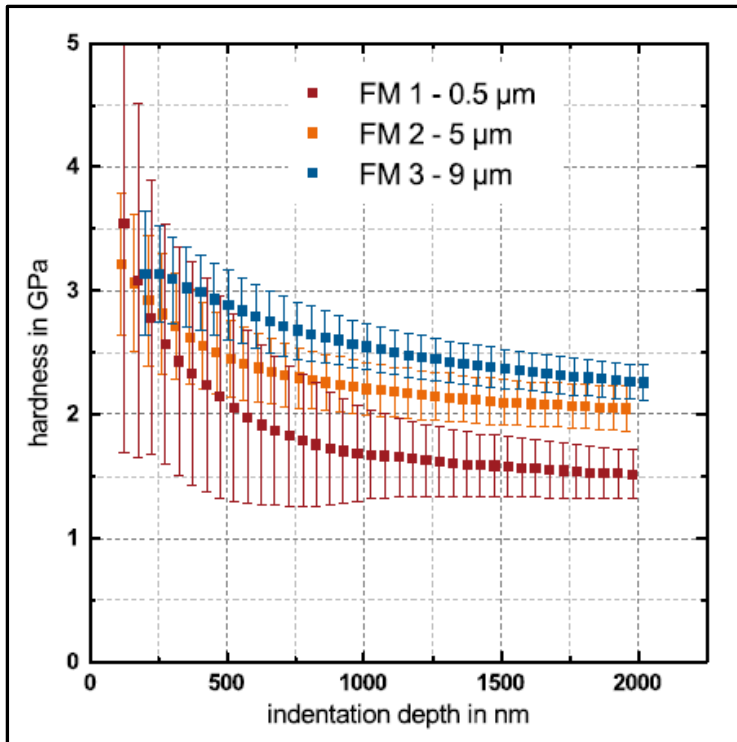


Figure A.26: Hardness of unworn disks.

The friction coefficient and wear for all three surfaces are plotted in Figures A.27 to A.29. It is noticeable that the friction coefficient during the first 32 hours, reaches steady state for FM1 and FM2. This is not the case for FM3 and the friction value is also much higher. The wear rate was also much lower for FM1 and FM2 after the running-in period. From these deeper deformations friction and wear increased, since larger volumes were subjected to mechanical rearrangements.

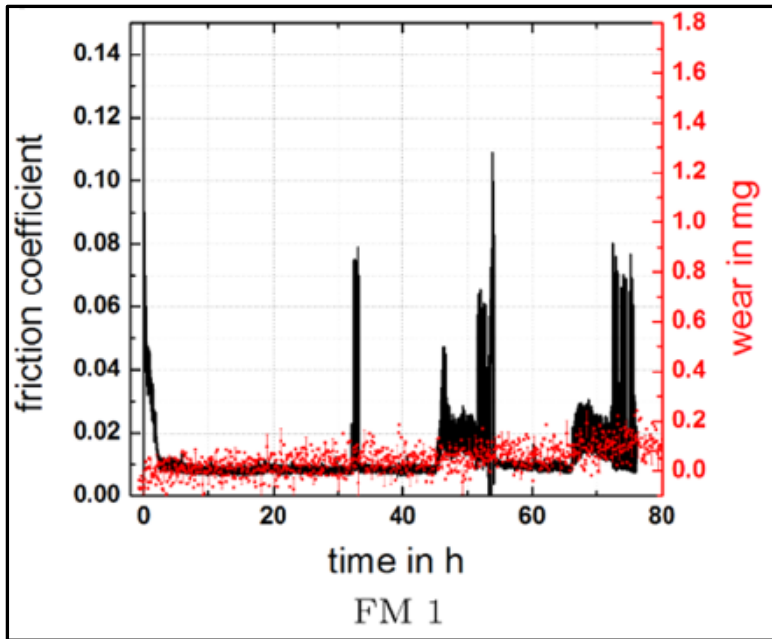


Figure A.27: Friction coefficient and wear for FM 1.

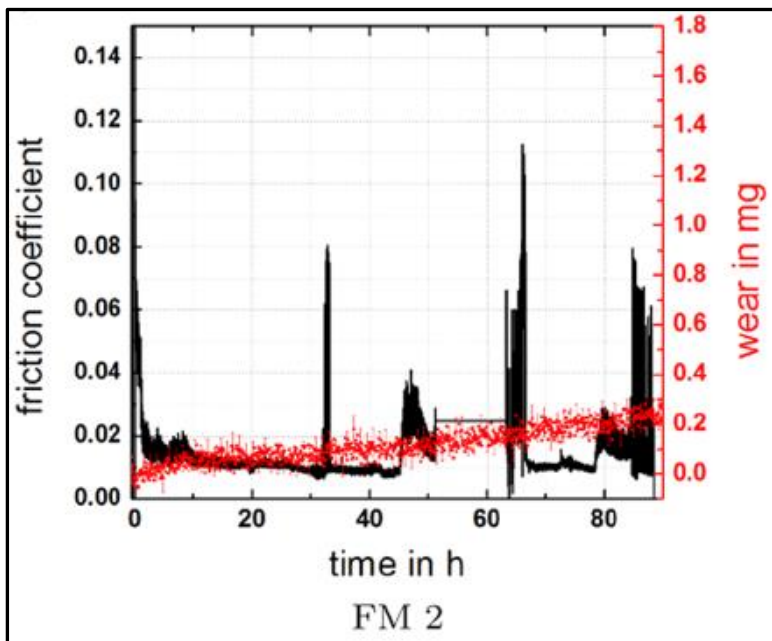


Figure A.28: Friction coefficient and wear for FM 2.

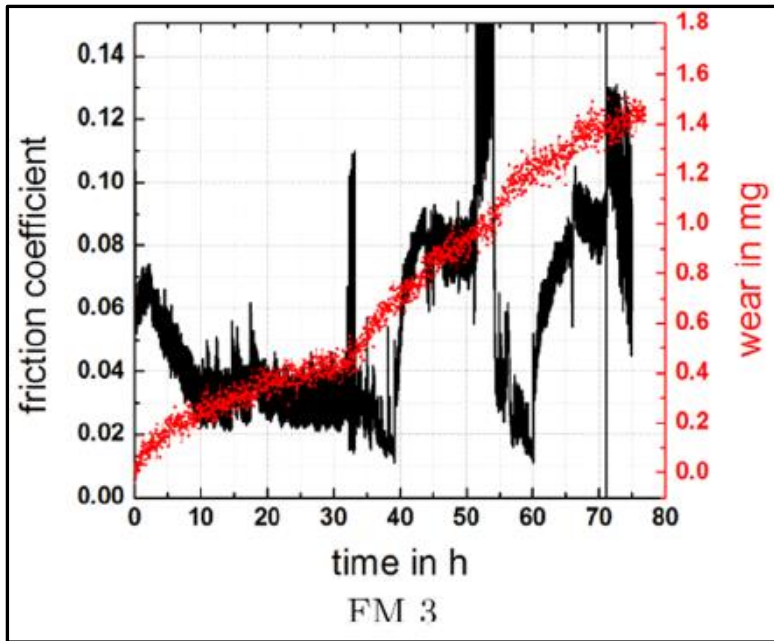


Figure A.29: Friction coefficient and wear for FM 3.

References

1. Akbarzadeh, S and Khonsari, MM (2010) "On the prediction of running-in behaviour in mixed-lubrication line contact", *Journal of Tribology ASME*, 132, 032102-1.
2. Batchelor, AW & Stachowiak, GW (2005) *Engineering Tribology*, Butterworth-Heinemann, USA.
3. Blau, PJ (1989) *Friction and wear transition of materials*, Noyes Publications, USA.
4. Blau, PJ, (2005) "On the nature of running-in", *Tribology International*, 38: 1007 – 1012.
5. de Vaal, PL & Langenhoven (2015) *The effects of humidity and soluble water content on the lubricity testing of a n-hexadecane and palmitic acid test fluid*, Dissertation for Master's degree, University of Pretoria, Pretoria, South Africa.
6. Farr, LPG (1975) "Molybdenum disulphide in lubrication: a review", *Wear*, 35: 1-22.
7. Feser, T, Stoyanov, P, Mohr, F and Dienwiebel, M (2013) "The running-in mechanisms of binary brass studied in-situ topography measurements", *Wear*, 303: 465-472.
8. Godet, M (1990) "Third-bodies in tribology", *Wear*, 136: 29–45.
9. Guo, F, Wang, W & Wong, PL (2004) "Application of partial elastohydrodynamic lubrication analysis in dynamic wear study for running-in", *Wear*, 257: 823 – 832.
10. Kumar, R, Prakash, B and Sethuramiah, A (2002) "A systematic methodology to characterise the running-in and steady state wear process", *Wear*, 252: 445-453.
11. Linsler, D, Scherge, M and Schröckert, F (2016) "Influence of subsurface plastic deformation on the running-in behavior of a hypoeutectic AlSi alloy", *Tribology International*, <http://dx.doi.org/10.1016/j.triboint.2016.01.033>.
12. Linsler, D, Scherge, M and Schlarb (2015) "The running-in corridor of lubricated metal-metal contacts", *Wear*, 342-343: 60-64.
13. Ludema, KC and Lee, Y (1990) "The shared-load wear model in lubricated sliding: scuffing criteria and wear coefficients", *Wear*, 138: 13-22.

14. Martin, JM, LeMogne, T, Chassagnette, C & Gardox, MN (1992) "Friction of hexagonal boron nitride in various environments", *Tribology Transactions*, 35: 463 – 472.
15. Nogueira, I, Dias, AM, Gras, R and Progri, R, (2002) "An experimental model for friction during running-in", *Wear*, 253: 541 – 549.
16. Okamoto, M, Jibiki, T, Ito, S and Motoda, T (2016) "Role of cross-grooved type texturing in acceleration of initial running-in under lubricated fretting", *Tribology International* 100: 126-131.
17. Patir, N (1978) "A numerical procedure for random generation of rough surfaces", *Wear*, 47: 263 – 277.
18. Savage, RH (1948) "Graphite lubrication", *Journal of Applied Physics*, 19: 1-10.
19. Svahn, F, Kassman-Rudolphi, A and Hogmark, S (2006) "On the effect of surface topography and humidity on lubricated running-in of a carbon based coating", *Wear*, 261: 1237 – 1246.
20. Winer, WO (1967) "Molybdenum disulphide as a lubricant: a review of the fundamental knowledge", *Wear*, 10: 422 – 452.

Appendix B.1: Friction Coefficient Graphs

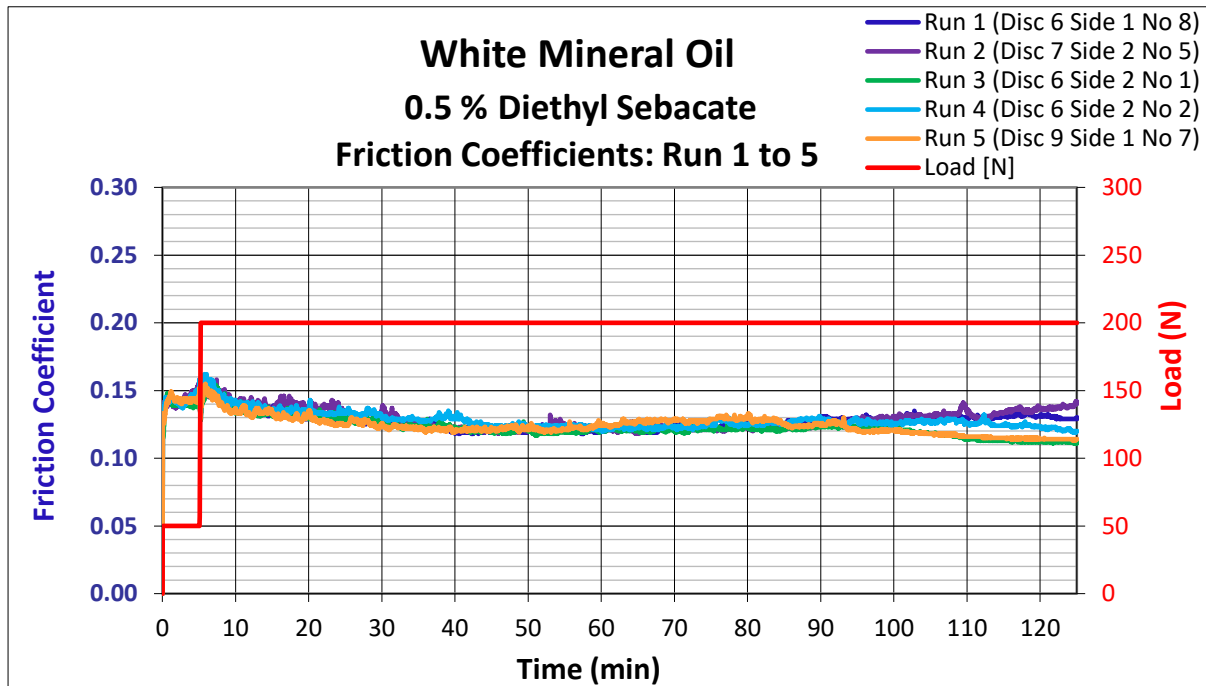


Figure B.1.1: Friction coefficient measurements for **white mineral oil (WMO) with 0.5 % (mass basis) diethyl sebacate**.

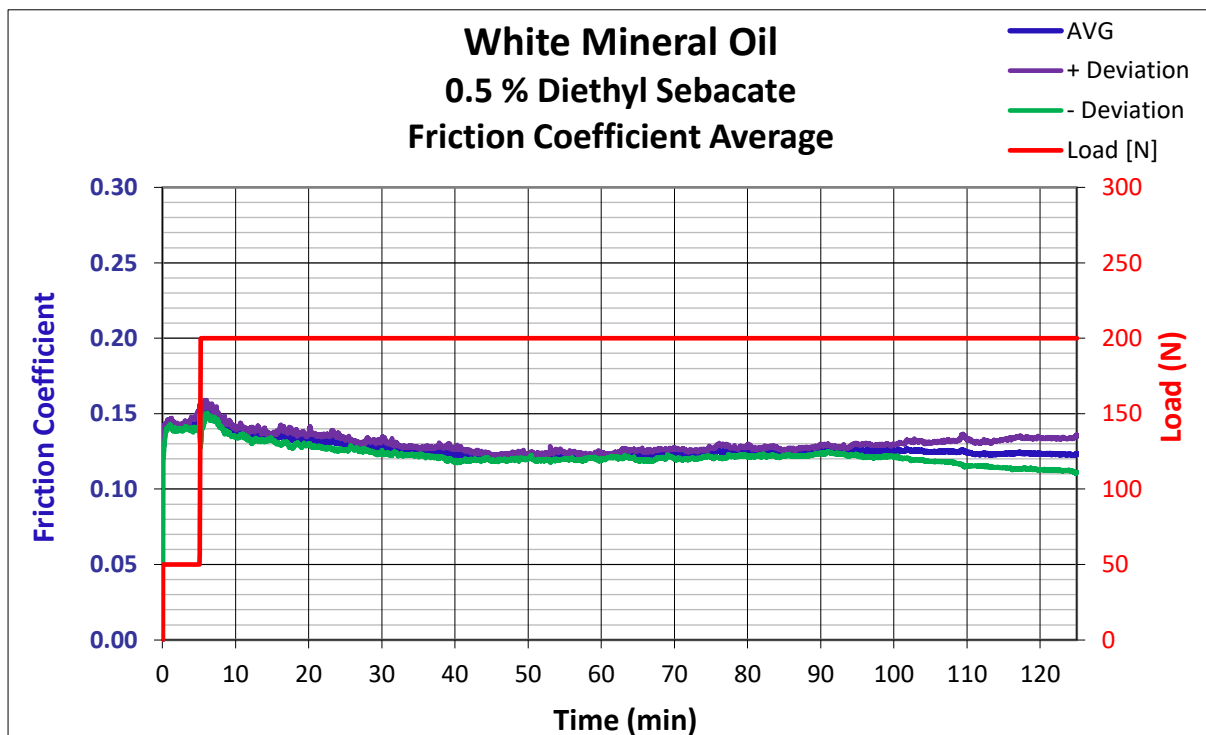


Figure B.1.2: Average of friction coefficient for **white mineral oil (WMO) with 0.5 % (mass basis) diethyl sebacate**.

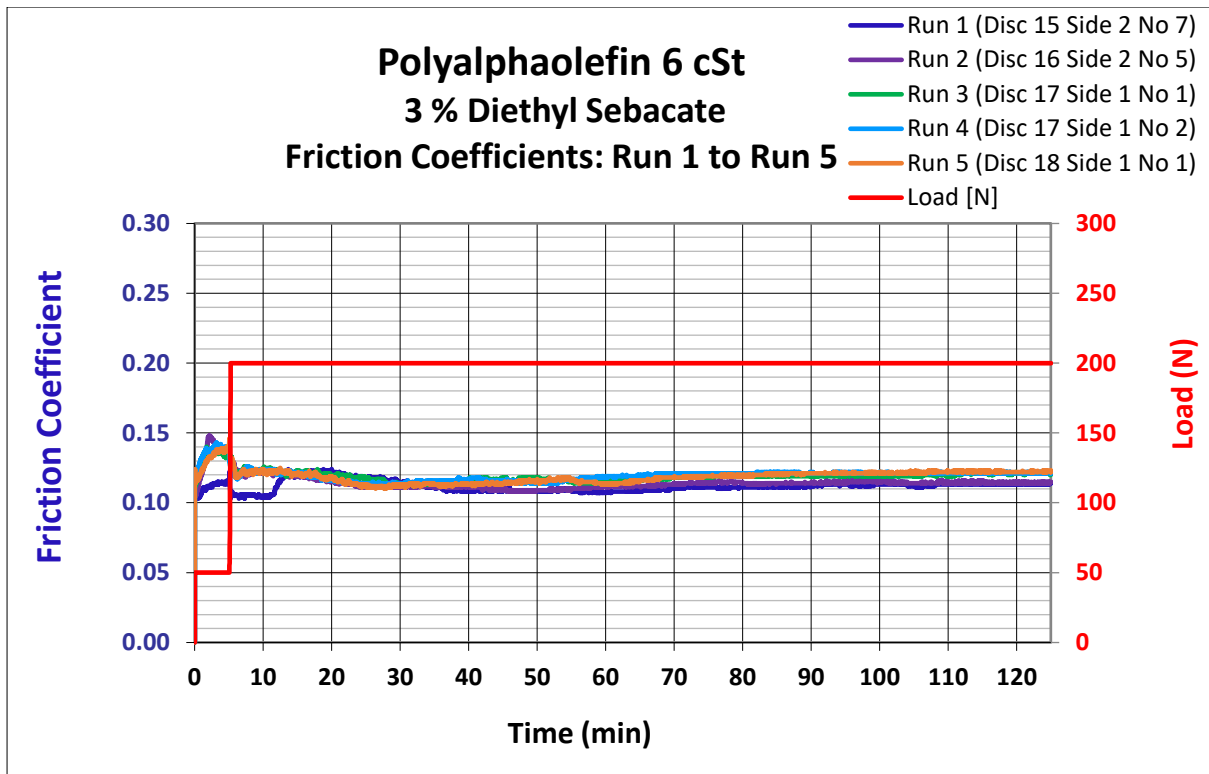


Figure B.1.3: Friction coefficient measurements for **polyalphaolefin 6 cSt (PAO 6)** with **3 % (mass basis) diethyl sebacate**.

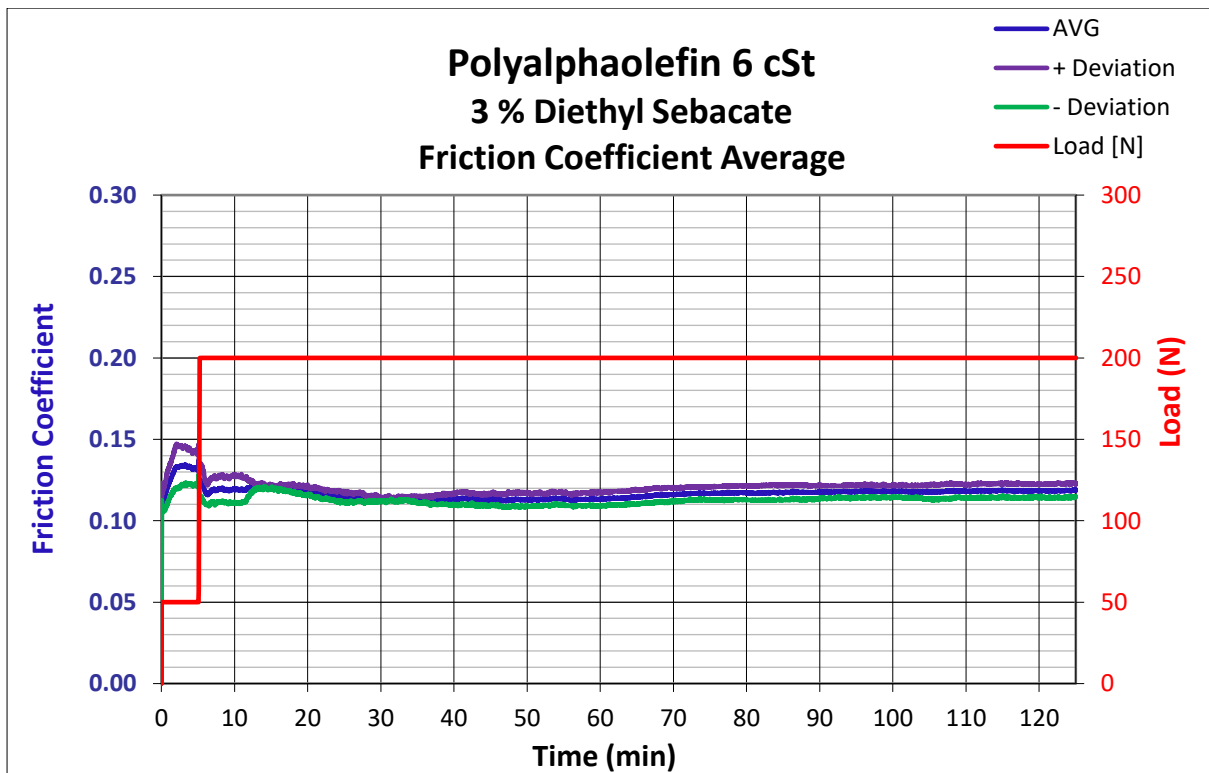


Figure B.1.4: Average of friction coefficient for **polyalphaolefin 6 cSt (PAO 6)** with **3 % (mass basis) diethyl sebacate**.

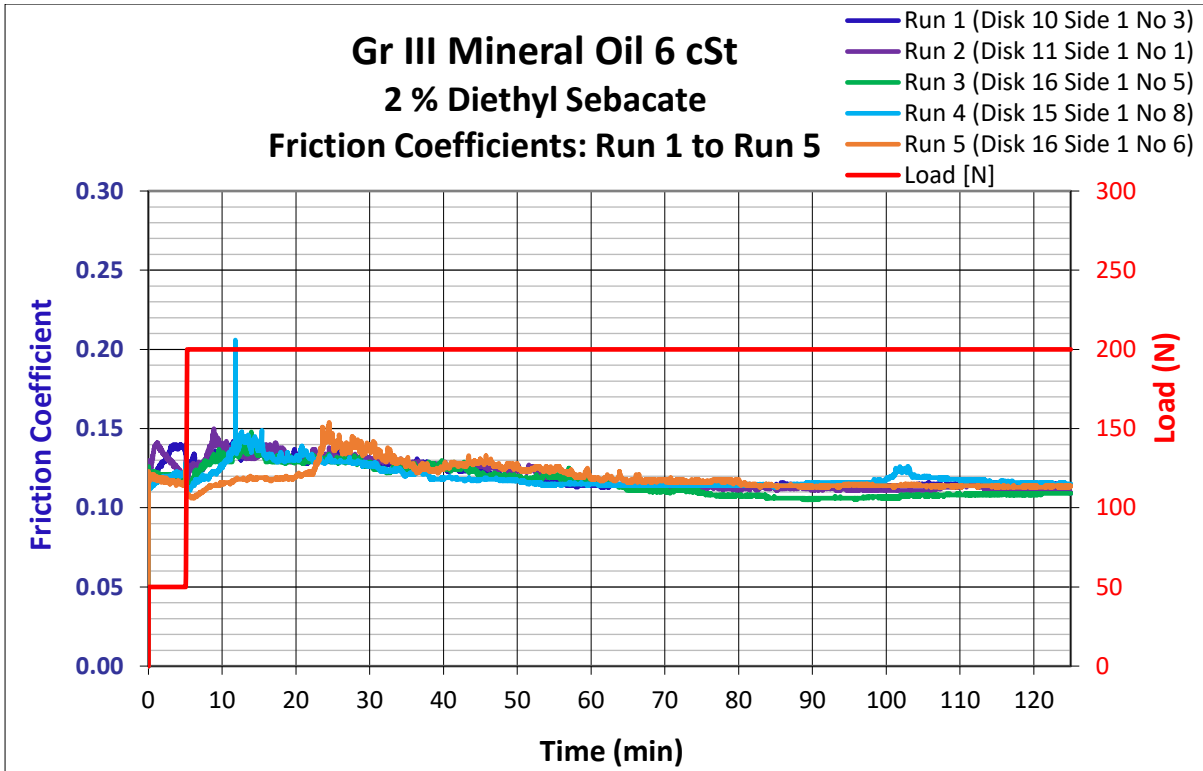


Figure B.1.5: Friction coefficient measurements for **Group III mineral oil 6 cSt (Gr III 6)** with **2 % (mass basis) diethyl sebacate**.

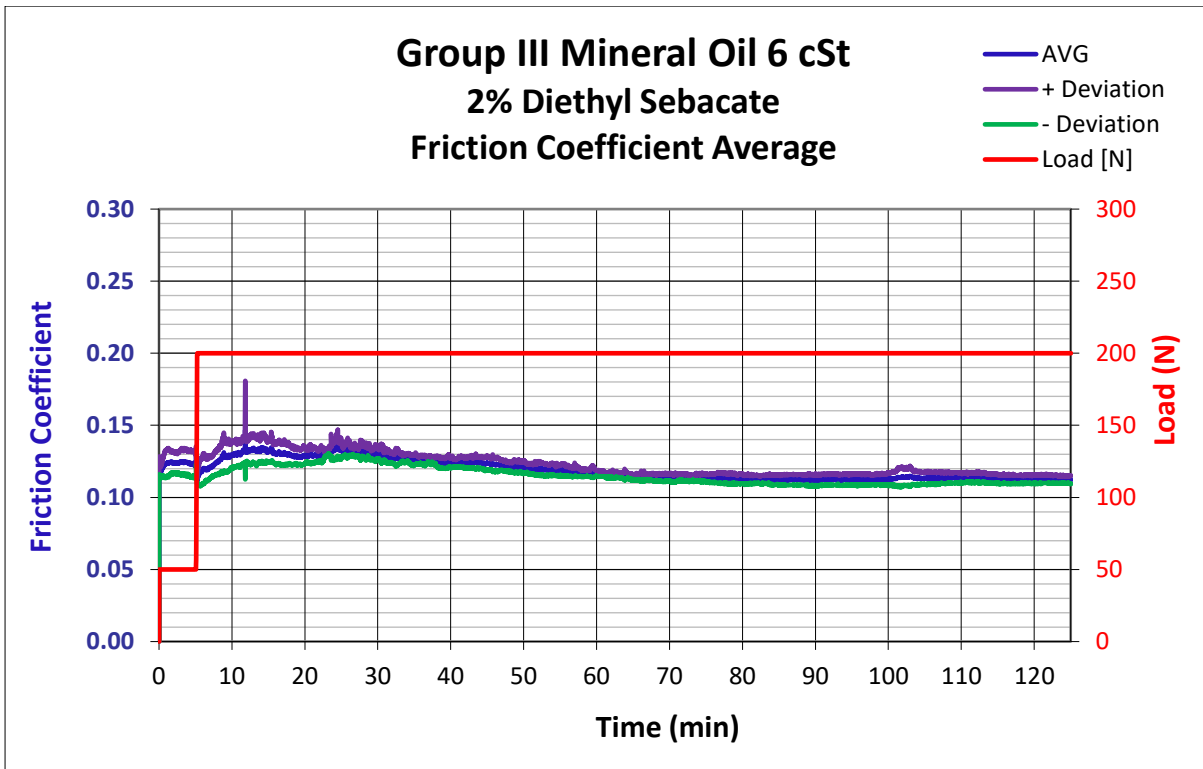


Figure B.1.6: Average of friction coefficient for **Group III mineral oil 6 cSt (Gr III 6)** with **2 % (mass basis) diethyl sebacate**.

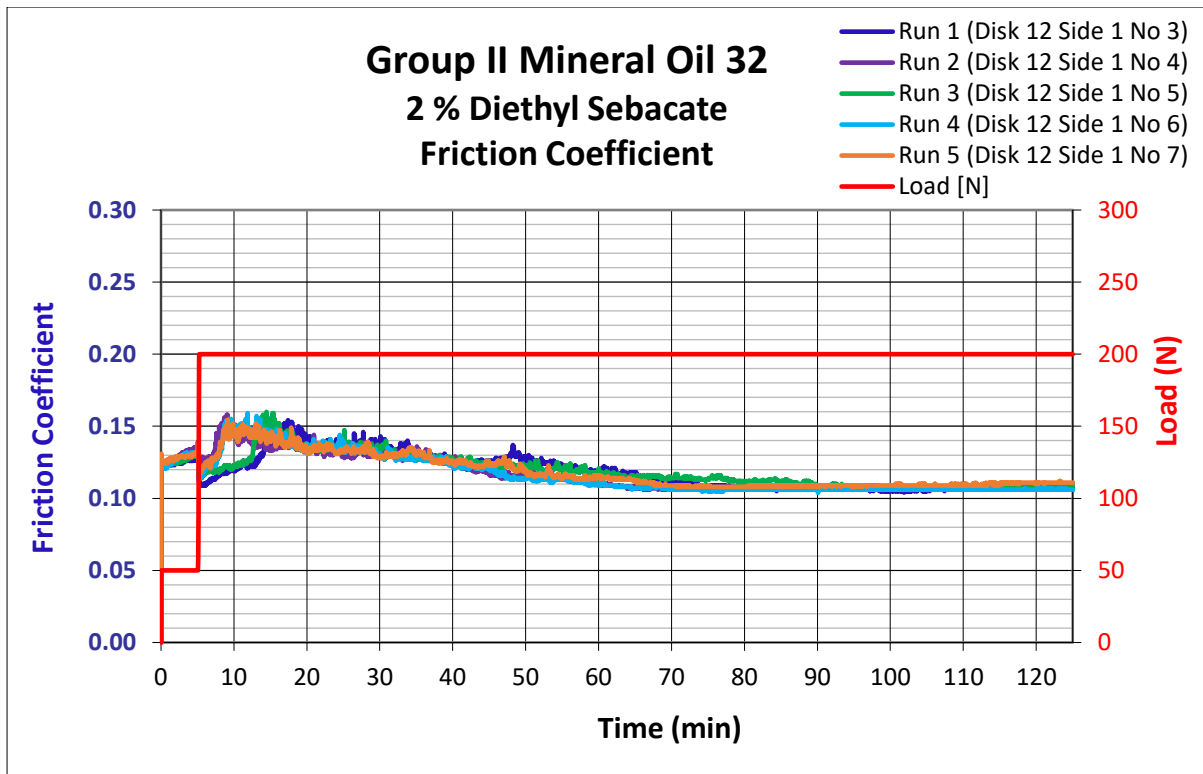


Figure B.1.7: Friction coefficient measurements for **Group II mineral oil, ISO VG 32, (Gr II 32)** with 2 % (mass basis) diethyl sebacate.

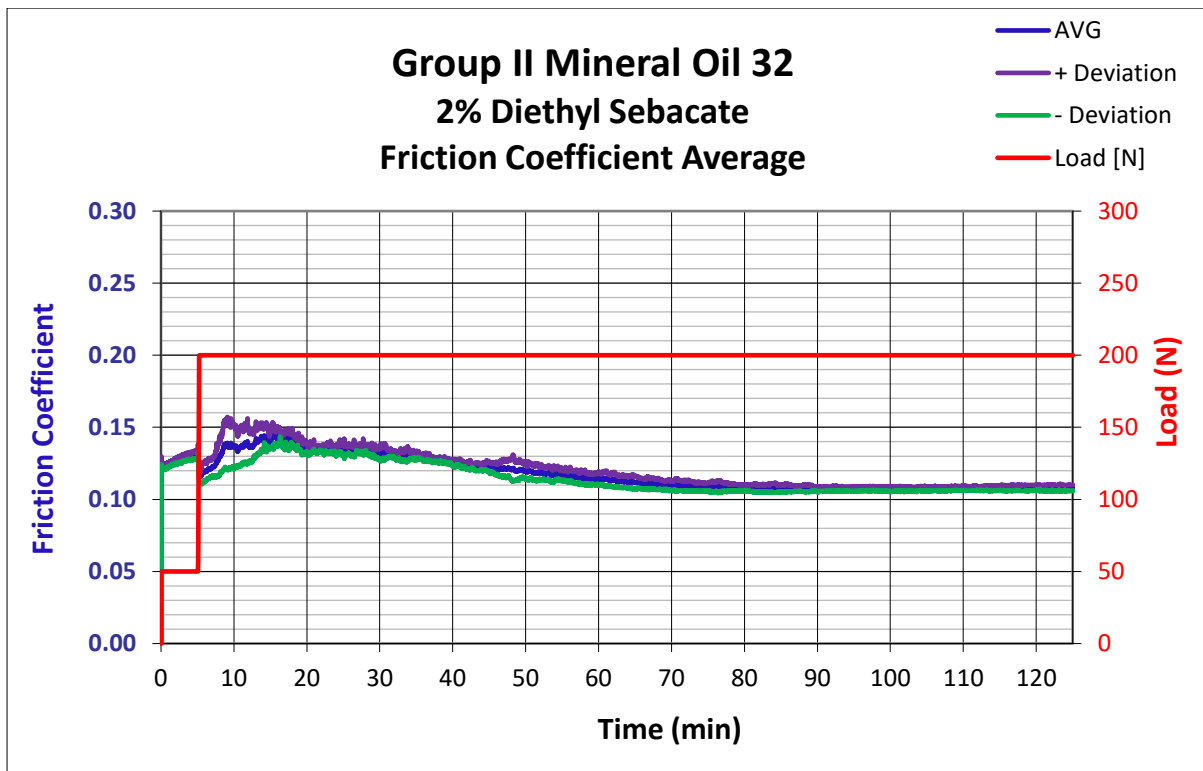


Figure B.1.8: Average of friction coefficient for **Group II mineral oil, ISO VG 32, (Gr II 32)** with 2 % (mass basis) diethyl sebacate.

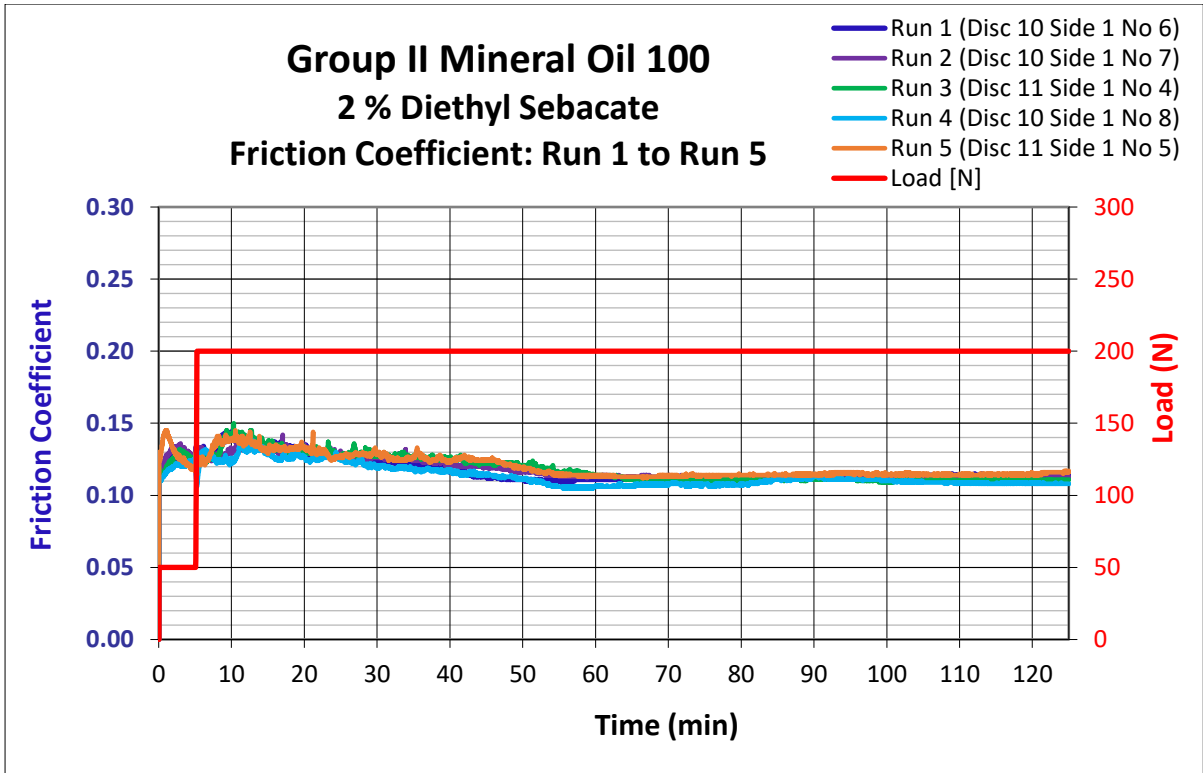


Figure B.1.9: Friction coefficient measurements for **Group II mineral oil, ISO VG 100, (Gr II 100)** with 2 % (mass basis) diethyl sebacate.

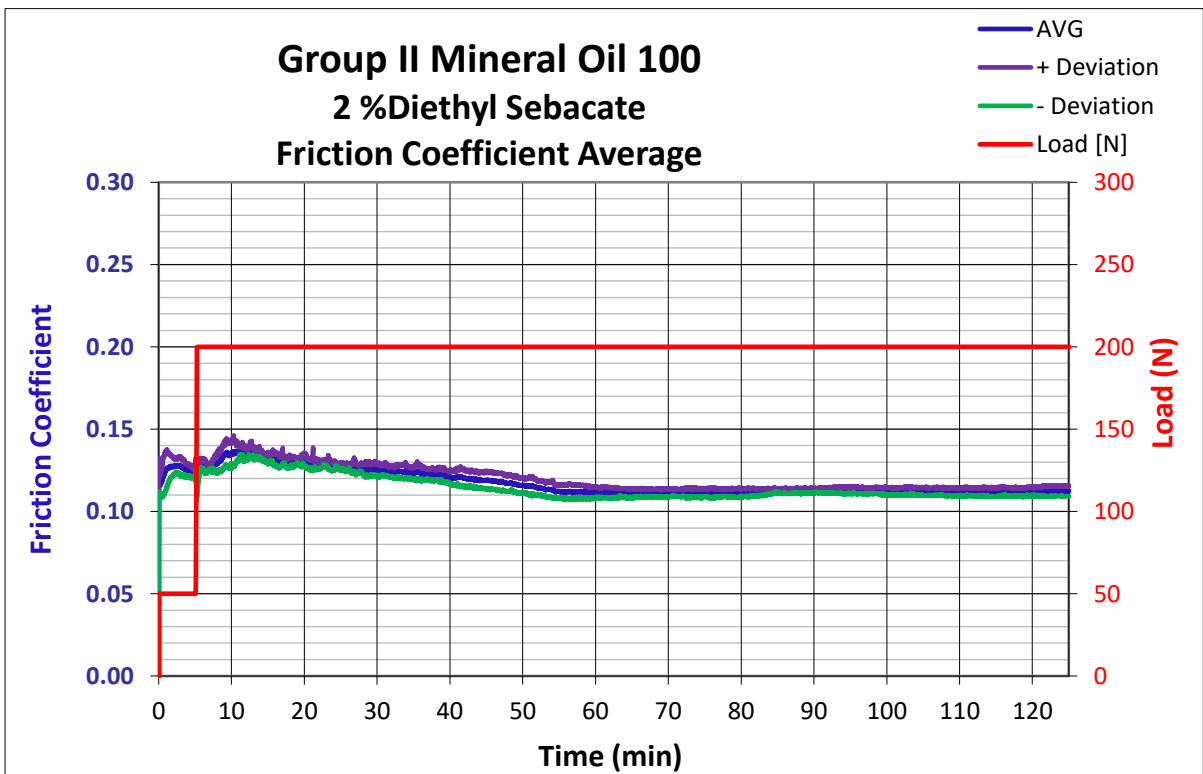


Figure B.1.10: Average of friction coefficient for **Group II mineral oil, ISO VG 100, (Gr II 100)** with 2 % (mass basis) diethyl sebacate.

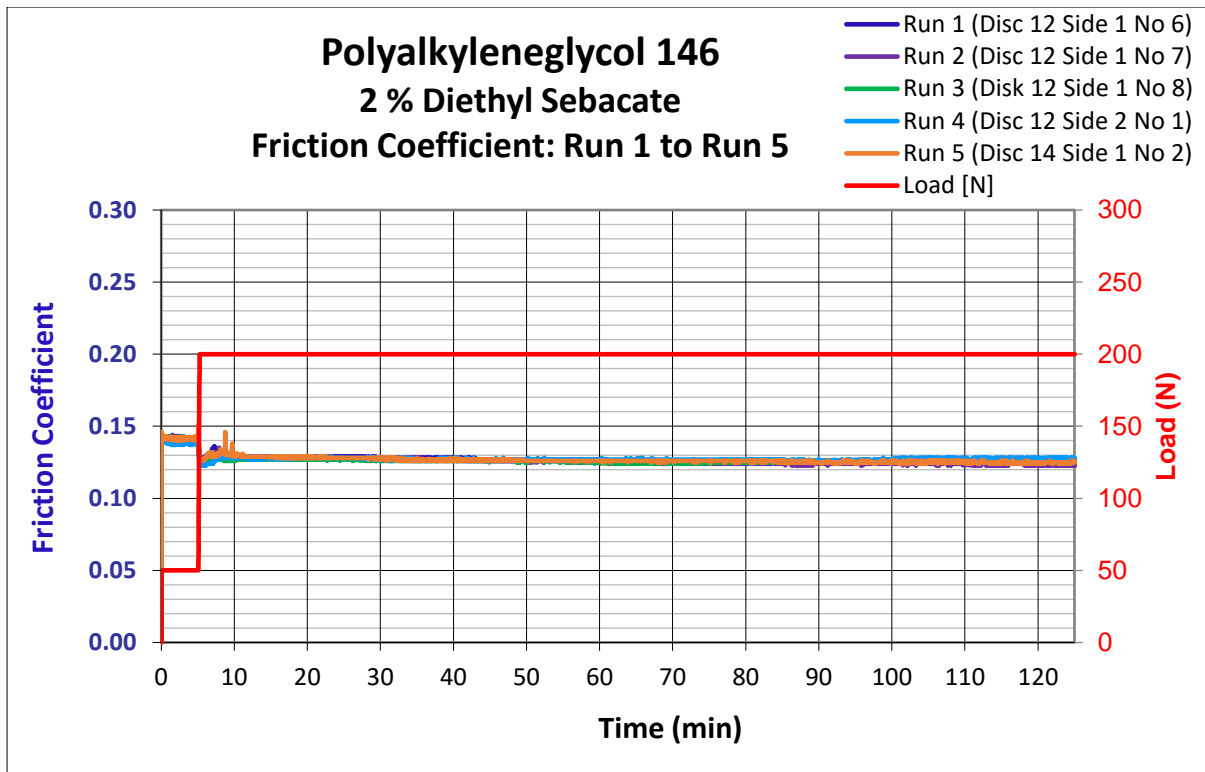


Figure B.1.11: Friction coefficient measurements for **polyalkylene glycol, ISO VG 146 (PAG 146)** with **0.5 % (mass basis) diethyl sebacate**.

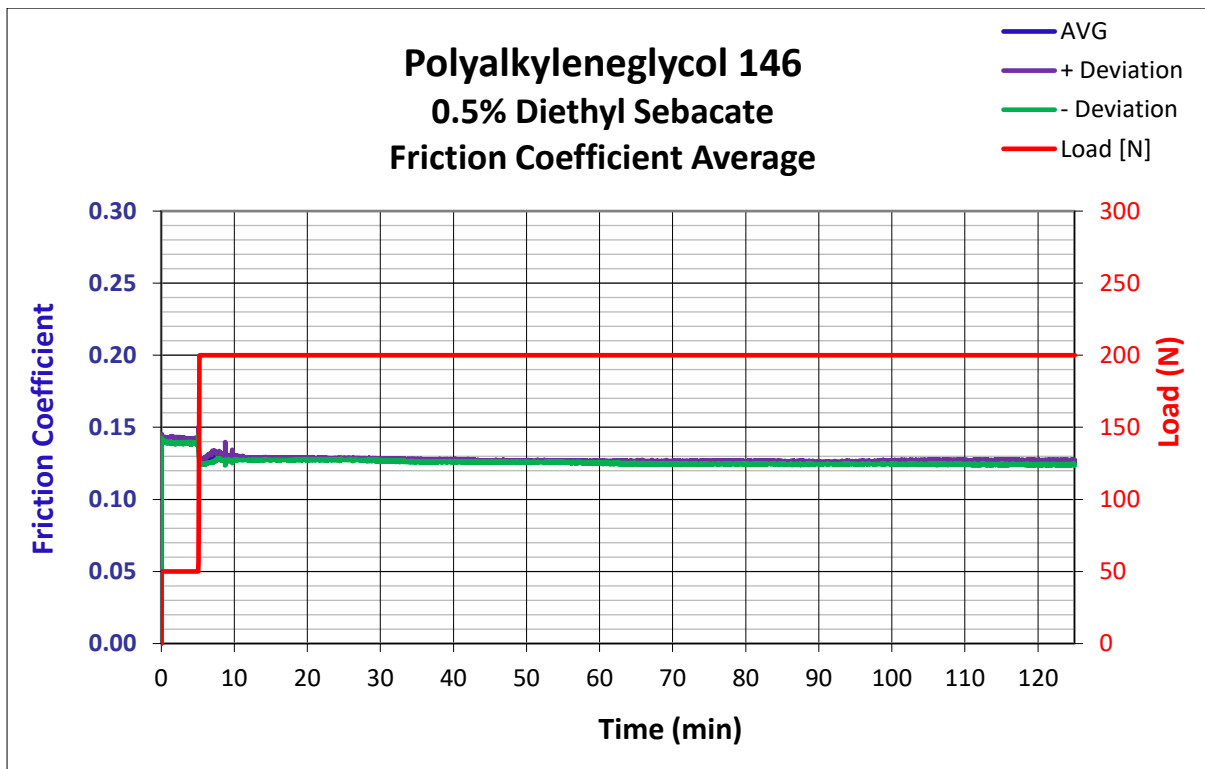


Figure B.1.12: Average of friction coefficient for **polyalkylene glycol, ISO VG 146, (PAG 146)** with **0.5 % (mass basis) diethyl sebacate**.

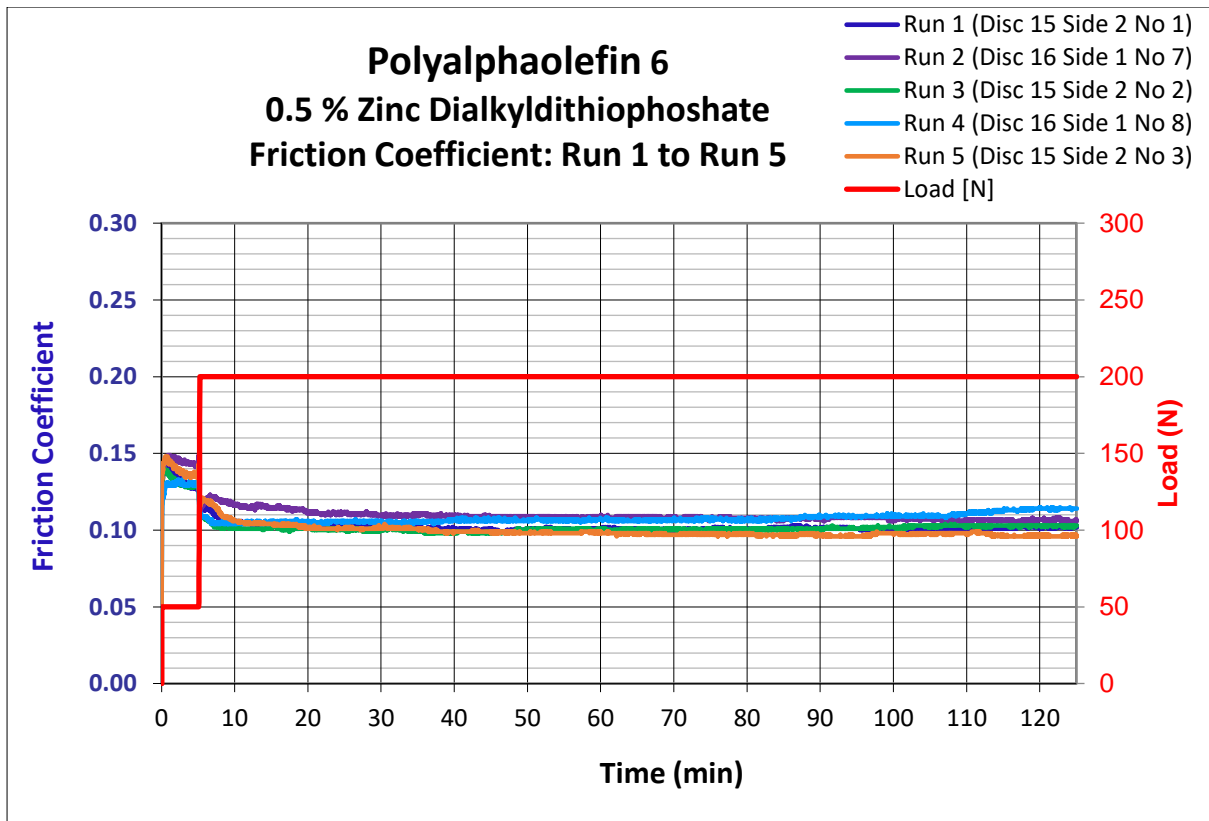


Figure B.1.13: Friction coefficient measurements for **polyalphaolefin, 6 cSt, (PAO 6)** with **0.5 % (mass basis) ZDDP**.

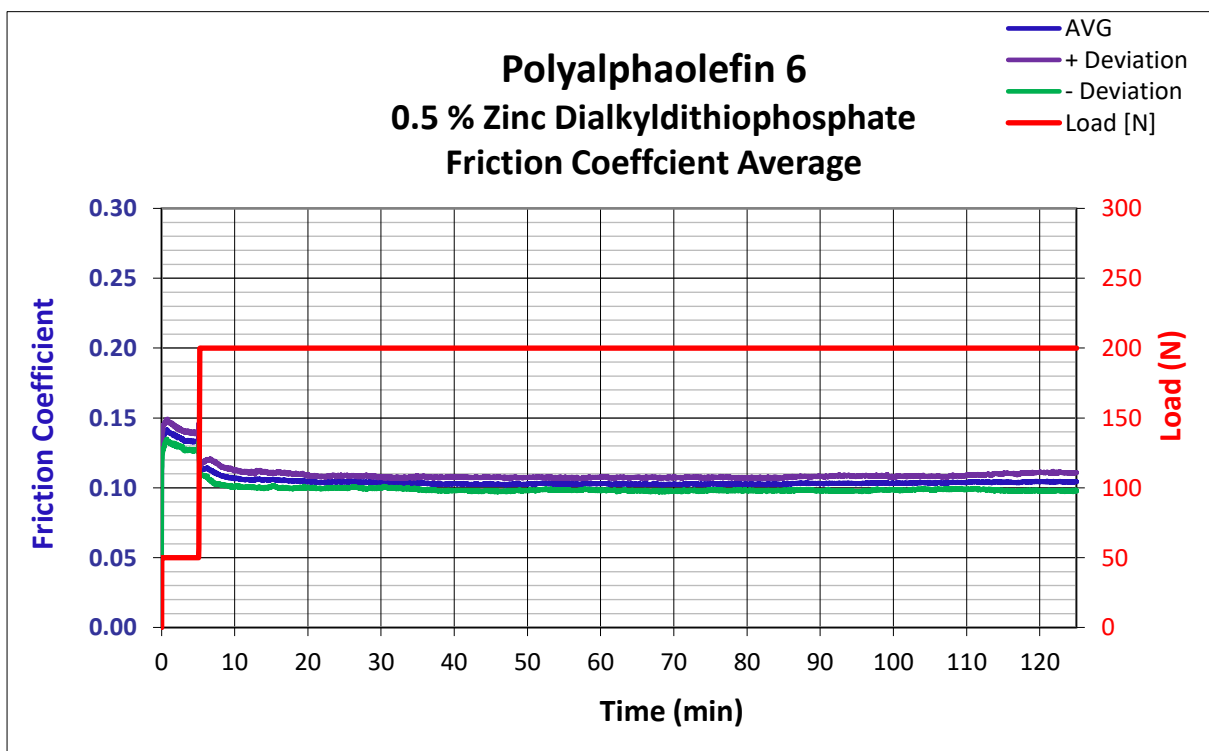


Figure B.1.14: Average friction coefficient for **polyalphaolefin, 6 cSt, (PAO 6)** with **0.5 % (mass basis) ZDDP**.

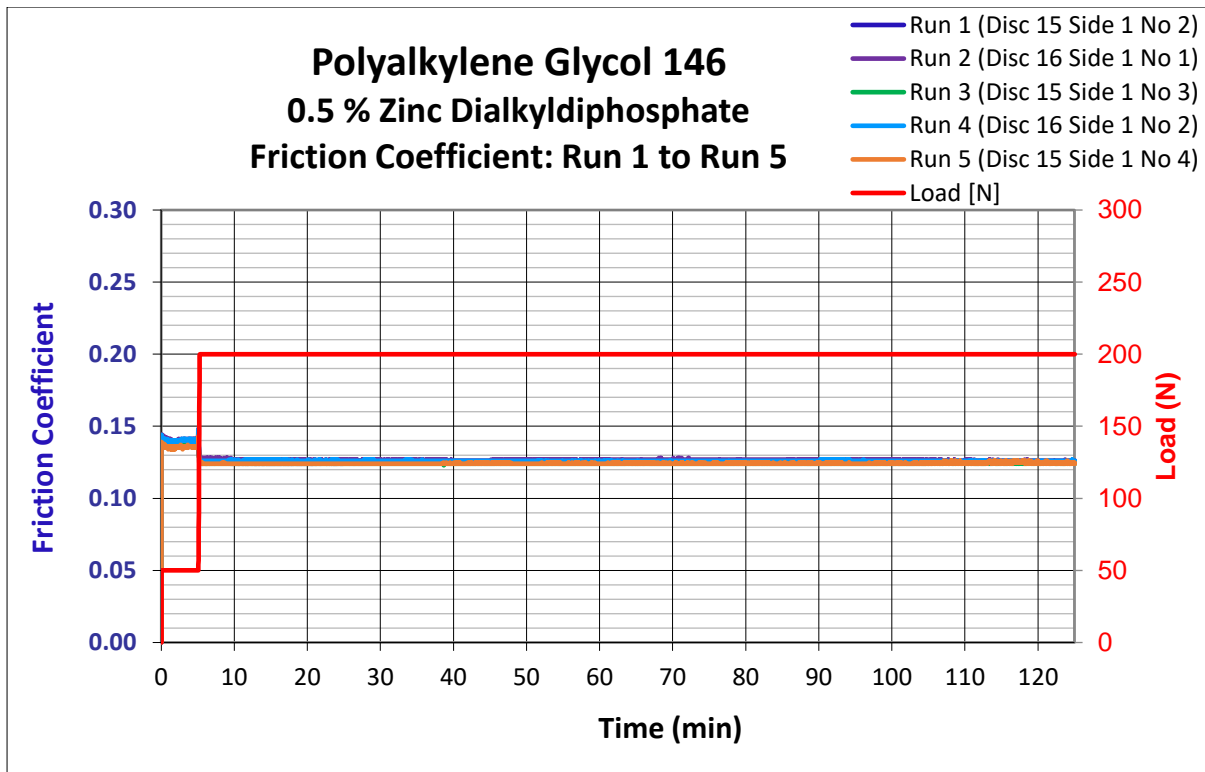


Figure B.1.15: Friction coefficient measurements for **polyalkylene glycol, ISO VG 146, (PAG 146) with 0.5 % (mass basis) ZDDP.**

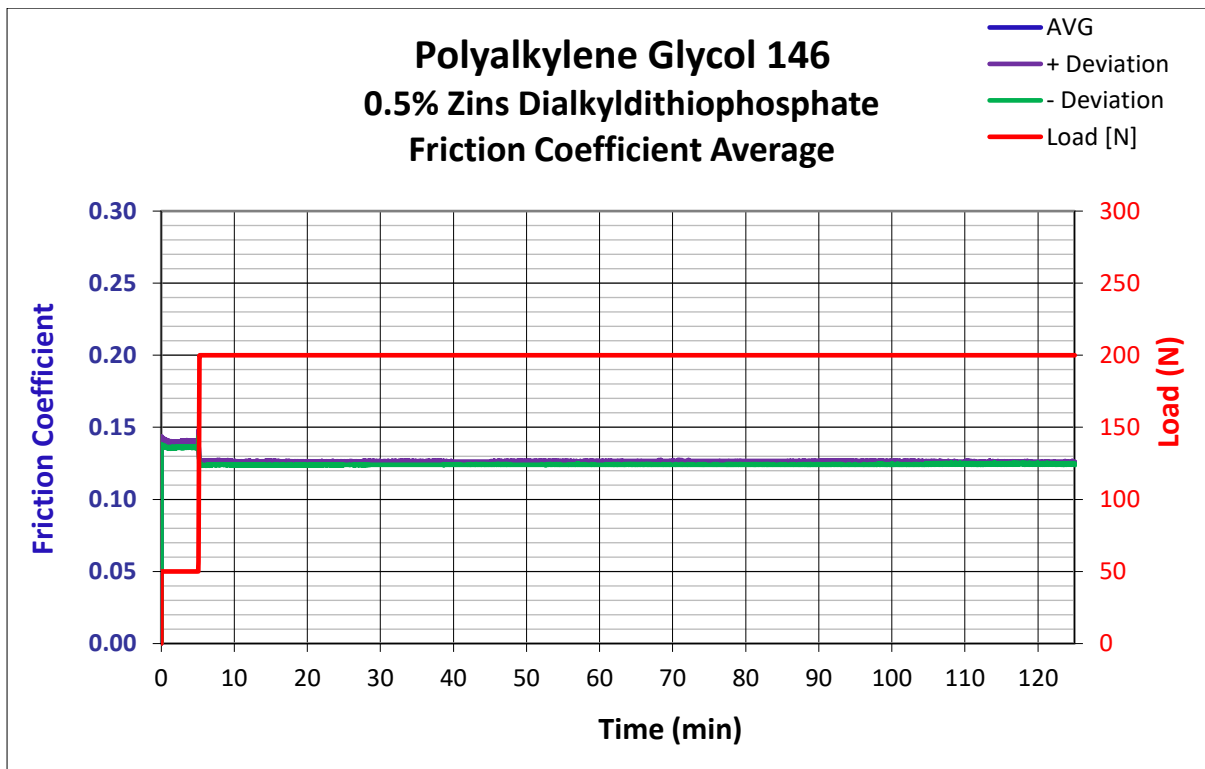
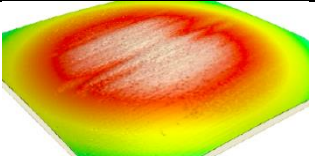
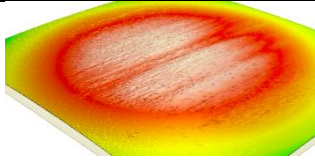
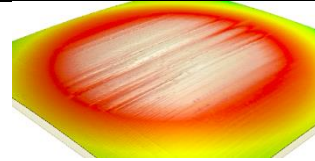
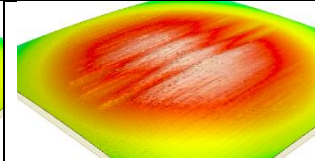
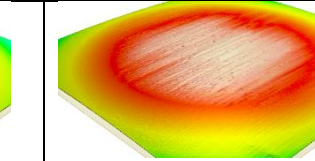
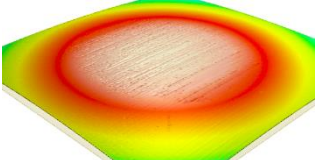
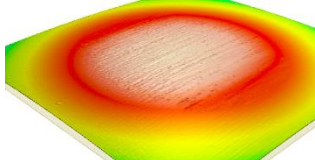
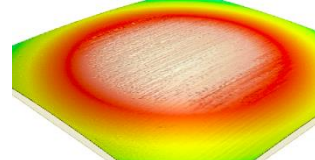
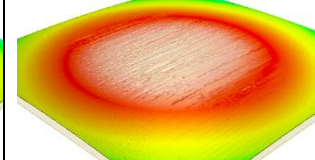
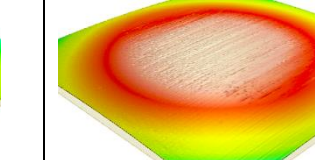
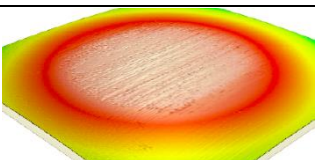
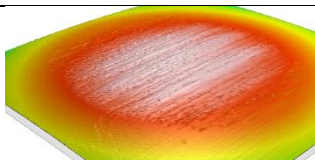
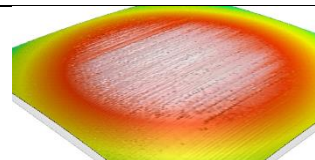
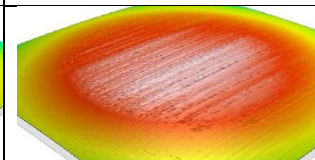
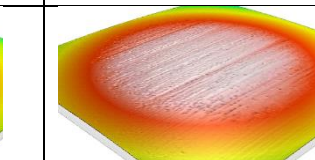
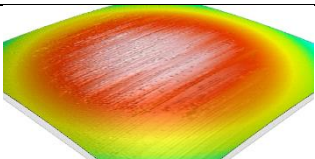
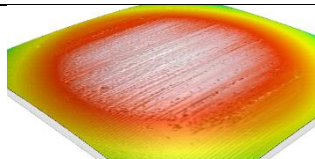
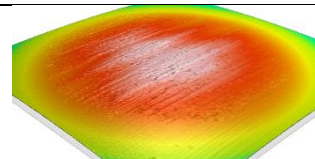
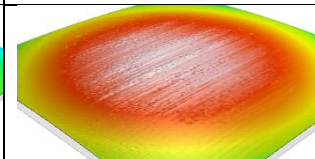
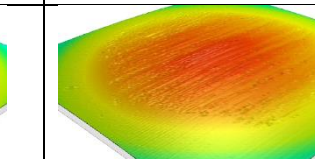
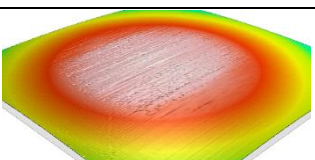
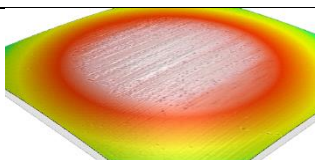
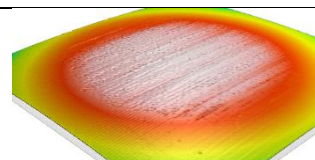
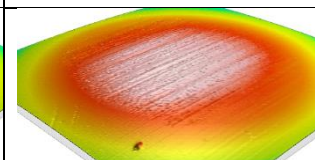
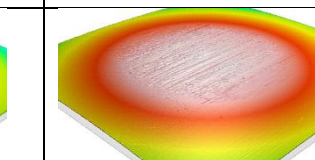


Figure B.1.16: Average friction coefficient for **polyalkylene glycol, ISO VG 146, (PAG 146) with 0.5 % (mass basis) ZDDP.**

Appendix B.2: Wear Scar and Wear Track 3 D images

Table B.2.1: 3 D images for wear scars obtained for test fluids evaluated on the SRV test rig.

Base Fluid	Run 1	Run 2	Run 3	Run 4	Run 5
WMO 0.5 % DES					
PAO 3 % DES					
Gr III 2 % DES					
Gr II 41.2 cSt 2 % DES					
Gr II 101 cSt 2 % DES					

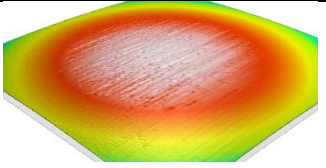
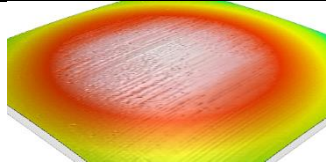
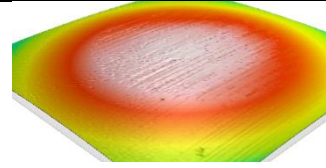
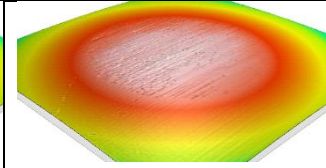
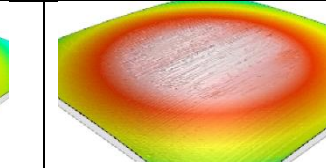
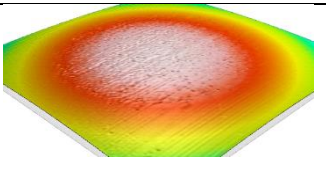
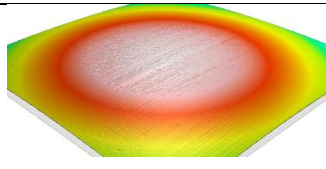
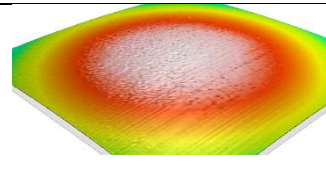
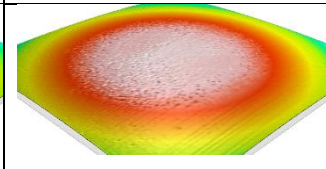
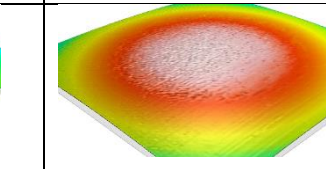
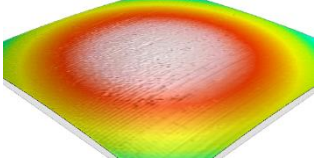
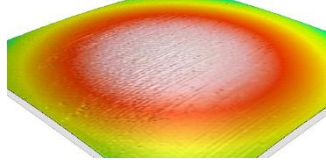
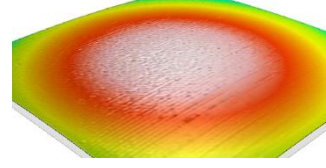
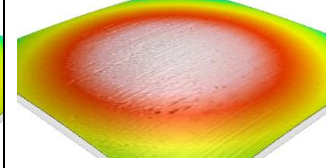
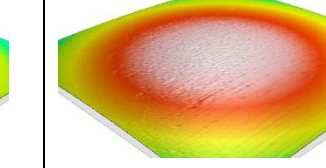
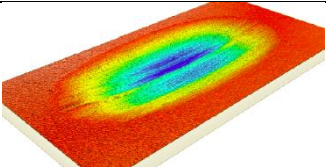
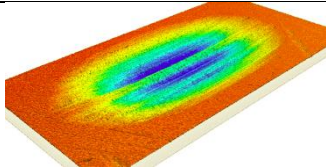
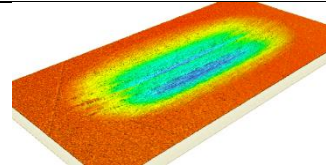
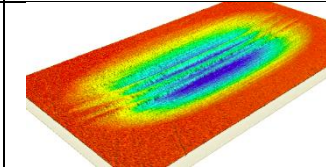
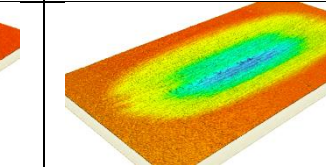
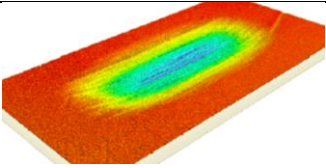
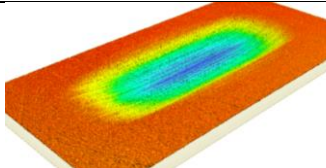
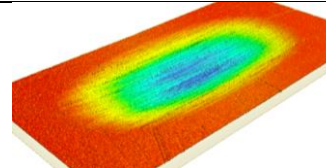
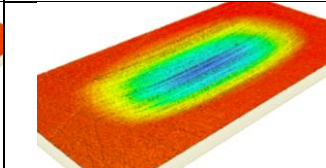
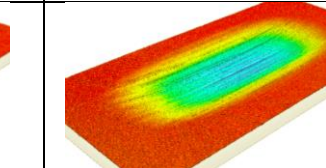
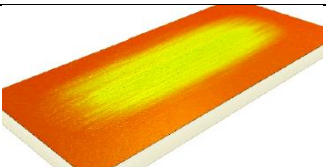
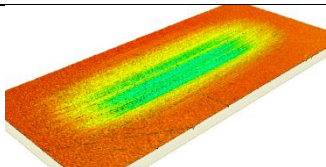
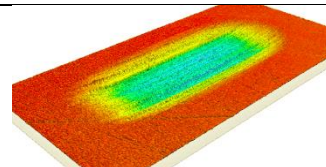
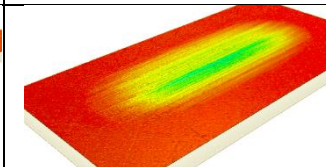
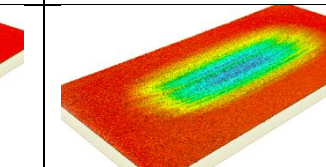
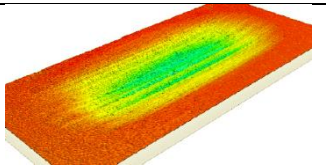
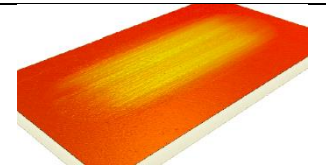
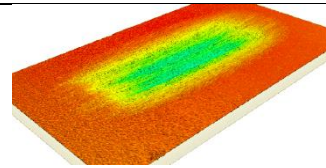
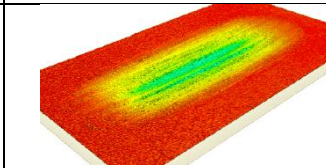
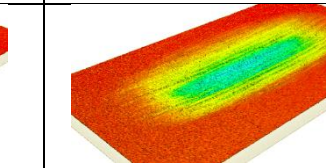
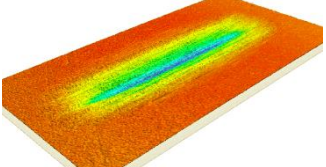
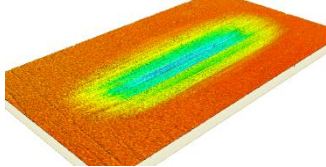
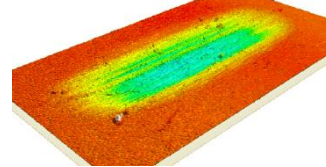
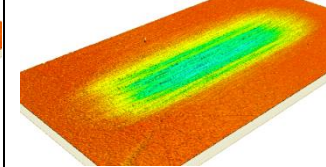
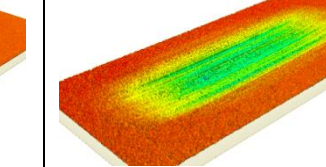
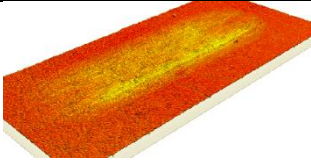
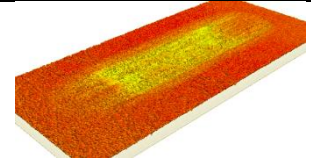
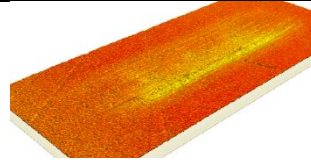
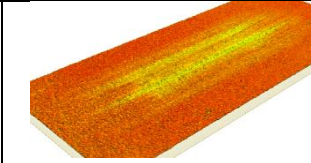
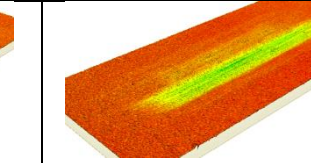
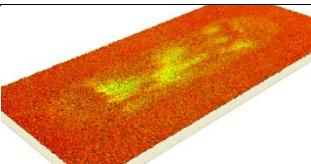

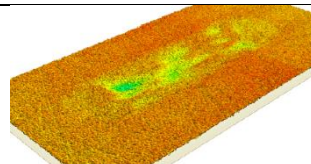
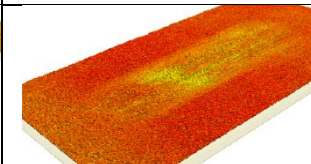
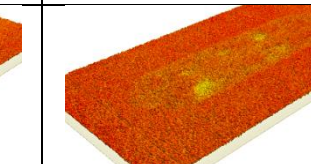
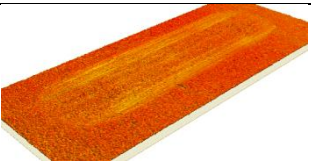


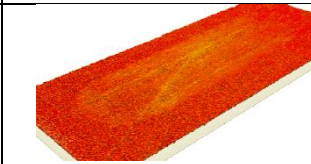
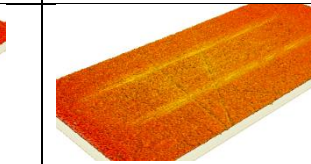
PAG 0.5 % DES					
PAO 0.5 % ZDDP					
PAG 0.5 % ZDDP					

Table B.2.2: 3 D images for wear tracks obtained for test fluids evaluated on the SRV test rig.

Base Fluid	Run 1	Run 2	Run 3	Run 4	Run 5
WMO 0.5 % DES					
PAO 3 % DES					
Gr III 2 % DES					
Gr II 41.2 cSt 2 % DES					
Gr II 101 cSt 2 % DES					

PAG 0.5 % DES					
PAO 0.5 % ZDDP					
PAG 0.5 % ZDDP					

Appendix B.3: Wear Surface Profiles

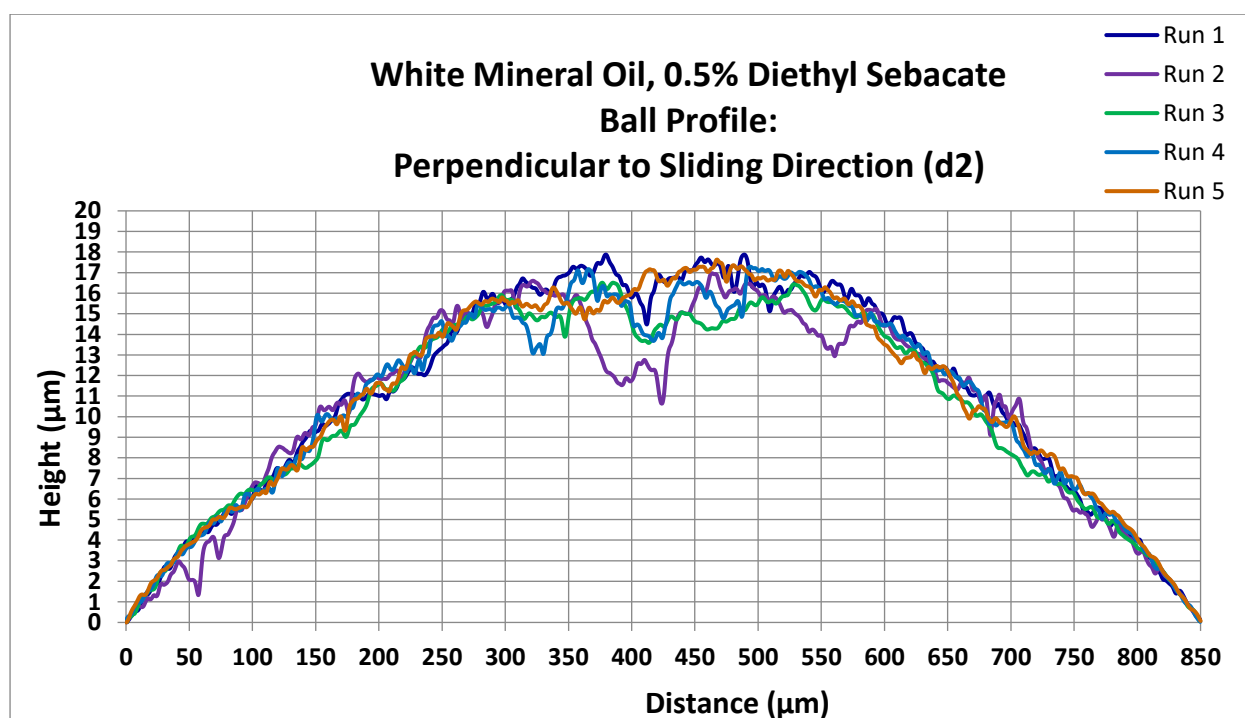


Figure B.3.1: Wear scar profiles perpendicular to sliding direction for **white mineral oil (WMO), 0.5 % diethyl sebacate**.

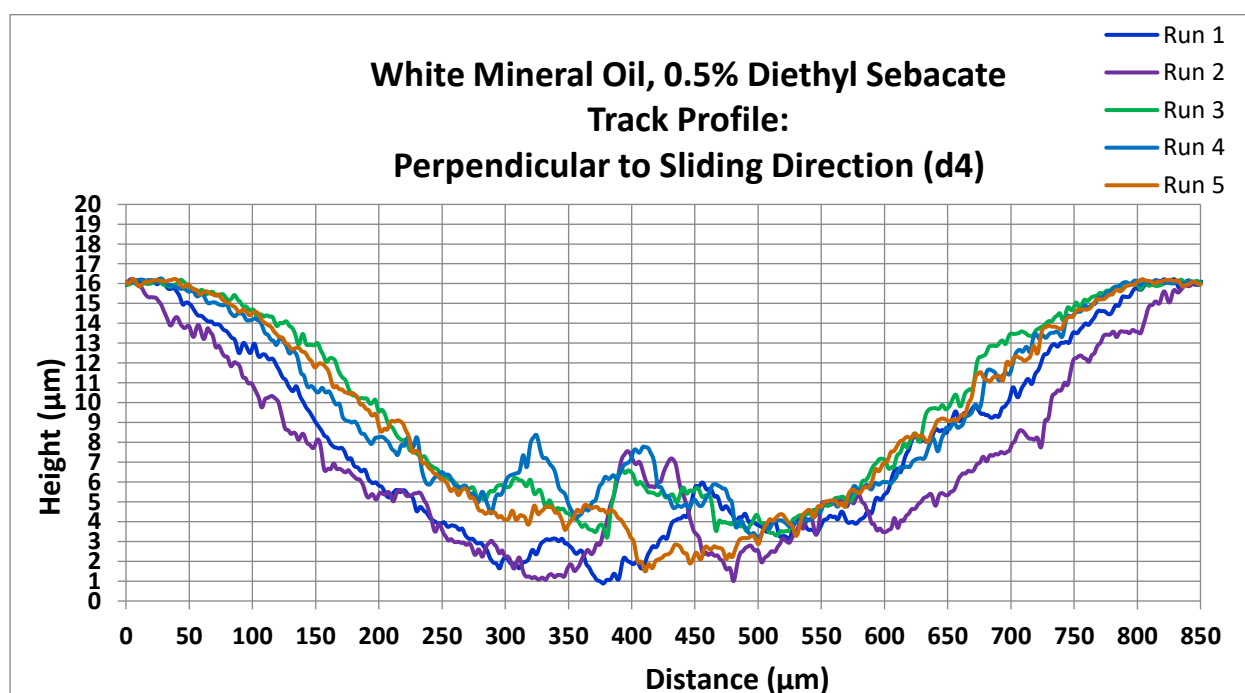


Figure B.3.2: Wear track profiles perpendicular to sliding direction for **white mineral oil (WMO), 0.5 % diethyl sebacate**.

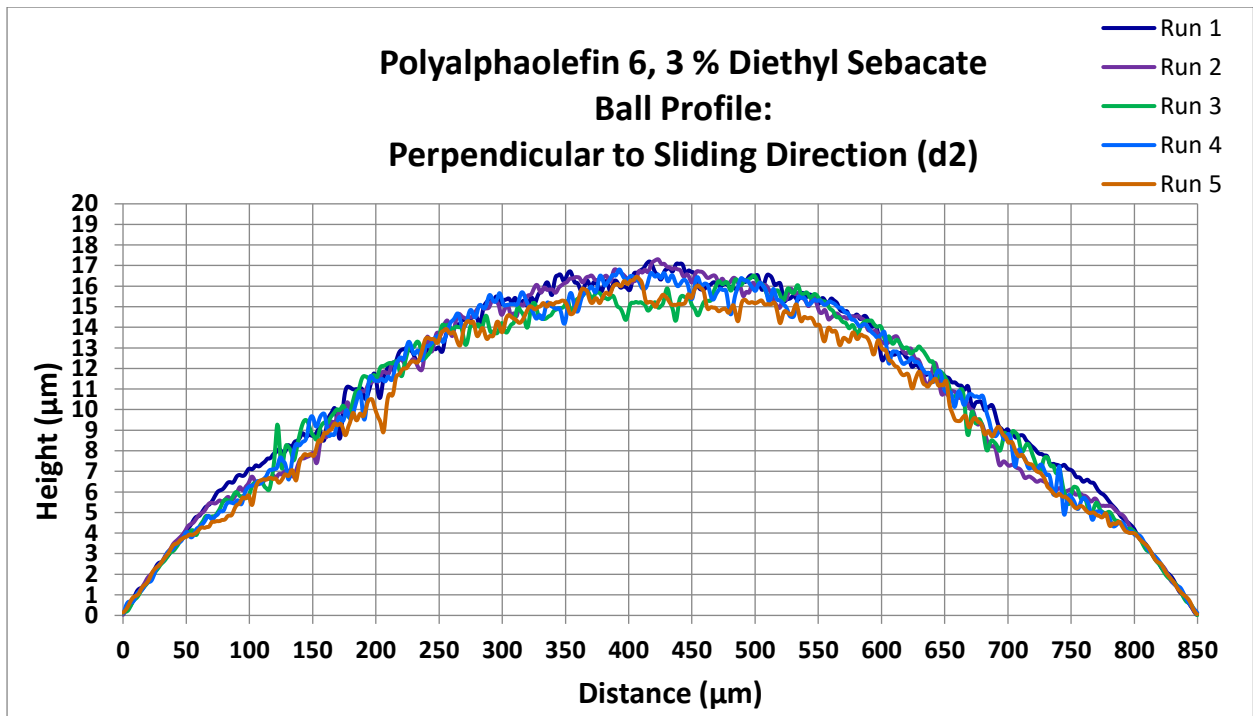


Figure B.3.3: Wear scar profiles perpendicular to sliding direction for **polyalphaolefin, 6 cSt, (PAO 6), 3 % diethyl sebacate**.

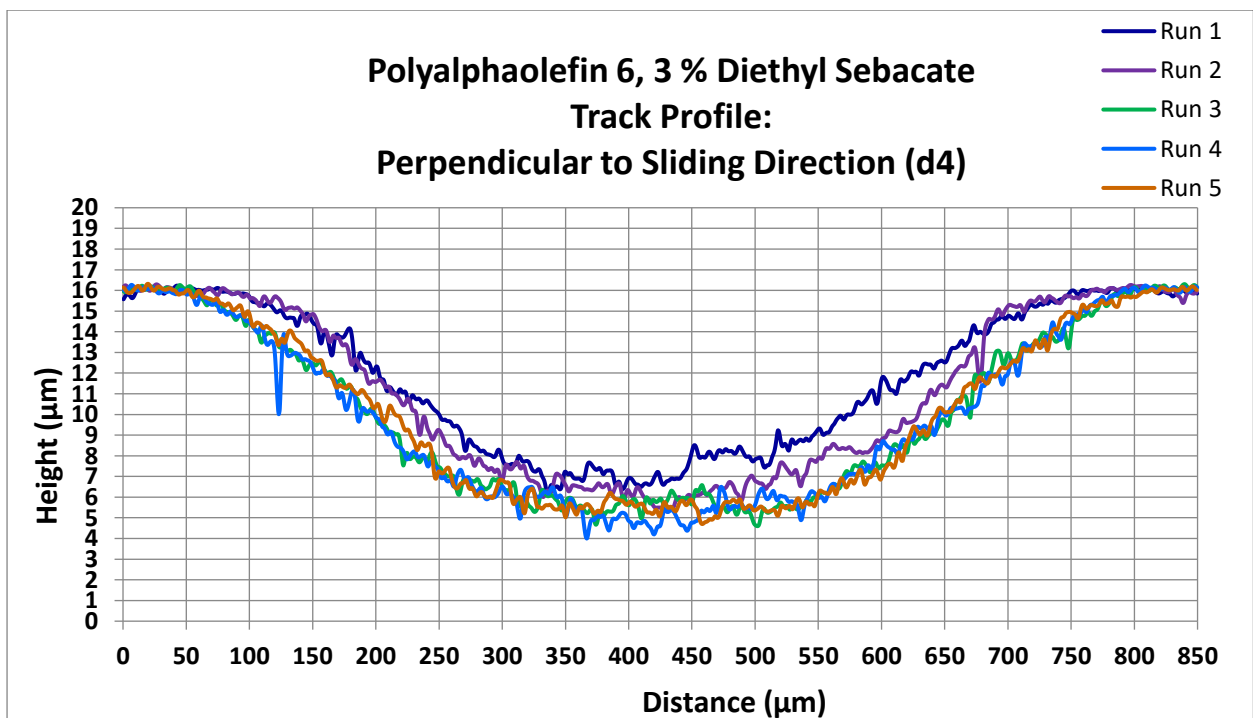


Figure B.3.4: Wear track profiles perpendicular to sliding direction for **polyalphaolefin, 6 cSt, (PAO 6), 3 % diethyl sebacate**.

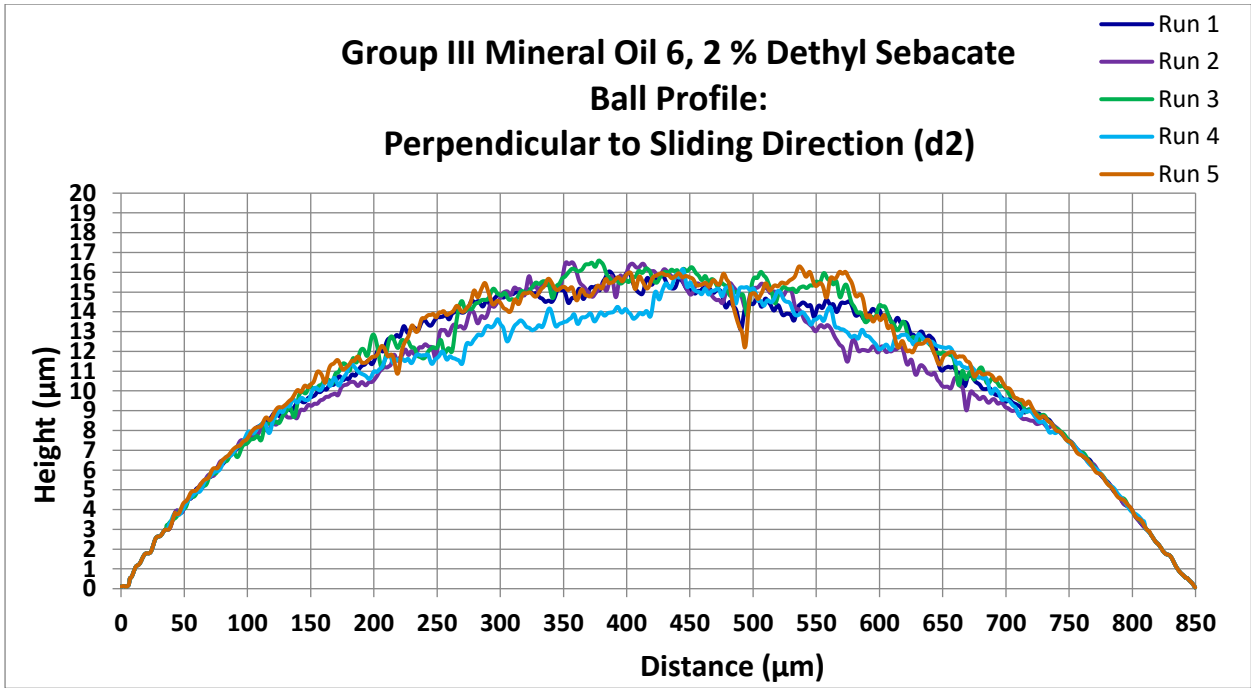


Figure B.3.5: Wear scar profiles perpendicular to sliding direction for **Group III mineral oil, 6 cSt, (Gr III 6) with 2 % diethyl sebacate.**

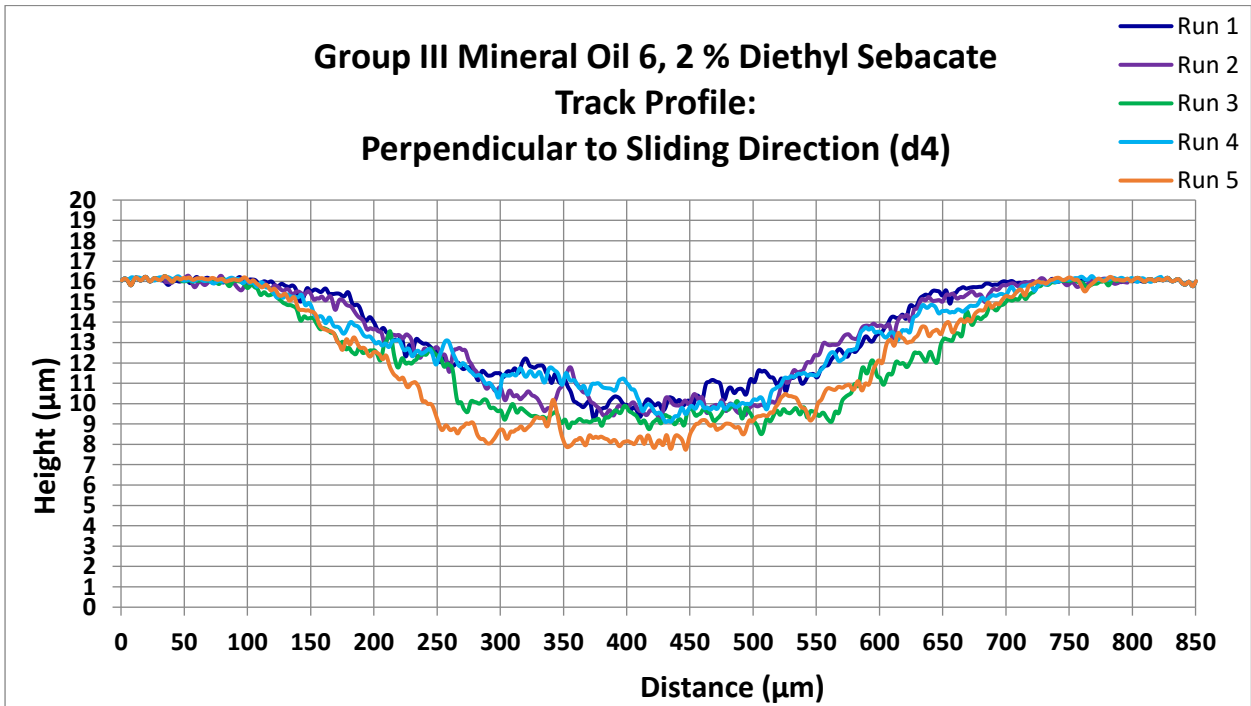


Figure B.3.6: Wear track profiles perpendicular to sliding direction for **Group III mineral oil, 6 cSt, (Gr III 6) with 2 % diethyl sebacate.**

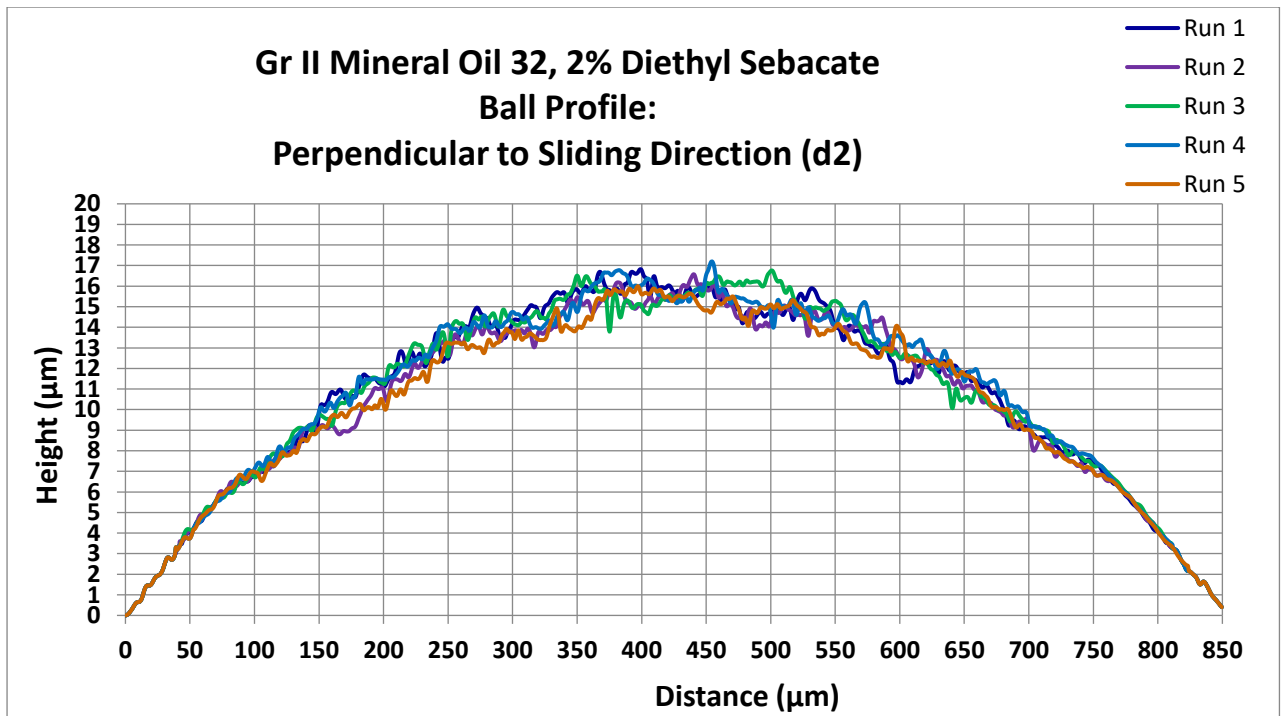


Figure B.3.7: Wear scar profiles perpendicular to sliding direction for **Group II mineral oil, ISO VG 32, (Gr II 32)** with 2 % diethyl sebacate.

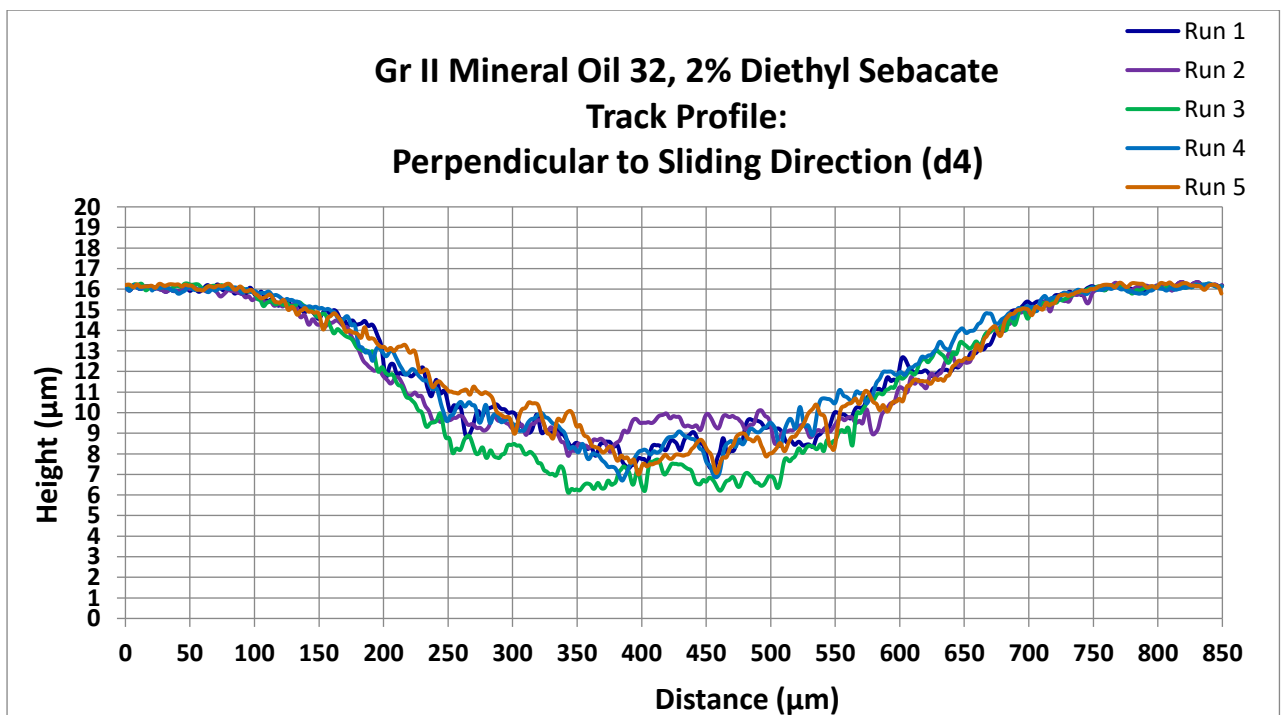


Figure B.3.8: Wear track profiles perpendicular to sliding direction for **Group II mineral oil, ISO VG 32, (Gr II 32)** with 2 % diethyl sebacate.

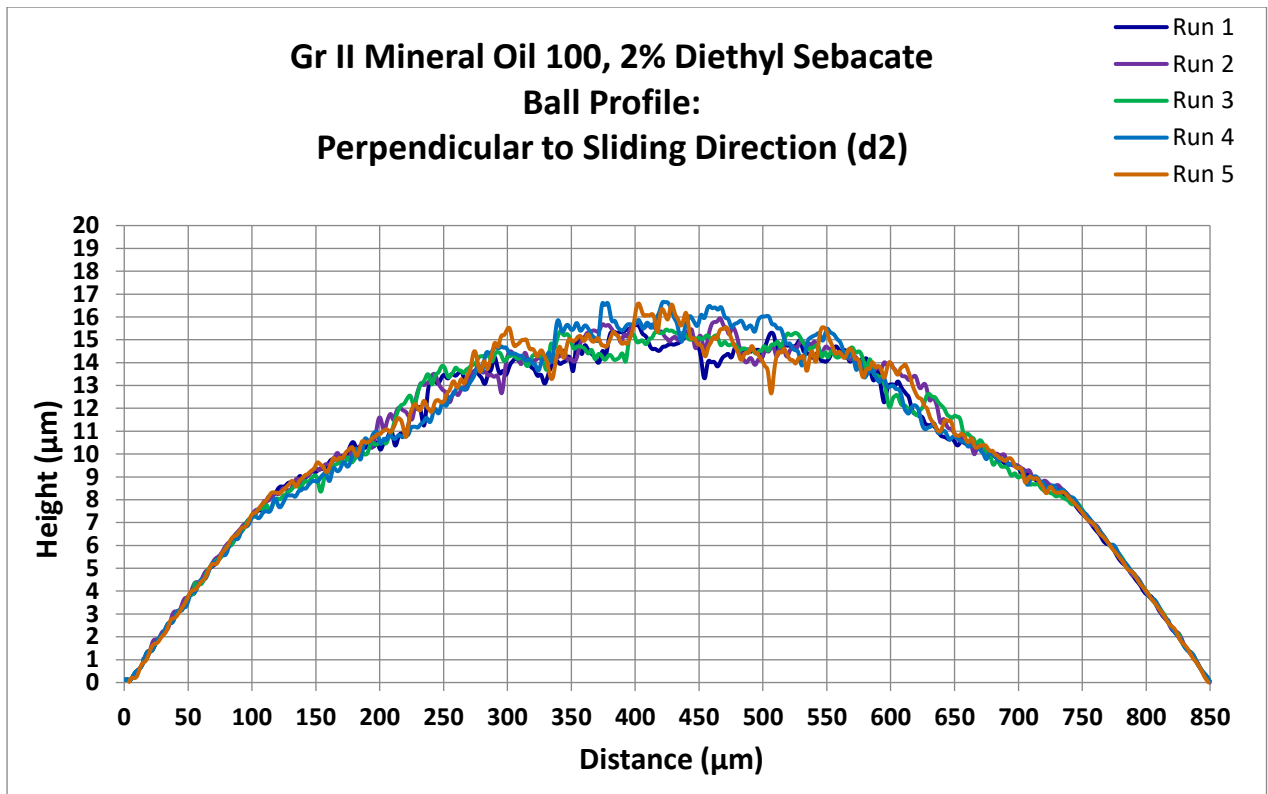


Figure B.3.9: Wear scar profiles perpendicular to sliding direction for **Group II mineral oil, ISO VG 100 (Gr II 100) with 2 % diethyl sebacate.**

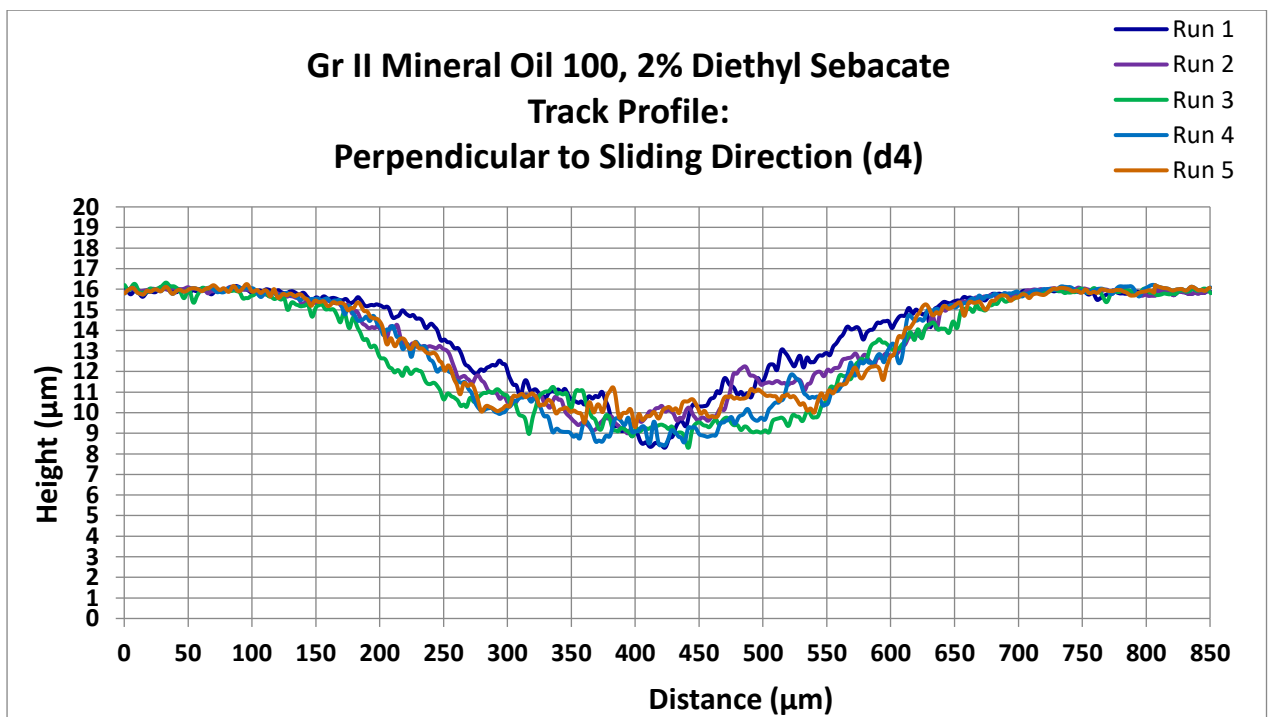


Figure B.3.10: Wear track profiles perpendicular to sliding direction for **Group II mineral oil, ISO VG 100, (Gr II 100) with 2 % diethyl sebacate.**

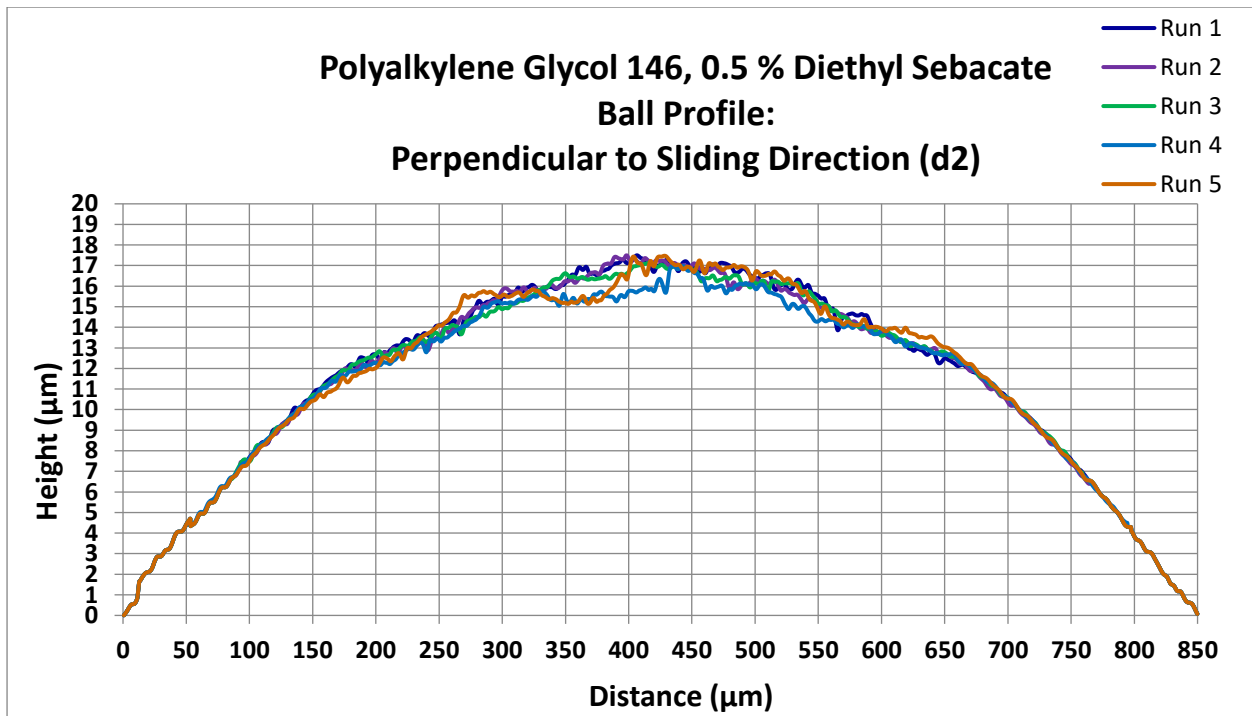


Figure B.3.11: Wear scar profiles perpendicular to sliding direction for **polyalkylene glycol**, ISO VG 146, (PAG 146) with 2 % diethyl sebacate.

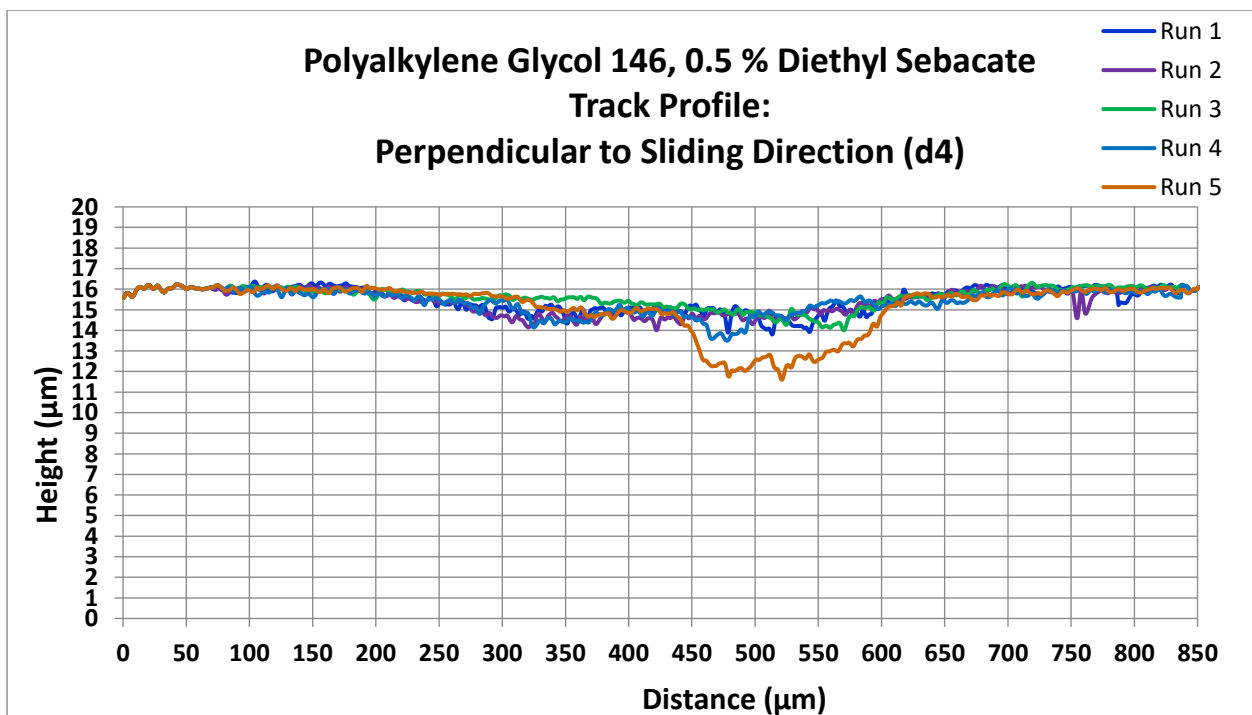


Figure B.3.12: Wear track profiles perpendicular to sliding direction for **polyalkylene glycol**, ISO VG 146, (PAG 146) with 2 % diethyl sebacate.

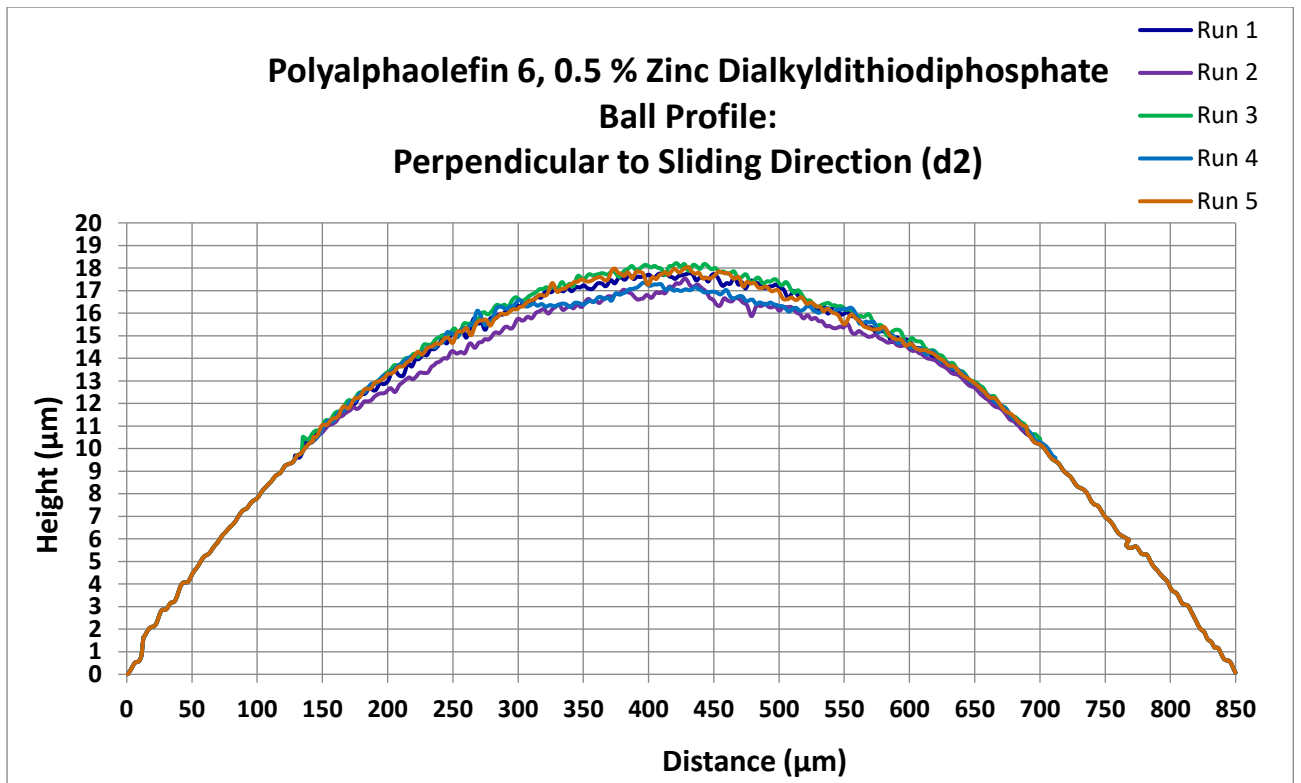


Figure B.3.13: Wear scar profiles perpendicular to sliding direction for polyalphaolefin, 6 cSt, (PAO 6) with 0.5 % ZDDP.

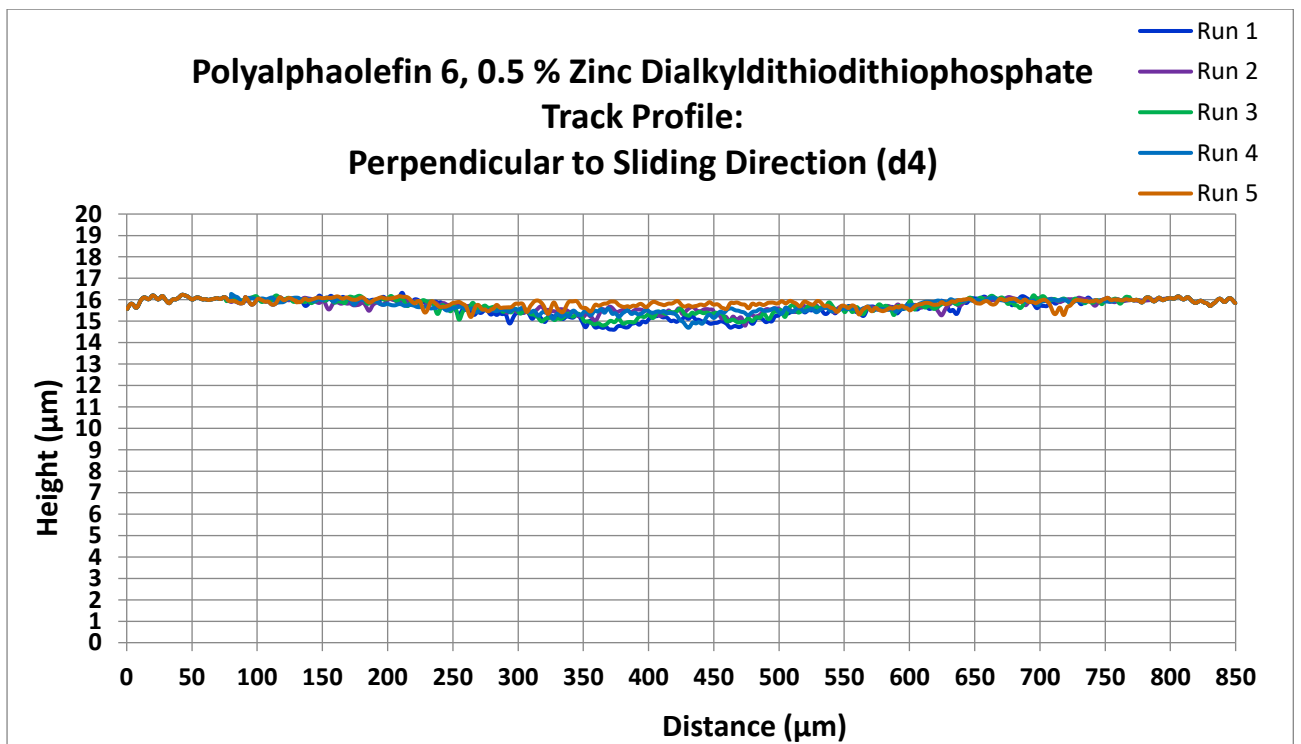


Figure B.3.14: Wear track profiles perpendicular to sliding direction for polyalphaolefin, 6 cSt, (PAO 6) with 0.5 % ZDDP.

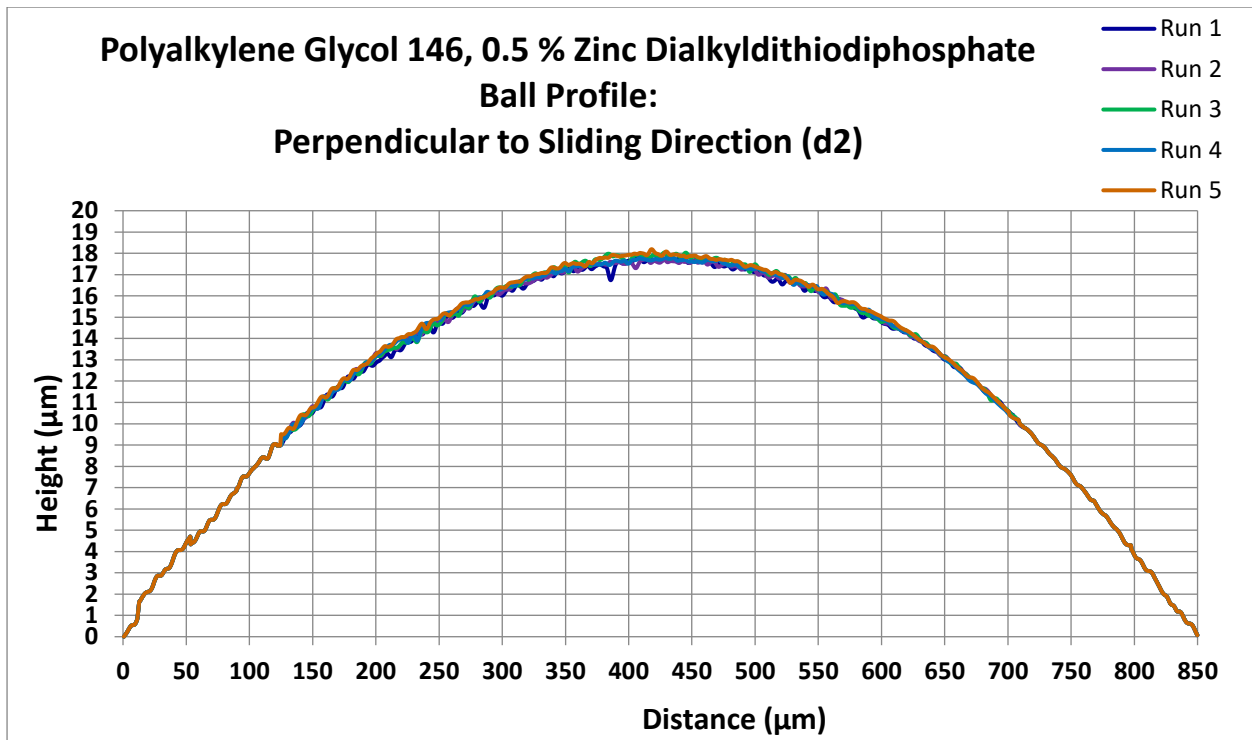


Figure B.3.15: Wear scar profiles perpendicular to sliding direction for **polyalkylene glycol**, ISO VG 146, (PAG 146) with 0.5 % ZDDP.

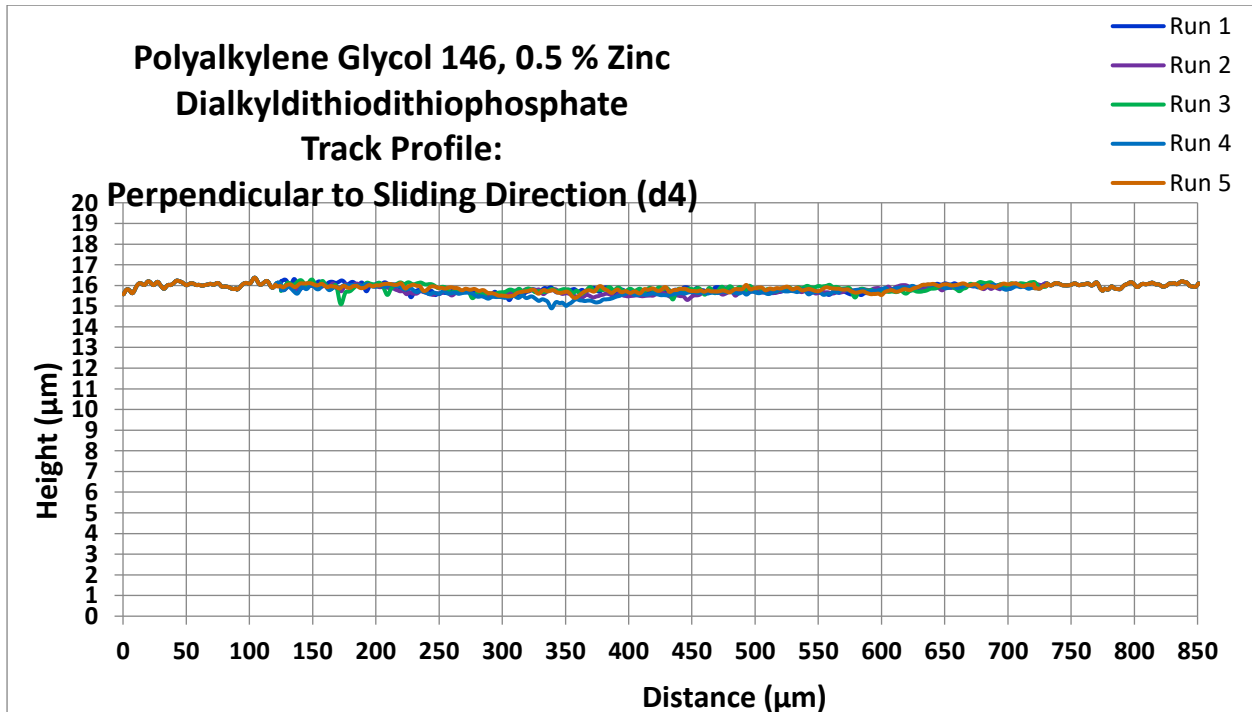


Figure B.3.16: Wear track profiles perpendicular to sliding direction for **polyalkylene glycol**, ISO VG 146, (PAG 146) with 0.5 % ZDDP.

Appendix B.4: Wear Volume Calculations

Wear volumes calculated according to ASTM D 7755-17.

Wear volume of the scar in mm³:

$$W_{v, ball} = \frac{\pi \cdot d_1^2 \cdot d_2^2}{64} \left(\frac{1}{R} - \frac{1}{\overline{R}_s} \right) \quad \text{B.4.1}$$

$$\overline{R}_s = \frac{d_2^3}{12 W_{q,flat}} \quad \text{B.4.2}$$

Where:

\overline{R}_s = resulting radius of the shape of the wear scar after the test in mm;

R = initial radius of the ball in mm;

d_1 = the wear scar diameter on the ball parallel to the sliding direction in mm;

d_2 = the wear scar diameter on the ball perpendicular to the sliding direction in

mm;

$W_{q,flat}$ = planimetric wear of the wear track in the middle of the wear track length and

seen perpendicular to the sliding direction in mm². Determined with MountainsMap[®] software.

Wear volume of the track mm^3 :

$$W_{v, flat} = \frac{\pi \cdot d_4^2 \cdot (d_3 - s)^2}{64} \cdot \frac{1}{\bar{R}_t} + s \cdot W_{q, flat} \quad \text{B.4.3}$$

And

$$\bar{R}_t = \frac{d_4^3}{12 W_{q, flat}} \quad \text{B.4.4}$$

d_3 = the total length of the wear track in sliding direction in mm.

d_4 = the width of the wear track in mm.

\bar{R}_t = resulting radius of the shape of the wear track after the test in mm.

s = stroke which is equal to 1 mm for all cases.

The measured values and calculated values for the wear volumes of the scar and track can be found in Table B.4.1 to Table B.4.8 for all the test fluids evaluated in part 1 of this investigation. These tables include the values for the wear volumes based on the adjusted wear scar diameter parallel to the sliding direction.

Table B.4.1: Wear volumes for scars and tracks for **white mineral oil (WMO) with 0.5 % diethyl sebacate**.

Run	Scar Dimensions		Track Dimensions			Scar Calculations			Track Calculations		
	d_1 (mm)		d_2 (mm)	d_3 (mm)	d_4 (mm)	$W_{q,flat}$ (mm ²)	\bar{R}_s (mm)	$W_{v, ball}$ (mm ³)		\bar{R}_t (mm)	$W_{v, flat}$ (mm ³)
	Meas.	Adj.						Meas.	Adj.		
1	0.745	0.618	0.792	1.667	0.783	0.00696	5.954	5.48E-04	3.77E-04	5.750	9.30E-03
2	0.765	0.646	0.829	1.688	0.825	0.00763	6.225	7.77E-04	5.55E-04	6.123	1.02E-02
3	0.726	0.629	0.751	1.692	0.788	0.00550	6.426	6.49E-04	4.86E-04	7.403	7.47E-03
4	0.759	0.631	0.761	1.688	0.754	0.00573	6.407	7.18E-04	4.96E-04	6.249	7.84E-03
5	0.700	0.614	0.759	1.662	0.751	0.00605	6.032	4.75E-04	3.65E-04	5.832	8.13E-03
AVG	0.739	0.628	0.778	1.679	0.780	0.00637	6.209	6.33E-04	4.56E-04	6.271	8.59E-03
STDEV	0.026	0.013	0.032	0.014	0.030	0.00090	0.214	1.23E-04	8.19E-05	0.665	1.13E-03

Table B.4.2: Wear volumes for scars and tracks for **polyalphaolefin, 6 cSt, (PAO 6) with 3 % diethyl sebacate.**

Run	Scar Dimensions		Track Dimensions			Scar Calculations			Track Calculations		
	d_1 (mm)		d_2 (mm)	d_3 (mm)	d_4 (mm)	$W_{q,flat}$ (mm ²)	\bar{R}_s (mm)	$W_{v, ball}$ (mm ³)		\bar{R}_t (mm)	$W_{v, flat}$ (mm ³)
	Meas.	Adj.						Meas.	Adj.		
1	0.619	0.563	0.683	1.578	0.677	0.00367	7.244	5.45E-04	4.50E-04	7.047	4.74E-03
2	0.643	0.598	0.715	1.608	0.714	0.00429	7.104	6.15E-04	5.31E-04	7.069	5.60E-03
3	0.658	0.608	0.746	1.618	0.747	0.00527	6.567	5.64E-04	4.83E-04	6.600	6.85E-03
4	0.656	0.605	0.746	1.615	0.746	0.00532	6.504	5.44E-04	4.63E-04	6.514	6.91E-03
5	0.664	0.622	0.759	1.618	0.754	0.00518	7.049	7.25E-04	6.37E-04	6.887	6.72E-03
AVG	0.648	0.599	0.730	1.607	0.728	0.00475	6.894	5.99E-04	5.13E-04	6.823	6.16E-03
STDEV	0.018	0.022	0.031	0.017	0.032	0.00073	0.335	7.63E-05	7.59E-05	0.255	9.59E-04

Table B.4.3: Wear volumes for scars and tracks for **Group III mineral oil, 6 cSt, (Gr III 6) with 2 % diethyl sebacate.**

Run	Scar Dimensions			Track Dimensions			Scar Calculations			Track Calculations	
	d_1 (mm)		d_2 (mm)	d_3 (mm)	d_4 (mm)	$W_{q,flat}$ (mm ²)	\bar{R}_s (mm)	$W_{v, ball}$ (mm ³)		\bar{R}_t (mm)	$W_{v, flat}$ (mm ³)
	Meas.	Adj.						Meas.	Adj.		
1	0.558	0.550	0.602	1.604	0.594	0.00209	8.723	4.74E-04	4.60E-04	8.366	2.84E-03
2	0.582	0.567	0.634	1.622	0.630	0.00224	9.467	6.31E-04	5.98E-04	9.302	3.05E-03
3	0.583	0.535	0.658	1.592	0.641	0.00295	8.035	5.45E-04	4.59E-04	7.442	3.90E-03
4	0.588	0.556	0.639	1.622	0.644	0.00237	9.169	6.31E-04	5.64E-04	9.368	3.21E-03
5	0.593	0.545	0.643	1.593	0.638	0.00323	6.865	3.89E-04	3.28E-04	6.690	4.28E-03
AVG	0.581	0.551	0.635	1.607	0.629	0.00258	8.452	5.34E-04	4.82E-04	8.234	3.46E-03
STDEV	0.013	0.012	0.021	0.015	0.020	0.00049	1.038	1.04E-04	1.06E-04	1.168	6.08E-04

Table B.4.4: Wear volumes for scars and tracks for **Group II mineral oil, ISO VG 100 (Gr II 100) with 2 % diethyl sebacate.**

Run	Scar Dimensions		Track Dimensions			Scar Calculations			Track Calculations		
	d_1 (mm)		d_2 (mm)	d_3 (mm)	d_4 (mm)	$W_{q,flat}$ (mm ²)	\bar{R}_s (mm)	$W_{v, ball}$ (mm ³)		\bar{R}_t (mm)	$W_{v, flat}$ (mm ³)
	Meas.	Adj.						Meas.	Adj.		
1	0.608	0.560	0.676	1.614	0.669	0.00319	8.094	6.35E-04	5.38E-04	7.843	4.24E-03
2	0.606	0.563	0.689	1.618	0.682	0.00327	8.333	6.85E-04	5.89E-04	8.063	4.36E-03
3	0.647	0.584	0.686	1.629	0.667	0.00383	7.012	5.54E-04	4.52E-04	6.446	5.17E-03
4	0.605	0.550	0.658	1.615	0.644	0.00302	7.860	5.66E-04	4.67E-04	7.371	4.06E-03
5	0.632	0.572	0.684	1.629	0.674	0.00323	8.257	7.23E-04	5.92E-04	7.894	4.34E-03
AVG	0.620	0.566	0.679	1.621	0.667	0.00331	7.911	6.33E-04	5.28E-04	7.52	4.43E-03
STDEV	0.019	0.013	0.012	0.007	0.014	0.00031	0.534	7.34E-05	6.60E-05	0.65	4.28E-04

Table B.4.5: Wear volumes for scars and tracks for **Group II mineral oil, ISO VG 100 (Gr II 100) with 2 % diethyl sebacate.**

Run	Scar Dimensions		Track Dimensions			Scar Calculations			Track Calculations		
	d_1 (mm)		d_2 (mm)	d_3 (mm)	d_4 (mm)	$W_{q,flat}$ (mm ²)	\bar{R}_s (mm)	$W_{v, ball}$ (mm ³)		\bar{R}_t (mm)	$W_{v, flat}$ (mm ³)
	Meas.	Adj.						Meas.	Adj.		
1	0.558	0.544	0.611	1.596	0.593	0.00178	10.727	6.11E-04	5.79E-04	9.784	2.40E-03
2	0.562	0.535	0.619	1.593	0.611	0.00214	9.219	5.44E-04	4.93E-04	8.884	2.87E-03
3	0.586	0.555	0.638	1.604	0.633	0.00254	8.522	5.67E-04	5.09E-04	8.338	3.40E-03
4	0.577	0.555	0.634	1.596	0.622	0.00242	8.758	5.64E-04	5.22E-04	8.268	3.24E-03
5	0.564	0.529	0.638	1.611	0.608	0.00222	9.722	6.17E-04	5.42E-04	8.429	3.03E-03
AVG	0.569	0.544	0.628	1.600	0.613	0.00222	9.390	5.81E-04	5.29E-04	8.74	2.99E-03
STDEV	0.012	0.012	0.012	0.007	0.015	0.00029	0.877	3.18E-05	3.32E-05	0.63	3.86E-04

Table B.4.6: Wear volumes for scars and tracks for **polyalkylene glycol, ISO VG 146, (PAG 146)** with 0.5 % diethyl sebacate.

Run	Scar Dimensions			Track Dimensions			Scar Calculations			Track Calculations	
	d_1 (mm)		d_2 (mm)	d_3 (mm)	d_4 (mm)	$W_{q,flat}$ (mm ²)	\bar{R}_s (mm)	$W_{v, ball}$ (mm ³)		\bar{R}_t (mm)	$W_{v, flat}$ (mm ³)
	Meas.	Adj.						Meas.	Adj.		
1	0.498	0.460	0.498	1.582	0.490	0.000538	19.090	4.44E-04	3.80E-04	18.272	7.56E-04
2	0.473	0.440	0.490	1.568	0.483	0.000568	17.276	3.75E-04	3.24E-04	16.575	7.91E-04
3	0.468	0.447	0.490	1.567	0.487	0.000438	22.380	4.01E-04	3.66E-04	21.943	6.08E-04
4	0.479	0.444	0.499	1.575	0.495	0.000506	20.517	4.25E-04	3.65E-04	19.956	7.04E-04
5	0.483	0.450	0.503	1.560	0.498	0.000743	14.253	3.76E-04	3.27E-04	13.864	1.02E-03
AVG	0.480	0.448	0.496	1.570	0.491	0.00056	18.703	4.04E-04	3.52E-04	18.12	7.76E-04
STDEV	0.011	0.008	0.006	0.008	0.006	0.00011	3.114	3.03E-05	2.53E-05	3.10	1.53E-04

Table B.4.7: Wear volumes for scars and tracks for **polyalphaolefin, 6 cSt, (PAO 6) with 0.5 % ZDDP**.

Run	Scar Dimensions			Track Dimensions			Scar Calculations			Track Calculations	
	d_1 (mm)		d_2 (mm)	d_3 (mm)	d_4 (mm)	$W_{q,flat}$ (mm ²)	\bar{R}_s (mm)	$W_{v, ball}$ (mm ³)		\bar{R}_t (mm)	$W_{v, flat}$ (mm ³)
	Meas.	Adj.						Meas.	Adj.		
1	0.424	0.424	0.452	1.531	0.420	0.000375	20.460	2.72E-04	2.72E-04	16.474	5.23E-04
2	0.453	0.453	0.464	1.548	0.458	0.000260	32.217	3.68E-04	3.68E-04	30.871	3.59E-04
3	0.431	0.431	0.411	1.545	0.404	0.000360	16.113	2.13E-04	2.13E-04	15.244	5.15E-04
4	0.431	0.431	0.405	1.545	0.458	0.000273	20.358	2.26E-04	2.26E-04	29.358	3.77E-04
5	0.437	0.437	0.430	1.549	0.421	0.000138	47.900	3.09E-04	3.09E-04	45.106	1.96E-04
AVG	0.435	0.435	0.432	1.544	0.432	0.00028	27.410	2.78E-04	2.78E-04	27.41	3.94E-04
STDEV	0.011	0.011	0.025	0.007	0.024	0.00009	12.929	6.33E-05	6.33E-05	12.21	1.34E-04

Table B.4.8: Wear volumes for scars and tracks for **polyalkylene glycol, ISO VG 146, (PAG 146) with 0.5 % ZDDP**.

Run	Scar Dimensions		Track Dimensions			Scar Calculations			Track Calculations		
	d_1 (mm)		d_2 (mm)	d_3 (mm)	d_4 (mm)	$W_{q,flat}$ (mm ²)	\bar{R}_s (mm)	$W_{v, ball}$ (mm ³)		\bar{R}_t (mm)	$W_{v, flat}$ (mm ³)
	Meas.	Adj.						Meas.	Adj.		
1	0.433	0.412	0.433	1.461	0.407	0.000177	38.339	4.44E-04	2.81E-04	31.821	2.31E-04
2	0.422	0.448	0.426	1.461	0.410	0.000162	39.773	3.75E-04	2.98E-04	35.469	2.11E-04
3	0.422	0.435	0.419	1.438	0.391	0.000186	32.884	4.01E-04	2.63E-04	26.8592	2.39E-04
4	0.420	0.433	0.419	1.495	0.403	0.000194	31.458	4.25E-04	2.54E-04	28.007	2.64E-04
5	0.407	0.425	0.409	1.475	0.377	0.000162	35.353	3.76E-04	2.52E-04	27.677	2.19E-04
AVG	0.480	0.425	0.421	1.466	0.398	0.00018	35.561	4.04E-04	2.70E-04	29.97	2.33E-04
STDEV	0.011	0.008	0.009	0.021	0.014	0.00001	3.518	3.03E-05	1.96E-05	3.62	2.05E-05

Appendix C.1: Friction Coefficient Graphs: Gradient vs. Step Load Increase

1.125 minutes

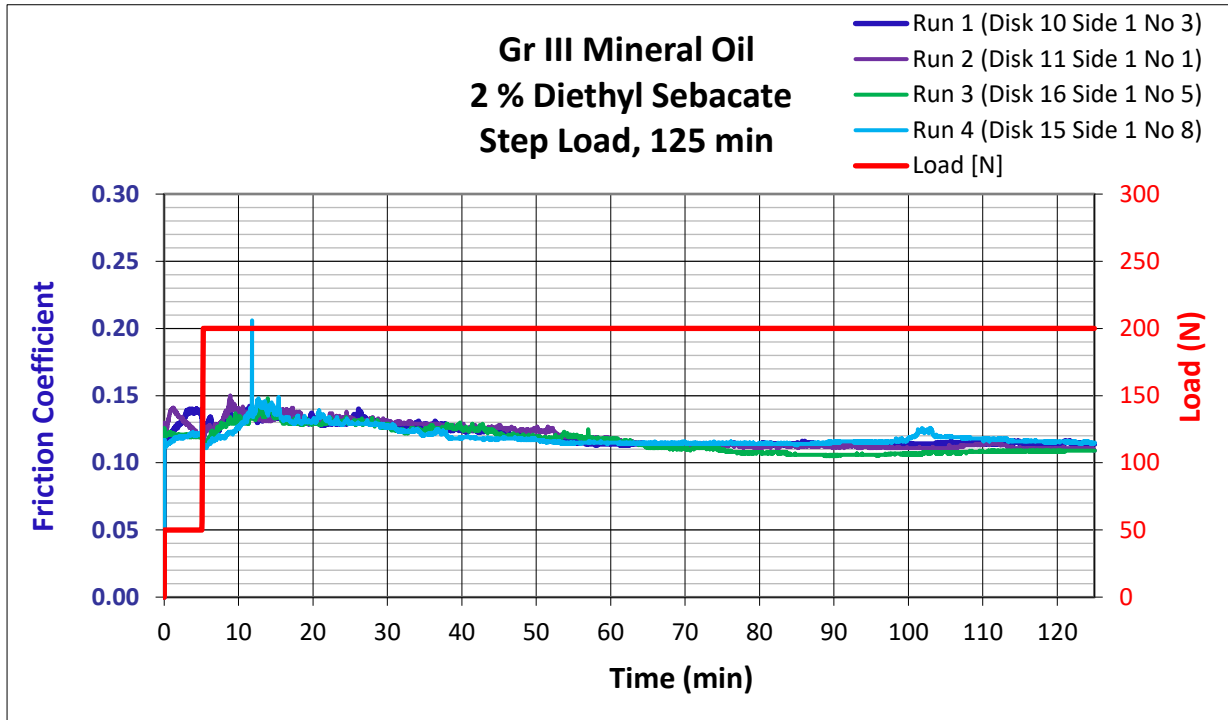


Figure C.1.1: Friction coefficient graphs for step load, 125 minutes.

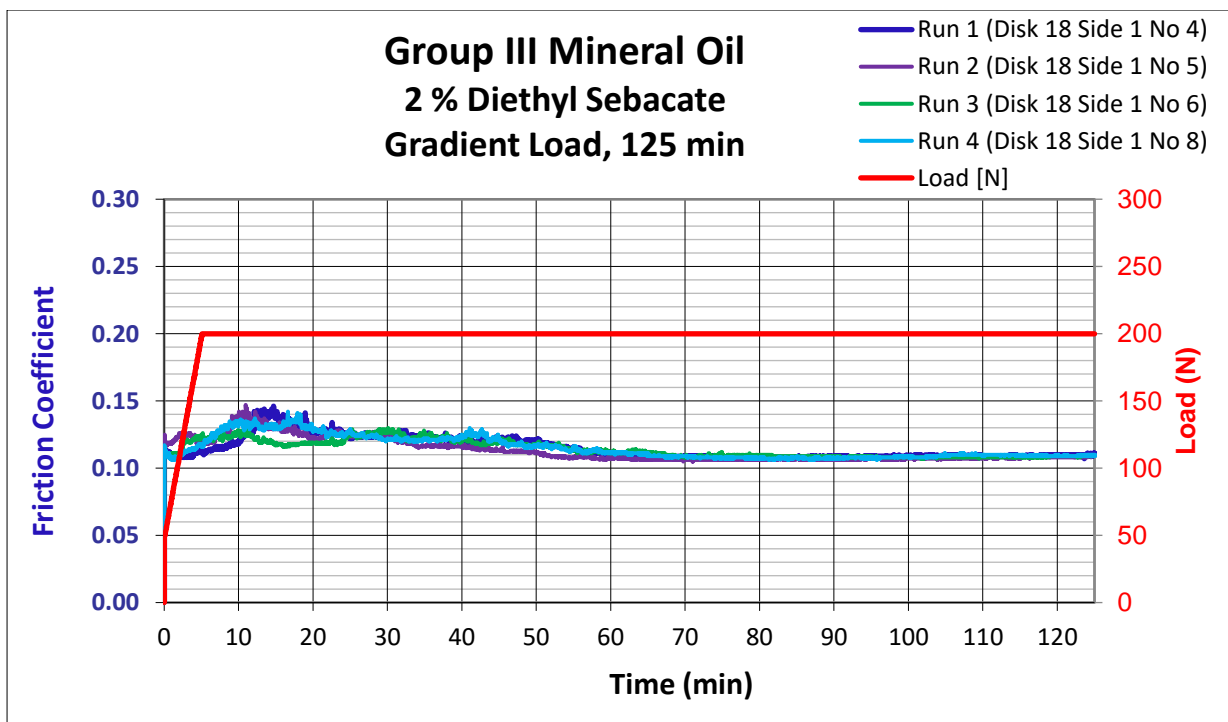


Figure C.1.2: Friction coefficient graphs for gradual load increase, 125 minutes.

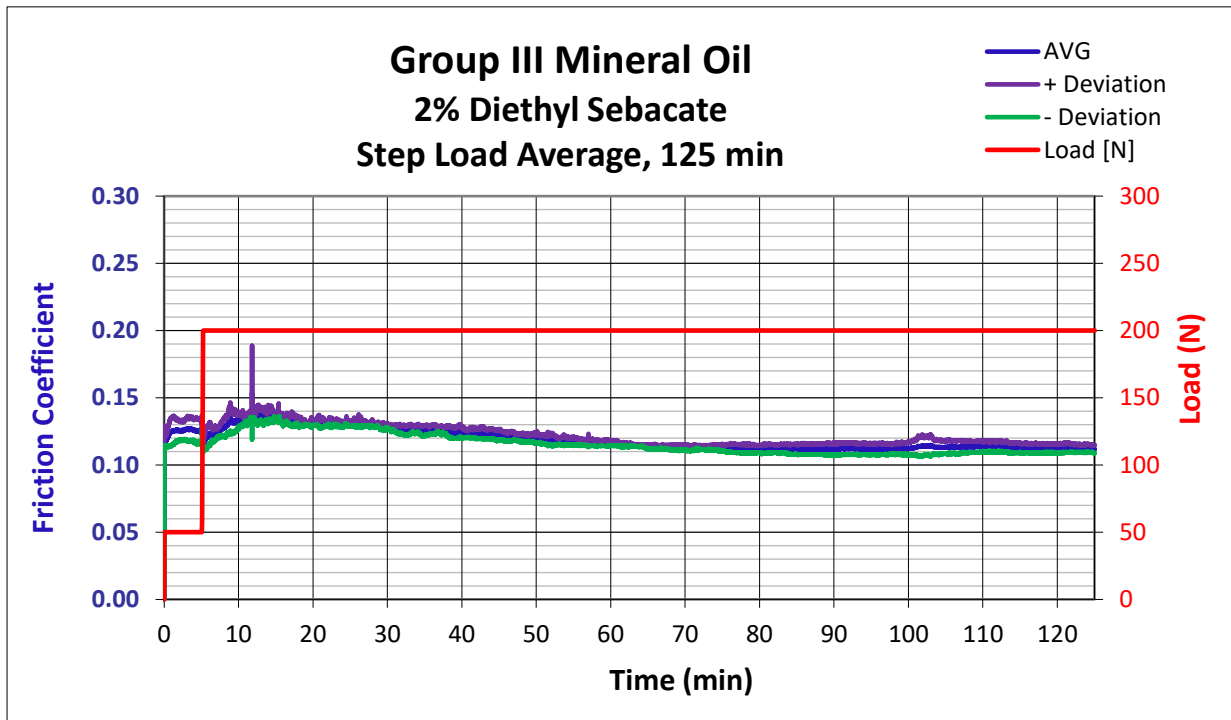


Figure C.1.3: Average of friction coefficient graphs for step load, 125 minutes.

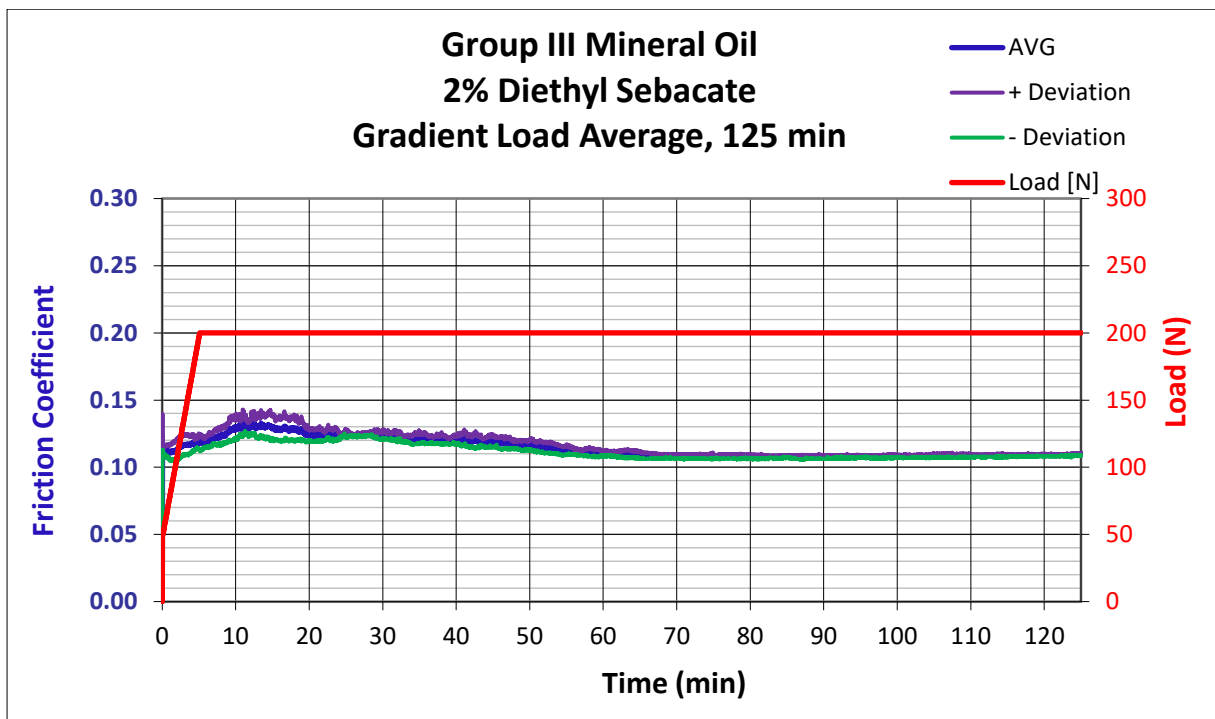


Figure C.1.4: Average of friction coefficient graphs for gradual load, 125 minutes.

2. 100 minutes

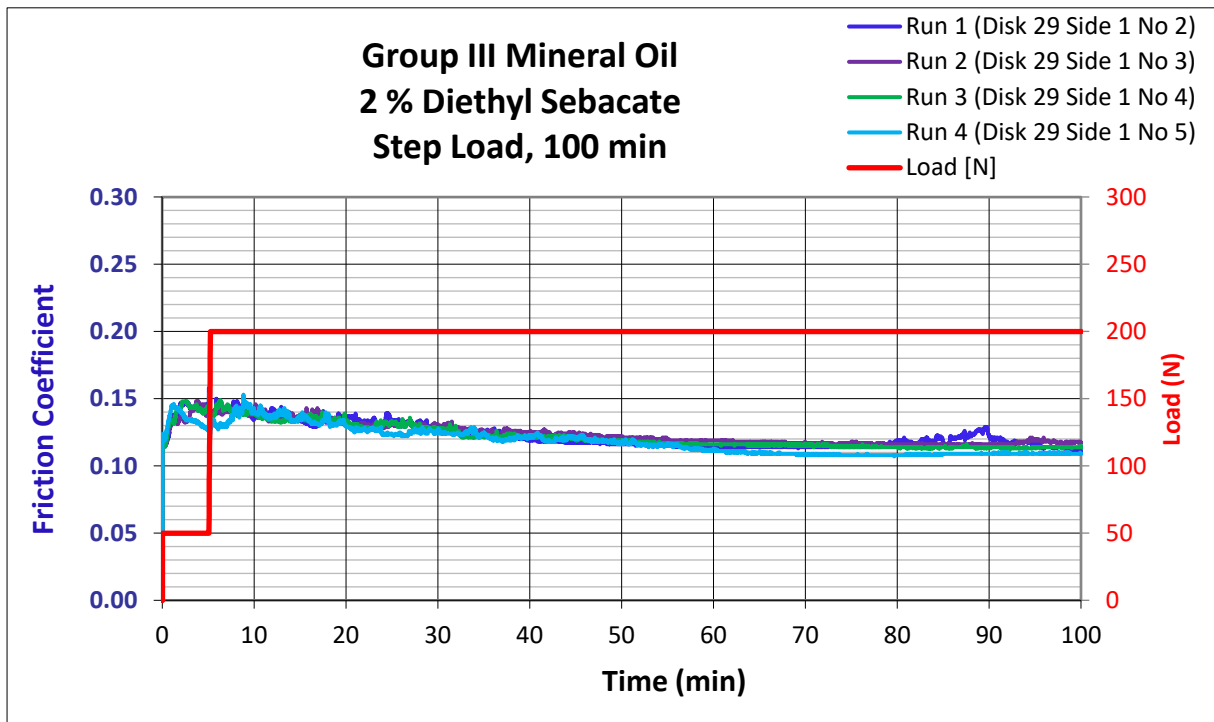


Figure C.1.5: Friction coefficient graphs for step load, 100 minutes.

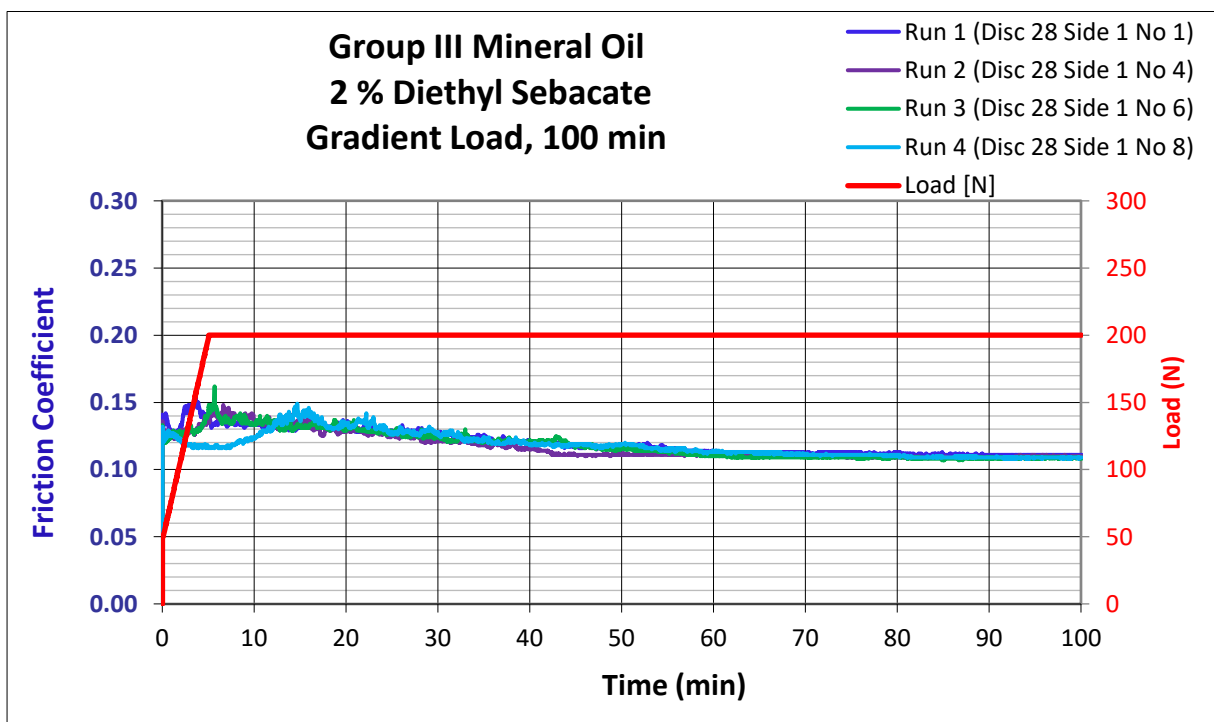


Figure C.1.6: Friction coefficient graphs for gradual load, 100 minutes.

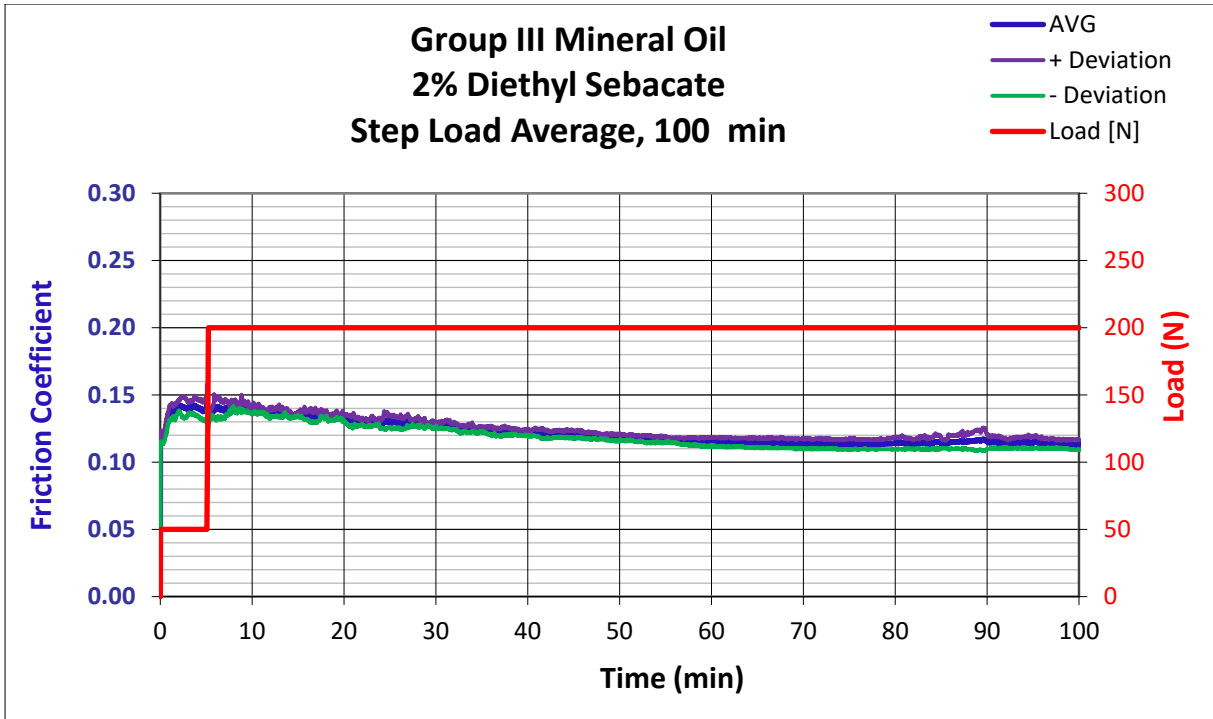


Figure C.1.7: Average of friction coefficient graphs for step load, 125 minutes.

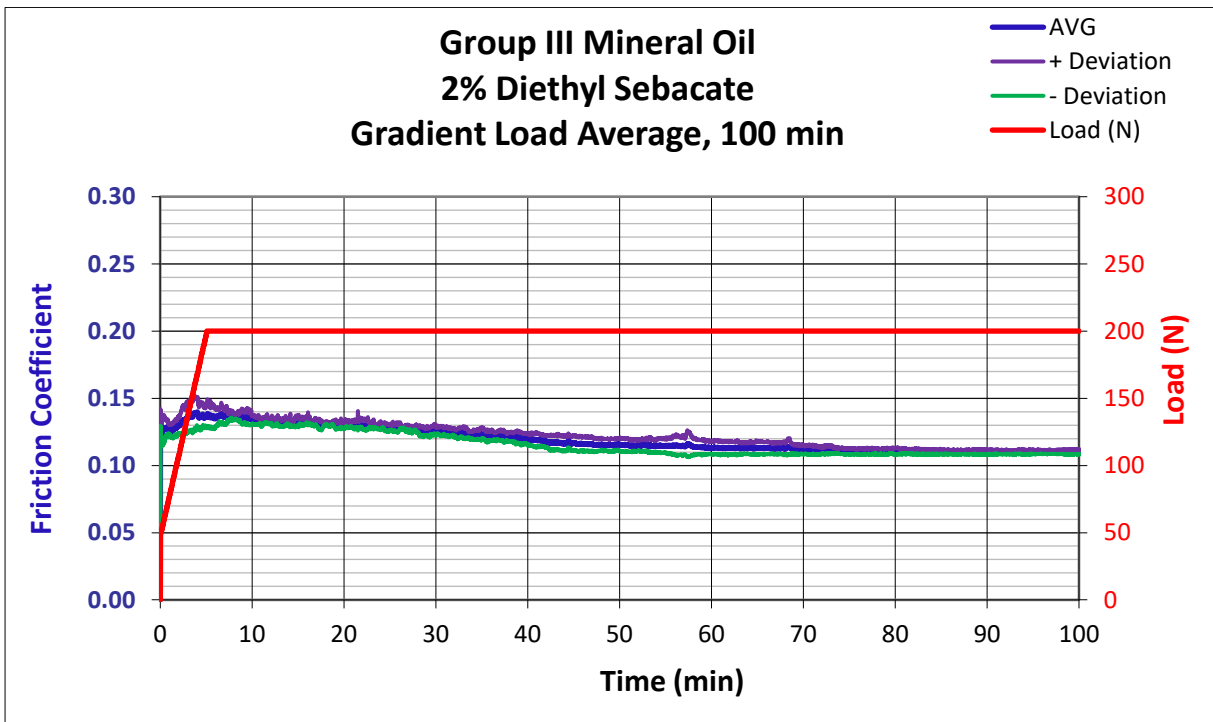


Figure C.1.8: Average of friction coefficient graphs for gradual load, 100 minutes.

3.75 minutes

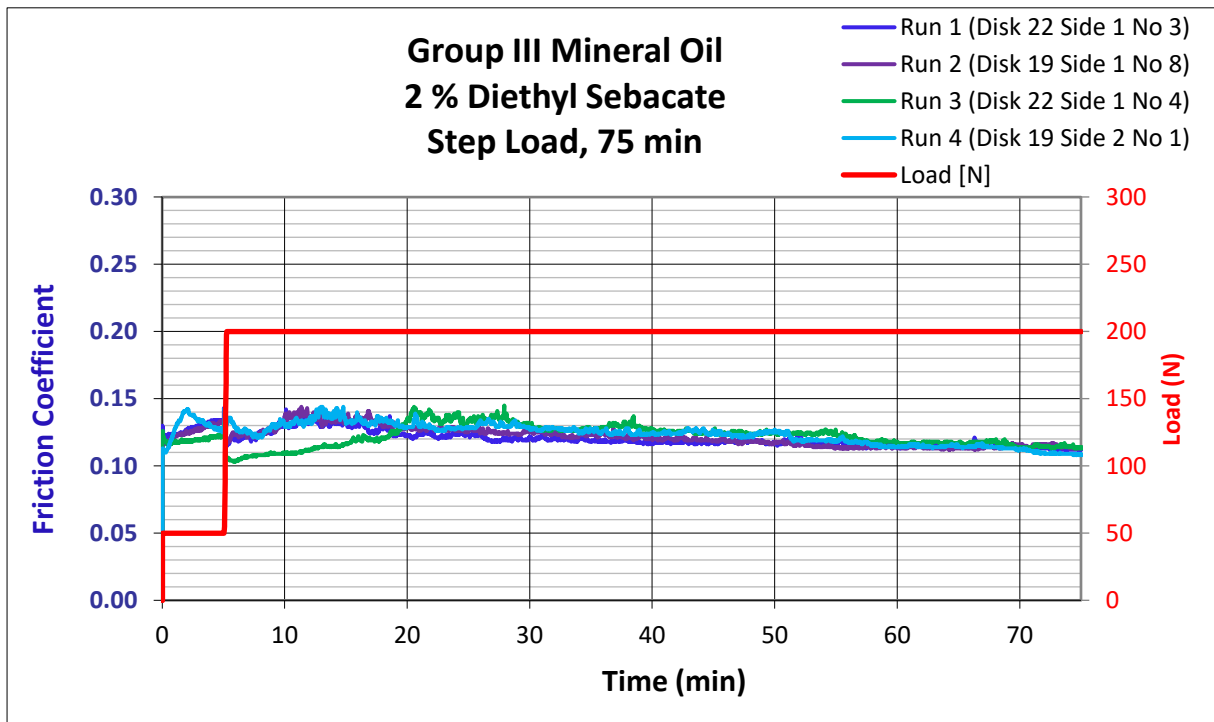


Figure C.1.9: Friction coefficient graphs for step load, 75 minutes.

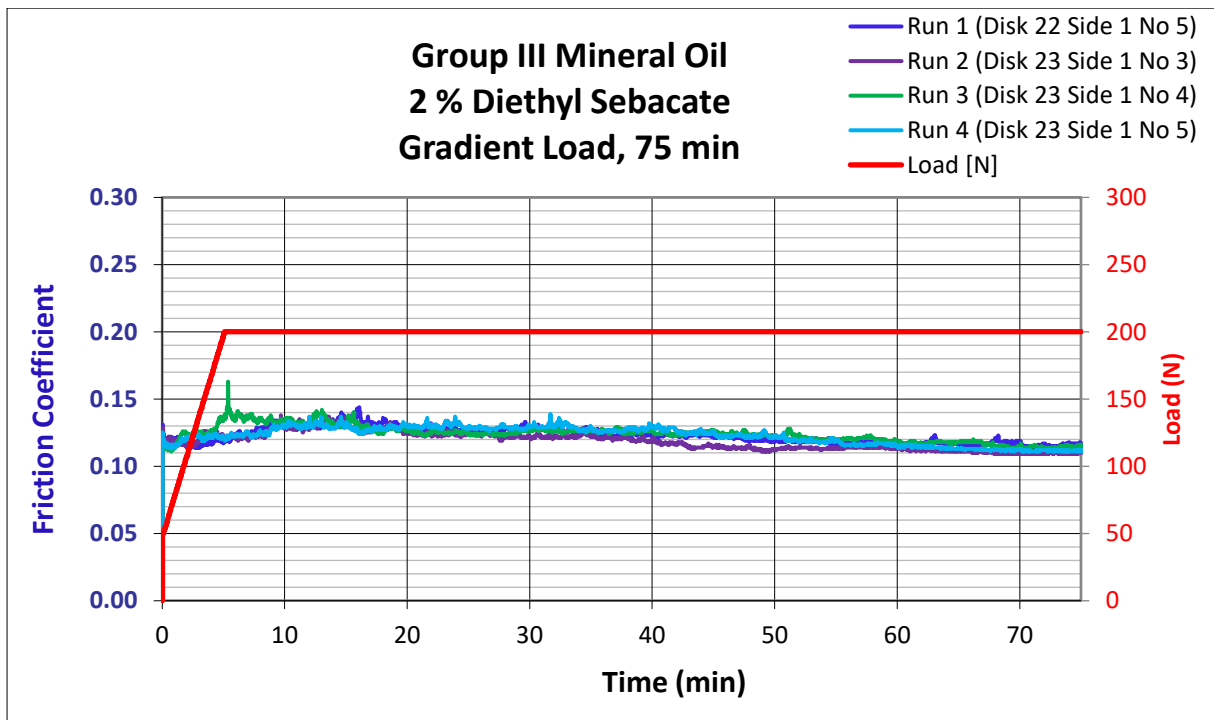


Figure C.1.10: Friction coefficient graphs for gradual load, 75 minutes.

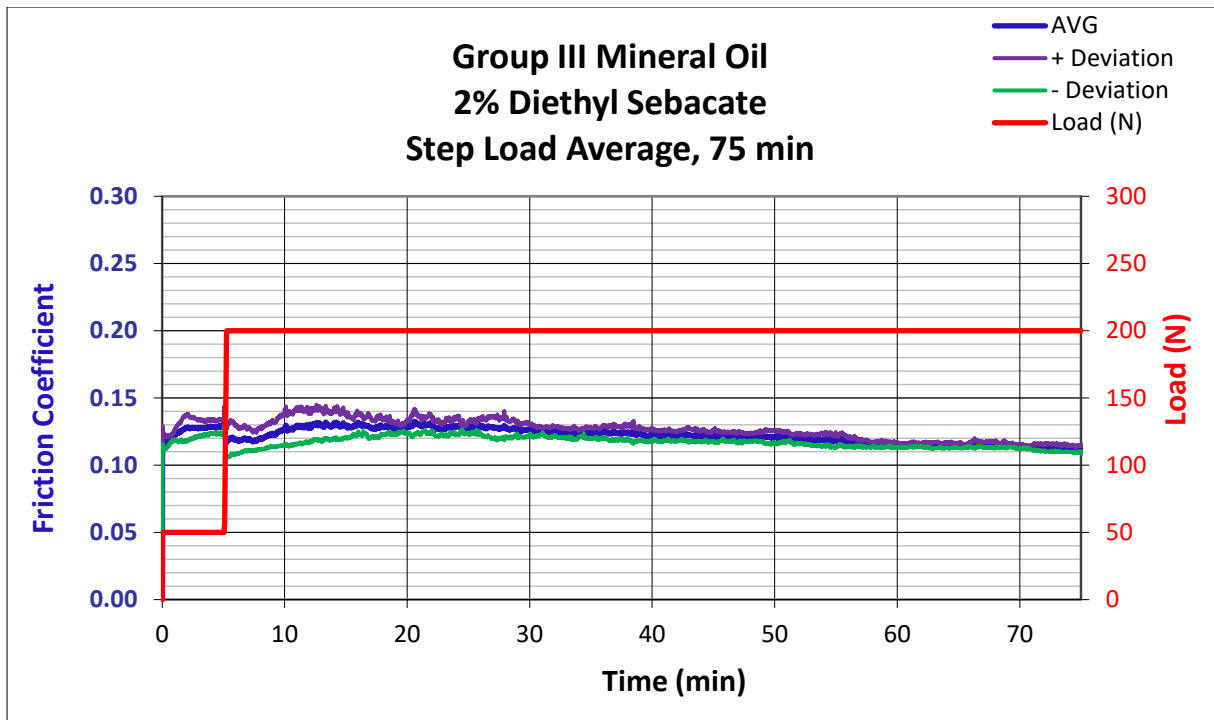


Figure C.1.11: Average of friction coefficient graphs for step load, 75 minutes.

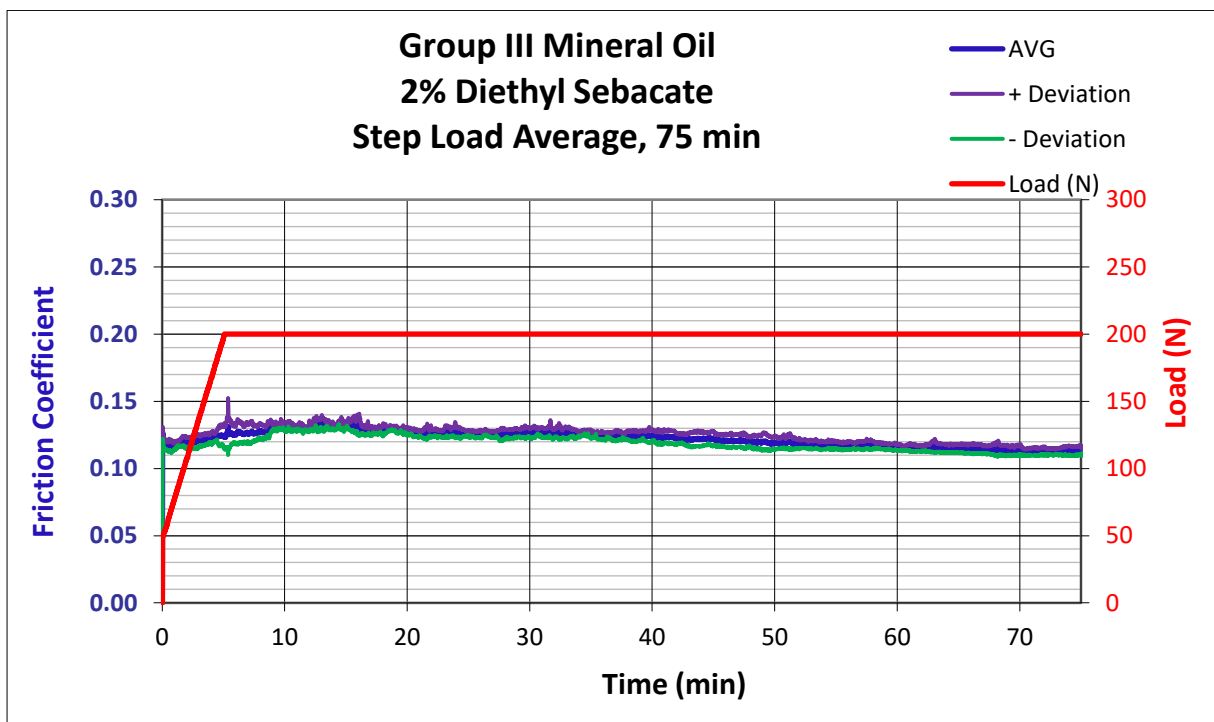


Figure C.1.12: Average of friction coefficient graphs for gradual load, 75 minutes.

4. 40 minutes

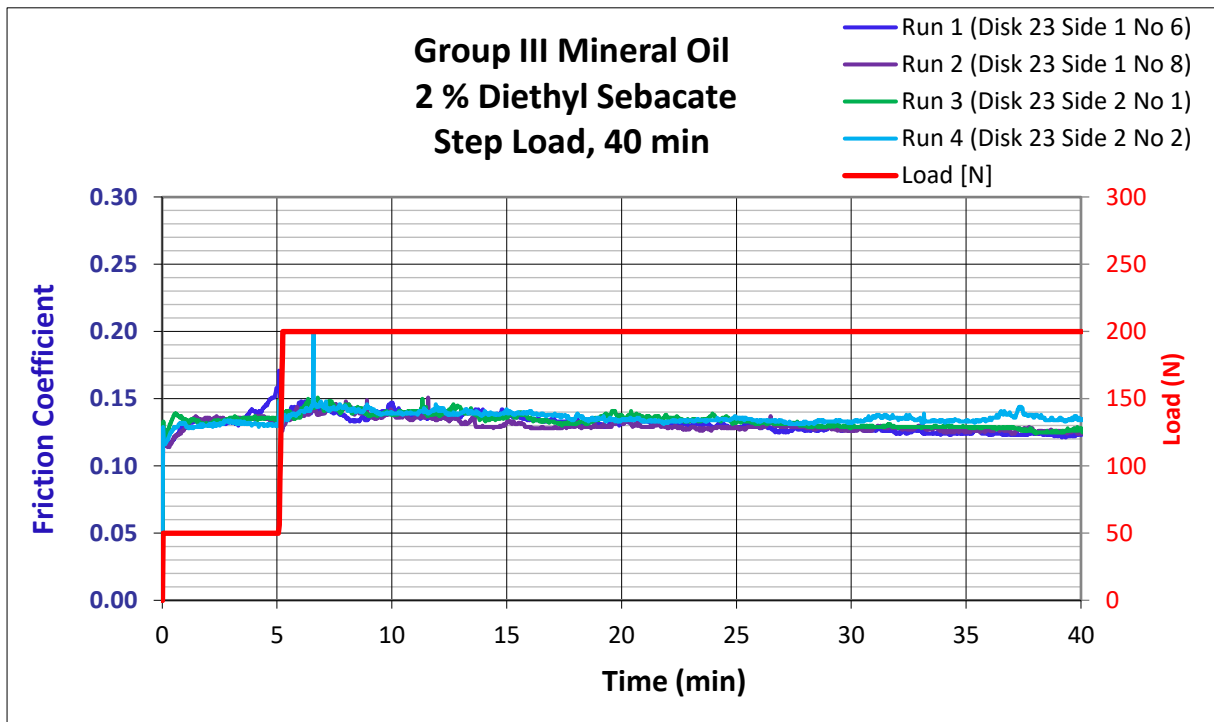


Figure C.1.13: Friction coefficient graphs for step load, 40 minutes.

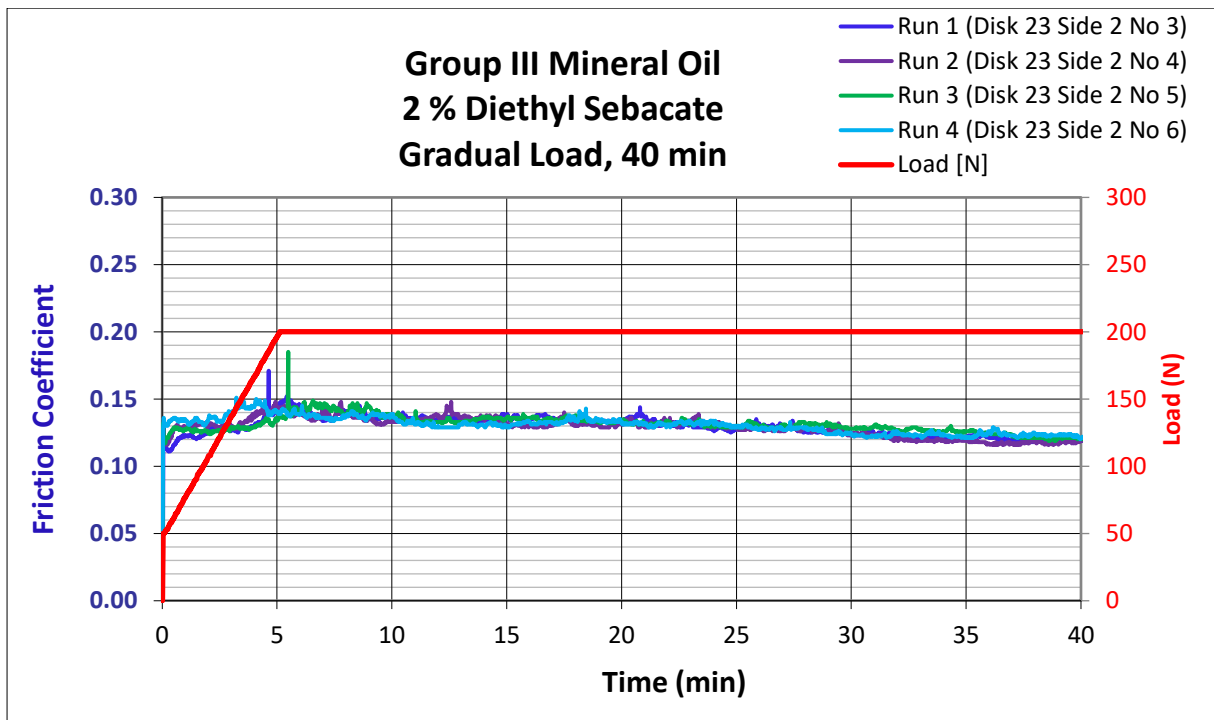


Figure C.1.14: Friction coefficient graphs for gradual load, 40 minutes.

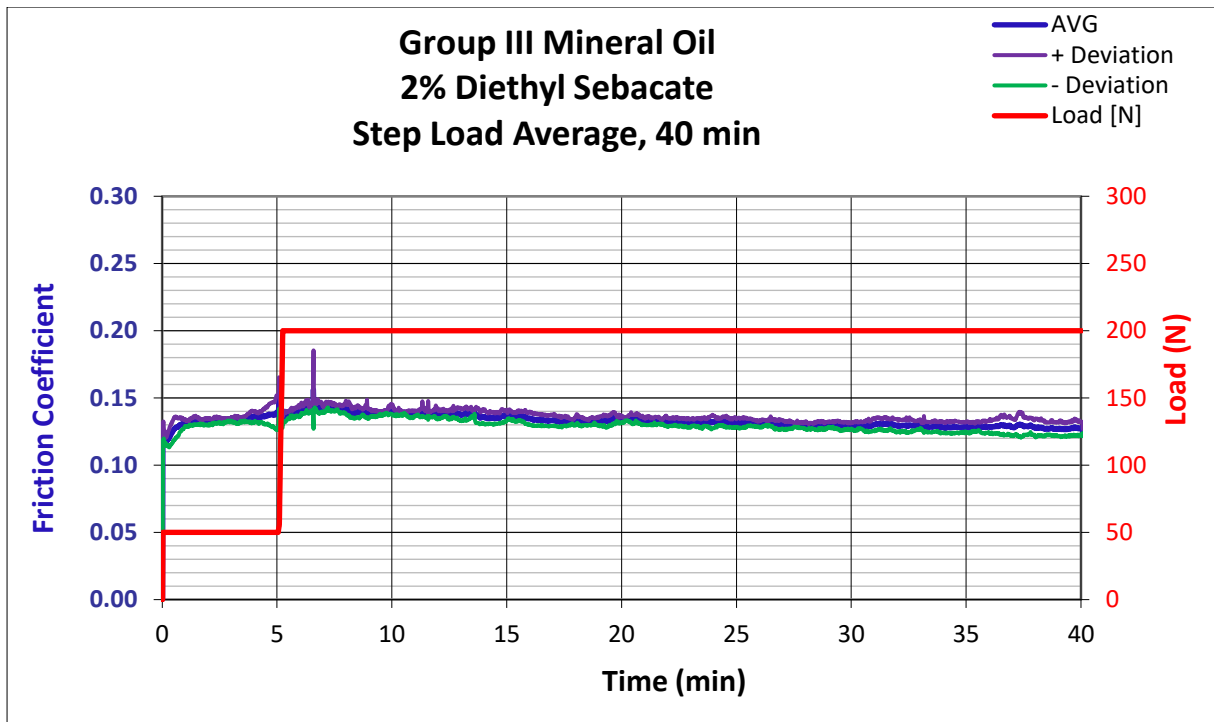


Figure C.1.15: Average of friction coefficient graphs for step load, 40 minutes.

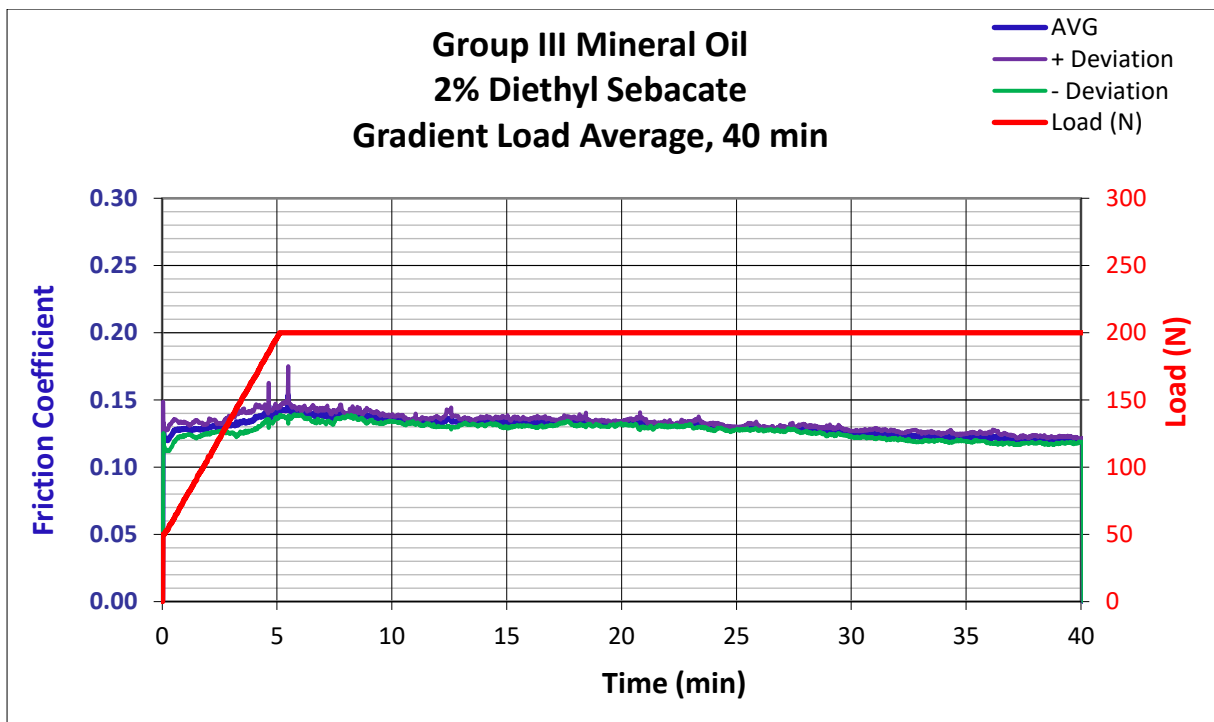


Figure C.1.16: Average of friction coefficient graphs for gradual load, 40 minutes.

5. 20 minutes

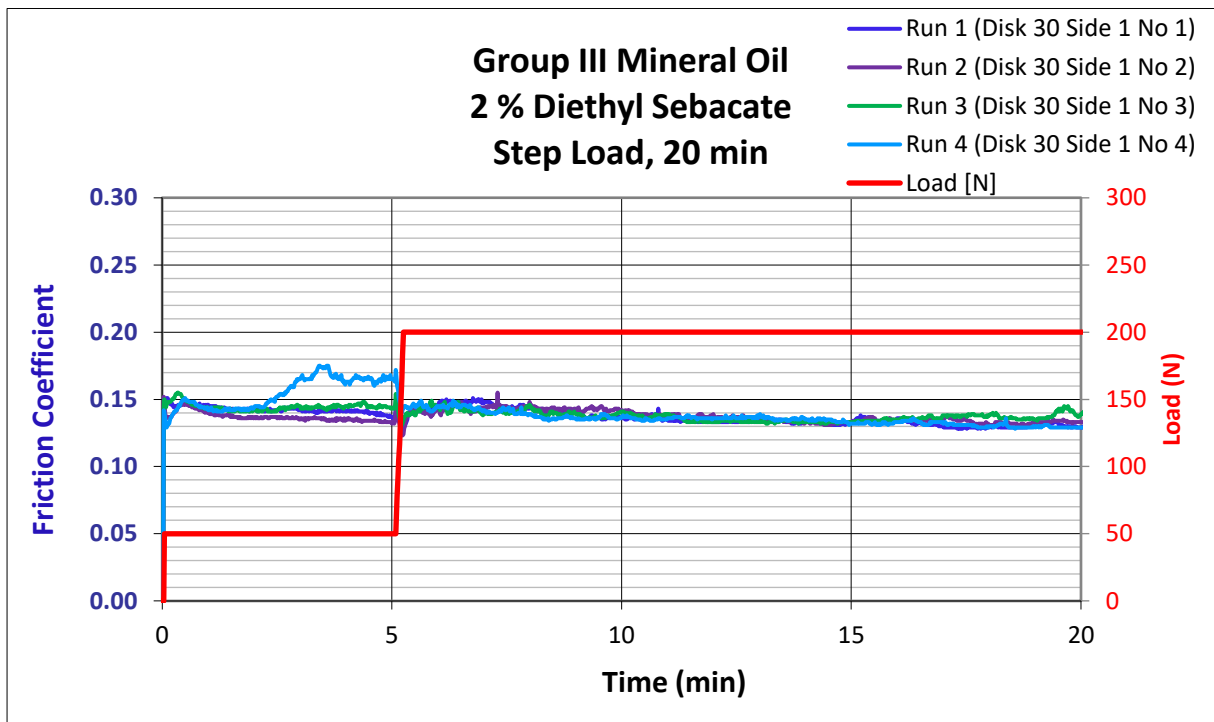


Figure C.1.17: Friction coefficient graphs for step load, 20 minutes.

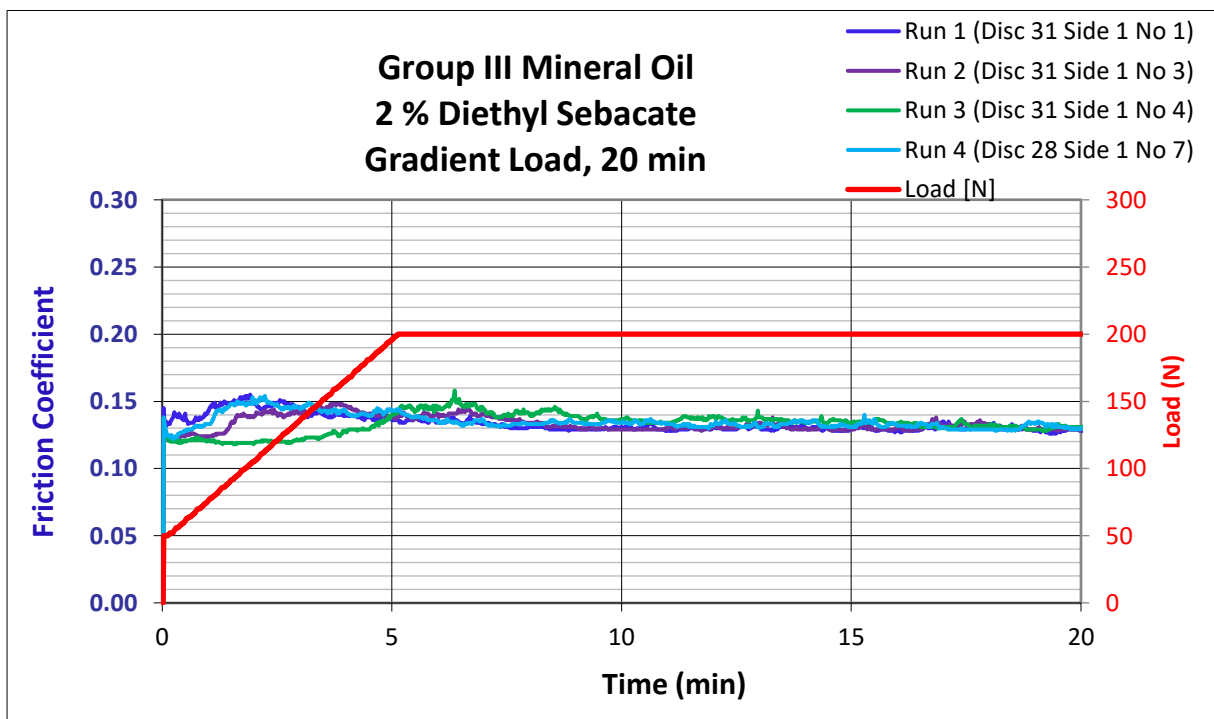


Figure C.1.18: Friction coefficient graphs for gradual load, 20 minutes.

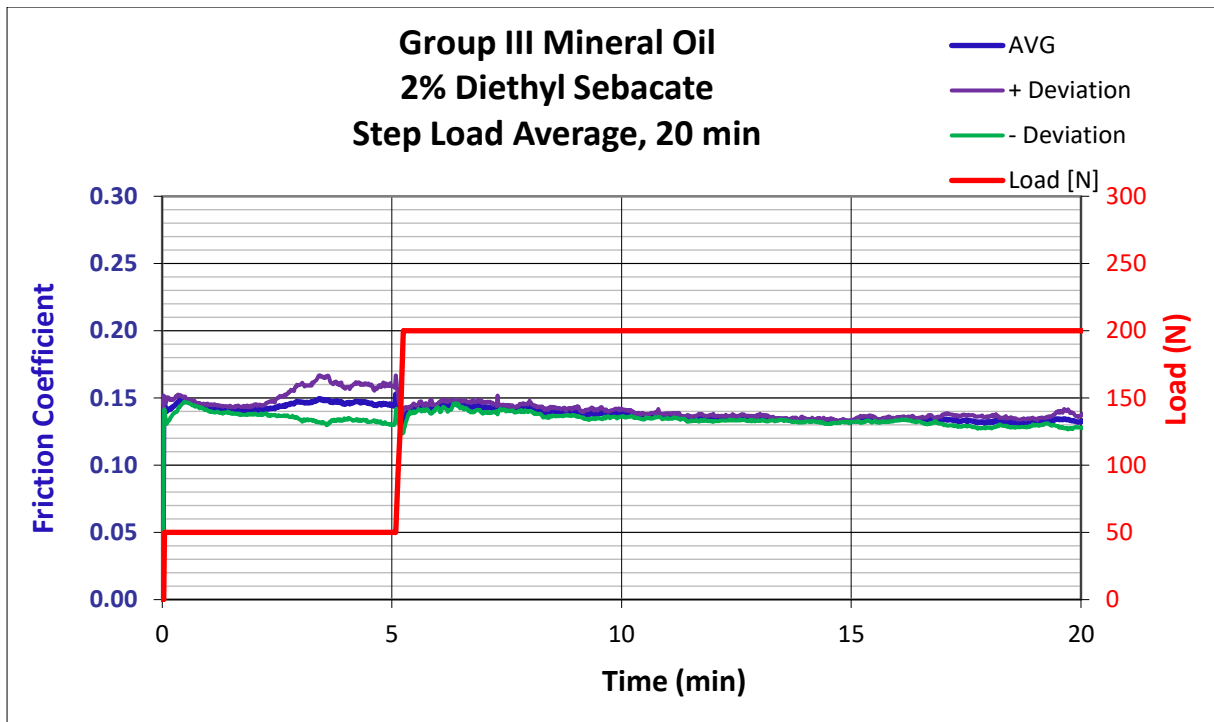


Figure C.1.19: Average of friction coefficient graphs for step load, 20 minutes.

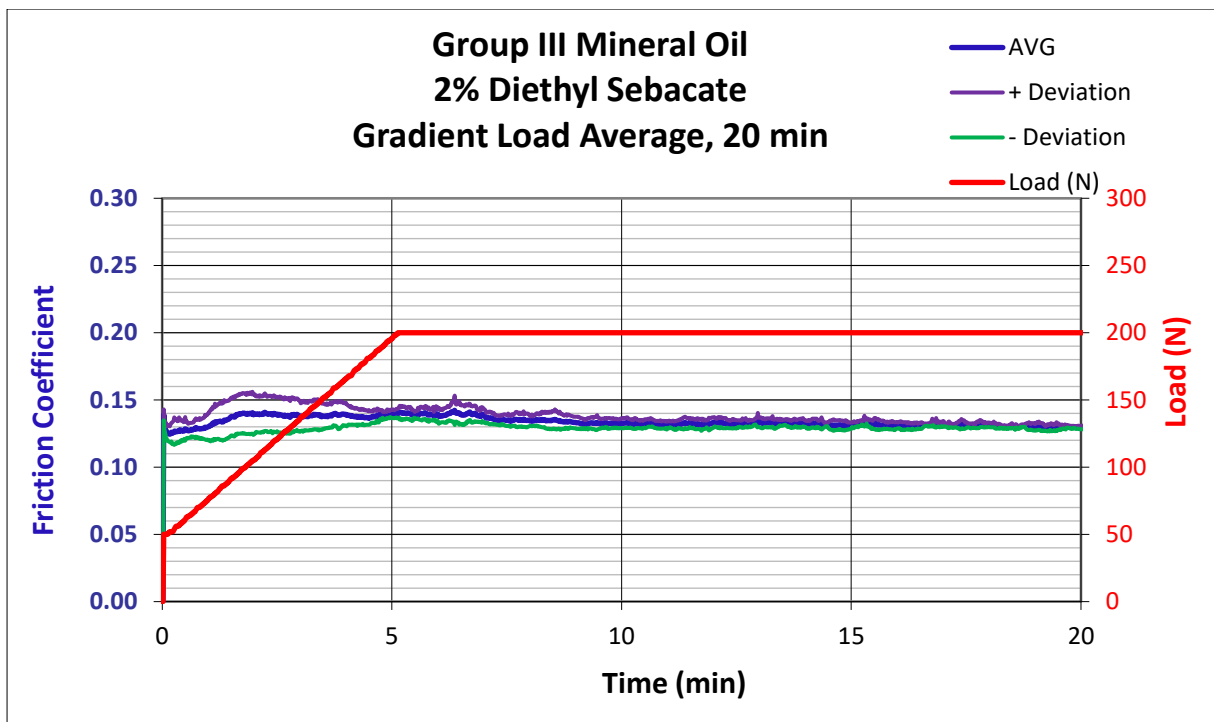


Figure C.1.20: Average of friction coefficient graphs for gradual load, 20 minutes.

6.5 Minutes

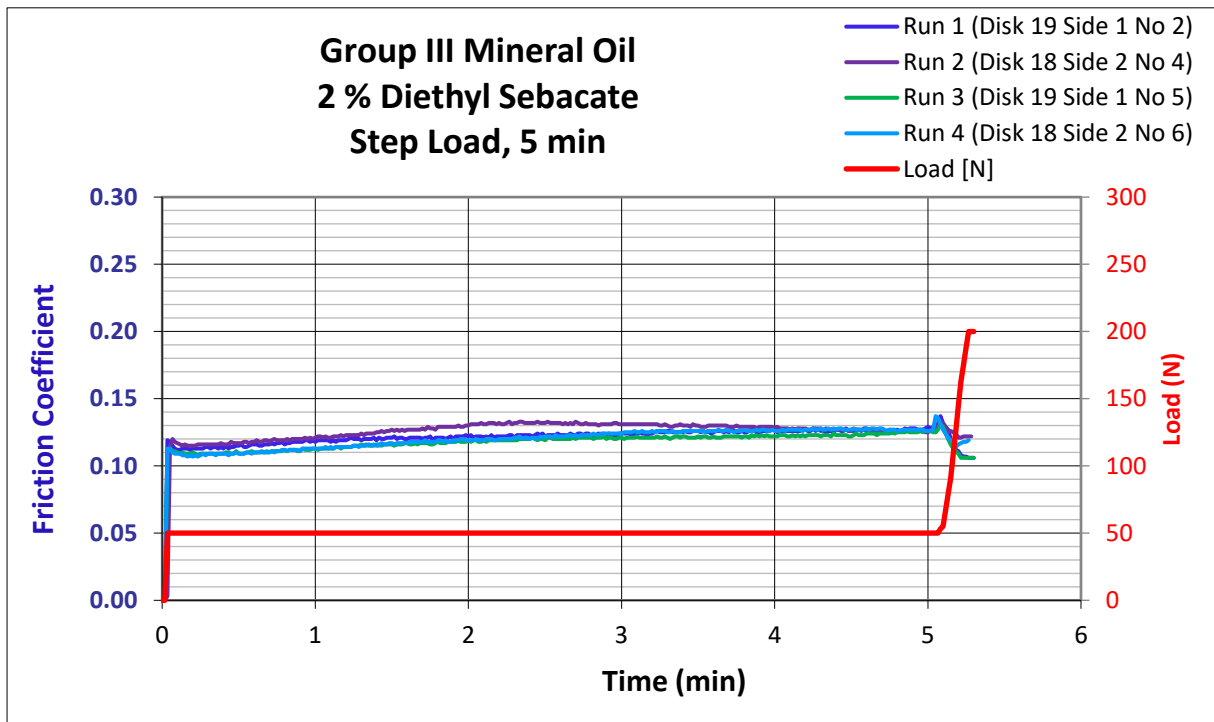


Figure C.1.21: Friction coefficient graphs for step load, 5 min.

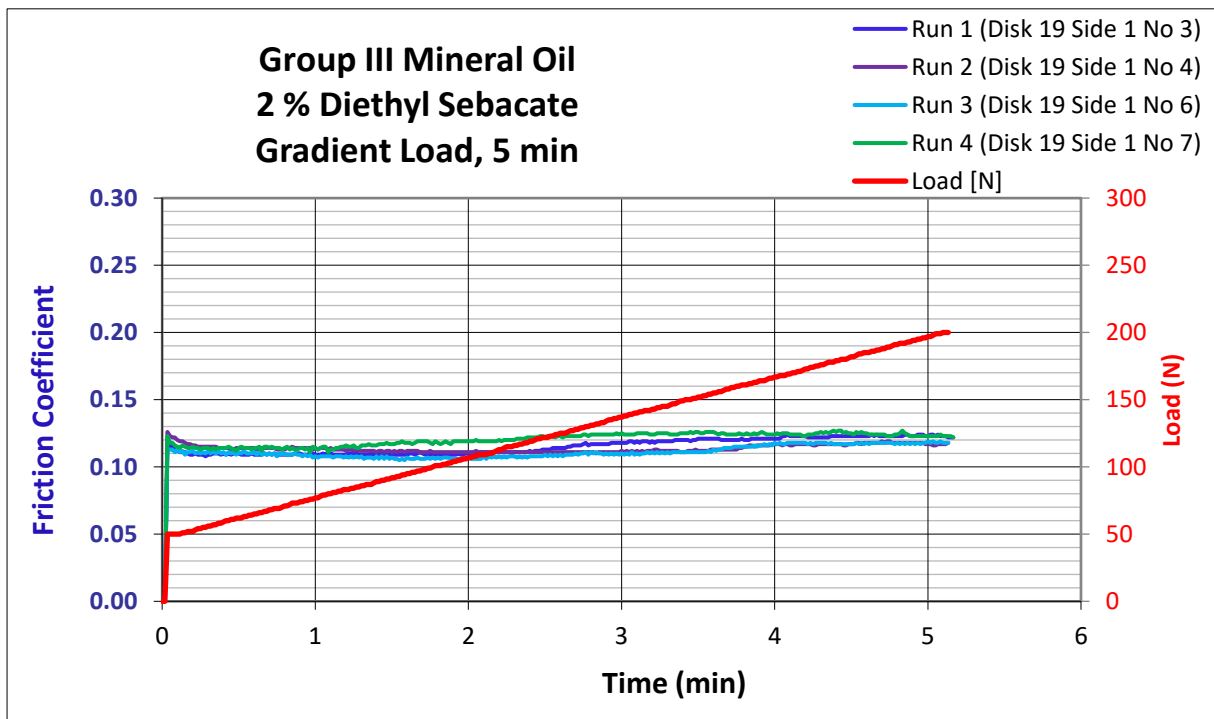


Figure C.1.22: Friction coefficient graphs for gradual load, 5 min.

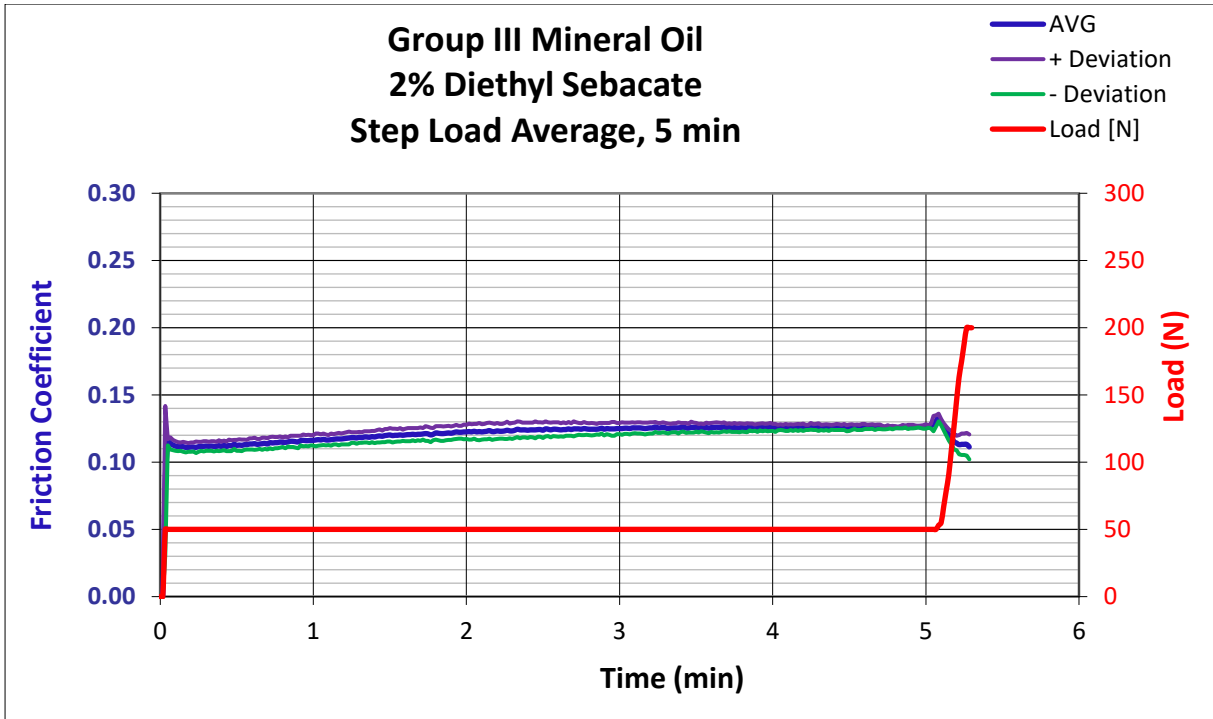


Figure C.1.23: Average of friction coefficient graphs for step load, 5 min.

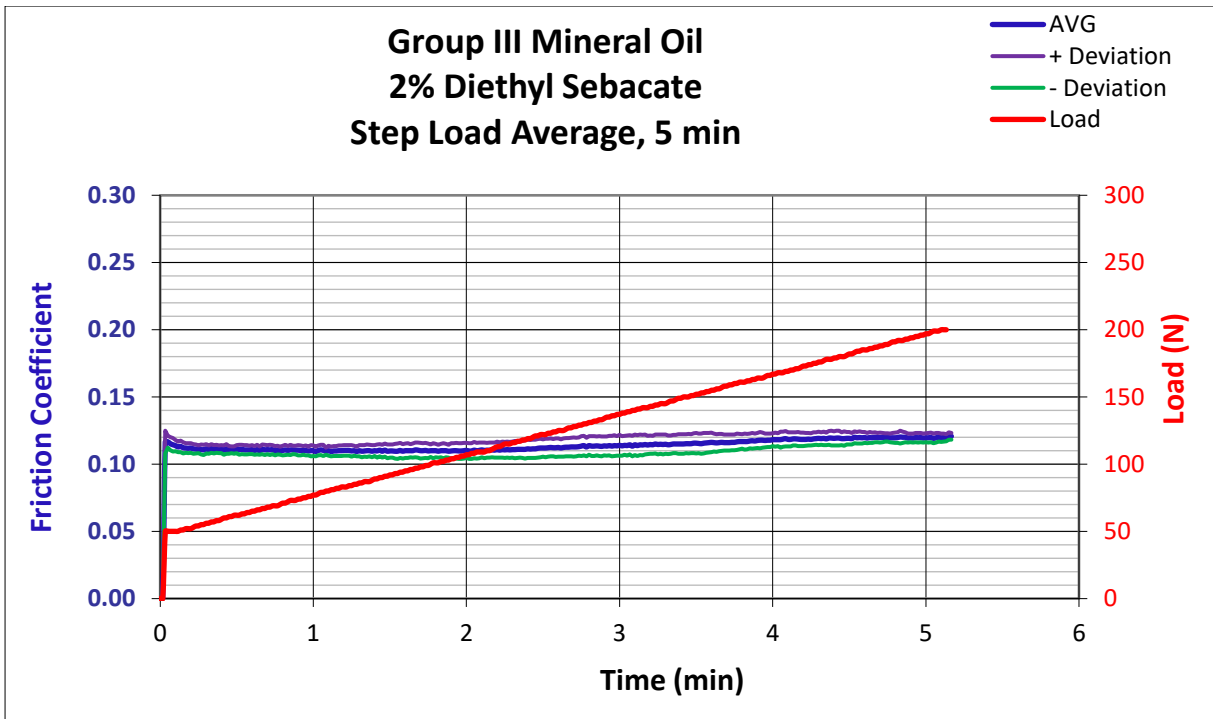


Figure C.1.24: Average of friction coefficient graphs for gradual load, 5 min.

Appendix C.2: Wear Surfaces 3 D Images; Step Load and Gradient Load

Table C.2.1: Wear scar surface 3D images, step load increase.

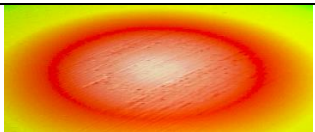
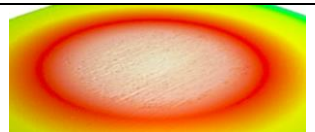
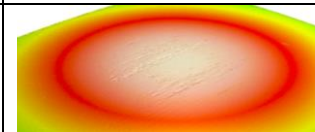
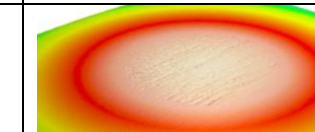
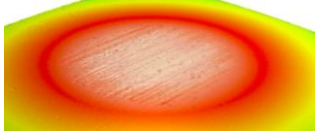
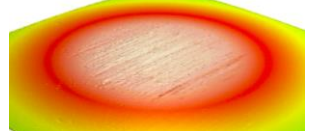
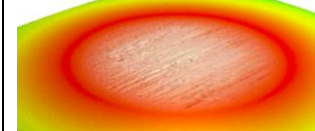
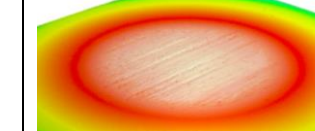

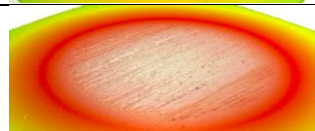
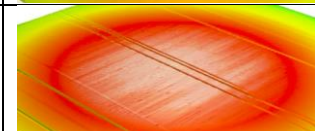
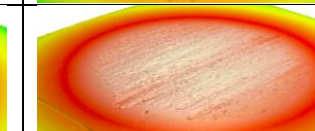
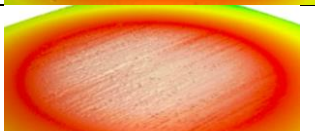
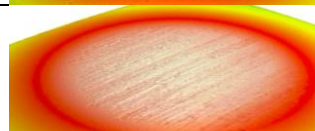
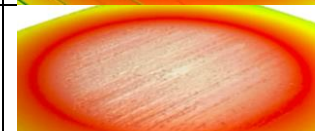
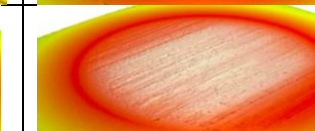
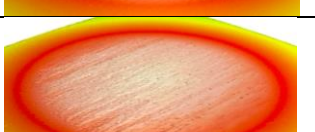
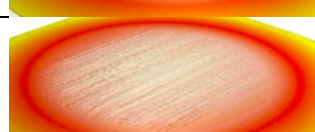
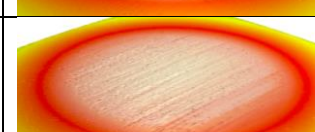
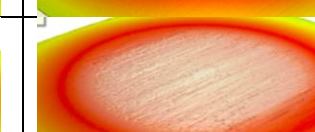

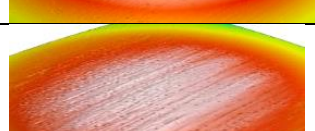
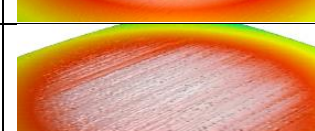
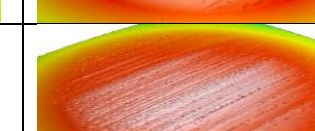
Step Load	Run 1	Run 2	Run 3	Run 4
5 min (After Load)				
20 min				
40 min				
75 min				
100 min				
125 min				

Table C.2.2: Wear track surface 3D images, step load increase.

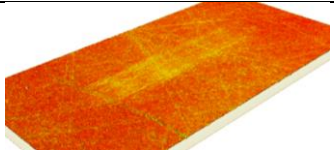
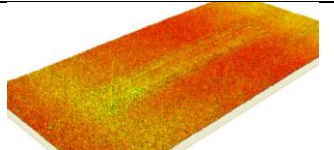
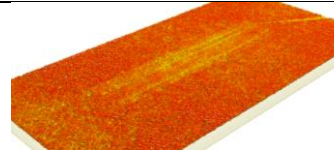
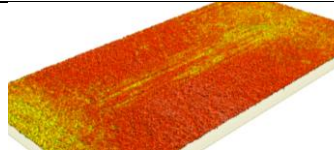
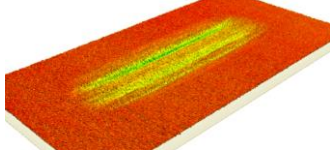
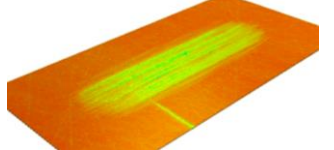
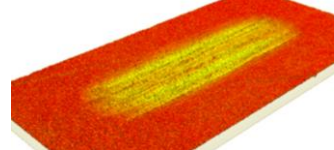
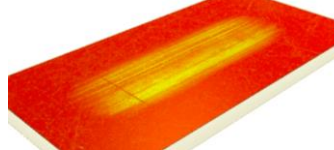
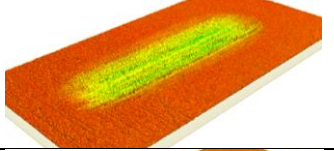
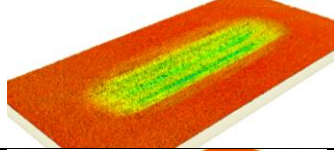
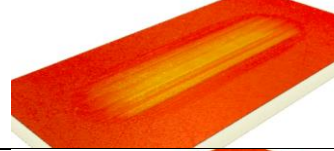
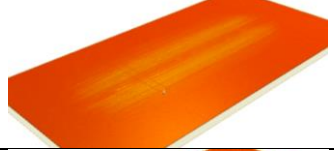
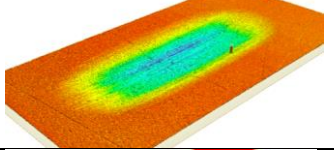
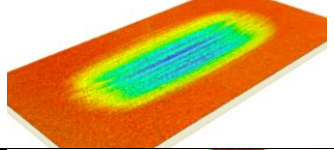
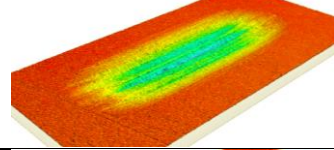
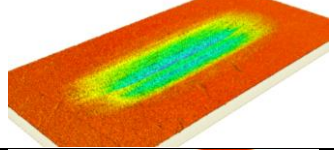
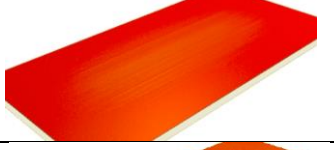
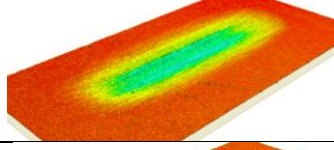
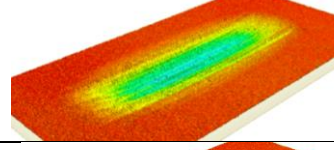
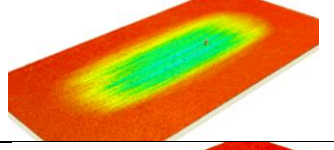
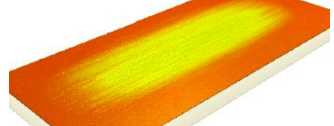
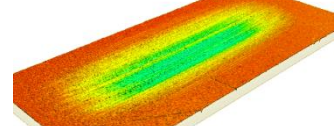
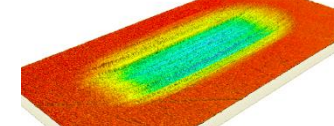
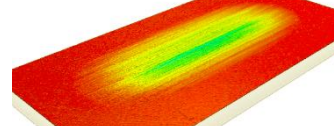
Step Load	Run 1	Run 2	Run 3	Run 4
5 min (After Running-in)				
20 min				
40 min				
75 min				
100 min				
125 min				

Table C.2.3: Wear scar surface 3D images, gradual load increase.

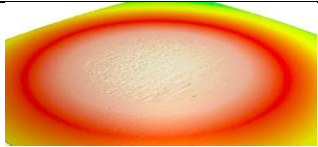
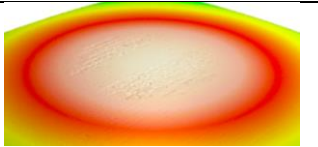
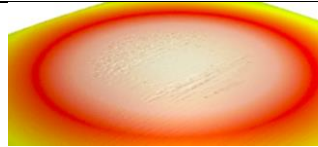
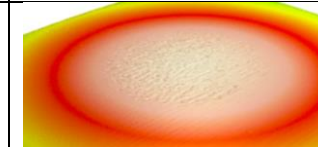
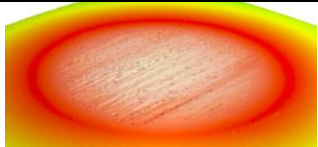
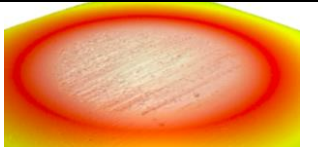
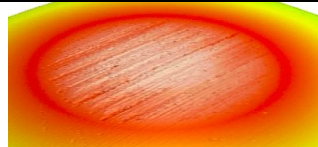
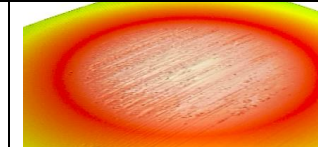
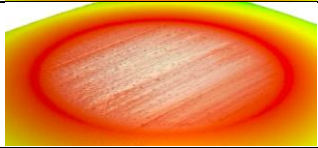
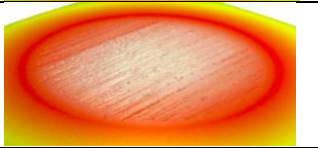
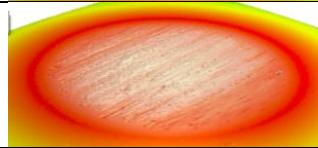
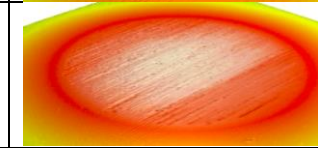
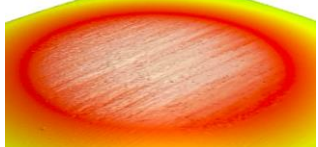
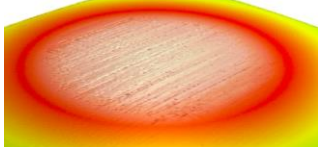
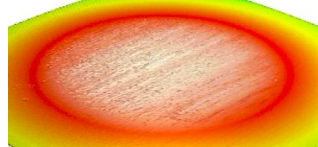
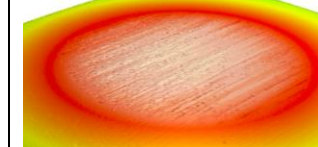
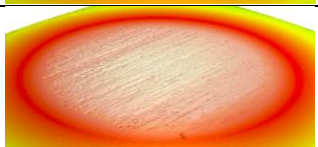
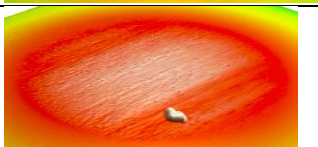

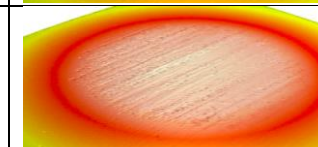
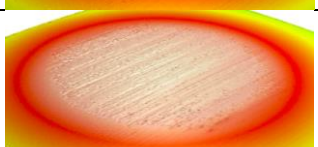
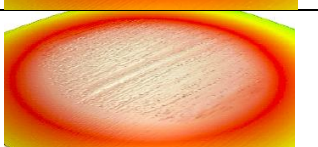
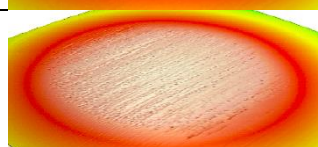
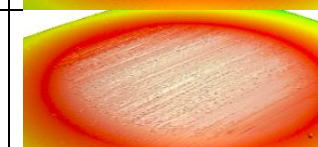
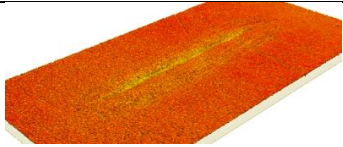
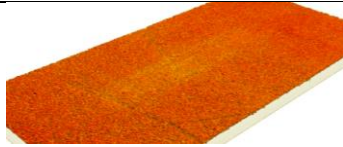
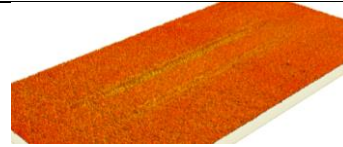
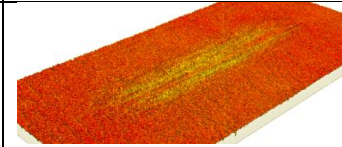
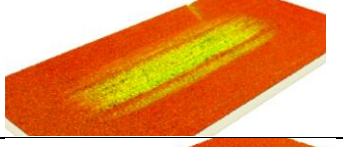
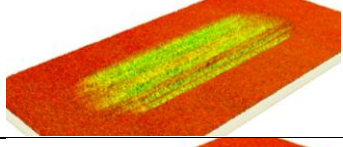
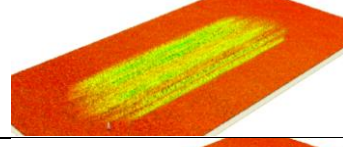
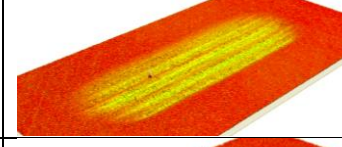
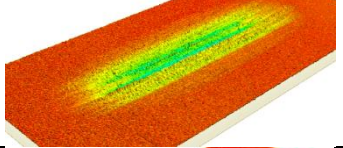
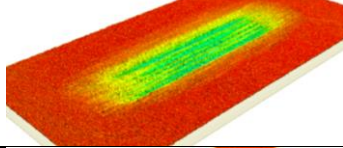
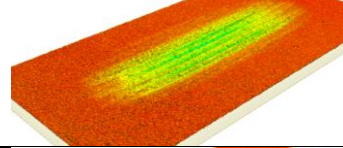
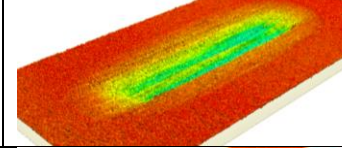
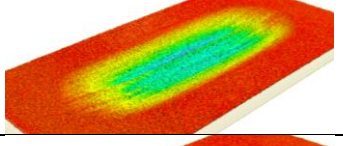
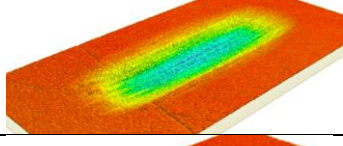
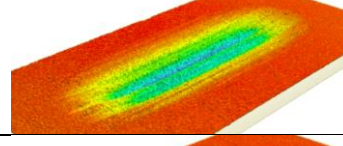
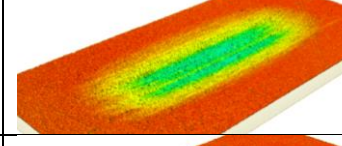
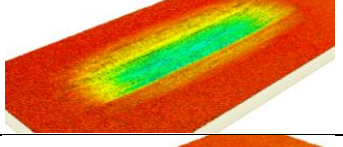
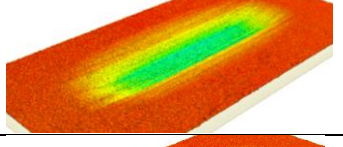
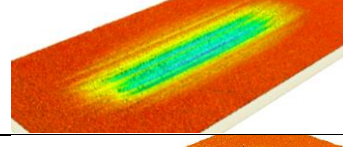
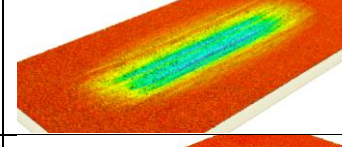
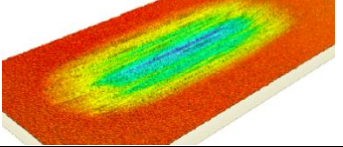
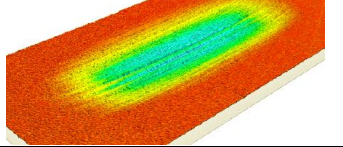
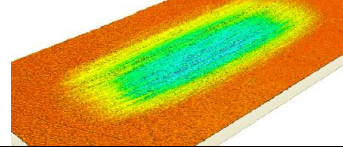
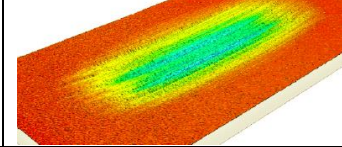
Gradual Load				
	Run 1	Run 2	Run 3	Run 4
5 min (After Running-in)				
20 min				
40 min				
75 min				
100 min				
125 min				

Table C.2.4: Wear track surface 3D images, gradual load increase.

Gradient Load				
	Run 1	Run 2	Run 3	Run 4
5 min (After Running-in)				
20 min				
40 min				
75 min				
100 min				
125 min				

Appendix C.3: Wear Surface Images: Step Load and Gradient Load

Table C.3.1: Wear scar surface images, step load increase.

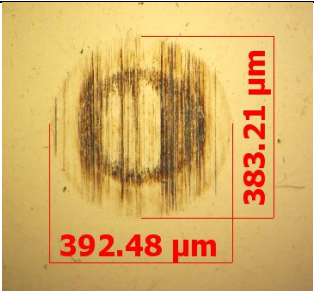
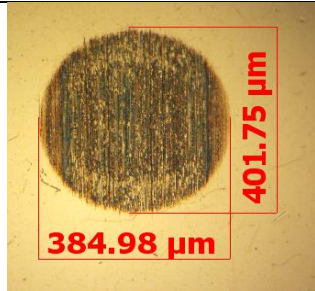

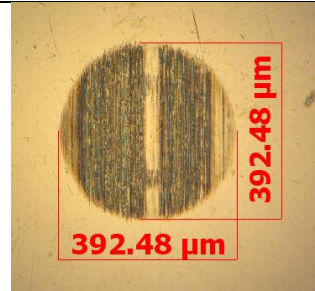
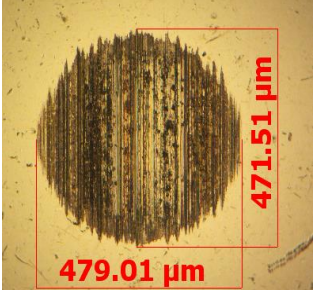
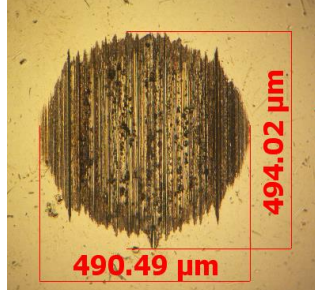
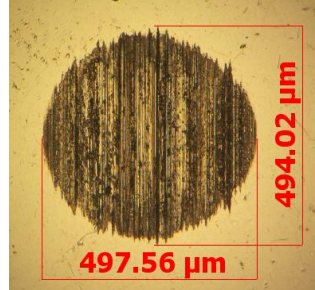
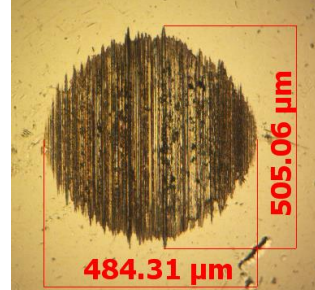
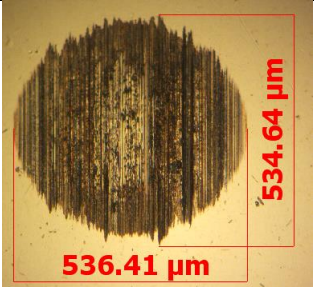
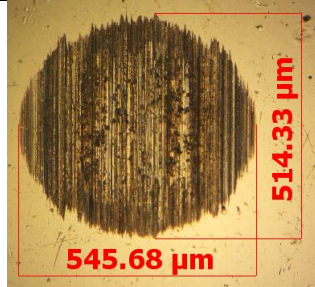
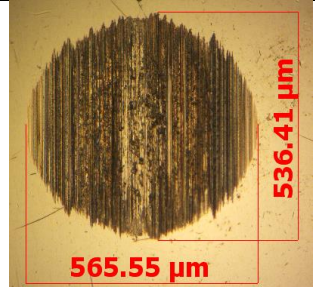
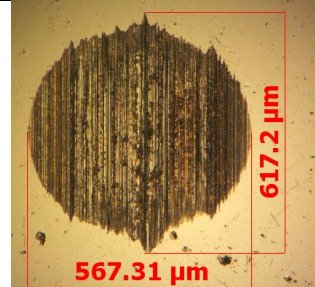
Step Load				
	Run 1	Run 2	Run 3	Run 4
5 min (After Load Increase)	 383.21 μm 392.48 μm	 401.75 μm 384.98 μm	 392.48 μm 387.18 μm	 392.48 μm 392.48 μm
20 min	 471.51 μm 479.01 μm	 494.02 μm 490.49 μm	 494.02 μm 497.56 μm	 505.06 μm 484.31 μm
40 min	 534.64 μm 536.41 μm	 514.33 μm 545.68 μm	 536.41 μm 565.55 μm	 617.2 μm 567.31 μm

Table C.3.1: (continued).

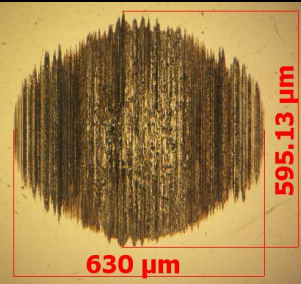
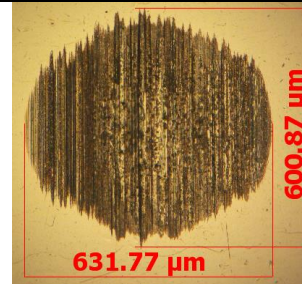
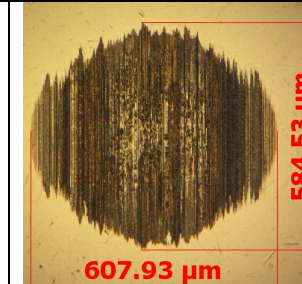
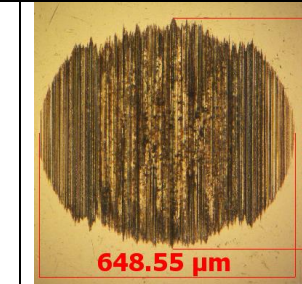
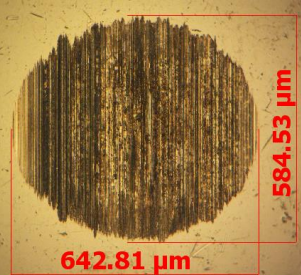
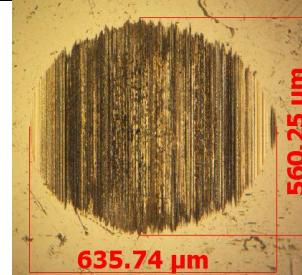
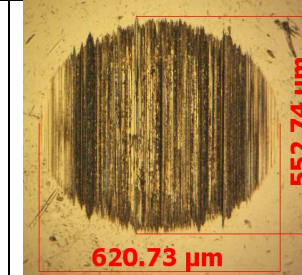
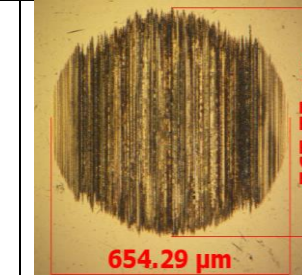
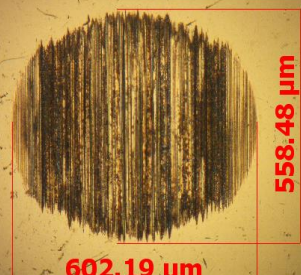
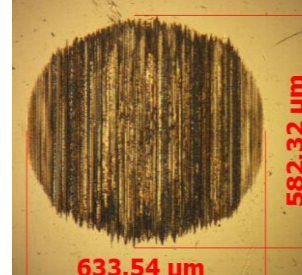
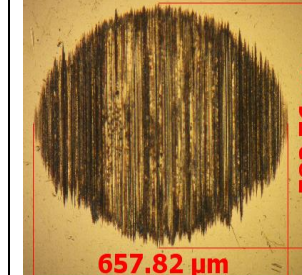
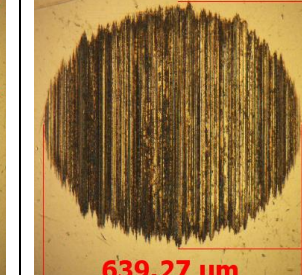
75 min	 <p>595.13 μm 630 μm</p>	 <p>600.87 μm 631.77 μm</p>	 <p>584.53 μm 607.93 μm</p>	 <p>591.59 μm 648.55 μm</p>
100 min	 <p>584.53 μm 642.81 μm</p>	 <p>560.25 μm 635.74 μm</p>	 <p>552.74 μm 620.73 μm</p>	 <p>567.75 μm 654.29 μm</p>
125 min	 <p>558.48 μm 602.19 μm</p>	 <p>582.32 μm 633.54 μm</p>	 <p>582.76 μm 657.82 μm</p>	 <p>588.06 μm 639.27 μm</p>

Table C.3.2: Wear track surface images, step load increase.

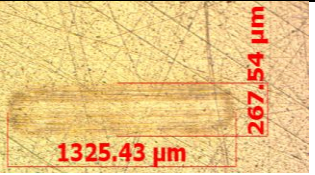
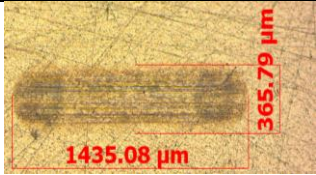
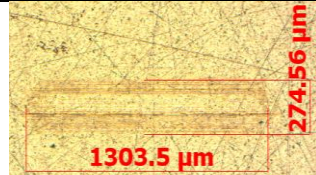
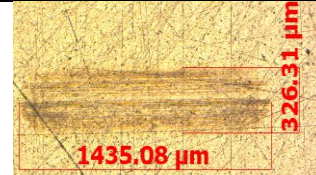
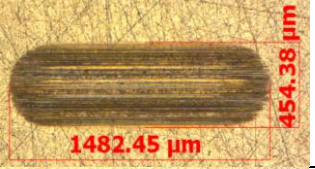
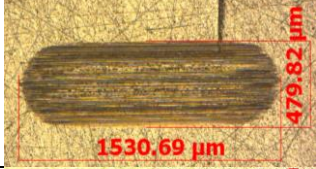
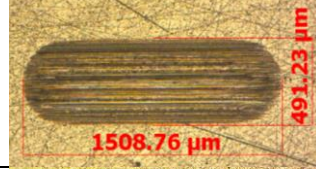
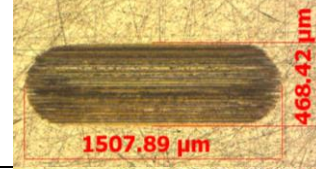
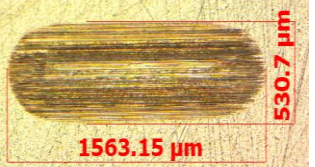

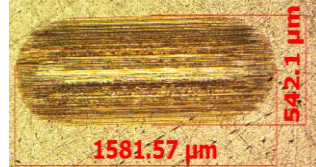

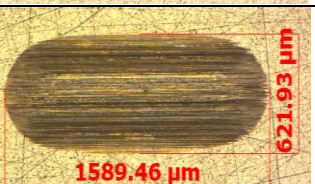
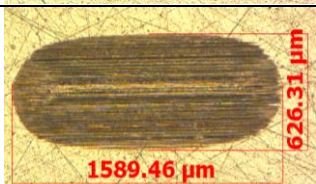


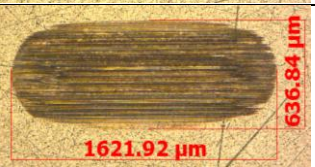
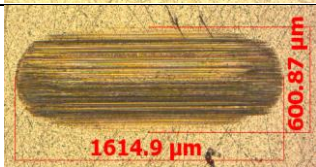
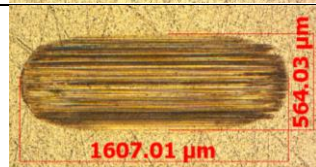
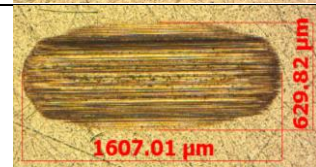
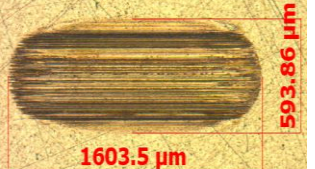
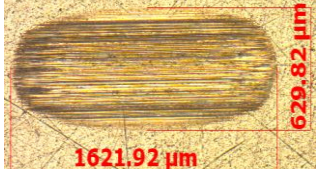
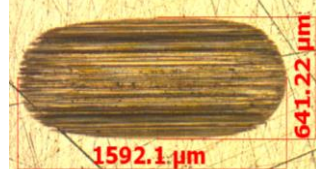
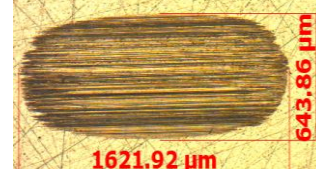
Step Load	Run 1	Run 2	Run 3	Run 4
5 min (After Running-in)				
20 min				
40 min				
75 min				
100 min				
125 min				

Table C.3.3: Wear scar surface images, gradual load increase.

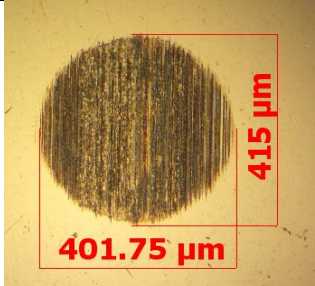
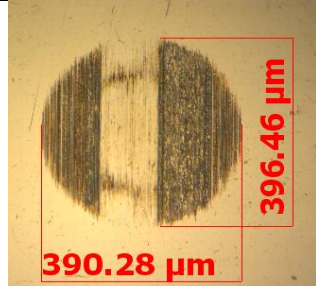
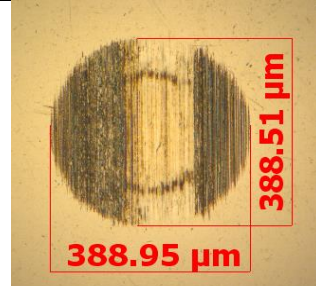
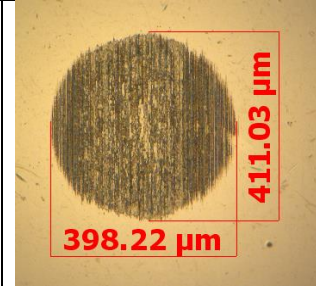
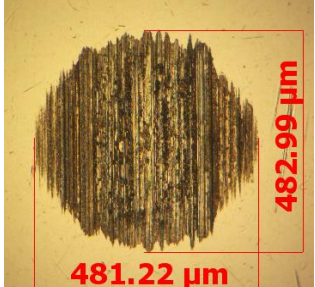
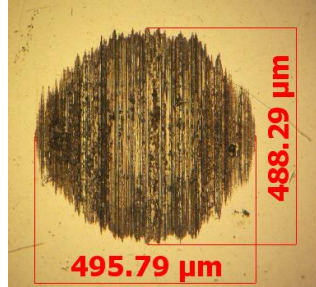
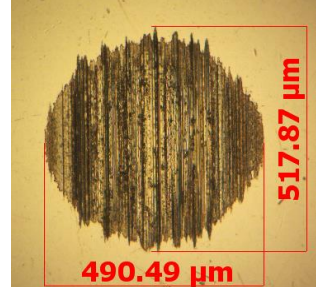
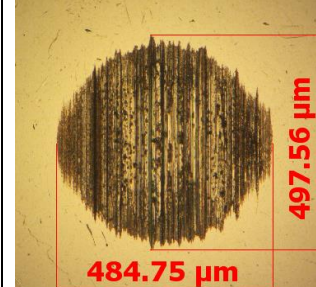
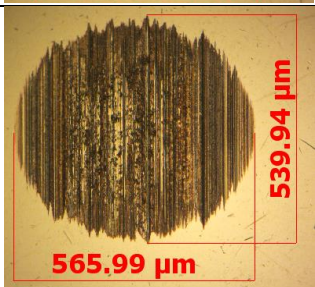

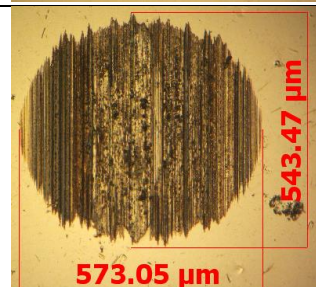
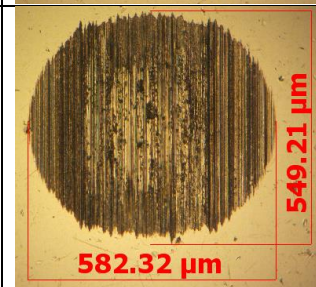
Gradual Load				
	Run 1	Run 2	Run 3	Run 4
5 min (After Running-in)	 401.75 μm (width) 415 μm (height)	 390.28 μm (width) 396.46 μm (height)	 388.95 μm (width) 388.51 μm (height)	 398.22 μm (width) 411.03 μm (height)
20 min	 481.22 μm (width) 482.99 μm (height)	 495.79 μm (width) 488.29 μm (height)	 490.49 μm (width) 517.87 μm (height)	 484.75 μm (width) 497.56 μm (height)
40 min	 565.99 μm (width) 539.94 μm (height)	 596.89 μm (width) 545.68 μm (height)	 573.05 μm (width) 543.47 μm (height)	 582.32 μm (width) 549.21 μm (height)

Table C.3.3: (continued).

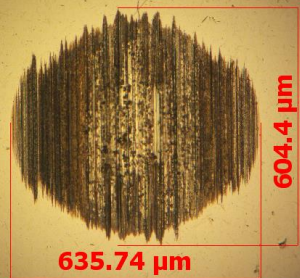
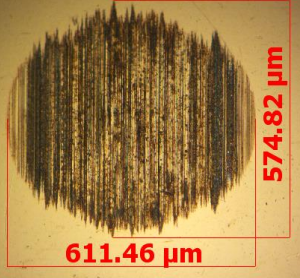
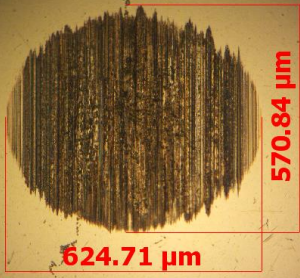
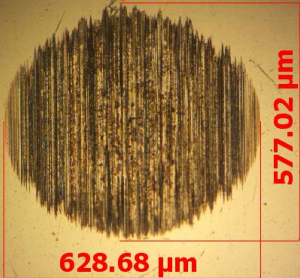
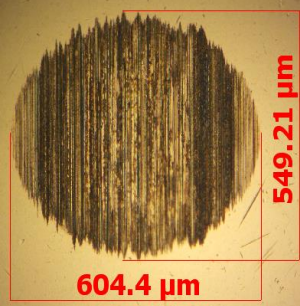
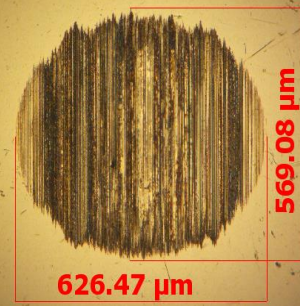
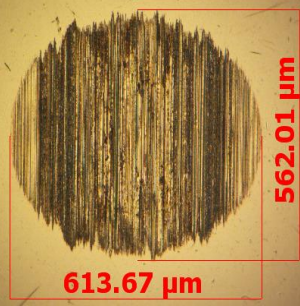
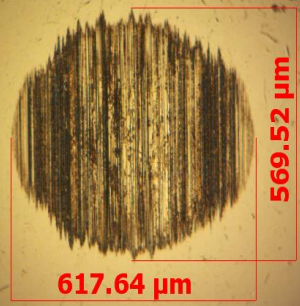
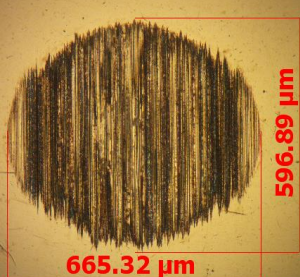
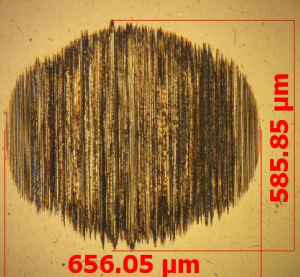
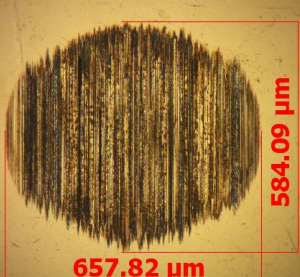
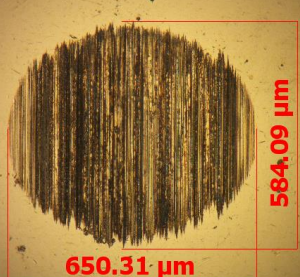
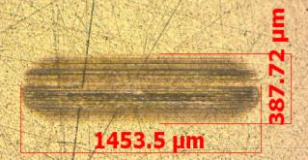
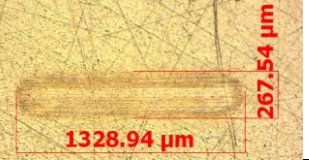

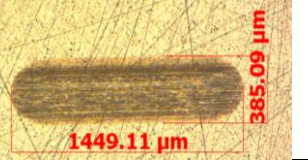
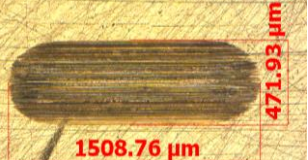


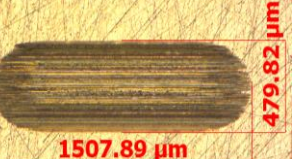
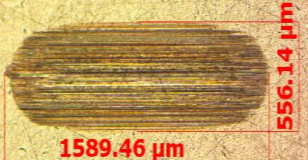

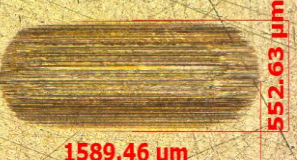
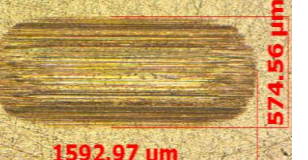
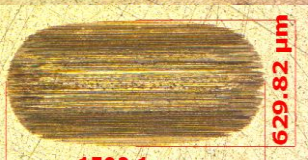
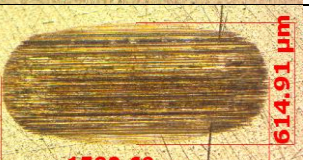
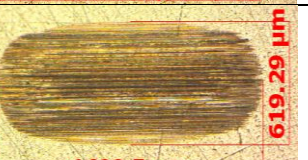
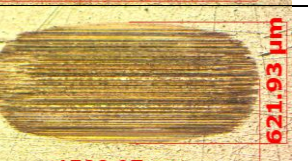







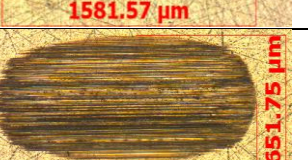
75 min					
100 min					
125 min					

Table C.3.4: Wear track surface images, gradual load increase.

Gradual Load				
	Run 1	Run 2	Run 3	Run 4
5 min (After Running-in)				
20 min				
40 min				
75 min				
100 min				
125 min				

Appendix C.4: Wear Surface Profiles

1. 125 min

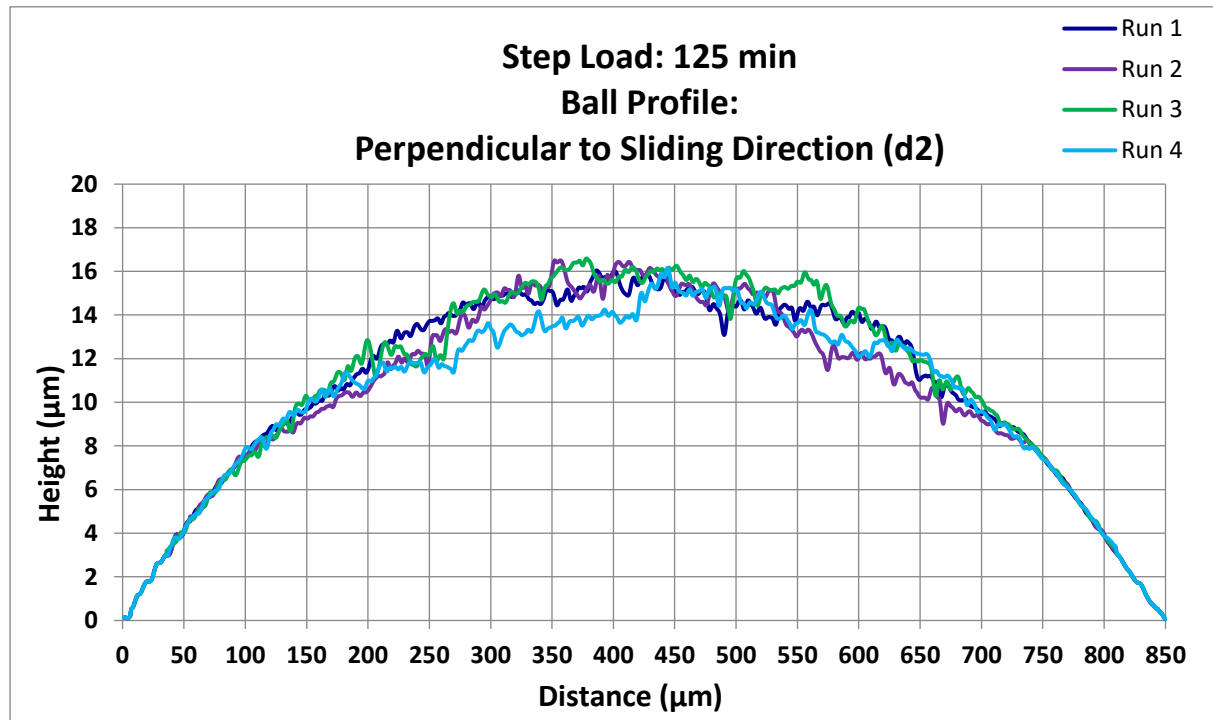


Figure C.4.1: Wear scar profiles perpendicular to sliding direction for **Group III mineral oil (Gr III) with 2 % diethyl sebacate** with step load increase, 125 minutes.

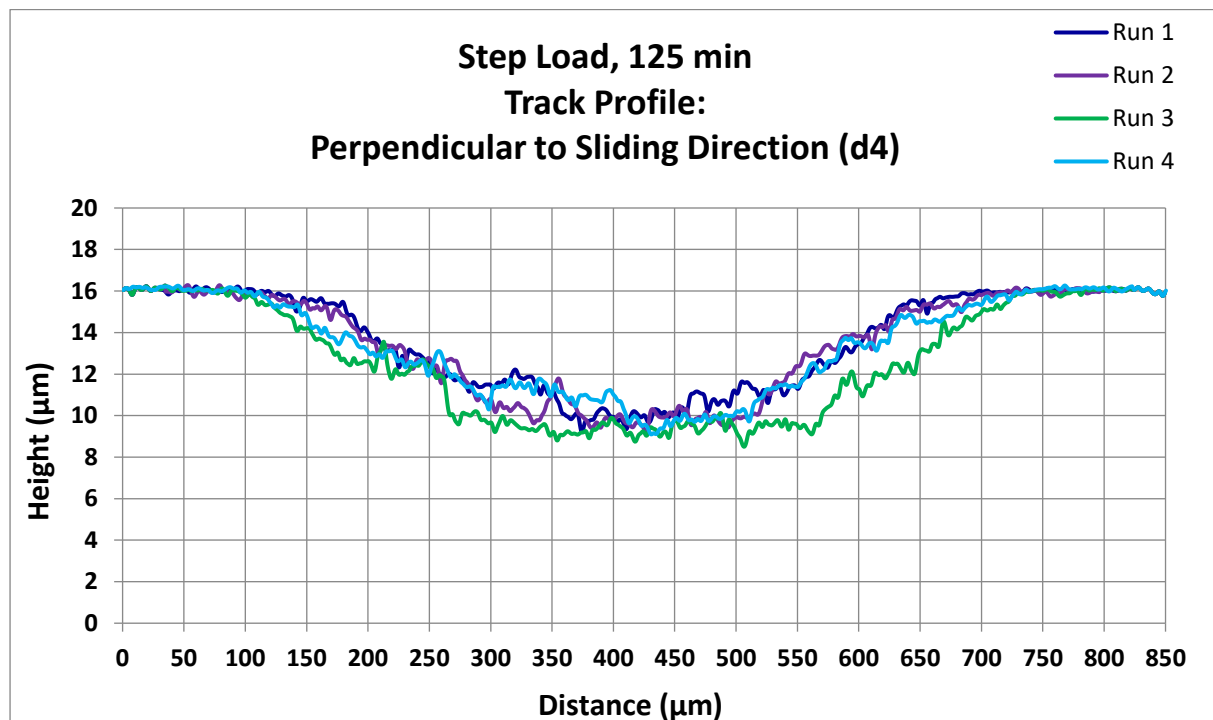


Figure C.4.2: Wear track profiles perpendicular to sliding direction for **Group III mineral oil (Gr III) with 2 % diethyl sebacate** with step load increase, 125 minutes.

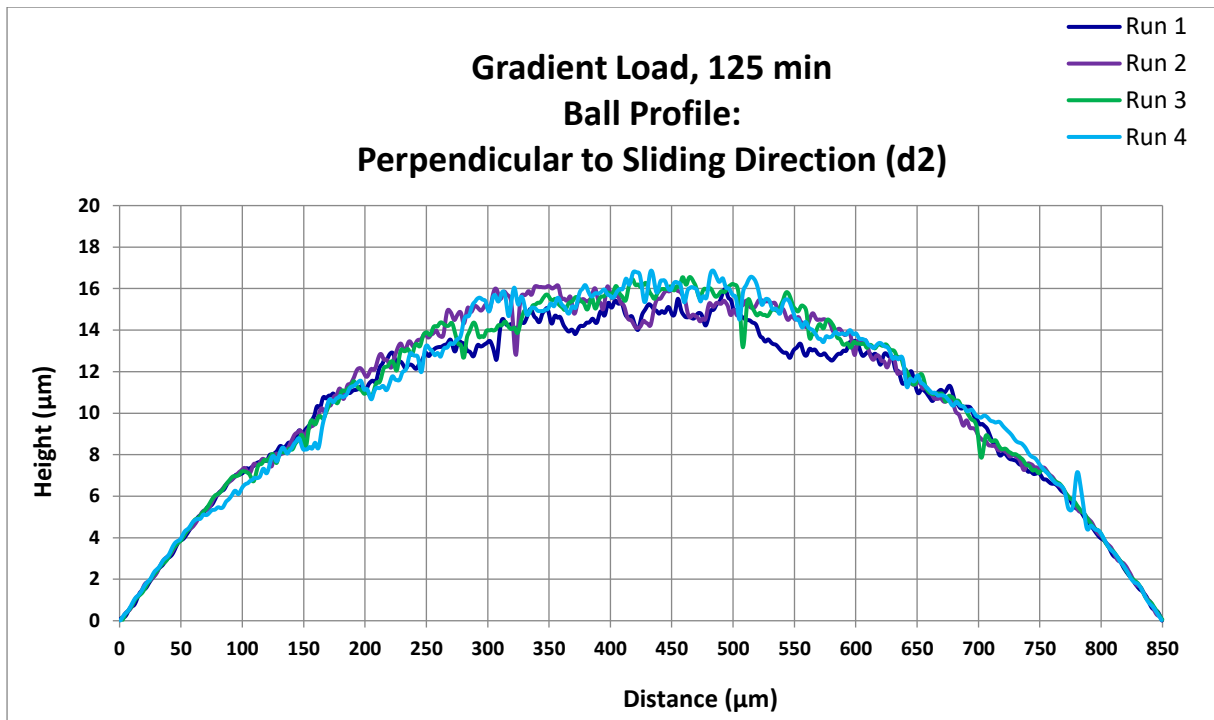


Figure C.4.3: Wear scar profiles perpendicular to sliding direction for **Group III mineral oil (Gr III) with 2 % diethyl sebacate** with gradual load increase, 125 minutes.

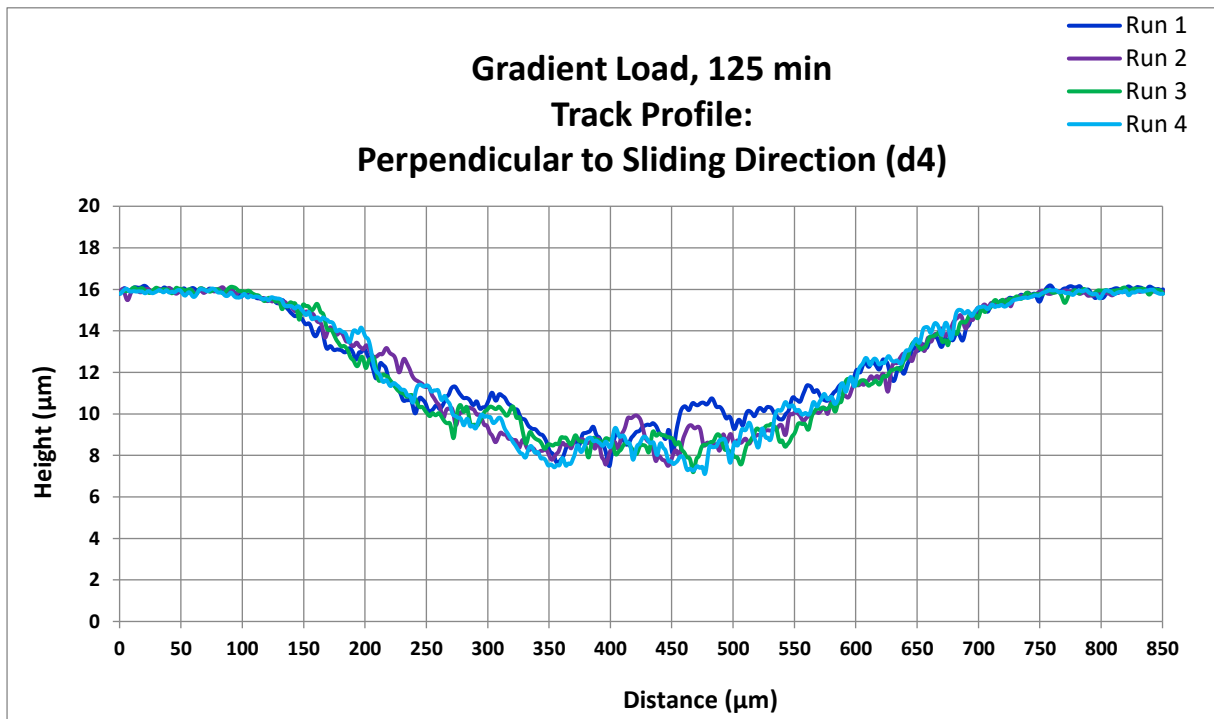


Figure C.4.4: Wear track profiles perpendicular to sliding direction for **Group III mineral oil (Gr III) with 2 % diethyl sebacate** with gradual load increase, 125 minutes.

2. 100 min

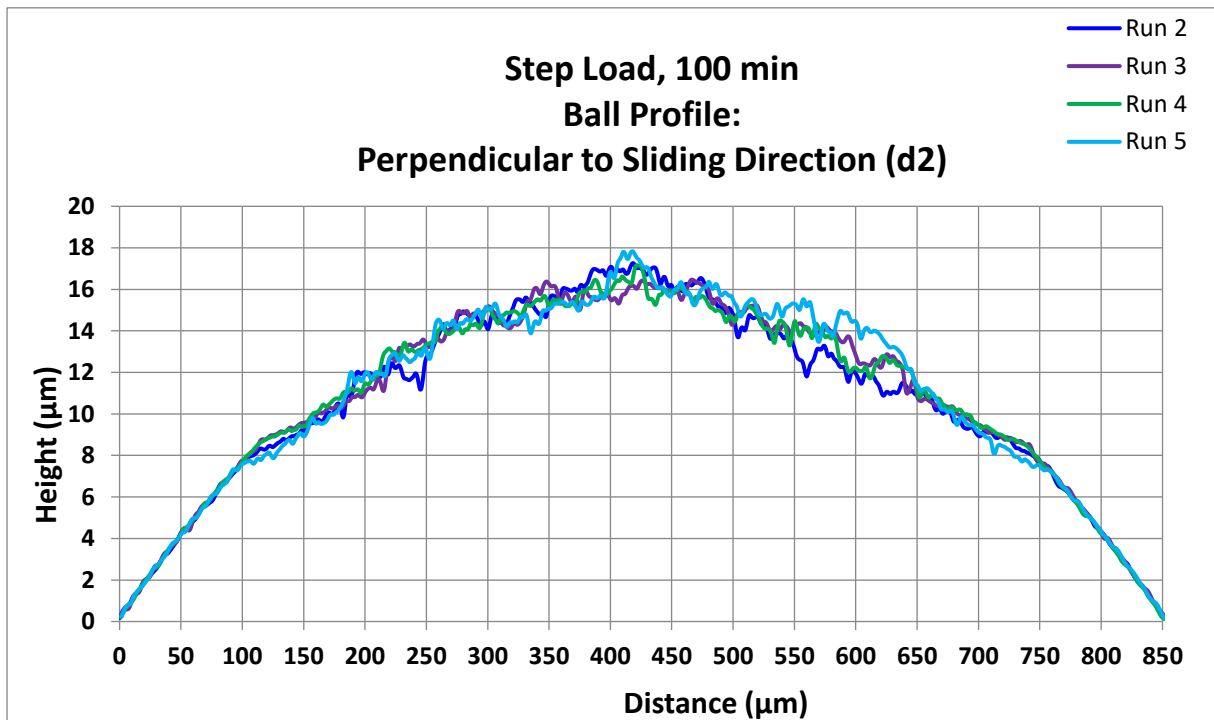


Figure C.4.5: Wear scar profiles perpendicular to sliding direction for **Group III mineral oil (Gr III)** with 2 % diethyl sebacate with step load increase, 100 minutes.

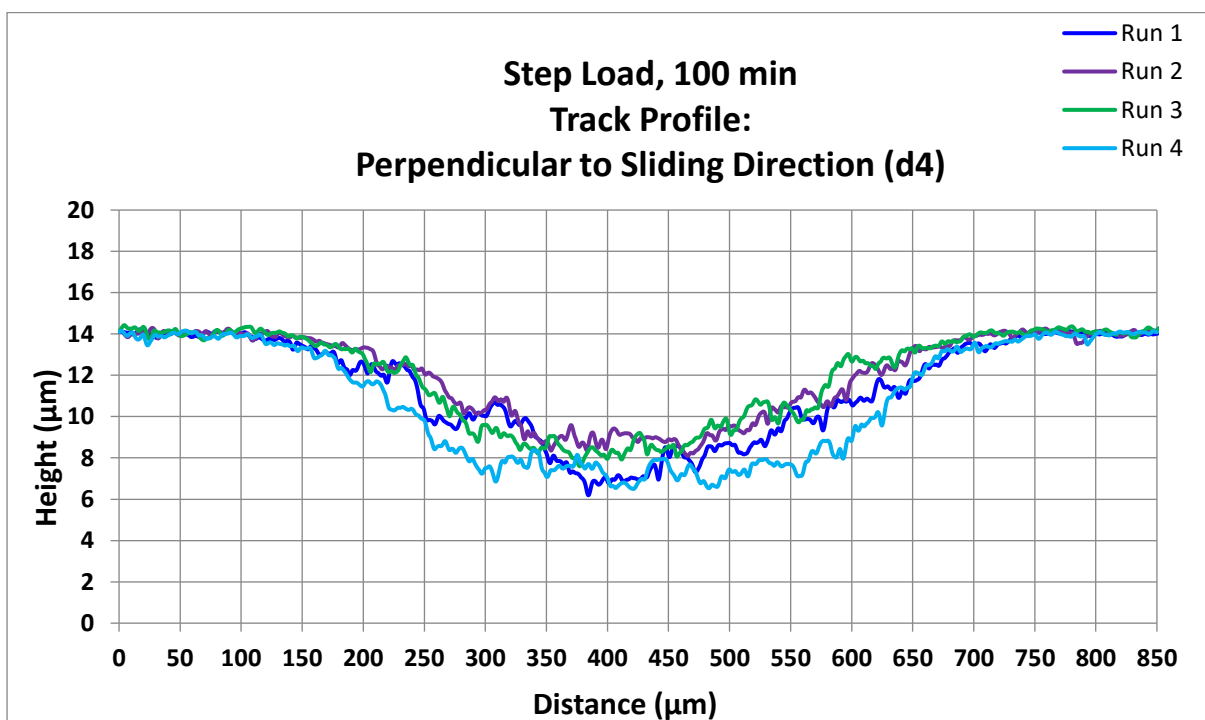


Figure C.4.6: Wear track profiles perpendicular to sliding direction for **Group III mineral oil (Gr III)** with 2 % diethyl sebacate with step load increase, 100 minutes.

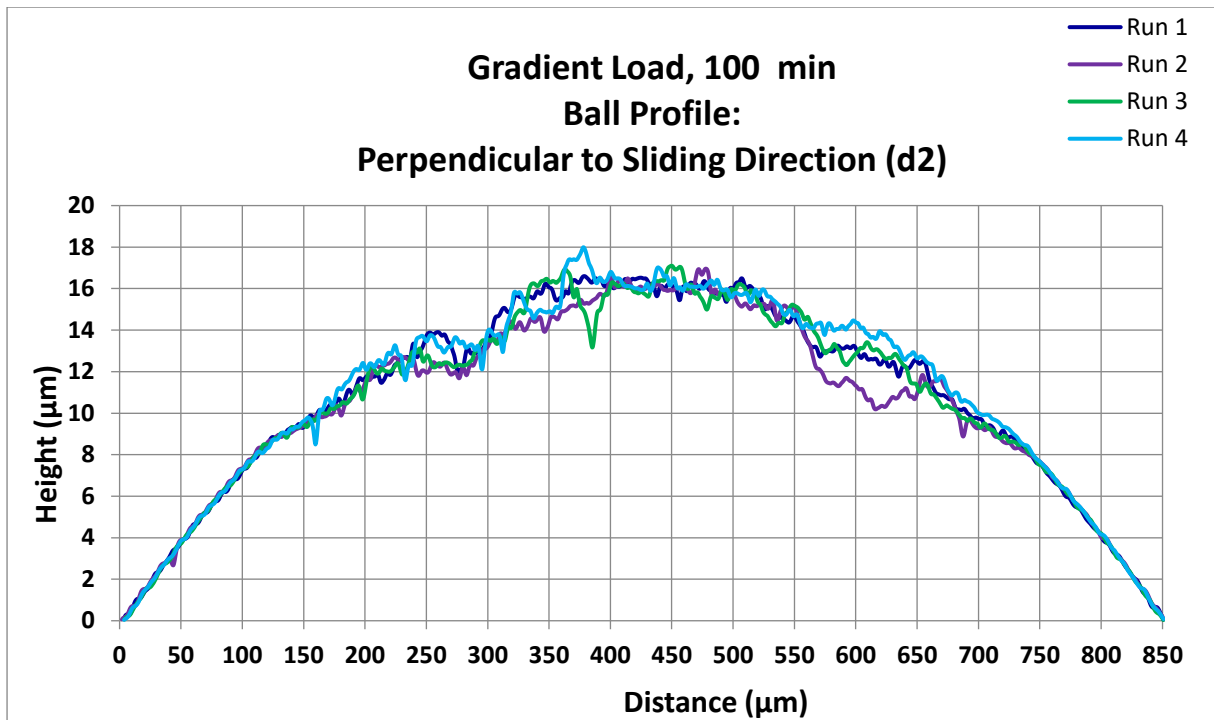


Figure C.4.7: Wear scar profiles perpendicular to sliding direction for **Group III mineral oil (Gr III) with 2 % diethyl sebacate** with gradual load increase, 100 minutes.

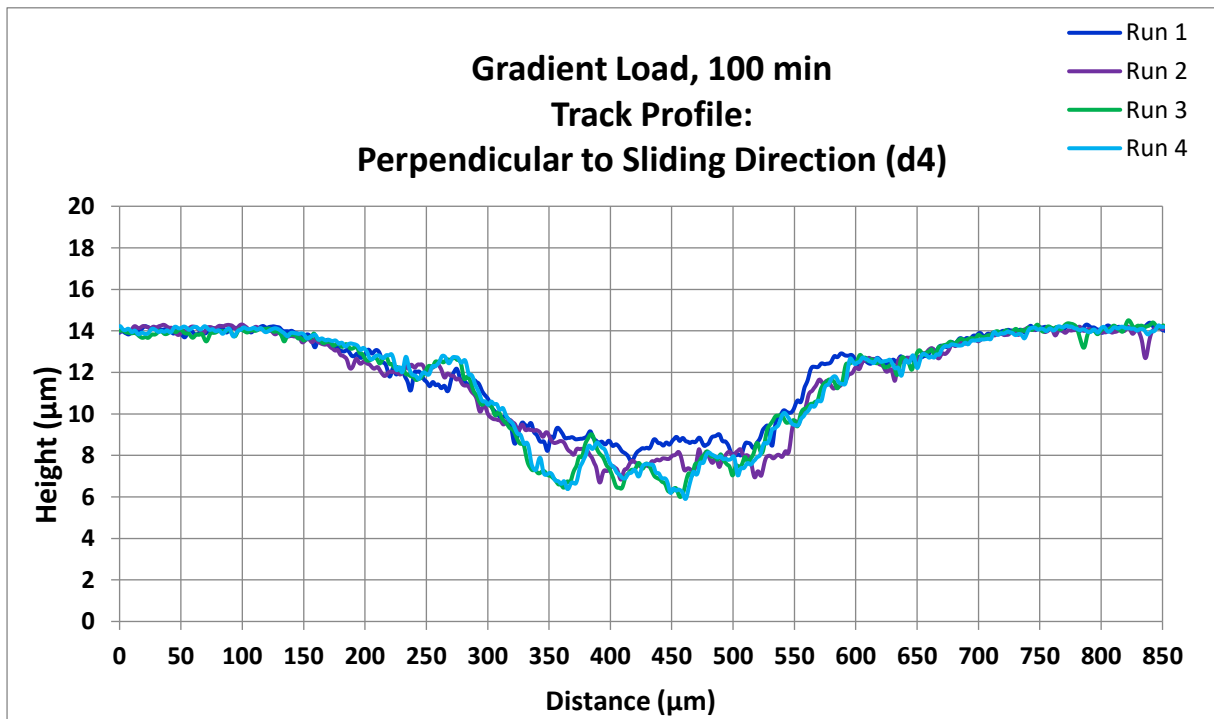


Figure C.4.8: Wear track profiles perpendicular to sliding direction for **Group III mineral oil (Gr III) with 2 % diethyl sebacate** with gradual load increase, 100 minutes.

3.75 min

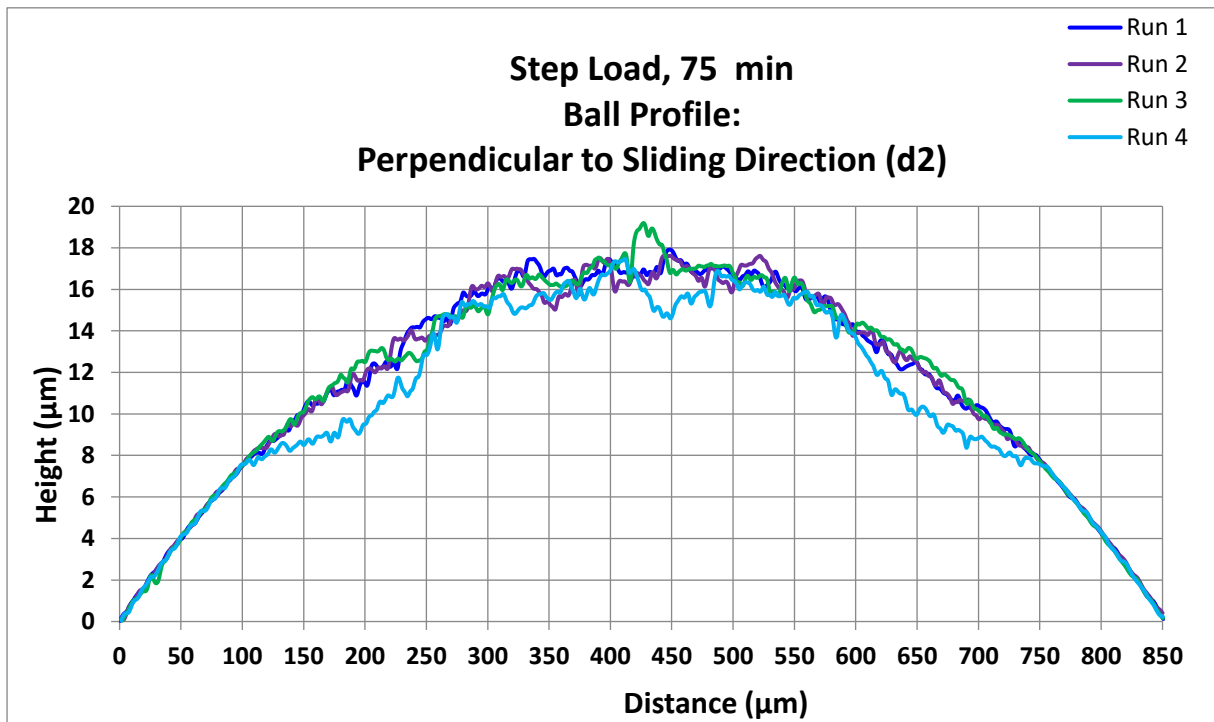


Figure C.4.9: Wear scar profiles perpendicular to sliding direction for **Group III mineral oil (Gr III) with 2 % diethyl sebacate** with step load increase, 75 minutes.

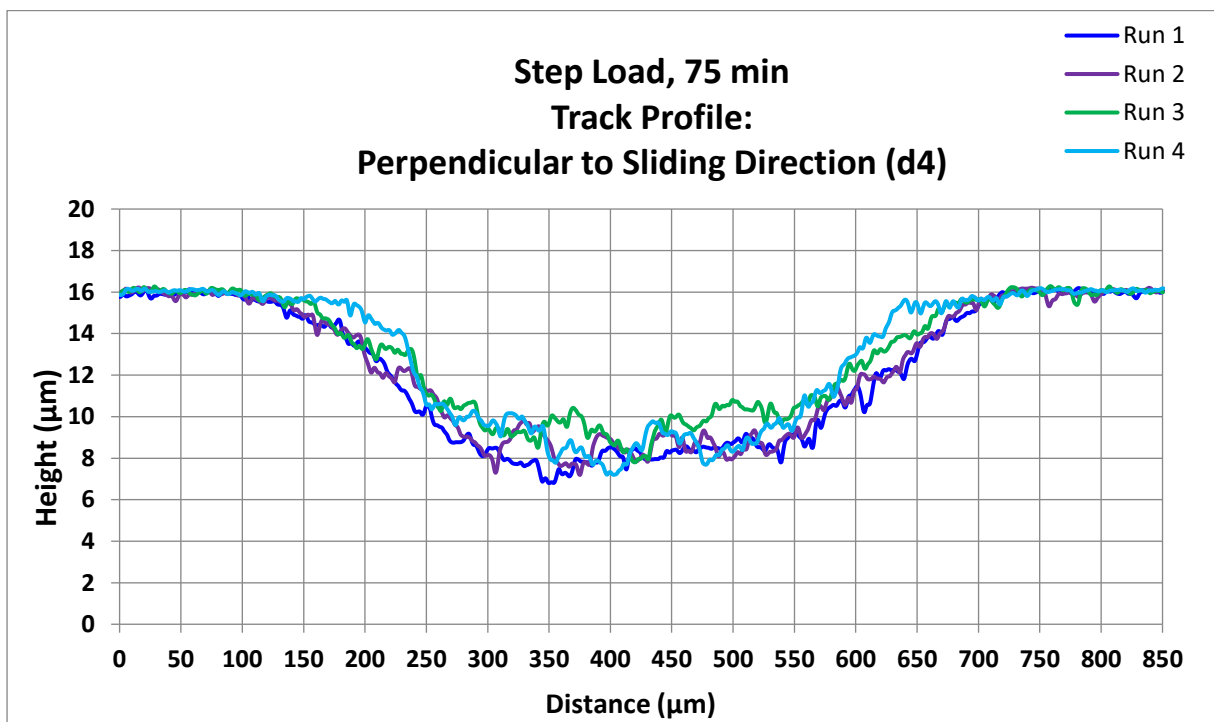


Figure C.4.10: Wear Track profiles perpendicular to sliding direction for **Group III mineral oil (Gr III) with 2 % diethyl sebacate** with step load increase, 75 minutes.

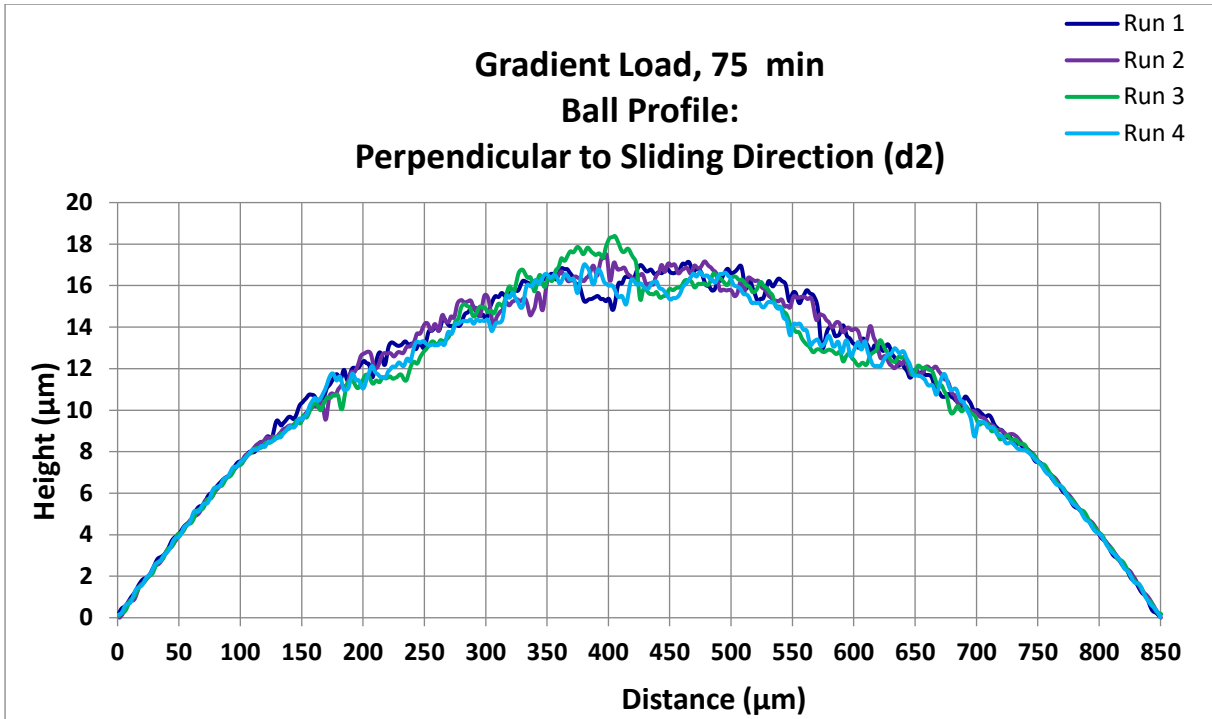


Figure C.4.11: Wear scar profiles perpendicular to sliding direction for **Group III** mineral oil (Gr III) with 2 % diethyl sebacate with gradual load increase, 75 minutes.

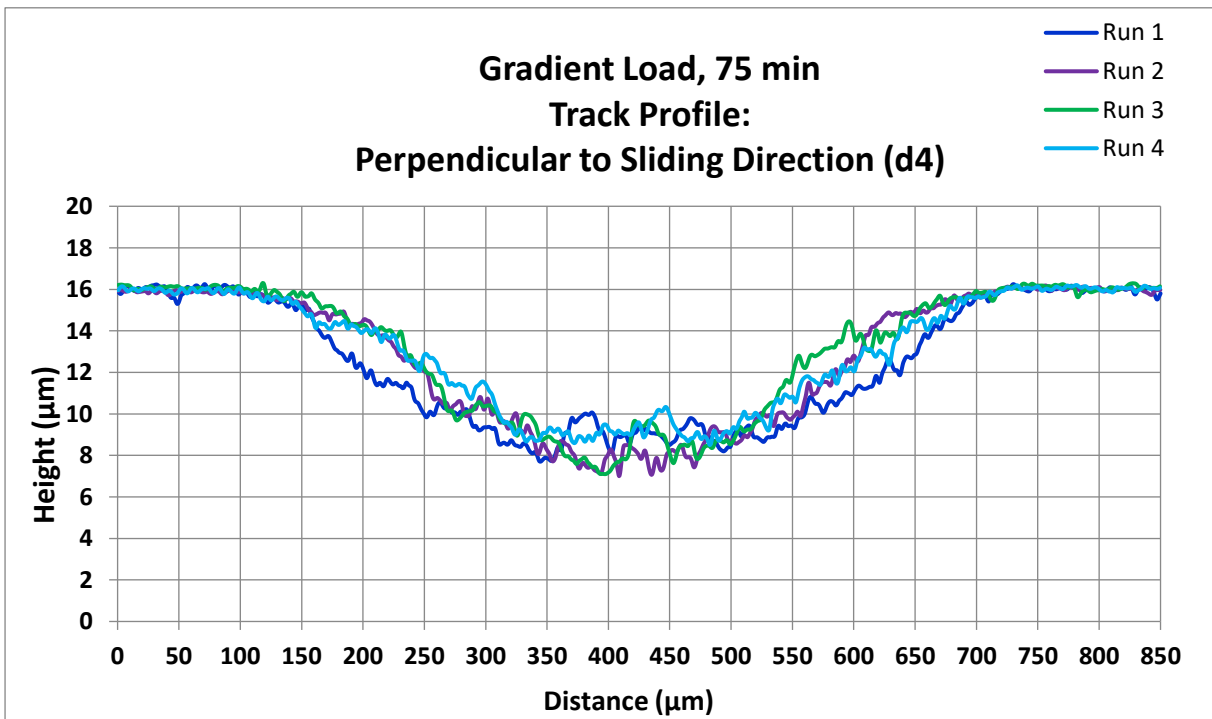


Figure C.4.12: Wear track profiles perpendicular to sliding direction for **Group III** mineral oil (Gr III) with 2 % diethyl sebacate with gradual load increase, 75 minutes.

4. 40 min

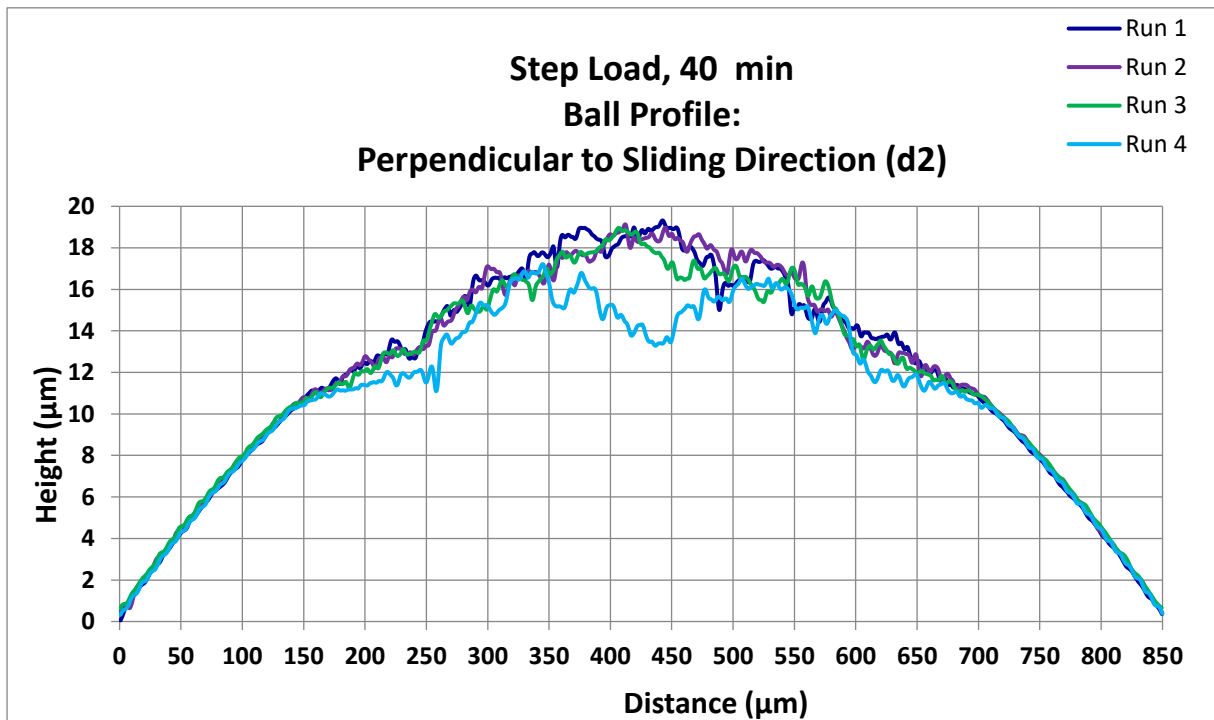


Figure C.4.13: Wear scar profiles perpendicular to sliding direction for **Group III mineral oil (Gr III) with 2 % diethyl sebacate** with step load increase, 40 minutes.

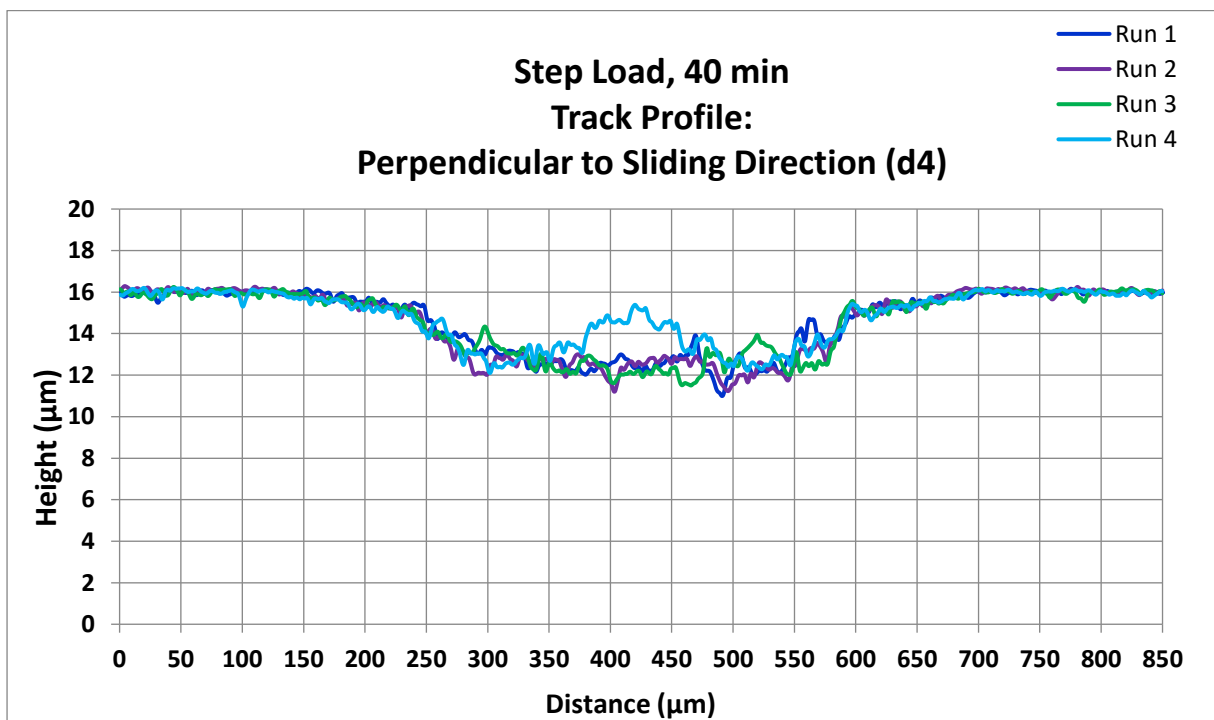


Figure C.4.14: Wear track profiles perpendicular to sliding direction for **Group III mineral oil (Gr III) with 2 % diethyl sebacate** with step load increase, 40 minutes.

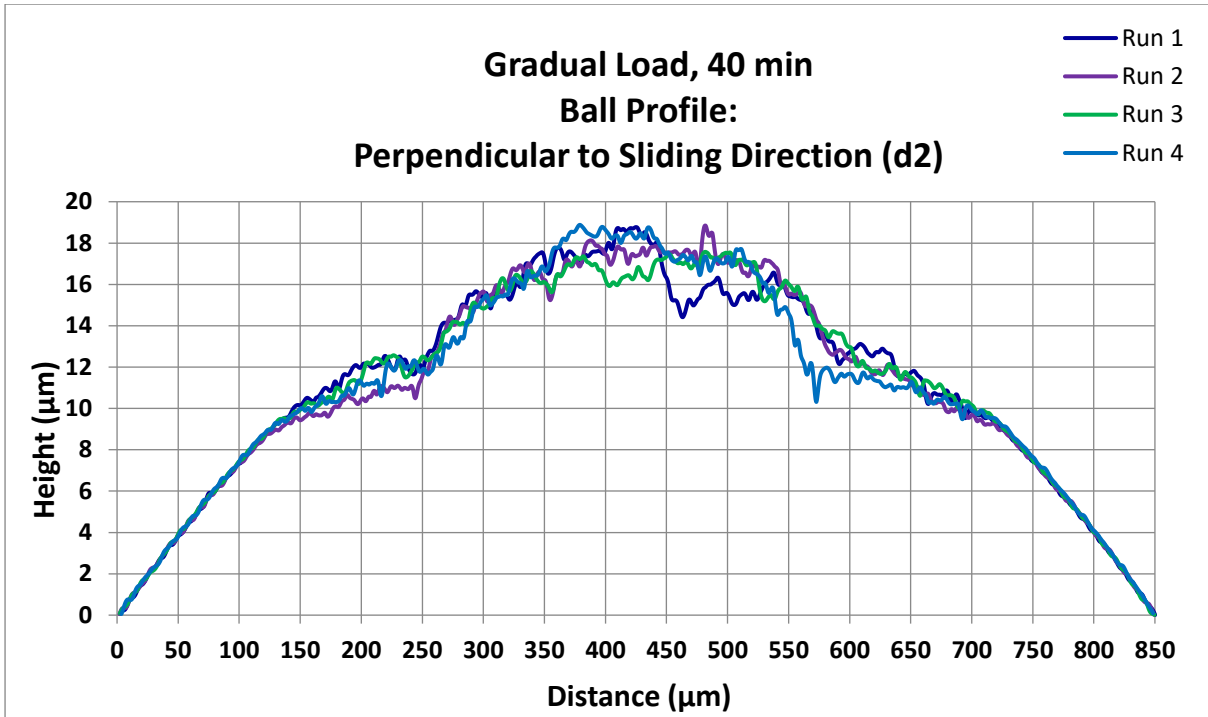


Figure C.4.15: Wear scar profiles perpendicular to sliding direction for **Group III** mineral oil (Gr III) with 2 % diethyl sebacate with gradual load increase, 40 minutes.

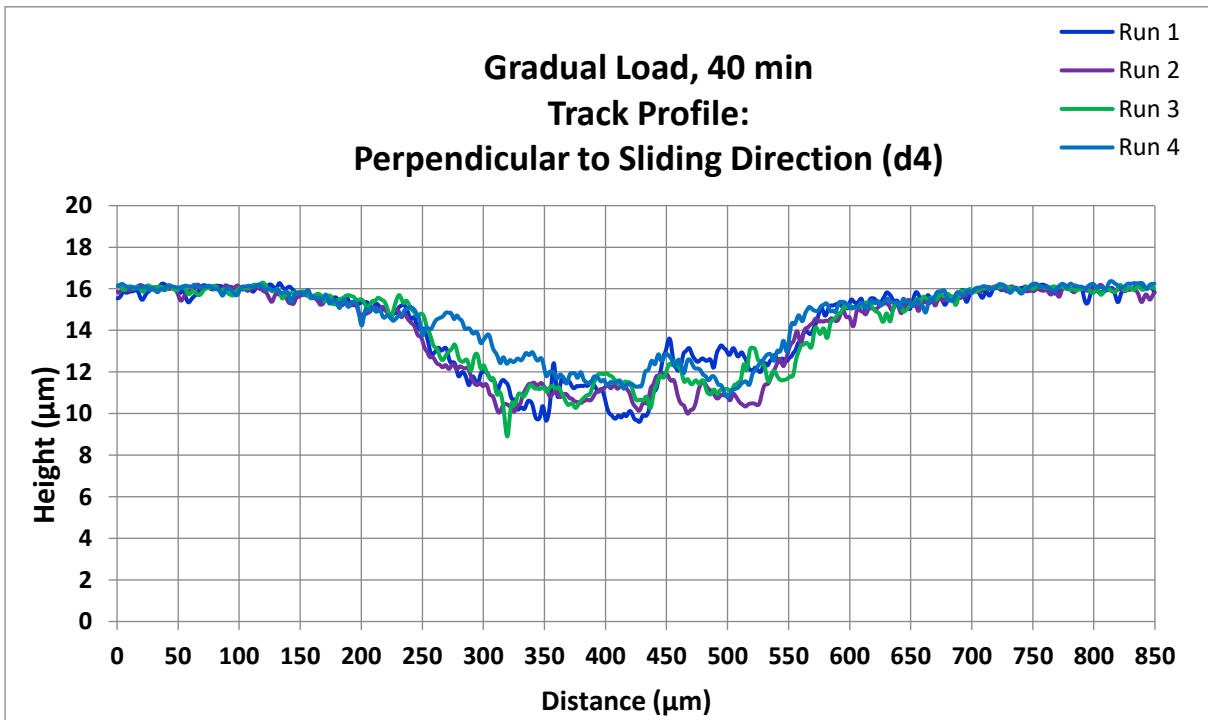


Figure C.4.16: Wear track profiles perpendicular to sliding direction for **Group III** mineral oil (Gr III) with 2 % diethyl sebacate with gradual load increase, 40 minutes.

5. 20 min

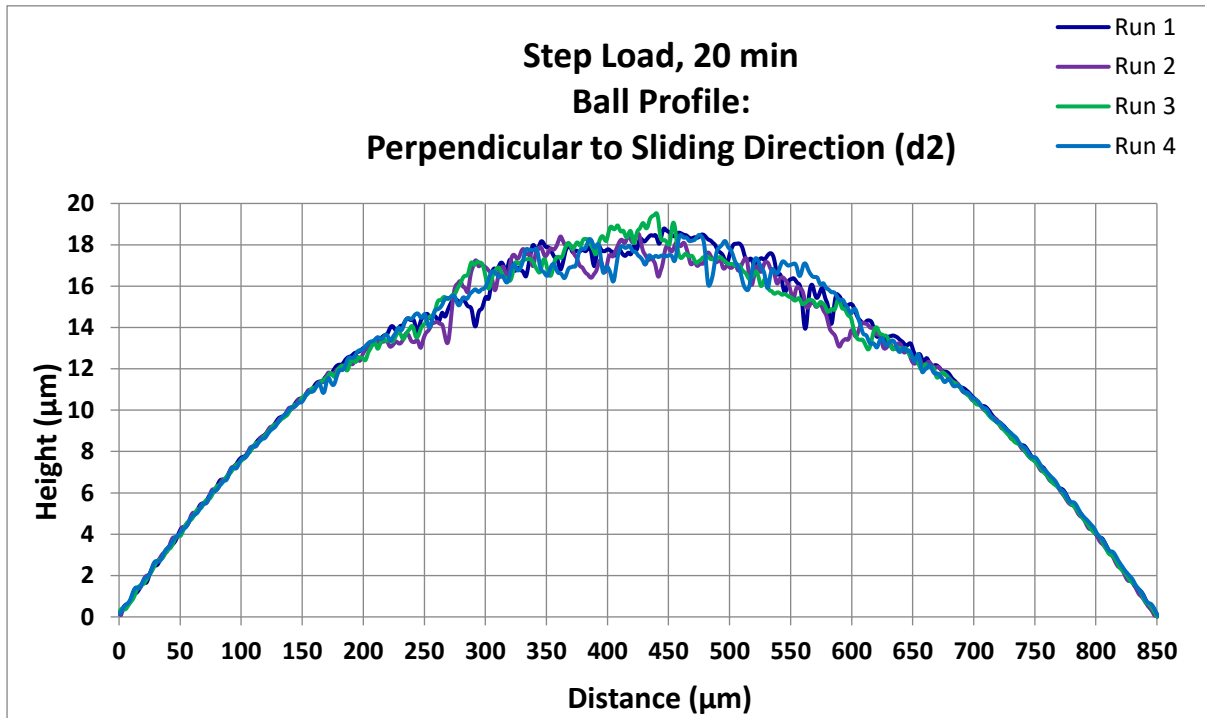


Figure C.4.17: Wear scar profiles perpendicular to sliding direction for **Group III** mineral oil (Gr III) with 2 % diethyl sebacate with step load increase, 20 minutes.

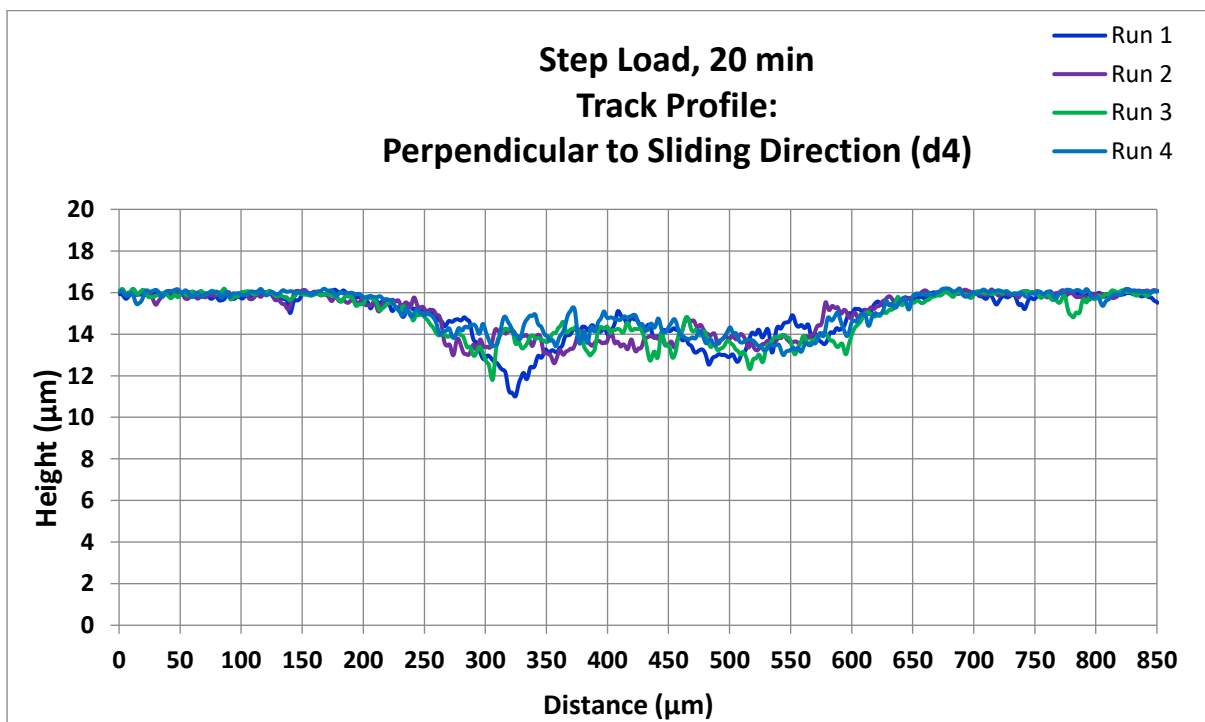


Figure C.4.18: Wear track profiles perpendicular to sliding direction for **Group III** mineral oil (Gr III) with 2 % diethyl sebacate with step load increase, 20 minutes.

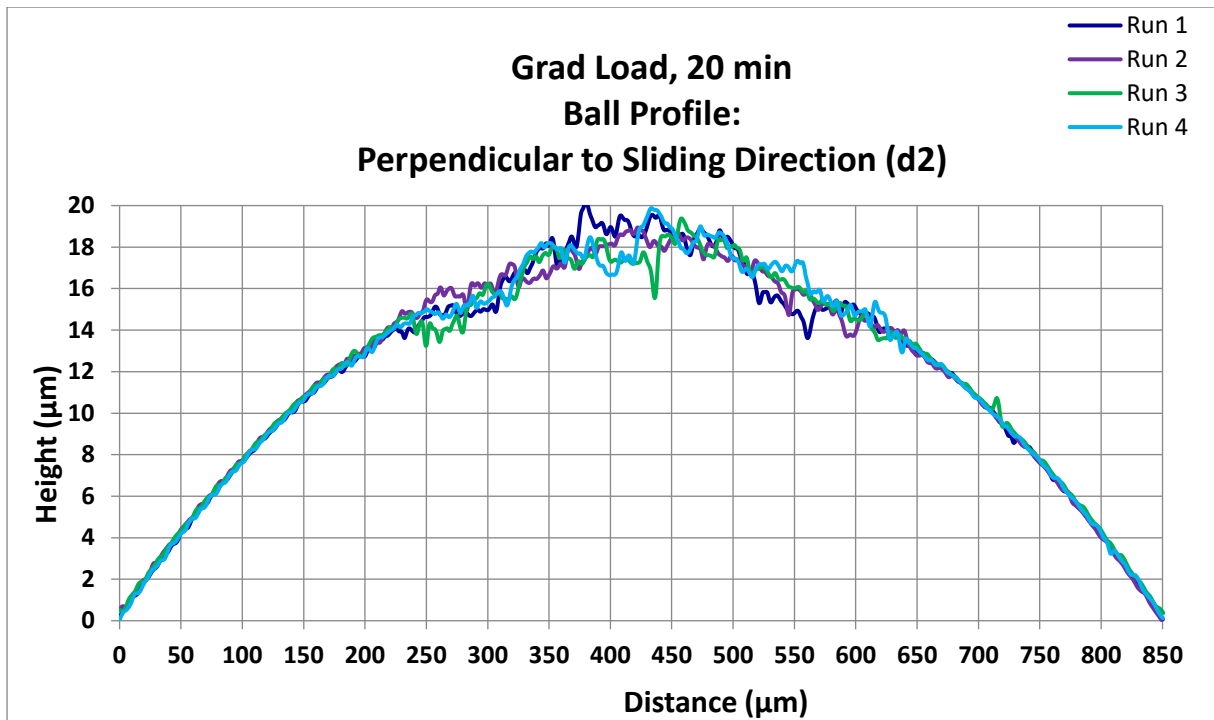


Figure C.4.19: Wear scar profiles perpendicular to sliding direction for **Group III mineral oil (Gr III) with 2 % diethyl sebacate** with gradual load increase, 20 minutes.

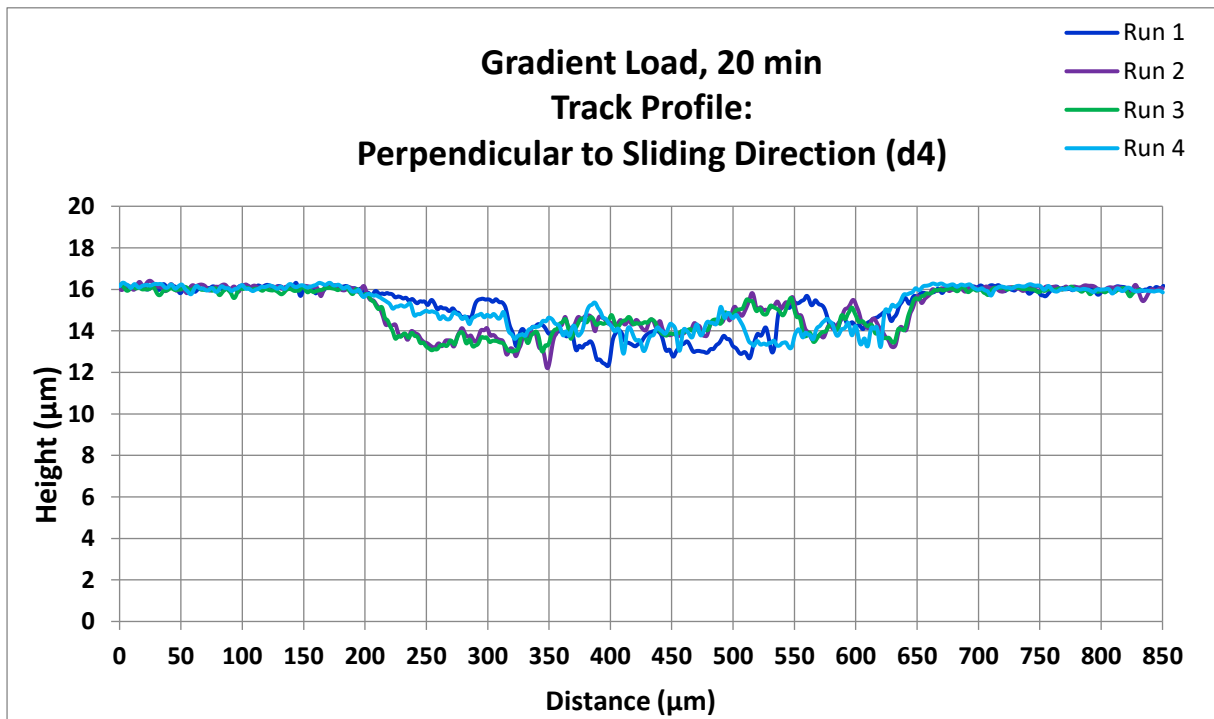


Figure C.4.20: Wear track profiles perpendicular to sliding direction for **Group III mineral oil (Gr III) with 2 % diethyl sebacate** with gradual load increase, 20 minutes.

6.5 Minutes

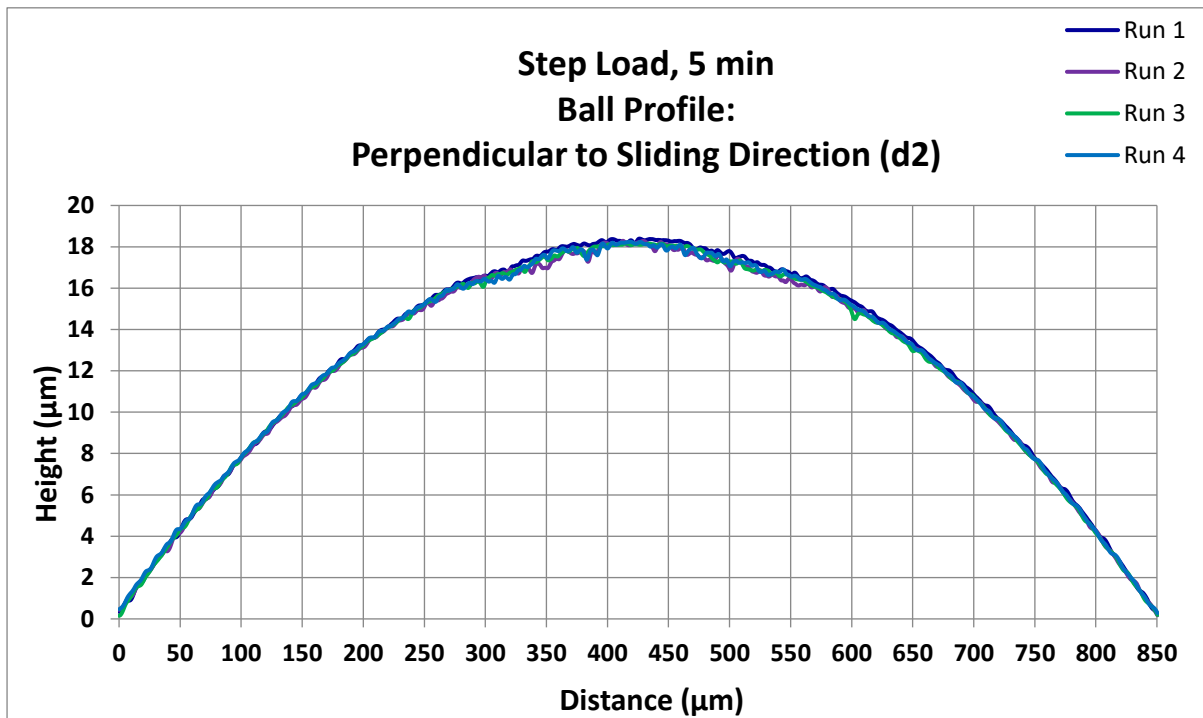


Figure C.4.21: Wear scar profiles perpendicular to sliding direction for **Group III** mineral oil (Gr III) with 2 % diethyl sebacate, 5 min.

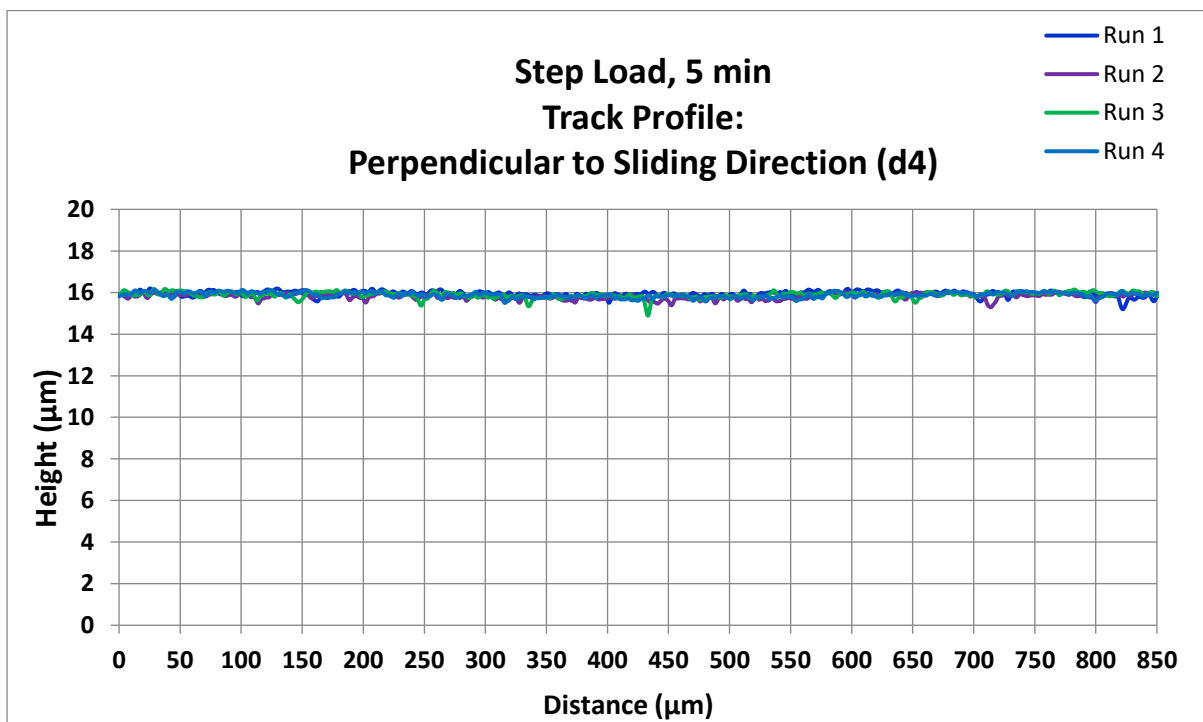


Figure C.4.22: Wear track profiles perpendicular to sliding direction for **Group III** mineral oil (Gr III) with 2 % diethyl sebacate, 5 min.

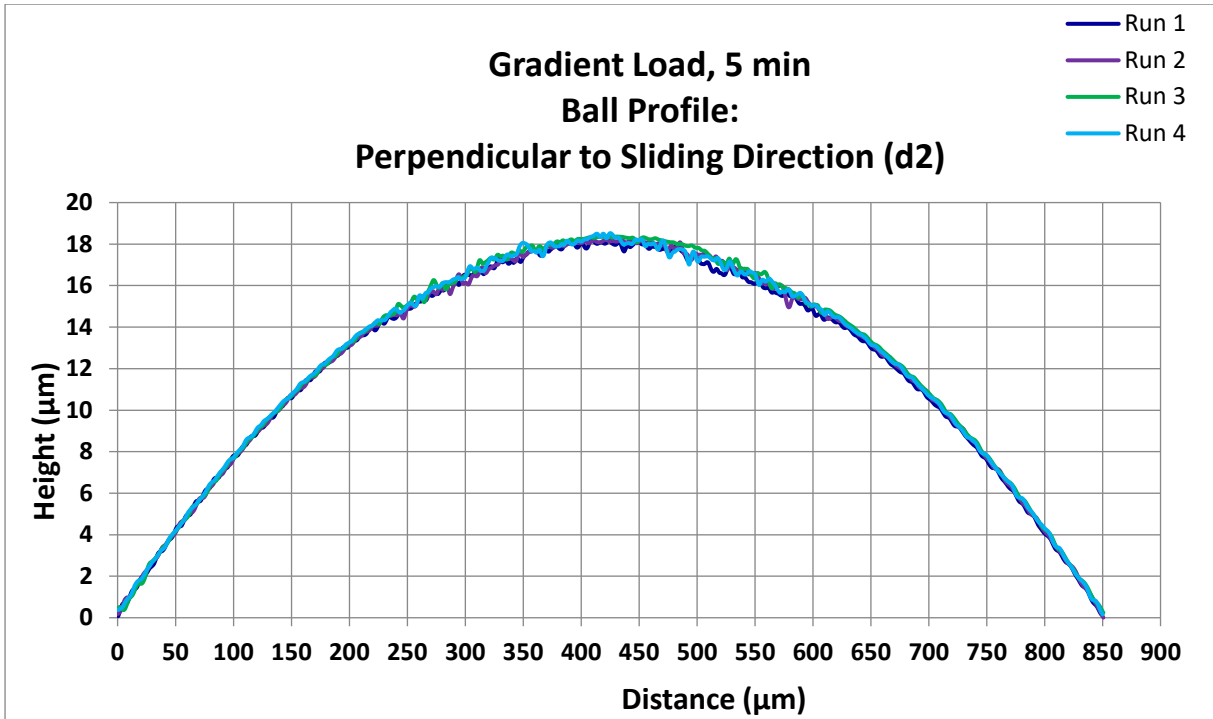


Figure C.4.23: Wear scar profiles perpendicular to sliding direction for **Group III** mineral oil (Gr III) with 2 % diethyl sebacate, 5 min.

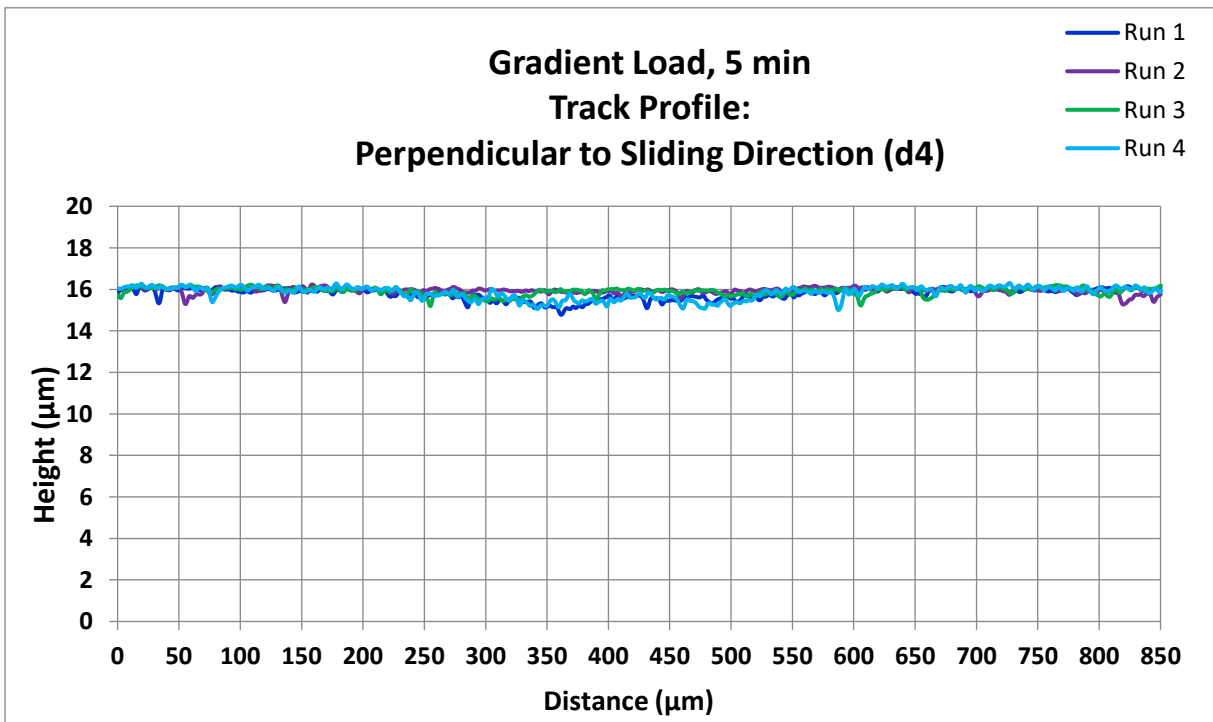


Figure C.4.24: Wear track profiles perpendicular to sliding direction for **Group III** mineral oil (Gr III) with 2 % diethyl sebacate, 5 min.

Appendix C.5: Wear Volume Calculations

Wear volumes calculated according to ASTM D 7755-17. Same formulas used as in Appendix B.5. The measured values and calculated values for the wear volumes of the scar and track can be found in Table C.5.1 to Table C.5.14 for all the wear surfaces.

Table C.5.1: Wear volume calculations for scars and tracks obtained with step load, 125 minutes.

Run	Scar Dimensions		Track Dimensions			Scar Calculations		Track Calculations	
	d_1 (mm)	d_2 (mm)	d_3 (mm)	d_4 (mm)	$W_{q,flat}$ (mm ²)	\bar{R}_s (mm)	$W_{v, ball}$ (mm ³)	\bar{R}_t (mm)	$W_{v, flat}$ (mm ³)
1	0.550	0.602	1.604	0.594	0.002	8.723	4.60E-04	8.366	2.84E-03
2	0.567	0.634	1.622	0.630	0.002	9.467	5.98E-04	9.302	3.05E-03
3	0.535	0.658	1.592	0.641	0.003	8.035	4.59E-04	7.442	3.90E-03
4	0.556	0.639	1.622	0.644	0.002	9.169	5.64E-04	9.368	3.21E-03
AVG	0.552	0.633	1.610	0.627	2.55E-03	8.849	5.2E-04	8.620	3.25E-03
STDEV	0.013	0.023	0.015	0.023	5.00E-04	0.623	7.15E-05	0.909	4.59E-04

Table C.5.2: Wear volume calculations for scars and tracks obtained with step load, 100 minutes.

Run	Scar Dimensions		Track Dimensions			Scar Calculations		Track Calculations	
	d_1 (mm)	d_2 (mm)	d_3 (mm)	d_4 (mm)	$W_{q,flat}$ (mm ²)	\bar{R}_s (mm)	$W_{v, ball}$ (mm ³)	\bar{R}_t (mm)	$W_{v, flat}$ (mm ³)
1	0.551	0.656	1.600	0.655	3.01E-03	7.806	4.61E-04	7.778	3.99E-03
2	0.557	0.658	1.596	0.656	3.19E-03	7.439	4.32E-04	7.383	4.21E-03
3	0.575	0.671	1.615	0.667	3.91E-03	6.434	3.26E-04	6.309	5.22E-03
4	0.594	0.650	1.596	0.652	3.04E-03	7.536	4.92E-04	7.586	4.02E-03
AVG	0.569	0.659	1.602	0.658	3.29E-03	7.304	4.28E-04	7.264	4.36E-03
STDEV	0.019	0.009	0.009	0.007	4.22E-04	0.600	7.21E-05	0.657	5.82E-04

Table C.5.3: Wear volume calculations for scars and tracks obtained with step load, 75 minutes.

Run	Scar Dimensions		Track Dimensions			Scar Calculations		Track Calculations	
	d_1 (mm)	d_2 (mm)	d_3 (mm)	d_4 (mm)	$W_{q,flat}$ (mm ²)	\bar{R}_s (mm)	$W_{v, ball}$ (mm ³)	\bar{R}_t (mm)	$W_{v, flat}$ (mm ³)
1	0.595	0.630	1.589	0.622	3.35E-03	6.227	2.72E-04	5.991	4.45E-03
2	0.601	0.632	1.589	0.626	3.19E-03	6.578	3.39E-04	6.409	4.24E-03
3	0.585	0.608	1.596	0.608	2.75E-03	6.801	3.28E-04	6.800	3.70E-03
4	0.592	0.649	1.611	0.648	2.78E-03	8.189	5.63E-04	8.177	3.72E-03
AVG	0.593	0.630	1.596	0.626	3.02E-03	6.949	3.76E-04	6.844	4.03E-03
STDEV	0.007	0.017	0.010	0.017	2.99E-04	0.860	1.28E-04	0.948	3.77E-04

Table C.5.4: Wear volume calculations for scars and tracks obtained with step load, 40 minutes.

Run	Scar Dimensions		Track Dimensions			Scar Calculations		Track Calculations	
	d_1 (mm)	d_2 (mm)	d_3 (mm)	d_4 (mm)	$W_{q,flat}$ (mm ²)	\bar{R}_s (mm)	$W_{v, ball}$ (mm ³)	\bar{R}_t (mm)	$W_{v, flat}$ (mm ³)
1	0.535	0.536	1.563	0.531	1.26E-03	10.246	4.13E-04	9.922	1.70E-03
2	0.514	0.546	1.549	0.534	1.42E-03	9.521	3.67E-04	8.933	1.90E-03
3	0.536	0.566	1.582	0.542	1.36E-03	11.045	4.95E-04	9.728	1.87E-03
4	0.617	0.567	1.622	0.564	1.12E-03	13.644	7.63E-04	13.409	1.57E-03
AVG	0.556	0.560	1.584	0.547	1.30E-03	11.403	5.42E-04	10.690	1.78E-03
STDEV	0.054	0.012	0.037	0.016	2.59E-04	2.085	2.02E-04	2.388	1.82E-04

Table C.5.5: Wear volume calculations for scars and tracks obtained with step load, 20 minutes.

Run	Scar Dimensions		Track Dimensions			Scar Calculations		Track Calculations	
	d_1 (mm)	d_2 (mm)	d_3 (mm)	d_4 (mm)	$W_{q,flat}$ (mm ²)	\bar{R}_s (mm)	$W_{v, ball}$ (mm ³)	\bar{R}_t (mm)	$W_{v, flat}$ (mm ³)
1	0.472	0.479	1.482	0.454	9.04E-04	10.137	2.54E-04	8.652	1.18E-03
2	0.494	0.490	1.531	0.480	8.76E-04	11.226	3.20E-04	10.509	1.18E-03
3	0.494	0.498	1.509	0.491	9.54E-04	10.760	3.18E-04	10.354	1.25E-03
4	0.505	0.484	1.508	0.468	8.25E-04	11.471	3.31E-04	10.379	1.09E-03
AVG	0.498	0.491	1.516	0.480	8.85E-04	11.152	3.23E-04	10.414	1.17E-03
STDEV	0.006	0.007	0.013	0.012	6.50E-05	0.361	7.00E-06	0.083	8.02E-05

Table C.5.6: Wear volume calculations for scars and tracks obtained with step load increase, 5 minutes.

Run	Scar Dimensions		Track Dimensions			Scar Calculations		Track Calculations	
	d_1 (mm)	d_2 (mm)	d_3 (mm)	d_4 (mm)	$W_{q,flat}$ (mm ²)	\bar{R}_s (mm)	$W_{v, ball}$ (mm ³)	\bar{R}_t (mm)	$W_{v, flat}$ (mm ³)
1	0.383	0.392	1.325	0.268	9.27E-05	54.370	2.02E-04	17.222	1.14E-04
2	0.402	0.385	1.435	0.366	1.14E-04	41.842	2.07E-04	35.892	1.48E-04
3	0.392	0.387	1.304	0.275	9.69E-05	49.902	2.04E-04	17.795	1.16E-04
4	0.392	0.392	1.435	0.326	1.16E-04	43.314	2.06E-04	24.892	1.56E-04
AVG	0.395	0.388	1.391	0.322	1.09E-04	45.019	2.06E-04	26.193	1.40E-04
STDEV	0.006	0.004	0.076	0.046	1.05E-05	4.292	1.53E-06	9.118	2.12E-05

Table C.5.7: Wear volume calculations for scars and tracks obtained with gradual load, 125 minutes.

Run	Scar Dimensions		Track Dimensions			Scar Calculations		Track Calculations	
	d_1 (mm)	d_2 (mm)	d_3 (mm)	d_4 (mm)	$W_{q,flat}$ (mm ²)	\bar{R}_s (mm)	$W_{v, ball}$ (mm ³)	\bar{R}_t (mm)	$W_{v, flat}$ (mm ³)
1	0.597	0.665	1.611	0.663	3.05E-03	8.055	5.87E-04	7.976	4.06E-03
2	0.586	0.656	1.600	0.655	3.01E-03	7.806	5.21E-04	7.778	3.99E-03
3	0.584	0.658	1.596	0.656	3.19E-03	7.439	4.75E-04	7.383	4.21E-03
5	0.584	0.650	1.596	0.652	3.04E-03	7.536	4.77E-04	7.586	4.02E-03
AVG	0.585	0.655	1.597	0.654	3.08E-03	7.594	4.91E-04	7.582	4.07E-03
STDEV	0.001	0.004	0.002	0.002	9.64E-05	0.190	2.60E-05	0.198	1.19E-04

Table C.5.8: Wear volume calculations for scars and tracks obtained with gradual load, 100 minutes.

Run	Scar Dimensions		Track Dimensions			Scar Calculations		Track Calculations	
	d_1 (mm)	d_2 (mm)	d_3 (mm)	d_4 (mm)	$W_{q,flat}$ (mm ²)	\bar{R}_s (mm)	$W_{v, ball}$ (mm ³)	\bar{R}_t (mm)	$W_{v, flat}$ (mm ³)
1	0.549	0.604	1.585	0.597	1.88E-03	9.762	5.28E-04	9.425	2.52E-03
2	0.569	0.626	1.589	0.611	2.11E-03	9.730	6.07E-04	9.044	2.81E-03
3	0.562	0.614	1.596	0.611	2.09E-03	9.205	5.33E-04	9.103	2.81E-03
4	0.570	0.618	1.582	0.604	2.09E-03	9.403	5.69E-04	8.772	2.78E-03
AVG	0.567	0.619	1.589	0.609	2.10E-03	9.446	5.70E-04	8.973	2.80E-03
STDEV	0.004	0.006	0.007	0.004	1.15E-05	0.265	3.70E-05	0.177	1.73E-05

Table C.5.9: Wear volume calculations for scars and tracks obtained with gradual load, 75 minutes.

Run	Scar Dimensions		Track Dimensions			Scar Calculations		Track Calculations	
	d_1 (mm)	d_2 (mm)	d_3 (mm)	d_4 (mm)	$W_{q,flat}$ (mm ²)	\bar{R}_s (mm)	$W_{v, ball}$ (mm ³)	\bar{R}_t (mm)	$W_{v, flat}$ (mm ³)
1	0.604	0.636	1.592	0.630	3.18E-03	6.726	3.72E-04	6.540	4.23E-03
2	0.575	0.611	1.581	0.615	2.76E-03	6.915	3.36E-04	7.033	3.65E-03
3	0.571	0.625	1.604	0.619	2.70E-03	7.529	4.19E-04	7.335	3.63E-03
4	0.577	0.629	1.593	0.622	2.67E-03	7.770	4.61E-04	7.522	3.55E-03
AVG	0.574	0.622	1.593	0.619	2.71E-03	7.405	4.05E-04	7.297	3.61E-03
STDEV	0.003	0.009	0.012	0.004	4.58E-05	0.441	6.36E-05	0.247	5.29E-05

Table C.5.10: Wear volume calculations for scars and tracks obtained with gradual load, 40 minutes.

Run	Scar Dimensions		Track Dimensions			Scar Calculations		Track Calculations	
	d_1 (mm)	d_2 (mm)	d_3 (mm)	d_4 (mm)	$W_{q,flat}$ (mm ²)	\bar{R}_s (mm)	$W_{v, ball}$ (mm ³)	\bar{R}_t (mm)	$W_{v, flat}$ (mm ³)
1	0.540	0.566	1.589	0.556	1.73E-03	8.712	3.91E-04	8.265	2.37E-03
2	0.546	0.597	1.589	0.586	1.85E-03	9.554	4.96E-04	9.039	2.50E-03
3	0.543	0.573	1.589	0.553	1.62E-03	9.688	4.61E-04	8.688	2.22E-03
4	0.549	0.582	1.593	0.575	1.47E-03	11.181	5.55E-04	10.740	2.00E-03
AVG	0.546	0.584	1.590	0.571	1.65E-03	10.141	5.04E-04	9.489	2.24E-03
STDEV	0.003	0.012	0.002	0.017	1.91E-04	0.903	4.75E-05	1.098	2.51E-04

Table C.5.11: Wear volume calculations for scars and tracks obtained with gradual load, 20 minutes.

Run	Scar Dimensions		Track Dimensions			Scar Calculations		Track Calculations	
	d_1 (mm)	d_2 (mm)	d_3 (mm)	d_4 (mm)	$W_{q,flat}$ (mm ²)	\bar{R}_s (mm)	$W_{v, ball}$ (mm ³)	\bar{R}_t (mm)	$W_{v, flat}$ (mm ³)
1	0.483	0.481	1.509	0.472	8.45E-04	10.996	2.89E-04	10.371	1.12E-03
2	0.488	0.496	1.516	0.490	8.36E-04	12.152	3.39E-04	11.756	1.10E-03
3	0.518	0.490	1.548	0.490	8.67E-04	11.343	3.54E-04	11.334	1.18E-03
4	0.498	0.485	1.508	0.480	8.82E-04	10.767	3.06E-04	10.442	1.16E-03
AVG	0.501	0.490	1.524	0.487	8.62E-04	11.421	3.33E-04	11.177	1.15E-03
STDEV	0.015	0.006	0.021	0.006	2.35E-05	0.696	2.46E-05	0.671	4.16E-05

Table C.5.12: Wear volume calculations for scars and tracks obtained with gradual load increase, 5 min.

Run	Scar Dimensions		Track Dimensions			Scar Calculations		Track Calculations	
	d_1 (mm)	d_2 (mm)	d_3 (mm)	d_4 (mm)	$W_{q,flat}$ (mm ²)	\bar{R}_s (mm)	$W_{v, ball}$ (mm ³)	\bar{R}_t (mm)	$W_{v, flat}$ (mm ³)
1	0.415	0.402	1.454	0.388	1.87E-04	28.950	2.26E-04	26.021	2.45E-04
2	0.396	0.390	1.329	0.268	1.00E-04	49.323	2.11E-04	15.888	1.24E-04
3	0.389	0.389	1.420	0.377	1.21E-04	40.651	1.97E-04	37.074	1.54E-04
4	0.411	0.398	1.449	0.385	2.71E-04	19.416	1.95E-04	17.558	3.55E-04
AVG	0.399	0.392	1.399	0.343	1.64E-04	36.463	2.01E-04	23.507	2.11E-04
STDEV	0.011	0.005	0.063	0.065	9.33E-05	15.387	8.72E-06	11.779	1.26E-04

Appendix C.6: Disk Hardness

1. Rockwell Hardness Disk 17

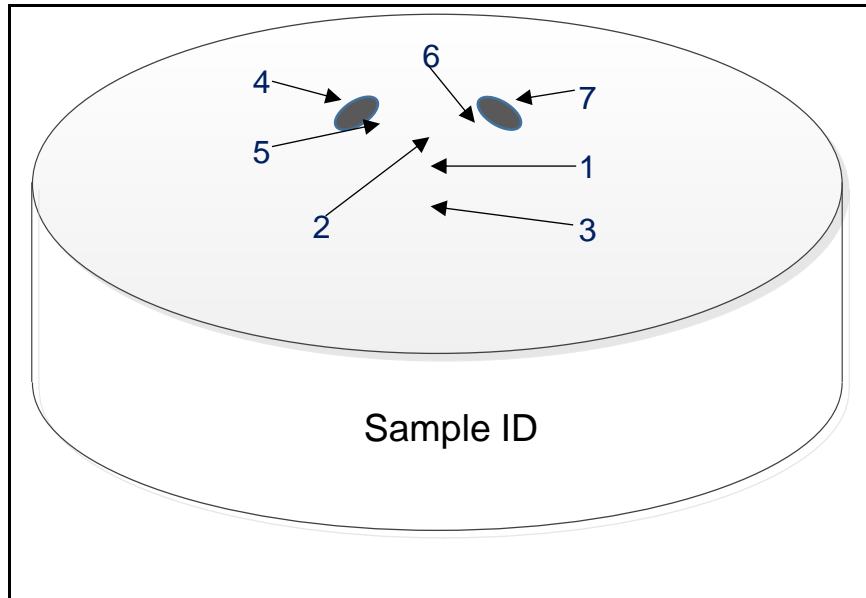


Figure C.6.1: Position on disk where hardness was measured.

Table C.6.1: Rockwell hardness of Disks 17.

Position on Disk	Rockwell Hardness
1	58.6
2	58.6
3	58.4
4	58.9
5	59.0
6	58.5
7	59.1

2. Rockwell Hardness Disk 18

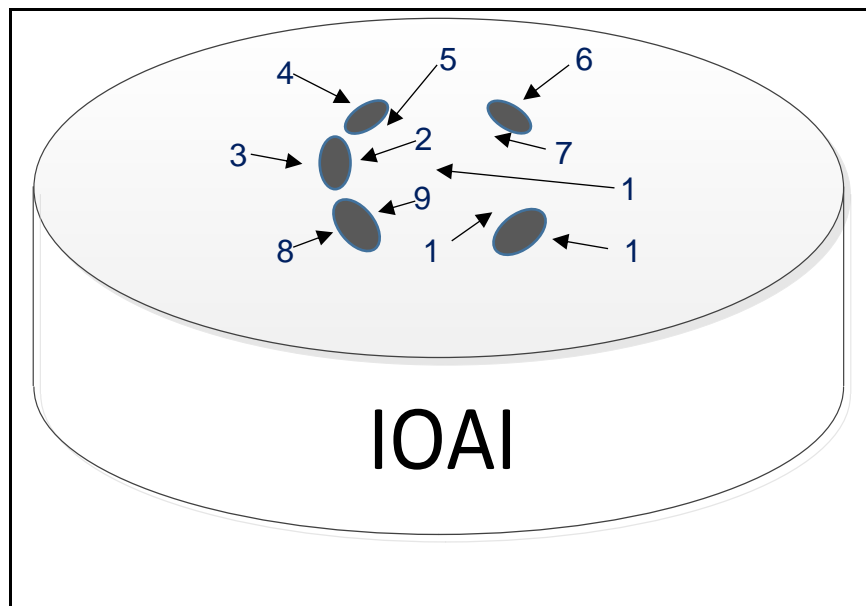


Figure C.6.2: Position on disk where hardness was measured.

Table C.6.2: Rockwell hardness of Disks 18.

Position on Disk	Rockwell Hardness
1	59.2
2	59.8
3	59.6
4	59.2
5	60.3
6	59.7
7	59.9
8	59.8
9	60.1
10	59.7
11	59.9

3. Rockwell Hardness Disk 19

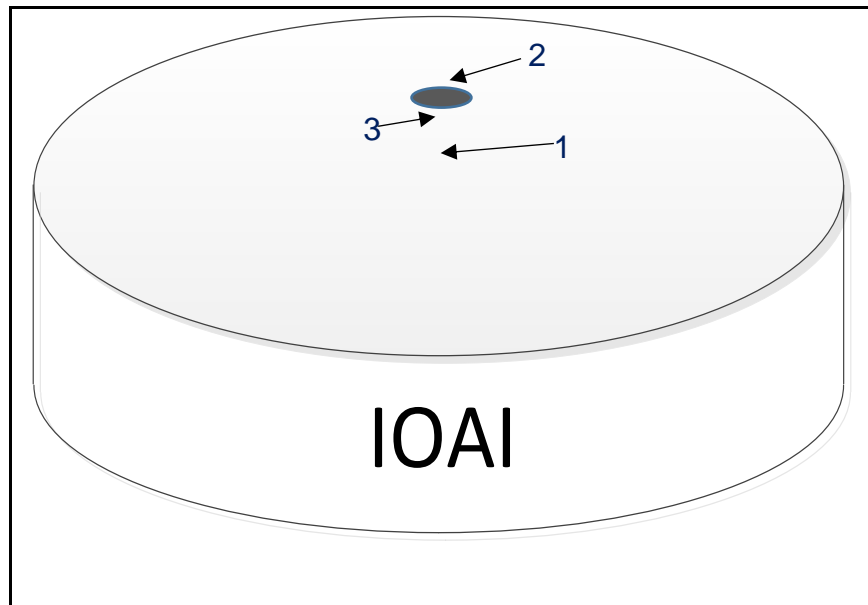


Figure C.6.3: Position on disk where hardness was measured.

Table C.6.3: Rockwell hardness of Disks 19.

Position on Disk	Rockwell Hardness
1	59.7
2	60.1
3	59.5

4. Rockwell Hardness Disk 20

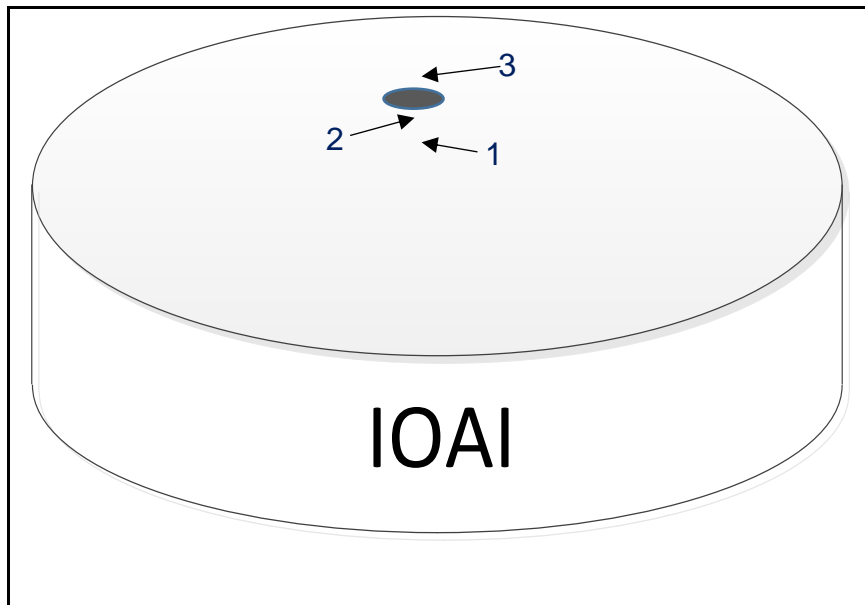


Figure C.6.4: Position on disk where hardness was measured.

Table C.6.4: Rockwell hardness of Disks 20.

Position on Disk	Rockwell Hardness
1	59.8
2	60.3
3	59.9